BEILSTEIN JOURNAL OF ORGANIC CHEMISTRY

Superstructures with cyclodextrins: Chemistry and applications IV

Edited by Gerhard Wenz

Imprint

Beilstein Journal of Organic Chemistry
www.bjoc.org
ISSN 1860-5397
Email: journals-support@beilstein-institut.de

The *Beilstein Journal of Organic Chemistry* is published by the Beilstein-Institut zur Förderung der Chemischen Wissenschaften.

Beilstein-Institut zur Förderung der Chemischen Wissenschaften
Trakehner Straße 7–9
60487 Frankfurt am Main
Germany
www.beilstein-institut.de

BEILSTEIN JOURNAL OF ORGANIC CHEMISTRY

Superstructures with cyclodextrins: Chemistry and applications IV

Gerhard Wenz

Editorial

Open Access

Address:
Saarland University, Organic Macromolecular Chemistry, Campus C4 2, 66123 Saarbrücken, Germany

Email:
Gerhard Wenz - g.wenz@mx.uni-saarland.de

Keywords:
cyclodextrins; superstructures

Beilstein J. Org. Chem. **2017,** *13,* 2157–2159.
doi:10.3762/bjoc.13.215

Received: 15 September 2017
Accepted: 25 September 2017
Published: 18 October 2017

This article is part of the Thematic Series "Superstructures with cyclodextrins: Chemistry and applications IV".

Guest Editor: G. Wenz

Superstructures are generally formed from molecules through non-covalent interactions, which can be either attractive or repulsive. The first examples of superstructures formed by attractive intermolecular forces were complexes of crown ethers [1], cryptands [2] and spherands [3], which were recognized by the 1987 Nobel Prize in Chemistry. In addition, inclusion compounds of cyclodextrins (CDs), cyclic oligomers of glucose, belong to this category and have been known since the pioneering work of Friedrich Cramer in 1951 [4,5]. Superstructures can also be held together by repulsive forces, so-called mechanical bonds [6], as exemplified in catenanes, rotaxanes, and knots [7]. Because of their restricted mobility, rotaxanes are well-suited for the design of molecular machines, which were the subject of the 2016 Nobel Prize in Chemistry [8,9]. Since superstructures are accessible through rational design, supramolecular chemistry had a great influence on organic and macromolecular chemistry as well as pharmacology and materials sciences. CDs in particular became the most important building blocks for superstructures because they are the only hosts that are non-toxic and available on an industrial scale. Recent developments in this exciting field are highlighted in the following.

α-CD forms one-dimensional superstructures with gold salts, such as $KAuBr_4$, which readily crystallize as fine needles [10]. Based on this finding, a new and environmentally friendly recovery process for gold from excavation material is under development.

Significant progress was achieved in the functionalization of CDs through the regioselective introduction of one, two, three or more equal or different substituents starting from the corresponding perbenzyl or permethyl derivatives [11,12]. In this way, hexaphyrine was attached threefold to α-CD to construct superstructures with switchable aromaticity [13]. Furthermore, buckminsterfullerene C_{60} was covalently linked to two γ-CD rings [14]. This conjugate is highly soluble in water because it forms a sandwich-like self-complex, which makes it particularly useful as a sensitizer for singlet oxygen $^1O_2$ generation [14].

Amphiphilic CD derivatives with oligoethylene oxide side chains form nanoparticles with the sensitizer Zn-phthalocyanine and the antineoplastic drug docetaxel. These materials might be applicable for dual cancer therapy [15]. Another self-assembled CD nanocarrier for the photoreactive dye squaraine that is useful for photodynamic therapy is described in this Thematic Series [16]. The group of Ravoo also conjugated arylazopyrazoles to amphiphilic cyclodextrin derivatives that form vesicles triggered by light [17]. A star-shaped polycationic CD derivative with many breakable, intrinsic, disulfide linkages forms nanoparticles with messenger RNA and drugs and is particularly useful for transport into HeLa cells [18].

Due to their hydrophilicity, CD-derived superstructures have become more and more interesting for the construction of biomaterials. In particular, interactions between cellular components and CDs might lead to "greener medical applications" as summarized in this Thematic Series in the article by Leclercq [19]. For example, β-CD was immobilized onto a silicon substrate and incubated with various bacteria. These bacteria could be captured nearly quantitatively at the surface and released again by competitive binding with free methylated β-CD [20]. The proteins insulin and lysozyme were also conjugated to the guest adamantane. The complexation of these conjugates by pegylated β-CD gives rise to superstructures which provide slow release and maintain full biological activity [21].

Significant progress was also achieved in the field of CD rotaxanes. A [3]-rotaxane was assembled from two monosubstituted α-CD rings, α,ω-dodecamethylene diazide axis, and two bulky alkyne stoppers through a copper-catalyzed [2 + 3] cycloaddition in one step. Because of the attached gadolinium complexes, this rotaxane showed a high NMR relaxivity, making it suitable as a probe for magnetic resonance imaging (MRI) [22]. Well-defined fluorescent polyrotaxanes with alternating, threaded cucurbit[6]uril and CD rings were assembled by Fraser Stoddart's group via an alkyne–azide click reaction exploiting supramolecular catalysis [23,24]. The concurrent radical copolymerization of 1,3-dienes and bulky stoppers in the presence of CDs (so-called *rotaxa*-polymerization) was further applied for the syntheses of water-soluble polyisoprene polyrotaxanes [25]. Furthermore, ABA-type block-copolyrotaxanes could be synthesized using this polymerization technique controlled by RAFT chain transfer agents [26].

The exciting world of CD polyrotaxanes, including self-healing materials [27], was highlighted at a special session "Smart Polymers and Materials from Cyclodextrins: Novel Designs and Functions" at the 253rd ACS National Meeting in San Francisco in spring 2017. This Thematic Series in the *Beilstein Journal of Organic Chemistry* also provides further insights into the synthesis and properties of CD superstructures, covering many aspects such as catalysis, molecular recognition, colloids, polyrotaxanes, drug delivery and more.

Gerhard Wenz

Saarbrücken, September 2017

References

1. Pedersen, C. J.; Frensdorff, H. K. *Angew. Chem.* **1972,** *84,* 16–26. doi:10.1002/ange.19720840104
2. Lehn, J.-M. *Acc. Chem. Res.* **1978,** *11,* 49–57. doi:10.1021/ar50122a001
3. Cram, D. J. *Angew. Chem.* **1988,** *100,* 1041–1052. doi:10.1002/ange.19881000804
4. Cramer, F. *Chem. Ber.* **1951,** *84,* 851–854. doi:10.1002/cber.19510840912
5. Cramer, F.; Hettler, H. *Naturwissenschaften* **1967,** *54,* 625–632. doi:10.1007/BF01142413
6. Bruns, C. J.; Stoddart, J. F. *The Nature of the Mechanical Bond: From Molecules to Machines;* John Wiley & Sons: Hoboken, 2016. doi:10.1002/9781119044123
7. Sauvage, J.; Dietrich-Buchecker, C., Eds. *Molecular Catenanes, Rotaxanes and Knots;* Wiley-VCH: Weinheim, Germany, 1999.
8. Stoddart, J. F. *Angew. Chem., Int. Ed.* **2017,** *56,* 11094–11125. doi:10.1002/anie.201703216
9. Sauvage, J.-P. *Angew. Chem., Int. Ed.* **2017,** *56,* 11080–11093. doi:10.1002/anie.201702992
10. Liu, Z.; Samanta, A.; Lei, J.; Sun, J.; Wang, Y.; Stoddart, J. F. *J. Am. Chem. Soc.* **2016,** *138,* 11643–11653. doi:10.1021/jacs.6b04986
11. Guieu, S.; Sollogoub, M. *J. Org. Chem.* **2008,** *73,* 2819–2828. doi:10.1021/jo7027085
12. Wang, B.; Zaborova, E.; Guieu, S.; Petrillo, M.; Guitet, M.; Blériot, Y.; Ménand, M.; Zhang, Y.; Sollogoub, M. *Nat. Commun.* **2014,** *5,* No. 5354. doi:10.1038/ncomms6354
13. Ménand, M.; Sollogoub, M.; Boitrel, B.; Le Gac, S. *Angew. Chem., Int. Ed.* **2016,** *55,* 297–301. doi:10.1002/anie.201508009
14. Zhu, X.; Quaranta, A.; Bensasson, R. V.; Sollogoub, M.; Zhang, Y. *Chem. – Eur. J.* **2017,** *23,* 9462–9466. doi:10.1002/chem.201700782
15. Conte, C.; Scala, A.; Siracusano, G.; Sortino, G.; Pennisi, R.; Piperno, A.; Miro, A.; Ungaro, F.; Sciortino, M. T.; Quaglia, F.; Mazzaglia, A. *Colloids Surf., B* **2016,** *146,* 590–597. doi:10.1016/j.colsurfb.2016.06.047
16. Kauscher, U.; Ravoo, B. J. *Beilstein J. Org. Chem.* **2016,** *12,* 2535–2542. doi:10.3762/bjoc.12.248
17. Stricker, L.; Fritz, E.-C.; Peterlechner, M.; Doltsinis, N. L.; Ravoo, B. J. *J. Am. Chem. Soc.* **2016,** *138,* 4547–4554. doi:10.1021/jacs.6b00484
18. Yang, W.; Yu, C.; Wu, C.; Yao, S. Q.; Wu, S. *Polym. Chem.* **2017,** *8,* 4043–4051. doi:10.1039/C7PY00666G
19. Leclercq, L. *Beilstein J. Org. Chem.* **2016,** *12,* 2644–2662. doi:10.3762/bjoc.12.261
20. Perez-Anes, A.; Szarpak-Jankowska, A.; Jary, D.; Auzély-Velty, R. *ACS Appl. Mater. Interfaces* **2017,** *9,* 13928–13938. doi:10.1021/acsami.7b02194
21. Hirotsu, T.; Higashi, T.; Motoyama, K.; Arima, H. *Carbohydr. Polym.* **2017,** *164,* 42–48. doi:10.1016/j.carbpol.2017.01.074

22. Fredy, J. W.; Scelle, J.; Ramniceanu, G.; Doan, B.-T.; Bonnet, C. S.; Tóth, É.; Ménand, M.; Sollogoub, M.; Vives, G.; Hasenknopf, B. *Org. Lett.* **2017,** *19,* 1136–1139. doi:10.1021/acs.orglett.7b00153
23. Hou, X.; Ke, C.; Zhou, Y.; Xie, Z.; Alngadh, A.; Keane, D. T.; Nassar, M. S.; Botros, Y. Y.; Mirkin, C. A.; Stoddart, J. F. *Chem. – Eur. J.* **2016,** *22,* 12301–12306. doi:10.1002/chem.201602954
24. Hou, X.; Ke, C.; Stoddart, J. F. *Chem. Soc. Rev.* **2016,** *45,* 3766–3780. doi:10.1039/C6CS00055J
25. Hilschmann, J.; Kali, G.; Wenz, G. *Macromolecules* **2017,** *50,* 1312–1318. doi:10.1021/acs.macromol.6b02640
26. Hilschmann, J.; Wenz, G.; Kali, G. *Beilstein J. Org. Chem.* **2017,** *13,* 1310–1315. doi:10.3762/bjoc.13.127
27. Kato, K.; Mizusawa, T.; Yokoyama, H.; Ito, K. *J. Phys. Chem. C* **2017,** *121,* 1861–1869. doi:10.1021/acs.jpcc.6b11362

License and Terms

BEILSTEIN JOURNAL OF ORGANIC CHEMISTRY

Cross-linked cyclodextrin-based material for treatment of metals and organic substances present in industrial discharge waters

Élise Euvrard[1], Nadia Morin-Crini[1], Coline Druart[1], Justine Bugnet[1], Bernard Martel[2], Cesare Cosentino[3], Virginie Moutarlier[4] and Grégorio Crini[*1]

Full Research Paper

Open Access

Address:
[1]Chrono-environnement, UMR 6249 usc INRA, University of Bourgogne Franche-Comté, 16 route de Gray, 25000 Besançon, France, [2]UMET UMR 8207, Ingénierie des Systèmes Polymères, University of Lille 1, 59655 Villeneuve d'Ascq, France, [3]G. Ronzoni Institute for Chemical and Biochemical Research, 81 via G. Colombo, 20133 Milano, Italy and [4]Chrono-environnement, Institut UTINAM, UMR 6213, University of Bourgogne Franche-Comté, 16 route de Gray, 25000 Besançon, France

Email:
Grégorio Crini[*] - gregorio.crini@univ-fcomte.fr

* Corresponding author

Keywords:
alkylphenols; adsorption; cyclodextrin; metals; polycyclic aromatic hydrocarbons

Beilstein J. Org. Chem. **2016,** *12,* 1826–1838.
doi:10.3762/bjoc.12.172

Received: 09 May 2016
Accepted: 29 July 2016
Published: 12 August 2016

This article is part of the Thematic Series "Superstructures with cyclodextrins: Chemistry and applications IV".

Guest Editor: G. Wenz

Abstract

In this study, a polymer, prepared by crosslinking cyclodextrin (CD) by means of a polycarboxylic acid, was used for the removal of pollutants from spiked solutions and discharge waters from the surface treatment industry. In spiked solutions containing five metals, sixteen polycyclic aromatic hydrocarbons (PAH) and three alkylphenols (AP), the material exhibited high adsorption capacities: >99% of Co^{2+}, Ni^{2+} and Zn^{2+} were removed, between 65 and 82% of the PAHs, as well as 69 to 90% of the APs. Due to the structure of the polymer and its specific characteristics, such as the presence of carboxylic groups and CD cavities, the adsorption mechanism involves four main interactions: ion exchange, electrostatic interactions and precipitation for metal removal, and inclusion complexes for organics removal. In industrial discharge waters, competition effects appeared, especially because of the presence of calcium at high concentrations, which competed with other pollutants for the adsorption sites of the adsorbent.

Introduction

Although considerable efforts have been made by the industrial sector over the last 30 years, the problem of water pollution still remains a significant concern. Particularly affected by this issue are the discharge waters (DWs) of the surface treatment (ST) industries known for using large amounts of water and chemicals in their manufacturing processes. Despite these industries

have their own treatment plants, generally physicochemical decontamination steps, the DWs still contain non-negligible amounts of pollutants. Among them, metals (in particular chromium, nickel and zinc) are commonly found at concentrations in the range of milligrams per liter, and organic molecules, such as polycyclic aromatic hydrocarbons (PAHs) and alkylphenols (APs) at concentrations varying from hundreds of nanograms per liter to some micrograms per liter [1].

However, it is extremely difficult to remove pollutants present at low concentrations (a few hundreds of micrograms per liter for some organic substances in DWs). For this purpose, specific systems can be added, called effluent finishing treatments. A sequential dual approach can be considered: firstly, adsorption onto carbon to remove organics (e.g., solvents, oils, PAHs and volatile organic compounds) combined with ion-exchange and/or chelation by means of organic resins to remove inorganic pollutants (e.g., metals and anions such as fluorides). Charles et al. [2] recently reported that this type of sequence is acknowledged for its efficiency. However, it is an approach to water treatment that combines two methods of separation using two distinct commercial materials. To our knowledge, materials able to combine the two functions are rare. Recently, bifunctional natural derivatives have been proposed for this purpose. For example, Zhao et al. [3] proposed a new cyclodextrin-based material for the simultaneous adsorption of metals and cationic dyes. Zhang et al. [4] studied the removal of cobalt and 1-naphthol onto magnetic nanoparticles containing cyclodextrin and iron and Yang et al. [5] proposed a new nanocomposite adsorbent for the simultaneous removal of organic and inorganic substances from water.

Here, we propose to use a single cross-linked cyclodextrin-based polymer for the removal of metals and organic pollutants present in polycontaminated effluents. Cyclodextrins (CDs), synthetic substances obtained from the enzymatic degradation of starch, belong to the family of cage molecules. They present remarkable encapsulation properties leading to a host–guest relationship with organic substances [6-9]. These cyclic oligosaccharides are water soluble in their native form and are often modified to prepare novel insoluble CD-based materials. Two patents published by Martel et al. [10], and Trotta et al. [11] can be consulted for the use of carboxylic acids and pyromellitic dianhydride, respectively, as agents to cross-linking CDs. Other cross-linking agents such as epichlorohydrin, ethylene glycol diglycidyl ether, glutaraldehyde, benzoquinone or isocyanates can be also used [1,12].

The main objective of the study was to investigate the adsorption capacities of a non-conventional and versatile CD-based material crosslinked with 1,2,3,4-butanetetracarboxylic acid (BTCA) toward several inorganic and organic elements. Performances of such systems were evaluated in the presence of spiked solutions and real DWs from ST industry containing five metals, 16 PAHs, three APs (model pollutants present in DWs from treatment-surface industries) in the presence and in the absence of calcium. The polymer showed high adsorption capacities in spiked solutions but adsorption strongly decreased in discharge waters due to some competition effects, notably between inorganics for adsorption sites.

Results

Material characterization

The cross-linked polymer used in this study is presented in Figure 1. In the control test (solution without pollutant), polymer addition led to large pH variations. The non-activated polyBTCA-CD (COOH form) decreased the pH value from 6 to 4.3 after 20 min of shaking whereas activated polyBTCA-CD (COO^-Na^+ form) led to a pH increase from 6 to 7.2 after 5 min shaking. In both cases the final pH remained constant over several hours.

The ion-exchange capacity (IEC) was equal to 0.705 mmol of COOH functions per gram of polymer. The point of zero charge (PZC) was plotted and followed the linear equations $y = -0.9639x + 6.1422$ and $y = -0.9233x + 3.138$ indicating a pH of 6.4 and 3.4 for the PZC of activated and non-activated polyBTCA-CD, respectively (Figure 2).

Figure 3 shows the XRD pattern of non-activated and activated polymers. These diffractograms indicate a wide amorphous peak between values of 2θ of 10 and 30°, highlighting that polymers are amorphous. No significant differences were observed between the two types of polymer.

Solid-state ^{13}C NMR spectra of the polymer are presented in Figure 4. The cross polarization magic angle spinning (CPMAS) spectrum shows the peaks of disordered cyclodextrin (broad signals) in the range of 50–110 ppm. Three strong broad bands attributable to the glucopyranose unit can be observed. The peak at 101 ppm is attributed to the anomeric carbon C-1: this confirms the presence of glucose units in the polymer. In the range of 50–110 ppm, the CH_2 signals of CD (C-6, C-6' and C-7) are completely hidden by the C-2, C-3 and C-5 peaks of the glucopyranose units. In the MAS spectrum, three CH_2 signals are clear and the signals at 65, 62.1 and 60.2 ppm are attributable to CH_2 in positions C-6', C-6 and C-7, respectively. These attributions were confirmed using cross-polarization with a polarization inversion sequence (CPPI spectrum not shown), which revealed three CH_2 signals due to the CD and also a peak at 30.15 ppm corresponding to CH_2 groups introduced by the cross-linking agent. As expected, the signals of the BTCA

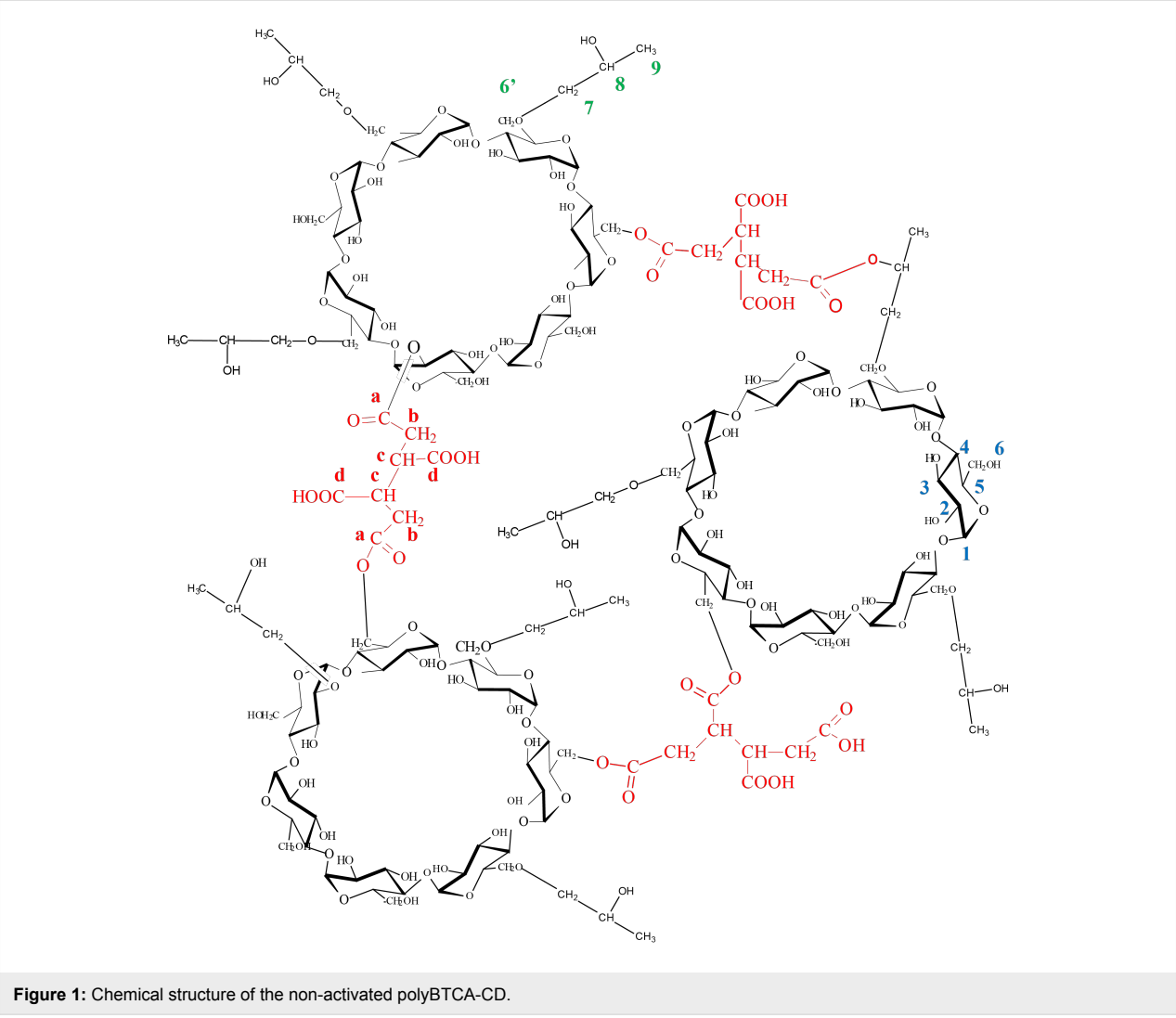

Figure 1: Chemical structure of the non-activated polyBTCA-CD.

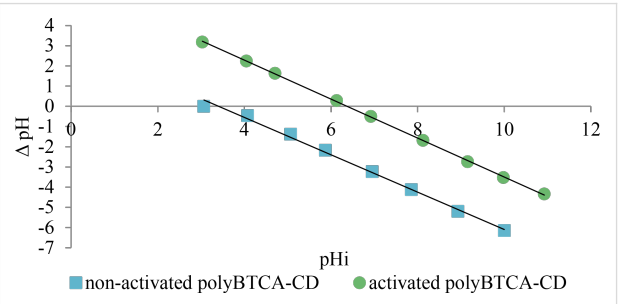

Figure 2: Determination of the PZC for the non-activated and activated polyBTCA-CD polymers (pHi: initial pH value, see also Experimental section).

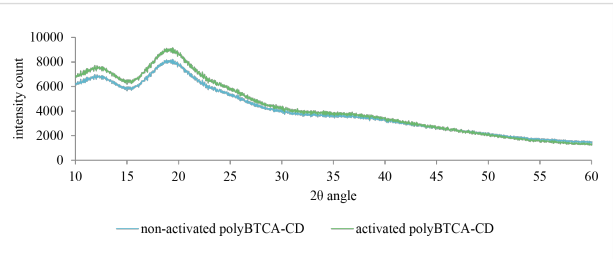

Figure 3: XRD pattern of the two polymers: non-activated and activated polyBTCA-CD.

crosslinking agent can be clearly distinguished (labeled a, b, c and d). In particular, the carbon of the carboxylic groups appears at 172.2 ppm. This peak (a,d) corresponds to esterified and free carboxylic groups of BTCA present in free carboxylic acids and in ester crosslinks, respectively. In the CPMAS spectrum we also note the presence of additional peaks due to the hydroxypropyl group present in the CD, and in particular the CH_3 group (C-9 carbon) at 15.3 ppm. The comparison between the CPMAS and MAS spectra shows a different intensity for this methyl signal reflecting the greater mobility of this group, as expected. Paradoxically, the intensity of the carbonyl signal does not increase in the MAS spectrum compared with the

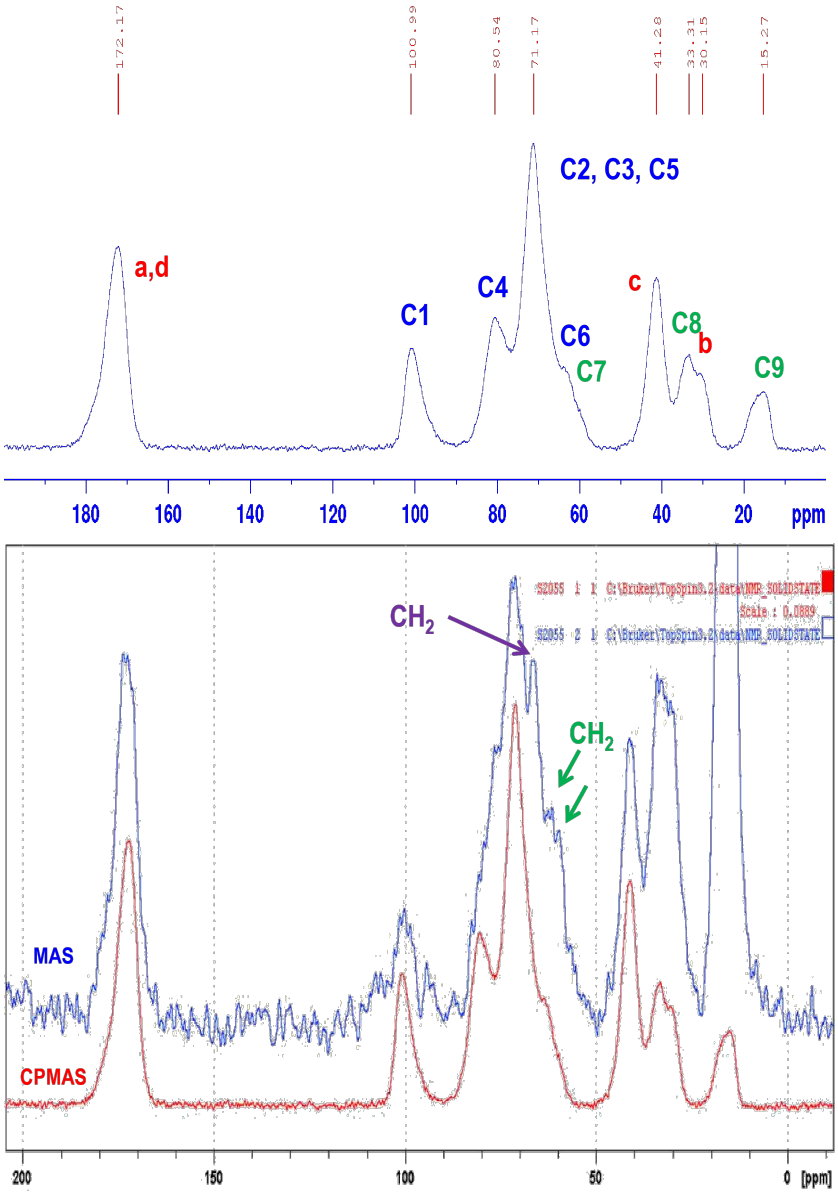

Figure 4: CPMAS and MAS spectra of polyBTCA-CD.

signal of the methyl group of CD. Finally, no significant differences were obtained between the non-activated polyBTCA-CD and the activated polyBTCA-CD spectra.

Metal adsorption

Effect of activation ($NaHCO_3$ treatment)

The activated polymer is more efficient than the non-activated polymer regardless of the dose (Figure 5). The activation enhanced the removal by 69%, 92%, 78%, 92% and 92% at a polymer concentration of 2 $g{\cdot}L^{-1}$ for Al^{3+}, Co^{2+}, Cr^{3+}, Ni^{2+} and Zn^{2+}, respectively. Moreover, it appears that a polymer concentration of 2 $g{\cdot}L^{-1}$ is enough to treat an inorganic load of 50 $mg{\cdot}L^{-1}$. Thus, for all the following experiments, the polymers were activated and a concentration of 2 $g{\cdot}L^{-1}$ was used.

Adsorption kinetics

Figure 6 shows the adsorption kinetics for two solutions containing five metals at 1 $mg{\cdot}L^{-1}$ and 10 $mg{\cdot}L^{-1}$. For these two concentrations, 100% removal was reached for most species except for Al1 and Cr1 systems, which reached a state of dynamic equilibrium. However, the adsorption time changed with the concentration and with the metals. At 1 $mg{\cdot}L^{-1}$ the adsorption kinetics was fast: in 5 min equilibrium was reached for the metals except for Al^{3+} (240 min). At 10 $mg{\cdot}L^{-1}$ for

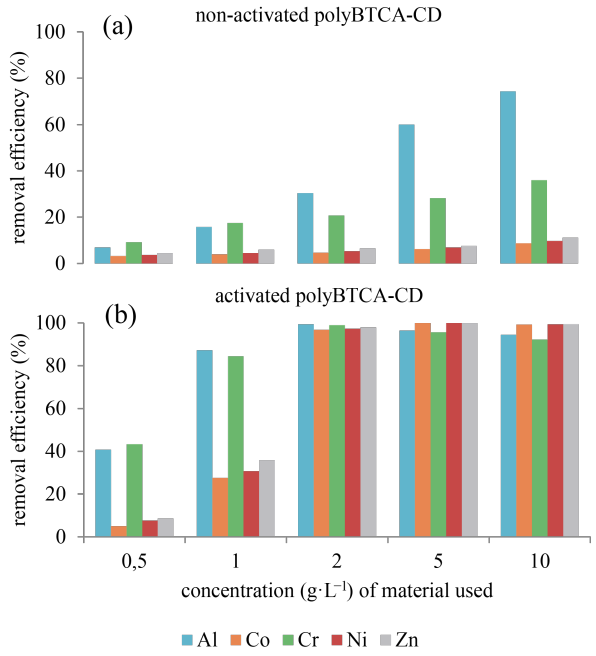

Figure 5: Adsorption capacity (%) of (a) the non-activated and (b) the activated ($NaHCO_3$ treatment) polyBTCA-CD at different concentrations for five metals (at 10 mg·L^{-1} metal).

Co^{2+}, Ni^{2+} and Zn^{2+}, equilibrium time increased to 30 min, while for Al^{3+} and Cr^{3+} it decreased to 30 min. These results were obtained in triplicate with small standard deviations, indicating the reproducibility of the experiments. For the two experiments we noted an increase of pH values ranging from 3.9 and 4.4 for the initial pH (pHi) to 6.2 and 7.3 for the final pH (pHf) for concentrations of 10 mg·L^{-1} and 1 mg·L^{-1}, respectively.

Influence of metal and calcium concentration

The results show that activated polyBTCA-CD is able to treat metal solutions from low concentrations (a few micrograms in SS3 and SS4 in Table 1) to high concentrations (ten milligrams for each metal (SS1 in Table 1). The exact composition of each spiked solution (SS) is given in the Experimental section. In addition, it was observed that without Ca^{2+} cations the removal efficiency was above 99%, except for aluminum and chromium (Table 1). When expressing these results in mmol of total metal retained per gram of polymer, it can be noted that for the highest concentration of metals (10 mg·L^{-1}), the polymer retained 0.466 mmol·g^{-1}. When calcium ions were added (SS5 in Table 1), Cr^{3+} was better retained than in the solution without calcium (85% compared to 38%) while the retention of Al^{3+} remained constant. For the three other metals, the retention dramatically decreased (<41%) in the presence of calcium.

PAH and AP adsorption

Figure 7a shows that the polyBTCA-CD can take up PAHs since the polymer removed between 74% and 79% of the global PAH load. It was also observed that removal was more efficient for heavy PAHs (89% adsorption) than for the lighter ones (62% adsorption). Following PAH adsorption the pH ranged from 6 to 7.6 at the end of the experiment. The polymer successfully removed APs as shown in Figure 7b. It can be noted that an increase of AP concentration led to a decrease in adsorp-

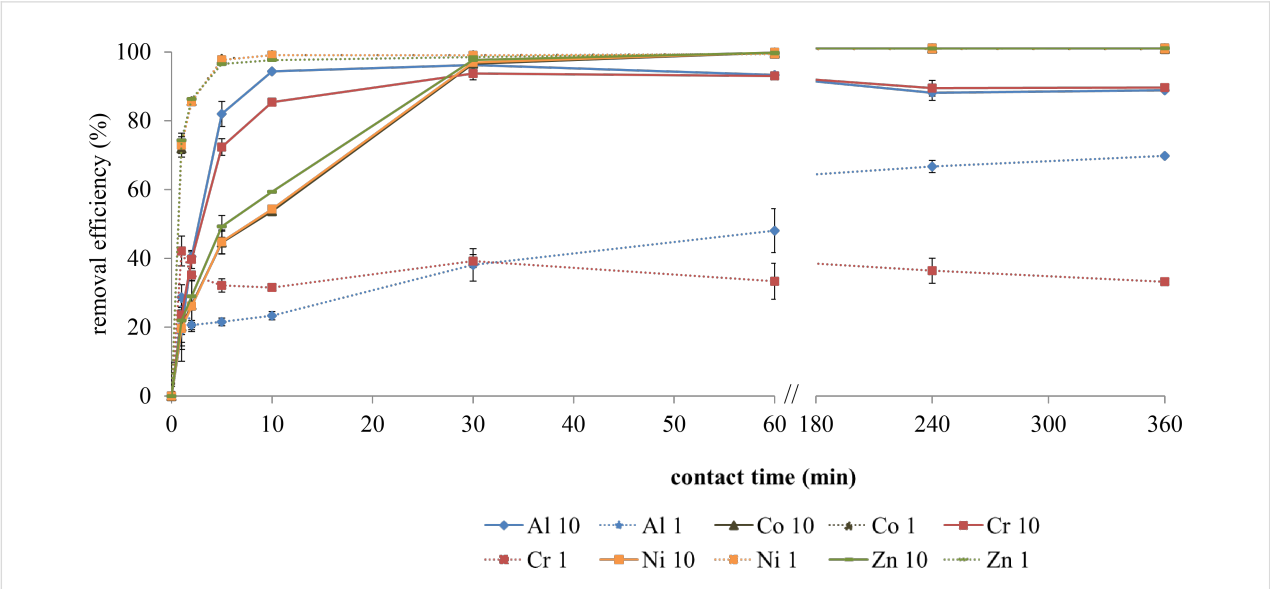

Figure 6: Adsorption kinetics for two solutions containing five metals at two concentrations (solution at 10 mg·L^{-1}: full lines; solution at 1 mg·L^{-1}: dashed lines) expressed as removal efficiency in % (n = 3).

Table 1: Efficiency of activated polyBTCA-CD expressed in % (concentration = 2 g·L^{-1}) to treat several metal spiked solutions SS (n = 3). See Experimental section for the exact compositions of the spiked solutions SS.

	Al^{3+}	Co^{2+}	Cr^{3+}	Ni^{2+}	Zn^{2+}	Ca^{2+}	pHi
SS1	87 ± 4	>99	88 ± 3	>99	>99	—	6.2
SS2	66 ± 4	>99	36 ± 1	>99	>99	—	7.3
SS3	87 ± 16	>99	45 ± 7	99 ± 0	>99	—	7.3
SS4	95 ± 2	>99	38 ± 2	99 ± 0	>99	—	7.3
SS5	97 ± 0	17 ± 2	85 ± 2	22 ± 2	41 ± 7	10 ± 4	4.7

tion capacities, notably for 4tOP (87% to 55%; Figure 7b). For the two solutions, the pH values ranged from 6 to 8.

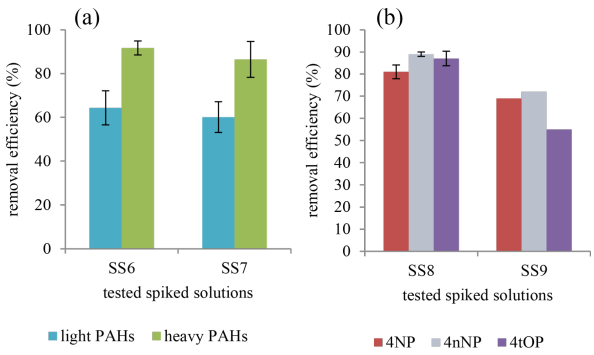

Figure 7: Removal efficiency (%) after treatment with activated polyBTCA-CD (concentration = 2 g·L^{-1}) for (a) two concentrations of PAHs: low for SS6 and high for SS7 (n = 3) and (b) two concentrations of APs: low for SS8 (n = 3) and high for SS9 (n = 1) (4NP: 4-nonylphenol, 4nNP: 4-*n*-nonylphenol, 4tOP: 4-*tert*-octylphenol).

Mixed metal and organic adsorption

Table 2 presents the adsorption results for the seven mixtures containing metals, PAHs, and APs. Firstly, it was noted that the removal efficiency observed in the solutions containing only one type of substance was similar to those observed in the previous experiments. The heavy PAHs were retained more than the lighter PAHs in each mixture. No adsorption difference was observed between the mixtures containing a single family of substance and those containing two or three families of substances.

Adsorption capacities with discharge waters

Metal adsorption in industrial discharge waters

The polymer was then tested on DWs from a ST company that is specialized in chemical coatings and any processes for the corrosion protection of metal parts intended for the automotive and building sectors. The average concentrations of the main elements present in the industrial DW are reported in Table 3.

In DWs, no pH variation was observed during the experiment (pHi = pHf = 8). The results indicate that the retention of the five metals studied above did not reach the removal efficiency obtained in SS, except for Al^{3+} (70% on average, Figure 8). Indeed, for Co^{2+}, Cr^{3+}, Ni^{2+} and Zn^{2+}, the removal efficiencies did not exceed 30%. Nevertheless, it appears that other elements in DWs were retained by the polymer (20%, 34%, 4%,

Table 2: Removal efficiency expressed in % of metals, PAHs and APs in solutions containing either one family of substances or mixtures after treatment by polyBTCA-CD (concentration = 2 g·L^{-1}, n = 3).

		metals	PAHs	APs	metals + PAHs	metals + APs	PAHs + APs	metals + PAHs + APs
metals	Al^{3+}	66 ± 4	—	—	65 ± 14	63 ± 5	—	65 ± 5
	Co^{2+}	>99	—	—	99 ± 1	99 ± 1	—	99 ± 1
	Cr^{3+}	36 ± 1	—	—	28 ± 8	25 ± 13	—	24 ± 13
	Ni^{2+}	>99	—	—	98 ± 2	98 ± 1	—	98 ± 1
	Zn^{2+}	>99	—	—	96 ± 4	96 ± 4	—	96 ± 4
PAHs	light	—	60 ± 7	—	63 ± 3	—	62 ± 8	62 ± 4
	heavy	—	87 ± 8	—	81 ± 10	—	87 ± 3	89 ± 5
APs	4NP	—	—	80 ± 3	—	82 ± 7	80 ± 11	81 ± 1
	4nNP	—	—	89 ± 1	—	90 ± 2	85 ± 1	81 ± 2
	4tOP	—	—	83 ± 3	—	86 ± 6	86 ± 6	82 ± 4
pHf		7.3	7.6	8	7.7	7.7	7.7	7.9

Table 3: Average concentrations expressed in mg·L^{-1} and standard errors of the main elements present in the DWs (n = 5).

Al^{3+}	Co^{2+}	Cr^{3+}	Ni^{2+}	Zn^{2+}	Ca^{2+}
1.48 ± 0.54	1.70 ± 0.74	0.04 ± 0.03	0.25 ± 0.11	0.90 ± 0.50	690 ± 156
Fe^{3+}	K^{+}	Mg^{2+}	Mn^{2+}	Sr^{2+}	
0.23 ± 0.12	73.3 ± 6.56	2.84 ± 0.31	0.12 ± 0.1	0.24 ± 0.03	

10%, 32%, and 18% for Ca^{2+}, Fe^{3+}, K^{+}, Mg^{2+}, Mn^{2+} and Sr^{2+}, respectively). Taking into account the initial concentrations of these elements (Table 3), this means that non-negligible amounts were retained. For instance, 134 mg·L^{-1} of Ca^{2+} was retained by the polymer, equivalent to 1.67 mmol·g^{-1}. However, when the initial polymer concentration increased, the removal efficiencies for the metals Co^{2+}, Cr^{3+}, Ni^{2+} and Zn^{2+} also increased (Table 4). For instance, with a polymer concentration of 10 g·L^{-1} (instead of 2 g·L^{-1} in Figure 5), retention reached 85%, 39%, 45% and 69% for Al^{3+}, Co^{2+}, Ni^{2+} and Zn^{2+}, respectively. At the same time, the retention of the other inorganic elements also increased (57%, 71%, 10%, 35%, 73% and 54% for Ca^{2+}, Fe^{3+}, K^{+}, Mg^{2+}, Mn^{2+} and Sr^{2+}, respectively).

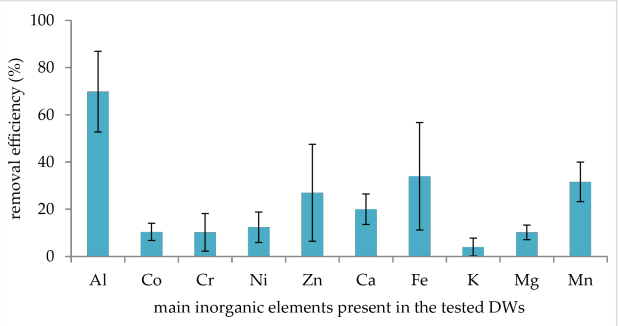

Figure 8: Removal efficiency (%) of inorganic elements after treatment of five DWs by polyBTCA-CD (concentrations = 2 g·L^{-1}, n = 5).

Detailed analysis of the discharge water after treatment with polyBTCA-CD

Among the 189 substances/parameters analyzed in the raw DW, 35 were detected: sixteen inorganic elements including twelve metals, and seven APs (Table 5). The treatment by activated polyBTCA-CD affected all water parameters and all substances detected in the raw DW except for Na. As in previous experiments on DWs, it was observed that the metals were not efficiently adsorbed by the polymer with a removal efficiency reaching 24%, 12%, 17% and 44% for Al^{3+}, Co^{2+}, Ni^{2+} and Zn^{2+}, respectively. Unlike metals, it appears that most of the organics were retained with removal efficiencies higher than 50%; for example 4tOP, 4nNP, monoethoxylate nonylphenol and monoethoxylate octylphenol were efficiently removed (81, 66, 83 and 77%, respectively). Moreover, some substances were retained in large quantities on the polyBTCA-CD such as chloride (130 mg·L^{-1}) and calcium (119 mg·L^{-1}), which is not reflected by the removal efficiency because of the large amounts present in the initial DW. The sodium concentration remained stable after adsorption due to the fact that the material was initially activated by $NaHCO_3$.

Discussion

To explain the adsorption performance of polyBTCA-CD, a chemisorption mechanism involving several interactions can occur including ion exchange, electrostatic interactions, inclusion complexation and/or precipitation [3,12-16].

Table 4: Removal efficiency of inorganic elements (%) in DW according to polymer concentration.

	removal efficiency (%)											
polymer concentration (g·L^{-1})	Al^{3+}	Co^{2+}	Cr^{3+}	Ni^{2+}	Zn^{2+}	Ca^{2+}	Fe^{3+}	K^{+}	Mg^{2+}	Mn^{2+}	Sr^{2+}	pH
5	81	27	>98	37	62	34	63	44	4	0	32	5
10	85	39	>98	47	69	57	71	42	9	35	56	5
15	88	46	>98	42	74	74	69	40	13	55	72	5
20	88	52	>98	47	74	86	70	36	22	72	84	5

Table 5: Extensive analysis on raw and treated DW by polyBTCA-CD (concentration = 2 g·L^{-1}).

		initial concentration	final concentration	removal (%)
physicochemical parameters (mg·L^{-1})	pH	8	8	—
	BOD-5	60	56	7
	COD	847	325	62
	hydrocarbon index C10-C40	0.8	0.2	75
	total cyanide	0.39	0.35	10
	AOX	1.6	0.9	42
	nitrites	121	105	13
	Kjeldahl nitrogen	44	30	31
	total nitrogen	200	182	9
inorganic elements (mg·L^{-1})	chloride	3140	3010	4
	sulphate	208	201	3
	potassium	98	94	4
	calcium	787	668	15
	magnesium	2.3	2.1	9
	manganese	0.11	0.09	17
	sodium	1666	1667	—
	sulfur	91	83	9
	aluminum	0.09	0.07	24
	cobalt	2.82	2.49	12
	iron	0.37	0.27	27
	molybdenum	0.07	0.06	9
	nickel	0.34	0.28	17
	selenium	0.1	0.09	10
	strontium	0.27	0.26	7
	zinc	0.9	0.5	44
organic substances (µg·L^{-1})	1,2-dichloroethane	1.2	0.7	42
	chloroform	4.4	3.2	27
	dichlorobromomethane	0.8	<0.5	>38
	4-*tert*-octylphenol	2.1	0.4	81
	4-nonylphenol	0.3	<0.1	>66
	monoethoxylate nonylphenol	5.62	0.97	83
	diethoxylate nonylphenol	2.05	0.96	53
	monoethoxylate octylphenol	177	41	77
	diethoxylate octylphenol	177	130	27
	4-*tert*-butylphenol	26	14	46

The polymer, without an activation step, removed 20% of the total metal load in spiked solutions (SS) containing five metals at 10 mg·L^{-1} each. This could be attributed to surface adsorption and diffusion into the polymer network. However, it was observed that an activation step in an aqueous solution of sodium bicarbonate was necessary to enhance metal retention, as also reported by Ducoroy et al. [17], allowing for a removal efficiency for metals higher than 99% for Co^{2+}, Ni^{2+} and Zn^{2+}, through both electrostatic interactions and ion exchange. Indeed, during the process of polymer synthesis, the cross-linking agent BTCA was used, this compound presents four carboxylic functions and a previous study [18] showed that only two of its carboxylic groups reacted with the CD units to form the polymer network, the two remaining ones being available to react with cations through chemisorption (electrostatic interactions and ion exchange). Moreover, this treatment only converted carboxylic groups into carboxylate without altering the amorphous structure of the polymer, as seen from the X-ray spectra.

Precipitation could also explain the removal efficiency enhancement observed with the activated polymer since it induced a strong pH increase. Indeed, for the solution of five metals at concentration of 1 mg·L^{-1} (SS2) treated with activated

polyBTCA-CD, the pH increased from 4.4 to 7.3, probably due to the basic character of the polymer, the COOH groups of which have been converted into COO^-Na^+ groups inducing metal precipitation, notably for Al^{3+} and Cr^{3+}.

With the highest concentration tested (10 $mg \cdot L^{-1}$, which corresponds to 5 mg of each metal per gram of polymer), the removal efficiency represents 0.466 mmol of metals adsorbed per gram of polymer, that is lower than the theoretical ion exchange capacity, estimated by titration to be 0.705 mmol of COOH functional groups per gram of polymer. In theory, in order to saturate the COOH functional groups, a concentration of 6.5 mg of each metal per gram of polymer (i.e., 13 $mg \cdot L^{-1}$) would have been necessary. In the DWs, focusing on Ca^{2+} only, 119 $mg \cdot L^{-1}$ were retained by the polymer, representing a concentration of 1.49 $mmol \cdot g^{-1}$ of material. Thus, the IEC of the polymer (0.705 $mmol \cdot g^{-1}$) was exceeded. This observation confirmed the fact that the inorganic elements were not only retained by ion exchange and/or electrostatic interactions, but other interactions occurred, such as precipitation and/or physical phenomena (surface adsorption, diffusion into the network and/or hydrogen bonding).

This study demonstrated the efficiency of activated polyBTCA-CD to treat the inorganic load, but also to treat the organic pollutants. It can be noted that the analysis of 26 substances present in the DW tested, showed that the polymer is able to adsorb 4-*tert*-butylphenol, 1,2-dichloroethane and chloroform, but also APs and the organo-halogenated compounds (represented by the AOX parameter). For the retention of APs, no difference was noted between 4NP, 4nNP and 4tOP. Heavy PAHs were better retained than light ones. This observation could be partially explained by the greater hydrophobicity of heavy PAHs compared with light ones [19]. Indeed, in the case of interactions with organics, CD units play an important role. The hydrophobic cavities of these molecules allow for the formation of inclusion complexes with PAH guest molecules (organic substances) [3,20]. If the guest compounds present an appropriate molecular size and structure to enter into the CD cavity the more hydrophobic the organic substances, the more stable the inclusion complexes.

The material was also able to efficiently treat complex solutions containing metals, PAHs, APs and other substances. However, although in spiked solutions no competition effect was revealed between substance groups, these phenomena appeared in more complex solution such as DWs. Indeed, the retention of inorganic elements decreased from an average of 87% for the five metals in SS to 26% in DWs. It appears that other elements present in DW were retained by the polymer, for instance Fe^{3+}, Mn^{2+}, Mg^{2+} and Ca^{2+}. Discharge waters from ST industries are complex matrices containing not only metals, PAHs or APs but also other elements including anions and salts, sometimes exceeding one gram per liter [21]. In this study, calcium and chlorides were present in the DWs at concentrations of 500 and 3 000 $mg \cdot L^{-1}$, respectively. In fact, a large amount of these other inorganic elements could interact with the polymer, notably Ca^{2+}, which was retained at 119 $mg \cdot L^{-1}$. Thus, the low retention of target metals (Al^{3+}, Co^{2+}, Cr^{3+}, Ni^{2+} and Zn^{2+}) by the adsorbent could be due to the simultaneous presence of high quantities of K^+, Na^+, Mg^{2+} or Ca^{2+}, which can saturate the carboxylate functions of the polymer and compete with the target metals for access to the active sites [22-25]. These observations were confirmed by the tests conducted in SS in the presence of calcium. An increase of polymer concentration in DWs (10 $g \cdot L^{-1}$ instead of 2 $g \cdot L^{-1}$) yielded better results in terms of removal efficiency for all metals. However, while the retention of Co^{2+}, Ni^{2+} and Zn^{2+} was reduced in the presence of Ca^{2+}, this was not always the case for Al^{3+} and Cr^{3+}. In some cases, Al^{3+} and Cr^{3+} exhibited unexpected behavior.

In solutions at low concentrations (SS2, SS3 and SS4), Al^{3+} and Cr^{3+} were removed with low efficiency compared to other metals, but in solutions at higher concentrations (SS1) or in the presence of calcium (SS5), an increase of removal efficiency was observed whereas for the three other metals, retention decreased. In the case of mixtures, the same observations were made, Al^{3+} and Cr^{3+} removal being systematically lower, whereas for the three other metals the removal efficiency remained as high as 99%. Moreover, in DWs, Al^{3+} was retained by an average of 60% while the others did not exceed a removal efficiency of 30%. No simple explanation could clarify these phenomena but some specific characteristics of these two metals must be pointed out. Indeed, the behavior of both Al^{3+} and Cr^{3+} is highly pH dependent, with complex speciation patterns [26-28]. Since the pH value was not kept constant during tests, the pH variations probably led to changes in speciation of the two metals, leading to this unexpected behavior compared to the other metals. Moreover, it can be noted that Al^{3+} and Cr^{3+} have the smallest ionic radii of the five metals and a low electronegativity, which are two parameters that decrease metal removal as described by Al-Rub and co-workers [29].

Conclusion

Throughout this study, it was demonstrated that polyBTCA-CD is a versatile sorbent able to retain substances present at concentrations close to a few milligrams per liter (metals and other inorganic elements) but also at trace concentrations ($\mu g \cdot L^{-1}$ for organics). Although ion exchange on the one hand, and host–guest inclusion on the other hand were the main phenomena interacting between adsorbent and solutes, the interpretation

of the results was made difficult due to the wide diversity of polluting species present in DWs, involving numerous other mechanisms in the adsorption (classified for instance as chemisorption and physisorption phenomena) [3,12,20]. Thus, further studies are needed to better understand how water parameters impact the different routes of pollutant retention, which is of great interest for future applications of non-conventional adsorbents in industry.

Experimental

Synthesis and characterization of the material

The cross-linked polymer (Figure 1) was prepared in a single step by crosslinking hydroxypropyl-β-cyclodextrin (HPβCD; Kleptose HPB®, DS = 0.62, Roquette, Lestrem, France) using 1,2,3,4-butanetetracarboxylic acid (BTCA; Aldrich, Milwaukee, WI). The synthesis procedure has already been described in detail by Martel et al. [10,30]. Based from their methodology, the typical cross-linking reaction was carried out as follows: in a reactor, 0.37 mol·L^{-1} of sodium dihydrogenophosphate ($Na_2H_2PO_2 \cdot H_2O$, catalyst), 0.85 mol·L^{-1} of BTCA and 0.18 mol·L^{-1} of HPβCD were dissolved; the resulting solution was then concentrated by evaporation, and the mixture heated to 140 °C. These last two steps were performed under vacuum in a rotary evaporator; the polymer formed was re-suspended through addition of water to the reactor; the polymer was then filtered and purified by several washings with water. It was dried at 50 °C until constant weight, yielding a white powder. The yield of the reaction was equal to 87.6 %.

To activate the polyBTCA-CD by converting the carboxylic functions to their carboxylate form, the material was stirred for 4 h in an aqueous solution of 4 g·L^{-1} $NaHCO_3$ (saturated) then extensively washed with osmosed water to remove unreacted reagents, and finally oven dried at 50 °C.

The ion exchange capacity (IEC) of the material was determined by pH-metric titration according to the calcium acetate method [31]. A solution of calcium acetate (2% w/w) was prepared in osmosed water. A weighed sample of dry polymer was stirred into the calcium acetate solution for 2 h following calibration with oxalic acid. Then, the solution was filtered, and the amount of acetic acid formed was measured by titration using a sodium hydroxide solution (0.05 M). The amount of ion exchange functions was equal to the amount of acetic acid present in solution. The results were expressed in mmol of COOH functional groups per gram of polymer.

The point of zero charge (PZC) values of both non-activated and activated polyBTCA-CD were determined by titration with the salt addition method. 50 mL of 0.1 M NaCl solution was placed in each of nine beakers. The pH of each solution was adjusted from 3 to 11 with one pH unit increment using a pH meter (pH meter, model 3110, WTW, Alès, France) with aqueous 0.1 M NaOH and 0.1 M HCl. Then 0.15 g of polymer was added to each beaker. The solutions were stirred for 48 h to reach equilibrium then the resulting pH (pHf) was measured. The difference between the initial and final pH values (ΔpH) was plotted against the initial pH. The PZC was represented by the point ΔpH = 0 [32].

X-ray diffraction analysis (XRD) was performed on a Bruker D8 Advance diffractometer using Cu Kα radiation with a wavelength of λ = 0.15406 nm produced at 40 kV and 40 mA. XRD data were collected over the 2θ range from 10° to 60° at every 0.02° with a scan speed of 0.5 s per step. For polymer, the diffraction profiles are divided into 2 parts: peaks related to diffraction of crystallites and a broad peak related to scattering of the amorphous phase. The assumption is that the areas are proportional to the scattering intensities of crystalline and amorphous phases. Thus, the percentage of polymer that is crystalline was determined from Equation 1 [33]:

$$\%\ \text{crystallinity} = \frac{\text{area under crystalline peaks}}{\text{total area under all peaks}} \times 100\,. \quad (1)$$

The polymer was also characterized by solid-state ^{13}C NMR techniques such as cross polarization magic angle spinning (CP MAS) and MAS. The spectra were recorded with a Bruker spectrometer operating at 75.47 MHz and 303 K. The compounds were placed in a zirconium rotor, 4 mm in diameter and 21 mm high. The chemical shifts were recorded relative to tetramethylsilane with benzene as secondary reference. The Hartmann–Hahn condition was satisfied during cross polarization magic angle with 1.5 ms of contact time under the following conditions: repetition time 8 s, 1H90° pulse length 4 μs, and spin rate at 10 kHz.

Adsorption tests

To determine the ability of the material to treat inorganic and organic load, several batch experiments were carried out with two kinds of solutions: spiked solutions (SS) containing different substances at several concentrations that are typical of ST discharge waters (DWs) [34] and real ST industrial DWs themselves.

SS contained metal sulfate salts ($Al_2(SO_4)_3 \cdot 16H_2O$; $CoSO_4 \cdot 7H_2O$; $CrK(SO_4)_2 \cdot 12H_2O$; $NiSO_4 \cdot 6H_2O$; $ZnSO_4 \cdot 7H_2O$) purchased from Aldrich and used without further purification. The sixteen PAHs of the US EPA list [35] and three APs were purchased from Supelco Sigma Aldrich (Saint-Quentin Fallavier, France) and used as received; eight light PAHs: naph-

thalene (NAP), acenaphthene (ACE), acenaphthylene (ACY), fluorene (FLU), phenanthrene (PHE), anthracene (ANT), fluoranthene (FLT) and pyrene (PYR); eight heavy PAHs: benz[*a*]anthracene (BaANT), chrysene (CHY), benzo[*b*]fluoranthene (BbFLT), benzo[*k*]fluoranthene (BkFLT), benzo[*a*]pyrene (BaPYR), dibenz[*a*,*h*]anthracene (dBahANT), indeno[1,2,3-*cd*]pyrene (IcdPYR) and benzo[*g*,*h*,*i*]perylene (BghiPL); three APs: 4-nonylphenol (4NP, CAS no. 84852-15-3), 4-*n*-nonylphenol (4nNP, CAS no. 104-40-5) and 4-*tert*-octylphenol (4tOP, CAS no. 140-66-9). Calcium chloride and sodium bicarbonate were purchased from Fischer Scientific (Illkirch, France) and used as received. Each SS was prepared from stock solutions in osmosed water.

Metal adsorption

In order to examine the effect of $NaHCO_3$ treatment (activation), the adsorption capacities of the non-activated and the activated polymer polyBTCA-CD were compared with a solution containing the five metals (Al^{3+}, Co^{2+}, Cr^{3+}, Ni^{2+} and Zn^{2+}) each at a concentration of 10 mg·L^{-1}. A kinetic study was also performed to determine the appropriate contact time between the material and the polymetallic solutions at concentrations of 1 and 10 mg·L^{-1} for each metal. Then, metal adsorption was determined by several polymetallic solutions containing the five metals described previously. Different concentrations of metals were tested: 10 mg·L^{-1} (SS1) and 1 mg·L^{-1} (SS2) for each metal and two solutions reproducing DW concentrations (SS3 and SS4). Moreover, two experiments were performed with metals in the absence (SS4) or presence (SS5) of $CaCl_2$ at DW concentrations, in order to observe the influence of salt concentrations (Table 6).

Table 6: Concentrations of metals and calcium expressed in mg·L^{-1} in the spiked solutions.

	Al^{3+}	Co^{2+}	Cr^{3+}	Ni^{2+}	Zn^{2+}	Ca^{2+}	pHi
SS1	9.12	9.71	10.05	9.46	9.37	<0.5	3.9
SS2	0.91	0.97	1.01	0.95	0.94	<0.5	4.4
SS3	0.95	0.76	0.015	0.10	0.36	<0.5	4.8
SS4	2.17	1.34	0.038	0.20	0.76	<0.5	4.8
SS5	2.26	1.33	0.035	0.20	0.75	457	4.7

PAH and AP adsorption

To determine the PAH adsorption, solutions were prepared with the sixteen PAHs: eight were considered as light PAHs, i.e., with a lower molecular weight, (NAP, ACY, ACE, FLU, PHE, ANT, FLT, PYR) and eight as heavy PAHs (BaANT, CHY, BbFLT, BkFLT, BaPYR, IcdPYR, dBahANT, BghiPL). Two PAH concentrations were tested: 3229 and 7243 ng·L^{-1} for the sum of the sixteen PAHs, i.e., for the first an average concentration of 1543 ± 261 ng·L^{-1} and 1686 ± 410 ng·L^{-1} (SS6; pHi 6), and for the second an average of 3508 ± 454 ng·L^{-1} and 3735 ± 333 ng·L^{-1} (SS7; pHi 6) for the sum of the light and the heavy PAHs, respectively. In the case of the APs, 4NP, 4nNP and 4tOP were used to prepare solutions at two concentrations: SS8 (pHi 6) containing 44, 53 and 59 µg·L^{-1} and SS9 (pHi 6) containing 662, 720 and 889 µg·L^{-1} 4NP, 4nNP and 4tOP, respectively.

Metals and organic adsorption in mixtures

To study adsorption capacities when substances are in mixture, seven solutions were prepared: mixture of five metals (pHi 4.4), mixture of sixteen PAHs (pHi 6), mixture of three APs (pHi 6), mixture of five metals + 16 PAHs (pHi 4.4), mixture of five metals + three APs (pHi 4.4), mixture of 16 PAHs + three APs (pHi 6.1) and mixture of five metals + 16 PAHs + three APs (pHi 4.4). In each solution, the average concentration was 1.08 ± 0.11 mg·L^{-1} for each metal, 365 ± 29 ng·L^{-1} for each light PAH, 419 ± 24 ng·L^{-1} for each heavy PAH and 53 ± 24 µg·L^{-1} for each AP.

Adsorption capacities in discharge waters

Five samples of real discharge waters (DWs) were collected from Zindel Industry located in Seloncourt (Doubs, France) which is specialized in chemical coatings and any processes for the corrosion protection of metal parts intended for the automotive and building sectors. Their process waters mainly contain metallic pollutants (e.g., Cr^{3+}, Ni^{2+} and Zn^{2+}) coming from rinsing and washing baths. Following the tests conducted on SS, metal retention capacity was also tested on five different industrial DWs. In one DW, the effect of polymer dose was tested: 5, 10, 15 and 20 g·L^{-1}. Moreover, one more detailed analysis was performed in order to see if the polymer can retain other substances present in the DW.

Batch experiments

In each experiment, 2 g·L^{-1} of material was stirred (250 rpm) with a fixed volume of polluted solution (with no modification of the initial pH value) at room temperature for 4 h. After treatment, the solutions were left to settle for 1 h, and the supernatant was analyzed. Chemical analyses were performed in the initial and in the treated solutions and the results expressed in concentration and removal efficiency. Under the same conditions, a control experiment was performed without pollutants in order to check whether pH variations occurred in non-activated and activated polyBTCA-CD.

Chemical analyses

For each SS or DW, initial and final pH values were measured. Metal concentrations were determined by inductively coupled plasma atomic emission spectroscopy (ThermoFisher, iCAP

6500 radial model, Courtaboeuf, France) after a step of acid digestion for DWs, following a previously reported method [21]. The analysis of the sixteen PAHs was performed by liquid–liquid extraction with hexane followed by separation and detection on a system composed of a GC apparatus and a triple quadrupole spectrometer (GC-MS/MS, Agilent, Massy, France) according to a method described in detail by Crini and co-workers [36]. Three APs (4NP, 4nNP, 4tOP) were analyzed by a certified laboratory (CARSO LSEHL, Lyon, France), by liquid–liquid extraction followed by separation and detection on GC-MS/MS according to the standard NF EN ISO 18857-1. For the detailed analysis, 189 substances and 17 water parameters were analyzed, before and after treatment of the DW, by a certified laboratory (CARSO LSEHL, Lyon, France).

Acknowledgements

The authors thank the Agence de l'Eau Rhône Méditerranée Corse, the FEDER (Fonds Européens de Développement Régional) and the Conseil Régional de Franche-Comté for financial support (NIRHOFEX Program 2013-2016) and Peter Winterton (University of Toulouse III, Toulouse, France) for English grammar and syntax review and his critical reading.

References

1. Morin-Crini, N.; Crini, G. *Prog. Polym. Sci.* **2013,** *38,* 344–368. doi:10.1016/j.progpolymsci.2012.06.005
2. Charles, J.; Bradu, C.; Morin-Crini, N.; Sancey, B.; Winterton, P.; Giangiacomo, T.; Badot, P.-M.; Crini, G. *J. Saudi Chem. Soc.* **2016,** *20,* 185–194. doi:10.1016/j.jscs.2013.03.007
3. Zhao, F.; Repo, E.; Yin, D.; Meng, Y.; Jafari, S.; Sillanpää, M. *Environ. Sci. Technol.* **2015,** *49,* 10570–10580. doi:10.1021/acs.est.5b02227
4. Zhang, X.; Wang, Y.; Yang, S. *Carbohydr. Polym.* **2014,** *114,* 521–529. doi:10.1016/j.carbpol.2014.08.072
5. Yang, W.; Yu, Z.; Pan, B.; Lv, L.; Zhang, W. *Chem. Eng. J.* **2015,** *268,* 399–407. doi:10.1016/j.cej.2015.01.051
6. Crini, G. *Chem. Rev.* **2014,** *114,* 10940–10975. doi:10.1021/cr500081p
7. Kayaci, F.; Aytac, Z.; Uyar, T. *J. Hazard. Mater.* **2013,** *261,* 286–294. doi:10.1016/j.jhazmat.2013.07.041
8. Szejtli, J. *Carbohydr. Polym.* **1990,** *12,* 375–392. doi:10.1016/0144-8617(90)90088-A
9. Mamba, B. B.; Krause, R. W.; Malefetse, T. J.; Nxumalo, E. N. *Environ. Chem. Lett.* **2007,** *5,* 79–84. doi:10.1007/s10311-006-0082-x
10. Martel, B.; Weltrowski, M.; Morcellet, J. Cyclodextrin polymers and/or cyclodextrin derivatives with complexing properties and ion-exchange properties and method for the production thereof. EP1165621B1, Feb 2, 2002.
11. Trotta, F.; Tumiatti, W. Cross-linked polymers based on cyclodextrins for removing polluting agents.. EP1492822A1, Jan 5, 2005.
12. Crini, G. *Prog. Polym. Sci.* **2005,** *30,* 38–70. doi:10.1016/j.progpolymsci.2004.11.002
13. Genç-Fuhrman, H.; Mikkelsen, P. S.; Ledin, A. *Water Res.* **2007,** *41,* 591–602. doi:10.1016/j.watres.2006.10.024
14. Tao, Z.; Chu, T.; Li, W.; Du, J.; Dai, X.; Gu, Y. *Colloids Surf., A* **2004,** *242,* 39–45. doi:10.1016/j.colsurfa.2004.04.044
15. Malamis, S.; Katsou, E. *J. Hazard. Mater.* **2013,** *252-253,* 428–461. doi:10.1016/j.jhazmat.2013.03.024
16. Saad, D. M.; Cukrowska, E. M.; Tutu, H. *Toxicol. Environ. Chem.* **2011,** *93,* 914–924. doi:10.1080/02772248.2011.575785
17. Ducoroy, L.; Bacquet, M.; Martel, B.; Morcellet, M. *React. Funct. Polym.* **2008,** *68,* 594–600. doi:10.1016/j.reactfunctpolym.2007.10.033
18. Ducoroy, L.; Martel, B.; Bacquet, M.; Morcellet, M. *J. Appl. Polym. Sci.* **2007,** *103,* 3730–3738. doi:10.1002/app.25249
19. Rollin, C.; Quiot, F. *Hydrocarbures aromatiques polycycliques - guide méthodologique - acquisition des données d'entrée des modèles analytiques ou numériques de transferts dans les sols et les eaux souterraines (in French);* Ministère de l'Ecologie et du Développement Durable, 2005; Vol. Report n° 66244-DESP-R01.
20. Steed, J. W.; Atwood, J. L. *Supramolecular chemistry,* 2nd ed.; John & Wiley: United Kingdom, 2009. doi:10.1002/9780470740880
21. Morin-Crini, N.; Druart, C.; Gavoille, S.; Lagarrigue, C.; Crini, G. *J. Environ. Prot.* **2013,** *4,* 53–60. doi:10.4236/jep.2013.47A007
22. Brusseau, M. L.; Wang, X.; Wang, W.-Z. *Environ. Sci. Technol.* **1997,** *31,* 1087–1092. doi:10.1021/es960612c
23. Reddad, Z.; Gerente, C.; Andres, Y.; Le Cloirec, P. *Environ. Sci. Technol.* **2002,** *36,* 2067–2073. doi:10.1021/es0102989
24. Schiewer, S.; Volesky, B. *Environ. Sci. Technol.* **1997,** *31,* 2478–2485. doi:10.1021/es960751u
25. Yang, S.; Li, J.; Lu, Y.; Chen, Y.; Wang, X. *Appl. Radiat. Isot.* **2009,** *67,* 1600–1608. doi:10.1016/j.apradiso.2009.03.118
26. Chen, T.; Zhou, Z.; Xu, S.; Wang, H.; Lu, W. *Bioresour. Technol.* **2015,** *190,* 388–394. doi:10.1016/j.biortech.2015.04.115
27. Gensemer, R. W.; Playle, R. C. *Crit. Rev. Environ. Sci. Technol.* **1999,** *29,* 315–450. doi:10.1080/10643389991259245
28. Kratochvil, D.; Pimentel, P.; Volesky, B. *Environ. Sci. Technol.* **1998,** *32,* 2693–2698. doi:10.1021/es971073u
29. Al-Rub, F. A. A.; El-Naas, M. H.; Ashour, I.; Al-Marzouqi, M. *Process Biochem.* **2006,** *41,* 457–464. doi:10.1016/j.procbio.2005.07.018
30. Martel, B.; Ruffin, D.; Weltrowski, M.; Lekchiri, Y.; Morcellet, M. *J. Appl. Polym. Sci.* **2005,** *97,* 433–442. doi:10.1002/app.21391
31. Ducoroy, L.; Martel, B.; Bacquet, B.; Morcellet, M. *J. Inclusion Phenom. Macrocyclic Chem.* **2007,** *57,* 271–277. doi:10.1007/s10847-006-9172-4
32. Tan, W.-f.; Lu, S.-j.; Liu, F.; Feng, X.-h.; He, J.-z.; Koopal, L. K. *Soil Sci.* **2008,** *173,* 277–286. doi:10.1097/SS.0b013e31816d1f12
33. Alexander, L. *J. Mater. Sci.* **1971,** *6,* 93. doi:10.1007/BF00550300
34. Druart, C.; Morin-Crini, N.; Euvrard, E.; Crini, G. *Environ. Processes* **2016,** *3,* 59–72. doi:10.1007/s40710-016-0125-7
35. Callahan, M. A.; Slimak, M. W.; Gabel, N. W.; May, I. P.; Fowler, C. F.; Freed, J. R.; Jennings, P.; Durfee, R. L.; Whitmore, F. C.; Maestri, B.; Mabey, W. R.; Holt, B. R.; Gould, C. *Water-related environmental fate of 129 priority pollutants, EPA-440/4-79-029a;* U. S. Environmental Protection Agency, Office of Water Planning and Standards and Office of Water and Waste Management, 1979.
36. Crini, N.; Druart, C.; Amiot, C.; Gavoille, S.; Crini, G. *Environ. Eng. Manage. J.* **2015,** *14,* 1195–1202.

BEILSTEIN JOURNAL OF ORGANIC CHEMISTRY

Radical polymerization by a supramolecular catalyst: cyclodextrin with a RAFT reagent

Kohei Koyanagi[1], Yoshinori Takashima[1], Takashi Nakamura[1,§], Hiroyasu Yamaguchi[1] and Akira Harada[*1,2]

Full Research Paper

Open Access

Address:
[1]Department of Macromolecular Science, Graduate School of Science, Osaka University, Toyonaka, Osaka 560-0043, Japan and [2]JST-ImPACT, Chiyoda-ku, Tokyo 100-8914, Japan

Email:
Akira Harada[*] - harada@chem.sci.osaka-u.ac.jp

* Corresponding author
§ Current affiliation: Faculty of Pure and Applied Sciences, University of Tsukuba.

Keywords:
cyclodextrin; radical polymerization; RAFT polymerization; substrate recognition site; supramolecular catalyst

Beilstein J. Org. Chem. **2016,** *12,* 2495–2502.
doi:10.3762/bjoc.12.244

Received: 26 August 2016
Accepted: 08 November 2016
Published: 22 November 2016

This article is part of the Thematic Series "Superstructures with cyclodextrins: Chemistry and applications IV".

Guest Editor: G. Wenz

Abstract

Supramolecular catalysts have received a great deal of attention because they improve the selectivity and efficiency of reactions. Catalysts with host molecules exhibit specific reaction properties and recognize substrates via host–guest interactions. Here, we examined radical polymerization reactions with a chain transfer agent (CTA) that has α-cyclodextrin (α-CD) as a host molecule (α-CD-CTA). Prior to the polymerization of *N*,*N*-dimethylacrylamide (DMA), we investigated the complex formation of α-CD with DMA. Single X-ray analysis demonstrated that α-CD includes DMA inside its cavity. When DMA was polymerized in the presence of α-CD-CTA using 2,2'-azobis[2-(2-imidazolin-2-yl)propane dihydrochloride (VA-044) as an initiator in an aqueous solution, poly(DMA) was obtained in good yield and with narrow molecular weight distribution. In contrast, the polymerization of DMA without α-CD-CTA produced more widely distributed polymers. In the presence of 1,6-hexanediol (C_6 diol) which works as a competitive molecule by being included in the α-CD cavity, the reaction yield was lower than that without C_6 diol.

Introduction

The folding of proteins in biological systems, the replication of DNA, and specific substrate recognition by enzymes play important roles in forming supramolecular structures, achieving functions, and maintaining life [1-6]. The crystal structures of RNA polymerase, DNA polymerase, and λ-exonuclease demonstrate that the cylindrical cavities of enzymes can effectively recognize substrates to produce biological polymers [1-6]. Cyclodextrins (CDs) have been widely used as substrate-recognition moieties in artificial enzymes [7-15], which have been used in the hydrolysis of activated esters [16-19] and as phase-

transfer catalysts [20-28]. Moreover, via complex formation, modern supramolecular catalysts [29-33] have been used to achieve various highly efficient and selective reactions, including hydrolysis reactions [10-15], C–H bond activation [34-36], olefin epoxidation [37-39], Diels–Alder reactions [40-42], 1,3-dipole cycloadditions [43,44], and polymerizations [45-47], among others. Selective substrate recognition and activation are essential functions of supramolecular catalysts.

CD derivatives are widely used in radical polymerization to dissolve hydrophobic monomers in aqueous solutions [48-54] and to control the aggregation of polymers [55-58]. Although supramolecular catalysts with CDs as monomer recognition sites and catalytic active sites have been designed for polymerization reactions, relatively few reports have described a catalytic design in which the catalytic active site does not leave the CD monomer recognition site during the growing step. In a previous design of radical initiators with CDs, the radical-initiating end group leaves the CD monomer recognition site [59,60]. With this molecular design, an included monomer is distant from the radical species and cannot be involved in the direct polymerization. Here, we will observe the effect of monomer recognition of CD on polymerization if a supramolecular polymerization catalyst capable of inserting the monomer between the active and binding sites can be designed. Based on this concept, we have reported that CDs can include and activate lactones to yield a polymer with a single CD at the end of the polymer chain [61-64]. Subsequently, we reported ring-opening metathesis polymerization involving the use of a Ru complex with a CD-derived monophosphine ligand [47]. In the design of the supramolecular polymerization catalysts, monomers are inserted between the initiating end group and the growing polymer chain.

In this study, the monomer recognition site is introduced to a reversible addition–fragmentation chain transfer (RAFT) polymerization system [65-69]. We have synthesized a chain transfer agent (CTA) bearing the CD moiety (CD-CTA) and have investigated this agent's polymerization behavior. The polymerization rate constant decreased with the addition of competitive molecules, indicating that complexation between CD-CTA and the monomer plays an important role in determining polymerization rate.

Results and Discussion

Preparation of α-CD-CTA

We designed a CTA reagent with α-CD or β-CD. Figure 1 illustrates the preparation of α-CD-CTA. Mercaptopropionic acid was reacted with benzyl bromide, K_3PO_4, and carbon bisulfide (CS_2) in acetone to afford a trithiocarbonyl derivative, a CTA with a carboxylic acid (CTA-COOH). α-CD-CTA was prepared in 50% yield by the reaction of CTA-COOH and 3-NH_2-α-CD with *N*,*N*'-dicyclohexylcarbodiimide (DCC)/1-hydroxybenzotriazole (HOBt) in DMF. The α-CD-CTA was purified using reverse-phase chromatography. β-CD-CTA was prepared using the same method as α-CD-CTA in 45% yield (see Supporting Information File 1). α-CD-CTA and β-CD-CTA can be dissolved in water. However, the solubility of β-CD-CTA in water was significantly low, leading to the formation of precipitates. β-CD-CTA forms a self-inclusion complex or a supramolecular dimer complex, which was characterized using 2D ROESY NMR (Supporting Information File 1, Figure S4).

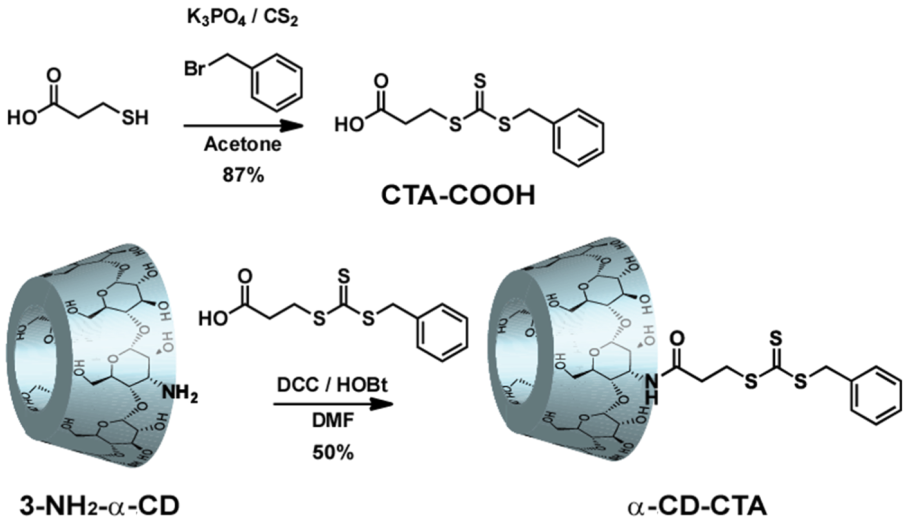

Figure 1: Preparation scheme of α-CD-CTA.

We focused on the polymerization activity of α-CD-CTA because the β-CD cavity of β-CD-CTA was capped by the CTA unit, inhibiting the molecular recognition property.

Crystal structure of the α-CD-DMA and β-CD-DMA complexes

We chose *N*,*N*-dimethylacrylamide (DMA), acrylic acid (AA), and acrylamide (AAm) as water-soluble vinyl monomers for radical polymerization. Prior to studying the polymerization of vinyl monomers, we investigated the complex formation of CDs with vinyl monomers. When mixing α-CD and DMA, we obtained single crystals suitable for X-ray crystallography analysis. The X-ray crystallography analysis is important to understand the complex in the condensed phase. Figure 2a shows the crystal structure of α-CD with DMA. α-CD formed a head-to-tail channel structure in the crystal. Figure 2b shows the schematic diagram of the crystal structure of α-CD/DMA. The stoichiometry of α-CD and encapsulated DMA was 1:1.

The *N*,*N*-dimethylamino group was located at the wider rim (secondary hydroxy group) of the α-CD cavity and the vinyl group was pointed toward the opposite direction. Based on the crystal structure, it is speculated that the modification of the wider rim of α-CD with the CTA group would bring the vinyl group of DMA and reactive radical species close together during the course of RAFT polymerization.

Figure S5a (Supporting Information File 1) shows the crystal structure of β-CD with DMA. β-CD formed a head-to-head dimeric structure in the crystal. Figure S5b shows a schematic diagram of the crystal structure of β-CD/DMA. The stoichiometry of β-CD and encapsulated DMA was 2:3. For two of the DMA molecules, the *N*,*N*-dimethylamino and the vinyl groups were located at the wider and the narrower rims of the β-CD cavity, respectively. The other one of the DMA molecules was packed between the two β-CD molecules in an equatorial plane.

When mixing α-CD and AA in water, we obtained a powder precipitate of a complex between α-CD and AA, although the crystal structure of α-CD and AA was not solved. The formation of precipitate implied the formation of a host-guest complex between them. A mixture of CDs (α-CD, β-CD and γ-CD) and AAm did not result in a precipitate, indicating that the affinities of the CDs for AAm were low.

Polymerization of vinyl monomers mediated by α-CD-CTA

α-CD-CTA-mediated polymerizations of water-soluble vinyl monomers were performed in aqueous media, where the strong molecular recognition property of α-CD is expected due to the hydrophobic effect. As a water-soluble radical initiator, we selected 2,2'-azobis[2-(2-imidazolin-2-yl)propane] dihydrochloride (VA-044). Two hundred equivalents (equiv) of monomers, 1 equiv of α-CD-CTA, and 0.4 equiv of VA-044 were mixed in water (monomer: 1 mol/kg). After the reactants were mixed and degassed, the sample tube was heated at 45 °C in an Ar atmosphere. After 24 hours, the polymer solution was lyophilized. The resulting polymers were dissolved in 8 mL MeOH or

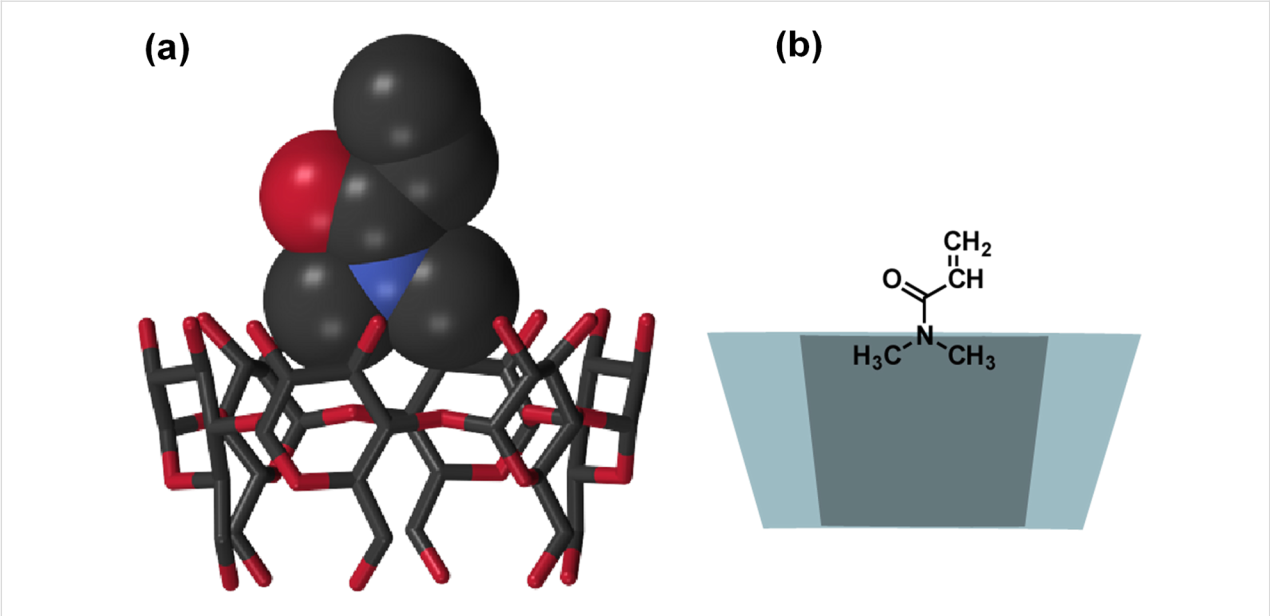

Figure 2: Crystal structure of α-CD with *N*,*N*-dimethylacrylamide (DMA). (a) The structure of an 1:1 inclusion complex between α-CD and DMA. One of the disordered pattern of DMA is shown. DMA molecules outside the α-CD, hydrogen atoms, and water molecules are omitted for clarity. Colors of the atoms are based on CPK coloring. DMA, space-filling model; CD, stick model. (b) A schematic diagram of the inclusion complex of α-CD/DMA.

chloroform, then reprecipitated into 80 mL diethyl ether. This cycle repeated twice to remove monomer. The structures of the obtained polymers were characterized by ^{1}H NMR spectroscopy (Figure S6, Supporting Information File 1). The ^{1}H NMR signals of the benzyl group and those of the CD moiety of α-CD-CTA were both observed in the obtained polymer, which indicates that both groups did not leave the polymer main chain after the radical polymerization and that α-CD-CTA functioned as a good chain transfer agent. Some end groups are formed from the VA 044 initiator.

Table 1 shows results for VA-044-initiated polymerizations of DMA, AA and AAm. Polymers' molecular weights and distributions were determined by gel permeation chromatography (GPC). The polymerization of DMA and AA mediated by α-CD-CTA gave polymers with similar molecular weights (12.8 and 14.8 kDa) and narrow distributions in good yields (85–88%) (Table 1, entries 2 and 5). In contrast, in the absence of α-CD-CTA, free radical polymerization with VA-044 gave polymers with higher molecular weights and wider distributions (Table 1, entries 1 and 4). In order to investigate the effect of encapsulation of monomer by α-CD moiety, the reactions in the presence of 1,6-hexanediol (C_6 diol) as a competitive guest molecule were also investigated. C_6 diol was selected as a non-ionic molecule with a high association constant to α-CD (K_a = 134 M^{-1}) [70]. In the presence of C_6 diol, the reaction yields dropped to 63–72%, whereas the molecular weights of the polymers increased (22.9 and 19.4 kDa in entries 3 and 6, respectively). It is considered that by inhibiting the molecular recognition of α-CD, the inclusion complexation ratio between the monomer and α-CD-CTA was decreased, which lead to lower yields and higher molecular weight of the resulting polymers due to preceding free radical polymerization. In the reaction of AAm monomer, which has a low affinity with α-CD, the properties of the obtained polymers were similar regardless of the presence of the α-CD-CTA or the competitive C_6 diol guest. The polymerization of AAm mediated by α-CD-CTA gave polymers with slightly narrower distributions. From the series of experiments, it was demonstrated that the molecular recognition property of α-CD-CTA effectively affected the chain transfer step.

Rate and mechanism of α-CD-CTA-mediated polymerization

We investigated the polymerization rate of DMA mediated by α-CD-CTA and the effect of the competitive molecule in water. A mixture of DMA (200 equiv), α-CD-CTA (1 equiv), and VA-044 (0.4 equiv) in D_2O (0.25 mol/kg) was degassed and heated at 45 °C in an Ar atmosphere. When a concentration of 1 mol/kg was used, the polymerization rate was too fast to trace during the initial stages of polymerization. Therefore, we chose to utilize a concentration of 0.25 mol/kg because this concentration allowed the polymerization rate to be easily followed. At regular time intervals, a 0.6 mL sample was collected and analyzed using ^{1}H NMR spectroscopy. The conversions were calculated using the ratio between the integral values for the polymer main chain and the vinyl group of the DMA monomer.

Figure 3a, b and c shows time-conversion curves, kinetic plots, and M_n-conversion for the polymerization of DMA mediated by α-CD-CTA. The time-conversion plots indicate the induction period in the presence and absence of C_6 diol. Kinetic rates were determined using the least-square method after the induction period. The presence of C_6 diol made a clear difference in the polymerization rate by α-CD-CTA. The kinetic rate was faster for α-CD-CTA (k = 2.2 h^{-1}) than for α-CD-CTA/C_6 diol (k = 1.7 h^{-1}). This finding supports that C_6 diol inhibits monomer recognition by the α-CD cavity, which was also indicated by the series of experiments in Table 1.

Table 1: Polymerizations of water-soluble vinyl monomers, mediated by α-CD-CTA[a].

Entry	CTA[b]	Monomer[b]	Competitor[c]	M_n / 10^3 [d]	M_w / M_n [d]	Yield%
1	–	DMA	–	9679	>10	96
2	α-CD-CTA	DMA	–	**12.8**	**1.2**	**85**
3	α-CD-CTA	DMA	C_6 diol	22.9	1.3	63
4	–	AA	–	45.9	>10	98
5	α-CD-CTA	AA	–	**14.8**	**1.2**	**88**
6	α-CD-CTA	AA	C_6 diol	19.4	1.2	72
7[e]	–	AAm	–	3841	>10	98
8[e]	α-CD-CTA	AAm	–	**10.4**	**1.3**	**98**
9[e]	α-CD-CTA	AAm	C_6 diol	9.9	1.4	99

[a]Polymerization was performed at 45 °C for 24 h, with VA-044 as an initiator. [b]$[Monomer]_0/[CTA]_0/[I]_0$ = 200/1/0.4 ($[Monomer]_0$ = 1 M). [c]$[Competitor]_0/[CTA]_0$ = 50/1. [d]M_n and M_w/M_n were determined by GPC using polystyrene sulfonate sodium salt (PSSNa) or polyacrylamide (PAAm) as references. [e]Polymerization of AAm was performed in acetate buffer [71,72].

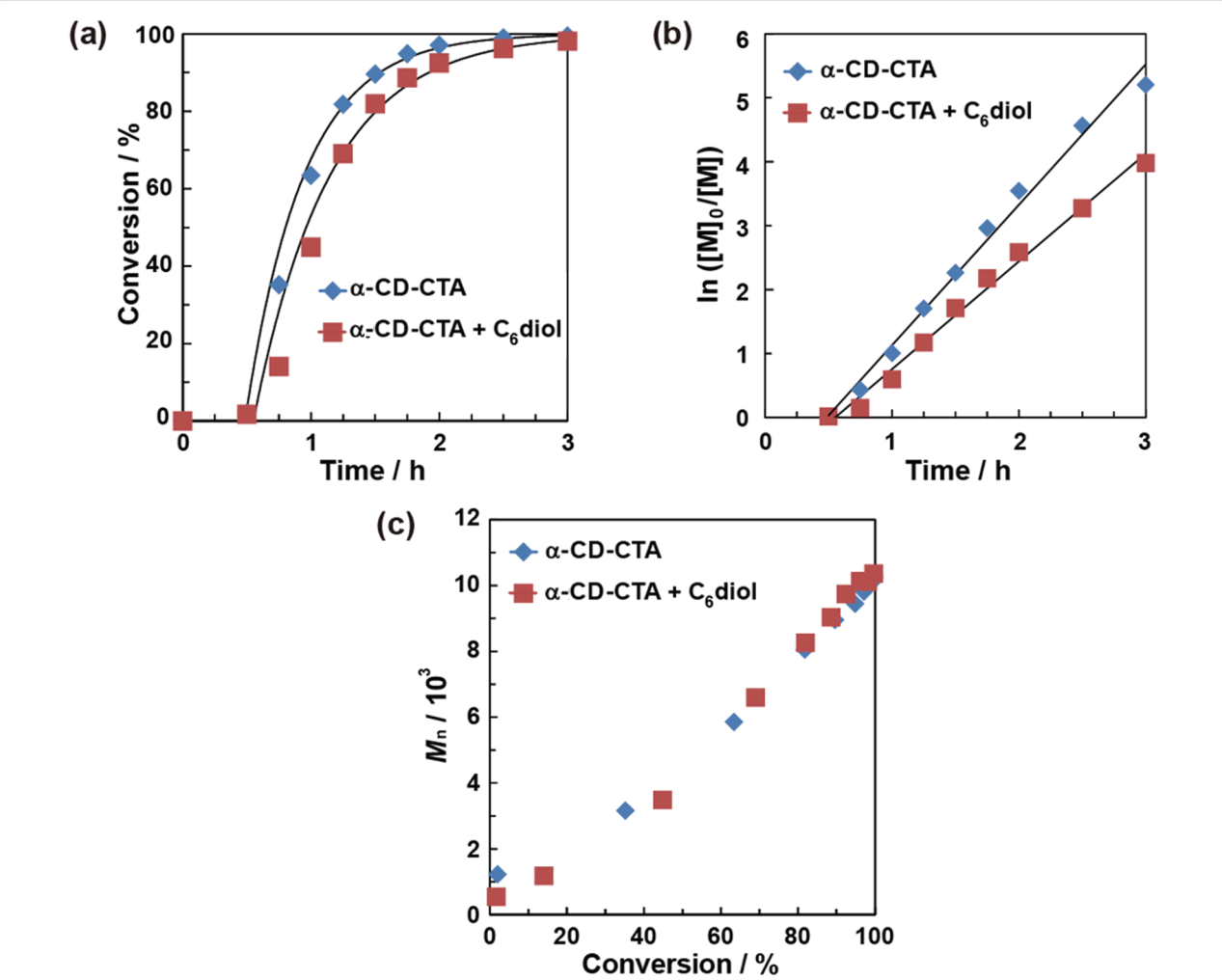

Figure 3: Time-conversion curves (a), kinetic plots (b) and plots of number-average molecular weight (M_n) versus conversion (c) for the α-CD-CTA-mediated polymerization of DMA. The blue rhombic plots correspond to the α-CD-CTA-mediated polymerization of DMA. The red square plots correspond to the α-CD-CTA/C_6 diol-mediated polymerization of DMA.

Figure 4 shows the proposed polymerization mechanism of a water-soluble vinyl monomer with α-CD-CTA. The radical (I$^\bullet$) derived from VA-044 attacks the monomer to produce a polymeric radical ($P_n^\bullet$). $P_n^\bullet$ reacts with α-CD-CTA to generate the intermediate α-CD-CTA-$P_n^\bullet$. α-CD-CTA-$P_n^\bullet$ is held in an equilibrium state with the macro-CTA, α-CD-CTA-P_n, and the benzyl radical (Bn$^\bullet$) with re-initiation activity. As demonstrated by the inhibition experiments, the yields and molecular weights of the polymers were affected by the molecular recognition property of α-CD-CTA. Based on these results, $P_n^\bullet$ and Bn$^\bullet$ preferentially attack the included monomer to afford the growing polymer in high yield. Therefore, the kinetic rate is faster for α-CD-CTA than for α-CD-CTA/C_6 diol, which produced polymers with narrow distribution. In the polymerization reaction, some of the polymer chains (P_n•) form dead chains through termination or irreversible chain transfer. However, the M_w/M_n of the polymer mediated by α-CD-CTA agents that the termination reaction is suppressed by α-CD-CTA compared to free radical polymerization.

Conclusion

We studied the radical polymerization of water-soluble vinyl monomers using CD-CTA with molecular recognition property. α-CD was found to include a DMA monomer in a 1:1 manner, which was characterized using single X-ray crystallography analysis. The polymerization of DMA with α-CD-CTA resulted in poly(DMA) with a narrow distribution in high yield, whereas a low yield was obtained for polymerization in the presence of C_6 diol, a competitive guest molecule for α-CD. In contrast, the polymerization of AAm, which had a lower affinity for α-CD, was not affected by α-CD-CTA in either the presence or absence of C_6 diol. These results indicate that the chain transfer reagent modified with a host molecule provided the site for a reaction between the end group of the growing polymer and

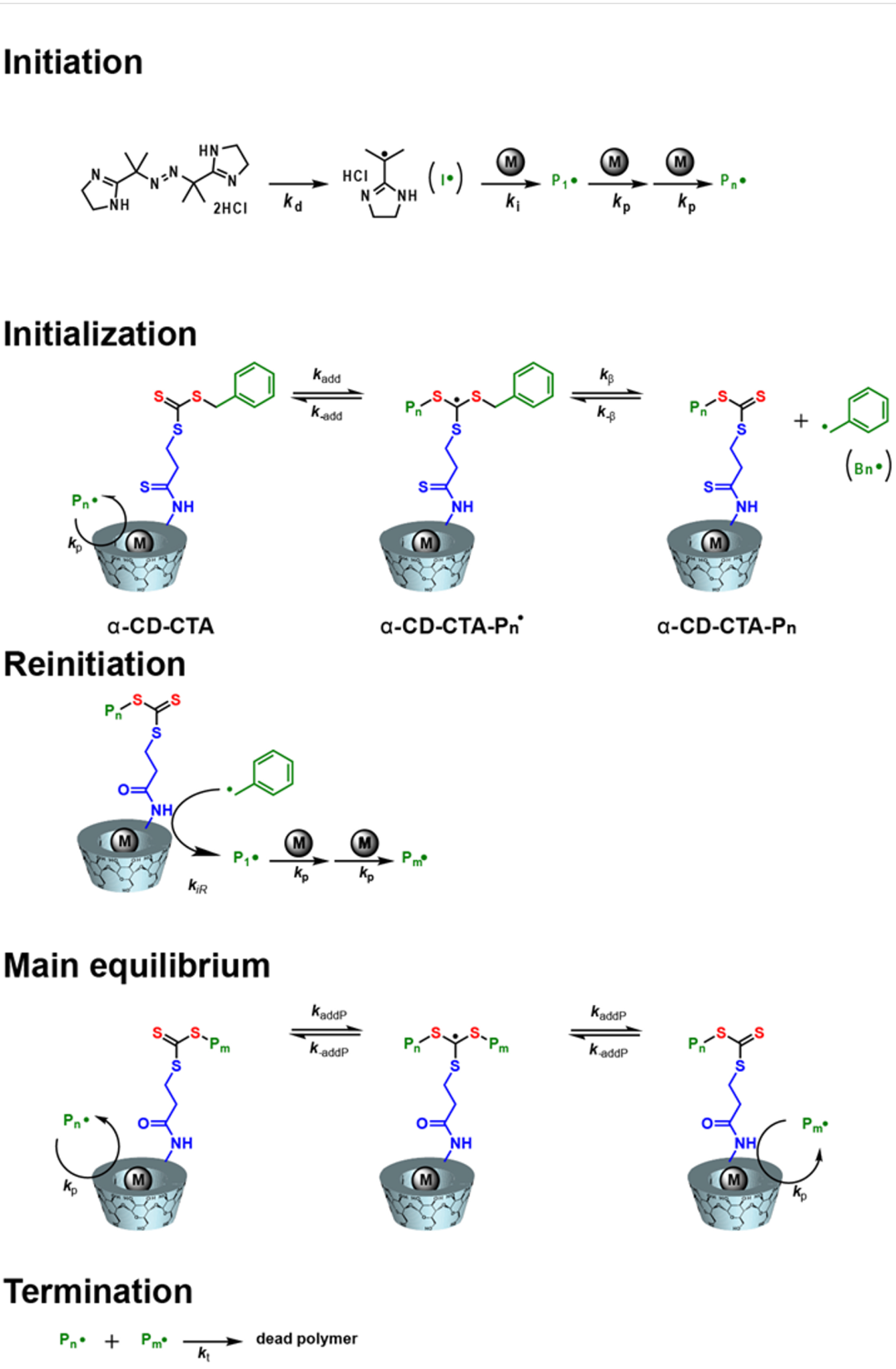

Figure 4: Proposed polymerization mechanism for a water-soluble vinyl monomer with α-CD-CTA as a chain transfer reagent. 2,2'-Azobis[2-(2-imidazolin-2-yl)propane] dihydrochloride (VA-044) was used as a water-soluble radical initiator.

monomers. Currently, we are investigating the preparation of supramolecular catalysts with a chain transfer reagent with two CDs to recognize monomers and the growing polymer chain, and exploring its function mimicking a biological molecular clamp.

Supporting Information

Supporting Information File 1

The preparation of α-CD-CTA and β-CD-CTA and typical polymerization methods.
[http://www.beilstein-journals.org/bjoc/content/supplementary/1860-5397-12-244-S1.pdf]

Supporting Information File 2

Crystallographic information file for α-CD-DMA.
[http://www.beilstein-journals.org/bjoc/content/supplementary/1860-5397-12-244-S2.cif]

Supporting Information File 3

Crystallographic information file for β-CD-DMA.
[http://www.beilstein-journals.org/bjoc/content/supplementary/1860-5397-12-244-S3.cif]

Acknowledgements

This work was financially supported by the ImPACT Program of Council for Science, Technology and Innovation (Cabinet Office, Government of Japan), a Grant-in-Aid for Scientific Research (B) (no. 26288062) from MEXT of Japan, and the Research Grant Program of the Asahi Glass Foundation.

References

1. Mooney, R. A.; Landick, R. *Cell* **1999,** *98,* 687–690. doi:10.1016/S0092-8674(00)81483-X
2. Kovall, R.; Matthews, B. W. *Science* **1997,** *277,* 1824–1827. doi:10.1126/science.277.5333.1824
3. Trakselis, M. A.; Alley, S. C.; Abel-Santos, E.; Benkovic, S. J. *Proc. Natl. Acad. Sci. U. S. A.* **2001,** *98,* 8368–8375. doi:10.1073/pnas.111006698
4. Benkovic, S. J.; Valentine, A. M.; Salinas, F. *Annu. Rev. Biochem.* **2001,** *70,* 181–208. doi:10.1146/annurev.biochem.70.1.181
5. Breyer, W. A.; Matthews, B. W. *Protein Sci.* **2001,** *10,* 1699–1711. doi:10.1110/ps.10301
6. Kool, E. T. *Acc. Chem. Res.* **1998,** *31,* 502–510. doi:10.1021/ar9602462
7. Mallick, I. M.; D'Souza, V. T.; Yamaguchi, M.; Lee, J.; Chalabi, P.; Gadwood, R. C.; Bender, M. L. *J. Am. Chem. Soc.* **1984,** *106,* 7252–7254. doi:10.1021/ja00335a070
8. D'Souza, V. T.; Hanabusa, K.; O'Leary, T.; Gadwood, R. C.; Bender, M. L. *Biochem. Biophys. Res. Commun.* **1985,** *129,* 727–732. doi:10.1016/0006-291X(85)91952-7
9. D'Souza, V. T.; Bender, M. L. *Acc. Chem. Res.* **1987,** *20,* 146–152. doi:10.1021/ar00136a004
10. Komiyama, M.; Breaux, E. J.; Bender, M. L. *Bioorg. Chem.* **1977,** *6,* 127–136. doi:10.1016/0045-2068(77)90015-3
11. Czarniecki, M. F.; Breslow, R. *J. Am. Chem. Soc.* **1978,** *100,* 7771–7772. doi:10.1021/ja00492a079
12. Breslow, R.; Czarniecki, M. F.; Emert, J.; Hamaguchi, H. *J. Am. Chem. Soc.* **1980,** *102,* 762–770. doi:10.1021/ja00522a054
13. Breslow, R.; Trainor, G. L.; Ueno, A. *J. Am. Chem. Soc.* **1983,** *105,* 2739–2744. doi:10.1021/ja00347a037
14. Breslow, R. *Acc. Chem. Res.* **1991,** *24,* 317–324. doi:10.1021/ar00011a001
15. Breslow, R. *Artificial Enzymes;* Wiley-VCH Verlag GmbH & Co. KGaA, 2006.
16. Tanaka, Y.; Sakuraba, H.; Nakanishi, H. *J. Chem. Soc., Chem. Commun.* **1983,** 947–948. doi:10.1039/C39830000947
17. Sakuraba, H.; Nakai, T.; Tanaka, Y. *J. Inclusion Phenom.* **1984,** *2,* 829–839. doi:10.1007/BF00662252
18. Trost, B. M.; Van Vranken, D. L. *J. Am. Chem. Soc.* **1990,** *112,* 1261–1263. doi:10.1021/ja00159a065
19. Trost, B. M.; Van Vranken, D. L. *J. Am. Chem. Soc.* **1993,** *115,* 444–458. doi:10.1021/ja00055a013
20. Harada, A.; Hu, Y.; Takahashi, S. *Chem. Lett.* **1986,** 2083–2084. doi:10.1246/cl.1986.2083
21. Hu, Y.; Harada, A.; Takahashi, S. *Synth. Commun.* **1988,** *18,* 1607–1610. doi:10.1080/00397918808081320
22. van Dongen, S. F. M.; Elemans, J. A. A. W.; Rowan, A. E.; Nolte, R. J. M. *Angew. Chem., Int. Ed.* **2014,** *53,* 11420–11428. doi:10.1002/anie.201404848
23. Hubert, C.; Denicourt-Nowicki, A.; Roucoux, A.; Landy, D.; Leger, B.; Crowyn, G.; Monflier, E. *Chem. Commun.* **2009,** 1228–1230. doi:10.1039/b818786j
24. Bricout, H.; Hapiot, F.; Ponchel, A.; Tilloy, S.; Monflier, E. *Curr. Org. Chem.* **2010,** *14,* 1296–1307. doi:10.2174/138527210791616920
25. Hapiot, F.; Bricout, H.; Tilloy, S.; Monflier, E. *Eur. J. Inorg. Chem.* **2012,** 1571–1578. doi:10.1002/ejic.201101316
26. Noël, S.; Léger, B.; Ponchel, A.; Philippot, K.; Denicourt-Nowicki, A.; Roucoux, A.; Monflier, E. *Catal. Today* **2014,** *235,* 20–32. doi:10.1016/j.cattod.2014.03.030
27. Hapiot, F.; Bricout, H.; Menuel, S.; Tilloy, S.; Monflier, E. *Catal. Sci. Technol.* **2014,** *4,* 1899–1908. doi:10.1039/c4cy00005f
28. Vanbésien, T.; Monflier, E.; Hapiot, F. *ACS Catal.* **2015,** *5,* 4288–4292. doi:10.1021/acscatal.5b00861
29. Lehn, J.-M. *Supramolecular Chemistry;* Wiley-VCH Verlag GmbH & Co. KGaA, 1995.
30. van Leeuwen, P. W. N. M. *Supramolecular Catalysis;* Wiley-VCH Verlag GmbH & Co. KGaA; Vol. 2008.
31. Raynal, M.; Ballester, P.; Vidal-Ferran, A.; van Leeuwen, P. W. N. M. *Chem. Soc. Rev.* **2014,** *43,* 1660–1733. doi:10.1039/C3CS60027K
32. Raynal, M.; Ballester, P.; Vidal-Ferran, A.; van Leeuwen, P. W. N. M. *Chem. Soc. Rev.* **2014,** *43,* 1734–1787. doi:10.1039/C3CS60037H
33. Vriezema, D. M.; Aragonès, M. C.; Elemans, J. A. A. W.; Cornelissen, J. J. L. M.; Rowan, A. E.; Nolte, R. J. M. *Chem. Rev.* **2005,** *105,* 1445–1490. doi:10.1021/cr0300688
34. Leung, D. H.; Fiedler, D.; Bergman, R. G.; Raymond, K. N. *Angew. Chem., Int. Ed.* **2004,** *43,* 963–966. doi:10.1002/anie.200352772
35. Das, S.; Incarvito, C. D.; Crabtree, R. H.; Brudvig, G. W. *Science* **2006,** *312,* 1941–1943. doi:10.1126/science.1127899

36. Leung, D. H.; Bergman, R. G.; Raymond, K. N. *J. Am. Chem. Soc.* **2006,** *128,* 9781–9797. doi:10.1021/ja061412w
37. Thordarson, P.; Bijsterveld, E. J. A.; Rowan, A. E.; Nolte, R. J. M. *Nature* **2003,** *424,* 915–918. doi:10.1038/nature01925
38. Coumans, R. G. E.; Elemans, J. A. A. W.; Nolte, R. J. M.; Rowan, A. E. *Proc. Natl. Acad. Sci. U. S. A.* **2006,** *103,* 19647–19651. doi:10.1073/pnas.0603036103
39. Jónsson, S.; Odille, F. G. J.; Norrby, P.-O.; Warnmark, K. *Chem. Commun.* **2005,** 549–551. doi:10.1039/B411978A
40. Walter, C. J.; Anderson, H. L.; Sanders, J. K. M. *J. Chem. Soc., Chem. Commun.* **1993,** 458–460. doi:10.1039/C39930000458
41. Marty, M.; Clyde-Watson, Z.; Twyman, L. J.; Nakash, M.; Sanders, J. K. M. *Chem. Commun.* **1998,** 2265–2266. doi:10.1039/a806070c
42. Yoshizawa, M.; Tamura, M.; Fujita, M. *Science* **2006,** *312,* 251–254. doi:10.1126/science.1124985
43. Mock, W. L.; Irra, T. A.; Wepsiec, J. P.; Adhya, M. *J. Org. Chem.* **1989,** *54,* 5302–5308. doi:10.1021/jo00283a024
44. Chen, J.; Rebek, J., Jr. *Org. Lett.* **2002,** *4,* 327–329. doi:10.1021/ol0168115
45. Armspach, D.; Matt, D.; Peruch, F.; Lutz, P. *Eur. J. Inorg. Chem.* **2003,** 805–809. doi:10.1002/ejic.200390109
46. Jouffroy, M.; Armspach, D.; Matt, D.; Osakada, K.; Takeuchi, D. *Angew. Chem., Int. Ed.* **2016,** *55,* 8367–8370. doi:10.1002/anie.201603191
47. Takashima, Y.; Uramatsu, K.; Jomori, D.; Harima, A.; Otsubo, M.; Yamaguchi, H.; Harada, A. *ACS Macro Lett.* **2013,** *2,* 384–387. doi:10.1021/mz4001942
48. Köllisch, H. S.; Barner-Kowollik, C.; Ritter, H. *Chem. Commun.* **2009,** 1097–1099. doi:10.1039/b818897a
49. Storsberg, J.; Ritter, H. *Macromol. Rapid Commun.* **2000,** *21,* 236–241. doi:10.1002/(SICI)1521-3927(20000301)21:5<236::AID-MARC236>3.0.CO;2-K
50. Glöckner, P.; Metz, N.; Ritter, H. *Macromolecules* **2000,** *33,* 4288–4290. doi:10.1021/ma992012e
51. Storsberg, J.; Hartenstein, M.; Müller, A. H. E.; Ritter, H. *Macromol. Rapid Commun.* **2000,** *21,* 1342–1346. doi:10.1002/1521-3927(20001201)21:18<1342::AID-MARC1342>3.0.CO;2-Z
52. Hetzer, M.; Schmidt, B. V. K. J.; Barner-Kowollik, C.; Ritter, H. *J. Polym. Sci., Part A: Polym. Chem.* **2013,** *51,* 2504–2517. doi:10.1002/pola.26644
53. Köllisch, H.; Barner-Kowollik, C.; Ritter, H. *Macromol. Rapid Commun.* **2006,** *27,* 848–853. doi:10.1002/marc.200600067
54. Choi, S. W.; Kretschmann, O.; Ritter, H.; Ragnoli, M.; Galli, G. *Macromol. Chem. Phys.* **2003,** *204,* 1475–1479. doi:10.1002/macp.200350010
55. Yao, F.; Xu, L.; Fu, G.-D.; Lin, B. *Macromolecules* **2010,** *43,* 9761–9770. doi:10.1021/ma102039n
56. Liu, Y.-Y.; Zhong, Y.-B.; Nan, J.-K.; Tian, W. *Macromolecules* **2010,** *43,* 10221–10230. doi:10.1021/ma1019973
57. Chechik, V.; Ionita, G. *Org. Biomol. Chem.* **2006,** *4,* 3505–3510. doi:10.1039/b607676a
58. Ionita, G.; Chechik, V. *Org. Biomol. Chem.* **2005,** *3,* 3096–3098. doi:10.1039/b508256k
59. Kakuchi, T.; Narumi, A.; Miura, Y.; Matsuya, S.; Sugimoto, N.; Satoh, T.; Kaga, H. *Macromolecules* **2003,** *36,* 3909–3913. doi:10.1021/ma021295z
60. Kakuchi, T.; Narumi, A.; Matsuda, T.; Miura, Y.; Sugimoto, N.; Satoh, T.; Kaga, H. *Macromolecules* **2003,** *36,* 3914–3920. doi:10.1021/ma021296r
61. Takashima, Y.; Osaki, M.; Harada, A. *J. Am. Chem. Soc.* **2004,** *126,* 13588–13589. doi:10.1021/ja047171e
62. Osaki, M.; Takashima, Y.; Yamaguchi, H.; Harada, A. *J. Am. Chem. Soc.* **2007,** *129,* 14452–14457. doi:10.1021/ja075140o
63. Harada, A.; Osaki, M.; Takashima, Y.; Yamaguchi, H. *Acc. Chem. Res.* **2008,** *41,* 1143–1152. doi:10.1021/ar800079v
64. Takashima, Y.; Osaki, M.; Ishimaru, Y.; Yamaguchi, H.; Harada, A. *Angew. Chem., Int. Ed.* **2011,** *50,* 7524–7528. doi:10.1002/anie.201102834
65. Chiefari, J.; Chong, Y. K.; Ercole, F.; Krstina, J.; Jeffery, J.; Le, T. P. T.; Mayadunne, R. T. A.; Meijs, G. F.; Moad, C. L.; Moad, G.; Rizzardo, E.; Thang, S. H. *Macromolecules* **1998,** *31,* 5559–5562. doi:10.1021/ma9804951
66. McCormick, C. L.; Lowe, A. B. *Acc. Chem. Res.* **2004,** *37,* 312–325. doi:10.1021/ar0302484
67. Moad, G.; Chong, Y. K.; Postma, A.; Rizzardo, E.; Thang, S. H. *Polymer* **2005,** *46,* 8458–8468. doi:10.1016/j.polymer.2004.12.061
68. Semsarilar, M.; Perrier, S. *Nat. Chem.* **2010,** *2,* 811–820. doi:10.1038/nchem.853
69. Barner-Kowollik, C., Ed. *Handbook of RAFT Polymerization;* Wiley-VCH Verlag GmbH & Co. KGaA, 2008. doi:10.1002/9783527622757
70. Bastos, M.; Briggner, L.-E.; Shehatta, I.; Wadsö, I. *J. Chem. Thermodyn.* **1990,** *22,* 1181–1190. doi:10.1016/0021-9614(90)90111-3
71. Thomas, D. B.; Sumerlin, B. S.; Lowe, A. B.; McCormick, C. L. *Macromolecules* **2003,** *36,* 1436–1439. doi:10.1021/ma025960f
72. Thomas, D. B.; Convertine, A. J.; Myrick, L. J.; Scales, C. W.; Smith, A. E.; Lowe, A. B.; Vasilieva, Y. A.; Ayres, N.; McCormick, C. L. *Macromolecules* **2004,** *37,* 8941–8950. doi:10.1021/ma048199d

License and Terms

BEILSTEIN JOURNAL OF ORGANIC CHEMISTRY

A self-assembled cyclodextrin nanocarrier for photoreactive squaraine

Ulrike Kauscher and Bart Jan Ravoo*

Full Research Paper

Open Access

Address:
Organic Chemistry Institute and Center for Soft Nanoscience, Westfälische Wilhelms-Universität Münster, Corrensstrasse 40, 48149 Münster, Germany

Email:
Bart Jan Ravoo* - b.j.ravoo@uni-muenster.de

* Corresponding author

Keywords:
cyclodextrin; host–guest chemistry; photodynamic therapy; self-assembly; squaraine

Beilstein J. Org. Chem. **2016,** *12,* 2535–2542.
doi:10.3762/bjoc.12.248

Received: 15 July 2016
Accepted: 04 November 2016
Published: 25 November 2016

This article is part of the Thematic Series "Superstructures with cyclodextrins: Chemistry and applications IV".

Guest Editor: G. Wenz

Abstract

Photoreactive squaraines produce cytotoxic oxygen species under irradiation and have significant potential for photodynamic therapy. Herein we report that squaraines can be immobilized on a self-assembled nanocarrier composed of amphiphilic cyclodextrins to enhance their photochemical activity. To this end, a squaraine was equipped with two adamantane moieties that act as anchors for the cyclodextrin vesicle surface. The supramolecular immobilization was monitored by using fluorescence spectroscopy and microscopy and the photochemistry of the squaraine was investigated by using absorption spectroscopy.

Introduction

Photodynamic therapy (PDT) has become a very attractive alternative to traditional cancer therapies due to its efficiency and selectivity [1-4]. PDT is based on a photosensitizer (PS), which is delivered to cancerous tissue followed by the irradiation with light of an appropriate wavelength. Irradiation of the PS causes its transition to the excited singlet state and, via intersystem crossing; the PS reaches its triplet state. Electron transfer occurs upon relaxation to the ground state. This process can take place in two ways distinguished as type I and II mechanisms [5]. The type I mechanism describes a direct interaction between the PS and the surrounding cell material. Electrons are transferred onto the cell material, causing the production of radicals that then react with oxygen to form reactive oxygen species. The type II mechanism, however, describes the interference of the PS with the triplet ground state of oxygen, leading to the production of singlet oxygen. In both mechanisms, the PS harvests the energy of incident light to form reactive oxygen species or singlet oxygen, which are highly cytotoxic [6,7].

Most clinically used PSs are based on porphyrins, which have the disadvantage of an absorption wavelength in the range of

visible light [8,9]. Visible light is scattered and absorbed by the inhomogeneous biological tissue. In order to optimise efficiency, it is vital to skew the absorption range of the PS towards the near infrared range. Then, the scattering and absorption by tissue is minimized and a more in-depth therapy becomes possible.

The search for more effective compounds with absorption in the near infrared includes amongst others cyanine [10], bodipy [11], and phthalocyanine [12] photosensitizers and has lately led to the consideration of a class of compounds known as squaraines [13-18]. Squaraines are a promising class of fluorescent dyes for PDT. In the past, squaraines showed a very low intersystem-crossing efficiency, leading to the premature conclusion that these dyes cannot be used in PDT [19]. Santos et al. showed that the intersystem-crossing efficiency of squaraines can be remarkably increased by incorporation of heavy atoms like selenium or sulfur and the addition of long aliphatic side chains [20,21]. The enhanced intersystem-crossing efficacy due to spin-orbital interactions makes modified squaraines a promising component of PDT [22,23].

Whether squaraines follow the type I or type II mechanism is discussed controversially in the literature. Santos et al. [19,20], Salice et al. [24] and Rapozzi et al. [25] investigated how benzothiazole-squaraines, which are also pursued in this project, cause cytotoxicity. Santos et al. postulated the production of singlet oxygen as a result of interaction between the squaraines and the ground state of oxygen [19,20]. A few years later, Salice et al. showed that squaraines are not efficient singlet oxygen producing agents, but can be applied successfully as singlet oxygen quenchers [23]. The authors discussed that this behaviour is based on charge-transfer processes between stacked squaraines as well as oxygen squaraine complexes. Within the same year, Rapozzi et al. described the photooxidation process of benzothiazol squaraines [24]. They showed that the irradiation of benzothiazole-squaraines results in a photodegradation process. Rapozzi et al. assume that oxidation probably involves through formation of a π-complex between the electron-rich enamine double bond and molecular oxygen. In comparison to the photo-oxidation of enaminon or other electron-rich double bonds, the complex can react further to produce 3-HBT (3-hexylbenzo[*d*]thiazol-2(3*H*)-one). The photogenerated oxidation products can then induce radical-chain reactions with the surrounding cell material, leading to cell toxicity.

However, like most PS, squaraines have poor water solubility, which leads to aggregation and inactivation under physiological conditions, causing a reduced production of reactive oxygen species [26]. To overcome this drawback, we considered to immobilize the squaraines onto a platform that provides spatial separation (Figure 1). Our platforms of choice are vesicles self-assembled from amphiphilic cyclodextrin [27]. Given their negligible toxicity cyclodextrins have been utilized as carriers in a number of studies [28,29]. Amphiphilic cyclodextrins substituted with hydrophobic alkyl groups on the primary side and hydrophilic oligo(ethylene glycol) units on the secondary side can be synthesized in a simple and straightforward three step synthesis [27,30]. Cyclodextrin vesicles (CDVs) can be easily prepared by sonication or extrusion in aqueous solution. CDVs have the unique possibility of versatile surface decoration by the simple addition of guest molecules to the aqueous solution of the vesicle [30]. The hydrophobic cyclodextrin cavities are well known to form size-selective inclusion complexes with apolar compounds such as adamantane [31]. In several publications, we have shown that CDVs retain this ability by keeping the cavity available for host–guest complexation. In that way, it was possible to decorate CDVs with carbohydrates [32,33], with peptides [34], and also with DNA [35]. Moreover

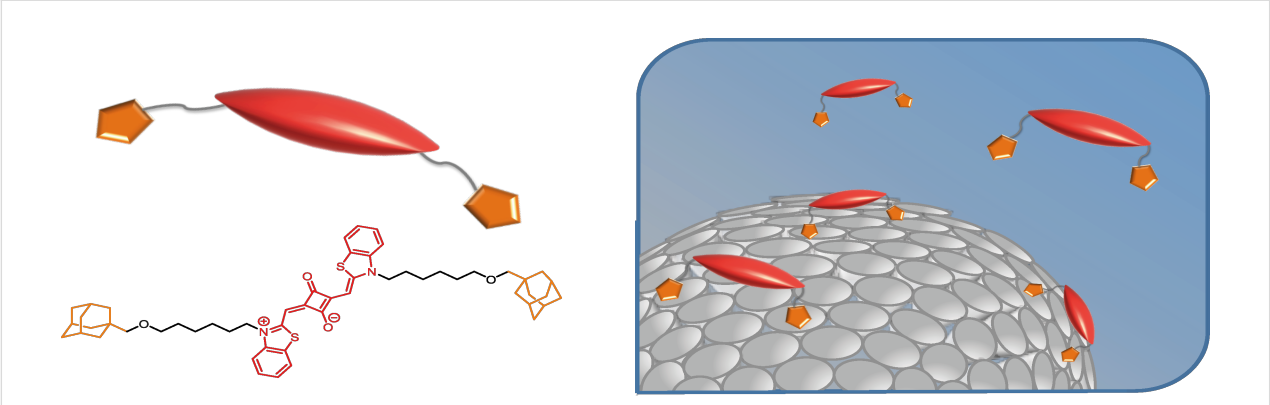

Figure 1: Schematic representation of adamantane-substituted squaraine (AdSq) binding as a divalent guest to the surface of cyclodextrin vesicles (CDV).

CDVs were also shown to form very dense membranes in combination with phospholipids and cholesterol [36]. Previous studies also showed promising results for PDT applications when a well-known PS, phthalocyanine, was used to decorate the cyclodextrin vesicles [37,38]. The immobilization led to an increased photoactivity of the phthalocyanines due to suppression of aggregation and inactivation of the PS at the surface of the CDVs.

In this contribution we show that squaraines can also be immobilized onto CDVs. For this purpose, the squaraines are equipped with two adamantane functions that bind into the cavities of cyclodextrin on the surface of the CDVs (Figure 1). The resulting divalent host–guest interaction should lead to a higher binding affinity of the squaraine for the CDV without affecting its photochemistry. In addition, it is expected that the aggregation of squaraine will be supressed by immobilization at the CDV surface. Ultimately, the photoactive squaraine can be combined with other functional guests, such as targeting units and tracers, to further enhance the potential of the nanocarrier.

Results and Discussion

Adamantane-substituted squaraine (AdSq) was synthesized in a three step synthesis. Benzothiazole rings were introduced to enlarge the π-system. The sulfur atoms of these moieties increase the intersystem crossing due to the heavy atom effect. Additionally hexyl alkane chains were introduced on both N-termini. Santos et al. showed that these lead to a higher intersystem crossing compared to shorter alkane chains [20,21]. The analytical data for AdSq (see Supporting Information File 1) are consistent with the molecular structure shown in Figure 1.

In a first set of experiments, we investigated the photochemical properties of AdSq in acetonitrile (Figure 2). The absorption spectrum shows a peak at 665 nm indicative of the presence of squaraine monomers in the solution. A shoulder around 610 nm indicates aggregation of the squaraine due to π–π stacking. A comparison of absorption spectra in different solvents revealed that the amount of aggregation is rather low in acetonitrile or ethanol but increases dramatically if water is used as a solvent (see Figure S1 in Supporting Information File 1). This is in agreement with literature and highlights the importance of introducing a platform for the immobilization of the squaraines as to provide steric separation and suppress aggregation.

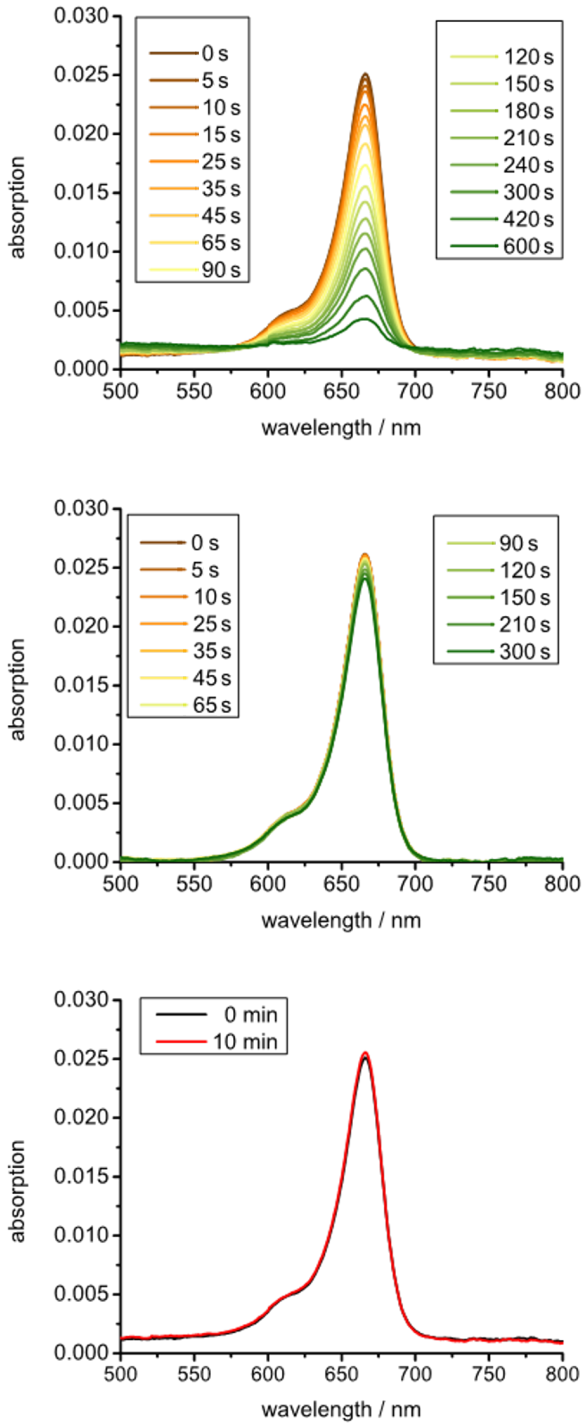

Figure 2: Absorption spectra of AdSq in acetonitrile. [AdSq] = 7.5 μM. Top: Absorption at different time points during irradiation. Middle: Absorption at different time points during irradiation of an argon equilibrated solution. Bottom: Absorption after and before storing in the dark for 10 min.

In the next step, we investigated the photoactivation under irradiation. To this end, a solution of AdSq was irradiated with light of a wavelength higher than 630 nm (250 W halogen lamp, long pass filter 630 nm). Absorption spectra were taken at different time points of irradiation. The obtained data show a decay of absorption with time of irradiation (Figure 2, top). Clearly, AdSq is undergoing a reaction under irradiation which leads to its decomposition. To verify that the proposed mechanism by Rapozzi (see above) is correct we carried out further

experiments. If the solution of AdSq in acetonitrile was equilibrated in an argon atmosphere to drive away any oxygen, the absorption spectra obtained show the same absorption intensity for all time points (Figure 2, middle). This reveals that AdSq undergoes no decomposition in absence of oxygen and that photodecomposition is definitely due to interaction with oxygen. To test if the decomposition mechanism is light driven, another set of absorption spectra were taken in an oxygen-equilibrated solution that was stored in the dark for 10 min. In this case, the absorption spectra show no decrease indicating that again no decomposition is obtained (Figure 2, bottom). Thus, AdSq is stable in solution if stored in the dark.

Next, we investigated the immobilization of AdSq by host–guest interaction with CDVs. Amphiphilic β-cyclodextrins substituted with 7 dodecylsulfide groups on the primary side and 7 oligo(ethylene glycol) units on the secondary side were obtained via a straightforward three step synthesis as described [27,30]. A thin film of these amphiphiles was obtained by evaporation of a chloroform solution in a round bottom flask. Hydration and extrusion with a Liposofast extruder and membranes with 100 nm pore size yield bilayer vesicles of an approximate size of 100 nm. CDVs were decorated with AdSq by simple addition of the AdSq to the aqueous dispersion of the CDVs.

Interestingly, the immobilization of AdSq on CDV can be directly observed by fluorescence spectrometry. To this end, solutions with different concentrations of CDV were prepared. AdSq was dissolved in acetonitrile in the dark and added to the vesicle solution. The percentage of acetonitrile in water was kept under 0.5%, so that any influence on solubility of AdSq, stability of CDVs or host guest interaction can be neglected. Fluorescence spectra were taken 20 min after addition of AdSq to assure the complete equilibration of the CDV dispersion. The fluorescence spectrum of AdSq without CDV shows no fluorescence, while increasing fluorescence intensity was detected with more CDV available (Figure 3, top). These results indicate that immobilization of the AdSq on the surface of CDV suppresses the aggregation of AdSq in aqueous solution and that the AdSq fluorescence is enhanced due to a suppression of intermolecular π–π stacking. The more CDV is available, the more AdSq is immobilized on the surface of the vesicles. To support this explanation, absorption spectra were taken of the solutions that were prepared for the fluorescence experiments. The absorption spectra show a decrease of the signal at 615 nm that indicates the presence of the aggregated form of AdSq (see Figure S2 in Supporting Information File 1).

The fluorescence spectra show a saturation of the intensity maximum for a concentration of 60 µM CDV. Assuming that

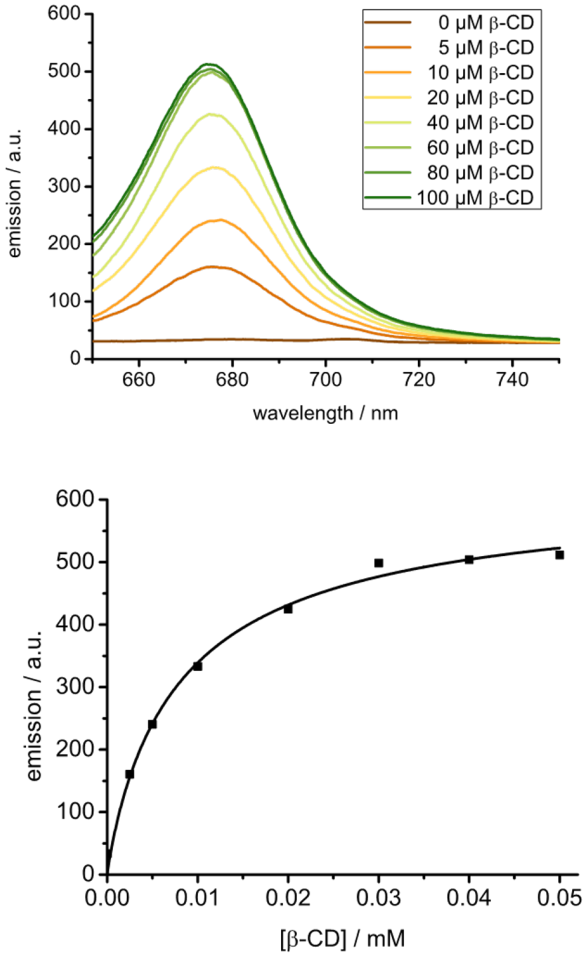

Figure 3: Top: Emission spectra (ex: 630 nm) of AdSq immobilized at CDV. [CDV] = 0–100 µM; [AdSq] = 5 µM. Bottom: Langmuir regression of a fluorescence titration of CDV to AdSq. [AdSq] = 10 µM, [CDV] = 0–100 µM. It is assumed that only cyclodextrins on the outer surface of the CDV are available for host–guest interactions.

the accessible concentration of cyclodextrin available for the complexation of guest is only 30 µM (since approximately 50% of the amphiphilic cyclodextrins reside at the interior surface of the CDV and AdSq is too large and too polar to pass the membrane), saturation is reached at a six-fold excess of host to guest, even though both are present in micromolar concentrations only. The binding constant of AdSq with the cyclodextrins in the CDV could be obtained by plotting the maximum fluorescence emission (at 676 nm) against the concentration of available cyclodextrin (Figure 3, bottom). The resulting Langmuir isotherm was fitted by linear regression (see Supporting Information File 1 for details) and the binding constant was determined to be $K_a = 1.2 \times 10^5\ M^{-1}$. The high-affinity binding of AdSq is a clear indication that both adamantanes are involved in binding to the CDV and that the interaction is effectively divalent.

In another set of experiments, giant unilamellar vesicles (GUVs) of amphiphilic cyclodextrins were formed by electroformation [35]. The obtained vesicles have a size of several micrometers and are thus directly visible by fluorescence microscopy. AdSq were added to a solution of the GUVs and immobilization of the molecules was examined with confocal fluorescence spectroscopy. The images taken show GUVs with a red luminescent membrane due to the squaraines bound to the GUV surface (Figure 4). Thus, fluorescence microscopy provided direct evidence for the immobilization of AdSq on the CDV.

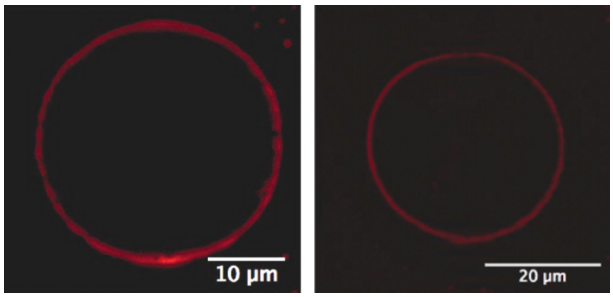

Figure 4: Confocal fluorescence microscopy of giant unilamellar vesicles (GUVs) of amphiphilic cyclodextrins with AdSq on their outer surface.

After the immobilization of AdSq on the surface of CDV was demonstrated, we investigated the photochemistry of AdSq on CDV. To this end, AdSq was added to an aqueous dispersion of CDV exactly as described above. The solution was irradiated for 600 s and absorption spectra were taken at various time points. As shown before in the acetonitrile solution, also AdSq immobilized on CDV photodecomposition (Figure 5). The decomposition of AdSq on the surface of CDV versus its decomposition in acetonitrile solution was compared (see Figure S3 in Supporting Information File 1). The immobilized squaraines showed a slower decay indicating a higher stability of squaraines on the CDV. To verify that the CDV are stable during this process, DLS spectra were taken. These reveal the same size for the vesicles before and after addition of squaraines as well as after irradiation, so that significant photodamage of the nanocarrier can be excluded. We note that our measurements are performed under atmospheric conditions. At these conditions the concentration of oxygen in water is 1.25 mM while the concentration of oxygen in acetonitrile is between 8.1–12.1 mM, depending on the type of measurement. [39]. The lower oxygen concentration in water can enhance the lifetime of AdSq on CDV.

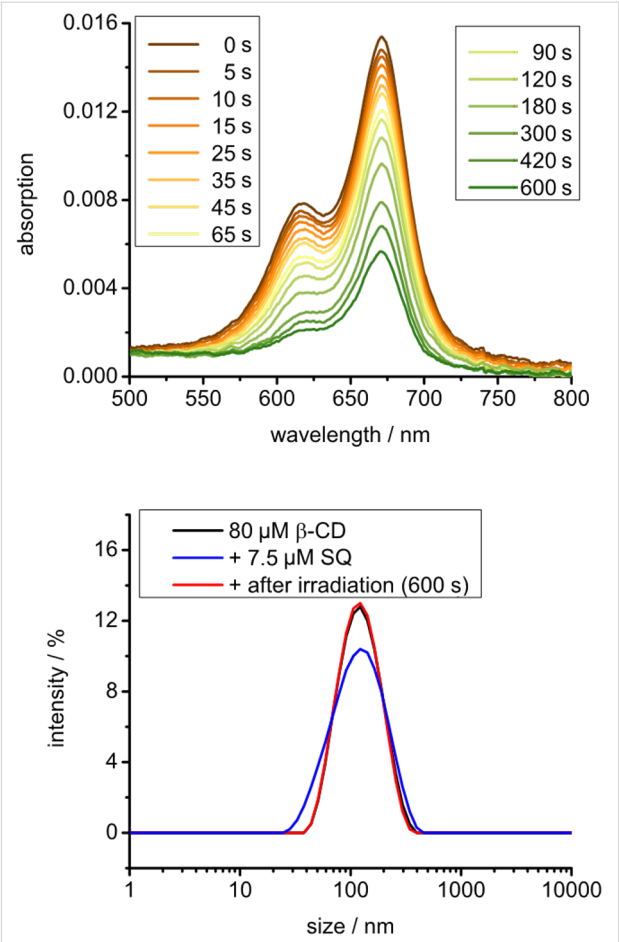

Figure 5: Top: Absorption spectra at different time points during irradiation of a CDV solution with AdSq immobilised on the vesicle surface. Bottom: DLS spectra before and after irradiation. [AdSq] = 7.5 µM, [CDV] = 80 µM.

Conclusion

We demonstrated the successful synthesis of a symmetric benzothiazol squaraine (AdSq) substituted with two adamantane groups. We showed that this squaraine can be activated by irradiation and undergoes an oxygen-dependent decomposition reaction as proposed by Rapozzi et al. for similar squaraines [25]. Host–guest inclusion between the adamantane groups and the cyclodextrin cavities at the surface of cyclodextrin vesicles (CDVs) results in efficient immobilization of the squaraine on a nanocarrier. In addition, π–π stacking (and hence inactivation) of the squaraine is supressed due to the steric separation of the squaraines on the vesicle surface. In short, the self-assembled nanosystem has several advantageous properties to be used as a PDT system. We envision that the photoactive squaraine can be combined with other functional guests, such as targeting units and tracers, to enhance the potential of the nanocarrier. Further studies have to be carried out to reveal the effectivity in medical applications.

Experimental

In the following the synthesis of AdSq is described (Figure 6). NMR spectra can be found in Supporting Information File 1. In

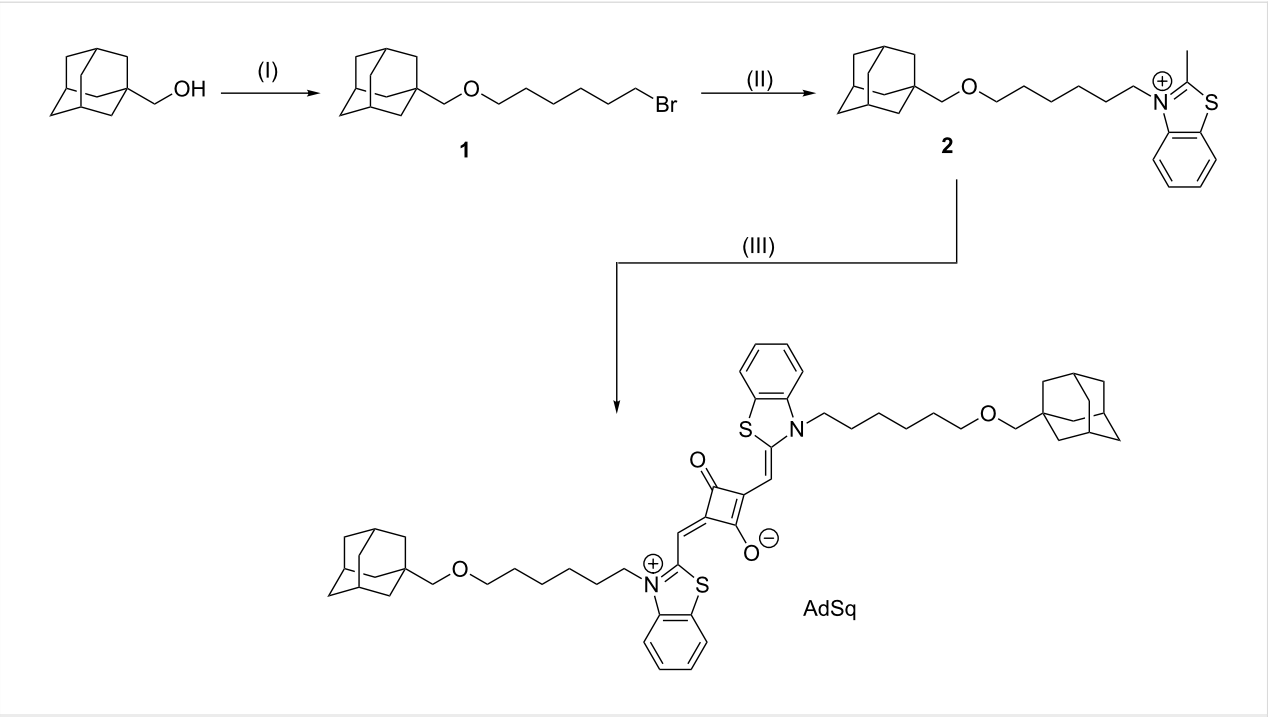

Figure 6: Synthesis of AdSq (I) NaH, DMF, 1,6-dibromohexane, 24 h, rt. (II) benzothiazole, acetonitrile, 12 h, 90 °C, 5%; (III) squaric acid, benzene, *n*-butanol, pyridine, 12 h, 120 °C, 26%.

the cases where the experimental protocol required an inert gas atmosphere, the Schlenk method was used under argon atmosphere.

1-[{(6-Bromohexyl)oxy}methyl]adamantane (1)

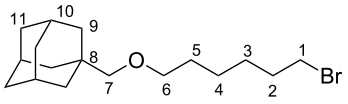

Adamantanyl-1-methanol (4.98 g, 29.95 mmol) and NaH (wt 60%, 2.38 g) were dissolved in dry DMF and stirred at room temperature for 90 minutes. 1,6-Dibromohexane (18.27 mL, 120 mmol) was then added drop-wise to the reaction mixture. The reaction mixture was stirred at room temperature for 24 hours and the excess NaH was subsequently quenched by addition of water. The product was then extracted from pentane (1×) and water (3×). The product was dried over $MgSO_4$ and excess solvent was removed by rotary evaporation. A fraction of crude product was then purifiied through silica column chromatography (EtOAc/cyclohexane (40:1), R_f: 0.6). Molecular formula: $C_{17}H_{29}BrO$. ^{1}H NMR (400 MHz, $CDCl_3$, 298 K) δ 3.33 (m, 4H, 1,6-H), 2.88 (s, 2H, 7-H), 1.89 (p, J = 3.1 Hz, 3H, 10-H), 1.84–1.75 (m, 2H, 2-H), 1.68–1.55 (m, 6H, 11-H), 1.54-1.25 (m, 14H, 2-5-9-H) ppm; ^{13}C NMR (75 MHz, $CDCl_3$, 298 K) δ 81.92 (CH_2, 7-C), 71.40 (CH_2, 6-C), 39.74 (3 CH_2, 9-C), 37.24 (3 CH_2, 11-C), 34.08 (C_q, 8-C), 33.96 (CH_2, 1-C), 32.78 (CH_2, 2-C), 29.38 (CH_2, 5-C), 28.29 (3 CH, 10-C), 28.01 (CH_2, 3-C), 25.37 (CH_2, 4-C) ppm; HRMS–ESI (*m*/*z*): calcd for $[C_{17}H_{29}BrO]^+$: 351.1294; found: 351.1299.

3-[6-{(Adamantan-1-yl)methoxy}hexyl]-2-methylbenzo[*d*]thiazole (2)

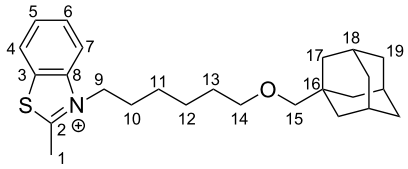

Methylbenzothiazole (0.89 g, 6 mmol) and 1-[{(6-bromohexyl)oxy}methyl]adamantane (**1**, 1.97 g, 6 mmol) were dissolved in 4 mL of acetonitrile and the resulted solution was stirred at 90 °C overnight. Afterwards the solvent was evaporated by rotary evaporation. The residue was washed with diethyl ether. The product was filtered and the precipitate was washed with diethyl ether. Afterwards the precipitate was redissolved in ethanol. The solvent was evaporated and the product was obtained as a dark red solid (0.119 g , 0.3 mmol, 5%). Molecular formula: $C_{25}H_{36}NOS$; ^{1}H NMR (300 MHz, $CDCl_3$, 298 K) δ 8.38 (m, 1H, 7-H), 7.98 (d, J = 8.5 Hz, 1H, 4-H), 7.75 (dd, J = 8.5, 1.3 Hz, 1H, 6-H), 7.71–7.56 (m, 1H, 5-H), 4.88 (t, J = 7.8 Hz, 2H, 9-H), 3.44 (s, 3H, 1-H), 3.32 (t, J = 6.0 Hz, 2H, 14-H),

2.90 (s, 2H, 15-H), 1.91 (m, 10-/18-H), 1.68–1.44 (m, 16H, 11-/12-/13-/17-/19-H), 1.22 (m, 2H) ppm; ^{13}C NMR (75 MHz, $CDCl_3$, 298 K) δ 175.66 (C_q, 2-C), 140.97 (C_q, 8-C), 129.88 (C_q, 3-C), 129.42, 128.58, 125.03, 116.40 (CH, 4-7-C), 82.02 (CH_2, 15-C), 71.24 (CH_2, 14-C), 51.04 (CH_2, 9-C), 39.81 (3 CH_2, 17-C), 37.29 (3 CH_2, 19-C), 34.16 (C_q, 16-C), 29.38 (CH_2, 13-C), 28.81 (CH_2, 10-C), 28.33 (3 CH, 18-C), 26.69 (CH_2, 11-C), 25.93 (CH_2, 12-C), 19.06 (CH_3, 1-C) ppm; HRMS–ESI (*m*/*z*): calcd for $[C_{25}H_{36}NOS]^+$: 398.2512; found: 398.2516.

2-((3-(6-((Adamantan-1-yl)methoxy)hexyl)benzo[*d*]thiazol-2(3*H*)-ylidene)methyl)-4-((3-(6-((adamantan-1-yl)methoxy)hexyl)benzo[*d*]thiazol-3-ium-2-yl)methylene)-3-oxocyclobut-1-en-1-olate, squaraine (AdSq)

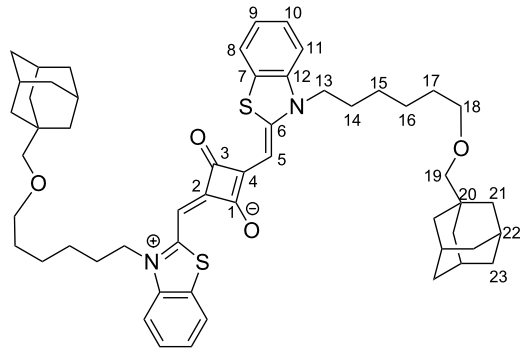

All solvents were dried and equilibrated with argon. The reaction was performed in the dark. Squaric acid (10 mg, 0.09 mmol) and compound (**2**, 70 mg, 0.18 mmol) were dissolved in a mixture of benzene, *n*-butanol and pyridine (2:1:1). The reaction was stirred for 12 h at 120 °C. The crude product was concentrated in vacuo and purified by column chromatography under argon atmosphere (DCM:MeOH 9:1, R_f: 0.6). The product was obtained as a dark blue solid (20 mg, 0.088 mmol, 26%). Molecular formula: $C_{54}H_{68}N_2O_4S_2$. ^{1}H NMR (600 MHz, $CDCl_3$, 298 K) δ 9.41 (dd, *J* = 18.1, 6.1 Hz, 2H, H_{ar}), 8.97–8.91 (m, 1H, H_{ar}), 8.55–8.45 (m, 2H, H_{ar}), 8.13 (t, *J* = 6.9 Hz, 2H, H_{ar}), 8.02 (dd, *J* = 8.0, 5.5 Hz, 1H, H_{ar}), 6.34 (s, 1H, 5-H), 4.96 (dd, *J* = 8.8, 6.2 Hz, 2H, 13-H), 4.63 (td, *J* = 6.6, 1.3 Hz, 1H, 5-H), 4.19 (qd, *J* = 11.0, 6.0 Hz, 2H, 13-H), 3.39–3.26 (m, 4H, 18-H), 2.94–2.89 (m, 4H, 19-H), 2.14–1.03 (m, 42H, 14-,16-,17-,21-,22-,23-H), 1.02–0.81 (m, 4H, 15-H) ppm; ^{13}C NMR (151 MHz, $CDCl_3$, 298 K) δ 198.35 (Cq, 3-C), 190.29 (Cq, 1-C), 187.25 (Cq, 6-C), 167.87 (Cq, 6-C), 145.25 (C_q, 2-C), 141.94, 140.97 (2CH, 12-C), 132.55, 130.99 (C_q, 7-C), 128.89, 128.59, 127.72, 127.27 (4CH, 9-,10-C), 124.95, 122.46 (CH, 8-,11-C), 112.36 (2CH, 5-C), 82.02 ($2CH_2$, 19-H), 73.01, 71.44, 71.31 ($2CH_2$, 18-C), 62.34 (CH, 13-C), 47.01 (CH, 13-C), 39.86 (CH, 21-C), 37.34 (CH, 23-C), 34.20 (C_q, C-20), 32.05, 31.99 ($2CH_2$, 17-C), 29.47, 29.38 ($2CH_2$, 14-C), 28.38 (2CH, 22-C), 26.09, 26.02 ($2CH_2$, 15-C), 25.99, 25.76 ($2CH_2$, 16-C), 18.69 ppm; MALDI–MS (*m*/*z*): calcd for $[C_{54}H_{68}N_2O_4S_2]^+$: 872,46; found: 872,47.

Supporting Information

Supporting Information File 1

Additional measurements and methods.
[http://www.beilstein-journals.org/bjoc/content/supplementary/1860-5397-12-248-S1.pdf]

Acknowledgments

Financial support from the DFG EXC 1003 Cells in Motion–Cluster of Excellence, Münster, Germany is gratefully acknowledged. We thank Lena Fischer-Riepe for her help with confocal microscopy.

References

1. Bonnett, R. *Chemical Aspects of Photodynamic Therapy;* Gordon and Breach Science Publishers: Amsterdam, 2000.
2. Bonnett, R. *Chem. Soc. Rev.* **1995,** *24,* 19–33. doi:10.1039/cs9952400019
3. Robertson, C. A.; Evans, D. H.; Abrahamse, H. *J. Photochem. Photobiol., B* **2009,** *96,* 1–8. doi:10.1016/j.jphotobiol.2009.04.001
4. Maisch, T. *Mini-Rev. Med. Chem.* **2009,** *9,* 974–983. doi:10.2174/138955709788681582
5. Felsher, D. W. *Nat. Rev. Cancer* **2003,** *3,* 375–379. doi:10.1038/nrc1070
6. Josefsen, L. B.; Boyle, R. W. *Met.-Based Drugs* **2008,** No. 276109. doi:10.1155/2008/276109
7. Ortel, B.; Shea, C. R.; Calzavara-Pinton, P. *Front. Biosci.* **2009,** *14,* 4157–4172. doi:10.2741/3520
8. Detty, M. R.; Gibson, S. L.; Wagner, S. J. *J. Med. Chem.* **2004,** *47,* 3897–3915. doi:10.1021/jm040074b
9. Cherno, N. K.; Krusir, G. V. *Prikl. Biokhim. Mikrobiol.* **2005,** *28,* 297–303.
10. Delaey, E.; van Laar, F.; De Vos, D.; Kamuhabwa, A.; Jacobs, P.; de Witte, P. *J. Photochem. Photobiol., B* **2000,** *55,* 27–36. doi:10.1016/S1011-1344(00)00021-X
11. Awuah, S. G.; Polreis, J.; Biradar, V.; You, Y. *Org. Lett.* **2011,** *13,* 3884–3887. doi:10.1021/ol2014076
12. Jiang, Z.; Shao, J.; Yang, T.; Wang, J.; Jia, L. *J. Pharm. Biomed. Anal.* **2014,** *87,* 98–104. doi:10.1016/j.jpba.2013.05.014
13. Sreejith, S.; Divya, K. P.; Ajayaghosh, A. *Angew. Chem., Int. Ed.* **2008,** *47,* 7883–7887. doi:10.1002/anie.200803194
14. Law, K. Y. *J. Phys. Chem.* **1987,** *91,* 5184–5193. doi:10.1021/j100304a012
15. Emmelius, M.; Pawloski, G.; Vollmann, H. W. *Angew. Chem., Int. Ed.* **1989,** *28,* 1445–1471. doi:10.1002/anie.198914453
16. Law, K. Y. *Chem. Rev.* **1993,** *93,* 449–486. doi:10.1021/cr00017a020
17. Dolmans, D. E. J. G. J.; Fukumura, D.; Jain, R. K. *Nat. Rev. Cancer* **2003,** *3,* 380–387. doi:10.1038/nrc1071

18. Yagi, S.; Nakazumi, H. *Syntheses and Applications of Squarylium Dyes*. In *Functional Dyes;* Kim, S.-H., Ed.; Elsevier B. V.: Amsterdam, 2006; pp 215–255. doi:10.1016/b978-044452176-7/50007-3
19. Kamat, P. V.; Das, S.; Thomas, K. G.; George, M. V. *J. Phys. Chem.* **1992,** *96,* 195–199. doi:10.1021/j100180a038
20. Santos, P. F.; Reis, L. V.; Almeida, P.; Oliveira, A. S.; Vieira Ferreira, L. F. *J. Photochem. Photobiol., A* **2003,** *160,* 159–161. doi:10.1016/S1010-6030(03)00203-X
21. Santos, P. F.; Reis, L. V.; Almeida, P.; Serrano, J. P.; Oliveira, A. S.; Vieira Ferreira, L. F. *J. Photochem. Photobiol., A* **2004,** *163,* 267–269. doi:10.1016/j.jphotochem.2003.12.007
22. Foote, C. S.; Lin, J. W.-P. *Tetrahedron Lett.* **1968,** *9,* 3267–3270. doi:10.1016/S0040-4039(00)89543-X
23. Mazur, S.; Foote, C. S. *J. Am. Chem. Soc.* **1970,** *92,* 3225–3226. doi:10.1021/ja00713a073
24. Salice, P.; Arnbjerg, J.; Pedersen, B. W.; Toftegaard, R.; Beverina, L.; Pagani, G. A.; Ogilby, P. R. *J. Phys. Chem. A* **2010,** *114,* 2518–2525. doi:10.1021/jp911180n
25. Rapozzi, V.; Beverina, L.; Salice, P.; Pagani, G. A.; Camerin, M.; Xodo, L. E. *J. Med. Chem.* **2010,** *53,* 2188–2196. doi:10.1021/jm901727j
26. Monge-Fuentes, V.; Muehlmann, L. A.; de Azevedo, R. B. *Nano Rev.* **2014,** *5,* No. 24381. doi:10.3402/nano.v5.24381
27. Ravoo, B. J.; Darcy, R. *Angew. Chem., Int. Ed.* **2000,** *39,* 4324–4326. doi:10.1002/1521-3773(20001201)39:23<4324::AID-ANIE4324>3.0.CO;2-O
28. Chauhan, P.; Hadad, C.; Sartorelli, A.; Zarattini, M.; Herreros-López, A.; Mba, M.; Maggini, M.; Prato, M.; Carofiglio, T. *Chem. Commun.* **2013,** *49,* 8525–8527. doi:10.1039/c3cc44852e
29. Uekama, K.; Hirayama, F.; Irie, T. *Chem. Rev.* **1998,** *98,* 2045–2076. doi:10.1021/cr970025p
30. Falvey, P.; Lim, C. W.; Darcy, R.; Revermann, T.; Karst, U.; Giesbers, M.; Marcelis, A. T. M.; Lazar, A.; Coleman, A. W.; Reinhoudt, D. N.; Ravoo, B. J. *Chem. – Eur. J.* **2005,** *11,* 1171–1180. doi:10.1002/chem.200400905
31. Chen, Y.; Liu, Y. *Chem. Soc. Rev.* **2010,** *39,* 495–505. doi:10.1039/B816354P
32. Voskuhl, J.; Stuart, M. C. A.; Ravoo, B. J. *Chem. – Eur. J.* **2010,** *16,* 2790–2796. doi:10.1002/chem.200902423
33. Kauscher, U.; Ravoo, B. J. *Beilstein J. Org. Chem.* **2012,** *8,* 1543–1551. doi:10.3762/bjoc.8.175
34. Versluis, F.; Tomatsu, I.; Kehr, S.; Fregonese, C.; Tepper, A. W. J. W.; Stuart, M. C. A.; Ravoo, B. J.; Koning, R. I.; Kros, A. *J. Am. Chem. Soc.* **2009,** *131,* 13186–13187. doi:10.1021/ja9026264
35. Nalluri, S. K. M.; Voskuhl, J.; Bultema, J. B.; Boekema, E. J.; Ravoo, B. J. *Angew. Chem., Int. Ed.* **2011,** *50,* 9747–9751. doi:10.1002/anie.201103707
36. Kauscher, U.; Stuart, M. C. A.; Drücker, P.; Galla, H.-J.; Ravoo, B. J. *Langmuir* **2013,** *29,* 7377–7383. doi:10.1021/la3045434
37. Voskuhl, J.; Kauscher, U.; Gruener, M.; Frisch, H.; Wibbeling, B.; Strassert, C. A.; Ravoo, B. J. *Soft Matter* **2013,** *9,* 2453–2457. doi:10.1039/c2sm27353e
38. Galstyan, A.; Kauscher, U.; Block, D.; Ravoo, B. J.; Strassert, C. A. *ACS Appl. Mater. Interfaces* **2016,** *8,* 12631–12637. doi:10.1021/acsami.6b02132
39. Li, Q.; Batchelor-McAuley, C.; Lawrence, N. S.; Hartshorne, R. S.; Compton, R. G. *J. Electroanal. Chem.* **2013,** *688,* 328–335. doi:10.1016/j.jelechem.2012.07.039

License and Terms

BEILSTEIN JOURNAL OF ORGANIC CHEMISTRY

Interactions between cyclodextrins and cellular components: Towards greener medical applications?

Loïc Leclercq

Review

Open Access

Address:
Univ. Lille, CNRS, ENSCL, UMR 8181 – UCCS - Equipe CÏSCO, F-59000 Lille, France

Email:
Loïc Leclercq - loic.leclercq@univ-lille1.fr

Keywords:
cellular interactions; cyclodextrins; endogenous substances; extraction; greener active ingredients; host–guest chemistry; lipids

Beilstein J. Org. Chem. **2016,** *12,* 2644–2662.
doi:10.3762/bjoc.12.261

Received: 12 September 2016
Accepted: 25 November 2016
Published: 07 December 2016

This article is part of the Thematic Series "Superstructures with cyclodextrins: Chemistry and applications IV".

Guest Editor: G. Wenz

Abstract

In the field of host–guest chemistry, some of the most widely used hosts are probably cyclodextrins (CDs). As CDs are able to increase the water solubility of numerous drugs by inclusion into their hydrophobic cavity, they have been widespread used to develop numerous pharmaceutical formulations. Nevertheless, CDs are also able to interact with endogenous substances that originate from an organism, tissue or cell. These interactions can be useful for a vast array of topics including cholesterol manipulation, treatment of Alzheimer's disease, control of pathogens, etc. In addition, the use of natural CDs offers the great advantage of avoiding or reducing the use of common petroleum-sourced drugs. In this paper, the general features and applications of CDs have been reviewed as well as their interactions with isolated biomolecules leading to the formation of inclusion or exclusion complexes. Finally, some potential medical applications are highlighted throughout several examples.

Introduction

Cyclodextrins (CDs) were discovered and identified over a century ago [1-3]. Between 1911 and 1935, Pringsheim and co-workers demonstrated the ability of CDs to form complexes with many organic molecules [4,5]. Since the 1970s, the structural elucidation of the three natural CDs, α-, β-, and γ-CDs composed of 6-, 7-, and 8-membered α-D-glucopyranoses linked by α-1,4 glycosidic bonds, allowed the development and the rational study of their encapsulation properties [6,7]. As their water solubility differs significantly, a great variety of modified CDs has been developed to improve the stability and the solubility of inclusion complexes [8-10]. Nowadays, CDs are widely applied in many fields [11-28] due to their host–guest properties, their origins (produced from starch by enzymatic conversion), their relatively low prices, their easy modifications, their biodegradability and their low toxicity. Moreover, CDs are able to interact with a wide range of biomol-

ecules opening the way for many biological applications. The majority of these researches are based on the ability of CDs to extract lipids from the cell membrane. The objective of this contribution is to focus on the potential use of natural and chemically modified CDs in the vast array of medical and biological applications.

Review

Cyclodextrins: synthesis, structure and physicochemical properties.

i) Native cyclodextrins

As mentioned earlier, the ordinary starch hydrolysis (e.g., corn starch) by an enzyme (i.e., cyclodextrin glycosyl transferase, CGTase) allows the production of the native CDs [13]. To reduce the separation and the purification costs, selective α-, β- and γ-CGTases have been developed in the last two decades [29]. Nevertheless, the cheapest remains the β-CD whereas the most expensive is the γ-CD. The molecular shape of the native CDs can be represented as a truncated cone with "hydrophobic" cavity which can accommodate hydrophobic compounds (Scheme 1). In aqueous solution, the complexation is enthalpically and entropically driven. In addition, complementary interactions (e.g., van der Waals forces, H-bonds, etc.) appear between the CD and the guest. The non-polar suitably-sized guest may be bound in numerous molar ratios (e.g., 1:1, 2:1, 1:2, etc.). In all cases, the knowledge of the binding constants (K_{ass}) is crucial because these values provide an index of host–guest binding forces. CDs can also form exclusion complexes where the CDs are bound to the guest through a H-bond network. For instance, the complexation of $[PMo_{12}O_{40}]$ anion by β- and γ-CD results in a one-dimensional columnar structure through a combination of intermolecular [C−H···O=Mo] and [O−H···O] interactions [30]. Unfortunately, the natural CDs as well as their inclusion complexes are of limited aqueous solubility leading to their precipitation. Fortunately, native CDs are effective templates for the generation of a wide range of molecular hosts through chemical modifications.

ii) Modified cyclodextrins

In order to meet specific requirements in the host–guest complex, chemical modifications make it possible to tailor CDs to a particular guest. The hydroxy groups serve as scaffolds on which substituents can easily be introduced. From a chemical synthesis point of view, the reactivity difference between the primary and secondary hydroxy groups allows selective functionalization on the narrow or the wider edge of the truncated cone (Table 1). Access to the gamut of functional groups greatly expands the utility of native and modified CDs in their numerous applications.

iii) Applications of cyclodextrins

As natural CDs and their derivatives are able to encapsulate a wide range of guest molecules into their cavity, they can be used in a wide range of applications including analytical chemistry [21,22,31], agriculture [15], food technology [16], catalysis [23-25,32], cosmetics [26], textile processing [28,33], and environmental protection technologies [27,34]. Nevertheless, the first global consumer of CDs is clearly the pharmaceutical industry [35,36]. Indeed, CDs are very useful to form inclusion complexes with a wide range of drugs and become a very valuable tool for the formulator in order to overcome delivery limitations [37,38]. As a result, numerous formulations that use CDs are now on the market worldwide (Table 2).

iv) Toxicity and biological effects of native and modified cyclodextrins

As safety and toxicity are important criteria for consideration before using CDs in pharmaceutical products, this section deals with toxicological issues. The native α- and β-CD, unlike γ-CD, cannot be hydrolyzed by pancreatic amylases and human salivary but can be fermented by the intestinal microflora. When administered orally, native CDs and hydrophilic derivatives are not absorbed from the human gastrointestinal tract and thus making them practically nontoxic due to their high molecular mass ranging from almost 1 000 to over 2 000 g/mol and their

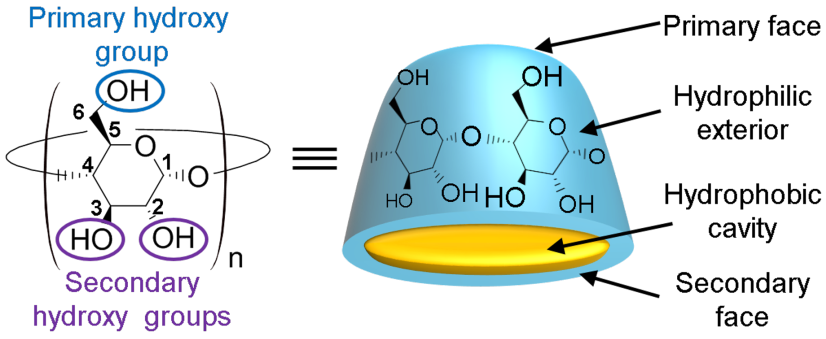

Scheme 1: Structure and conventional representation of native CDs.

Table 1: Structures, acronyms and characteristics of some modified cyclodextrins.[a]

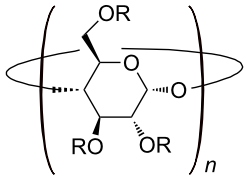

Abbreviation	Substituents (R)	Characteristics
ME	–H or $–CH_3$	soluble in cold water and organic solvents, hemolytic
HP	–H or $–CH_2CH(OH)CH_3$	highly water-soluble, low toxicity
S	–H or $-SO_3Na$	pK_a > 1, water soluble
SBE	–H or $–(CH_2)_4SO_3H$	water soluble
G1	–H or –glucosyl	highly water soluble
G2	–H or –maltosyl	low toxicity

[a]ME: methyl; HP: 2-hydroxypropyl; S: sulfate; SBE: sulfobutyl ether; G1 glucosyl; G2: maltosyl.

Table 2: Some marketed pharmaceutical formulations with CD.[a]

CD	Drug	Formulation	Trade name	Market
α-CD	Alprostadil	IV solution	Rigidur	Europe, USA
α-CD	Cefotiam hexetil	Oral tablet	Pansporin T	Japan
β-CD	Iodine	Topical solution	Mena-Gargle	Japan
β-CD	Nicotine	Sublingual tablet	Nicorette	Europe
β-CD	Piroxicam	Oral tablet	Flogene	Brazil, Europe
HP-β-CD	Hydrocortisone	Topical cream	Dexocort	Europe
HP-β-CD	Itraconazole	IV solution	Sporanox	Europe, USA
HP-β-CD	Mitomycin	IV solution	Mitozytrex	USA
ME-β-CD	Chloramphenicol	ED solution	Clorocil	Europe
SBE-β-CD	Voriconazole	IV solution	Vfend	Europe, USA
SBE-β-CD	Ziprasidone	IM solution	Zeldox	Canada, USA
γ-CD	Minoxidil	Topical solution	Alopexy	Europe
HP-γ-CD	Diclofenac	ED solution	Voltarenopthta	Europe

[a]Note that the list is not exhaustive and that only one trade name is given (IV: intravenous, IM: intramuscular, ED: eye drop). Adapted from [37].

hydrophilic nature with a significant number of H-bond donors and acceptors [39]. Indeed, CDs violate three criteria of the Lipinski's rule: i) no more than 5 H-bond donors, ii) no more than 10 H-bond acceptors, iii) a molecular mass less than 500 g/mol, and iv) an octanol–water partition coefficient (log *P*) not greater than 5 [40]. As these criteria apply only to absorption by passive diffusion of compounds through cell membranes, the absorption of the native CDs and their hydrophilic derivatives are not allowed in their intact form and any cellular absorption, if it occurs, is by passive transport through cytoplasmic membranes (i.e., by transporter proteins) [41]. In contrast, lipophilic derivatives (e.g., ME-β-CD) interact more readily with membranes than the hydrophilic derivatives, they cannot readily permeate cell membranes (see below) [42]. Moreover, oral administration of alkylated CD derivatives, such as ME-β-CD, is limited by its potential toxicity [43]. Indeed, ME-β-CD is partially absorbed from the gastrointestinal tract into the systemic circulation. Moreover, they have been shown to be toxic after parenteral administration. The opposite holds for hydrophilic CD derivatives, such as HP-β-CD and SBE-β-CD, which are considered safe for parenteral administration. In a general way, the γ-CD, HP-β-CD and SBE-β-CD, S-β-CD and G2-β-CD appear to be globally safer than α-, β- and alkylated CDs which are less suitable for parental administration [44,45]. Table 3 presents the pharmacokinetics and safety overview of some natural and modified CDs. When administered, natural and hydrophilic CD derivatives disappear rapidly from systemic circulation and are distributed to various tissues of the body such as kidney, liver, urinary bladder, etc. Nevertheless, they are mainly renally excreted intact. At high concentrations, α-, β-

Table 3: Pharmacokinetics and safety overview of some native and modified CDs for rats.[a]

CD	Fraction excreted unchanged in urine	Oral adsorption	LD_{50} oral (g/kg)	LD_{50} IV (g/kg)
α-CD	≈90%	2–3%	>10	0.5–0.75
β-CD	≈90%	1–2%	>5	0.45–0.79
γ-CD	≈90%	<0.02%	>>8	4
HP-β-CD	≈90%	≤3%	>2	10
G_2-β-CD	–	–	>5	–
ME-β-CD	>95%	0.5–12%	>8	1.5–2.1
SBE-β-CD	–	–	>10	>15

[a]Taken from [44,47-53]. [b] Randomly methylated β-CD.

and alkylated CDs present renal damage and dysfunction [46]. In 2008, Stella and He discussed the detailed studies of toxicology, mutagenicity, teratogenicity and carcinogenicity of various CDs [45]. Overt signs of acute toxicity are not apparent for CDs (i.e., no inflammatory response and no cell degeneration). They are also not genotoxic, not teratogenic or mutagenic. However, CDs affect the human organism only at extremely high concentrations. Nevertheless, the principal side effect of natural and modified CDs is probably the cell toxicity. This effect is directly correlated to their hemolytic activities. Indeed, several in vitro studies reported erythrocyte lysis although the toxicological implication in vivo is negligible. The lysis mechanism is related to their capacity to draw phospholipids and cholesterol out of the biological membrane (see below). Based on this, the complexation of endogenous substances are of potential interest for many applications.

Biomolecule/cyclodextrin inclusions complexes

Native and modified CDs can be used to complex certain chemicals produced naturally present in cells and tissues (i.e., endogenous substances). Indeed, CDs are able to form complexes with various biomolecules including lipids, carbohydrates, proteins and nucleic acids. In this section, some biomolecule/CD inclusion complexes are presented.

i) Complexation of lipids and consequences

Lipids are hydrophobic or amphiphilic molecules very diverse, including, among other fats, waxes, sterols, fat-soluble vitamins, phospholipids, mono-, di- and triglycerides, etc. Their amphiphilic nature causes the molecules of certain lipids to organize into liposomes when they are in aqueous medium. This property allows the formation of biological membranes. Indeed, cells and organelles membranes are composed of lipids. Lipids also provide various other biological functions, including cell signaling and storage of metabolic energy by lipogenesis. Biological lipids are basically due to two types of compounds acting as “building blocks”: ketoacyl groups and isoprene units. From this point of view, they can be divided into eight categories: fatty acids (and their derivatives: mono-, di- and triglycerides and phospholipids), acylglycerols, phosphoglycerides, sphingolipids, glycolipids and polyketides, which result from the condensation of ketoacyl groups, sterols (e.g., cholesterol) and prenols, which are produced from condensation of isoprene units [54]. These compounds can be easily included inside the CDs because they are hydrophobic or amphiphilic molecules. As mentioned earlier, and as it will become exceeding clear throughout the following sections, the majority of research involving CDs has revolved around their ability to manipulate lipid (phospholipids and cholesterol) composition in different cells [55-58]. Although numerous studies deal of this topic, the mechanism of this process is poorly investigated (i.e., only the consequences of this phenomenon are reported). For sake of clarity, only some typical examples are reported in this section.

The first well-documented effect of CDs is probably hemolysis which corresponds to the lysis of red blood cells (erythrocytes) and the release of their contents into surrounding fluid (blood plasma). In 1982, Irie and co-workers reported that native CDs are able to cause hemolysis of human erythrocytes [59]. This behavior occurs at relatively high concentrations (>1 mM) and that the degree of cholesterol extraction is a function of the CD used, its concentration, incubation time, temperature. For instance, in given conditions (isotonic solution with similar incubation time and temperature), the observed hemolysis is in the order γ-CD < α-CD < β-CD.

This different effect, observed for native CDs, has been explained by Ohtani et al. in 1989 [58]. As the membrane of erythrocytes is composed of proteins (43%) associated with lipids (49%) and carbohydrates (8%) and as the fraction of cholesterol is 25% of total membrane lipids [54], the proposed

explanation is based on the specific interaction of natural CDs with the erythrocyte membrane components. Indeed, α- and β-CD are excellently suited to solubilize phospholipids and cholesterol, respectively, whereas γ-CD is generally less lipid-selective. In more detail, the CD affinity for solubilizing various lipid components of the erythrocyte membranes are in the order γ-CD << β-CD < α-CD for phospholipids and α-CD < γ-CD << β-CD for cholesterol [58]. These findings are corroborated by the work of Leventis and Silvius which have reported that β- and γ-CD accelerate the rate of cholesterol transfer by a larger factor than they accelerate the transfer of phospholipid, whereas the opposite is true for α-CD [60]. The hemolytic properties of CDs are a general behavior not limited to human erythrocytes: All mammalian red blood cells are affected by the parent CDs. For instance, dog erythrocytes are also affected by native CDs in the order γ-CD < α-CD < β-CD [61]. Thus, the magnitude of the hemolytic activity observed for dog erythrocytes is consistent with the order of magnitude of human erythrocytes (see discussion above). However, the hemolytic activity is largely influenced by the substituents attached to the CDs. The presence of hydrophilic substituents (e.g., glucosyl, 2-hydroxypropyl, 3-hydroxypropyl, maltosyl, sulfate, sulfobutyl ether, etc.) reduces the hemolytic activity in comparison with the parent CDs while the lipophilic ones (e.g., methylated CDs) demonstrate the strongest hemolytic activities [62]. As for parent CDs, these differences are ascribed to the different solubilization effects of lipid components and their sequestration in the external aqueous phase.

As the hemolysis is attributed to the removal of erythrocyte membrane components, particularly phospholipids and cholesterol, the value of the binding constants between CDs and lipids can be very relevant. To the author's knowledge there is only one paper in the literature that describes the binding constants between CDs (α- or γ-CD) and short phospholipids (i.e., diheptanoylphosphatidylcholine, DHPC) [63]. In this study, the association constants were estimated from ^{1}H NMR measurements. The results proved that the K_1 values are in the order α-CD < γ-CD while the K_2 values are in the order γ-CD < α-CD. This behavior was attributed to the large cavity of γ-CD which is able to incorporate both alkyl chains of DHPC simultaneously. In contrast, the formation of a 1:2 inclusion complex with α-CD is easier than with γ-CD. These findings are corroborated by Fauvelle and co-workers who reported that α-CD has the strongest affinity to phospholipids (e.g., phosphatidylinositol) [64,65]. In 2000, Nishijo et al. studied the interactions of various CDs with dipalmitoyl, distearoyl, and dimyristoylphosphatidylcholine liposomes. This study highlights that the liposome-CD interaction depends on the length of the fatty acid chain of the phospholipid, the cavity size, and the nature of the substituents at the CD [66]. In the literature, the binding constant between cholesterol and β-CD was estimated around 1.7×10^4 M^{-1} from a solubility method [67,68]. This value proves the good stability of the inclusion complex because of the driving force of complexation: hydrophobic interaction. Despite there is no information on the binding constant observed for the inclusion of cholesterol in γ-CD, the cavity internal diameter of the β-CD and its derivatives perfectly matches the size of the sterol molecules contrary to γ-CD (too large) [69,70]. Moreover, the positive correlation observed between the hemolytic activities of various modified CDs and their ability to solubilize cholesterol reveal that HP-β-CD was shown to be a more efficient cholesterol-acceptor molecule than HP-γ-CD. This is apparently due to the diameter of its internal cavity that matches the size of this molecule. Finally, it is noteworthy that all CDs lose their abilities to induce hemolysis, when their cavities are occupied with guest molecules due to a reduced interaction with the erythrocyte membranes [71]. All these observations support the aforementioned affinities of α-CD for phospholipids and of β-CD for cholesterol.

In addition, sub-hemolytic concentrations of native CDs are also demonstrated to cause shape changes in human erythrocytes. The hemolytic effect is concomitant with shape changes (from biconcave discocyte to stomatocyte or echinocyte) depending on the cavity size of the CDs. For instance, α- and γ-CD induce progressive shape changes from discocytes into stomatocytes and from stomatocytes into spherocytes [58]. In contrast, β-CD leads only to swelling of erythrocytes. Similar effects are found for chemically modified CDs. For instance, Motoyama et al. have reported morphological changes in erythrocytes induced by methylated CDs such as 2,6-di-*O*-methyl-α-CD and 2,6-di-*O*-methyl-β-CD (DM-α-CD and DM-β-CD) [72,73]. The authors reported that DM-α-CD induces morphological changes in rabbit erythrocytes leading to stomatocytes, while DM-β-CD leads to echinocytes. This difference is ascribed to the cavity size of the CDs and their ability to extract either sphingomyelin and/or cholesterol of lipid rafts. Lipid rafts are constituted of cholesterol, glycolipids, and sphingomyelin. Nevertheless, their structures have heterogeneity with the presence of cholesterol-rich and sphingomyelin-rich domains. Consequently, DM-α-CD extract sphingomyelin form sphingomyelin-rich domains while DM-β-CD extract cholesterol from cholesterol-rich lipid rafts (Scheme 2). This assertion is supported by the work of Nishijo et al. which reported the binding constants of the 1:1 and 1:2 (cholesterol:DM-β-CD) complexes (1.09×10^2 M^{-1} and 5.68×10^4 M^{-1}, respectively, at 25 °C) [74]. Finally, it is noteworthy that the presence of DM-α-CD and DM-β-CD also leads to hemolysis. As cholesterol interacts with markedly higher affinity with sphingolipids (e.g., sphingomyelin) than with

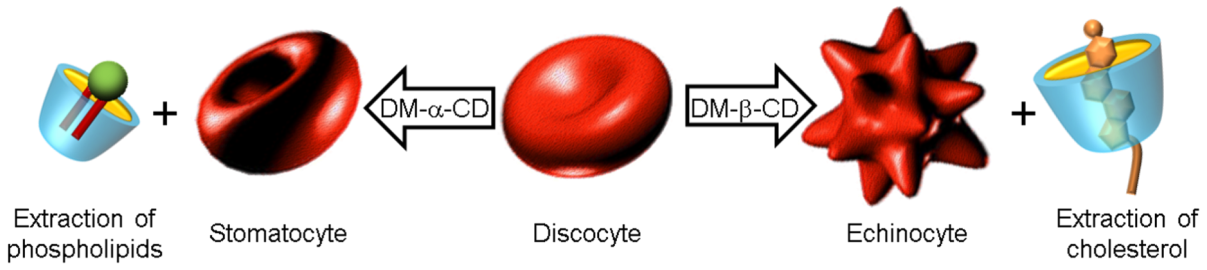

Scheme 2: Proposed mechanism for morphological changes in erythrocytes induced by methylated CDs.

common membrane phospholipids, the extraction of cholesterol by DM-β-CD or sphingomyelin by DM-α-CD leads to strong modification of the cholesterol-rich or sphingomyelin-rich lipid rafts, respectively [60]. Therefore, even if the target is significantly different, the final effect is the same (i.e., hemolysis).

It should be noted that this cholesterol and/or phospholipids extraction is not limited to erythrocytes. Indeed, all eukaryotic or prokaryotic cells are affected by the presence of CDs. For instance, the cytotoxicity of native, methylated, and hydroxypropylated α-, β-, and γ-CDs have been studied on an in vitro model of blood-brain barrier by Monnaert and co-workers [75]. The results prove that the native CDs are the most toxic (γ-CD < β-CD < α-CD). As expected, lipid effluxes on the brain capillary endothelial cells in the presence of native CDs reveal that α-CD extracts only phospholipids whereas β-CD is able to remove phospholipids and cholesterol. In contrast, γ-CD is less lipid-selective than the other native CDs. This differential effect compared to the order of magnitude of hemolytic activity (γ-CD < α-CD < β-CD) could be ascribed to the lower cholesterol content in blood–brain barrier cells compared to erythrocytes. Indeed, the cholesterol fraction is markedly higher in erythrocytes than in other cells. As for hemolysis, the presence of hydrophilic substituents (e.g., 2-hydroxypropyl and sulfobutyl ether) annihilates the cytotoxicity while the presence of methyl residues induces cell death of various cells (Caco-2, TR146, PC-12, etc.) [76-78]. For instance, cell death induced by DM-β-CD is caused by a marked apoptosis mechanism (i.e., a process by which cells trigger their self-destruction in response to a signal which leads to cell changes prior to death) for NR8383, A549 and Jurkat cells [79]. This apoptosis process results from cholesterol extraction leading to inhibition of the activation of PI3K-Akt-Bad pathway. The presence of DM-α-CD had repercussions that were totally opposite to the DM-β-CD. Indeed, the cell death results from a non-apoptotic mechanism (i.e., necrosis). This differential effect could be attributed to a dissimilarity of interaction between the methylated CDs with the cholesterol-rich lipid rafts and with the sphingomyelin-rich domains for DM-β-CD and DM-α-CD, respectively. These results suggest that lipid rafts of cell membranes would be involved in cell death and cellular function.

However, the mechanism of cholesterol extraction mediated by CDs is still open to discussion. For instance, Yancey et al. proposed that CDs diffuse into the proximity of the erythrocyte membrane leading to lipid complexation without complete desorption in the aqueous phase [80]. In contrast, Besenicar et al. proposed that CDs complex lipids during their naturally exchange from the membrane to the aqueous phase [81]. Stella and He supposed that the CDs interact directly with the membrane of the cells prior to lipid efflux [45]. In the same idea, Mascetti et al. proposed that CDs interact directly with cholesterol [82]. Based on molecular simulations, López et al. proposed the following mechanism: i) association of CDs in aqueous solution to form dimers, ii) binding of dimers at the membrane surface, iii) extraction and complexation of cholesterol, and iv) desorption of CD/cholesterol in the aqueous solution [83]. However, whatever the molecular mechanism, the lipid efflux mediated by CDs is clearly different from those of surfactants. Indeed, at low concentrations, the mechanism involves the penetration of the detergent molecules into the lipid membrane leading to increase its fluidity. In contrast, at higher concentrations, the extraction of membrane constituents is ensured by micellar solubilization [84,85].

ii) Complexation of peptides and proteins and some applications

Proteins are polymers of amino acids covalently linked through peptide bonds. The nature of the proteins is determined primarily by their amino acid sequence, which constitutes their primary structure. Amino acids have very different chemical properties; their arrangement along the polypeptide chain determines their spatial arrangement. This is described locally by their secondary and tertiary structures. The secondary structure describes the arrangement of amino acid residues observed at the atomic scale stabilized mainly by H-bonds (e.g., α-helix,

β-sheet and turns). The tertiary structure corresponds to the general shape of the observable protein across the whole molecule. It describes the interactions between the different elements of the secondary structure. Finally, the assembly of several protein subunits to form a functional complex is described by the quaternary structure [54]. As some amino acids have hydrophobic side chains (e.g., alanine, valine, leucine, isoleucine, proline, phenylalanine, tryptophan, cysteine and methionine), they can be easily included inside the CDs. This complexation leads to modification of the protein. For sake of clarity, only some typical examples are reported in this section.

In their paper on the differential effects of natives CDs, Ohtani and co-workers highlighted that, in addition to the extraction of lipids, these CDs are also able to solubilize proteins in the order α-CD < γ-CD << β-CD [58]. In 1991, Sharma and Janis studied the interaction of CDs with hydrophobic proteins leading to the formation of soluble and insoluble complexes [86]. CDs caused the precipitation of lipoproteins in the order γ-CD < α-CD < β-CD. This behavior could be ascribed to the formation of inclusion complexes. However, the presented data did not exclude the formation of exclusion complexes.

Several years later, Horský and Pitha reported a study on the interaction of CDs with peptides containing aromatic amino acids [87]. From competitive spectrophotometry measurements, with *p*-nitrophenol as a competing reagent at pH 7.4, the authors determined the stability constants of aromatic amino acids and their oligopeptides with α-, β-, HP-β-, and ME-β-CD. The estimated constants of free L-phenylalanine (Phe) increased in the order ME-β-CD ≈ HP-β-CD < α-CD < β-CD. Moreover, the results proved that the stability of oligopeptides containing Phe is higher than that of Phe itself. For instance, the binding constant of free Phe with β-CD was estimated at 17 M^{-1} whereas with the Gly-Gly-Phe tripeptide, the binding constant was 89 M^{-1}. Nevertheless, the complexation occurs when the native functional form of the proteins is unfolded.

In 1996, Bekos et al. investigated the role of the L-tyrosine (Tyr) residue in the binding of pentapeptides to α- and β-CD [88]. The two peptides used in this study were: Tyr-Ile-Gly-Ser-Arg (YIGSR) and Tyr-Gly-Gly-Phe-Leu (YGGFL). The former interacts specifically with the integrin receptors on specific neuronal cells whereas the latter is known to bind to brain receptor sites. From steady-state fluorescence spectroscopy, the estimated constants of free Tyr increased in the order α-CD < β-CD. As in the previous study, the stability constants of pentapeptides containing Tyr with β-CD were higher than that of Tyr itself (48, 224, and 123 M^{-1} for free Try, YIGSR, and YGGFL, respectively). Therefore, the pentapeptide conformation affects the stability of the pentapeptide/β-CD inclusion complex. In contrast, the pentapeptide/α-CD inclusion complex was not affected by the oligopeptide conformation (27, 20, and 20 M^{-1} for free Try, YIGSR, and YGGFL, respectively).

The same year, Lovatt and co-workers investigated the dissociation of bovine insulin oligomers induced by aqueous solution of α-, HP-β-, and ME-β-CD [89]. The energetics of the dissociation of insulin oligomers have been investigated by microcalorimetry. As expected, the dissociation of insulin oligomers is increased upon the addition of CDs. This dissociation is clearly related to the interaction of these CDs with the protein side chains. Indeed, the dissociation of insulin oligomers is endothermic without CDs whereas in the presence of α-CD, the dissociation is less endothermic due to the exothermic binding of α-CD to exposed groups on insulin monomers after dissociation. Therefore, the α-CD facilitates the oligomer dissociation. In contrast, the dissociation is observed to be more endothermic in the presence of HP-β- and ME-β-CD although oligomer dissociation is induced. The authors suggest that the binding of HP-β- and ME-β-CD is endothermic and entropy driven.

As native and modified CDs are able to complex some amino acids which constitute peptides and proteins, these molecules can be useful for their separation by capillary zone electrophoresis. In this context, Rathore and Horváth reported that carboxymethyl-β-CD (CM-β-CD) in the electrophoretic medium (aqueous buffer solution, pH 2.5) enhanced the separation in capillary zone electrophoresis (raw fused-silica) of standard proteins such as α-chymotrypsinogen A, cytochrome *c*, lysozyme and ribonuclease A [90]. The obtained results proved that the separation of peptides and proteins can be enhanced by adding CDs to the electrophoretic medium. Unfortunately, only certain CDs can be used as selectivity enhancers. Indeed, in contrast to CM-β-CD, the addition of DM-β-CD had no effect on the separation of the mentioned proteins and peptides.

In 2006, the group of Yamamoto studied the effect of β-, γ-, G1-β-, and Me-α-CD on the thermal stability of an aqueous buffered solution of chicken egg white lysozyme by circular dichroism and fluorescence spectroscopy [91]. The thermal stability is significantly lowered in the presence of β-, γ-, and G1-β-CD whereas the opposite is true for the Me-α-CD. It should be noted that the thermal stability reduction is very important for G1-β-CD. Based on fluorescence spectroscopy, the authors suggested that CDs include the side chains of tryptophan (Trp) residues of lysozyme within their internal cavities to diminish the hydrophobicity of the hydrophobic core of lysozyme and consequently to lower the thermal stability (Scheme 3). In addition, some CD molecules persist in binding to the side chains of Trp residues to retard the renaturation of lysozyme.

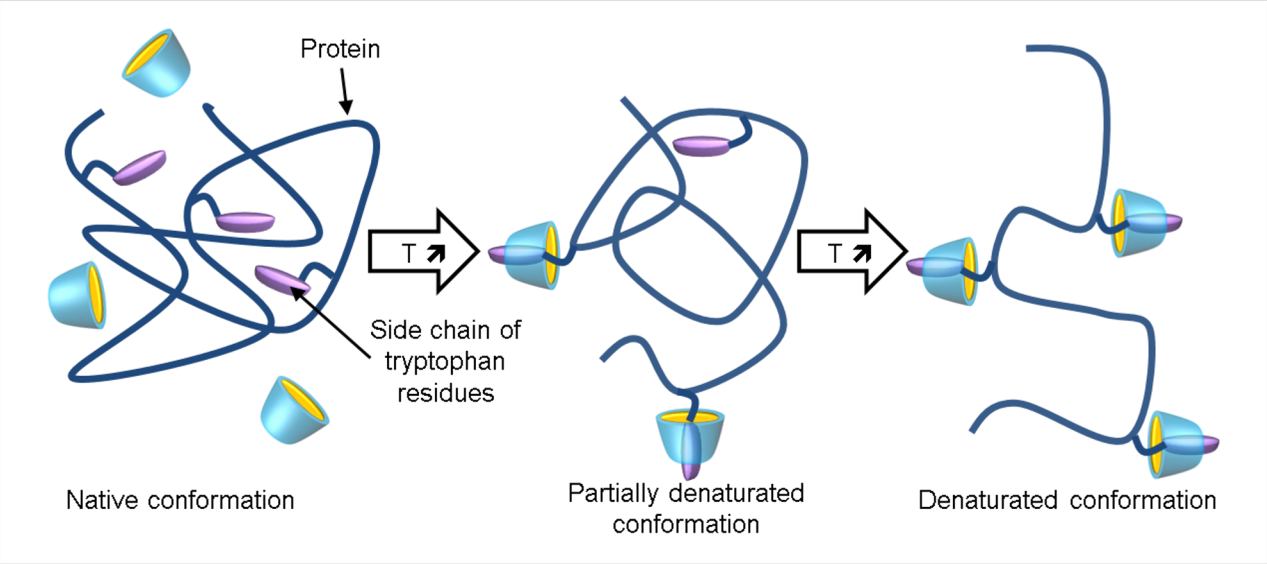

Scheme 3: Proposed mechanism for the conformational change of egg white lysozyme with temperature elevating in the presence of modified CDs.

From the findings described above, it can be presumed that the effect of CD is directly linked to its ability to complex Trp and the behavior of Me-α-CD can be related to its cavity size. The binding constants are always weaker with modified α-CD than with functionalized β-CD (see discussion above). In 2009, a ^{1}H NMR spectroscopic study revealed that the ^{1}H NMR signals corresponding to Trp residues were shifted upon the addition of G1-β-CD due to encapsulation of the tryptophan residues in the G1-β-CD cavity [92]. In addition, the ^{1}H NMR signals for cysteine 64 and isoleucine 98 were also influenced to a considerable extent with the addition of G1-β-CD. This allows the conclusion that these hydrophobic amino acid residues are also included by this CD. These results are highly compatible with the very important thermal stability reduction observed in the presence of G1-β-CD. Therefore, the interaction of CDs with proteins is very complicated due to the presence of many binding sites.

Thaumatins refer to a family of proteins present in the sweetness of the katemfe fruit (*Thaumatococcus daniellii* Bennett) endemic in West Africa. It is used worldwide in human nutrition and pharmacology as a sweetener, flavor enhancer or to mask bitterness and it is 100,000 times sweeter than sucrose. Thaumatin has been shown to bind to G-protein-coupled receptors (GPCRs) which are transmembrane proteins, responsible for signal transduction. Therefore, the interaction of CDs with thaumatin could be used to modify the interaction of thaumatin with GPCRs and to modify its sweet-taste profile. In this context, Thordarson et al. studied the interaction of α-CD with thaumatin [93]. The 1D and 2D NMR experiments revealed that α-CD binds to aromatic residues of thaumatin with a binding constant of 8.5 M^{-1}. As the active binding site of the thaumatin protein is known, the authors have synthesized a heptapeptide (Lys-Thr-Gly-Asp-Arg-Gly-Phe) that mimics this binding site of thaumatin. The results show that α-CD binds to the C-terminal solvent accessible phenylalanine residue with a binding constant of 8.8 M^{-1}. As the α-CD may interact with the active binding site on thaumatin, the regulation of the interaction of thaumatin with GPCRs is probably possible.

Varca et al. published on the possible applications in the formulations of protein-like structures, such as enzymes, peptides and amino acids, for pharmaceutical applications [94]. The authors highlight that the formation of cyclodextrin/protein supramolecular complexes can be used to improve their stabilizations. However, the intrinsic characteristics of guest proteins can be also modified. In addition, it is exceedingly clear throughout this paragraph that peptides and proteins have moderate binding constants with CDs compared to lipids.

iii) Complexation of carbohydrates

The International Union of Pure and Applied Chemistry (IUPAC) defines carbohydrates as a class of organic compounds containing a carbonyl group (aldehyde or ketone) and at least two hydroxy residues (OH). It is noteworthy that substances derived from monosaccharides by reduction of the carbonyl group, by oxidation of at least one functional group at the end of the chain in carboxylic acid, by replacement of one or more hydroxy groups by a hydrogen atom, an amine, a thiol or any similar group are also called carbohydrates. Carbohydrates are, with proteins and lipids, essential constituents of living organisms because they are key biological intermediates for energy storage. In autotrophs, such as plants, sugars are converted into starch whereas for heterotrophic organisms, such as

animals, they are stored as glycogen. However, polysaccharides serve also as structural components: cellulose for plants and chitin for arthropods. Moreover, saccharides and their derivatives play key roles in the immune system, fertilization, blood clotting, information transfer, etc. For instance, the 5-carbon monosaccharide ribose forms the backbone of the genetic molecule RNA (see below) and is also an important component of coenzymes (ATP, FAD and NAD).

In 1992, Aoyama et al. reported on the selective complexation of pentoses and hexoses by β-CD [95]. Based on competitive inhibition of the 8-anilinonaphthalene-1-sulfonate binding followed by fluorescence measurements, the binding constants can be estimated. The obtained results reveal that D-ribose, D- and L-arabinose, D-xylose, D-lyxose, D-2-deoxyribose, and methyl β-D-ribopyranoside were complexed by β-CD (binding constants ≤14 M^{-1}). In contrast, aldohexoses and their derivatives (D-glucose, D-galactose, D-mannose, D- and L-fucose, and methyl α-D-fucopyranoside) were not complexed (binding constants ≈ "0" M^{-1}). These binding constants can be directly correlated to the hydrophobicity of the sugar. Nevertheless, the H-bonds between the hydroxy groups of bound sugar and the OH groups of β-CD are also extremely important for determining the structure and for the selectivity of the complex.

It is noteworthy that several other publications have studied the interaction of D-glucose with native CDs. For instance, Hirsh and co-workers estimated the binding constants of D-glucose to α-CD and β-CD at 450 and 420 M^{-1}, respectively, from blood glucose meter [96]. In contrast, Hacket et al. determined the binding constant of D-glucose to β-CD at 0.6 M^{-1} by fluorimetric competition titrations [97]. The results obtained by Hacket et al. are closer to the values published by Aoyama and co-workers. In addition, it is quite logical that D-glucose interacts weakly with native CDs due to its size and its hydrophilic property. However, from these conflicting results, Turner proposed to use kinetic measurements to determine the association constants of several sugars with β-CD [98]. This new method has been published in 2000 [99] and the binding constants obtained by these three groups are reported in Table 4.

Table 4: Association constants for the sugar/β-CD complexes (*K*).

	Guest	*K* (M^{-1})		
Pentoses	D-arabinose	0.7[a]	1.5[b]	0.9[c]
	D-ribose	5.3[a]	6.3[b]	4.8[c]
	D-xylose	1.0[a]	1.6[b]	1.6[c]
Hexoses	D-galactose	"0"[a]	0.5[b]	0.3[c]
	D-glucose	"0"[a]	0.6[b]	0.4[c]
	D-mannose	"0"[a]	1.0[b]	0.7[c]

[a]Taken from [95]. [b]Taken from [97]. [c]Taken from [98].

These values are relatively close to each other and the sugar/β-CD binding constants increase in the order of D-galactose ≈ D-glucose < D-mannose < D-arabinose < D-xylose < D-ribose. This magnitude is consistent with the order of magnitude of the sugar hydrophobicity scale determined by Janado and Yano in 1985 (Scheme 4) [100]. This hydrophobicity scale is corroborated by Wei and Pohorille for the hexose series [101]. Therefore, even if all the literature values for the binding constants obtained by the different methods are not especially self-consistent, it is clear that β-CD can selectively recognize pentoses in contrast to hexoses [102]. However, the binding constants remain very small (see Table 4). Based on all these results, the interaction of CDs with carbohydrates in aqueous solution can be completely neglected. Similar conclusions were made by Paal and Szeijtli [103].

iv) Complexation of nucleic acids

Nucleic acids are macromolecules, where the monomer is the nucleotide. Each nucleotide has three components: a 5-carbon sugar, a phosphate group, and a nitrogenous base. These nucleotides are joined by phosphodiester bonds. There are two types of nucleic acids according to the sugar: deoxyribose and ribose for deoxyribonucleic acid, DNA, and ribonucleic acid, RNA. Nucleic acids function in encoding, transmitting and expressing genetic information. As nucleic acids allow the synthesis of proteins their modifications result in numerous consequences. As earlier mentioned, CDs are used for numerous

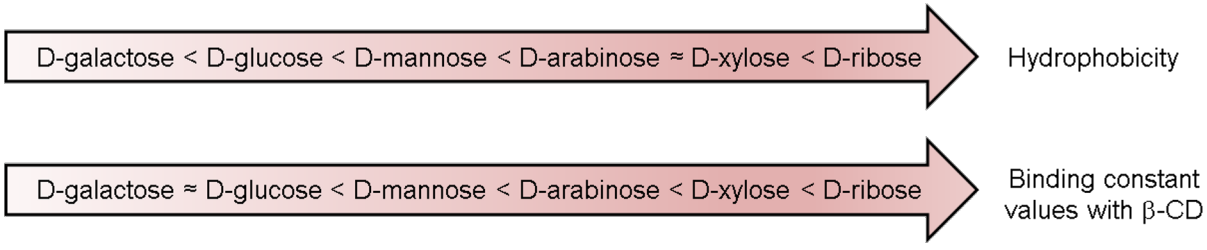

Scheme 4: Sugar hydrophobicity scale according to Janado and Yano and correlation with the binding constant values observed with β-CD.

commercial applications. Therefore, the investigation of nucleic acid interactions (e.g., DNA or RNA) with various types of CDs is important to evaluate possible intracellular effects of CDs.

The interactions between native CDs and nucleic acids are still a subject of intense discussion along the past years. For instance, the results found in the literature for the α-CD are contradictory. Indeed, the works of Komiyama [104], Tee [105], and Spies et al. [106] suggested that α-CD cannot interact with DNA because the cavity of this molecule is too small to accommodate DNA base pairs. All these results support the work of Hoffmann and Bock who examined the complex formation between different CDs and nucleotides [107]. In contrast, in a more recent work, Jaffer et al. have found that α-CD can form H-bonds with DNA base pairs that flip out spontaneously at room temperature leading to DNA denaturation [108]. Consequently, exclusion and inclusion complexes are achieved with α- and β-CD, respectively. Nevertheless, it is noteworthy that when a complex is formed with β-CD, the ribose and phosphate groups of the nucleotides exert also a stabilizing effect by establishing H-bonds with the outer rim of the CD molecules. Interestingly, the extent of complexation depends significantly on the base composition and the double- or triple-helical structures. In contrast to native CDs, cationic CDs are known to interact strongly with DNA [109,110]. As consequence, CDs can be used to complex DNA and to encapsulate it into liposomes for potential gene therapy applications [111]. However, other formulation can be used to obtain non-viral vectors [112].

Since anthrylamines have potent DNA-intercalating properties, Ikeda et al. have attached an anthrylamine to a β-CD [113]. The obtained anthryl(alkylamino)-β-CD was used as chemically switched DNA intercalator. However, as the anthryl residue is locked in the CD cavity, its intercalation into DNA is not possible in aqueous solution. Upon addition of a ligand that is tightly bound in the CD cavity (e.g., 1-adamantanol), the host molecule releases the anthryl unit, which then leads to strong intercalation with the double-stranded DNA molecule leading to structural distortions (Scheme 5). This behavior was clearly established from ^{1}H NMR spectroscopy (shifts and broadening of anthryl signals) in the presence of the 1-adamantanol guest. This concept could be very useful in nucleic acid reactions of medicinal and biotechnological importance for new drug delivery systems. Unfortunately, the binding constants between CDs and nucleic acids remain relatively modest and close to those observed for peptides and proteins (see above).

Current and potential medical and biological applications

As mentioned earlier, CDs are able to complex biomolecules. Unfortunately, the strength of this behavior depends of the molecular structure. For instance, the binding constants increased in the order carbohydrates << nucleic acids << proteins < lipids. Consequently, the majority of biological investigations about CDs involved their ability to extract lipids (cholesterol or phospholipids) from the plasma membrane. As expected, this capacity can be very useful for numerous applications. For sake of clarity, only some typical applications of CD/cellular interactions are reported.

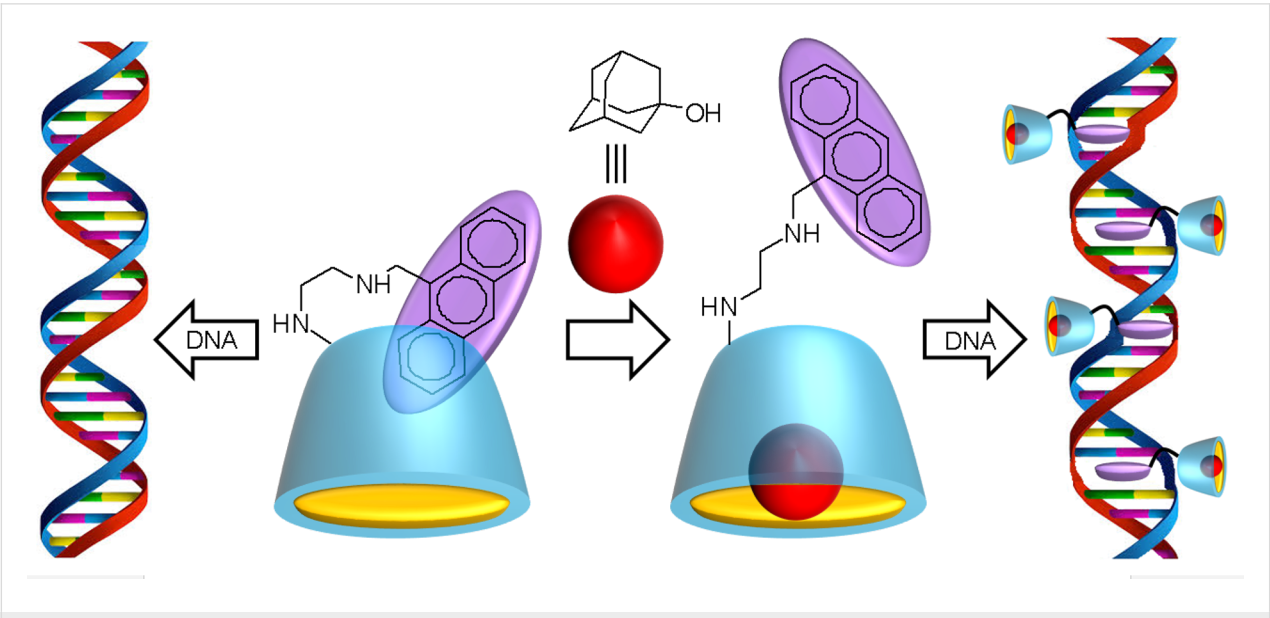

Scheme 5: Principle of chemically switched DNA intercalators based on anthryl(alkylamino)-β-CD/1-adamantanol (Left: unchanged DNA strand. Right: DNA strand intercalated at four locations).

i) Cell membrane cholesterol efflux

As previously mentioned, CDs are able to interact and to complex cholesterol and others lipids [114]. A great number of publications deals with this topic and with the consequences of this phenomenon (e.g., hemolysis or cytotoxicity, see section above). Since the nineties, β-CDs are known to have a high affinity, in vitro, for sterols as compared to other lipids [58,115]. Consequently, these molecules can be used to manipulate the cellular cholesterol content, to modify cholesterol metabolism [115,116] and to stimulate the removal of cholesterol from a variety of cells in culture [80,117-119]. It should be noted that the cholesterol extraction by CDs is both time and dose dependent. In addition, the exposure of cells to modified β-CD in the 10–100 mM concentration range results in high rates of cell cholesterol efflux. Some typical examples are presented in this section.

CDs have been used to demonstrate the presence of different kinetic pools of cholesterol within cell models. Indeed, CDs have been used recently to monitor the movement of cholesterol from monolayers [57] or liposome bilayers [60]. For instance, a typical paper has been published in 2001 by Leventis and Silvius [60]. In order to characterize the CDs capacity to bind cholesterol, the authors examined the catalytic transfer of cholesterol between liposomes composed of 1-stearoyl-2-oleoyl phosphatidylcholine (SOPC) or SOPC/cholesterol. In the steady state under such conditions where a negligible fraction of the sterol is bound to CD (i.e., in the presence of submillimolar concentrations), β- and γ-CDs accelerate considerably the rate of cholesterol transfer between lipid vesicles (63- and 64-fold, respectively). This improvement is clearly greater than the transfer of phospholipid. The opposite is true for α- and methyl-β-CD. The kinetics of CD-mediated cholesterol transfer indicates that the transbilayer flip-flop of cholesterol is very rapid (halftime < 1–2 min at 37 °C). In the case of β-CD, the author reported on the relative affinities of cholesterol for different phospholipids. As expected, strong variations in cholesterol affinity were observed depending on the degree of chain unsaturation and the headgroup structure. The transfer revealed that cholesterol interacts with markedly higher affinity with sphingolipids than with other membrane phospholipids. As extension of this work, Huang and London highlighted the possibility of preparing asymmetric vesicles during the exchange of membrane lipids between different vesicles by selective inclusion of phospholipids and/or cholesterol into the CD cavity [120]. Moreover, CDs can also be used to monitor the intracellular movement of cholesterol in tissue culture cells [121].

As the cholesterol extraction by CDs occurs usually at very high rates, CDs have been used to demonstrate the presence of different kinetic pools of cholesterol within cells. Unfortunately, only few papers have studied the dynamics of this process on cells. For instance, the kinetics of cholesterol efflux have been examined in different cell lines such as fibroblasts [117], human erythrocytes [122], rat cerebellar neurons [123], differentiated human neurons and astrocytes [124], etc. All these results indicated that CDs induce cholesterol, sphingolipids, and phospholipids extraction from the cytoplasmic membrane typically in a range of 50–90% of the original amount. Castagne and co-workers studied the cholesterol extraction of native and modified β-CDs on endothelial cells (HUVEC) [125]. The measurement of the residual cholesterol content of cells reveals that cholesterol was extracted in a dose dependent relationship. As expected, a correlation was obtained between the cytotoxicity and the affinity for cholesterol. The affinity of CDs for cholesterol was classified in the order β-CD < HP-β-CD < Me-β-CD. Similar results are obtained with other biological membranes [117-126]. Another typical example has been published by Steck et al. The authors investigated the cholesterol movement created by the treatment of human erythrocytes with Me-β-CD [122]. The results show that the rate of efflux is approximately three orders of magnitude higher than the cholesterol transfer from cells to synthetic vesicles. Therefore, Me-β-CDs are very efficient to extract large amounts of membrane cholesterol at a very high rate. CDs can also catalyze the exchange of cholesterol between serum lipoproteins and cells [56].

ii) Cardiovascular diseases

The atherosclerosis vascular disease (ASVD) is caused by an inflammation of the arterial wall that is caused by increased cholesterol blood levels and an accumulation of cholesterol crystals in the subendothelial spaces leading to arteriosclerotic plaque formation [127]. It is noteworthy that the cholesterol represents a maximum of 10% of the total mass of plaque. Consequently, the elasticity of the artery walls is reduced, pulse pressure can be modified and blood clot can be formed (Scheme 6). Cardiovascular disease is currently the leading cause of death worldwide. As plasma levels of cholesterol are associated with cardiovascular morbidity and mortality, the use of CDs to solubilize and to remove cholesterol (and plaque) is very promising to combat this deadly condition.

It is noteworthy that high concentrations of modified β-CDs result in rates of cell cholesterol efflux far in excess of those achieved with physiological cholesterol acceptors such as high-density lipoproteins (HDL). Indeed, plasma levels of HDL are inversely associated with cardiovascular morbidity and mortality because this lipoprotein is responsible for transporting cholesterol to the liver where it can be eliminated [128]. The opposite holds for low-density lipoproteins (LDL). Their function is to transport cholesterol, free or esterified, in the

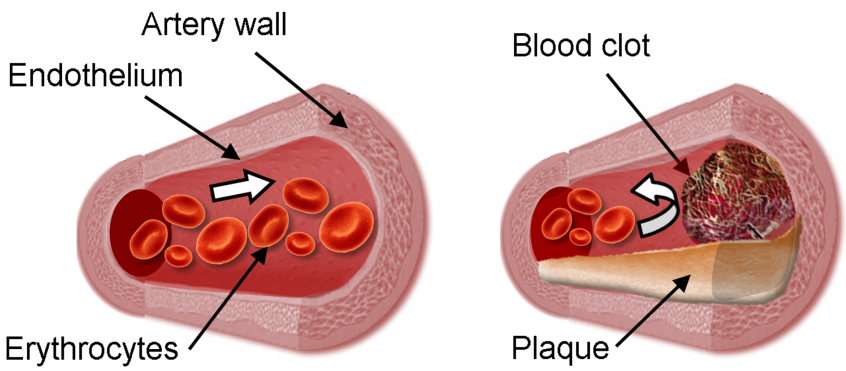

Scheme 6: Normal (left) and diseased artery (right).

blood and through the body to bring them to the cells. HDL particles also reduce macrophage accumulation, and thus help prevent or even regress atherosclerosis. The alteration of cellular cholesterol regulation, named the reverse cholesterol transport, RCT, could be used to block atheroprogression associated with different severity degrees of atherosclerosis pathogenesis. From the pioneering works of Irie et al., it became clear that CDs can be useful to prevent atherosclerosis [115,129].

As the critical step in the formation of atherosclerosis plaque is the recruitment of monocytes (a type of white blood cells), which can differentiate into macrophages and ingest LDL, Murphy et al. proposed to prevent the activation/expression of monocyte adhesion [130]. For this cell adhesion, molecules such as CD11b are required. Therefore, the authors reported that β-CD, but not its cholesterol complex, inhibits CD11b activation. As the cholesterol content of lipid rafts diminished after treatment with the cholesterol acceptors, the authors proposed that the cholesterol efflux from serum monocytes is the main mechanism and is probably an effective means of inhibiting the development of atherosclerotic plaques.

In 2015, Montecucco et al. reported the anti-atherosclerotic action of KLEPTOSE® CRYSMEB (a mixture of methylated β-CD where 2-*O*-methylations are dominant) in atherosclerotic mouse models [131]. As expected, their interfering action with cholesterol metabolism has a positive impact on atherogenesis, lipid profile and atherosclerotic plaque inflammation. In addition to reduce triglyceride serum levels, this CD reduces cholesterol accumulation in atherosclerotic plaques by the modification of HDL-cholesterol levels. It is noteworthy that HDL and apolipoprotein A-I (ApoA-I) cause a dose-dependent reduction in the activation of CD11b (i.e., anti-inflammatory effect on monocytes) through interactions with several receptors and ABCA1 for HDL and ApoA-I, respectively.

However, the process, which leads to an aberrant accumulation of cholesterol in artery walls forming atherosclerotic plaques, is complex. Thus the alteration of RCT as well as the expression and the functionality of transporters (ABCA1, ABCG1, and SR-BI) involved in this process could be very useful in the fight against atherosclerosis pathogenesis. As pointed out by Coisne and co-workers, "*RCT alterations have been poorly studied at the arterial endothelial cell and smooth muscle cells levels*" [132]. Consequently, the authors investigated the effect of different methylated β-CDs on the RCT of arterial endothelial and smooth muscle cells. It should be noted that these two cell types express basal levels of ABCA1 and SR-BI whereas ABCG1 was solely found in arterial endothelial cells. The authors highlighted the correlation between the percentages of cholesterol extraction and the methylation degree of the CDs. This effect was clearly independent of the membrane composition. The expression levels of ABCA1 and ABCG1, as well as the cholesterol efflux to ApoA-I and HDL, were reduced due to cholesterol-methylated β-CD interaction. Consequently, the cellular cholesterol involved in atherosclerotic lesions is lowered and the expression of ABCA1 and ABCG1 transporters involved in RCT is clearly modulated.

In 2016, Zimmer et al. published on the effect of HP-β-CD in order to reduce atherosclerotic plaques [133]. The HP-β-CD can be used to dissolve cholesterol crystal (responsible for the complex inflammatory response) which can be excreted from the body in urine. Mice were fed with a cholesterol-rich diet for 12 weeks in order to promote fatty plaques in their blood vessels (i.e., to obtain atherosclerotic mice). After 8 weeks, they started the injection of HP-β-CD (2 injections by week). Over the remaining four weeks, the authors observed a plaque reduction in atherosclerotic mice that had consumed HP-β-CD compared with plaques in the blood vessels of untreated animals (≈46% reduction). From a mechanistic point of view, the researchers suspect that the CD boosts the activity of macro-

phages, enabling them to attack excess cholesterol without causing inflammation. Indeed, CD increases liver X receptor (LXR) involved in the antiatherosclerotic and anti-inflammatory effects as well as in the RCT improvement.

Moreover, α-CD can also be used to reduce LDL cholesterol and alters plasma fatty acid profile [134,135]. In 2016, a double blind, placebo-controlled clinical trial has been published on the effect of oral α-CD [136]. After 12 to 14 weeks, a daily 6 gram dose of α-CD allowed to reduce fasting plasma glucose levels (1.6%, $p < 0.05$) and insulin index (11%, $p < 0.04$) in 75 healthy men and women. In addition, the LDL cholesterol levels were reduced by 10% ($p < 0.045$) compared with placebo. This CD was well tolerated and no serious adverse events were reported. Only about 8% of patients treated with α-CD reported side effect such as minor gastrointestinal symptoms (3% for the placebo). Consequently, the use of α-CD, safe and well tolerated, showed a reduction in LDL cholesterol, and an improvement of fasting plasma glucose.

The ability of CDs to change the contractibility of arterial smooth muscles indicates that the cellular cholesterol level is an extremely important factor for the cardiovascular system. Continued research on this front could potentially lead to major advancement in the fight against heart disease.

iii) Neurologic diseases

Like in other body systems, the cells of the nervous system are also susceptible to cholesterol extraction mediated by CDs. In the present section, for sake of clarity, only the potential applications of CDs to fight the Alzheimer's and Niemann–Pick type C diseases (AD and NPC, respectively) are reported.

AD is a chronic neurodegenerative disease which represents 60% to 70% of cases of dementia. This disease is characterized by the formation of amyloid plaques in the brain and is often associated to the cerebral accumulation of amyloidogenic peptides (Aβ42). This production is mediated by two neuronal enzymes (β- and γ-secretase) which can be inhibited by methylated β-CDs via cholesterol depletion [137]. Additionally, Yao and co-workers demonstrated that HP-β-CD reduces cell membrane cholesterol accumulation in N2a cells overexpressing Swedish mutant APP (SwN2a) [138]. Moreover, this CD dramatically lowered the levels of Aβ42 in cells as well as the amyloid plaque deposition by reduction of APP protein β cleavage and by up-regulation of the gene expression involved in cholesterol transport. In cell models, this CD also improved clearance mechanisms.

CDs also exert significant beneficial effects in NPC disease, which shares neuropathological features with AD. This disorder is characterized by an abnormal endosomal/lysosomal storage disease associated with genetic mutations in NPC1 and NPC2 genes coding for proteins involved in the intracellular cholesterol transport. Consequently, functions of the impaired proteins cause a progressive neurodegeneration as well as liver and lung diseases. As these two proteins act in tandem and promote the export of cholesterol from endosomes/lysosomes, CDs can bypass the functions of NPC1 and NPC2 and can trap and transport membrane-stored cholesterol from endosomes/lysosomes [139]. This ability of CDs to sequester and to transport cholesterol could potentially lead to major advancements in our ability to fight neurodegenerative diseases.

iv) Antipathogen activities

Cholesterol levels in the plasma membrane are extremely important in many parts of the viral infection process such as the entry and release of virions from the host cell as well as for the transport of various viral proteins. CDs have a clear antiviral activity against influenza virus [140], human immunodeficiency virus (HIV-1) [141], murine corona virus [142], poliovirus [143], human T cell leukemia virus (HTLV-1) [144], Newcastle virus [145,146], varicella-zoster [147], duck and human hepatitis B virus [148,149], bluetongue virus [150], etc. In these cases, the ability of CDs to decrease membrane cholesterol was proposed as antiviral mechanism. Nevertheless, the biological effects of the CDs can be classified according to their role: i) to impede the viral entry in the host cell, ii) to decrease the relative infectivity of the virions, iii) to decrease the observed viral titer, and iv) to disrupt the surface transport of influenza virus hemagglutinin. Few typical examples of the CD effect on the pathogenicity of several viruses are reported.

The HIV is a widely studied virus in terms of the effects of CDs. For instance, sulfated CDs are able to inhibit HIV infection [151,152]. In 1998, Leydet et al. demonstrated anti-HIV and anticytomegalovirus activity of several charged CD derivatives [153]. In 2008, Liao et al. reported that HP-β-CD exhibits also an anti-HIV activity based on cholesterol depletion [154]. However, the mechanism had not yet been determined. Since the membrane cholesterol [155] and lipid raft-based receptors [156] are strictly required for infectivity and HIV entry, CDs are excellent candidates for its use as a chemical barrier for AIDS prophylaxis.

Another common viral disease is caused by herpes simplex virus (HSV) leading to several distinct medical disorders including orofacial and genital herpes or encephalitis [157]. In this context, the anti-HSV properties of native CDs (α- and β-CD) have been estimated against HSV-1 and HSV-2 [158]. The antiviral properties were clearly dependent on the cavity size: α-CD exhibited no significant antiherpetic activity, while,

under similar conditions, β-CD reduced both the cell-free and cell-associated virus more effectively than acyclovir (i.e., antiherpetic drug). Indeed, the results reveal an almost complete protection of Vero cells against acyclovir-sensitive and acyclovir-resistant strains of HSV. The ability of β-CD to impede virus replication is proposed as antiviral mechanism.

The potential occurrence of synergistic effects presents a special case, and may occur when one substance increases the activity of another. Currently, gaps in our knowledge of the circumstances under which such effects may occur (e.g., mixture composition, contact time, species, and exposure concentrations) often hamper predictive approaches. However, since the CDs are able to extract cholesterol and other lipids from the viral membrane, it is likely that their combination with virucides or antiviral drugs which act on the same target results in a synergistic effect. Based on this assumption, our group studied the combination of di-*n*-decyldimethylammonium chloride, [DiC_{10}][Cl] (the most widely used cationic surfactant with intrinsic virucidal activity), and native CDs (α-, β- and γ-CD) [159]. A marked synergism was observed with γ-CD against lipid-containing deoxyribonucleic and ribonucleic acid viruses (HSV-1, respiratory syncytial virus, RSV), and vaccinia viruses, VACV). Indeed, noticeable reductions of the [DiC_{10}][Cl] concentration (i.e., active virucide) were obtained: 72, 40 and 85% against HSV-1, RSV and VACV, respectively. In all cases, submillimolar [DiC_{10}][Cl] and γ-CD concentrations were required to obtain a "6-log reduction" (equivalent to 99.9999% reduction) of the viral titer. Therefore, for these diluted solutions, free CD and [DiC_{10}] species prevail due to the Le Châtelier's principle. Moreover, the micellization equilibrium is not relevant as the virucidal activity was clearly obtained in the premicellar region. Thus, the proposed mechanism of the synergy is based on the ability of CD to extract rapidly cholesterol from the viral envelope. Indeed, γ-CD catalyzes the rapid exchange of cholesterol between the viral envelope and the aqueous solution. The sequestration of cholesterol in the bulk phase facilitates the [DiC_{10}] insertion within the lipid envelope which leads to the virus inactivation (Scheme 7). This means that γ-CD accelerates the rate of cholesterol extraction by a larger factor than α- or β-CD. The proposed mechanism is highly compatible with the results of Leventis and Silvius (see above) [60]. These results demonstrate a clear effect of CDs on the "viability" of enveloped viruses and provide evidences of their potential use in order to improve the efficiency of common antiviral medications.

As cholesterol extraction is general and not limited to viral infections, a whole range of studies have shown that the presence of CDs impedes the entry of bacteria, fungi and parasites into host cells. This effect has been demonstrated for *Plasmodium* species [160], *Campylobacter jejuni* [161], *Leishmania donovani* [162], etc. and this behavior can be explained by the vital role of the lipid rafts in the binding and the entry of pathogens into host cells. Therefore, synergistic effects can also

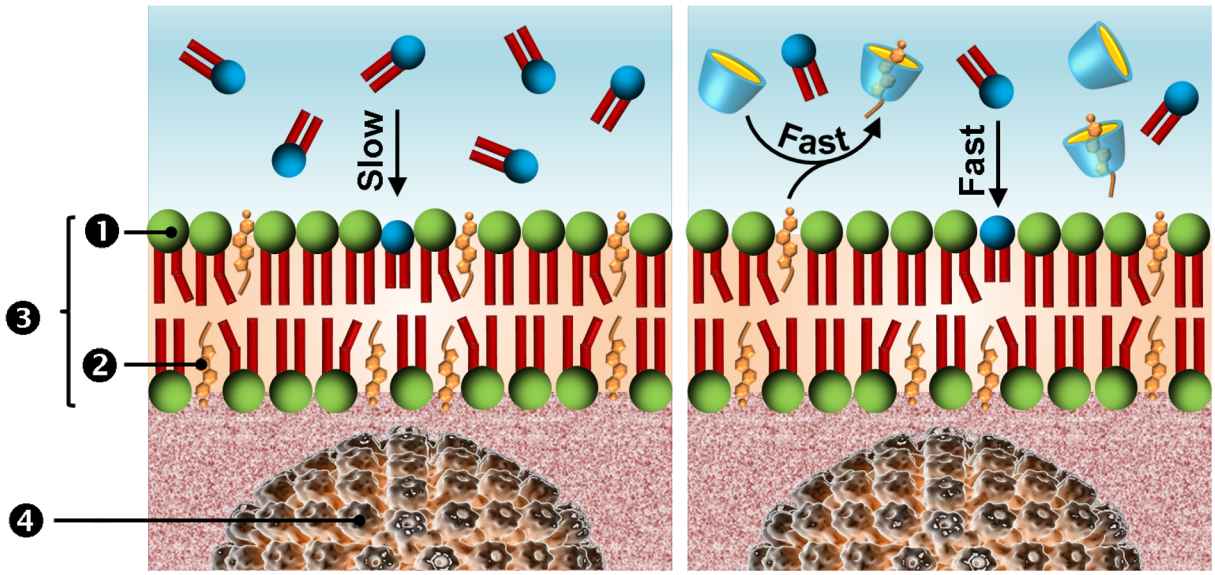

Scheme 7: Kinetics of [DiC_{10}] insertion into the viral envelope without (left) or with γ-CD (right). Note that, after this step, the presence of [DiC_{10}] cations induces morphological changes that enhance the envelope fluidity and lead to the virus inactivation after envelope disruption (1. phospholipid, 2. cholesterol, 3. envelope, and 4. nucleocapsid).

be obtained for bacteria, fungi and parasites. For instance, the combination of $[DiC_{10}][Cl]$ and β-CD allows a clear reduction of the minimum inhibitory concentration, MIC, against *Candida albicans* compared to $[DiC_{10}][Cl]$ alone. This effect was only observed for the β-CD/$[DiC_{10}]$ mixture: the MIC values for α- and γ-CD/$[DiC_{10}]$ mixtures were similar to that of $[DiC_{10}][Cl]$ alone. This behavior was attributed to the interaction of β-CD with the lipid membrane components [163]. Other relevant examples can be found in the review of Macaev et al. [164].

Conclusion

This review proposes an overview of the current and potential applications of CDs throughout their interactions with endogenous substances that originate from within an organism, tissue or cell. The majority of these applications are based on the capacity of CDs to withdraw cholesterol of the plasma membrane. This behavior presents several applications such as cholesterol manipulation, control of viral and bacterial infections, treatment of Alzheimer's and heart diseases, etc. Moreover, CDs present a viable basis in the context of "green pharmacy and medicine". In the last decade, the concept of "eco-friendly pharmacy" emerged in response to the Kreisberg's question: "*what clinicians can do to reduce the environmental impacts of medications"* [165]? Of course, the answers are based on similar principles than green chemistry initially developed by Anastas and Warner [166]. The principles cover various concepts such as: i) the use of bio-sourced ingredients, ii) the use of "green concepts" during the production (chemicals, synthesis processes, life cycle engineering, packaging, waste management), iii) the reduction of the negative impact of medication transportations, iv) the reduction of healthcare environmental footprint, v) the reduction of the use of pharmaceuticals and, vi) the improvement of the ultimate drug disposal with the use of take-back programs [167]. As CDs are bio-sourced compounds with very low toxicity dangers and easily biodegradable, they can be used to obtain more sustainable drug formulations in which CDs act as an active green ingredient and not only as an excipient. It is noteworthy that these CDs can be used alone or in combination with common petro-sourced medications. If a synergistic effect between the two molecules is obtained, a significant amount of the drug can be replaced by eco- and biocompatible CDs whilst maintaining the same biological activity. This is particularly interesting as it solves at least partially the negative impact of pharmaceutical formulations to the environment. Consequently, in this context of "greener pharmacy", CDs will contribute without doubt to preserve our planet in the coming years.

Acknowledgments

This review is dedicated to the memory of Michel Teeten who taught me experimental biology.

References

1. Villiers, A. *Compt. Rend. Acad. Sci.* **1891,** *112,* 536–538.
2. Schardinger, F. *Z. Untersuch. Nahr. u. Genussm.* **1903,** *6,* 865–880. doi:10.1007/BF02067497
3. Schardinger, F. *Zentralbl. Bakteriol. Parasitenk. Abt. II* **1911,** *29,* 188–197.
4. Pringsheim, H.; Langhans, A. *Ber. Dtsch. Chem. Ges.* **1912,** *45,* 2533–2546. doi:10.1002/cber.191204502156
5. Pringsheim, H. *Angew. Chem.* **1931,** *44,* 677–682. doi:10.1002/ange.19310443302
6. Crini, G. *Chem. Rev.* **2014,** *114,* 10940–10975. doi:10.1021/cr500081p
7. Saenger, W.; Jacob, J.; Gessler, K.; Steiner, T.; Hoffmann, D.; Sanbe, H.; Koizumi, K.; Smith, S. M.; Takaha, T. *Chem. Rev.* **1998,** *98,* 1787–1802. doi:10.1021/cr9700181
8. Sabadini, E.; Cosgrovea, T.; Do Carmo Egídio, F. *Carbohydr. Res.* **2006,** *341,* 270–274. doi:10.1016/j.carres.2005.11.004
9. Szejtli, J. *Chem. Rev.* **1998,** *98,* 1743–1754. doi:10.1021/cr970022c
10. Khan, A. R.; Forgo, P.; Stine, K. J.; D'Souza, V. T. *Chem. Rev.* **1998,** *98,* 1977–1996. doi:10.1021/cr970012b
11. Rekharsky, M. V.; Inoue, Y. *Chem. Rev.* **1998,** *98,* 1875–1918. doi:10.1021/cr970015o
12. Uekama, K.; Hirayama, F.; Irie, T. *Chem. Rev.* **1998,** *98,* 2045–2076. doi:10.1021/cr970025p
13. Noujeim, N.; Leclercq, L.; Schmitzer, A. R. *Curr. Org. Chem.* **2010,** *14,* 1500–1516. doi:10.2174/138527210791616830
14. Frömming, K. H.; Szejtli, J. *Cyclodextrins in pharmacy;* Kluwer Academic Publishers: Dordrecht, 1994. doi:10.1007/978-94-015-8277-3
15. Campos, E. V. R.; De Oliveira, J. L.; Fraceto, L. F. *Adv. Sci., Eng. Med.* **2014,** *6,* 373–387. doi:10.1166/asem.2014.1538
16. Szente, L.; Szejtli, J. *Trends Food Sci. Technol.* **2004,** *15,* 137–142. doi:10.1016/j.tifs.2003.09.019
17. Funasaki, N.; Ishikawa, S.; Neya, S. *Pure Appl. Chem.* **2008,** *80,* 1511–1524. doi:10.1351/pac200880071511
18. Leclercq, L.; Nardello-Rataj, V. *Eur. J. Pharm. Sci.* **2016,** *82,* 126–137. doi:10.1016/j.ejps.2015.11.017
19. Ivancic, A.; Macaev, F.; Aksakal, F.; Boldescu, V.; Pogrebnoi, S.; Duca, G. *Beilstein J. Nanotechnol.* **2016,** *7,* 1208–1218. doi:10.3762/bjnano.7.112
20. Singh, M.; Sharma, R.; Banerjee, U. C. *Biotechnol. Adv.* **2002,** *20,* 341–359. doi:10.1016/S0734-9750(02)00020-4
21. van De Manakker, F.; Vermonden, T.; Van Nostrum, C. F.; Hennink, W. E. *Biomacromolecules* **2009,** *10,* 3157–3175. doi:10.1021/bm901065f
22. Bjerre, J.; Rousseau, C.; Marinescu, L.; Bols, M. *Appl. Microbiol. Biotechnol.* **2008,** *81,* 1–11. doi:10.1007/s00253-008-1653-5
23. Leclercq, L.; Bricout, H.; Tilloy, S.; Monflier, E. *J. Colloid Interface Sci.* **2007,** *307,* 481–487. doi:10.1016/j.jcis.2006.12.001
24. Leclercq, L.; Lacour, M.; Sanon, S. H.; Schmitzer, A. R. *Chem. – Eur. J.* **2009,** *15,* 6327–6331. doi:10.1002/chem.200900763
25. Leclercq, L.; Compagny, R.; Mühlbauer, A.; Mouret, A.; Aubry, J.-M.; Nardello-Rataj, V. *ChemSusChem* **2013,** *6,* 1533–1540. doi:10.1002/cssc.201300081
26. Buschmann, H.-J.; Schollmeyer, E. *J. Cosmet. Sci.* **2002,** *53,* 185–191.
27. Baudin, C.; Pean, C.; Perly, B.; Goselin, P. *Int. J. Environ. Anal. Chem.* **2000,** *77,* 233–242. doi:10.1080/03067310008032685

28. Szejtli, J. *Starch/Staerke* **2003,** *55,* 191–196. doi:10.1002/star.200390050
29. Biwer, A.; Antranikian, G.; Heinzle, E. *Appl. Microbiol. Biotechnol.* **2002,** *59,* 609–617. doi:10.1007/s00253-002-1057-x
30. Wu, Y.; Shi, R.; Wu, Y.-L.; Holcroft, J. M.; Liu, Z.; Frasconi, M.; Wasielewski, M. R.; Li, H.; Stoddart, J. F. *J. Am. Chem. Soc.* **2015,** *137,* 4111–4118. doi:10.1021/ja511713c
31. Xiao, Y.; Ng, S.-C.; Tan, T. T. Y.; Wang, Y. *J. Chromatogr. A* **2012,** *1269,* 52–68. doi:10.1016/j.chroma.2012.08.049
32. Leclercq, L.; Hapiot, F.; Tilloy, S.; Ramkisoensing, K.; Reek, J. N. H.; Van Leeuwen, P. W. N. M.; Monflier, E. *Organometallics* **2005,** *24,* 2070–2075. doi:10.1021/om048994f
33. Leclercq, L. Smart medical textiles based on cyclodextrins for curative or preventive patient care. In *Active coatings for smart textiles;* Hu, J., Ed.; Woodhead Publishing: Duxford, U.K., 2016; pp 391–427. doi:10.1016/B978-0-08-100263-6.00017-4
34. Boyle, D. *J. Environ. Manage.* **2006,** *80,* 380–386. doi:10.1016/j.jenvman.2005.09.017
35. Jambhekar, S. S.; Breen, P. *Drug Discovery Today* **2016,** *21,* 356–362. doi:10.1016/j.drudis.2015.11.017
36. Jambhekar, S. S.; Breen, P. *Drug Discovery Today* **2016,** *21,* 363–368. doi:10.1016/j.drudis.2015.11.016
37. Loftsonn, T.; Jarho, P.; Másson, M.; Järvinen, T. *Expert Opin. Drug Delivery* **2005,** *2,* 335–351. doi:10.1517/17425247.2.1.335
38. Agrawal, R.; Gupta, V. *Int. J. Pharm. Front. Res.* **2012,** *2,* 95–112.
39. Matsuda, H.; Arima, H. *Adv. Drug Delivery Rev.* **1999,** *36,* 81–99. doi:10.1016/S0169-409X(98)00056-8
40. Lipinski, C. A.; Lombardo, F.; Dominy, B. W.; Feeney, P. J. *Adv. Drug Delivery Rev.* **1997,** *23,* 3–25. doi:10.1016/S0169-409X(96)00423-1
41. Amidon, G. L.; Lennernäs, H.; Shah, V. P.; Crison, J. R. *Pharm. Res.* **1995,** *12,* 413–420. doi:10.1023/A:1016212804288
42. Tötterman, A. M.; Schipper, N. G.; Thompson, D. O.; Mannermaa, J.-P. *J. Pharm. Pharmacol.* **1997,** *49,* 43–48. doi:10.1111/j.2042-7158.1997.tb06750.x
43. Marttin, E.; Verhoef, J. C.; Merkus, F. W. H. M. *J. Drug Targeting* **1998,** *6,* 17–36. doi:10.3109/10611869808997878
44. Del Valle, E. M. M. *Process Biochem. (Oxford, U. K.)* **2004,** *39,* 1033–1046. doi:10.1016/S0032-9592(03)00258-9
45. Stella, V. J.; He, Q. *Toxicol. Pathol.* **2008,** *36,* 30–42. doi:10.1177/0192623307310945
46. Thompson, D. O. *Crit. Rev. Ther. Drug Carrier Syst.* **1997,** *14,* 1–104. doi:10.1615/CritRevTherDrugCarrierSyst.v14.i1.10
47. Davis, M. E.; Brewster, M. E. *Nat. Rev. Drug Discovery* **2004,** *3,* 1023–1035. doi:10.1038/nrd1576
48. Irie, T.; Uekama, K. *J. Pharm. Sci.* **1997,** *86,* 147–162. doi:10.1021/js960213f
49. De Bie, A. T. H. J.; Van Ommen, B.; Bär, A. *Regul. Toxicol. Pharmacol.* **1998,** *27,* 150–158. doi:10.1006/rtph.1998.1219
50. Van Ommen, B.; De Bie, A. T. H. J.; Bär, A. *Regul. Toxicol. Pharmacol.* **2004,** *39,* 57–66. doi:10.1016/j.yrtph.2004.05.011
51. Matsuda, K.; Mera, Y.; Segawa, Y.; Uchida, I.; Yokomine, A.; Takagi, K. *Ogo Yakuri* **1983,** *26,* 287–291.
52. Lina, B. A. R.; Bär, A. *Regul. Toxicol. Pharmacol.* **2004,** *39,* 14–26. doi:10.1016/j.yrtph.2004.05.006
53. Lina, B. A. R.; Bär, A. *Regul. Toxicol. Pharmacol.* **2004,** *39,* 27–33. doi:10.1016/j.yrtph.2004.05.005
54. Voet, D. In *Biochemistry,* 4th ed.; Voet, J. G., Ed.; John Willey & Sons Inc.: New York, USA, 2011.
55. Zidovetzki, R.; Levitan, I. *Biochim. Biophys. Acta* **2007,** *1768,* 1311–1324. doi:10.1016/j.bbamem.2007.03.026
56. Atger, V. M.; de la Llera Moya, M.; Stoudt, G. W.; Rodrigueza, W. V.; Phillips, M. C.; Rothblat, G. H. *J. Clin. Invest.* **1997,** *99,* 773–780. doi:10.1172/JCI119223
57. Ohvo, H.; Slotte, J. P. *Biochemistry* **1996,** *35,* 8018–8024. doi:10.1021/bi9528816
58. Ohtani, Y.; Irie, T.; Uekama, K.; Fukunaga, K.; Pitha, J. *Eur. J. Biochem.* **1989,** *186,* 17–22. doi:10.1111/j.1432-1033.1989.tb15171.x
59. Irie, T.; Otagiri, M.; Sunada, M.; Uekama, K.; Ohtani, Y.; Yamada, Y.; Sugiyama, Y. *J. Pharmacobio-Dyn.* **1982,** *5,* 741–744. doi:10.1248/bpb1978.5.741
60. Leventis, R.; Silvius, J. R. *Biophys. J.* **2001,** *81,* 2257–2267. doi:10.1016/S0006-3495(01)75873-0
61. Arikan, S.; Yigit, A. A.; Zengin, N. *Rev. Med. Vet. (Toulouse, Fr.)* **2004,** *155,* 500–503.
62. Arima, H.; Motoyama, K.; Irie, T. Recent findings on safety profiles of cyclodextrins, cyclodextrin conjugates, and polypseudorotaxanes. In *Cyclodextrins in pharmaceutics, cosmetics, and biomedicine: current and future industrial applications;* Bilensoy, E., Ed.; Wiley: Hoboken, USA, 2011; pp 91–122. doi:10.1002/9780470926819.ch5
63. Ishikawa, S.; Neya, S.; Funasaki, N. *J. Phys. Chem. B* **1998,** *102,* 2502–2510. doi:10.1021/jp9729066
64. Fauvelle, F.; Debouzy, J. C.; Crouzy, S.; Göschl, M.; Chapron, Y. *J. Pharm. Sci.* **1997,** *86,* 935–943. doi:10.1021/js9602453
65. Debouzy, J. C.; Fauvelle, F.; Crouzy, S.; Girault, L.; Chapron, Y.; Göschl, M.; Gadelle, A. *J. Pharm. Sci.* **1998,** *87,* 59–66. doi:10.1021/js970180j
66. Nishijo, J.; Shiota, S.; Mazima, K.; Inoue, Y.; Mizuno, H.; Yoshida, J. *Chem. Pharm. Bull.* **2000,** *48,* 48–52. doi:10.1248/cpb.48.48
67. Shiotani, K.; Uehata, K.; Irie, T.; Uekama, K.; Thompson, D. O.; Stella, V. J. *Pharm. Res.* **1995,** *12,* 78–84. doi:10.1023/A:1016238720701
68. Frijlink, H. W.; Eissens, A. C.; Hefting, N. R.; Poelstra, K.; Lerk, C. F.; Meijer, D. K. F. *Pharm. Res.* **1991,** *8,* 9–16. doi:10.1023/A:1015861719134
69. Ravichandran, R.; Divakar, S. *J. Inclusion Phenom. Mol. Recognit. Chem.* **1998,** *30,* 253–270. doi:10.1023/A:1007912809965
70. Betzel, C.; Saenger, W.; Hingerty, B. E.; Brown, G. M. *J. Am. Chem. Soc.* **1984,** *106,* 7545–7557. doi:10.1021/ja00336a039
71. Uekama, K.; Irie, T.; Sunada, M.; Otagiri, M.; Tsubaki, K. *J. Pharmacobio-Dyn.* **1981,** *4,* 142–144. doi:10.1248/bpb1978.4.142
72. Motoyama, K.; Arima, H.; Toyodome, H.; Irie, T.; Hirayama, F.; Uekama, K. *Eur. J. Pharm. Sci.* **2006,** *29,* 111–119. doi:10.1016/j.ejps.2006.06.002
73. Motoyama, K.; Toyodome, H.; Onodera, R.; Irie, T.; Hirayama, F.; Uekama, K.; Arima, H. *Biol. Pharm. Bull.* **2009,** *32,* 700–705. doi:10.1248/bpb.32.700
74. Nishijo, J.; Moriyama, S.; Shiota, S. *Chem. Pharm. Bull.* **2003,** *51,* 1253–1257. doi:10.1248/cpb.51.1253
75. Monnaert, V.; Betbeder, D.; Fenart, L.; Bricout, H.; Lenfant, A. M.; Landry, C.; Cecchelli, R.; Monflier, E.; Tilloy, S. *J. Pharmacol. Exp. Ther.* **2004,** *311,* 1115–1120. doi:10.1124/jpet.104.071845

76. Kiss, T.; Fenyvesi, F.; Bácskay, I.; Váradi, J.; Fenyvesi, É.; Iványi, R.; Szente, L.; Tósaki, Á.; Vecsernyés, M. *Eur. J. Pharm. Sci.* **2010,** *40,* 376–380. doi:10.1016/j.ejps.2010.04.014
77. Boulmedarat, L.; Bochot, A.; Lesieur, S.; Fattal, E. *J. Pharm. Sci.* **2005,** *94,* 1300–1309. doi:10.1002/jps.20350
78. Kiss, T.; Fenyvesi, F.; Pasztor, N.; Feher, P.; Varadi, J.; Kocsan, R.; Szente, L.; Fenyvesi, E.; Szabo, G.; Vecsernyes, M.; Bacskay, I. *Pharmazie* **2007,** *62,* 557–558.
79. Motoyama, K.; Kameyama, K.; Onodera, R.; Araki, N.; Hirayama, F.; Uekama, K.; Arima, H. *Eur. J. Pharm. Sci.* **2009,** *38,* 249–261. doi:10.1016/j.ejps.2009.07.010
80. Yancey, P. G.; Rodrigueza, W. V.; Kilsdonk, E. P. C.; Stoudt, G. W.; Johnson, W. J.; Phillips, M. C.; Rothblat, G. H. *J. Biol. Chem.* **1996,** *271,* 16026–16034. doi:10.1074/jbc.271.27.16026
81. Beseničar, M. P.; Bavdek, A.; Kladnik, A.; Maček, P.; Anderluh, G. *Biochim. Biophys. Acta* **2008,** *1778,* 175–184. doi:10.1016/j.bbamem.2007.09.022
82. Mascetti, J.; Castano, S.; Cavagnat, D.; Desbat, B. *Langmuir* **2008,** *24,* 9616–9622. doi:10.1021/la8004294
83. López, C. A.; de Vries, A. H.; Marrink, S. J. *PLoS Comput. Biol.* **2011,** *7,* e1002020. doi:10.1371/journal.pcbi.1002020
84. Moore, S. L.; Denyer, S. P.; Hanlon, G. W.; Olliff, C. J.; Lansley, A. B.; Rabone, K.; Jones, M. *Int. J. Antimicrob. Agents* **2006,** *28,* 503–513. doi:10.1016/j.ijantimicag.2006.08.023
85. Nardello-Rataj, V.; Leclercq, L. *Int. J. Pharm.* **2016,** *511,* 550–559. doi:10.1016/j.ijpharm.2016.07.045
86. Sharma, A.; Janis, L. S. *Clin. Chim. Acta* **1991,** *199,* 129–137. doi:10.1016/0009-8981(91)90104-K
87. Horský, J.; Pitha, J. *J. Inclusion Phenom. Mol. Recognit. Chem.* **1994,** *18,* 291–300. doi:10.1007/BF00708735
88. Bekos, E. J.; Gardella, J. A., Jr.; Bright, F. V. *J. Inclusion Phenom. Mol. Recognit. Chem.* **1996,** *26,* 185–195. doi:10.1007/BF01053537
89. Lovatt, M.; Copper, A.; Camilleri, P. *J. Inclusion Phenom. Mol. Recognit. Chem.* **1996,** *25,* 169–172. doi:10.1007/BF01041562
90. Rathore, A. S.; Horváth, C. *J. Chromatogr. A* **1998,** *796,* 367–373. doi:10.1016/S0021-9673(97)00994-1
91. Yamamoto, T.; Fukui, N.; Hori, A.; Matsui, Y. *J. Mol. Struct.* **2006,** *782,* 60–66. doi:10.1016/j.molstruc.2005.01.024
92. Yamamoto, T.; Kobayashi, T.; Yoshikiyo, K.; Matsui, Y.; Takahashi, T.; Aso, Y. *J. Mol. Struct.* **2009,** *920,* 264–269. doi:10.1016/j.molstruc.2008.10.058
93. Healey, R. D.; Prasad, S.; Rajendram, V.; Thordarson, P. *Supramol. Chem.* **2015,** *27,* 414–419. doi:10.1080/10610278.2014.956745
94. Varca, G. H. C.; Andreo-Filho, N.; Lopes, P. S.; Ferraz, H. G. *Curr. Protein Pept. Sci.* **2016,** *11,* 255–263. doi:10.2174/138920310791233387
95. Aoyama, Y.; Nagai, Y.; Otsuki, J.-i.; Kobayashi, K.; Toi, H. *Angew. Chem., Int. Ed. Engl.* **1992,** *31,* 745–747. doi:10.1002/anie.199207451
96. Hirsch, W.; Muller, T.; Pizer, R.; Ricatto, P. J. *Can. J. Chem.* **1995,** *73,* 12–15. doi:10.1139/v95-003
97. Hacket, F.; Coteron, J.-M.; Schneider, H.-J.; Kazachenko, V. P. *Can. J. Chem.* **1997,** *75,* 52–55. doi:10.1139/v97-007
98. Turner,, I. The study of b-cyclodextrin interactions with sugars using “inhibition kinetics” and the bromination of pyrimidine derivatives. Ph.D. Thesis, Concordia University, 1999.
99. Tee, O. S.; Hussein, S. M. I.; Turner, I. E.; Yazbeck, O. J. *Can. J. Chem.* **2000,** *78,* 436–443. doi:10.1139/v00-033
100. Janado, M.; Yano, Y. *J. Solution Chem.* **1985,** *14,* 891–902. doi:10.1007/BF00646298
101. Wei, C.; Pohorille, A. *J. Am. Chem. Soc.* **2009,** *131,* 10237–10245. doi:10.1021/ja902531k
102. Walker, D. B.; Joshi, G.; Davis, A. P. *Cell. Mol. Life Sci.* **2009,** *66,* 3177–3191. doi:10.1007/s00018-009-0081-8
103. Paal, T.; Szejtli, J. *Acta Chim. Acad. Sci. Hung.* **1981,** *106,* 9–15.
104. Komiyama, M. *J. Am. Chem. Soc.* **1989,** *111,* 3046–3050. doi:10.1021/ja00190a045
105. Tee, O. S. *Adv. Phys. Org. Chem.* **1994,** *29,* 1–85. doi:10.1016/S0065-3160(08)60075-1
106. Spies, M. A.; Schowen, R. L. *J. Am. Chem. Soc.* **2002,** *124,* 14049–14053. doi:10.1021/ja012272n
107. Hoffman, J. L.; Bock, R. M. *Biochemistry* **1970,** *9,* 3542–3550. doi:10.1021/bi00820a007
108. Jaffer, S. S.; Ghosh, P.; Das, A.; Purkayastha, P. *Nanoscale* **2010,** *2,* 1420–1422. doi:10.1039/c0nr00184h
109. Siman, L.; Carrasco, I. S. S.; da Silva, J. K. L.; de Oliveira, M. C.; Rocha, M. S.; Mesquita, O. N. *Phys. Rev. Lett.* **2012,** *109,* 248103. doi:10.1103/PhysRevLett.109.248103
110. Alves, P. S.; Mesquita, O. N.; Rocha, M. S. *J. Phys. Chem. Lett.* **2015,** *6,* 3549–3554. doi:10.1021/acs.jpclett.5b01603
111. Tavares, G. D.; Viana, C. M.; Araujo, J. G. V. C.; Ramaldes, G. A.; Carvalho, W. S.; Pesquero, J. L.; Vilela, J. M. C.; Andrade, M. S.; de Oliveira, M. C. *Chem. Phys. Lett.* **2006,** *429,* 507–512. doi:10.1016/j.cplett.2006.08.043
112. O’Mahony, A. M.; Ogier, J.; Darcy, R.; Cryan, J. F.; O’Driscoll, C. M. *PLoS One* **2013,** *8,* e66413. doi:10.1371/journal.pone.0066413
113. Ikeda, T.; Yoshida, K.; Schneider, H.-J. *J. Am. Chem. Soc.* **1995,** *117,* 1453–1454. doi:10.1021/ja00109a040
114. Khuntawee, W.; Wolschann, P.; Rungrotmongkol, T.; Wong-ekkabut, J.; Hannongbua, S. *J. Chem. Inf. Model.* **2015,** *55,* 1894–1902. doi:10.1021/acs.jcim.5b00152
115. Irie, T.; Fukunaga, K.; Pitha, J. *J. Pharm. Sci.* **1992,** *81,* 521–523. doi:10.1002/jps.2600810609
116. Riottot, M.; Olivier, P.; Huet, A.; Caboche, J.-J.; Parquet, M.; Khallou, J.; Lutton, C. *Lipids* **1993,** *28,* 181–188. doi:10.1007/BF02536637
117. Kilsdonk, E. P. C.; Yancey, P. G.; Stoudt, G. W.; Bangerter, F. W.; Johnson, W. J.; Phillips, M. C.; Rothblat, G. H. *J. Biol. Chem.* **1995,** *270,* 17250–17256. doi:10.1074/jbc.270.29.17250
118. Kritharides, L.; Kus, M.; Brown, A. J.; Jessup, W.; Dean, R. T. *J. Biol. Chem.* **1996,** *271,* 27450–27455. doi:10.1074/jbc.271.44.27450
119. Christian, A. E.; Haynes, M. P.; Phillips, M. C.; Rothblat, G. H. *J. Lipid Res.* **1997,** *38,* 2264–2272.
120. Huang, Z.; London, E. *Langmuir* **2013,** *29,* 14631–14638. doi:10.1021/la4031427
121. Neufield, E. B.; Cooney, A. M.; Pitha, J.; Dawidowicz, E. A.; Dwyer, N. K.; Pentchev, P. G.; Blanchette-Mackie, E. J. *J. Biol. Chem.* **1996,** *271,* 21604–21613. doi:10.1074/jbc.271.35.21604
122. Steck, T. L.; Ye, L.; Lange, Y. *Biophys. J.* **2002,** *83,* 2118–2125. doi:10.1016/S0006-3495(02)73972-6
123. Ottico, E.; Prinetti, A.; Prioni, S.; Giannotta, C.; Basso, L.; Chigorno, V.; Sonnino, S. *J. Lipid Res.* **2003,** *44,* 2142–2151. doi:10.1194/jlr.M300247-JLR200

124. Swaroop, M.; Thorne, N.; Rao, M. S.; Austin, C. P.; McKew, J. C.; Zheng, W. *J. Biomol. Screening* **2012,** *17,* 1243–1251. doi:10.1177/1087057112456877
125. Castagne, D.; Fillet, M.; Delattre, L.; Evrard, B.; Nusgens, B.; Piel, G. *J. Inclusion Phenom. Macrocyclic Chem.* **2009,** *63,* 225–231. doi:10.1007/s10847-008-9510-9
126. Visconti, P. E.; Galantino-Homer, H.; Ning, X. P.; Moore, G. D.; Valenzuela, J. P.; Jorgez, C. J.; Alvarez, J. G.; Kopf, G. S. *J. Biol. Chem.* **1999,** *274,* 3235–3242. doi:10.1074/jbc.274.5.3235
127. George, S. J.; Lyon, C. Pathogenesis of Atherosclerosis. In *Atherosclerosis: Molecular and Cellular Mechanisms;* George, S. J.; Johnson, J., Eds.; Wiley-VCH: Weinheim, Germany, 2010; pp 3–20. doi:10.1002/9783527629589.ch1
128. Slatter, T. L.; Williams, M. J. A.; Frikke-Schmidt, R.; Tybjærg-Hansen, A.; Morison, I. M.; McCormick, S. P. A. *Atherosclerosis* **2006,** *187,* 393–400. doi:10.1016/j.atherosclerosis.2005.09.019
129. Irie, T.; Fukunaga, K.; Garwood, M. K.; Carpenter, T. O.; Pitha, J.; Pitha, J. *J. Pharm. Sci.* **1992,** *81,* 524–528. doi:10.1002/jps.2600810610
130. Murphy, A. J.; Woollard, K. J.; Hoang, A.; Mukhamedova, N.; Stirzaker, R. A.; McCormick, S. P. A.; Remaley, A. T.; Sviridov, D.; Chin-Dusting, J. *Arterioscler., Thromb., Vasc. Biol.* **2008,** *28,* 2071–2077. doi:10.1161/ATVBAHA.108.168690
131. Montecucco, F.; Lenglet, S.; Carbone, F.; Boero, S.; Pelli, G.; Burger, F.; Roth, A.; Bertolotto, M.; Nencioni, A.; Cea, M.; Dallegri, F.; Fraga-Silva, R. A.; Fougère, L.; Elfakir, C.; Gassner, A.-L.; Rudaz, S.; Parissaux, X.; Wils, D.; Salomé, M.; Vuilleumier, N.; Poggi, A.; Mach, F. *Vasc. Pharmacol.* **2015,** *72,* 197–208. doi:10.1016/j.vph.2015.04.008
132. Coisne, C.; Hallier-Vanuxeem, D.; Boucau, M.-C.; Hachani, J.; Tilloy, S.; Bricout, H.; Monflier, E.; Wils, D.; Serpelloni, M.; Parissaux, X.; Fenart, L.; Gosselet, F. *Front. Physiol.* **2016,** *7,* 185. doi:10.3389/fphys.2016.00185
133. Zimmer, S.; Grebe, A.; Bakke, S. S.; Bode, N.; Halvorsen, B.; Ulas, T.; Skjelland, M.; De Nardo, D.; Labzin, L. I.; Kerksiek, A.; Hempel, C.; Heneka, M. T.; Hawxhurst, V.; Fitzgerald, M. L.; Trebicka, J.; Björkhem, I.; Gustafsson, J.-Å.; Westerterp, M.; Tall, A. R.; Wright, S. D.; Espevik, T.; Schultze,, J. L.; Nickenig, G.; Lütjohann, D.; Latz, E. *Sci. Transl. Med.* **2016,** *8,* 333ra50. doi:10.1126/scitranslmed.aad6100
134. Artiss, J. D.; Brogan, K.; Brucal, M.; Moghaddam, M.; Jen, K.-L. C. *Metabolism* **2006,** *55,* 195–202. doi:10.1016/j.metabol.2005.08.012
135. Wagner, E. M.; Jen, K.-L. C.; Artiss, J. D.; Remaley, A. T. *Metab., Clin. Exp.* **2008,** *57,* 1046–1051. doi:10.1016/j.metabol.2008.02.020
136. Amar, M. J. A.; Kaler, M.; Courville, A. B.; Shamburek, R.; Sampson, M.; Remaley, A. T. *Lipids Health Dis.* **2016,** *15,* 115. doi:10.1186/s12944-016-0284-6
137. Grimm, M. O. W.; Grimm, H. S.; Tomic, I.; Beyreuther, K.; Hartmann, T.; Bergmann, C. *J. Biol. Chem.* **2008,** *283,* 11302–11311. doi:10.1074/jbc.M801520200
138. Yao, J.; Ho, D.; Calingasan, N. Y.; Pipalia, N. H.; Lin, M. T.; Beal, M. F. *J. Exp. Med.* **2012,** *209,* 2501–2513. doi:10.1084/jem.20121239
139. Vance, J. E.; Karten, B. *J. Lipid Res.* **2014,** *55,* 1609–1621. doi:10.1194/jlr.R047837
140. Barman, S.; Nayak, D. P. *J. Virol.* **2007,** *81,* 12169–12178. doi:10.1128/JVI.00835-07
141. Liao, Z.; Graham, D. R.; Hildreth, J. E. K. *AIDS Res. Hum. Retroviruses* **2004,** *19,* 675–687. doi:10.1089/088922203322280900
142. Thorp, E. B.; Gallagher, T. M. *J. Virol.* **2004,** *78,* 2682–2692. doi:10.1128/JVI.78.6.2682-2692.2004
143. Danthi, P.; Chow, M. *J. Virol.* **2004,** *78,* 33–41. doi:10.1128/JVI.78.1.33-41.2004
144. Wielgosz, M. M.; Rauch, D. A.; Jones, K. S.; Ruscetti, F. W.; Ratner, L. *AIDS Res. Hum. Retroviruses* **2005,** *21,* 43–50. doi:10.1089/aid.2005.21.43
145. Laliberte, J. P.; McGinnes, L. W.; Peeples, M. E.; Morrison, T. G. *J. Virol.* **2006,** *80,* 10652–10662. doi:10.1128/JVI.01183-06
146. Laliberte, J. P.; McGinnes, L. W.; Morrison, T. G. *J. Virol.* **2007,** *81,* 10636–10648. doi:10.1128/JVI.01119-07
147. Hambleton, S.; Steinberg, S. P.; Gershon, M. D.; Gershon, A. A. *J. Virol.* **2007,** *81,* 7548–7558. doi:10.1128/JVI.00486-07
148. Funk, A.; Mhamdi, M.; Hohenberg, H.; Heeren, J.; Reimer, R.; Lambert, C.; Prange, R.; Sirma, H. *J. Virol.* **2008,** *82,* 10532–10542. doi:10.1128/JVI.00422-08
149. Bremer, C. M.; Bung, C.; Kott, N.; Hardt, M.; Glebe, D. *Cell. Microbiol.* **2009,** *11,* 249–260. doi:10.1111/j.1462-5822.2008.01250.x
150. Bhattacharya, B.; Roy, P. *J. Virol.* **2008,** *82,* 10600–10612. doi:10.1128/JVI.01274-08
151. Schols, D.; De Clercq, E.; Witvrouw, M.; Nakashima, H.; Snoeck, R.; Pauwels, R.; van Schepdael, A.; Claes, P. *Antiviral Chem. Chemother.* **1991,** *2,* 45–53. doi:10.1177/095632029100200108
152. Weiner, D. B.; Williams, W. V.; Weisz, P. B.; Greene, M. I. *Pathobiology* **1992,** *60,* 206–212. doi:10.1159/000163724
153. Leydet, A.; Moullet, C.; Roque, J. P.; Witvrouw, M.; Panneccouque, C.; Andrei, G.; Snoeck, R.; Neyts, J.; Schols, D.; de Clercq, E. *J. Med. Chem.* **1998,** *41,* 4927–4932. doi:10.1021/jm970661f
154. Liao, Z.; Cimakasky, L. M.; Hampton, R.; Nguyen, D. H.; Hildreth, J. E. K. *AIDS Res. Hum. Retroviruses* **2001,** *17,* 1009–1019. doi:10.1089/088922201300343690
155. Campbell, S.; Gaus, K.; Bittman, R.; Jessup, W.; Crowe, S.; Mak, J. *J. Virol.* **2004,** *78,* 10556–10565. doi:10.1128/JVI.78.19.10556-10565.2004
156. Popik, W.; Alce, T. M.; Au, W.-C. *J. Virol.* **2002,** *76,* 4709–4722. doi:10.1128/JVI.76.10.4709-4722.2002
157. Aitken, C.; Jeffries, D. J. *Clin. Microbiol. Rev.* **2001,** *14,* 528–546. doi:10.1128/CMR.14.3.528-546.2001
158. Carlson, R. M.; Kent Froberg, M.; Ayub Khan, M.; Rice, S. A.; Wallace, K. B. Cyclodextrin compositions and methods of treating viral infections. U.S. Patent 20030220294, Nov 27, 2003.
159. Leclercq, L.; Dewilde, A.; Aubry, J.-M.; Nardello-Rataj, V. *Int. J. Pharm.* **2016,** *512,* 273–281. doi:10.1016/j.ijpharm.2016.08.057
160. Crandall, I. E.; Szarek, W. A.; Vlahakis, J. Z.; Xu, Y.; Vohra, R.; Sui, J.; Kisilevsky, R. *Biochem. Pharmacol.* **2007,** *73,* 632–642. doi:10.1016/j.bcp.2006.10.030
161. Lin, C.-D.; Lai, C.-K.; Lin, Y.-H.; Hsieh, J.-T.; Sing, Y.-T.; Chang, Y.-C.; Chen, K.-C.; Wang, W.-C.; Su, H.-L.; Lai, C.-H. *Infect. Immun.* **2011,** *79,* 3563–3575. doi:10.1128/IAI.05175-11
162. Pucadyil, T. J.; Tewary, P.; Madhubala, R.; Chattopadhyay, A. *Mol. Biochem. Parasitol.* **2004,** *133,* 145–152. doi:10.1016/j.molbiopara.2003.10.002
163. Leclercq, L.; Lubart, Q.; Dewilde, A.; Aubry, J.-M.; Nardello-Rataj, V. *Eur. J. Pharm. Sci.* **2012,** *46,* 336–345. doi:10.1016/j.ejps.2012.02.017

164. Macaev, F.; Boldescu, V.; Geronikaki, A.; Sucman, N. *Curr. Top. Med. Chem.* **2013,** *13,* 2677–2683. doi:10.2174/15680266113136660194
165. Kreisberg, J. *Integr. Med.* **2007,** *6,* 50–52.
166. Anastas, P. T.; Warner, J. C. *Green Chemistry: Theory and Practice;* Oxford University Press: New York, 1998; p 30.
167. Kümmerer, K. Why Green and Sustainable Pharmacy?. In *Green and sustainable pharmacy;* Kümmerer, K.; Hempel, M., Eds.; Springer-Verlag: Berlin, Germany, 2010; pp 3–10. doi:10.1007/978-3-642-05199-9_1

License and Terms

BEILSTEIN JOURNAL OF ORGANIC CHEMISTRY

Stabilization of nanosized titanium dioxide by cyclodextrin polymers and its photocatalytic effect on the degradation of wastewater pollutants

Tamás Zoltán Agócs[1,2], István Puskás[1], Erzsébet Varga[1], Mónika Molnár[2] and Éva Fenyvesi[*1]

Full Research Paper

Open Access

Address:
[1]CycloLab Cyclodextrin R&D Laboratory Ltd, Illatos út 7, Budapest, 1097, Hungary and [2]Department of Applied Biotechnology and Food Science, Budapest University of Technology and Economics, Szent Gellért tér 4, Budapest, 1111, Hungary

Email:
Éva Fenyvesi[*] - fenyvesi.e@cyclolab.hu

* Corresponding author

Keywords:
carboxymethyl β-cyclodextrin polymer; colloid stability; ibuprofen; methylene blue; nanoTiO$_2$; synergetic effect; wastewater treatment

Beilstein J. Org. Chem. **2016,** *12,* 2873–2882.
doi:10.3762/bjoc.12.286

Received: 27 September 2016
Accepted: 19 December 2016
Published: 28 December 2016

This article is part of the Thematic Series "Superstructures with cyclodextrins: Chemistry and applications IV".

Guest Editor: G. Wenz

Abstract

Advanced oxidation processes (AOPs) are considered highly competitive water treatment technologies for the removal of organic pollutants. Among AOP techniques, photocatalysis has recently been the most widely studied. Our aims were to investigate how the dispersion of nanosized titanium dioxide (nanoTiO$_2$) applied in photodegradation-based procedures can be stabilized with cyclodextrins in order to obtain a new, more efficient photocatalyst for the purification of waters polluted by xenobiotics applying UV irradiation. During our work, on the one hand, we studied the behavior and stability of nanoTiO$_2$ in cyclodextrin solutions. On the other hand, we used various monomer and polymer cyclodextrin derivatives, and assessed the options for nanoTiO$_2$ stabilization in the presence of various salts and tap water on the basis of turbidity tests. The physical stability of nanoTiO$_2$ dispersions is diminished in the presence of the salts found in tap water (and occurring also in surface waters and ground water) and they are precipitated immediately. This colloidal instability can be improved by cyclodextrin derivatives. Based on the results of our studies we have selected carboxymethyl β-cyclodextrin polymer (CMBCD-P) for stabilization of nanoTiO$_2$ dispersions. The photocatalytic degradation of methylene blue and ibuprofen as model organic pollutants in various media (distilled water, NaCl solution and tap water) has been studied using nanoTiO$_2$ as catalyst stabilized by CMBCD-P. CMBCD-P itself showed a catalytic effect on the UV degradation of methylene blue. In addition to enhancing the colloid stability of nanoTiO$_2$ CMBCD-P showed also synergistic effects in catalyzing the photodecomposition process of the dye. On the other hand, ibuprofen as a model pharmaceutical, a pollutant of emerging concern (EP), was protected by CMBCD-P against the photocatalytic degradation showing that inclusion complex formation can result in opposite effects depending on the structure of the host–guest complex.

Introduction

The wastewater purification and reuse are key challenges of our society. Globally 330 km^3year^{-1} municipal wastewater is produced [1]. According to the European Investment Bank, by 2025, 800 million people will be living in regions in shortage of drinking water [2]. The recently recognized harmful xenobiotics (contaminants of emerging concern, such as pharmaceutical residues, personal care products, industrial additives) impose a high risk on the environment and also on human because they usually do not degrade in nature, appear in surface waters and groundwater, and may accumulate in living organisms [3,4]. From time to time, these microcontaminants can also be detected in tap water and may pose a risk for human, too [5]. These microcontaminants are xenobiotics for the microbes used in the secondary treatment (after sedimentation, which is the primary treatment) of wastewater, so these compounds are not efficiently eliminated with the conventional technologies from the effluent. To avoid the contamination of the receiving environment (sea, river, lake, wetlands, ground, etc.) it is essential that efficient and economical treatment procedure(s) are elaborated for the removal of such microcontaminants. Various sorbents containing cyclodextrin (CD) have been developed aiming at the removal of pharmaceutical residues, pesticides and other endocrine disrupting compounds from purified wastewater [6,7]. CDs are cyclic oligosaccharides consisting of 6–8 glucose units (α-, β- and γ-CD) primarily used in the pharmaceutical, cosmetic and household chemical industry [8]. They form non-covalent inclusion complexes with a great number of the organic contaminants in soil (petroleum hydrocarbons, polycyclic aromatic hydrocarbons, etc.) and microcontaminants occurring in water (pharmaceutical and cosmetic active agents, pesticides, etc.). The CD derivatives, which are well soluble in water, such as hydroxypropyl and methylated CDs, can enhance desorption of the contaminants from the soil and are useful in soil remediation technologies (e.g., in situ/ex situ microbial degradation and chemical oxidation of contaminants in soil) [9,10]. Immobilizing CDs either by crosslinking or by coupling to the surface of natural or synthetic polymers CD-based sorbents are obtained in the form of beads, nanosponges, microfibers, etc., which are able to remove microcontaminants from purified wastewater [11-17] and can be also used as samplers [12]. Further methods applying CDs for wastewater purification include CD-intensified biodegradation of contaminants [18], and oxidation of micropollutants adsorbed on cyclodextrin polymer (CDP) using $KMnO_4$ [19].

Advanced oxidation processes (AOPs) based on in situ generation of highly reactive species can mineralize organic contaminants into relatively harmless compounds. Research activities have been recently focused on photocatalysis belonging to these AOP techniques [20-24]. The photodegradation is a technology utilizing the energy of light for decomposition of the contaminants. CD can catalyse or inhibit the photodecomposition of a compound depending on the position of the light-sensitive bonds of the included compound. For instance, photodegradation of bisphenol A was enhanced in aqueous solutions containing β-CD [25], while the photodecomposition of pesticides of similar structure (parathion and paraoxon) was inhibited or catalyzed, respectively, by β-CD [26]. The complex formation can either protect the drug from the effect of light or accelerate the decomposition [27,28].

Recently, various photocatalysts modified by CDs have been described. For instance, reduced graphene oxide/β-CD/titanium dioxide showed enhanced removal of phenol and Cr(VI) [29], graphene nanosheets with self-assembled nanolayer of TiO_2 stabilized by β-CD resulted in improved photodegradation of methylene blue [24], and CD-functionalized Fe_3O_4/TiO_2 was efficient catalyst in photodecomposition of endocrine disrupting compounds, such as bisphenol A and dibutyl phthalate [30].

Producing strong oxidizing radicals (hydroxyl and superoxide radical ions) titanium dioxide is a widely used catalyst for photodecomposition of various organic pollutants [31]. The photocatalytic reactions take place on the surface of the catalyst on the effect of solar light or of artificial UV light irradiation. In the practice, TiO_2 is immobilized on a surface, e.g., glass wool mats or ceramic plates and a thin layer of waste water is treated by solar light to achieve the decomposition of the organic pollutants [32]. Another way of enhancing the surface is the application of nanoparticles (nanoTiO_2). Such nanosized particles can readily aggregate forming larger agglomerates of reduced surface and reduced catalytic activity. The aggregation is a slow process in distilled water, but happens instantly in the presence of salts, e.g., in tap water, surface waters and waste waters. β-CD can be used for stabilization of colloidal TiO_2 systems [33] – at least in distilled water – as it is adsorbed on the surface of the nanoparticles (with its wider secondary side, Figure 1) [34]. In addition to the improvement of the colloidal stability, also the efficiency of the photocatalytic performance of nanoTiO_2 particles can be enhanced by adsorption of β-CD. The latter plays electron-donating and hole-capturing roles when linked to nanoTiO_2 colloids leading to restriction of charge–hole recombination [35]. The efficiency is further improved by keeping the ligands close to the surface of nanoTiO_2 via inclusion complexation. In other studies the presence of CDs caused a delay in the photocatalytic degradation of toluene [36].

Although several operating parameters (concentration of pollutants, pH, irradiation time etc.) have already been investigated

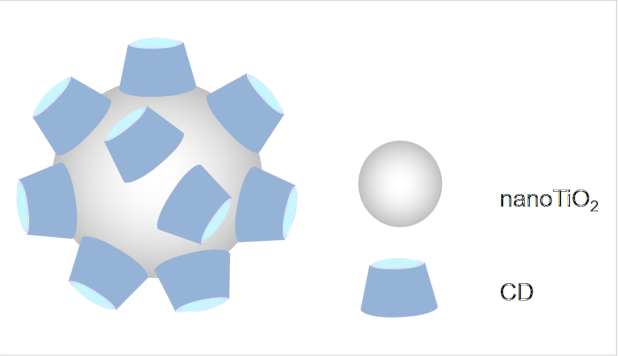

Figure 1: Adsorption of β-CD on the surface of nanoTiO$_2$ [37].

most of the experiments published so far were performed only in distilled water [23,38-40]. In the present work we aimed at finding a cyclodextrin derivative which effectively protects nanoTiO$_2$ in aqueous media against the precipitating effect of different salts in tap water. We used turbidity and light scattering measurements for studying the aggregation behavior of nanoTiO$_2$. In a second step, the photocatalytic properties of the stabilized nanoTiO$_2$ dispersions have been studied for degradation of some model organic pollutants (methylene blue and ibuprofen) under UV-A light irradiation.

Results and Discussion

Selection of the CD derivative for stabilizing nanoTiO$_2$ dispersions

In aqueous dispersions, in the presence of salts the nanoparticles of TiO$_2$ start to aggregate and form larger particles enhancing the turbidity of dispersion. The turbidity (the haziness of the dispersion caused by particles invisible for the naked eye) was measured to monitor the aggregation of the particles of nanoTiO$_2$. Various monomer and polymer CD derivatives were studied how they influence the stability of nanoTiO$_2$ in the presence of NaCl (0.1%) by recording the turbidity. We used neutral and charged CD derivatives, such as non-ionic 2-hydroxypropyl-β-cyclodextrin monomer (M) and polymer (P) (HPBCD-M/P), anionic carboxymethyl-β-cyclodextrin monomer and polymer (CMBCD-M/P) and quaternary ammonium β-cyclodextrin polymer (QABCD-P) in a concentration of 1% (50 mg/5 mL). The polymers were prepared by crosslinking the proper monomers with epichlorohydrin and contained 4–200 β-CD units. None of the monomers could hinder the aggregation of nanoTiO$_2$ in 0.1% NaCl solution while the polymers showed stabilizing effect (Table 1).

The effects of the polymer concentration (1% and 5%) and its average molecular weight (90 kDa, 200 kDa, 300 kDa) on the colloidal stability of the nanoTiO$_2$ dispersion were also studied using the neutral HPBCD-P. It was clearly shown that the stabilization effect was not influenced by the average molecular weight and there was no remarkable difference between the samples with 1% and 5% polymer concentration (the turbidity in salt solution changed to 102–107% and 102–105% related to the initial after 120 min, respectively. Results are not presented here.)

After diluting nanoTiO$_2$ dispersions with tap water immediate precipitation was observed. Among the CD polymers studied the QABCD-P could not hinder this precipitation, the HPBCD-P slowed down the precipitation process, while in the presence of CMBCD-P no precipitation occurred in 120 min (Figure 2).

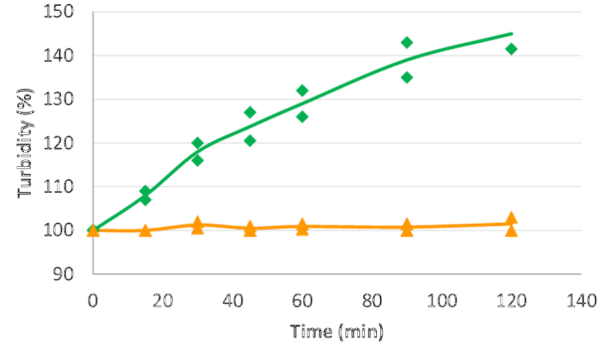

Figure 2: Turbidity of nanoTiO$_2$ dispersion (0.02%) in the presence of 1% HPBCD-P (green diamond) and 1% CMBCD-P (yellow triangle) in tap water.

As the lowest enhancement in turbidity both in NaCl solution and in tap water was obtained with the polymer of the carboxymethyl β-CD derivative (CMBCD-P), this material was selected for further studies.

The colloidal stability of nanoTiO$_2$ dispersions in various salt solutions was examined in the presence of some selected ions typical in tap water. Without the CD polymer additive the

Table 1: Turbidity of 0.02% nanoTiO$_2$ dispersions in the presence of 1% CD polymers in distilled water and in 0.1% NaCl solution at 120 min related to the initial turbidity (100%).

	No CD	HPBCD-P	CMBCD-P	QABCD-P
Distilled water	100 ± 2%	104 ± 2%	101 ± 2%	101 ± 2%
0.1% NaCl solution	209 ± 5%	107 ± 2%	101 ± 2%	103 ± 2%

nanoTiO$_2$ was immediately precipitated in the solution of 0.1% Na_2SO_4, and a fast enhancement of the turbidity was observed in the presence of the other salts: Ca/$MgCl_2$ and Na_2CO_3. The dispersion was stable at as low concentration as 1% CMBCD-P and the turbidity remained <105% within 120 min of observation (Table 2).

The stabilizing effect of the CD-based polymers especially of CMBCD-P can be attributed to steric effects caused by the adsorption of the polymer on the surface of nanoTiO$_2$ particles. It forms a layer, which inhibits their aggregation. The negative charge contributes to the stabilizing effect by i) electrostatic attraction of the sorbed layer to the positively charged holes on the nanoTiO$_2$ particles and ii) repulsion between the particles covered by the polymer layer.

Aggregation studies

Based on particle size measurements the aggregation behavior of nanoTiO$_2$ in the presence and absence of polymer was compared in different media. We studied the effect of NaCl and tap water.

The applied nanoTiO$_2$ consists of crystallites of 10–20 nm diameter as evidenced by scanning electron micrographs provided by Evonik [41]. However, in aqueous dispersion prepared in our laboratory, these nanocrystallites form – still relatively small – aggregates having a mean size of 50–60 nm (Figure 3 and Figure 4, red curves).

The particle size distribution of nanoTiO$_2$ in the absence of destabilizing ions is relatively narrow and nearly harmonic (mean aggregate size: 55 nm) as shown in Figure 3 and Figure 4. In the presence of 0.1% NaCl, the loss of stability is indicated by the increase of the mean size to 3150 nm two hours after addition. When CMBCD-P is adsorbed onto the nanoTiO$_2$, only partial aggregation was observed. A bimodal distribution was obtained. The smaller sized fraction (71% of the total sample) had a mean size of 90 nm, while the larger sized fraction (29% of the total sample) had a mean size of 1060 nm two hours after addition. As the photocatalytic degradation experiments were carried out for 60 min even this partial stabilizing effect of the polymer seemed to be enough for keeping the catalytic efficiency of the nanocatalyst.

Table 2: The effect of salts (0.1%) on the turbidity of nanoTiO$_2$ aqueous dispersions (0.02%) in the presence and absence of CMBCD-P (1%)[a].

	Relative turbidity (%)				
	NaCl	$CaCl_2$	$MgCl_2$	Na_2CO_3	Na_2SO_4
No CD	209%	>200%*	>200%**	220%*	immediate precipitation
CMBCD-P	100.1%	100.2%	100.1%	100.4%	100.0%

[a]Turbidity after 120 min (*20 min, ** 60 min) related to the initial value.

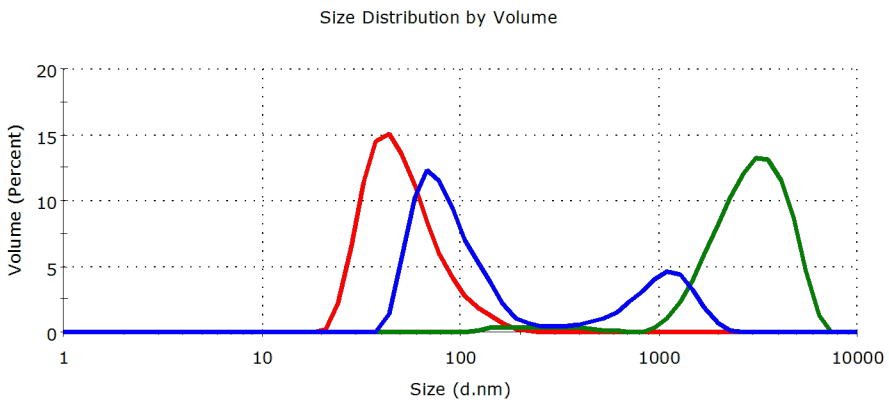

Figure 3: Aggregation effect of 0.1% NaCl on 0.02% nanoTiO$_2$ dispersion in the absence (green curve) and presence of CMBCD-P polymer (blue curve). The red curve shows the particle size distribution in the absence of destabilizing ions.

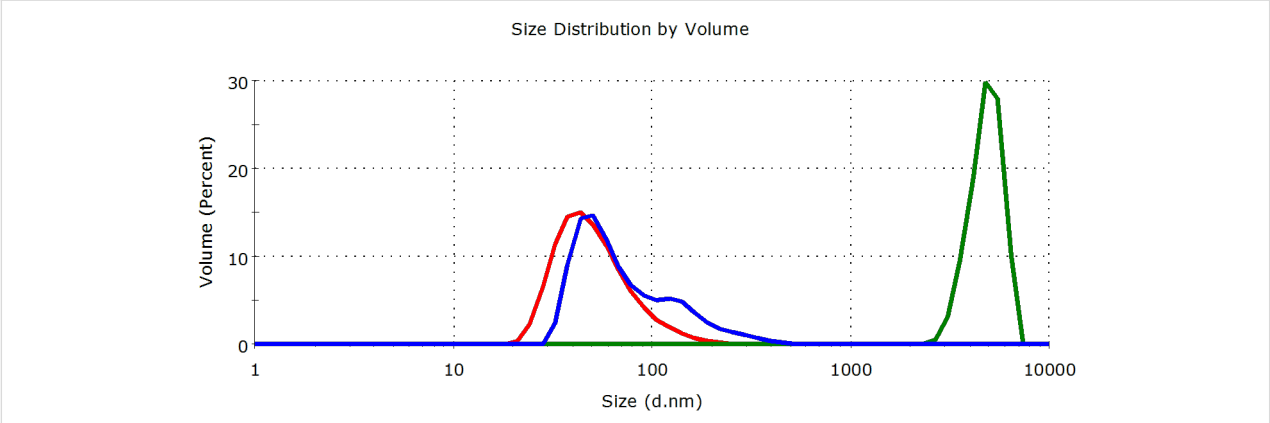

Figure 4: Aggregation effect of tap water on 0.02% nanoTiO2 dispersion in the absence (green curve) and presence of CMBCD-P polymer (blue curve). The red curve shows the particle size distribution in the absence of destabilizing ions.

In tap water, the stability of nanoTiO$_2$ is similarly diminished as observed for 0.1% NaCl. The mean particle size increased to 4880 nm. It is notable that CMBCD-P proved to be more effective in this medium than in 0.1% NaCl solution. The initial particle size distribution of nanoTiO$_2$ was nearly preserved, the mean size increased only to 59 nm, however, the distribution profile became slightly wider and a shoulder peak at 168 nm appeared on the curve.

Photocatalytic effect of the CMBCD-P stabilized nanoTiO$_2$ dispersions

The photocatalytic effect of nanoTiO$_2$ on the decomposition of two model contaminants: a dye (methylene blue, MB) and a drug (ibuprofen, IBR) was studied in various media (distilled water, NaCl solution and tap water) in the presence and absence of the polymer. The concentrations of the model compounds were measured as a function of time and the half-life time values were calculated to characterize the reaction rate of the degradation. For comparison, the decomposition of the model compounds was measured also without any additives and in the presence of CMBCD-P only. The results for MB are summarized in Figure 5 and Table 3.

Interestingly, without catalyst MB was decomposed faster in tap water than in distilled water most probably due to the small concentration of iron present. Fe(III) and organic carboxylic acid, which coexist in natural environments, can set up a photo-Fenton system with H_2O_2 produced in situ generating OH radicals of high oxidizing capacity [42,43]. Nitrate could also produce OH radicals when absorbing UV light, but the low concentration of nitrate in tap water can insignificantly contribute to enhancing photodegradation.

The polymer itself showed some catalytic effect: the rate of degradation of MB was slightly increased in all the three media

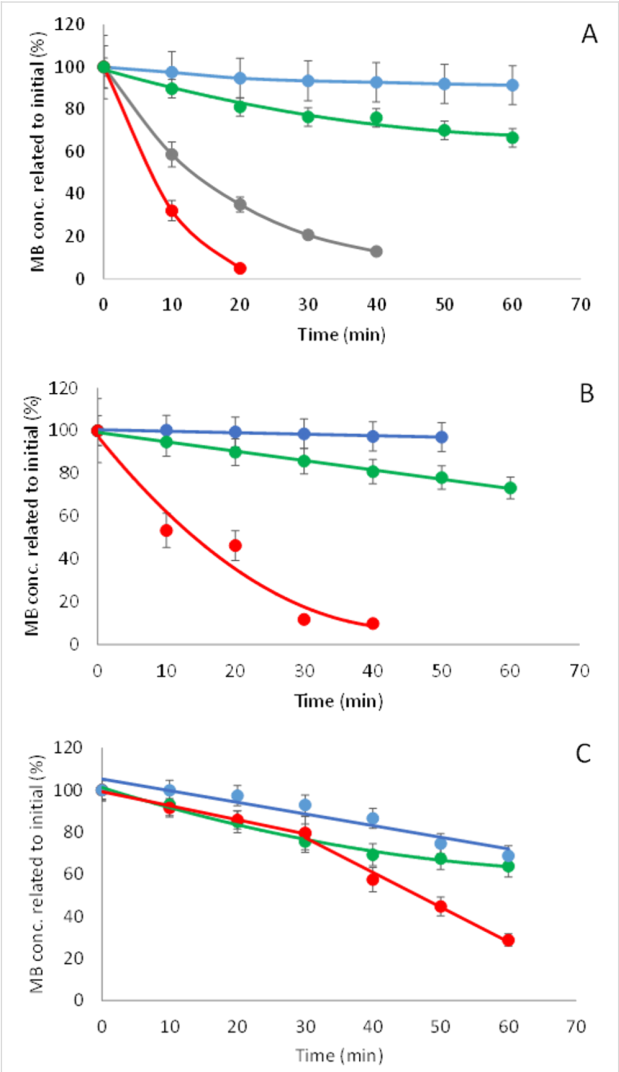

Figure 5: Photodegradation of MB in aqueous solutions: distilled water (A), 0.1% NaCl solution (B) and tap water (C) examining the dye itself (blue), in the presence of 1% CMBCD-P (green), of 0.02% nanoTiO$_2$ (grey) and 0.02% nanoTiO$_2$ stabilized by 1% CMBCD-P (red).

Table 3: Half-life time (min) of photodegradation of MB in aqueous solutions in the absence and presence of CMBCD-P (1%), nanoTiO$_2$ (0.02%) and nanoTiO$_2$ (0.02%) stabilized by CMBCD-P (1%).

Medium	MB	MB + CMBCD-P	MB + nanoTiO$_2$	MB + nanoTiO$_2$ + CMBCD-P
Distilled water	495 ± 45	108 ± 11	13.5 ± 2.5	4.6 ± 0.5
NaCl solution (0.1%)	990 ± 70	136 ± 12	precipitation	11.3 ± 1.3
Tap water	107 ± 10	88.8 ± 7	precipitation	94.2 ± 0.5 (phase 1) 24.6 ± 3.6 (phase 2)

resulting in the shortest half-life time in tap water similarly to the dye alone.

The catalytic effect of nanoTiO$_2$ itself could be measured only in distilled water, as both in NaCl solution and in tap water it was precipitated if not stabilized by CMBCD-P. In any media studied the reaction rate followed the order of: no additive < CMBCD-P < nanoTiO$_2$ < nanoTiO$_2$/CMBCD-P.

Applying the nanoTiO$_2$ stabilized by the polymer synergistic effect was observed in distilled water. In NaCl solution the rate of decomposition was lower partly attributed to adsorption of chloride on TiO$_2$ surface. There might be a competition between dyes and anions for the adsorption sites and the anions may modify the superficial properties of TiO$_2$ [44]. The total concentration of inorganic ions in tap water is much lower than 0.1%, therefore this competition for the sorption sites is probably less pronounced even if we take into account that hydrogencarbonate, hydrogenphosphate and sulfate ions hinder the MB adsorption in a higher extent compared to chloride [44].

The nanoTiO$_2$ stabilized by the polymer showed peculiar behavior in tap water: MB was decomposed in two distinct phases. In the first 30 min a slow degradation was observed (similar to that observed with the polymer only) and it was followed by fast decomposition (Figure 5 and Table 3). Similar two-stage degradation was observed for the photocatalytic decomposition of pharmaceutical residues, such as carbamazepine and ibuprofen in wastewater with TiO$_2$ catalyst [42,45]. It was proved that the natural organic matter (NOM) which are the humic substances present in surface waters and tap water had an initial inhibiting effect: after the decomposition of NOM the drug degradation was enhanced [42,45]. The tap water (our test solution) also contained some dissolved organic components (1–2 mg/L) and this would explain our observation.

A different behavior was witnessed in the case of ibuprofen in our experiments. This drug was slowly decomposed in distilled water without any additives (Figure 6 and Table 4) and a slight enhancement in the degradation rate was obtained with nanoTiO$_2$. In the presence of the polymer the rate of degradation decreased suggesting that the complex formation of ibuprofen has a protective effect. Using the CMBCD-P-stabilized nanoTiO$_2$ as additive hardly any decrease in the drug concentration upon UV irradiation was measured especially in tap water.

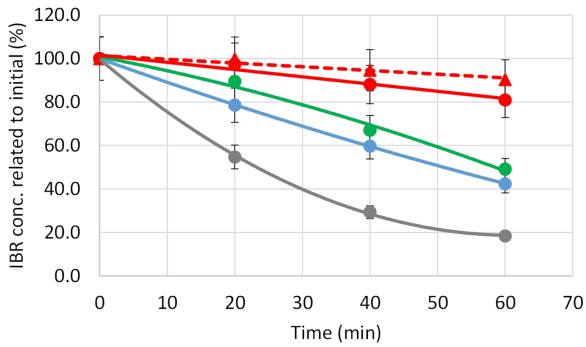

Figure 6: Photodegradation of IBR in distilled water examining the drug itself (blue circle), and in the presence of 1% CMBCD-P (green circle), of 0.02% nanoTiO$_2$ (grey circle), 0.02% nanoTiO$_2$ stabilized by 1% CMBCD-P (red circle), and 0.02% nanoTiO$_2$ stabilized by 1% CMBCD-P in tap water (red triangle).

It is well-known that the complexation often has a protective effect on the included guest molecules [8]. Either catalysis or

Table 4: Half life time (min) of photodecomposition of IBR in distilled and tap water.

Medium	IBR	IBR + CMBCD-P	IBR + nanoTiO$_2$	IBR + nanoTiO$_2$ + CMBCD-P
Distilled water	31 ± 13	61 ± 18	25 ± 6	201 ± 56
Tap water	no data	no data	precipitation	331 ± 54

inhibition of the light-induced cleavage can occur depending on the conformation of the host–guest complex (if the light-sensitive part of the molecule is located within or outside of the cavity), on the complex association constant and on the concentration ratio of the guest to the CD. It was shown that the photodecomposition of MB was enhanced by stabilizing Ag/TiO_2 nanoparticles with β-CD, but applying β-CD in excess the rate of degradation decreased dramatically [46]. The association constant of IBR/β-CD complex falls in the range of 10^3–10^4 M^{-1} [47,48], while that of MB/β-CD is less than 10^3 M^{-1} [49,50]. According to NMR studies IBR is deeply included into the cavity [51], while MB is too large to be completely shielded by complexation. The too strong association between IBR and the cavities of CMBCD-P can be a possible reason of protection instead of catalytic decomposition in this process. Further experiments are needed to clarify why enhanced protection was observed when the polymer was present together with TiO_2.

In order to check if the polymer itself is degraded similarly to the model pollutants as a control experiment, the CMBCD-P solution with and without nanoTiO_2 was irradiated under identical conditions as the photodegradation of the pollutants. Size exclusion chromatography (HPLC) was used to characterize the composition of the polymer. This method enables to discriminate between the smaller and larger components and to monitor the degradation of the polymer. The chromatograms of the samples before and after irradiation match within the experimental error proving that no significant change in the polymer structure occurred upon UV light irradiation even in the presence of nanoTiO_2 under the applied conditions (irradiation for 1 h). Lannoy et al. published the photodegradation of toluene in the presence of nanoTiO_2 stabilized by native β-cyclodextrin and its random methylated derivative (BCD and RAMEB, respectively.) [36]. In the first hour 88% and 97% of the initial CD concentration was measured by phenolphthalein complexation, respectively, and 34% and 18% of these CDs were degraded in 5 hours. These results show that the substituted CDs are of higher stability compared to the unsubstituted one. The CMBCD-P is an epichlorohydrin-crosslinked polymer with the number of substituents/CD of approximately 10 (in RAMEB ≈12). Although the conditions of the photodegradation experiments published by Lannoy [36] are different from ours, the <5% degradation of CMBCD-P within 1 h seems to be in agreement with 3% degradation of RAMEB within the same time period. Further experiments are needed to reveal the fate of CMBCD-P during longer irradiation.

Conclusion

We have successfully selected a potential stabilizing agent, carboxymethyl β-cyclodextrin polymer for improving the colloidal stability of nanosized TiO_2. Dynamic light scattering measurements proved that the aggregation of TiO_2 nanoparticles was hindered by the presence of this polymer additive. Studying its influence on the photocatalytic effect on nanosized TiO_2 on one hand a synergistic photocatalytic effect was observed for photodecomposition of the methylene blue in tap water, on the other hand a protective effect of CMBCD-P was observed for the ibuprofen degradation. The efficiency of the CMBCD-P-stabilized nanosized TiO_2 photocatalytic system will be studied on further model compounds selected among the emerging pollutants.

Experimental

Materials

Applying the procedure of CycloLab Ltd. Budapest Hungary a dispersion of 9.96% nanoTiO_2 has been prepared from the Degussa-Evonik (Japan) titanium dioxide sample (Aeroxide P90 consisting of anatase 90% and rutile 10% with a specific surface area of 90–100 m^2/g and mean particle size 14 nm**)**. This dispersion (pH was about 2) was diluted to 0.02% for the experiments. The cyclodextrins characterized by the degree of substitution (DS) in the case of monomers and by the CD content in the case of polymers (Table 5) are all CycloLab's

Table 5: Cyclodextrins used during the experiments.

	Abbreviation	Characteristics	Average molecular weight (M_w)[a]
hydroxypropyl-β-cyclodextrin	HPBCD-M	DS ≈4,2	1.38 kDa
hydroxypropyl-β-cyclodextrin polymer crosslinked with epichlorohydrin	HPBCD-P	CD content: ≈65–70%	90 kDa; 200 kDa; 300 kDa
carboxymethyl-β-cyclodextrin	CMBCD-M	DS ≈4	1.36 kDa
carboxymethyl-β-cyclodextrin-polymer crosslinked with epichlorohydrin	CMBCD-P	DS 2–3; CD content: ≈65–70%	33 kDa
quaternary ammonium β-cyclodextrin polymer crosslinked with epichlorohydrin	QABCD-P	DS ≈0.2 CD content: ≈65–70%	≈6 kDa

[a]For monomers it is calculated, for polymers data were obtained by static light scattering.

products. The DS and the CD content were determined by NMR as described earlier [52]. The molecular weights were determined by static light scattering as described by Puskás et al. [53]. The salts (NaCl, $CaCl_2$, $MgCl_2$, Na_2CO_3, Na_2SO_4), NaOH and the model pollutants (methylene blue, MB and ibuprofen, IBR) are analytical grade chemicals purchased from Molar (Hungary).

Composition of tap water

The tap water in the district where the laboratory is located contains the following minerals according to the Budapest Potable Water Analysis [54]: Cl^- 21 mg/L, Na 11 mg/L, Ca^{2+} 60 mg/L, SO_4^{2-} 27 mg/L, HCO_3^- 150 mg/L, NO_3^- 5 mg/L, orthophosphate <5 mg/L. The electric conductivity is 480 μS/cm and pH 7.5. Total organic carbon content (TOC) 1–2 mg/L.

Methods

Turbidity measurements

Turbidity of the nanoTiO_2 dispersions was measured at 410 nm by Agilent 8453 spectrophotometer. The samples were measured in glass cuvettes of 1 cm.

Determinations of moisture content

The moisture content of the CMBCD-P has been determined using a 'Karl Fischer V20' type auto-titration device (Mettler Toledo).

Light scattering measurements

Determination of average molecular weight by static light scattering: The average molecular weight of the water-soluble polymers has been determined by static light scattering method using a Malvern Zetasizer Nano Series ZS device manufactured by Malvern Instruments Ltd., UK. The analysis was performed as described elsewhere [53].

Particle size analysis by dynamic light scattering: Determination of the particle size distribution of the nanoTiO_2 particles and aggregates was performed by dynamic light scattering method (also known as photon correlation spectroscopy) using a Malvern Zetasizer Nano ZS instrument using a He-Ne laser of 4 mW power and 633 nm wavelength and avalanche photodiode detector. Triplicate measurements were carried out for all samples, each averaged of at least 10 runs at 25 °C. The volume size distribution was utilized for aggregate state analysis.

Photodegradation experiments

The degradation of methylene blue and ibuprofen was studied using an optical bench with medium pressure mercury-vapor lamp of 200 W (Tunsgram, Hungary) emitting mainly in the UV-A range. The light was focused by an optical lens on the quartz cuvette containing the sample. The concentration of MB and IBR was measured by spectrophotometry and by HPLC, respectively. The presence of polymer did not affect the spectrophotometric determination. The concentration of MB and IBR solutions was set to 20 and 50 μM, respectively before irradiation.

The half-life time was calculated postulating first order rate kinetics. Representing the concentration of MB or IBR in natural logarithmic scale as a function of time linear relationships were obtained proving the first order kinetics of degradation. The regression coefficients were in the range of 0.98–1.00. Three parallel measurements were evaluated.

Determination of methylene blue concentration

The concentration of the dye was measured by spectrophotometry using Agilent 8453 spectrophotometer at $\lambda = 664$ nm using 750 nm as reference.

Determination of ibuprofen concentration by HPLC

An Agilent 1100 HPLC system equipped with a diode array detector (254 nm) was used with a Waters ODS C18 (250 mm × 4.6 mm, 5 μm) analytical column and elution with 45% acetonitrile and 0.05% formic acid in water at a flow rate of 1.0 mL/min. The column temperature was set to 40 °C. The samples were diluted with 50% acetonitrile in 1:1 ratio before injecting 5 μL.

Characterization of the molecular weight distribution by HPLC

The same equipment was used with refractive index detector and TSK gel G2000SW silicagel based column (TosoHaas) (7.5 × 300 mm, 10 μm (molecular weight ranges: 1–30 kDa)), and guard column (7.5 × 75 mm) for size exclusion chromatography of CMBCD-P. The mobile phase (water, pH adjusted to 2.7 with cc. H_3PO_4) was eluted with 1 mL/min. The temperature of the column and of the RI detector was adjusted to 30 °C and 40 °C, respectively. The samples containing 10 mg/mL CMBCD-P were diluted to 5 mg/mL with the mobile phase and 20 μL was injected.

Acknowledgements

The authors thank to Katalin Csabai for the size exclusion chromatography of the polymer.

References

1. Matero-Sagasta, J.; Raschid-sally, L.; Thebo, A. Global Wastewater and Sludge Production, Treatment and Use. In *Wastewater. Economic Asset in an Urbanizing World;* Drechsel, P.; Qadir, M.; Wicheins, D., Eds.; Springer: Berlin, 2015; pp 15–38.

2. EIB Water and Waste water management. http://www.eib.org/projects/sectors/water-and-waste-water-management/index.htm (accessed July 27, 2016).
3. Petrie, B.; Barden, R.; Kasprzyk-Hordern, B. *Water Res.* **2015,** *72,* 3–27. doi:10.1016/j.watres.2014.08.053
4. US Environmental Protection Agency. https://www.epa.gov/wqc/contaminants-emerging-concern-including-pharmaceuticals-and-personal-care-products (accessed June 20, 2016).
5. WHO Information sheet. http://www.who.int/water_sanitation_health/emergencies/en/ (accessed June 20, 2016).
6. Nagy, Z. M.; Molnár, M.; Fekete-Kertész, I.; Molnár-Perl, I.; Fenyvesi, É.; Gruiz, K. *Sci. Total Environ.* **2014,** *485–486,* 711–719. doi:10.1016/j.scitotenv.2014.04.003
7. Jurecska, L.; Dobosy, P.; Barkács, K.; Fenyvesi, É.; Záray, G. *J. Pharm. Biomed. Anal.* **2014,** *98,* 90–93. doi:10.1016/j.jpba.2014.05.007
8. Szejtli, J.; Osa, T., Eds. *Cyclodextrins; Comprehensive Supramolecular Chemistry*, Vol. 3; Pergamon: Oxford, UK, 1996.
9. Fenyvesi, É.; Molnár, M.; Leitgib, L.; Gruiz, K. *Land Contam. Reclam.* **2009,** *17,* 585–597.
10. Villaverde, J.; Morillo, E. Remediation of contaminated soils and long-term risk assessment of organic residues by using cyclodextrins. In *Cyclodextrins in Pharmaceutics, Cosmetics, and Biomedicine;* Bilensoy, E., Ed.; John Wiley & Sons, Inc.: Hoboken, N. J., 2011; pp 199–233.
11. Crini, G.; Morcellet, M. *J. Sep. Sci.* **2002,** *25,* 789–813. doi:10.1002/1615-9314(20020901)25:13<789::AID-JSSC789>3.0.CO;2-J
12. Gruiz, K.; Molnár, M.; Fenyvesi, É.; Hajdu, C.; Atkári, A.; Barkács, K. *J. Inclusion Phenom. Macrocyclic Chem.* **2011,** *70,* 299–306. doi:10.1007/s10847-010-9909-y
13. Sawicki, R.; Mercier, L. *Environ. Sci. Technol.* **2006,** *40,* 1978–1983. doi:10.1021/es051441r
14. Ertas, Y.; Celebioglu, A.; Uyar, T. In *Abstract Book of 18th International Cyclodextrin Symposium,* Gainesville, Florida, May 19–21, 2016; p 91.
15. Chen, C.-Y.; Chen, C.-C.; Chung, C.-Y. *Bioresour. Technol.* **2007,** *98,* 2578–2583. doi:10.1016/j.biortech.2006.09.009
16. Forouharshad, M.; Putti, M.; Basso, A.; Prato, M.; Monticelli, O. *ACS Sustainable Chem. Eng.* **2015,** *3,* 2917–2924. doi:10.1021/acssuschemeng.5b00892
17. Alsbaiee, A.; Smith, B. J.; Xiao, L.; Ling, Y.; Helbling, D. E.; Dichtel, W. R. *Nature* **2016,** *529,* 190–194. doi:10.1038/nature16185
18. Furuta, T.; Ikefuji, S.; Tokunaga, K.; Neoh, T. L.; Yoshii, H. *J. Inclusion Phenom. Macrocyclic Chem.* **2007,** *57,* 21–27. doi:10.1007/s10847-006-9168-0
19. Cai, X.; Liu, Q.; Xia, C.; Shan, D.; Du, J.; Chen, J. *Environ. Sci. Technol.* **2015,** *49,* 9264–9272. doi:10.1021/acs.est.5b01734
20. Gaya, U. I.; Abdullah, A. H. *J. Photochem. Photobiol., C: Photochem. Rev.* **2008,** *9,* 1–12. doi:10.1016/j.jphotochemrev.2007.12.003
21. Chan, S. H. S.; Wu, T. Y.; Juan, J. C.; Teh, C. Y. *J. Chem. Technol. Biotechnol.* **2011,** *86,* 1130–1158. doi:10.1002/jctb.2636
22. Chakrabarti, S.; Dutta, B. K. *J. Hazard. Mater.* **2004,** *112,* 269–278. doi:10.1016/j.jhazmat.2004.05.013
23. Pitchaimuthu, S.; Rajalakshmi, S.; Kannan, N.; Velusamy, P. *Appl. Water Sci.* **2015,** *5,* 201–208. doi:10.1007/s13201-014-0181-y
24. Wang, G.; Wang, X.; Yu, R.; Deng, N. *Fresenius Environ. Bull.* **2008,** *17,* 1054–1060.
25. Wang, G.; Wu, F.; Zhang, X.; Luo, M.; Deng, N. *J. Chem. Technol. Biotechnol.* **2006,** *81,* 805–811. doi:10.1002/jctb.1513
26. Kamiya, M.; Nakamura, K.; Sasaki, C. *Chemosphere* **1994,** *28,* 1961–1966. doi:10.1016/0045-6535(94)90146-5
27. Glass, B. D.; Brown, M. E.; Daya, S.; Worthington, M. S.; Drummond, P.; Antunes, E.; Lebete, M.; Anoopkumar-Dukie, S.; Maharaj, D. *Int. J. Photoenergy* **2001,** *3,* 205–211. doi:10.1155/S1110662X01000277
28. Sortino, S.; Giuffrida, S.; De Guidi, G.; Chillemi, R.; Petralia, S.; Marconi, G.; Condorelli, G.; Sciuto, S. *Photochem. Photobiol.* **2001,** *73,* 6–13. doi:10.1562/0031-8655(2001)0730006TPOFAI2.0.CO2
29. Shen, J.; Li, N.; Ye, M. *J. Alloys Compd.* **2013,** *580,* 239–244. doi:10.1016/j.jallcom.2013.05.090
30. Sharavath, V.; Sarkar, S.; Gandla, D.; Ghosh, S. *Electrochim. Acta* **2016,** *210,* 385–394. doi:10.1016/j.electacta.2016.05.177
31. Chalasani, R.; Vasudevan, S. *ACS Nano* **2013,** *7,* 4093–4104. doi:10.1021/nn400287k
32. Hashimoto, K.; Irie, H.; Fujishima, A. *Jpn. J. Appl. Phys.* **2005,** *44,* 8269–8285. doi:10.1143/JJAP.44.8269
33. Willner, I.; Eichen, Y. *J. Am. Chem. Soc.* **1987,** *109,* 6862–6863. doi:10.1021/ja00256a056
34. Zhang, X.; Wu, F.; Deng, N. *J. Hazard. Mater.* **2011,** *185,* 117–123. doi:10.1016/j.jhazmat.2010.09.005
35. Willner, I.; Eichen, Y.; Willner, B. *Res. Chem. Intermed.* **1994,** *20,* 681–700. doi:10.1163/156856794X00487
36. Lannoy, A.; Kania, N.; Bleta, R.; Fourmentin, S.; Machut-Binkowski, C.; Monflier, E.; Ponchel, A. *J. Colloid Interface Sci.* **2016,** *461,* 317–325. doi:10.1016/j.jcis.2015.09.022
37. Fenyvesi, E. *Cyclodextrin News* **2014,** *28,* 1–9.
38. Subramanian, R.; Sakthivel, P.; Nagarathinam, K.; Ponnusamy, V. *Appl. Water Sci.* **2014,** 1–14.
39. Gao, Z.; Mi, Y.; Gao, L. Titania photocatalyst bonded with carboxymethyl-beta-cyclodextrin. Chin. Pat. 1698961, Nov 23, 2005. *Chem. Abstr.* **2005,** *145,* 302705.
40. Evonic Industries: AEROXIDE®, AERODISP® and AEROPERL® Titanium Dioxide as Photocatalyst. Technical Information 1243. http://www.aerosil.com/sites/lists/RE/DocumentsSI/TI-1243-Titanium-Dioxide-as-Photocatalyst-EN.pdf (accessed July 27, 2016).
41. Aerodisp® product information. https://www.aerosil.com/www2/uploads/productfinder/VP-Disp-W-2730-X-EN.pdf (accessed July 27, 2016).
42. He, Y.; Sutton, N. B.; Rijnaarts, H. H. H.; Langenhoff, A. A. M. *Appl. Catal., B: Environ.* **2016,** *182,* 132–141. doi:10.1016/j.apcatb.2015.09.015
43. Feng, W.; Nansheng, D. *Chemosphere* **2000,** *41,* 1137–1147. doi:10.1016/S0045-6535(00)00024-2
44. Guillard, C.; Puzenat, E.; Lachheb, H.; Houas, A.; Herrmann, J.-M. *Int. J. Photoenergy* **2005,** *7,* 1–9. doi:10.1155/S1110662X05000012
45. Doll, T. E.; Frimmel, F. H. *Water Res.* **2005,** *39,* 403–411. doi:10.1016/j.watres.2004.09.016
46. Attarchi, N.; Montazer, M.; Toliyat, T. *Appl. Catal., A* **2013,** *467,* 107–116. doi:10.1016/j.apcata.2013.07.018
47. Reijenga, J. C.; Ingelse, B. A.; Everaerts, F. M. *J. Chromatogr. A* **1997,** *792,* 371–378. doi:10.1016/S0021-9673(97)00644-4
48. Mura, P.; Manderioli, A.; Bettinetti, G. P.; Bramanti, G. 1st World Meeting on Pharmaceutics, Biopharmaceutics and Pharmaceutical Technology, Budapest, Hungary, May 9–11, 1995; pp 595–596.

49. Hirai, H.; Toshima, N.; Uenoyama, S. *Bull. Chem. Soc. Jpn.* **1985,** *58,* 1156–1164. doi:10.1246/bcsj.58.1156
50. Scott, J.; Tidball, A.; Uitvlugt, J. M.; Lucia, M.; Griend, D. A. V.; Douglas, A.; Louters, L. L. *Biochimie* **2007,** *91,* 271–276. doi:10.1016/j.biochi.2008.10.003
51. Liu, W.; Zhang, Y.; Zhao, B. *J. Chin. Chem. Soc.* **2012,** *59,* 1155–1158. doi:10.1002/jccs.201200071
52. Malanga, M.; Bálint, M.; Puskás, I.; Tuza, K.; Sohajda, S.; Jicsinszky, L.; Szente, L.; Fenyvesi, É. *Beilstein J. Org. Chem.* **2014,** *10,* 3007–3018. doi:10.3762/bjoc.10.319
53. Puskás, I.; Szemjonov, A.; Fenyvesi, E.; Malanga, M.; Szente, L. *Carbohydr. Polym.* **2013,** *94,* 124–128. doi:10.1016/j.carbpol.2013.01.025
54. Budapest Potable Water Analysis (in Hungarian). http://www.egyutteuropaert.eu/wp-content/uploads/2013/01/Budapesti_ivovizvizsgalat.pdf (accessed Dec 7, 2016).

License and Terms

BEILSTEIN JOURNAL OF ORGANIC CHEMISTRY

Versatile synthesis of end-reactive polyrotaxanes applicable to fabrication of supramolecular biomaterials

Atsushi Tamura, Asato Tonegawa, Yoshinori Arisaka and Nobuhiko Yui*

Full Research Paper

Open Access

Address:
Department of Organic Biomaterials, Institute of Biomaterials and Bioengineering, Tokyo Medical and Dental University, 2-3-10 Kanda-Surugadai, Chiyoda, Tokyo 101-0062, Japan

Email:
Nobuhiko Yui* - yui.org@tmd.ac.jp

* Corresponding author

Keywords:
azide group; biomaterials; click chemistry; cyclodextrin; polyrotaxane

Beilstein J. Org. Chem. **2016,** *12,* 2883–2892.
doi:10.3762/bjoc.12.287

Received: 26 September 2016
Accepted: 15 December 2016
Published: 28 December 2016

This article is part of the Thematic Series "Superstructures with cyclodextrins: Chemistry and applications IV".

Guest Editor: G. Wenz

Abstract

Cyclodextrin (CD)-threaded polyrotaxanes (PRXs) with reactive functional groups at the terminals of the axle polymers are attractive candidates for the design of supramolecular materials. Herein, we describe a novel and simple synthetic method for end-reactive PRXs using bis(2-amino-3-phenylpropyl) poly(ethylene glycol) (PEG-Ph-NH_2) as an axle polymer and commercially available 4-substituted benzoic acids as capping reagents. The terminal 2-amino-3-phenylpropyl groups of PEG-Ph-NH_2 block the dethreading of the α-CDs after capping with 4-substituted benzoic acids. By this method, two series of azide group-terminated polyrotaxanes (benzylazide: PRX-Bn-N_3, phenylazide: PRX-Ph-N_3,) were synthesized for functionalization via click reactions. The PRX-Bn-N_3 and PRX-Ph-N_3 reacted quickly and efficiently with *p*-(*tert*-butyl)phenylacetylene via copper-catalyzed click reactions. Additionally, the terminal azide groups of the PRX-Bn-N_3 could be modified with dibenzylcyclooctyne (DBCO)-conjugated fluorescent molecules via a copper-free click reaction; this fluorescently labeled PRX was utilized for intracellular fluorescence imaging. The method of synthesizing end-reactive PRXs described herein is simple and versatile for the design of diverse functional PRXs and can be applied to the fabrication of PRX-based supramolecular biomaterials.

Introduction

Polyrotaxanes (PRXs) are a class of interlocked polymers that consist of an inclusion complex of cyclodextrins (CDs) and a linear axle polymer capped with bulky stopper molecules [1-3]. Because the threading CDs are associated along the polymer chain via non-covalent intermolecular interactions, they can move freely along the polymer chain. This free mobility of threading CDs in PRXs is attractive for the development of functional supramolecular materials [4-6]. In PRX applications, chemical modification of the threading CDs is important to reduce intermolecular interactions of the PRXs, impart solu-

bility in organic solvents and water, and introduce functional molecules [7-9]. In this regard, various methods of introducing functional groups at the threading CD moieties of PRXs are used. Among the various chemical modifications, the introduction of azide or alkynyl groups at the threading CDs of the PRX is particularly attractive, because these functional groups undergo efficient azide–alkyne Huisgen [2 + 3] dipolar cycloaddition reactions, or click reactions [10-12]. Indeed, our group has reported on PRXs bearing azide groups at the threading CDs for the introduction of ligands and fluorescent molecules in biomaterials applications [13,14].

PRXs bearing reactive azide or alkynyl groups at the terminals of the axle polymers have an attractive designs for the fabrication of biomaterials, because the terminal azide or alkynyl groups in the PRXs can be utilized for the modification of other polymer chains and functional molecules. In general, PRXs comprising an inclusion complex of a linear polymer and threading CDs are typically synthesized via a two-step reaction: the preparation of pseudopolyrotaxanes, and the subsequent modification of the end groups of an axle polymer using bulky stopper molecules to prevent CD dethreading [1-3]. For the synthesis of end-reactive PRXs, the introduction of reactive functional groups during the preparation of PRXs is both simple and convenient. However, although the capping of pseudopolyrotaxanes via click reactions between azide (or alkyne)-terminated axle polymers and bulky stoppers containing alkyne (or azide) groups is employed broadly [15-21], few have reported on the synthesis of PRXs bearing terminal azides or alkynes [22,23]. This is probably because of the difficulties in synthesizing sufficient amounts of bulky stopper molecules containing azide or alkynyl groups for the capping reaction.

Herein, we describe a simple synthesis method for end-reactive PRXs using commercially available 4-substituted benzoic acids. Typically, 4-substituted benzoic acids are unsuitable for the capping of pseudopolyrotaxanes because they are insufficiently bulky. In this study, bis(2-amino-3-phenylpropyl) poly(ethylene glycol) (PEG-Ph-NH_2) (**3**) was utilized as an axle polymer for the synthesis of end-reactive PRXs [24]. The terminal 2-amino-3-phenylpropyl groups in PEG-Ph-NH_2 allow the formation of a pseudopolyrotaxane with α-CDs and simultaneously contribute to increasing the bulkiness of the terminal stopper groups after the capping reaction. This allows us to synthesize PRXs using small stopper molecules (e.g., 4-substituted benzoic acids) that cannot block the dethreading of α-CDs themselves. In this study, the synthesis and characterization of PRXs bearing azide groups and their reactivity against model alkynes via copper-catalyzed click reactions are performed. Additionally, fluorescence labeling of the PRX and intracellular fluorescence imaging were performed as an example application.

Results and Discussion

Synthesis of azide-terminated PRXs using bis(2-amino-3-phenylpropyl) poly(ethylene glycol) and 4-substituted benzoic acids

To investigate whether PRXs could be obtained via 4-substituted benzoic acids, the end capping reaction of commonly utilized pseudopolyrotaxanes comprising bis(aminopropyl) PEG (PEG-NH_2) (**1**) and α-CD was performed using 4-azidobenzoic acid as a model compound (Scheme 1A).

The synthesis of PRXs was assessed with size exclusion chromatography (SEC) measurements in dimethyl sulfoxide (DMSO), in which the unreacted pseudopolyrotaxanes were readily dissociated into their constituent compounds. If PRXs were produced, the peak of the PRXs would be observed at an earlier elution volume than the PEG axle polymer (elution volume: 3.7 mL) or α-CD (elution volume: 4.5 mL) in the SEC chart. Figure 1 shows the SEC chart of the crude products of the PEG-NH_2/α-CD pseudopolyrotaxane treated with 4-(azidomethyl)benzoic acid (**2a**) in the presence of 4-(4,6-dimethoxy-1,3,5-triazin-2-yl)-4-methylmorpholinium chloride (DMT-MM). However, the PRX peak is not detected, presumably because of the dethreading of α-CDs, even though the terminal groups of the axle polymer are capped with **2a**. Therefore, **2a** is insufficient bulky to prevent the dethreading of CDs from PRXs. To achieve the synthesis of end-reactive polyrotaxanes using 4-substituted benzoic acids as capping reagents, it is necessary to increase the bulkiness of the terminal group of the axle polymer.

In this regard, we next performed the capping reaction of pseudopolyrotaxanes composed of bis(2-amino-3-phenylpropyl) PEG (PEG-Ph-NH_2) (**3**) as an axle polymer and threading α-CDs using the same 4-substituted benzoic acids (Scheme 1B). The reaction was performed in a heterogeneous system to prevent the dethreading of the α-CDs. The terminal 2-amino-3-phenylpropyl groups were introduced in **3** to increase the bulkiness after capping with **2a**. As a result of the capping reaction, the PRX peak is clearly observed at the elution volume of 3.3 mL in the SEC chart of the crude products (Figure 1). This result indicates that the successful synthesis of the end-reactive PRX (**4a**) was achieved by using **3** as an axle polymer. The yield of **4a** was determined to be 21.9% (calculated based on the molecular equivalents of the PEG axle). Many mechanisms can reduce the yield of PRXs including dethreading of CDs from the axle polymer in the process of the end capping reaction, the limited reaction efficiency of the stopper molecules in a heterogeneous system, and the loss of PRXs in the process of purification. Therefore, optimization of the reaction conditions and purification methods are required to increase the PRX yield.

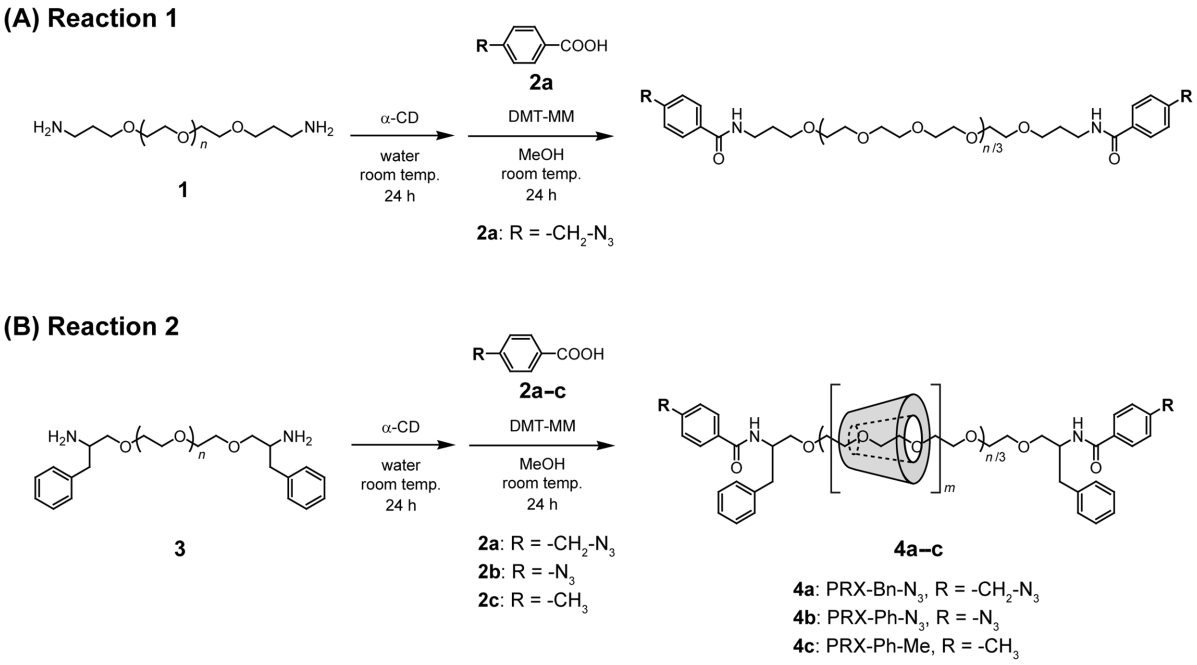

Scheme 1: Scheme for the end-capping of the PEG-NH_2 (**1**)/α-CD pseudopolyrotaxane with 4-(azidomethyl)benzoic acid (**2a**) (Reaction 1). Synthesis of end-reactive PRXs (**4a–c**) by the end-capping of the PEG-Ph-NH_2 (**3**)/α-CD pseudopolyrotaxane with **2a–c** (Reaction 2).

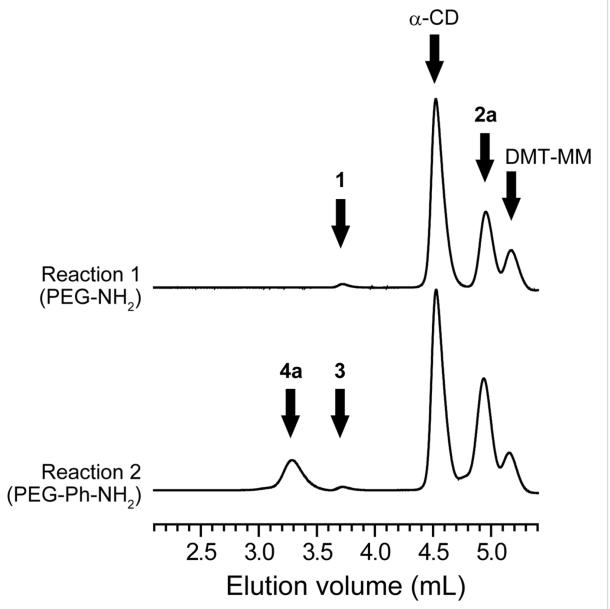

Figure 1: SEC charts for crude products of reaction 1 (upper chart) and 2 (lower chart).

Next, to investigate whether other 4-substituted benzoic acids can be used as capping reagents for the preparation of the PEG-Ph-NH_2/α-CD-based PRXs, the same capping reaction was demonstrated using 4-azidobenzoic acid (**2b**) and 4-methylbenzoic acid (**2c**). SEC charts of the resulting PRXs clearly demonstrated the successful synthesis of the PEG-Ph-NH_2/α-CD-based PRXs (**4a–c**) using **2b** and **2c** (Figure 2A). The chemical composition of the resulting PRXs is summarized in Table 1. The number of threading α-CDs in **4a–c** is almost equal among the products, suggesting that the chemical composition of the obtained PRXs is not affected by the capping reagents. Additionally, **4a–c** exhibit narrow molecular weight distributions (Table 1) and negligible contamination by free α-CDs (Figure 2A). According to these results, **3** is an optimal axle polymer to synthesize PRXs with a variety of 4-substituted benzoic acids.

To confirm the introduction of reactive azide groups at the terminals of PRX-Bn-N_3 (**4a**) and PRX-Ph-N_3 (**4b**), Fourier-transform infrared (FTIR) spectra of the obtained PRXs were measured (Figure 2B, expanded views of FTIR spectra are shown in Supporting Information File 1, Figure S1). In the FTIR spectrum of **4a**, the asymmetric stretching mode of the terminal benzylazide groups is clearly observed at 2102 cm^{-1} [25,26]. For **4b**, the symmetric and asymmetric stretching modes of the terminal phenylazide groups are observed at 2127 and 2092 cm^{-1}, respectively [27]. PRX-Ph-Me (**4c**) exhibits negligible peaks in this region. In addition, proton nuclear magnetic resonance (^{1}H NMR) spectra of **4a–c** are well characterized by the chemical structures of the products (Supporting Information File 1, Figure S2). These results clearly demonstrate the successful synthesis of PRXs with well-defined terminal structures.

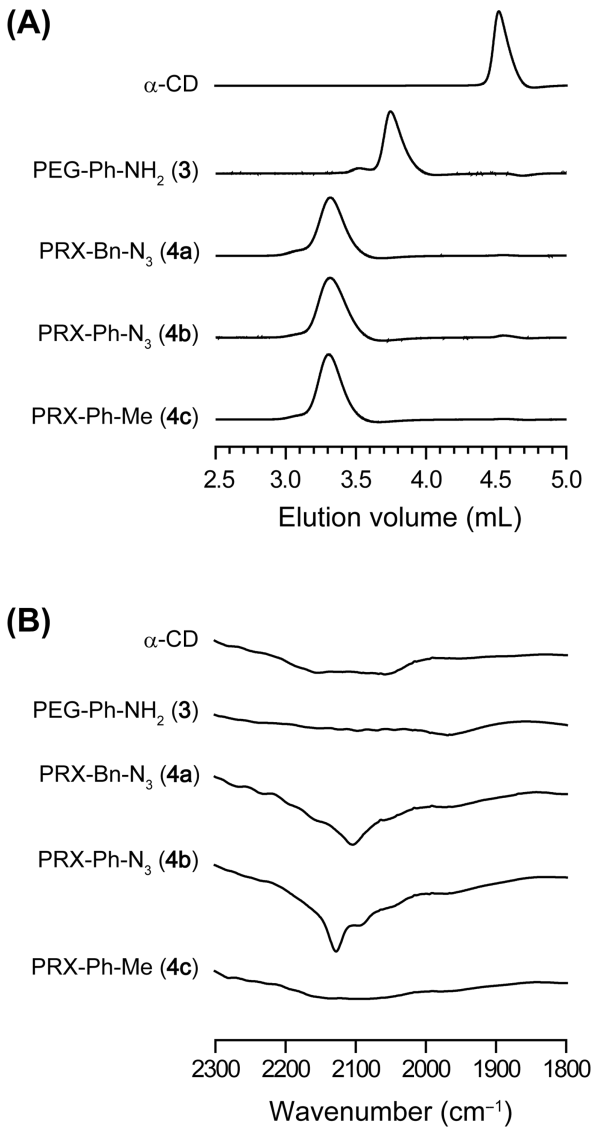

Figure 2: (A) SEC charts of α-CD, PEG-Ph-NH_2 (**3**), PRX-Bn-N_3 (**4a**), PRX-Ph-N_3 (**4b**), and PRX-Ph-Me (**4c**). (B) FTIR transmission spectra of α-CD, PEG-Ph-NH_2 (**3**), PRX-Bn-N_3 (**4a**), PRX-Ph-N_3 (**4b**), and PRX-Ph-Me (**4c**).

Reactivity of terminal azide groups in PRXs with alkynes via copper-catalyzed click reaction

The reactivity of the terminal azide groups of **4a** and **4b** with alkynes via the copper-catalyzed click reaction was examined. In this experiment, *p*-(*tert*-butyl)phenylacetylene was utilized as the model alkyne. One equivalent of *p*-(*tert*-butyl)phenylacetylene was allowed to react with the terminal azide groups of the PRXs in the presence of $CuSO_4$ and sodium ascorbate (Scheme 2). After 60 min of reaction, ^{1}H NMR spectra of the obtained products (**5a–c**) were measured (Figure 3A). In the ^{1}H NMR spectra of **5a** and **5b**, the protons assignable to 1,2,3-triazole linkages are observed at 8.5 and 9.4 ppm, respectively, which were consistent with the previous report [28]. These results suggest that the copper-catalyzed click reaction with *p*-(*tert*-butyl)phenylacetylene proceeds for both **4a** and **4b**. However, the ^{1}H NMR spectra of **4c** and **5c** are almost identical, despite the click reaction being conducted. This result indicates that the copper-catalyzed click reaction with *p*-(*tert*-butyl)phenylacetylene is selective for the terminal azide groups of **4a** and **4b**.

Next, the kinetics for the reaction between **4a**,**b** and *p*-(*tert*-butyl)phenylacetylene was investigated. Briefly, 1 mol equivalent of *p*-(*tert*-butyl)phenylacetylene was allowed to react with the terminal azide groups of the PRXs. The ratio of terminal azide groups in the PRXs reacted with *p*-(*tert*-butyl)phenylacetylene molecules was determined by ^{1}H NMR. This reveals that the copper-catalyzed click reaction between azide-terminated **4a**,**b** and *p*-(*tert*-butyl)phenylacetylene proceeds rapidly, reaching a plateau value within 60 min (Figure 3B). In addition, approximately 80% of azide groups reacted with *p*-(*tert*-butyl)phenylacetylene after 60 min, suggesting that the click reaction with the terminal azide groups of **4a,b** occurred quickly and efficiently. In general, aliphatic azide groups (i.e., benzylazide) are more reactive than aromatic azide groups (i.e., phenylazide) in the click reaction with alkynes [28]. In our experiments, **4a** and **4b** exhibited similar reaction efficiencies with *p*-(*tert*-butyl)phenylacetylene, but this may change with the reaction conditions and alkyne species.

Table 1: Reaction conditions and characterizations of the PRXs.

Sample code	Feed [α-CD]/[PEG-Ph-NH_2] molar ratio	Number of threading α-CDs[a]	$M_{n,NMR}$[b]	M_w/M_n[c]
PRX-Bn-N_3 (**4a**)	51.3	40.9 (36.7%)	50,100	1.12
PRX-Ph-N_3 (**4b**)	51.3	42.8 (38.4%)	51,900	1.14
PRX-Ph-Me (**4c**)	51.3	41.5 (37.3%)	50,700	1.13

[a]Determined by ^{1}H NMR in NaOD/D_2O. The values in parentheses denote the percentage of α-CD coverage on the PEG chain, assuming one α-CD molecule includes two repeating units of ethylene glycol. [b]Calculated based on the chemical composition of the PRXs determined by ^{1}H NMR. [c]Determined by SEC in DMSO containing 10 mM LiBr at 65 °C.

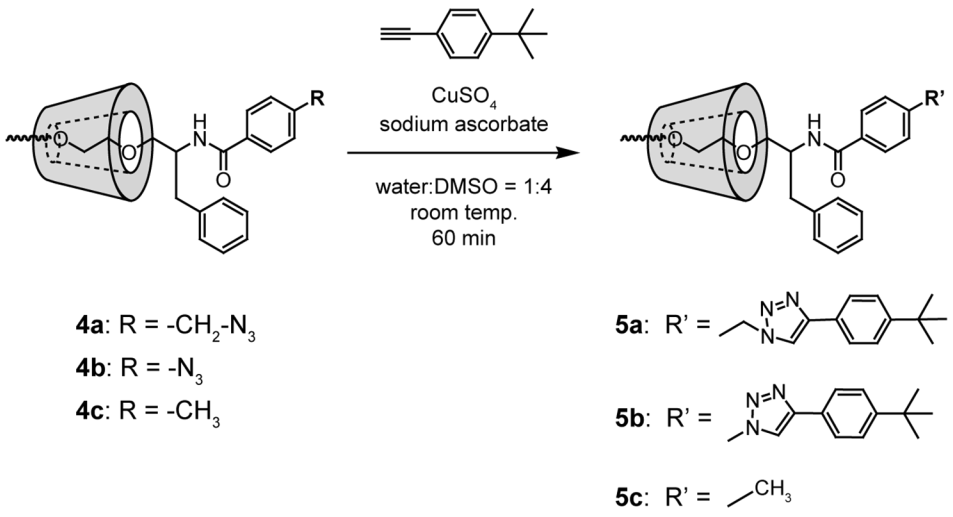

Scheme 2: End-group modification of **4a-c** with model alkyne via copper-catalyzed click reaction.

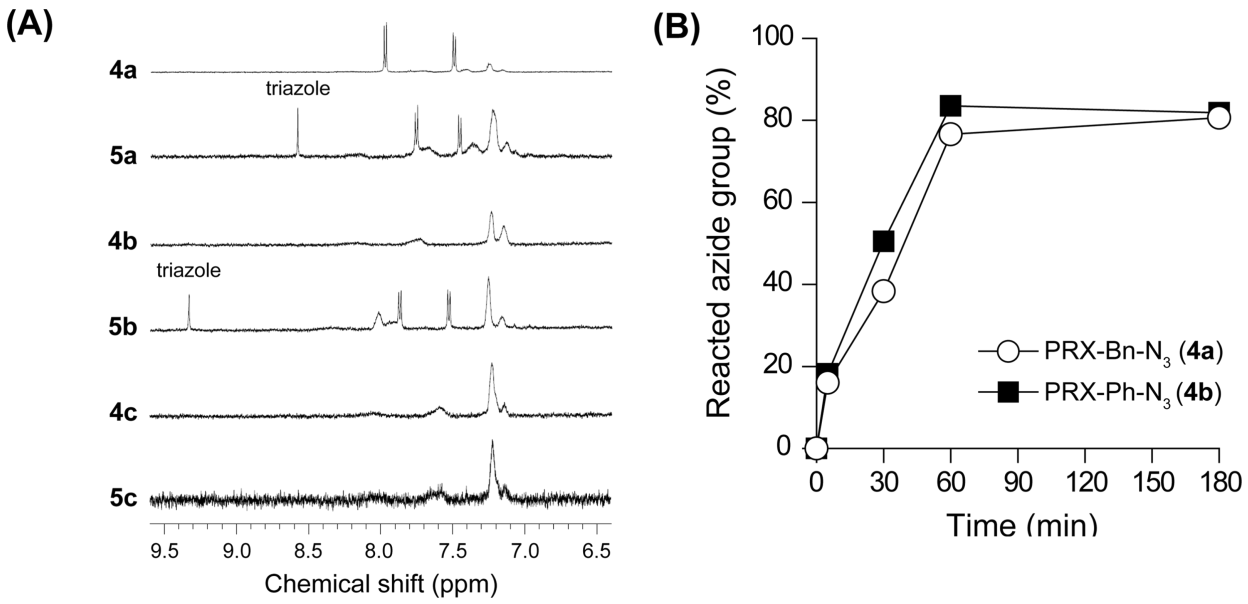

Figure 3: (A) ^{1}H NMR spectra of the PRXs before (**4a**, **4b**, **4c**) and after copper-catalyzed click reactions with *p*-(*tert*-butyl)phenylacetylene for 60 min (**5a**, **5b**, **5c**). Spectra were recorded in DMSO-d_6. (B) Time-course of click reaction between the azide-terminated PRXs (**4a**: open circles, **4b**: closed squares) and *p*-(*tert*-butyl)phenylacetylene.

End-group functionalization of PRXs for fluorescence imaging

Terminal reactive groups in the PRXs can be utilized in various biomaterials applications, such as the fabrication of cross-linked materials (e.g., hydrogels) [29], direct surface immobilization onto alkyne-immobilized surfaces [30], and the modification of other functional molecules for drug delivery [31]. Herein, alkynyl group-bearing fluorescent molecules were modified at the terminal azide group of the PRXs, and intracellular fluorescence imaging of the PRXs was performed to verify whether the terminally modified fluorescent molecules could be used for fluorescence imaging. First, **4a** was modified with 2-(2-hydroxyethoxy)ethyl (HEE) groups to impart water solubility, which was necessary for in vitro cellular experiments (Scheme 3) [32,33]. Then, the terminal benzylazide groups of HEE-PRX-Bn-N_3 (**6**) were modified with dibenzylcyclooctyne (DBCO)-conjugated fluorescent molecules (DF488) via a copper-free click reaction (Scheme 3) [34,35].

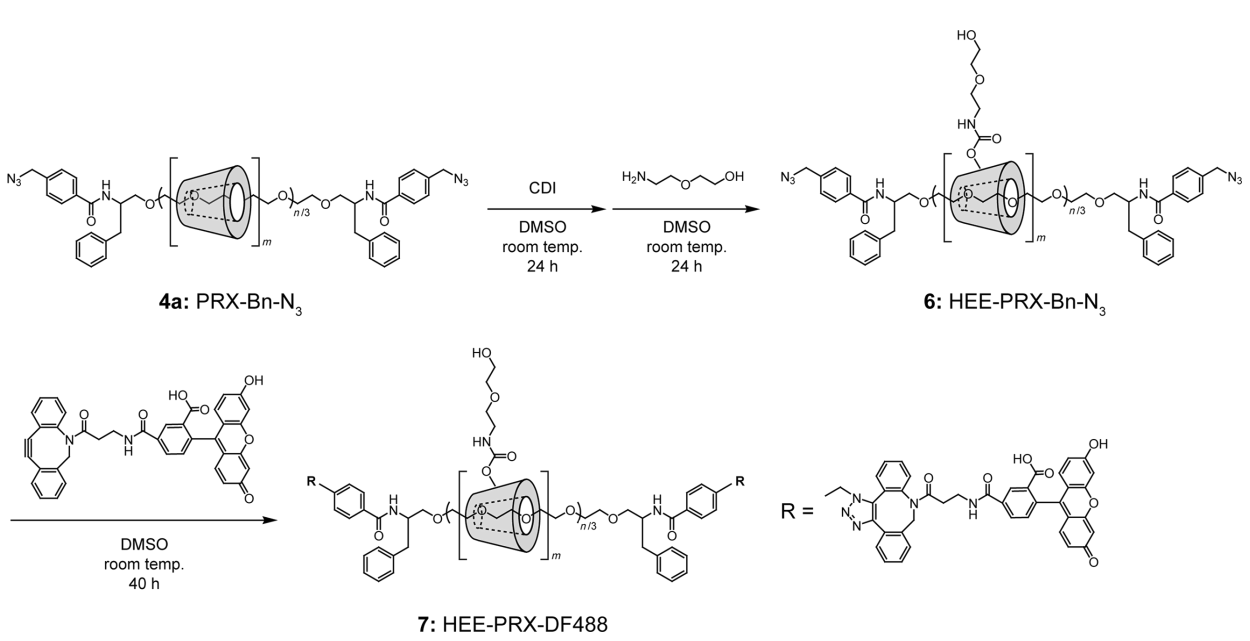

Scheme 3: Scheme of the synthesis of water-soluble PRX (**6**) and the following end group modification with copper-free click reaction (**7**).

After the modification, the introduction of DF488 at the terminal of **6** is confirmed by SEC measurements equipped with a fluorescence detector (Figure 4). Compound **6** exhibits negligible peaks in fluorescence detection, whereas a unimodal peak is observed in refractive index detection. Meanwhile, HEE-PRX-DF488 (**7**) exhibits a unimodal peak in both fluorescence and refractive index detection, clearly indicating the successful modification of the fluorescent molecules via the copper-free click reaction. Additionally, the terminal azide groups in **6** were almost entirely modified with fluorescent molecules.

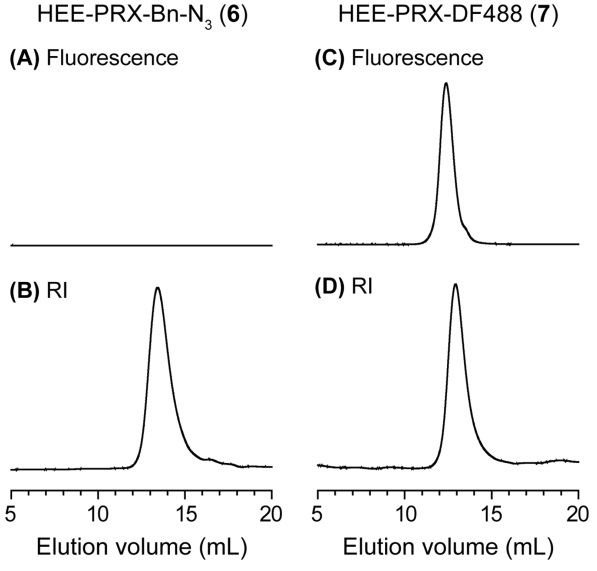

Figure 4: SEC charts of the HEE-PRX-Bn-N_3 (**6**) (A, B) and the HEE-PRX-DF488 (**7**) (C, D) monitored with fluorescence detector (excitation wavelength: 488 nm, emission wavelength: 515 nm) (A, C) and refractive index (RI) detector (B, D).

In our previous study relating to drug delivery applications of PRXs, fluorescent molecules were modified on the threading α-CDs in the PRXs to monitor intracellular uptake and localization of the PRXs [14,32,36,37]. To verify whether **7** could be utilized for monitoring the intracellular internalization of the PRXs, the intracellular uptake of **7** was investigated. HeLa cells were treated with **7** for 26 h, before observation by confocal laser scanning microscopy (CLSM) (Figure 5). The punctate **7** is clearly observed at the perinuclear region of the HeLa cells. The **7** puncta is highly co-localized with the LysoTracker Red, indicating that **7** was internalized into the cells via endocytosis and localized in acidic endosomes and lysosomes. This intracellular uptake pathway and localization of **7** is consistent with our previous reports [14,32,36,37]. Accordingly, we concluded that the terminal azide groups in **4a** can be utilized as installation moieties for fluorescent molecules to monitor intracellular fate of PRXs. Although the number of installation sites in the azide-terminated PRXs is limited to two, it is considered that the installation of two fluorescent molecules at the terminals of the PRX is sufficient for detecting the intracellular trafficking and biodistribution of PRXs by fluorescence microscopy [38]. In addition, the terminal azide groups in the PRXs can act as installation moieties for magnetic resonance imaging (MRI)

contrast agents and positron emission tomography (PET) probes for in vivo studies.

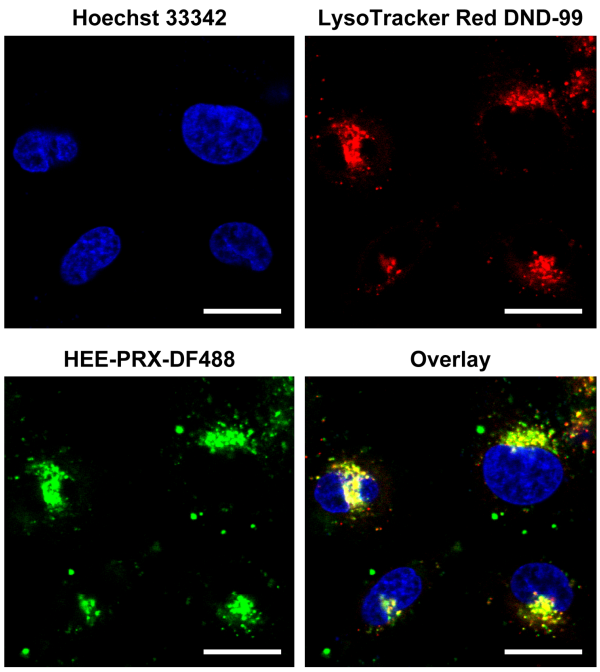

Figure 5: CLSM images of HeLa cells treated with HEE-PRX-DF488 (**7**) (500 μg/mL) for 26 h (scale bars: 20 μm). The acidic endosomes/lysosomes and nuclei are stained with LysoTracker Red DND-99 and Hoechst 33342, respectively.

Conclusion

In this study, we described a novel preparation method for end-reactive PRXs using **3** as an axle polymer for the PRXs. The terminal 2-amino-3-phenylpropyl groups of **3** prevent the dethreading of α-CDs after end-capping with 4-substituted benzoic acids such as **2a** and **2b**. The terminal azide groups of **4a** and **4b** exhibited fast and efficient reactions with *p*-(*tert*-butyl)phenylacetylene via a copper-catalyzed click reaction. In addition, the terminal azide groups of **4a** were modified with DBCO-conjugated fluorescent molecules via a copper-free click reaction. Finally, successful intracellular fluorescence imaging was achieved using the fluorescently labeled compound **7**. In addition to such fluorescent molecules, many functional molecules could be introduced at the terminal of the PRXs via copper-catalyzed or copper-free click reactions, including ligand molecules for active targeting, radioactive molecules for in vivo imaging, hydrophobic polymers for the surface immobilization of PRXs, and hydrophilic polymers for acquiring water solubility. Accordingly, the azide group-terminated end-reactive **4a** and **4b** are expected to be useful candidates in the fabrication or functionalization of supramolecular biomaterials, such as cross-linked hydrogels, surface immobilization, and drug delivery carriers for biomolecules [6]. Further studies relating to the biomaterials applications of azide group-terminated PRXs are currently underway in our laboratory and will be reported elsewhere.

Experimental

Materials

α,ω-Bis(2-amino-3-phenylpropyl) poly(ethylene glycol) (PEG-Ph-NH_2) (M_n = 10,060, M_w/M_n = 1.02) was synthesized according to our previous report [24]. α,ω-Bisaminopropyl PEG (PEG-NH_2) (M_n = 10,200, M_w/M_n = 1.03) was obtained from NOF Corporation (Tokyo, Japan). α-Cyclodextrin (α-CD) was obtained from Ensuiko Sugar Refining (Tokyo, Japan). 4-(Azidomethyl)benzoic acid was synthesized according to the previous report [27]. 4-Azidobenzoic acid, 4-methylbenzoic acid, *p*-(*tert*-butyl)phenylacetylene, and 2-(2-hydroxyethoxy)-ethylamine (HEEA) were obtained from TCI (Tokyo, Japan). 4-(4,6-Dimethoxy-1,3,5-triazin-2-yl)-4-methylmorpholinium chloride (DMT-MM) and copper(II) sulfate pentahydrate ($CuSO_4$) were obtained from Wako Pure Chemical Industries (Osaka, Japan). *N*,*N*'-Carbonyldiimidazole (CDI) and (+)-sodium L-ascorbate were obtained from Sigma-Aldrich (St. Louis, MO, USA). Dibenzocyclooctyne-fluor 488 (DF488) was obtained from Click Chemistry Tools (Scottsdale, AZ, USA). Other solvents were obtained from Kanto Chemicals (Tokyo, Japan).

Characterization of PRXs

SEC was performed out on an HLC-8120 system (Tosoh, Tokyo, Japan) equipped with a combination of TSKgel AW-4000 and AW-2500 columns (150 mm × 6 mm ID) (Tosoh), eluted with dimethylsulfoxide (DMSO) containing 10 mM LiBr at a flow rate of 0.15 mL/min at 65 °C. The polydispersity index (M_w/M_n) was calculated from a calibration curve of standard PEGs (Agilent Technologies, Wilmington, DE, USA). For SEC with fluorescence detection, the measurements were performed on a Gulliver system (Jasco, Tokyo, Japan) consisting of a DG-2080–53 degasser (Jasco), a PU-980 pump (Jasco), an AU-950 autosampler (Jasco), a CO-965 column oven (Jasco), an FP-920 fluorescence detector (excitation wavelength: 488 nm, emission wavelength: 515 nm) (Jasco), an RI-2031 Plus refractive index detector (Jasco), and a combination of TSKgel α-4000 and TSKgel α-2500 columns (300 mm × 7.8 mm ID) (Tosoh). The solutions (50 μL) were injected into the SEC system, and the system was eluted with a mixture of water and DMSO (volume ratio 50:50) at a flow rate of 0.3 mL/min at 40 °C. ^{1}H NMR spectra were recorded on a Bruker Avance III 500 MHz spectrometer (Bruker BioSpin, Rheinstetten, Germany). FTIR spectra were recorded on a Spectrum 100 FTIR spectrometer (Perkin Elmer, Wellesley, MA, USA). The sample powder was mixed with KBr and pellets were prepared for FTIR measurements.

Synthesis of benzylazide group-terminated PRX (**4a**)

PEG-Ph-NH_2 (300 mg, 29.9 μmol) dissolved in a small aliquot of water was added to the α-CD aqueous solution (10.3 mL, 145 mg/mL), and the mixture was stirred for 24 h at room temperature. After the reaction, the precipitate was collected by centrifugation and freeze-dried for 1 day to obtain a pseudopolyrotaxane as powder (yield 1.37 g). Then, 4-(azidomethyl)benzoic acid (106 mg, 597 μmol), DMT-MM (165 mg, 597 μmol), and the pseudopolyrotaxane were allowed to react in methanol (14 mL) for 24 h at room temperature. The precipitate was collected by centrifugation and washed three times with methanol, and then dissolved in DMSO and reprecipitated into water. This reprecipitation process was repeated until all free α-CD was removed. The recovered precipitate was dispersed into water and freeze-dried to obtain a benzylazide group-terminated PRX (**4a**) (327.9 mg, 21.9% yield based on PEG mol %). The number of threading α-CDs in **4a** was determined by ^{1}H NMR in DMSO-d_6. ^{1}H NMR (500 MHz, D_2O) δ 3.2–4.1 (m, PEG backbone and H_2, H_3, H_4, H_5, and H_6 protons of α-CD), 4.43 (s, -CH_2- of benzylazide), 4.95 (m, H_1 proton of α-CD), 7.2–7.3 (m, aromatics of benzyl group), 7.42 (d, aromatics of benzylazide), 7.59 (d, aromatics of benzylazide).

Synthesis of phenylazide group-terminated PRX (**4b**)

The PRXs capped with 4-azidobenzoic acid were synthesized as described above (48.8% yield based on PEG mol %). ^{1}H NMR (500 MHz, D_2O) δ 3.2–3.8 (m, PEG backbone and H_2, H_3, H_4, H_5, and H_6 protons of α-CD), 4.95 (m, H_1 proton of α-CD), 7.04 (d, aromatics of phenylazide), 7.1–7.3 (m, aromatics of benzyl group), 7.54 (d, aromatics of phenylazide).

Synthesis of 4-methylphenyl group-terminated PRX (**4c**)

The PRXs capped with 4-methylbenzoic acid were synthesized as described above (48.5% yield based on PEG mol %). ^{1}H NMR (500 MHz, D_2O) δ 2.28 (m, -CH_3 of methylphenyl group), 3.2–4.1 (m, PEG backbone and H_2, H_3, H_4, H_5, and H_6 protons of α-CD), 4.95 (m, H_1 proton of α-CD), 7.1–7.3 (m, aromatics of benzyl group and methylphenyl group), 7.43 (d, aromatics of methylphenyl group).

Reactivity of terminal azide groups in PRXs with alkynes via copper-catalyzed click reaction (**5a**, **5b**)

The typical procedure for investigating the reactivity of **4a** was as follows: **4a** (122.2 mg, 2.31 μmol of PRX, 4.62 mM of azide groups) and *p*-(*tert*-butyl)phenylacetylene (0.82 μL, 4.62 μmol, 1 mol equivalent to azide group in **4a**) were dissolved in DMSO (6.4 mL). Then, $CuSO_4$ (16.1 mg, 81.1 μmol) and sodium ascorbate (40.2 mg, 161 μmol) were dissolved in water (1.6 mL) and added to the reaction mixture (the concentration of $CuSO_4$ and sodium ascorbate in the reaction mixture were 10.1 mM and 20.1 mM, respectively). The reaction mixture was allowed to stir at room temperature. At prescribed time periods, an aliquot of the reaction mixture was collected (2 mL) and purified by dialysis against water for three days (molecular weight cut-off of 3500; Fast Gene, Nippon Genetics, Tokyo, Japan). The recovered solutions were freeze-dried to obtain the PRXs as powders. The ratio of terminal azide groups in **4a** reacted with *p*-(*tert*-butyl)phenylacetylene was calculated from the ^{1}H NMR peak area between 1.3 ppm (-C(CH_3) of *p*-(*tert*-butyl)phenylacetylene) and 4.8 ppm (H_1 proton of α-CD threading onto **4a**). ^{1}H NMR (500 MHz, DMSO-d_6) δ 1.29 (-C(CH_3)$_3$ of *tert*-butylphenyl group), 3.2–3.8 (m, PEG backbone and H_2, H_3, H_4, H_5, and H_6 protons of α-CD), 4.45 (m, O_6H of α-CD), 4.80 (m, H_1 of α-CD), 5.49 (m, O_3H of α-CD), 5.65 (m, O_2H of α-CD), 7.1–7.3 (m, aromatics derived from 2-amino-3-phenylpropyl group), 7.36 (br, aromatics derived from 4-(azidomethyl)benzoic acid), 7.46 (d, aromatics of *tert*-butylphenyl group), 7.68 (br, aromatics derived from 4-(azidomethyl)benzoic acid), 7.76 (d, aromatics of *tert*-butylphenyl group), 8.53 (s, triazole).

The same reaction was performed for **4b** and **4c** according to the above described procedure.

Synthesis of water-soluble benzylazide group-terminated PRX (**6**)

To solubilize **4a** into an aqueous solutions, 2-(2-hydroxyethoxy)ethyl (HEE) groups were modified onto the threading α-CDs of **4a** [28,29]. Briefly, **4a** (100 mg, 2 μmol of PRX, 81.6 μmol of α-CD) and CDI (132 mg, 816 μmol) were dissolved in dehydrated DMSO (5 mL), and the solution was stirred for 24 h at room temperature under a nitrogen atmosphere. Then, HEEA (81 μL, 816 μmol) was added to the reaction mixture and the solution was stirred for an additional 24 h at room temperature under a nitrogen atmosphere. After the reaction, the PRX was purified by dialysis against water for three days (molecular weight cut-off of 12,000–14,000, Fast Gene, Nippon Genetics). The recovered solution was freeze-dried to obtain **6** as powder (117.7 mg, 73.8% yield). The number of HEE groups in **6** was determined to be 226.6 by comparing the ^{1}H NMR peak area between 3.12 ppm (-NH-CH_2-CH_2-O- of HEE group) and 4.7–5.2 ppm (H_1 proton of α-CD). The M_n of **6** was determined to be 79,800 from the ^{1}H NMR. ^{1}H NMR (500 MHz, DMSO-d_6) δ 3.12 (m, -NH-CH_2-CH_2- of HEE group), 3.2–4.5 (m, PEG backbone and H_2, H_3, H_4, H_5, and H_6 protons of α-CD), 4.57 (m, O_6H of α-CD), 4.84 (m, H_1 of α-CD), 5.60 (m, O_2H and O_3H of α-CD), 7.04 (m, -NH-CH_2-CH_2- of HEE group), 6.9–7.3 (m, aromatics

derived from 2-amino-3-phenylpropyl group and 4-(azidomethyl)benzoic acid).

Terminal modification of **6** via copper-free click reaction

6 (46.2 mg, 576 nmol of PRX, 1.15 μmol of azide groups) and DF488 (1.0 mg, 6.36 μmol, 5.5 mol equivalent to azide group in the HEE-PRX-Bn-N_3) were dissolved in DMSO (4 mL) and the reaction mixture was allowed to stir for 40 h at room temperature. Then, the PRX was purified by dialysis against water for three days (molecular weight cut-off of 10,000, Thermo Fisher Scientific, Waltham, MA, USA). The recovered solutions were freeze-dried to obtain HEE-PRX-DF488 (**7**) as a yellow powder (43.2 mg, 92.0% yield). The degree of DF488 in the terminals of **7** was determined to be 96.1% by ^{1}H NMR spectroscopy. ^{1}H NMR (500 MHz, DMSO-d_6) δ 3.14 (m, -NH-CH_2-CH_2- of HEE group), 3.2–4.4 (m, PEG backbone and H_2, H_3, H_4, H_5, and H_6 protons of α-CD), 4.58 (m, O_6H of α-CD), 4.85 (m, H_1 of α-CD), 5.63 (m, O_2H and O_3H of α-CD), 7.05 (m, -N*H*-CH_2-CH_2- of HEE group), 6.4-8.8 (m, aromatics derived from 2-amino-3-phenylpropyl group, 4-(azidomethyl)benzoic acid, and DF488).

Cellular internalization

HeLa cells derived from human cervical carcinoma were obtained from the Japanese Collection of Research Bioresources (JCRB, Osaka, Japan). The cells were cultured in Dulbecco's modified Eagle's medium (DMEM) (Wako Pure Chemical Industries) containing 10% fetal bovine serum (FBS) (Sigma-Aldrich), 100 units/mL penicillin, and 100 μg/mL streptomycin (Wako Pure Chemical Industries) in a humidified 5% CO_2 atmosphere at 37 °C. HeLa cells were plated on 35 mm glass-bottom dishes (Iwaki, Tokyo, Japan) at a density of 1×10^4 cells/dish and incubated overnight. After the medium was exchanged with fresh DMEM (135 μL), the cells were treated with **7** (15 μL) (concentration: 500 μg/mL) for 26 h. Then, the cells were stained with LysoTracker Red DND-99 (Thermo Fisher Scientific) (500 nM) for 30 min, followed by staining with Hoechst 33342 (Dojindo Laboratories, Kumamoto, Japan) (1 μg/mL) for 10 min at 37 °C. CLSM images were acquired with a FluoView FV10i (Olympus, Tokyo, Japan) equipped with a 60x water-immersion objective lens (N/A 1.2) and a diode laser.

Supporting Information

Supporting Information File 1

FTIR and ^{1}H NMR spectra of the PRXs.
[http://www.beilstein-journals.org/bjoc/content/supplementary/1860-5397-12-287-S1.pdf]

Acknowledgements

This work was supported by the Grant-in-Aid for Scientific Research (A) from Japan Society for the Promotion of Science (JSPS) (No. 16H01852 to N.Y.): Grant-in-Aid for Challenging Exploratory Research from JSPS (No. 16K12893 to N.Y.).

References

1. Harada, A.; Li, J.; Kamachi, M. *Nature* **1992,** *356,* 325–327. doi:10.1038/356325a0
2. Harada, A.; Hashidzume, A.; Yamaguchi, H.; Takashima, Y. *Chem. Rev.* **2009,** *109,* 5974–6023. doi:10.1021/cr9000622
3. Wenz, G.; Han, B.-H.; Müller, A. *Chem. Rev.* **2006,** *106,* 782–817. doi:10.1021/cr970027+
4. Araki, J.; Ito, K. *Soft Matter* **2007,** *3,* 1456–1473. doi:10.1039/B705688E
5. Li, J.; Loh, X. J. *Adv. Drug Delivery Rev.* **2008,** *60,* 1000–1017. doi:10.1016/j.addr.2008.02.011
6. Tamura, A.; Yui, N. *Chem. Commun.* **2014,** *50,* 13433–13446. doi:10.1039/c4cc03709j
7. Inomata, A.; Sakai, Y.; Zhao, C.; Ruslim, C.; Shinohara, Y.; Yokoyama, H.; Amemiya, Y.; Ito, K. *Macromolecules* **2010,** *43,* 4660–4666. doi:10.1021/ma100259t
8. Araki, J.; Ito, K. *J. Polym. Sci., Part A: Polym. Chem.* **2006,** *44,* 6312–6323. doi:10.1002/pola.21717
9. Yui, N.; Katoono, R.; Yamashita, A. *Adv. Polym. Sci.* **2009,** *222,* 115–173. doi:10.1007/12_2008_8
10. Kolb, H. C.; Finn, M. G.; Sharpless, K. B. *Angew. Chem., Int. Ed.* **2001,** *40,* 2004–2021. doi:10.1002/1521-3773(20010601)40:11<2004::AID-ANIE2004>3.0.CO;2-5
11. Lutz, J.-F.; Zarafshani, Z. *Adv. Drug Delivery Rev.* **2008,** *60,* 958–970. doi:10.1016/j.addr.2008.02.004
12. Binder, W. H.; Sachsenhofer, R. *Macromol. Rapid Commun.* **2007,** *28,* 15–54. doi:10.1002/marc.200600625
13. Hyun, H.; Yui, N. *Macromol. Rapid Commun.* **2011,** *32,* 326–331. doi:10.1002/marc.201000631
14. Yokoyama, N.; Seo, J.-H.; Tamura, A.; Sasaki, Y.; Yui, N. *Macromol. Biosci.* **2014,** *14,* 359–368. doi:10.1002/mabi.201300198
15. Loethen, S.; Ooya, T.; Choi, H. S.; Yui, N.; Thompson, D. H. *Biomacromolecules* **2006,** *7,* 2501–2506. doi:10.1021/bm0602076
16. Zeng, K.; Zheng, S. *Macromol. Chem. Phys.* **2009,** *210,* 783–791. doi:10.1002/macp.200800605
17. Wu, J.; Gao, C. *Macromol. Chem. Phys.* **2009,** *210,* 1697–1708. doi:10.1002/macp.200900281
18. Wu, J.; He, H.; Gao, C. *Macromolecules* **2010,** *43,* 2252–2260. doi:10.1021/ma902255v
19. Yu, S.; Zhang, Y.; Wang, X.; Zhen, X.; Zhang, Z.; Wu, W.; Jiang, X. *Angew. Chem., Int. Ed.* **2013,** *52,* 7272–7277. doi:10.1002/anie.201301397
20. Jiang, L.; Ye, L.; Zhang, A.-y.; Feng, Z.-g. *Macromol. Chem. Phys.* **2014,** *215,* 1022–1029. doi:10.1002/macp.201400047
21. Yu, S.; Yuan, J.; Shi, J.; Ruan, X.; Wang, Y.; Gao, S.; Du, Y. *J. Mater. Chem. B* **2015,** *3,* 5277–5283. doi:10.1039/C5TB00627A
22. Dam, H. H.; Caruso, F. *ACS Nano* **2012,** *6,* 4686–4693. doi:10.1021/nn301045z
23. Tardy, B. L.; Dam, H. H.; Kamphuis, M. M. J.; Richardson, J. J.; Caruso, F. *Biomacromolecules* **2014,** *15,* 53–59. doi:10.1021/bm401244a

24. Tamura, A.; Tanaka, H.; Yui, N. *Polym. Chem.* **2014,** *5,* 4511–4520. doi:10.1039/c4py00379a
25. Akhrass, S. A.; Ostaci, R.-V.; Grohens, Y.; Drockenmuller, E.; Reiter, G. *Langmuir* **2008,** *24,* 1884–1890. doi:10.1021/la702984w
26. Jiang, J.; Wu, X.; Li, D.; Ma, B.; Liu, R.; Wang, X.; Zhang, J.; Zhu, H.; Cui, Q. *J. Phys. Chem. B* **2015,** *119,* 513–518. doi:10.1021/jp510178s
27. Shi, F.; Niu, J.; Liu, Z.; Wang, Z.; Smet, M.; Dehaen, W.; Qiu, Y.; Zhang, X. *Langmuir* **2007,** *23,* 1253–1257. doi:10.1021/la062391m
28. Wrobel, M.; Aubé, J.; König, B. *Beilstein J. Org. Chem.* **2012,** *8,* 1027–1036. doi:10.3762/bjoc.8.115
29. DeForest, C. A.; Anseth, K. S. *Nat. Chem.* **2011,** *3,* 925–931. doi:10.1038/nchem.1174
30. Yang, W. J.; Cai, T.; Neoh, K.-G.; Kang, E.-T.; Teo, S. L.-M.; Rittschof, D. *Biomacromolecules* **2013,** *14,* 2041–2051. doi:10.1021/bm400382e
31. Lallana, E.; Sousa-Herves, A.; Fernandez-Trillo, F.; Riguera, R.; Fernandez-Megia, E. *Pharm. Res.* **2012,** *29,* 1–34. doi:10.1007/s11095-011-0568-5
32. Tamura, A.; Yui, N. *J. Biol. Chem.* **2015,** *290,* 9442–9454. doi:10.1074/jbc.M115.636803
33. Tamura, A.; Nishida, K.; Yui, N. *Sci. Technol. Adv. Mater.* **2016,** *17,* 361–374. doi:10.1080/14686996.2016.1200948
34. Ning, X.; Guo, J.; Wolfert, M. A.; Boons, G. J. *Angew. Chem., Int. Ed.* **2008,** *47,* 2253–2255. doi:10.1002/anie.200705456
35. Jewett, J. C.; Bertozzi, C. R. *Chem. Soc. Rev.* **2010,** *39,* 1272–1279. doi:10.1039/B901970G
36. Tamura, A.; Yui, N. *Biomaterials* **2013,** *34,* 2480–2491. doi:10.1016/j.biomaterials.2012.12.006
37. Tamura, A.; Yui, N. *Sci. Rep.* **2014,** *4,* No. 4356. doi:10.1038/srep04356
38. Murakami, M.; Cabral, H.; Matsumoto, Y.; Wu, S.; Kano, M. R.; Yamori, T.; Nishiyama, N.; Kataoka, K. *Sci. Transl. Med.* **2011,** *3,* 64ra2. doi:10.1126/scitranslmed.3001385

License and Terms

BEILSTEIN JOURNAL OF ORGANIC CHEMISTRY

Synthesis of multi-lactose-appended β-cyclodextrin and its cholesterol-lowering effects in Niemann–Pick type C disease-like HepG2 cells

Keiichi Motoyama[1], Rena Nishiyama[1], Yuki Maeda[1,2], Taishi Higashi[1], Yoichi Ishitsuka[1], Yuki Kondo[1], Tetsumi Irie[1,2], Takumi Era[3] and Hidetoshi Arima[*1,2,§]

Full Research Paper

Open Access

Address:
[1]Graduate School of Pharmaceutical Sciences, Kumamoto University, 5-1 Oe-honmachi, Chuo-ku, Kumamoto 862-0973, Japan, [2]Program for Leading Graduate Schools "HIGO (Health life science: Interdisciplinary and Glocal Oriented) Program", Kumamoto University, 5-1 Oe-honmachi, Chuo-ku, Kumamoto 862-0973, Japan and [3]Department of Cell Modulation, Institute of Molecular Embryology and Genetics, Kumamoto University, 2-2-1 Honjo, Chuo-ku, Kumamoto 860-0811, Japan

Email:
Hidetoshi Arima[*] - arimah@gpo.kumamoto-u.ac.jp

* Corresponding author
§ Tel: +81 96 371 4160, Fax: +81 96 371 4160

Keywords:
asialoglycoprotein receptor; cholesterol; cyclodextrin; lactose; Niemann–Pick type C disease

Beilstein J. Org. Chem. **2017,** *13,* 10–18.
doi:10.3762/bjoc.13.2

Received: 24 September 2016
Accepted: 01 December 2016
Published: 03 January 2017

This article is part of the Thematic Series "Superstructures with cyclodextrins: Chemistry and applications IV".

Guest Editor: G. Wenz

Abstract

Niemann–Pick type C (NPC) disease, characterized by intracellular accumulation of unesterified cholesterol and other lipids owing to defects in two proteins NPC1 and NPC2, causes neurodegeneration and other fatal neurovisceral symptoms. Currently, treatment of NPC involves the use of 2-hydroxypropyl-β-cyclodextrin (HP-β-CD). HP-β-CD is effective in the treatment of hepatosplenomegaly in NPC disease, albeit at a very high dose. One of the methods to reduce the required dose of HP-β-CD for treatment of NPC is to actively targeting hepatocytes with β-cyclodextrin (β-CD). The aim of the present study was to synthesize a novel multi-lactose-appended β-CD (multi-Lac-β-CD) and to evaluate its cholesterol-lowering effect in U18666A-treated HepG2 (NPC-like HepG2) cells. Further, the study aimed at delivering β-CD to hepatocytes via cholesterol-accumulated HepG2 cells, and indicated that the newly synthesized multi-Lac-β-CD had an average degree of substitution of lactose (DSL) of 5.6. This newly synthesized multi-Lac-β-CD was found to significantly decrease the concentration of intracellular cholesterol with negligible cytotoxicity as compared to HP-β-CD. An increased internalization of TRITC-multi-Lac-β-CD (DSL 5.6) as compared to TRITC-HP-β-CD was observed in NPC-like HepG2 cells. Further, the dissociation constant of peanut lectin with multi-Lac-β-CD (DSL5.6) was found to be extremely low (2.5×10^{-8} M). These results indicate that multi-Lac-β-CD (DSL5.6) diminished intracellular cholesterol levels in NPC-like HepG2 cells via asialoglycoprotein receptor (ASGPR)-mediated endocytosis.

Introduction

The Niemann–Pick type C (NPC) disease is a lipid storage disorder with the accumulation of membrane lipids such as cholesterol and multiple sphingolipids especially in lysosomes. The excessive accumulation of these lipids results in a progressive neurologic and visceral dysfunction [1-3]. A mutation in the *NPC1* and/or *NPC2* gene causes the NPC disease. The majority of the mutations occur in the *NPC1* gene that produces NPC1 protein responsible for binding [3] and transporting of cholesterol to the endolysosomes [4,5]. Meanwhile the remaining mutations are located in the *NPC2* gene that encodes the NPC2 protein as a lysosomal protein. Excessive accumulation of cholesterol in endolysosomes in children, results in severe hepatosplenomegaly and neurodegeneration [3,6]. Hence, the sequestration of cholesterol is an important factor in the development of the NPC disease.

Cyclodextrins (CDs) are cyclic glucose oligosaccharides used by the pharmaceutical industry to enhance solubility, stability, and bioavailability of drugs. CDs improve the above properties of drugs through complex formation, when formulated as injectable solutions, sprays, eye drops, powders, and tablets [7,8]. In recent years, the efficacy of 2-hydroxypropyl-β-cyclodextrin (HP-β-CD) in the treatment of the NPC disease has attracted considerable attention [9,10]. Administration of HP-β-CD to *NPC1*-knockout ($Npc1^{-/-}$) mice significantly prolonged the survival rate by reducing the cholesterol levels [9-11]. In addition, therapeutic effects of HP-β-CD have been observed in mouse models of NPC disease. These studies have led to the initiation of two human clinical trials, a phase I/IIa trial in 2013 and a phase IIb/III trial in 2015, by the National Institutes of Health (NIH), USA. However, the administration of high doses of HP-β-CD is inevitable to obtain the effects in vivo because HP-β-CD cannot enter the cells owing to its hydrophilicity and relatively high molecular weight.

The asialoglycoprotein receptor (ASGPR), a hepatic galactose or *N*-acetylglucosamine (GlcNAc) receptor, is highly expressed on the sinusoidal cell surface of hepatocytes. ASGPR is responsible for the binding, internalization, and subsequent clearance of glycoproteins containing terminal galactose or GlcNAc residues from the circulation [12]. Hence, galactosylated nanocarriers have been utilized for the selective delivery of drugs to the liver via ASGPR-mediated endocytosis [13]. In fact, ASGPR-mediated endocytosis is one of the promising approaches for delivery of CDs into hepatocytes for the treatment of hepatosplenomegaly in NPC disease. In our previous report, monolactosylated β-CD (mono-Lac-β-CD) diminished the cholesterol accumulation in U18666A-treated HepG2 cells (NPC-like HepG2 cells), as a model of NPC hepatocytes, as much as HP-β-CD [14]. Further, ASGPR recognizes galactose moieties at three points, collectively known as the "golden triangle" [15,16]. However, as mono-Lac-β-CD can bind to only one point in the golden triangle of ASGPR, it has insufficient binding ability to ASGPR.

Consequently, in the present study, we synthesized a novel multi-lactose-appended β-CD (multi-Lac-β-CD) to enhance the targeting ability to ASGPR, and evaluated its cholesterol-lowering effect in NPC-like HepG2 cells.

Results and Discussion

Synthesis of multi-Lac-β-CD

In the present study, we fabricated multi-Lac-β-CD (**5**) to obtain a hepatocyte-specific cholesterol-lowering agent. The schematic representation of the synthesis of multi-Lac-β-CD (**5**) is shown in Figure 1. Briefly, *per*-NH_2-β-CD (**4**) was synthesized by chlorination (*per*-chloro-β-CD (**2**)) and azidation (*per*-azido-β-CD (**3**)) of primary hydroxy groups of β-CD **1**, as reported previously [17]. It may be possible to use *per*-iodo- or *per*-bromo-β-CD instead of *per*-chloro-β-CD. However, the iodo-β-CD may be unstable due to the too high reactivity. Therefore, we prepared *per*-chloro-β-CD with sufficient reactivity. Finally, lactose groups were inserted in *per*-amino-β-CD by treatment with cyanotrihydroborate in dimethyl sulfoxide (DMSO) at 90 °C for 24 h. The product yield of multi-Lac-β-CD was 25%, and no unreacted compounds were confirmed by thin-layer chromatography (TLC). The MALDI–TOF MS spectrum of multi-Lac-β-CD revealed several peaks at *m*/*z* 2804, *m*/*z* 3006, *m*/*z* 3139, *m*/*z* 3296, and *m*/*z* 3454, corresponding to tri-, tetra-, penta-, hexa- and hepta-lactose-substituted β-CDs, respectively (Figure 2A). Further, the ^{1}H NMR spectrum indicated that the degree of substitution of lactose (DSL) was 5.6. This value was obtained from the integral values of the anomeric protons of lactose and glucose in β-CD (Figure 2B). These results indicate the successful synthesis of multi-Lac-β-CD (DSL5.6).

Cytotoxicity of multi-Lac-β-CD (DSL5.6)

To evaluate the cytotoxicity of multi-Lac-β-CD (DSL5.6), cell viability was examined after treatment with multi-Lac-β-CD (DSL5.6) by the water-soluble tetrazolium (WST)-1 method (Figure 3). U18666A-treated HepG2 cells were used as NPC-like cells in this experiment because U18666A can inhibit cholesterol trafficking in cells and simulate NPC disease phenotypes [18]. No significant changes in cytotoxicity were observed in NPC-like HepG2 cells after treatment with 0.01–1 mM multi-Lac-β-CD (DSL5.6) for 24 h.

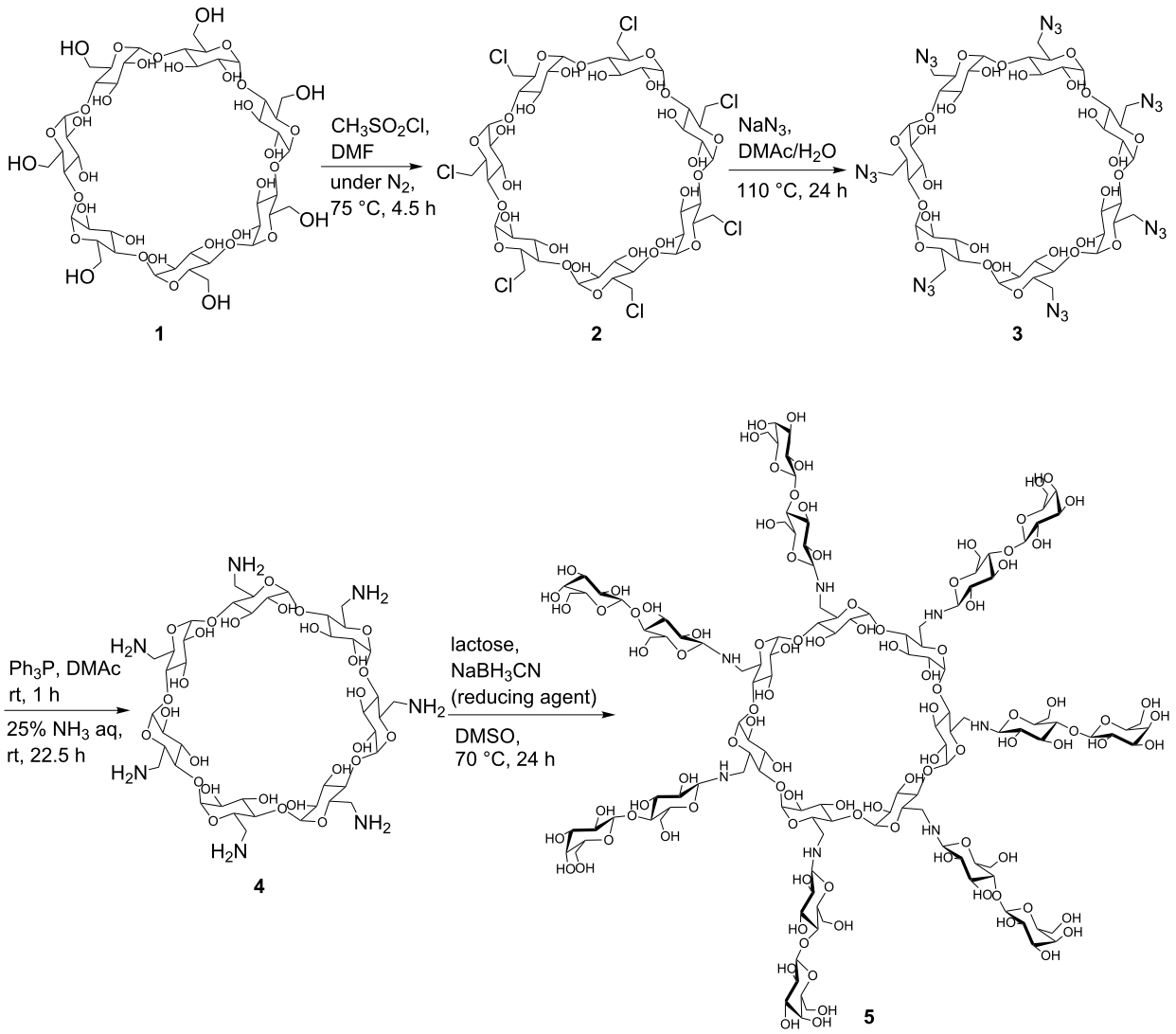

Figure 1: Schematic representation for synthesis of multi-Lac-β-CD (**5**), β-CD (**1**), *per*-chloro-β-CD (**2**), *per*-azido-β-CD (**3**), *per*-amino-β-CD, (**4**), multi-Lac-β-CD (DSL5.6), DSL, degree of substitution of lactose, DMAc, dimethylacetamide.

Interaction between multi-Lac-β-CD (DSL5.6) and peanut agglutinin

We initially attempted to clarify the role of the lactose moieties in multi-Lac-β-CD for binding to ASGPR by determining the dissociation constant of multi-Lac-β-CD (DSL5.6) with peanut agglutinin (PNA), a galactose-binding lectin, using the quartz crystal microbalance method (QCM) (Figure 4A). The dissociation constant of multi-Lac-β-CD (DSL5.6) was found to be 2.6×10^{-8} M, which was comparable with that obtained for the positive control asialofetuin (AF; 3×10^{-8} M). In contrast, β-CD did not show any response in the frequency of detection unit of QCM, thus indicating a negligible interaction with PNA (Figure 4B). Hence, the data indicated specific galactose-binding ability of multi-Lac-β-CD (DSL5.6).

Intracellular distribution of TRITC-multi-Lac-β-CD (DSL5.6)

Next, to investigate whether multi-Lac-β-CD (DSL5.6) can enter ASGPR-expressing cells, we examined the intracellular distribution of tetramethylrhodamine isothiocyanate (TRITC)-multi-Lac-β-CD (DSL5.6) in NPC-like HepG2 cells (ASGPR positive cells) Figure 5. The cellular uptake of TRITC-multi-Lac-β-CD (DSL5.6) was observed in NPC-like HepG2 cells 24 h post incubation (Figure 5A). Additionally, TRITC-multi-Lac-β-CD (DSL5.6) was co-localized with the endolysosomes stained by LysoTracker®. The fluorescence intensity of TRITC in cells was measured using the software of the BZ-II analyzer (Figure 5B). Meanwhile, the intracellular levels of TRITC-β-CD and TRITC-HP-β-CD in NPC-like HepG2 cells were ob-

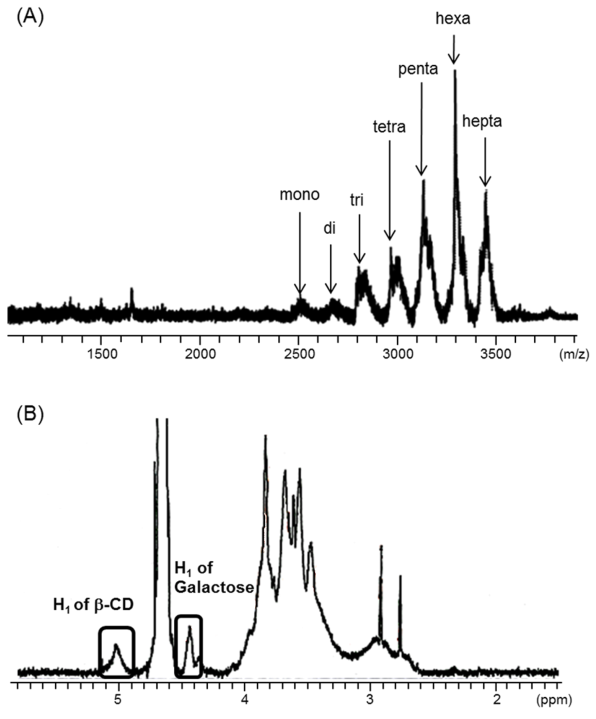

Figure 2: MALDI–TOFMS (A) and ^{1}H NMR spectra (B) of multi-Lac-β-CD (DSL5.6)

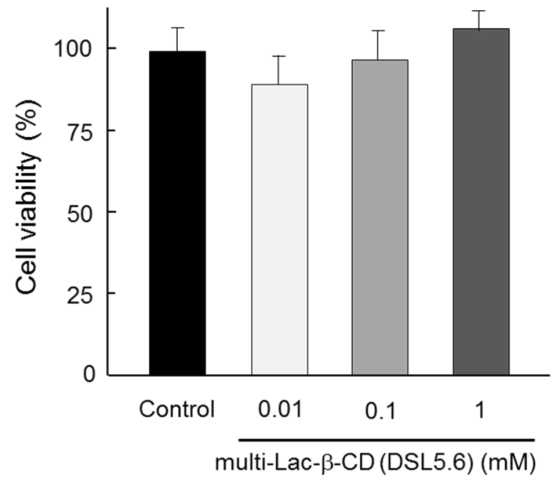

Figure 3: Cytotoxicity of multi-Lac-β-CD in NPC-like HepG2 cells after treatment for 24 h. NPC-like HepG2 cells were incubated with 150 μL of media [FBS (–)] containing multi-Lac-β-CD (DSL5.6) at 37 °C for 24 h. Data represents mean ± S.E.M. for six experiments.

served to be lower than that of TRITC-multi-Lac-β-CD (DSL5.6) (Figure 5B). In summary, these results indicate that multi-Lac-β-CD (DSL5.6) was distributed to the endolysosomes after cellular uptake by the NPC-like HepG2 cells.

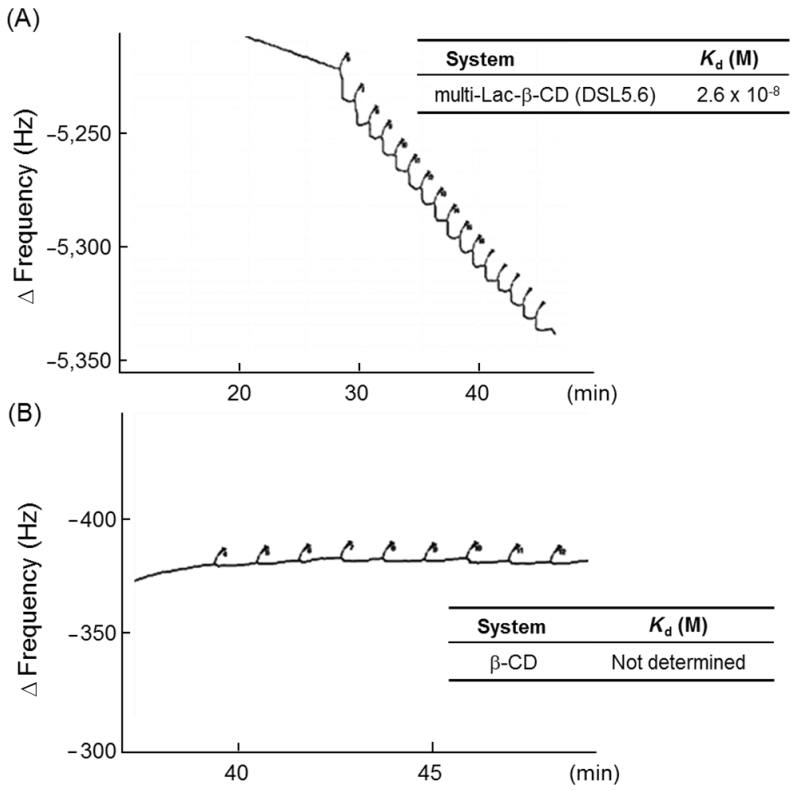

Figure 4: Binding curves of multi-Lac-β-CD (DSL5.6) (A) and β-CD (B) with peanut agglutinin (PNA). The binding curves for multi-Lac-β-CD (DSL5.6) and β-CD were determined by the quartz crystal microbalance (QCM) method. Phosphate-buffered saline (pH 7.4) was used as the sample buffer.

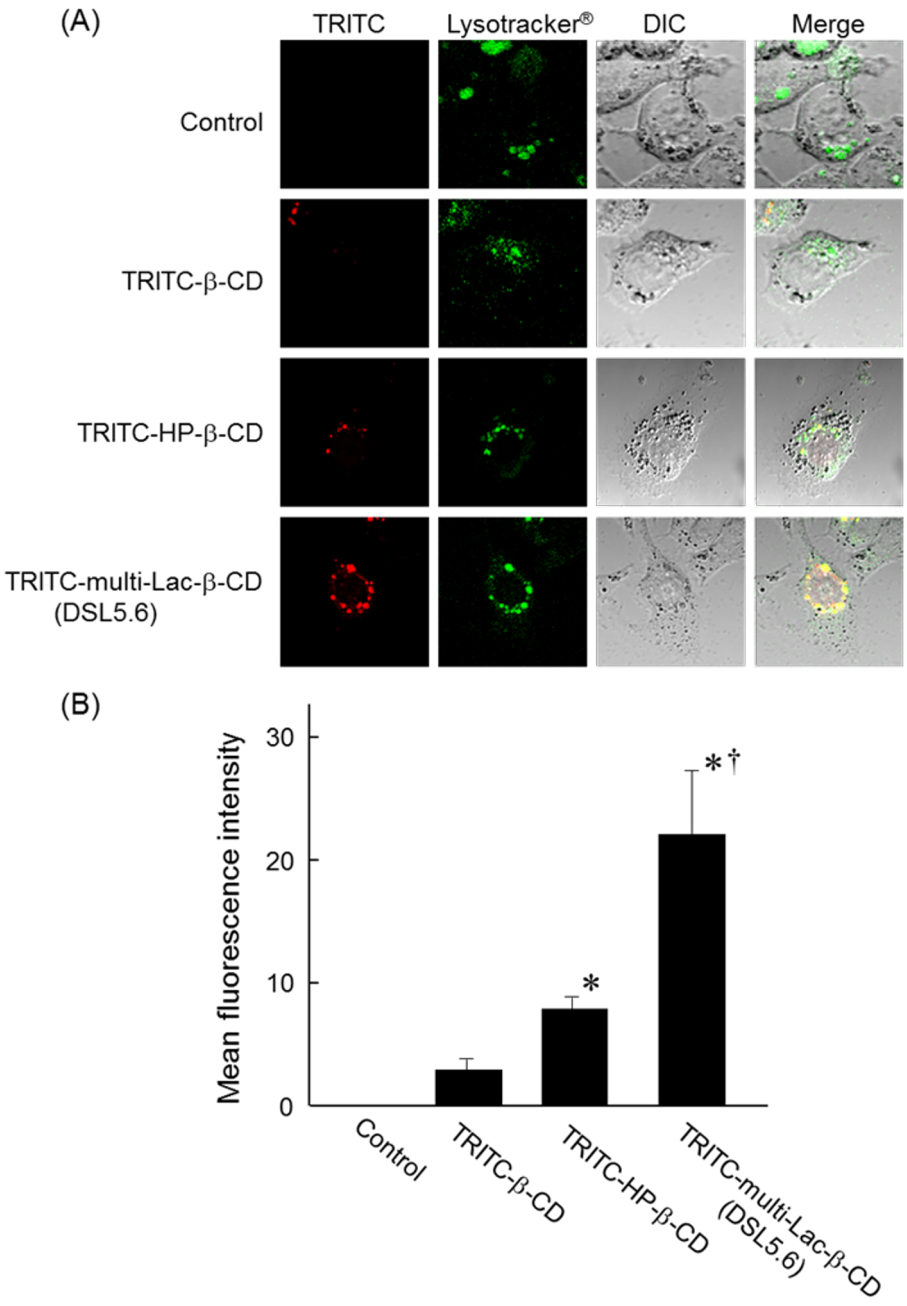

Figure 5: Intracellular distribution of TRITC-multi-Lac-β-CD (DSL5.6) in NPC-like HepG2 cells. Cells were incubated in medium [FBS (−)] with or without 100 μM TRITC-CDs for 24 h. (B) The fluorescence intensities of TRITC-CDs were determined in ten randomly selected cells per image by confocal laser scanning microscopy and BZ-II analyzer. Data represents mean ± S.E.M. of three experiments. *p < 0.05, compared with TRITC-β-CD. †p < 0.05, compared with 100 μM TRITC-HP-β-CD.

Effects of multi-Lac-β-CD (DSL5.6) on intracellular cholesterol levels

The effects of β-CD, HP-β-CD, mono-Lac-β-CD and multi-Lac-β-CD (DSL5.6) on intracellular cholesterol levels were studied in NPC-like HepG2 cells using Filipin III, which can specifically bind to unesterified cholesterol (Figure 6). Treatment of cells with 1 mM HP-β-CD, mono-Lac-β-CD and multi-Lac-β-CD (DSL5.6) for 24 h diminished the Filipin III-derived fluorescence intensity, when compared to that with β-CD (Figure 6A). These results indicated a significant cholesterol-lowering effect of multi-Lac-β-CD (DSL5.6) with statistical difference, as compared to that of β-CD or HP-β-CD (Figure 6B). In addition, the cholesterol-lowering effect of multi-Lac-β-CD (DSL5.6) tended to be stronger than that of

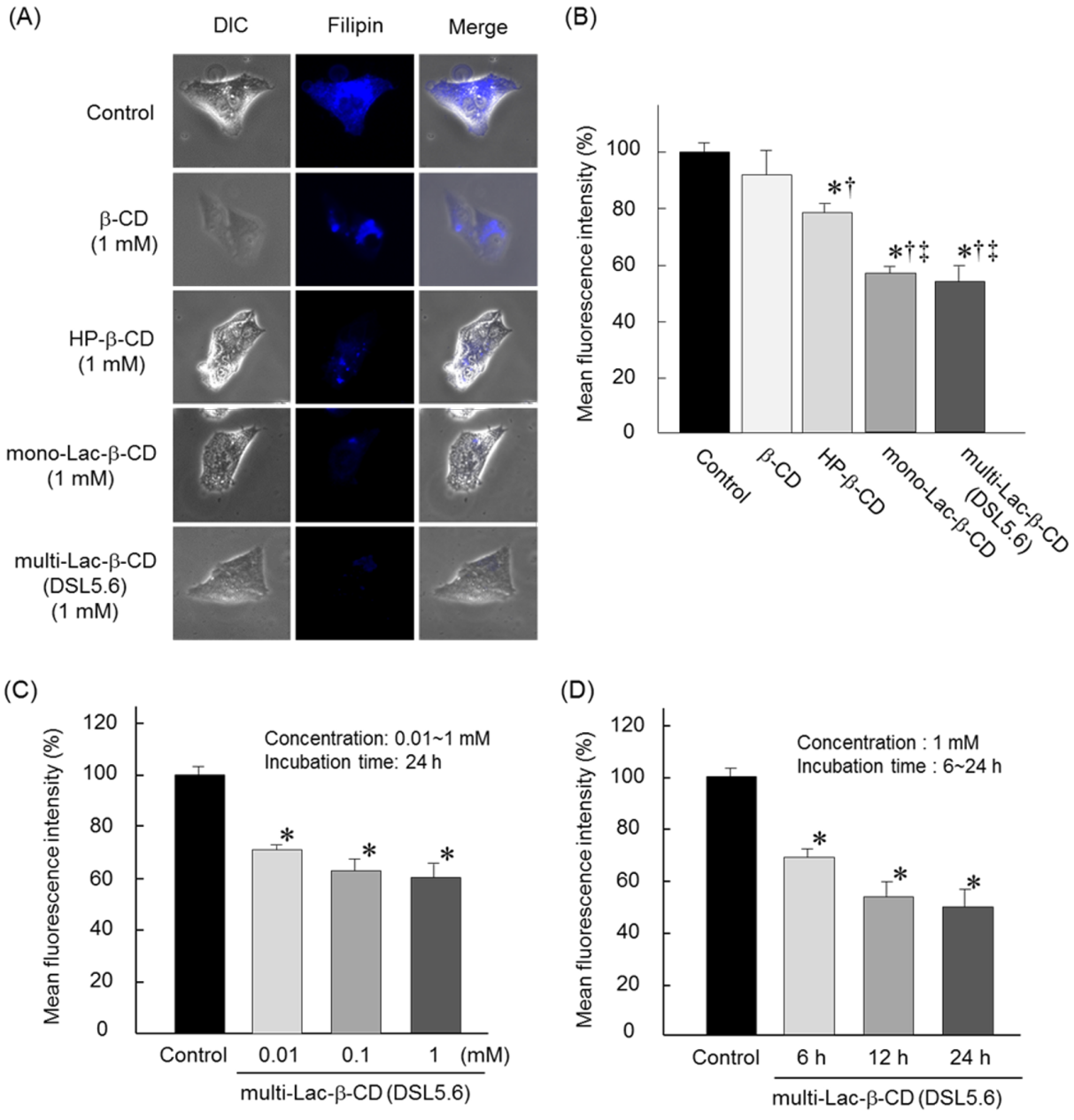

Figure 6: Intracellular distribution of cholesterol in NPC-like HepG2 cells. (A) NPC-like HepG2 cells (1×10^5 cells/35 mm dish) were treated with β-CD, HP-β-CD, mono-Lac-β-CD or multi-Lac-β-CD (DSL5.6) for 24 h at a concentration of 1 mM. (B) Fluorescence intensities of Filipin III in ten randomly selected cells were determined by the fluorescence microscope and BZ-II analyzer. (C) Effects of varying concentrations of multi-Lac-β-CD (DSL5.6) on cholesterol levels. (D) Effects of incubation time of multi-Lac-β-CD (DSL5.6) on cholesterol levels. Data represent mean ± S.E.M. of three experiments. *$p < 0.05$, compared with control. †$p < 0.05$, compared with β-CD. ‡$p < 0.05$, compared with HP-β-CD.

mono-Lac-β-CD, although there was no significant difference between these Lac-β-CDs (Figure 6A and 6B). Furthermore, this cholesterol-lowering effect of multi-Lac-β-CD (DSL5.6) was concentration- and time-dependent (Figure 6C and 6D). Hence, these results indicated that multi-Lac-β-CD (DSL5.6) decreased intracellular cholesterol levels in HPC-like HepG2 cells.

HP-β-CD, one of the therapeutic candidates for the treatment of NPC disease, attenuates free cholesterol accumulation in various organs and prolongs the lifespan of *Npc1*$^{-/-}$ mice and NPC-diseased human fibroblasts [9,10,19]. Toxicological studies indicate that HP-β-CD is generally safe. However, a recent study has found that repeated administration of high doses of HP-β-CD causes hearing loss in cats [20,21]. There-

fore, the targeting technique is one of promising approaches to reduce the dose of CDs. Importantly, the multi-Lac-β-CD (DSL5.6) showed more potent cholesterol-lowering effects in NPC-like HepG2 cells than HP-β-CD. Accordingly, multi-Lac-β-CD (DSL5.6) may attenuate the risk of hearing loss due to its hepatocyte-selectivity. In order to evaluate the liver accumulation of multi-Lac-β-CD (DSL5.6), the biodistribution studies need to be performed in NPC disease model mice in future.

The galactose density is a crucial factor for regulation of galactose affinity to ASGPR. Stokmaier et al. revealed that the binding affinity of galactose to ASGPR elevated 100–1000 fold from mono- to triantennary galactose structures, probably due to clustering effects [22]. The dissociation constant of monosaccharide with ASGPR was 10^{-4} M, whereas those of triantennary and tetraantennary compounds with ASGPR were 5×10^{-9} M and 9×10^{-9} M, respectively [22]. Previously, we synthesized the mono-Lac-β-CD and revealed the reduction in accumulation of intracellular cholesterol in NPC-like HepG2 cells [14]. ASGPR is known to recognize the galactose moiety at three points in the golden triangle [15,16]. Therefore, the binding affinity of multi-Lac-β-CD (DSL5.6) to ASGPR is likely to be much higher than that of mono-Lac-β-CD. In fact, multi-Lac-β-CD (DSL5.6) has a quite low dissociation constant (2.6×10^{-8} M) with PNA, probably a result of its clustering effect in ASGPR recognition. The further elaborate studies to compare the binding affinity of multi-Lac-β-CD (DSL5.6) to PNA with mono-Lac-β-CD are necessary. In addition, to demonstrate the ASGPR-expressing cell-selective binding and cholesterol-lowering effects of multi-Lac-β-CD (DSL5.6), the comparative studies using ASGPR-negative cells are also needed.

Several lines of evidence indicate that the lowering effect of CDs on the accumulation of cholesterol is attributed to endocytosed CD [23]. The CDs can enter the cells via pinocytosis and reach the interior of the endolysosomes [24] and should remain intact because mammalian cells lack the enzymes for degradation of CDs [8]. A current study indicates that endocytosed CDs are capable of replacing the function of NPC1 [23]. However, it is still unclear how the endocytosed CDs can bypasses the functional NPC1. NPC1, a transmembrane protein expressed in endolysosomes, can bind to cholesterol [25]. NPC2 interacts with NPC1 and delivers cholesterol to the limiting membranes [25], while β-CDs form inclusion complexes with cholesterol. Hence, β-CDs may have the potential to bypass the functional NPC1 or NPC2 and deliver cholesterol directly to the limiting membranes. Once the cholesterol exits the endolysosomes, it is delivered to other organelles by the cholesterol transport system. To elucidate the detailed mechanism of cholesterol-lowering effects of multi-Lac-β-CD (DSL5.6), further elaborate studies on not only the interaction of multi-Lac-β-CD (DSL5.6) with endolysosomes membranes, but also cholesterol trafficking are necessary.

Conclusion

In this study, we developed multi-Lac-β-CD (DSL5.6) to reduce cholesterol levels in NPC-like HepG2 cells. The multi-Lac-β-CD (DSL5.6) was internalized in NPC-like HepG2 cells via ASGPR-mediated endocytosis and was found to diminish the accumulation of cholesterol in the endolysosomes. In conclusion, the findings from the present study may be crucial for the development of an active targeting CD-based therapy for the treatment of hepatosplenomegaly in NPC disease.

Experimental

Materials

β-CD was a kind gift from Nihon Shokuhin Kako (Tokyo, Japan). Lactose monohydrate was purchased from Wako Pure Chemical Industries (Osaka, Japan). Tetramethylrhodamine isothiocyanate (TRITC) was obtained from Funakoshi (Tokyo, Japan). Biotinylated-peanut agglutinin (PNA) and bovine serum albumin (BSA) were purchased from Cosmo Bio (Tokyo, Japan) and Boehringer Mannheim K.K. (Tokyo, Japan), respectively.

Synthesis of multi-Lac-β-CD (DSL5.6)

per-6-Amino-β-CD (**4**) was synthesized as reported previously [17]. Lactose residues were introduced in the primary amino groups of *per*-6-amino-β-CD. For this experiment, 20 mL of DMSO containing *per*-6-amino-β-CD (**4**, 0.1 g), lactose monohydrate (1.52 g), and sodium cyanotrihydroborate (2.79 g) were mixed and incubated at 70 °C for 24 h. After dialysis by Spectra/pore (MWCO: 1000) in water at room temperature for 48 h, the sample was concentrated in a rotary evaporator and freeze-dried to obtain multi-Lac-β-CD. ^{1}H NMR spectra for multi-Lac-β-CD consisted of protons of both β-CD and lactose. The ratios of peak areas of the anomeric proton of β-CD and protons of the lactose were approximately 5.6. This result indicated that β-CD covalently binds to lactose in a molar ratio of 1:5.6 (Figure 2B). A 25% yield of multi-Lac-β-CD was obtained after synthesis. ^{1}H NMR (500 MHz, D_2O) δ (from TMS), 5.00 (H1, β-CD), 3.84−3.62 (H3, H5, H6, β-CD), 3.54−3.43 (H2, H4, β-CD), 4.56−4.41 (anomeric proton of lactose).

Cell culture

HepG2 cells (human hepatocellular carcinoma cell line) were grown in Dulbecco's Modified Eagle's Medium (DMEM, Nissui Pharmaceuticals, Tokyo, Japan), containing penicillin (1×10^5 mU/mL), streptomycin (0.1 mg/mL) and supplemented with 10% fetal bovine serum (FBS), in a humidified incubator with 5% CO_2. NPC-like HepG2 cells accumulated

with high amounts of cholesterol were obtained after 48 h treatment with DMEM containing 1.25 μM U18666A.

Cytotoxicity

The viability of NPC-like HepG2 cells treated with multi-Lac-β-CD (DSL5.6) was assayed by the WST-1 method. A cell counting kit (CCK) from Wako Pure Chemical Industries (Osaka, Japan) was used for the analysis. The WST-1 method has been described in-depth in our previous publication [14].

Quartz crystal microbalance (QCM)

The molecular interaction of multi-Lac-β-CD (DSL5.6) with PNA, one of galactose-binding lectins, was analyzed with a QCM analyzer (Single-Q, SCINICS, Tokyo, Japan). Avidin was used for immobilizing biotinylated-PNA on the sensor cuvette. The biotinylated-PNA was blocked with 1% BSA in PBS (pH 7.4). Two μL of multi-Lac-β-CD (DS5.6) (final concentration: 1 mM) was added to PBS (pH 7.4). The binding curves and dissociation constants (K_d) were obtained using Q-UP software equipped in the Single-Q.

Intracellular distribution of multi-Lac-β-CD (DSL5.6)

The intracellular distribution of TRITC-multi-Lac-β-CD (DS5.6) in NPC-like HepG2 cells was assayed by confocal laser scanning microscopy, as reported previously [14].

Intracellular cholesterol levels post treatment with multi-Lac-β-CD (DSL5.6)

The intracellular cholesterol levels in multi-Lac-β-CD (DS5.6) treated NPC-like HepG2 cells were detected by a cholesterol cell-based detection assay kit (Cayman Chemical Company, Ann Arbor, MI, USA), as reported previously [14]. The fluorescence intensities of Filipin III in ten randomly selected cells were calculated as the ratio of Filipin III area to cell area by the fluorescence microscope and BZ-II analyzer.

Data analysis

Quantitative data was expressed as the mean ± standard error of the mean (S.E.M.), while the statistical comparisons were made using the Scheffe's test. A p-value < 0.05 was considered statistically significant.

Acknowledgements

The research was funded by the Ministry of Health, Labor, and Welfare of Japan.

References

1. Patterson, M. C.; Vecchio, D.; Prady, H.; Abel, L.; Wraith, J. E. *Lancet Neurol.* **2007,** *6,* 765–772. doi:10.1016/S1474-4422(07)70194-1
2. Pentchev, P. G.; Comly, M. E.; Kruth, H. S.; Vanier, M. T.; Wenger, D. A.; Patel, S.; Brady, R. O. *Proc. Natl. Acad. Sci. U. S. A.* **1985,** *82,* 8247–8251. doi:10.1073/pnas.82.23.8247
3. Vanier, M. T. *Orphanet J. Rare Dis.* **2010,** *5,* No. 16. doi:10.1186/1750-1172-5-16
4. Higgins, M. E.; Davies, J. P.; Chen, F. W.; Ioannou, Y. A. *Mol. Genet. Metab.* **1999,** *68,* 1–13. doi:10.1006/mgme.1999.2882
5. Neufeld, E. B.; Wastney, M.; Patel, S.; Suresh, S.; Cooney, A. M.; Dwyer, N. K.; Roff, C. F.; Ohno, K.; Morris, J. A.; Carstea, E. D.; Incardona, J. P.; Strauss, J. F., III; Vanier, M. T.; Patterson, M. C.; Brady, R. O.; Pentchev, P. G.; Blanchette-Mackie, E. J. *J. Biol. Chem.* **1999,** *274,* 9627–9635. doi:10.1074/jbc.274.14.9627
6. Naureckiene, S.; Sleat, D. E.; Lackland, H.; Fensom, A.; Vanier, M. T.; Wattiaux, R.; Jadot, M.; Lobel, P. *Science* **2000,** *290,* 2298–2301. doi:10.1126/science.290.5500.2298
7. Szente, L.; Szejtli, J. *Adv. Drug Delivery Rev.* **1999,** *36,* 17–28. doi:10.1016/S0169-409X(98)00092-1
8. Davis, M. E.; Brewster, M. E. *Nat. Rev. Drug Discovery* **2004,** *3,* 1023–1035. doi:10.1038/nrd1576
9. Liu, B.; Turley, S. D.; Burns, D. K.; Miller, A. M.; Repa, J. J.; Dietschy, J. M. *Proc. Natl. Acad. Sci. U. S. A.* **2009,** *106,* 2377–2382. doi:10.1073/pnas.0810895106
10. Davidson, C. D.; Ali, N. F.; Micsenyi, M. C.; Stephney, G.; Renault, S.; Dobrenis, K.; Ory, D. S.; Vanier, M. T.; Walkley, S. U. *PLoS One* **2009,** *4,* e6951. doi:10.1371/journal.pone.0006951
11. Porter, F. D.; Scherrer, D. E.; Lanier, M. H.; Langmade, S. J.; Molugu, V.; Gale, S. E.; Olzeski, D.; Sidhu, R.; Dietzen, D. J.; Fu, R.; Wassif, C. A.; Yanjanin, N. M.; Marso, S. P.; House, J.; Vite, C.; Schaffer, J. E.; Ory, D. S. *Sci. Transl. Med.* **2010,** *2,* 56ra81. doi:10.1126/scitranslmed.3001417
12. Rigopoulou, E. I.; Roggenbuck, D.; Smyk, D. S.; Liaskos, C.; Mytilinaiou, M. G.; Feist, E.; Conrad, K.; Bogdanos, D. P. *Autoimmun. Rev.* **2012,** *12,* 260–269. doi:10.1016/j.autrev.2012.04.005
13. Guo, H.; Zhang, D.; Li, T.; Li, C.; Guo, Y.; Liu, G.; Hao, L.; Shen, J.; Qi, L.; Liu, X.; Luan, J.; Zhang, Q. *J. Pharm. Sci.* **2014,** *103,* 987–993. doi:10.1002/jps.23875
14. Motoyama, K.; Hirai, Y.; Nishiyama, R.; Maeda, Y.; Higashi, T.; Ishitsuka, Y.; Kondo, Y.; Irie, T.; Era, T.; Arima, H. *Beilstein J. Org. Chem.* **2015,** *11,* 2079–2086. doi:10.3762/bjoc.11.224
15. Lee, Y. C.; Lee, R. T. *Acc. Chem. Res.* **1995,** *28,* 321–327. doi:10.1021/ar00056a001
16. Rice, K. G.; Lee, Y. C. *J. Biol. Chem.* **1990,** *265,* 18423–18428.
17. Okamatsu, A.; Motoyama, K.; Onodera, R.; Higashi, T.; Koshigoe, T.; Shimada, Y.; Hattori, K.; Takeuchi, T.; Arima, H. *Bioconjugate Chem.* **2013,** *24,* 724–733. doi:10.1021/bc400015r
18. Sugimoto, Y.; Ninomiya, H.; Ohsaki, Y.; Higaki, K.; Davies, J. P.; Ioannou, Y. A.; Ohno, K. *Proc. Natl. Acad. Sci. U. S. A.* **2001,** *98,* 12391–12396. doi:10.1073/pnas.221181998
19. Ramirez, C. M.; Liu, B.; Taylor, A. M.; Repa, J. J.; Burns, D. K.; Weinberg, A. G.; Turley, S. D.; Dietschy, J. M. *Pediatr. Res.* **2010,** *68,* 309–315. doi:10.1203/PDR.0b013e3181ee4dd2
20. Crumling, M. A.; Liu, L.; Thomas, P. V.; Benson, J.; Kanicki, A.; Kabara, L.; Hälsey, K.; Dolan, D.; Duncan, R. K. *PLoS One* **2012,** *7,* e53280. doi:10.1371/journal.pone.0053280
21. Ward, S.; O'Donnell, P.; Fernandez, S.; Vite, C. H. *Pediatr. Res.* **2010,** *68,* 52–56. doi:10.1203/PDR.0b013e3181df4623

22. Stokmaier, D.; Khorev, O.; Cutting, B.; Born, R.; Ricklin, D.; Ernst, T. O. G.; Böni, F.; Schwingruber, K.; Gentner, M.; Wittwer, M.; Spreafico, M.; Vedani, A.; Rabbani, S.; Schwardt, O.; Ernst, B. *Bioorg. Med. Chem.* **2009,** *17,* 7254–7264. doi:10.1016/j.bmc.2009.08.049
23. Rosenbaum, A. I.; Maxfield, F. R. *J. Neurochem.* **2011,** *116,* 789–795. doi:10.1111/j.1471-4159.2010.06976.x
24. Mukherjee, S.; Ghosh, R. N.; Maxfield, F. R. *Physiol. Rev.* **1997,** *77,* 759–803.
25. Kwon, H. J.; Abi-Mosleh, L.; Wang, M. L.; Deisenhofer, J.; Goldstein, J. L.; Brown, M. S.; Infante, R. E. *Cell* **2009,** *137,* 1213–1224. doi:10.1016/j.cell.2009.03.049

BEILSTEIN JOURNAL OF ORGANIC CHEMISTRY

Phosphated cyclodextrins as water-soluble chiral NMR solvating agents for cationic compounds

Cira Mollings Puentes and Thomas J. Wenzel*

Full Research Paper

Open Access

Address:
Department of Chemistry, Bates College, Lewiston, Maine 04240 USA

Email:
Thomas J. Wenzel* - twenzel@bates.edu

* Corresponding author

Keywords:
chiral; chiral differentiation; cyclodextrin; enantiomer; enantiomeric purity; NMR

Beilstein J. Org. Chem. **2017,** *13,* 43–53.
doi:10.3762/bjoc.13.6

Received: 30 September 2016
Accepted: 22 December 2016
Published: 06 January 2017

This article is part of the Thematic Series "Superstructures with cyclodextrins: Chemistry and applications IV".

Guest Editor: G. Wenz

Abstract

The utility of phosphated α-, β- and γ-cyclodextrins as water-soluble chiral NMR solvating agents for cationic substrates is described. Two sets of phosphated cyclodextrins, one with degrees of substitution in the 2–6 range, the other with degrees of substitution in the 6–10 range, are examined. Results with 33 water-soluble cationic substrates are reported. We also explored the possibility that the addition of paramagnetic lanthanide ions such as praseodymium(III) and ytterbium(III) further enhances the enantiomeric differentiation in the NMR spectra. The chiral differentiation with the phosphated cyclodextrins is compared to prior results obtained with anionic carboxymethylated cyclodextrins. There are a number of examples where a larger differentiation is observed with the phosphated cyclodextrins.

Introduction

Chiral NMR solvating agents are commonly used for determining enantiomeric purity. In some cases, these compounds cause reproducible perturbations in chemical shifts that can be used in the assignment of the absolute stereochemistry [1-7]. Since chiral solvating agents associate with the compound being studied through non-covalent interactions, they are easy to use and involve merely mixing the reagent with the compound in an NMR tube.

Cyclodextrins (CDs), which are cyclic oligosaccharides containing D-glucose units, represent an important and versatile class of chiral NMR solvating agents (Figure 1). The most common representatives are α-, β- and γ-CD, which contain six, seven and eight glucose rings, respectively. Many substrates form inclusion complexes with CDs and the differing sizes of α-, β- and γ-CD allow the study of substrates of different sizes. Furthermore, the secondary hydroxy groups at the 2 and 3-posi-

tions and the primary hydroxy groups at the 6-position of CDs can be derivatized with a variety of functional groups. Such derivatization can be used to alter the solubility, binding properties of substrates, and ultimately enantioselectivity properties of the CDs. The cavity of CDs has the secondary hydroxy groups at one opening and the primary ones at the other and the opening to the cavity at the secondary side is larger than that at the primary side.

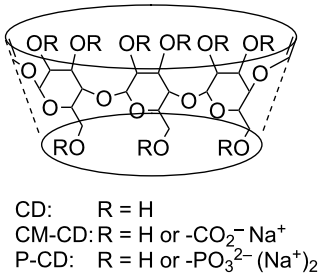

Figure 1: Structure of cyclodextrins (CD) and their carboxymethylated (CM-CD) and phosphated (P-CD) derivatives.

Native, underivatized CDs are effective chiral NMR solvating agents in water [8,9]. Water-soluble substrates with hydrophobic moieties such as aryl rings typically form inclusion complexes by insertion of the aryl ring into the CD cavity. Neutral CDs with permethylated [10-12], benzylated [13], benzoylated [13,14], carbamoylated [15-18], and acetylated [19,20] hydroxy groups have been studied in NMR applications. The permethylated CDs can be used in both aqueous and organic solvents whereas the other neutral derivatives are typically useful in organic solvents such as chloroform-*d*. In addition to the aforementioned modifications, the hydroxy groups of CDs can also be derivatized with ionic substituents. CDs with anionic carboxymethyl [21-32] (CM-CD, Figure 1), sulfate [29,30,33-35], sulfobutylether [22-24,36,37] and thiocarboxymethyl [38] groups also have been studied as chiral NMR solvating agents. The general findings of these studies are that anionic CDs are more effective chiral NMR solvating agents for cationic substrates than neutral native CDs. Similarly cationic CDs containing amine [39,40], xylylenediamine [41], and trialkylammonium groups [42-44] are found to be more effective for anionic substrates than the neutral native CDs.

An important consideration with derivatized CDs is the degree of substitution (DS) of the hydroxy groups. When preparing ionic CD derivatives, it is often difficult if not impossible to derivatize all of the hydroxy groups. Whether the functionalization takes place preferentially at the primary or secondary hydroxy groups can have a significant impact on the enantioselectivity of the resulting derivative. Carboxymethyl- and trimethylammonio-substituted CDs are commercially available but often have a low DS of about 2. Previous reports have found that randomly substituted ionic CDs with higher degrees of carboxymethylation and trimethylammonium groups (DS = 11 for β-CD) [21,43] are considerably more effective than derivatives with lower DS. Unfortunately, CM-CDs with high DS are not commercially available and investigators wishing to use these compounds in chiral NMR applications would have to synthesize and purify them.

Phosphated CD derivatives (P-CDs, Figure 1) have been utilized as effective enantioselectors in capillary electrophoresis [45-48]. Various phosphated α-, β- and γ-CD are commercially available with different degrees of substitutions from low (2–6) to high DS (6–10). This report will describe the utilization of P-CDs as water-soluble chiral NMR solvating agents. Thirty-three cationic substrates with a wide range of structural features are examined and enantiomeric differentiation obtained with P-CDs is compared to prior results acquired with CM-CDs.

Results and Discussion

Thirty-three substrates including α-methylbenzylamine (**1**), *N*,α-dimethylbenzylamine (**2**), *N*,*N*-dimethyl-1-phenethylamine (**3**), *N*-allyl-α-methylbenzylamine (**4**), β-methylphenethylamine (**5**), 1-methyl-3-phenylpiperazine (**6**), ephedrine (**7**), α-(methylaminoethyl)benzyl alcohol (**8**), 2-*tert*-butylamino-1-phenylethanol (**9**), α-(1-aminoethyl)-4-hydroxybenzyl alcohol (**10**), tyrosinol (**11**), 3-dimethylamino-2-methylpropiophenone (**12**), *cis*-(2-benzylamino)cyclohexanemethanol (**13**), alanine methyl ester (**14**), 2-phenylglycine methyl ester (**15**), phenylalanine methyl ester (**16**), tyrosine (**17**), 4-chlorophenylalanine methyl ester (**18**), 4-chlorophenylalanine ethyl ester (**19**), carbobenzyloxy serine (**20**), 2-methylindoline (**21**), *trans*-1-amino-2-indanol (**22**), *cis*-1-amino-2-indanol (**23**), tryptophan (**24**), tryptophan methyl ester (**25**), 1-methyltryptophan methyl ester (**26**), 1-(1-naphthyl)ethylamine (**27**), *N*,*N*-dimethyl-1-(1-naphthyl)ethylamine (**28**), propranolol (**29**), pheniramine (**30**), brompheniramine (**31**), doxylamine (**32**), and carbinoxamine (**33**) (Figure 2) in their protonated cationic form were individually tested with six different P-CDs at cyclodextrin concentrations of 5, 10 and 20 mM.

All substrates, except for **14**, have aromatic rings in their structures. Previous studies [21,31,32] and observations made herein with the P-CDs indicate that host–guest complexes through insertion of the aryl ring into the cavity of the CDs occur which is supported by NMR measurements. In the NMR spectra the resonances of the P-CD H3 and H5 protons, which are located inside the CD cavity, are perturbed to lower frequencies in the spectra due to shielding of these protons by the inserted aryl

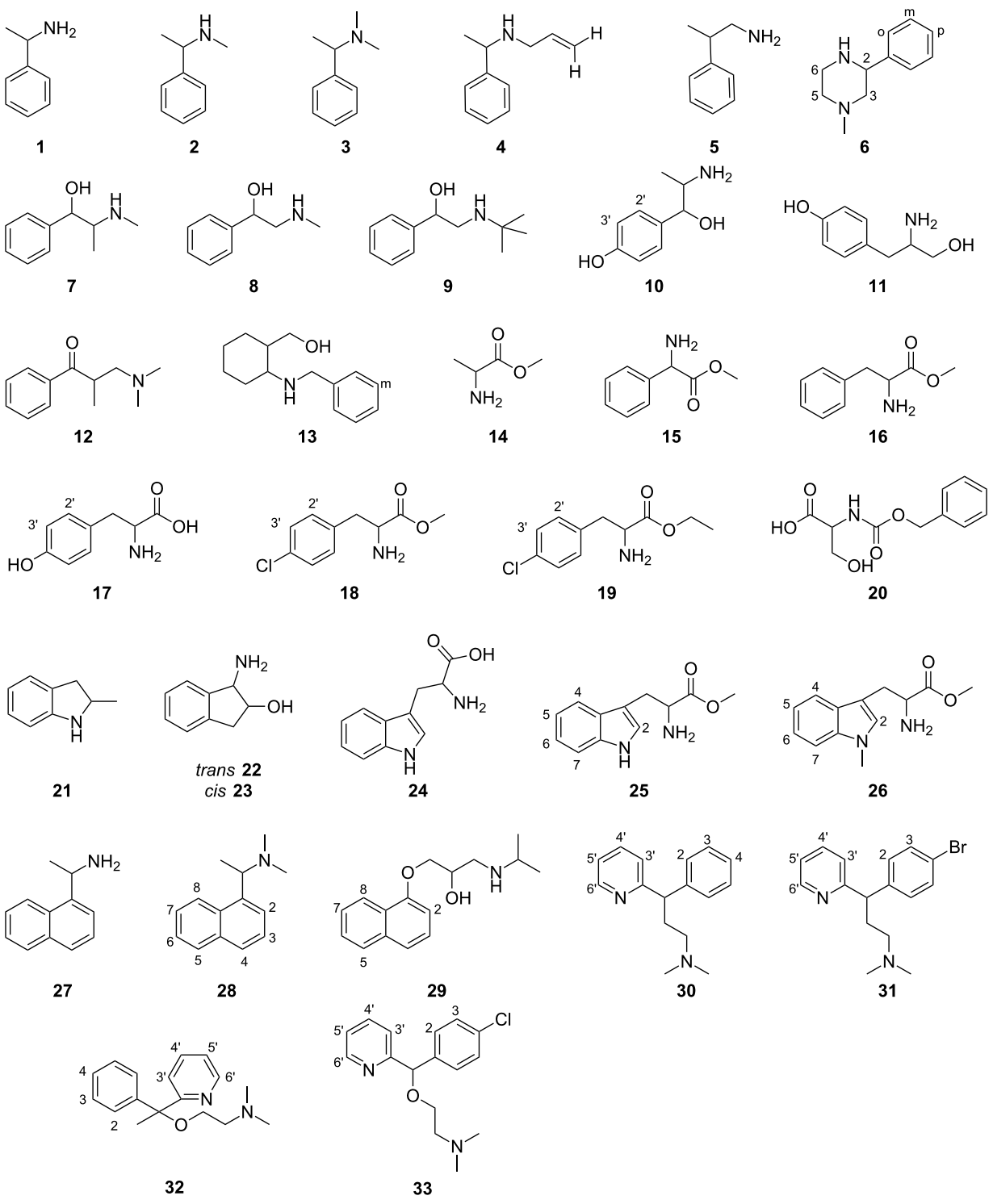

Figure 2: Structures of substrates included in the study. All compounds were examined in their protonated forms with the P-CDs.

ring. The largest magnitude of enantiomeric differentiation observed in the ^{1}H NMR spectra of the substrates with each P-CD at 5, 10 or 20 mM (P-α-CD-L_{DS}, DS = 2–6; P-α-CD-H_{DS}, DS = 6–10; P-β-CD-L_{DS}, DS = 2–6; P-β-CD-H_{DS}, DS = 6–10; P-γ-CD-L_{DS}, DS = 2–6; P-γ-CD-H_{DS}, DS = 6–10) is reported herein.

Equation 1 and Equation 2 show the association of the (*R*)- and (*S*)-enantiomers of a substrate (Sub) with a chiral solvating agent (CSA).

$$\text{CSA} + (R)\text{-Sub} = \text{CSA–}(R)\text{-Sub}, K_R \quad (1)$$

$$\text{CSA} + (S)\text{-Sub} = \text{CSA–}(S)\text{-Sub}, K_S \quad (2)$$

Provided that the exchange of substrates with the CSA is fast on the NMR time scale, there are two mechanisms through which chiral solvating agents (CSAs) can cause enantiomeric differentiation. The first is that the complexes of the two enantiomers of the substrate with the enantiomerically pure CSA are diastereomers and therefore exhibit different chemical shifts. The second relies on a frequently observed difference in the association constants of the two enantiomers with the CSA (K_R and K_S). Under the conditions of fast exchange, one of the enantiomers will preferentially bind with the CSA compared to the other and the time-averaged solvation of the two enantiomers will be different. It is often not possible to determine which mechanism dominates when enantiomeric differentiation is observed in the NMR spectrum, and in many cases both mechanisms likely contribute to some extent.

In cases where enantiomeric differentiation occurs through the formation of diastereomeric CD–substrate complexes, best results in the NMR spectrum would be expected at 20 mM P-CD because of a higher degree of complexation. However, in some spectra there have been an overlap of one of the substrate resonances with other resonances of the substrate or CD in such a way that it was not possible to determine in a regular one-dimensional NMR spectrum whether enantiomeric differentiation was present.

In those cases where enantiomeric differentiation occurs solely through differences in association constants of the two enantiomers of the substrate with the P-CD, the magnitude of the enantiomeric differentiation may decrease at increasing P-CD concentrations from 5 to 20 mM. In this situation, the enantiomer of the substrate with the higher association constant has a higher proportion complexed with the P-CD at 5 mM than the substrate enantiomer with the lower association constant. Therefore, resonances of the substrate with the higher association constant are more perturbed in the NMR spectrum. At higher concentrations of P-CD (10 or 20 mM), also a higher proportion of the enantiomer with the lower association constant binds to the P-CD, thus enhancing perturbations in the NMR spectrum of this enantiomer and thereby diminishing the extent of enantiomeric differentiation. In some cases, the position of the resonances of the two enantiomers in the NMR spectrum may reverse their order as the concentration of the CSA is raised from low to high values. A detailed analysis of this situation has been reported in the literature [49].

Substrates **1**–**6** contain amine and aryl moieties. An enantiomeric differentiation is observed in the ^{1}H NMR spectra of **1**–**3** in the presence of P-CD, whereas no differentiation is observed in the spectra of **4**–**6** with any of the P-CDs (Table 1). Table 1 and others herein also provide data for enantiomeric differentiation in the spectra of **1**–**6** that was previously reported with a series of carboxymethylated cyclodextrins (CM-CD) [21,31,32]. The differentiation only occurs in the aliphatic resonances of **1**–**6** with P-CDs and CM-CDs. The degree of enantiomeric differentiation in the spectra of **1**–**3** with the different P-CDs show that there is no consistent trend as to which P-CD derivative is more effective at causing enantiomeric differentiation. P-α-CD-H_{DS} is especially effective for substrate **3**, but it is ineffective for the other substrates in this group.

Table 1: Enantiomeric differentiation in ppm in the ^{1}H NMR spectra (400 MHz) of **1**–**6** (10 mM) with P-CDs and CM-CD [31,32] in D_2O. The concentration of the cyclodextrin is 20 mM unless otherwise indicated.

		P-α-CD-L_{DS}	P-α-CD-H_{DS}	P-β-CD-L_{DS}	P-β-CD-H_{DS}	P-γ-CD-L_{DS}	P-γ-CD-H_{DS}	CM-CD
1	CH	0	0	0	0	0	0.004	0.010 - β
	CH_3	0	0	0	0	0	0.007	0
2	CH	0	0	0.008	0	0	0	0
	N-CH_3	0	0	0.006	0	0	0	0.013 - β
	C-CH_3	0	0	0	0	0	0	0.008 - β
3	CH	0.040[a]	0.048[a]	0	0	0	0	0
	C-CH_3	0.029[b]	0.027[a]	0.016	0.026	0.027	0	0.010 - β
4	CH_3	0	0	0	0	0	0	0.010 - α
5	CH_3	0	0	0	0	0	0	0.007 - β
6	CH_3	0	0	0	0	0	0	0.008 - β

[a]10 mM; [b]5 mM.

P-β-CD-L_{DS} is the only P-CD that is effective for **2**, whereas P-γ-CD-H_{DS} is the only one effective for **1**. Figure 3 shows a comparison of the *C*-methyl resonance of **3** (10 mM) in the presence of P-α-CD-H_{DS}, P-β-CD-H_{DS}, and P-γ-CD-H_{DS} at a concentration of 10 mM. The most significant degree of enantiomeric differentiation in the spectrum with P-α-CD-H_{DS} is apparent (Figure 3b), as is the smaller differentiation with P-β-CD-H_{DS} (Figure 3c) and the non-existent differentiation with P-γ-CD-H_{DS} (Figure 3d). While CM-CDs causes greater enantiomeric differentiation of more resonances in the NMR spectra of **1**–**6**, there are only a few examples where the P-CDs are more effective. The enantiomeric differentiation of the methine and methyl resonances of **3** with some of the P-CDs is noteworthy.

Another group of tested substrates contains aryl, amine and either hydroxy (**7**–**11**, **13**) or carbonyl (**12**) moieties. Within this group, the NMR spectra of **7**, **9** and **10** exhibit enantiomeric differentiation in the presence of one or more of the P-CDs (Table 2). Of particular note is the effectiveness of P-β-CD-L_{DS} for **7** as the CH and CHOH resonances exhibit enantiomeric differentiation on the order of 0.03 ppm. As with compounds **1**–**6**,

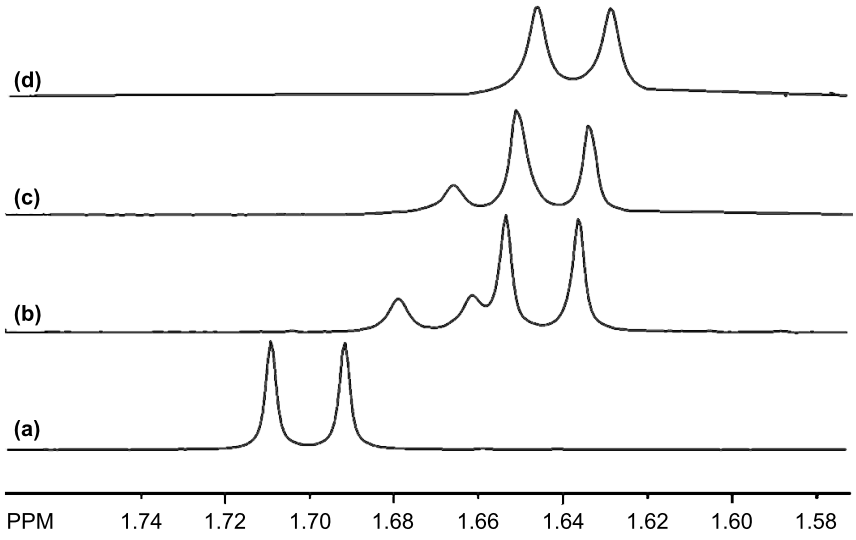

Figure 3: The (a) *C*-methyl resonance of **3** (10 mM, enriched in the (*R*)-enantiomer) in the presence of (b) P-α-CD-H_{DS} (10 mM), (c) P-β-CD-H_{DS} (10 mM) and (d) P-γ-CD-H_{DS} (10 mM).

Table 2: Enantiomeric differentiation in ppm in the ^{1}H NMR spectra (400 MHz) of **7**–**10** (10 mM) with P-CDs and CM-CD [32] in D_2O. The concentration of the cyclodextrin is 20 mM unless otherwise indicated.

		P-α-CD-L_{DS}	P-α-CD-H_{DS}	P-β-CD-L_{DS}	P-β-CD-H_{DS}	P-γ-CD-L_{DS}	P-γ-CD-H_{DS}	CM-CD
7	CH	0	0	0.034	0.026	0	0	0
	CH-OH	0	0	0.030	0.010	0.024	0	0
	N-CH_3	0	0	0.008	0.004[a]	0	0.006[b]	0.010 - β
	C-CH_3	0	0	0.005	0	0	0	0
8	N-CH_3	0	0	0	0	0	0	0.015 - β
9	CH-OH	0	0	0	0.025	0	0	
	CH_2	0	0	0.008	0	0	0	
	CH_2'	0	0.009	0.008	0	0	0	
10	CH-OH	0.006[b]	0	0	0	0	0	0
	CH_3	0	0	0	0.004	0	0	0.008 - α
	H2'	0	0	0	0	0	0	0.021 - β
	H3'	0	0	0	0	0	0	0.014 - β

[a]5 mM; [b]10 mM.

none of the P-CDs is consistently most effective, either among the different cavity sizes between the α-, β- and γ-P-CDs or among the low and high-DS derivatives. Figure 4 shows a comparison of the methine resonance of the carbinol carbon and the *N*-methyl resonance of **7** with the six different P-CDs. The pronounced enantiomeric differentiation of the methine resonance with P-β-CD-L_{DS} and P-γ-CD-L_{DS} in Figure 4d and f, respectively, is apparent. The smaller enantiomeric differentiation with the P-β-CD-L_{DS} and P-β-CD-H_{DS} and the absence of enantiomeric differentiation of the methine resonance with P-α-CD-L_{DS} and P-α-CD-H_{DS} is also apparent in the spectra shown in Figure 4. For the *N*-methyl resonance, the largest enantiomeric differentiation is also observed with P-β-CD-L_{DS}, whereas no enantiomeric differentiation is observed with P-γ-CD-L_{DS}. Another interesting observation is that P-β-CD-H_{DS} and P-γ-CD-H_{DS} cause partial enantiomeric differentiation of the *N*-methyl resonance, but the order of the two enantiomers in the spectrum ((1*S*,2*R*) more shielded) is different from that with P-β-CD-L_{DS} ((1*R*,2*S*) more shielded). The use of P-CDs and CM-CDs for **7**–**10** is complementary as several of the resonances show larger enantiomeric differentiation in the NMR spectra with one of the CM-CDs, whereas others are more differentiated with one of the P-CDs.

Substrates **14**–**20** are a series of amino acids either in their ester (**14**,**16**, **18**, **19**) or acid (**17**, **20**) form. At least one resonance of **14**–**20** exhibits enantiomeric differentiation in the presence of one or more of the P-CDs (Table 3). In most cases, the enantiomeric differentiation is rather minimal with the P-CDs. However, some exceptions include the aryl hydrogen resonances of **19** with P-β-CD-L_{DS} and P-β-CD-H_{DS}, one of the methylene resonances of **19** with P-γ-H_{DS}, and the methine resonances of **16** with P-γ-CD-L_{DS}. The difference in the enantiomeric differentiation of the aryl resonances of **18** and **19** with P-β-CD-L_{DS} and P-β-CD-H_{DS} is noteworthy, as the only difference between the two substrates is that **19** is the ethyl ester and **18** is the methyl ester of 4-chlorophenylalanine. The small change from a methyl to ethyl group obviously has a significant, favorable influence on the enantiomeric differentiation of the aryl resonances while having considerably less effect on the other hydrogen resonances of **18** and **19**. Five of the substrates reported in Table 3 were previously examined with CM-CDs and while one of the CM-CDs is often more effective than the P-CDs, there are examples of resonances of **15**, **16**, **18** and **20** where one of the P-CDs causes the largest enantiomeric differentiation.

Substrates **21**–**26** contain bicyclic indoline, indane and indole rings. The P-CDs were only effective at causing enantiomeric differentiation in the ^{1}H NMR spectra of a few resonances of **21**, **24** and **26** (Table 4). With only two exceptions, the methylene resonance of **24** with P-α-CD-H_{DS} and the *O*-methyl resonance of **26** with P-γ-CD-H_{DS} and P-β-CD-L_{DS}, the CM-CDs are more effective at causing enantiomeric differentiation in the ^{1}H NMR spectra of the substrates **21**–**26**.

Substrates **27**–**29** contain naphthyl rings. Naphthyl-containing compounds form inclusion complexes more favorably with the larger β- and γ-cyclodextrins so the general ineffectiveness of P-α-CD-L_{DS} and P-α-CD-H_{DS} for **27**–**29** is not surprising (Table 5). Both the P-β-CDs and P-γ-CDs are effective at

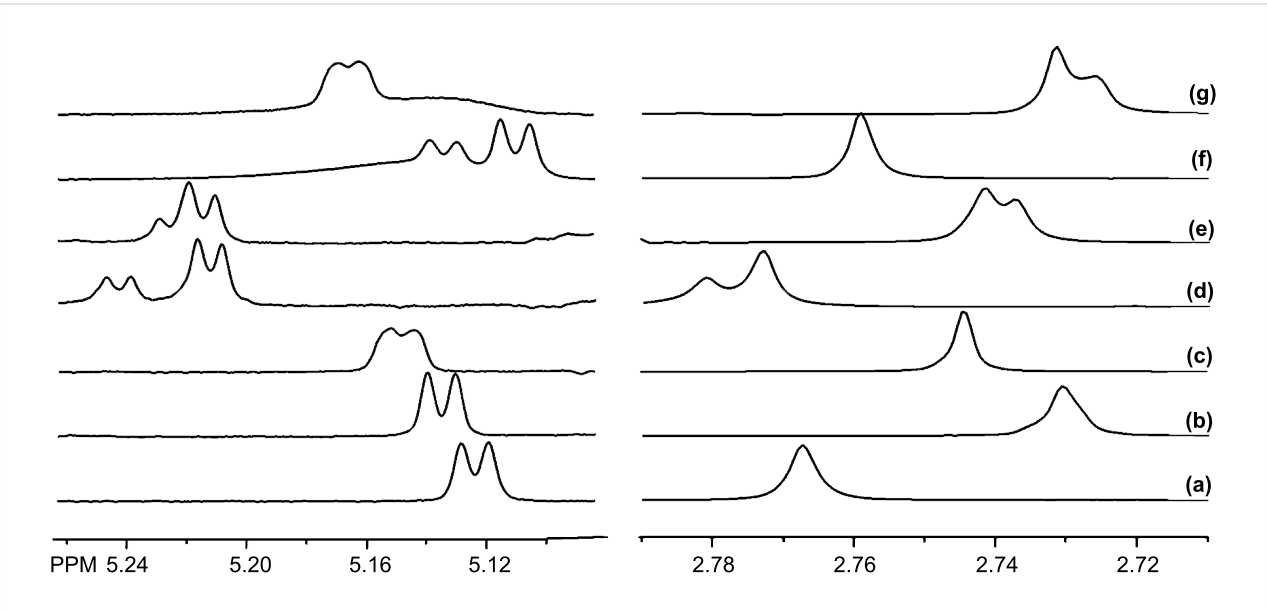

Figure 4: The (a) methine resonance of the carbinol carbon (5.124 ppm) and *N*-methyl resonance (2.768 ppm) of **7** (10 mM, enriched in (1*S*,2*R*)-enantiomer) with 20 mM of (b) P-α-CD-L_{DS}, (c) P-α-CD-H_{DS}, (d) P-β-CD-L_{DS}, (e) P-β-CD-H_{DS}, (f) P-γ-CD-L_{DS} and (g) P-γ-CD-H_{DS}.

Table 3: Enantiomeric differentiation in ppm in the ^{1}H NMR spectra (400 MHz) of **14**–**20** (10 mM) with P-CDs and CM-CD [31] in D_2O. The concentration of the cyclodextrin is 20 mM unless otherwise indicated.

		P-α-CD-L_{DS}	P-α-CD-H_{DS}	P-β-CD-L_{DS}	P-β-CD-H_{DS}	P-γ-CD-L_{DS}	P-γ-CD-H_{DS}	CM-CD
14	CH	0.007[a]	0	0	0	0	0	
15	CH	0	0	0	0	0	0	0.019 - α
	O-CH_3	0	0	0	0.007[b]	0	0	0
16	CH	0	0	0	0	0.044	0	0.016 - α
	CH_2	0	0	0	0	0	0	0.007 - α
	O-CH_3	0.002	0.002	0.003	0.005	0	0.003	0.012 - β
17	CH	0	0	0	0	0.004[a]	0	0.019 - α
	CH_2	0.007	0	0	0	0.003[a]	0	0.009 - α
	H2’	0	0	0	0	0	0	0.006 - β
	H3’	0	0	0	0	0	0	0.005 - β
18	CH	0	0	0	0.004[a]	0	0	0.004 - β
	CH_2	0	0	0	0.009[a]	0	0	0.008 - β
	O-CH_3	0.005[a]	0	0.004[a]	0.004[a]	0.004[a]	0.004[a]	0.012 - β
	H2’	0	0.010	0.009	0.009[a]	0	0	0.006 - β
	H3’	0	0.009	0	0	0	0	0.009 - β
19	CH	0.004	0	0	0.003[a]	0	0	
	CH_2	0	0	0	0.005[a]	0	0.035[a]	
	CH_2’	0.005	0	0	0	0	0	
	CH_3	0	0	0	0.002	0	0	
	H2’	0	0	0.021	0.021	0	0	
	H3’	0	0	0.037[a]	0.034	0	0	
20	Ar-CH_2	0.013[a]	0.014	0.006	0	0	0	0

[a]10 mM; [b]5 mM.

Table 4: Enantiomeric differentiation in ppm in the ^{1}H NMR spectra (400 MHz) of **21** and **24**–**26** (10 mM) with P-CDs and CM-CD [31] in D_2O. The concentration of the cyclodextrin is 20 mM unless otherwise indicated.

		P-α-CD-L_{DS}	P-α-CD-H_{DS}	P-β-CD-L_{DS}	P-β-CD-H_{DS}	P-γ-CD-L_{DS}	P-γ-CD-H_{DS}	CM-CD
21	CH_2	0.007	0.002	0	0	0	0	0.009 - β
	CH_3	0.005	0	0	0	0.009[a]	0	0.015 - β
24	CH_2	0.004[b]	0.007[a]	0	0.004[b]	0	0	0
25	CH	0	0	0	0	0	0	0.036 - γ
	CH_2	0	0	0	0	0	0	0.013 - α
	H2	0	0	0	0	0	0	0.010 - γ
	H4	0	0	0	0	0	0	0.008 - γ
	H5	0	0	0	0	0	0	0.019 - β
	H6	0	0	0	0	0	0	0.019 - β
	H7	0	0	0	0	0	0	0.022 - β
26	CH	0	0	0	0	0	0	0.016 - β
	O-CH_3	0	0	0.010[b]	0	0	0.012[b]	0
	H2	0	0	0	0	0	0	0.011 - β
	H5	0	0	0	0	0	0	0.019 - β
	H6	0	0	0	0	0	0	0.019 - β
	H7	0	0	0	0	0	0	0.020 - β

[a]10 mM; [b]5 mM.

Table 5: Enantiomeric differentiation in ppm in the ^{1}H NMR spectra (400 MHz) of **27**–**29** (10 mM) with P-CDs and CM-CD [31] in D_2O. The concentration of the cyclodextrin is 20 mM unless otherwise indicated.

		P-α-CD-L_{DS}	P-α-CD-H_{DS}	P-β-CD-L_{DS}	P-β-CD-H_{DS}	P-γ-CD-L_{DS}	P-γ-CD-H_{DS}	CM-CD
27	CH_3	0.004[a]	0.004[a]	0	0	0.004[a]	0.005[a]	
28	CH	0	0	0	0.020	0	0	
	N-CH_3	0	0	0.016[a]	0.011[a]	0.016[a]	0	
	C-CH_3	0	0	0	0	0.011[a]	0	
	H4	0	0	0	0	0.013[a]	0	
	H8	0	0	0	0	0.011[a]	0	
29	N-CH_2	0	0	0.006[a]	0.008	0.007[b]	0.008[a]	0
	O-CH_2	0	0	0	0	0	0.006[b]	0
	C-CH_3	0	0	0.027	0.009	0	0	0
	H2	0	0	0	0	0	0	0.017 - γ
	H8	0	0	0	0	0	0	0.022 - γ

[a]10 mM; [b]5 mM.

causing enantiomeric differentiation in resonances of **27**–**29**. An interesting observation is the ineffectiveness of P-γ-CD-H_{DS} at causing enantiomeric differentiation of in the spectrum of **28**, whereas the P-γ-CD-L_{DS} causes enantiomeric differentiation of four resonances. Similarly, enantiomeric differentiation of the *C*-methyl resonance of **29** with P-β-CD-L_{DS} is much larger (0.027 ppm) than that with P-β-CD-H_{DS} (0.009 ppm). Substrate **29** is also examined with CM-CDs, further confirming the conclusion that the CM-CDs and P-CDs provide complementary results. CM-γ-CD causes enantiomeric differentiation of two of the aryl resonances of **29** that is not observed with the P-CDs. However, the P-β- and P-γ-CDs cause enantiomeric differentiation of aliphatic resonances of **29** that is not observed with the CM-CDs.

Substrates **30**–**33** are a series of antihistamines that have both an aryl and a pyridyl ring. Of all the compounds examined previously with the CM-CDs, **30**–**33** were noteworthy for both the number of resonances that exhibited enantiomeric differentiation and the magnitude of the distinction. Many resonances exhibit enantiomeric differentiation greater than 0.02 ppm, with one as high as 0.08 ppm, for **30**–**33** with CM-CDs (Table 6). While the P-CDs are not nearly as effective for **30**–**33** as the CM-CDs, there are still eight resonances of **30**–**33** where one of the P-CDs caused larger enantiomeric differentiation than any of the CM-CDs. As with many of the other compounds examined herein, the P-CDs tend to be most effective at causing enantiodifferentiation for the aliphatic resonances.

Earlier studies with the CM-CDs demonstrated the effectiveness of adding paramagnetic lanthanide ions such as praseodymium(III) and ytterbium(III) to enhance the enantiomeric differentiation in the NMR spectra of cationic substrates [29-32]. The lanthanide cation binds to the anionic carboxymethyl group on the CM-CD and the magnetic field of the paramagnetic lanthanide ion perturbs the chemical shifts of the substrate bound in the cyclodextrin cavity by a through-space (pseudocontact) mechanism. The ability of paramagnetic lanthanide ions to improve the enantiomeric differentiation in the spectra of substrates in mixtures with P-CDs was next explored.

In some cases, mixing praseodymium(III) or ytterbium(III) nitrate with the P-CD resulted in the formation of a precipitate. In those cases where the addition of lanthanide(III) nitrates to P-CD–substrate mixtures did not result in the formation of a precipitate, the spectra were often broadened. One reason for the broadening may be caused by the slower exchange within the larger ternary lanthanide–P-CD–substrate complex. Another is because the paramagnetic species shortens the relaxation time of the excited nuclei causing uncertainty broadening.

One example where the addition of a lanthanide ion did produce a large enhancement in enantiomeric differentiation is shown in Figure 5 for the *N*-methyl resonance of **7**. The series of spectra in Figure 5 is for a mixture of **7** (10 mM) and P-β-CD-L_{DS} (20 mM) with increasing concentrations of ytterbium(III) nitrate. The *N*-methyl resonance of **7** with only P-β-CD-L_{DS} shown in Figure 5a exhibits a small degree of enantiomeric differentiation (0.008 ppm). The mixture with ytterbium(III) at 16 mM exhibits an enantiomeric differentiation of 0.109 ppm. An interesting observation is that the resonance of the (1*S*,2*R*)-enantiomer is more shielded on the addition of ytterbium(III) whereas the resonance of the (1*R*,2*S*)-enantiomer is deshielded. The equation that predicts the magnitude of the through-space shifts caused by a lanthanide ion has an angle term that can be either

Table 6: Enantiomeric differentiation in ppm in the ^{1}H NMR spectra (400 MHz) of **30**–**33** (10 mM) with P-CDs and CM-CD [21,31] in D_2O. The concentration of the cyclodextrin is 20 mM unless otherwise indicated.

		P-α-CD-L_{DS}	P-α-CD-H_{DS}	P-β-CD-L_{DS}	P-β-CD-H_{DS}	P-γ-CD-L_{DS}	P-γ-CD-H_{DS}	CM-CD
30	CH	0	0	0	0	0	0	0.039 - α
	N-CH_2	0	0	0.010	0.011[a]	0	0	0
	N-CH_2'	0	0	0.013	0.013[a]	0	0	0
	H4	0	0	0	0	0	0	0.018 - γ
	H3'	0	0	0	0	0	0	0.075 - α
	H4'	0	0	0.004	0.005[a]	0	0.004	0.080 - α
	H6'	0	0	0	0	0	0	0.042 - β
31	CH	0	0	0.013	0.008[a]	0.015	0	0.021 - α
	N-CH_3	0.011	0.016	0	0	0	0	0
	H2	0	0	0.005	0	0	0.005	0.034 - β
	H3	0	0	0.013	0.014	0	0	0.040 - γ
	H3'	0	0	0	0	0.012[a]	0	0.069 - α
	H4'	0	0	0.015	0.015	0	0	0.074 - β
	H5'	0	0	0	0	0	0.017	0
	H6'	0	0	0	0	0	0	0.047 - β
32	N-CH_2	0	0	0.011[a]	0	0	0	0
	O-CH_2	0.011[a]	0	0	0	0	0	0
	C-CH_3	0	0.005	0	0.006	0	0	0.021 - β
	H3'	0	0.008	0.009	0.007	0	0	0.010 - γ
	H4'	0	0	0	0	0	0	0.021 - β
	H5'	0	0	0.020	0.021	0	0.004	0
	H6'	0	0	0.018[a]	0.012	0	0	0.013 - β
33	CH	0.016[a]	0.019[a]	0	0	0	0.020	0.013 - β
	H2	0.019	0.019	0	0	0	0	0.021 - γ
	H3	0	0	0	0	0	0	0.004 - β
	H4'	0	0	0	0	0	0	0.020 - α
	H6'	0	0	0	0	0	0	0.027 - γ

[a]10 mM.

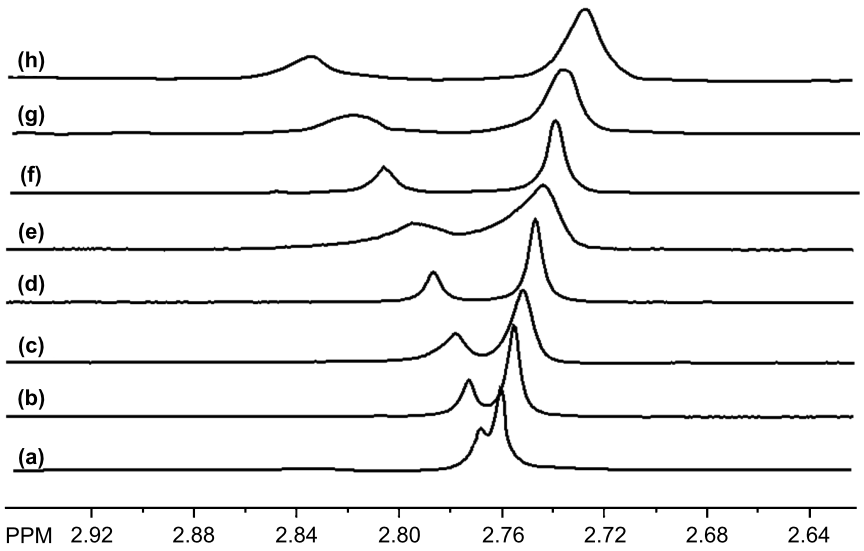

Figure 5: The *N*-methyl resonance of **7** (10 mM, enriched in (1S,2R)-enantiomer) with P-β-CD-L_{DS} (20 mM) and concentrations of ytterbium(III) nitrate of (a) 0 mM, (b) 2 mM, (c) 4 mM, (d) 6 mM, (e) 8 mM, (f) 10 mM, (g) 12 mM and (h) 16 mM.

positive or negative depending on the geometry of the complex and the position of a nucleus relative to the principle magnetic axis of the complex. In all likelihood, the behavior seen in the spectra in Figure 5 reflects differences in the sign of this angle term for the two enantiomers [31,32].

Conclusion

Twenty-three out of the 33 substrates were studied with the P-CDs and CM-CDs. Overall, 54 different resonances exhibited larger enantiomeric differentiation with one of the CM-CDs, whereas 26 different resonances exhibited larger distinction with one of the P-CDs. For 16 of the 23 substrates, there is at least one resonance where larger enantiomeric differentiation was observed with one of the P-CDs. With substrates **3**, **20** and **24**, at least one of the P-CDs caused enantiomeric differentiation whereas none of the CM-CDs was effective. In some cases, it is also possible to add a paramagnetic lanthanide ion such as praseodymium(III) or ytterbium(III) to enhance the enantiomeric differentiation in the ^{1}H NMR spectrum of a substrate mixed with a P-CD. Given these observations and the fact that the P-CDs are commercially available, their use as potential chiral NMR reagents for water-soluble cationic compounds is warranted.

Experimental

I. Reagents

Sodium salts of phosphated α-, β- and γ-cyclodextrin with low (2–6) and high DS (6–10) were obtained from CarboMer Inc., San Diego, California. The P-CDs were refrigerated between 2–8 °C until use as recommended by the manufacturer. Substrates were obtained from commercial sources either as hydrochloride salts or neutral compounds. Neutral substrates were converted to their hydrochloride salts in deuterium oxide (D_2O) by adding a slight excess of deuterium chloride (DCl).

II. Apparatus

Proton (^{1}H) NMR spectra were obtained using a Bruker Avance 400 MHz NMR spectrometer. Samples were run in D_2O with 8 scans at ambient probe temperature.

III. Procedure

Stock solutions of the P-α-CDs (40 mM), P-γ-CDs (40 mM) and cationic substrates (20 mM), which were enriched in one enantiomer when available, were prepared in D_2O. P-CD and substrate solutions were kept at ambient temperature. Appropriate aliquots of P-α or P-γ-CD, substrate, and D_2O were combined in NMR tubes to obtain a 600 μL solution of 20, 10, or 5 mM P-CD and 10 mM substrate. The P-β-CDs were not soluble in D_2O at 40 mM and 20 mM stock solutions were used in preparing P-β-CD samples at 5 and 10 mM. An appropriate amount of the P-β-CD was weighed for 20 mM solutions.

Supporting Information

Supporting Information File 1

Complete ^{1}H NMR spectra are provided for the samples in Figures 3 and 4. Additional regions of the spectra of Figure 5 are provided.
[http://www.beilstein-journals.org/bjoc/content/supplementary/1860-5397-13-6-S1.pdf]

Acknowledgements

We thank the National Science Foundation (Research at Undergraduate Institutions Program Grant CHE-1145061; Major Research Instrumentation Program, Grant CHE-0115579) for supporting this work.

References

1. Uccello-Barretta, G.; Balzano, F. *Top. Curr. Chem.* **2013,** *341,* 69–131. doi:10.1007/128_2013_445
2. Wenzel, T. J.; Chisholm, C. D. *Prog. Nucl. Magn. Reson. Spectrosc.* **2011,** *59,* 1–63. doi:10.1016/j.pnmrs.2010.07.003
3. Wenzel, T. J. *Discrimination of chiral compounds using NMR spectroscopy;* Wiley Press: Hoboken, NJ, 2007.
4. Webb, T. H.; Wilcox, C. S. *Chem. Soc. Rev.* **1993,** *22,* 383–395. doi:10.1039/CS9932200383
5. Parker, D. *Chem. Rev.* **1991,** *91,* 1441–1457. doi:10.1021/cr00007a009
6. Pirkle, W. H.; Hoover, D. J. *Top. Stereochem.* **1982,** *13,* 263–331. doi:10.1002/9780470147221.ch4
7. Uccello-Baretta, G.; Balzano, F.; Salvadori, P. *Curr. Pharm. Des.* **2006,** *12,* 4023–4045. doi:10.2174/138161206778743628
8. Greatbanks, D.; Pickford, R. *Magn. Reson. Chem.* **1987,** *25,* 208–215. doi:10.1002/mrc.1260250306
9. Casy, A. F.; Mercer, A. D. *Magn. Reson. Chem.* **1988,** *26,* 765–774. doi:10.1002/mrc.1260260908
10. Uccello-Barretta, G.; Balzano, F.; Caporusso, A. M.; Salvadori, P. *J. Org. Chem.* **1994,** *59,* 836–839. doi:10.1021/jo00083a026
11. Uccello-Barretta, G.; Balzano, F.; Caporusso, A. M.; Iodice, A.; Salvadori, P. *J. Org. Chem.* **1995,** *60,* 2227–2231. doi:10.1021/jo00112a050
12. Uccello-Barretta, G.; Balzano, F.; Menicagli, R.; Salvadori, P. *J. Org. Chem.* **1996,** *61,* 363–365. doi:10.1021/jo951314l
13. Uccello-Barretta, G.; Cuzzola, A.; Balzano, F.; Menicagli, R.; Salvadori, P. *Eur. J. Org. Chem.* **1998,** 2009–2012. doi:10.1002/(SICI)1099-0690(199809)1998:9<2009::AID-EJOC2009>3.0.CO;2-V
14. Uccello-Barretta, G.; Cuzzola, A.; Balzano, F.; Menicagli, R.; Iuliano, A.; Salvadori, P. *J. Org. Chem.* **1997,** *62,* 827–835. doi:10.1021/jo961562x
15. Uccello-Barretta, G.; Ferri, L.; Balzano, F.; Salvadori, P. *Eur. J. Org. Chem.* **2003,** 1741–1748. doi:10.1002/ejoc.200210504
16. Yashima, E.; Yamada, M.; Yamamoto, C.; Nakashima, M.; Okamoto, Y. *Enantiomer* **1997,** *2,* 225–240.
17. Uccello-Barretta, G.; Balzano, F.; Sicoli, G.; Scarselli, A.; Salvadori, P. *Eur. J. Org. Chem.* **2005,** 5349–5355. doi:10.1002/ejoc.200500506

18. Kuroda, Y.; Suzuki, Y.; He, J.; Kawabata, T.; Shibukawa, A.; Wada, H.; Fujima, H.; Go-oh, Y.; Imai, E.; Nakagawa, T. *J. Chem. Soc., Perkin Trans. 2* **1995,** 1749–1759. doi:10.1039/P29950001749
19. Holzgrabe, U.; Mallwitz, H.; Branch, S. K.; Jefferies, T. M.; Wiese, M. *Chirality* **1997,** *9,* 211–219. doi:10.1002/(SICI)1520-636X(1997)9:3<211::AID-CHIR2>3.0.CO;2-I
20. Branch, S. K.; Holzgrabe, U.; Jefferies, T. M.; Mallwitz, H.; Oxley, F. J. R. *J. Chromatogr. A* **1997,** *758,* 277–292. doi:10.1016/S0021-9673(96)00734-0
21. Dignam, C. F.; Randall, L. A.; Blacken, R. D.; Cunningham, P. R.; Lester, S.-K. G.; Brown, M. J.; French, S. C.; Aniagyei, S. E.; Wenzel, T. J. *Tetrahedron: Asymmetry* **2006,** *17,* 1199–1208. doi:10.1016/j.tetasy.2006.04.006
22. Endresz, G.; Chankvetadze, B.; Bergenthal, D.; Blaschke, G. *J. Chromatogr. A* **1996,** *732,* 133–142. doi:10.1016/0021-9673(95)01244-3
23. Owens, P. K.; Fell, A. F.; Coleman, M. W.; Berridge, J. C. *J. Chromatogr. A* **1998,** *797,* 149–164. doi:10.1016/S0021-9673(97)00982-5
24. Owens, P. K.; Fell, A. F.; Coleman, M. W.; Kinns, M.; Berridge, J. C. *J. Pharm. Biomed. Anal.* **1997,** *15,* 1603–1619. doi:10.1016/S0731-7085(97)00030-7
25. Chankvetadze, B.; Schulte, G.; Bergenthal, D.; Blaschke, G. *J. Chromatogr. A* **1998,** *798,* 315–323. doi:10.1016/S0021-9673(97)00999-0
26. Chankvetadze, B.; Burjanadze, N.; Bergenthal, D.; Strickmann, D.; Blaschke, G.; Pintore, G.; Cerri, R. *Electrophoresis* **1998,** *19,* 2101–2108. doi:10.1002/elps.1150191210
27. Park, K.-L.; Kim, K. H.; Jung, S.-H.; Lim, H.-M.; Hong, C.-H.; Kang, J.-S. *J. Pharm. Biomed. Anal.* **2002,** *27,* 569–576. doi:10.1016/S0731-7085(01)00580-5
28. Lee, S.-H.; Yi, D.-H.; Jung, S.-H. *Bull. Korean Chem. Soc.* **2004,** *25,* 216–220. doi:10.5012/bkcs.2004.25.2.216
29. Smith, K. J.; Wilcox, J. D.; Mirick, G. E.; Wacker, L. S.; Ryan, N. S.; Vensel, D. A.; Readling, R.; Domush, H. L.; Amonoo, E. P.; Shariff, S. S.; Wenzel, T. J. *Chirality* **2003,** *15,* S150–S158. doi:10.1002/chir.10254
30. Wenzel, T. J.; Amoono, E. P.; Shariff, S. S.; Aniagyei, S. E. *Tetrahedron: Asymmetry* **2003,** *14,* 3099–3104. doi:10.1016/j.tetasy.2003.07.019
31. Provencher, K. A.; Weber, M. A.; Randall, L. A.; Cunningham, P. R.; Dignam, C. F.; Wenzel, T. J. *Chirality* **2010,** *22,* 336–346. doi:10.1002/chir.20748
32. Provencher, K. A.; Wenzel, T. J. *Tetrahedron: Asymmetry* **2008,** *19,* 1797–1803. doi:10.1016/j.tetasy.2008.07.024
33. Chankvetadze, B.; Burjanadze, N.; Maynard, D. M.; Bergander, K.; Bergenthal, D.; Blaschke, G. *Electrophoresis* **2002,** *23,* 3027–3034. doi:10.1002/1522-2683(200209)23:17<3027::AID-ELPS3027>3.0.CO;2-V
34. Kahle, C.; Deubner, R.; Schollmayer, C.; Scheiber, J.; Baumann, K.; Holzgrabe, U. *Eur. J. Org. Chem.* **2005,** 1578–1589. doi:10.1002/ejoc.200400673
35. Zhou, Z.; Thompson, R.; Reamer, R. A.; Lin, Z.; French, M.; Ellison, D.; Wyvratt, J. *Electrophoresis* **2003,** *24,* 2448–2455. doi:10.1002/elps.200305510
36. Chankvetadze, B.; Endresz, G.; Bergenthal, D.; Blaschke, G. *J. Chromatogr. A* **1995,** *717,* 245–253. doi:10.1016/0021-9673(95)00489-4
37. Owens, P. K.; Fell, A. F.; Coleman, M. W.; Berridge, J. C. *J. Inclusion Phenom. Macrocyclic Chem.* **2000,** *38,* 133–151. doi:10.1023/A:1008123229006
38. Kano, K.; Hasegawa, H. *J. Am. Chem. Soc.* **2001,** *123,* 10616–10627. doi:10.1021/ja0112644
39. Kano, K.; Hasegawa, H. *J. Inclusion Phenom. Macrocyclic Chem.* **2001,** *41,* 41–47. doi:10.1023/A:1014429907212
40. Brown, S. E.; Coates, J. H.; Duckworth, P. A.; Lincoln, S. F.; Easton, C. J.; May, B. L. *J. Chem. Soc., Faraday Trans.* **1993,** *89,* 1035–1040. doi:10.1039/FT9938901035
41. Park, K. K.; Lim, H. S.; Park, J. W. *Bull. Korean Chem. Soc.* **1999,** *20,* 211–213.
42. Rekharsky, M.; Yamamura, H.; Kawai, M.; Inoue, Y. *J. Am. Chem. Soc.* **2001,** *123,* 5360–5361. doi:10.1021/ja003810j
43. Chisholm, C. D.; Wenzel, T. J. *Tetrahedron: Asymmetry* **2011,** *22,* 62–68. doi:10.1016/j.tetasy.2010.12.001
44. Dowey, A. E.; Puentes, C. M.; Carey-Hatch, M.; Sandridge, K. L.; Krishna, N. B.; Wenzel, T. J. *Chirality* **2016,** *28,* 299–305. doi:10.1002/chir.22582
45. Tanaka, Y.; Yanagawa, M.; Terabe, S. International Symposium on Chromatography, Yokohama, Japan, Jan 22–25, 1995; Hatano, H.; Hanai, T., Eds.; World Scientific, 1995; pp 395–400.
46. Nishi, H. *J. High Resolut. Chromatogr.* **1995,** *18,* 659–664. doi:10.1002/jhrc.1240181009
47. Juvancz, Z.; Jicsinszky, L.; Markides, K. E. *J. Microcolumn Sep.* **1997,** *9,* 581–589. doi:10.1002/(SICI)1520-667X(1997)9:8<581::AID-MCS1>3.0.CO;2-Y
48. Yanes, E. G.; Gratz, S. R.; Sutton, R. M. C.; Stalcup, A. M. *Fresenius' J. Anal. Chem.* **2001,** *369,* 412–417. doi:10.1007/s002160000643
49. Klika, K. D. *Tetrahedron: Asymmetry* **2009,** *20,* 1099–1102. doi:10.1016/j.tetasy.2009.03.036

License and Terms

BEILSTEIN JOURNAL OF ORGANIC CHEMISTRY

Dynamics and interactions of ibuprofen in cyclodextrin nanosponges by solid-state NMR spectroscopy

Monica Ferro[1], Franca Castiglione[*1], Nadia Pastori[1], Carlo Punta[1], Lucio Melone[2], Walter Panzeri[3], Barbara Rossi[4,5], Francesco Trotta[6] and Andrea Mele[*1,3]

Full Research Paper

Open Access

Address:
[1]Department of Chemistry, Materials and Chemical Engineering "G. Natta", Politecnico di Milano, Piazza L. da Vinci 32 – 20133 Milano, Italy, [2]Università degli Studi e-Campus, Via Isimbardi 10, 22060 Novedrate, Como, Italy, [3]CNR-ICRM, Via L. Mancinelli 7, 20131 Milano, Italy, [4]Elettra – Sincrotrone Trieste, Strada Statale 14 km 163.5, Area Science Park, 34149 Trieste, Italy, [5]Department of Physics, University of Trento, via Sommarive 14, 38123 Povo, Trento, Italy and [6]Department of Chemistry, University of Torino, Via Pietro Giuria 7, 10125 Torino, Italy

Email:
Franca Castiglione* - franca.castiglione@polimi.it; Andrea Mele* - andrea.mele@polimi.it

* Corresponding author

Keywords:
cross-polarization; cyclodextrin; ibuprofen; nanosponges; solid-state NMR

Beilstein J. Org. Chem. **2017,** *13,* 182–194.
doi:10.3762/bjoc.13.21

Received: 31 October 2016
Accepted: 12 January 2017
Published: 27 January 2017

This article is part of the Thematic Series "Superstructures with cyclodextrins: Chemistry and applications IV".

Guest Editor: G. Wenz

Abstract

Two different formulations of cyclodextrin nanosponges (CDNS), obtained by polycondensation of β-cyclodextrin with ethylenediaminetetraacetic acid dianhydride (EDTAn), were treated with aqueous solutions of ibuprofen sodium salt (IbuNa) affording hydrogels that, after lyophilisation, gave two solid CDNS-drug formulations. ^{1}H fast MAS NMR and ^{13}C CP-MAS NMR spectra showed that IbuNa was converted in situ into its acidic and dimeric form (IbuH) after freeze-drying. ^{13}C CP-MAS NMR spectra also indicated that the structure of the nanosponge did not undergo changes upon drug loading compared to the unloaded system. However, the ^{13}C NMR spectra collected under variable contact time cross-polarization (VCT-CP) conditions showed that the polymeric scaffold CDNS changed significantly its dynamic regime on passing from the empty CDNS to the drug-loaded CDNS, thus showing that the drug encapsulation can be seen as the formation of a real supramolecular aggregate rather than a conglomerate of two solid components. Finally, the structural features obtained from the different solid-state NMR approaches reported matched the information from powder X-ray diffraction profiles.

Introduction

In the last ten years cyclodextrin nanosponges (CDNS) polymer materials received great attention as promising new materials in several fields of applications such as bio-catalysis, agriculture, analytical chemistry [1,2] and in pharmaceutical research. Their wide applicability is mostly due to their nanoporous structure, along with their high chemical and thermal stabilities. Consid-

ering the pharmaceutical applications, they received interest as drug carriers, since these materials are able to accommodate small drug molecules within their porous network made of CD lipophilic cavities and more hydrophilic polymer channels originated during the cross-linking process with suitable cross-linking agents (CL). The polymer is obtained by condensation reaction of the OH groups of the glucopyranose units of cyclodextrins (CD) with a poly-functional cross-linking agent [3]. CDNS have been characterized, in the solid state, by a repertoire of physical methods such as solid-state ^{13}C CP-MAS NMR, FTIR and Raman spectroscopy [4-6]. Moreover, in many of their formulations, CDNS showed good swelling capability when contacted with water solutions, giving rise to homogeneous hydrogels potentially useful as drug carriers [7]. In order to obtain an effective control over the drug delivery procedure, several efforts have been made to explore how the nanoporous polymer structure influences the delivery property of entrapped drugs [8]. In particular the transport properties of ibuprofen sodium salt (IbuNa) entrapped in CDNS polymer gels has been investigated by high resolution magic angle spinning (HR-MAS) NMR technique [9] as a paradigmatic case of an active pharmaceutical ingredient (API) entrapped in a polymeric scaffold. The results pointed out that the motion of a small drug molecule drastically changes from subdiffusive to slightly superdiffusive regimes depending on the cyclodextrin to CL molar ratio, and hence on the CDNS polymeric structure. Ibuprofen is the API of many nonsteroidal anti-inflammatory formulations widely used in the treatment of fever, rheumatoid arthritis and other inflammatory diseases [10]. From the chemical viewpoint, ibuprofen is the (*RS*)-2-(4-(2-methylpropyl)phenyl)propanoic acid. Its sodium salt is water-soluble and absorbed in blood plasma more quickly than the undissociated acid [11]. In the following, we will refer to the undissociated acid as IbuH and to the sodium salt as IbuNa. For both IbuH and IbuNa, the desired pharmacological effects are due to the *S*-enantiomer. Nevertheless, the commercially available drug is the racemic mixture (*R,S*)-ibuprofen. Moreover, solid-state NMR spectra revealed that in all tablet samples, ibuprofen is present in acidic form IbuH with different contents of bound water within tablets [12] depending on the formulation.

In this work the racemic (*R,S*)-ibuprofen sodium salt (IbuNa) was encapsulated in cyclodextrin nanosponges (CDNS) obtained by cross-linking of β-cyclodextrin with ethylenediaminetetraacetic acid dianhydride (EDTAn) in two different preparations: CDNS(1:4) and CDNS(1:8), where the 1:*n* notation indicates the CD to EDTAn molar ratio used for the synthesis. The solid state products were prepared via freeze-drying of the hydrogels obtained by swelling the nanosponge with aqueous solutions of IbuNa. The main purpose of the present work is to investigate the structural changes of the host CDNS material as well as the drug chemical and structural modifications in the polymer network in the solid state. The methodological approach here presented relies upon two different solid state NMR methodologies and it is finally supported by powder X-ray diffraction (PXRD) data. In particular, here we present the use of variable contact time (VCT) cross-polarization ^{13}C NMR as a novel and powerful source of information on the drug loaded polymers, complementary to the chemical shift data achievable with the commonly employed ^{13}C CP-MAS NMR spectra. In a typical VCT experimental session, an array of CP-MAS spectra are collected by modulating the contact time needed for cross polarization. The experimental data can be fitted by using suitable theoretical models. When feasible, the fitting procedure affords important relaxation parameters such as the proton spin-lattice relaxation times $T_{1\rho}$(H) and the ^{1}H–^{13}C cross-polarization time constant T_{CH}. In general, the outcome of VCT data processing is a "dynamic fingerprint" that can be used for the characterization of the polymer-drug system.

In general, the CP-VCT methodology can be exploited to provide a dynamic characterization of polymeric systems which are expected to be structurally similar, as recently demonstrated for molecular imprinted epichlorohydrin–cyclodextrin polymers [13]. In the present work, CDNS(1:4) and CDNS(1:8), along with the corresponding ibuprofen loaded systems, are used as a paradigmatic case. The CDNS do not show significant chemical shift variations on passing from the unloaded polymers to the drug-loaded systems, thus making their characterization difficult. The dynamic fingerprint provided by the VCT data allows overcoming this problem. In a broader sense, CP-VCT techniques can be considered a convenient approach for systems in which the common NMR parameters, like chemical shift and line-width, may fail to provide an acceptable characterization due to high structural similarity at molecular level.

Finally yet importantly, in the present work we also report on solid state ^{1}H NMR spectra of the examined compounds acquired under fast magic angle spinning (Fast MAS) conditions. As detailed in the Discussion, this technique is quite rarely used. The results of the ^{1}H Fast MAS NMR experiments provided further structural details of the state of the drug molecule loaded in the CDNS materials.

Theoretical Aspects

The CP-MAS experiment and CP dynamics

Cross-polarization (CP) is a SSNMR technique originally developed for enhancing the signal intensities of low-abundance spins, generally referred to as *S* spins (typically ^{13}C, ^{15}N, ^{29}Si etc.) by polarization transfer from high-abundance spins, in turn labelled as *I* spins (usually protons). The transfer of magnetiza-

tion occurs via heteronuclear dipolar interaction between the two spin species (*I*–*S*) when the Hartmann–Hahn condition is met. In the present work only ^{1}H,^{13}C magnetization transfer will be considered, thus the Hartmann–Hahn condition can be expressed as: $\gamma(^{1}H)B_1(^{1}H) = \gamma(^{13}C)B_1(^{13}C)$, where γ are the gyromagnetic ratios of the nuclei and B_1 is the so-called spin-lock field generated by the spectrometer acquisition hardware. The efficiency of the CP process strongly depends on the structural and dynamic properties of the system, in particular molecular conformational changes, rotational dynamics and internuclear distances in the solid state. The CP dynamic regime can be explored by acquiring several experiments at increasing contact time (CT). This methodology is called Variable Contact Time (VCT); generally, the CT is increased from few μs to some ms. A quantitative analysis of the CP data can be performed by fitting the experimental curves of the CP intensity, *I*(t), versus the contact time *t*. The fitting procedure follows several theoretical models. A complete description of the theory and practical considerations is reported in the review article of Kolodziejski and Klinowski [14]. In the following, we will describe in detail two models: the classical *I*–*S* model and the *I*–*I**–S model.

The classical *I*–*S* model

This theoretical model, initially developed by Mehring [15], is based on the classical spin thermodynamics. The system is described as consisting of a lattice with a huge heat capacity and two subsystems, the isolated *S* spins and an extended network of coupled *I* spins. The heat capacity of the rare *S* spins is much lower than that of *I* spins. According to this model, the spins *I* are characterized by a rapid spin diffusion so that they behave as a single spin system at a uniform spin temperature.

After the initial excitation pulse of the *I* spins, when the Hartmann–Hahn condition is met the magnetization is transferred from the *I* spins to the observed *S* spins. The schematic representation of the CP process is shown in the left-hand part of Figure 1.

The enhanced signal of the *S* spins detected as a function of the of cross-polarization contact time, *t*, is expressed as follows (Equation 1):

$$S(t) = I_0 \frac{k_{IS}}{(k_{IS} + k_S) - k_I}\left[\exp^{-k_I t} - \exp^{-(k_{IS}+k_S)t}\right] \quad (1)$$

where k_{IS} is the rate constant for the "heat flow" between the I and S spins, and k_I, k_S are the inverse of the spin-lattice relaxation times in the rotating frame for the spin *I* ($T_{1\rho}$(H)) and *S* ($T_{1\rho}$(S)), respectively. The simplified Equation (2) is obtained assuming that: 1) $k_S < k_{IS}$ (k_S is negligible), 2) $k_{IS} + k_S > k_I$, the system is in the fast CP regime.

$$S(t) = I_0 \frac{k_{IS}}{k_{IS} - k_I}\left[\exp^{-k_I t} - \exp^{-k_{IS} t}\right] \quad (2)$$

According to Equation 2, the magnetization of the *S* spins rises with the CP rate constant k_{IS}, reaches the maximum S_{CPMAX} at time t_{MAX} and, subsequently, decreases with the time constant k_I. Some experimental curves showing the trends mentioned before are shown in Figure 7. Finally, the two relaxation parameters T_{CH} and $T_{1\rho}$(H) can be determined, in principle, by fitting the experimental curves with the bi-exponential Equation 2.

The *I*–*I**–*S* model

In the *I*–*I**–*S* model, the reservoir of the *I* (^{1}H) nuclei surrounding a given *S* (^{13}C) nucleus is divided into two subsets: *I** indicates the protons closest to the observed S nucleus, *I* the nuclei at longer distances. This model was proposed to explain the case when the proton spin diffusion rate $1/T_{Diff}$ is not fast

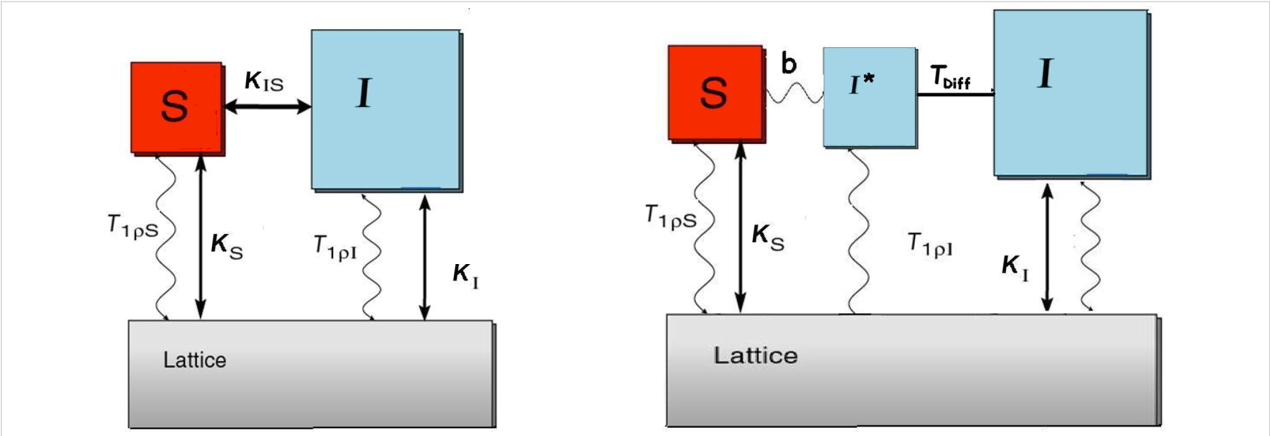

Figure 1: Schematic thermodynamic description of the CP process and time constants. The *I*-*S* model (left), the *I*–*I**–*S* model (right). Adapted with permission from [14]. Copyright 2002 American Chemical Society.

enough so that the *I* spins do not behave as a whole spin system. The *I**–*S* spin pairs are isolated from the spin network and exchange polarization in an oscillatory mode. The oscillations are damped by the spin-diffusion contact with the whole *I* spin system. A schematic representation of the physical process is reported in the right-hand side panel of Figure 1. The oscillatory CP kinetics is described [16] by the Equation 3:

$$S(t) = I_0 \exp^{-k_1 t}\left[1-\frac{1}{2}\exp^{-\frac{t}{T_{\mathrm{Diff}}}}-\frac{1}{2}\exp^{-\frac{3t}{2T_{\mathrm{Diff}}}}\cos\left(\frac{2\pi bt}{2}\right)\right] \quad (3)$$

where *b* is the heteronuclear dipolar coupling. Further mathematical developments allow determining the composition of the spin cluster.

The oscillatory behaviour of the signal intensity in ^{1}H–^{13}C VCT experiments was observed for the first time on single crystals [16-18]. It was found that the frequency of oscillation depends on the heteronuclear dipolar coupling *b* due to the orientation of the single crystal respect to the external magnetic field. Later on, similar results have been found for other systems, including powders, bilayers, and supramolecular complexes [19].

Comparing the two models, it was demonstrated that the *I*–*I**–*S* model applies in special cases when the whole spin system has strong *I**–*S* dipolar interactions and weak homonuclear *I*-*I** dipolar couplings [14]. In the opposite case, i.e., when weak *I**−*S* and strong *I*−*I** couplings are present, the CP kinetics follow the more general *I*−*S* model. As a final remark, we wish to stress that the oscillatory behaviour described above has not been reported frequently so far, and that the data reported and discussed in the following of this work represent an example.

Results and Discussion

Solid-state NMR

^{1}H MAS NMR spectroscopy

^{1}H high-resolution spectra of small organic molecules, characterised by the isotropic chemical shift and *J* couplings, are easily obtained in solution. By contrast, for rigid solids, the corresponding solid-state ^{1}H NMR spectrum generally shows broad, featureless lines due to the strong homonuclear dipolar couplings among protons, which in many cases exceed the range of chemical shifts. Consequently, solid-state ^{1}H NMR spectra are seldom reported, the assignment of the ^{1}H resonances and quantitative analysis of *SS* ^{1}H NMR spectra is still very challenging. The spectral resolution can be improved by applying line narrowing techniques such as magic angle sample spinning (MAS) [20], usually combined with complex homonuclear decoupling pulse sequences designed ad hoc [21,22]. The resolution of the solid-state NMR signals strongly depends on the sample spinning speed, for diluted nuclei (^{13}C or ^{15}N) slow or moderate speeds are enough to obtain resolved spectra, while fast or very fast spinning (spinning regime >50 kHz) conditions are needed to obtain “liquid like spectra”.

We begin the spectroscopic investigation of the systems by discussing the proton MAS spectra of the two nanosponges CDNS(1:8) and CDNS(1:4) free and IbuNa loaded according to the procedure described in the experimental section. The ^{1}H MAS NMR spectra of both nanosponges CDNS(1:8) and CDNS(1:4) (Figure 2b), acquired at 20 kHz spinning speed, exhibit broad lines characteristic of a rigid solid due to a not complete averaging of the strong homonuclear ^{1}H–^{1}H dipolar interactions. A different NMR pattern is observed for the CDNS-drug samples. The ^{1}H spectrum of the sample CDNS(1:8)-IbuNa (Figure 2a) shows narrow resolved signals of the drug molecule and a broad line for the polymeric network. Similarly, the ^{1}H MAS spectrum (Figure 2b) of CDNS(1:4)-IbuNa shows resolved peaks (line widths of 40–50 Hz) of the drug molecule.

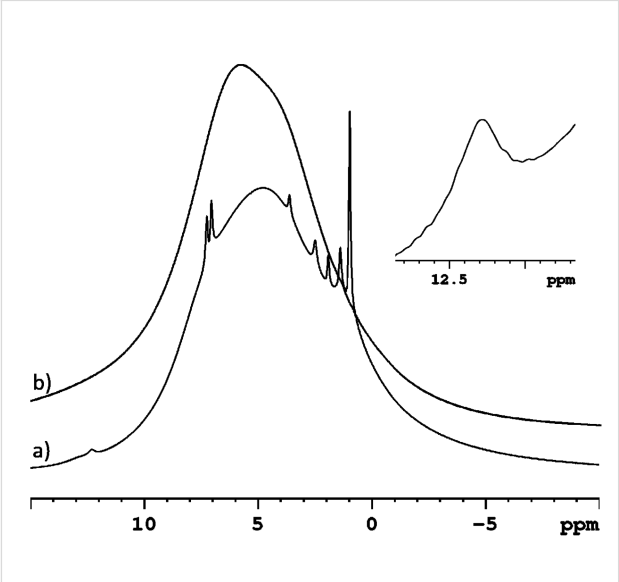

Figure 2: ^{1}H MAS NMR spectra of a) CDNS(1:8)-IbuNa and b) CDNS(1:8). The inset (top right) shows the expansion of the spectral region where the hydrogen bonded protons of the carboxylic functional groups resonate. The notation CDNS-IbuNa indicates the original preparation, irrespective of the conversion of the sodium salt into the undissociated acid.

Signal resolution further increases under fast MAS (40 kHz spinning) conditions (Figure 3c). The observed high resolution of the IbuNa spectral lines is the consequence of the efficient averaging of the homonuclear ^{1}H–^{1}H dipolar interactions due to fast rotation of the sample at the magic angle. All the resonances can be easily assigned. The peak at 0.96 ppm is due to the methyl groups, small peaks belonging to the alkyl protons

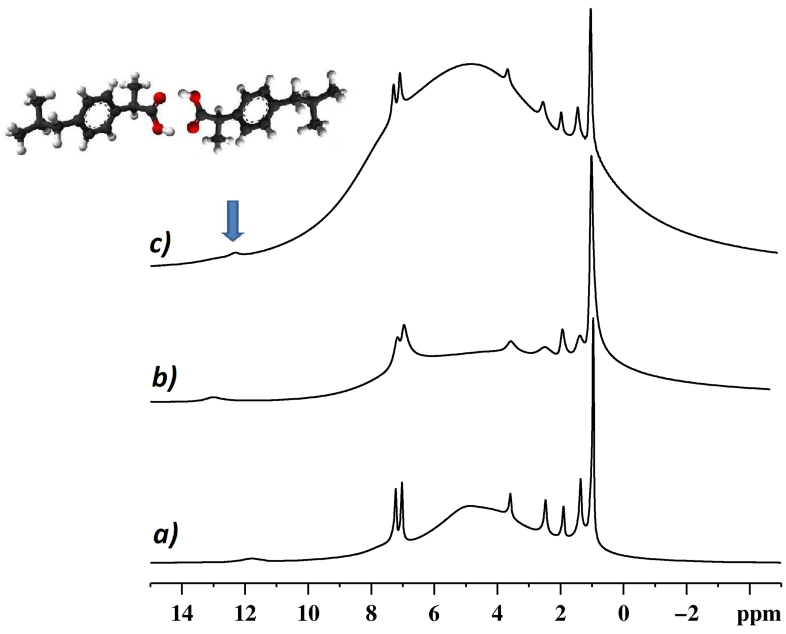

Figure 3: The effect of the spinning speed on the spectral features. ^{1}H MAS NMR spectra of a) CDNS(1:4)-IbuNa under conditions of fast spinning speed (40 kHz), b) CDNS(1:4)-IbuNa recorded at lower spinning speed (20 kHz), c) CDNS(1:8)-IbuNa recorded at 20 kHz spinning speed. The notation CDNS-IbuNa indicates the original preparation, irrespective of the conversion of the sodium salt into the undissociated acid. The arrow indicates the peak assigned to the hydrogen bonded dimer, sketched in the inset.

are in the range 1.4–3.6 and the resonances at 7–7.23 are due to the phenyl group. It is important to observe a high frequency signal at 12.05 ppm for CDNS(1:8) and at 13 ppm for CDNS(1:4). This peak is indeed unexpected, as it is assignable to carboxylic protons involved in hydrogen bonds. The presence of such a signal provides evidence for two remarkable facts: i) the drug entrapped in the nanosponge is in the acidic form, and ii) the ibuprofen molecules hosted in the CDNS are fully involved in a hydrogen-bond network. This point is worth of a comment: racemic IbuH was reported [23] to form dimers in the crystal state, as assessed by the combined single crystal X-ray and pulsed neutron diffraction techniques. In the present study, the observed ^{1}H NMR peak assignable to a hydrogen bonded proton seems to indicate a similar situation, i.e., dimeric IbuH confined in CDNS linked by IbuH···IbuH interactions. However, it should be kept in mind that other types of hydrogen bonds may be established, such as those between IbuH and the free OH groups of CD or the COOH and amino functional groups of the cross-linker. The acidic IbuH form present in the network can be motivated by considering that, even if the swelling of CDNS is achieved by adding an aqueous basic solution of sodium carbonate [9], the final pH of the hydrogel is slightly acidic. Moreover, water removal by lyophilisation induces an increased protonation of IbuH, due to the concentration of the system.

^{13}C CP-MAS NMR spectroscopy

In order to get more information on the CDNS polymer structure, polymer–drug interactions and drug mobility, we recorded the ^{13}C CP-MAS spectra for several samples of free CDNS and the corresponding drug-loaded samples. Three different types of samples were studied: 1) free polymers CDNS(1:4) and CDNS(1:8); 2) pure IbuNa; 3) CDNS(1:4)-IbuNa and CDNS(1:8)-IbuNa.

Both spectra of the CDNS polymers, reported in Figure 4, show broad lines characteristic of amorphous materials. The top trace of Figure 4 shows the characteristic spectrum of crystalline β-CD, along with the peak assignment already known from the literature. The peak assignment is a guide for the interpretation of the spectra of CDNS. The observed chemical shifts follow the order C(1), C(4), [C(5), C(3) and C(2)] and C(6), in increasing order of shielding. For both CDNS polymers, the peak assignment is reported in Table 1.

The ^{13}C CP-MAS spectrum of IbuNa is reported in Figure 5 (top trace). It was acquired as reference spectrum of the drug molecule and the resonances assigned according to Geppi et al. [24]. The spectrum shows sharp lines (line-width range: 80–100 Hz) specific of a crystalline sample. Ibuprofen is a small molecule characterized by an interesting internal dynamic

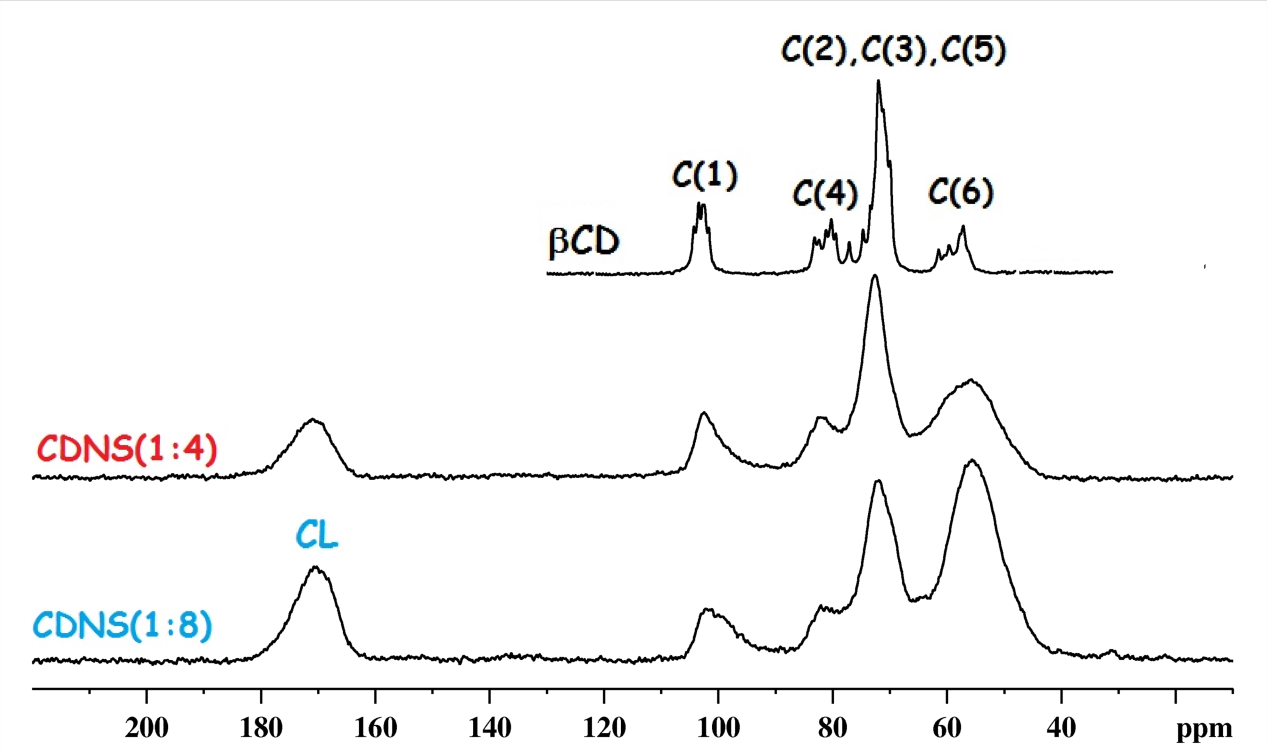

Figure 4: ^{13}C CP-MAS NMR spectra for samples of β-CD (top), CDNS(1:4) (middle) and CDNS(1:8) polymers (bottom). CL indicates the carbonyl group of the cross-linking agent.

behaviour due to two main molecular fragments: the alkyl chain and the aromatic ring. The internal motion was studied in detail using solid-state ^{13}C NMR spectroscopy at different temperatures by Carignani et al. [25]. The authors identified two types of motion with a different time scale: 1) the rotations of the two methyl groups of the isobutyl moiety, occurring in the fast regime, 2) the π-flip of the phenyl ring belonging to the intermediate motional regime.

Both rotational motions are fast enough to observe an average isochronous signal for the methyl carbon atoms (12 and 13) as well as for the aromatic protonated carbons (5,6–7,8). It is worth reminding that a different mobility was observed for ibuprofen in its acid form (IbuH) which shows hindered rotational motion for both molecular fragments.

The ^{13}C CP-MAS NMR spectra of the CDNS samples without and with ibuprofen are also shown in Figure 5. A comparison of the reported spectra does not highlight any observable change of the linewidth and chemical shift of the CDNS signals after loading the polymers with IbuNa. This is a clear indication that adding the drug to the CDNS does not influence significantly the nanosponge porous structure. From the point of view of the encapsulated drug, the ^{13}C CP-MAS spectra show that the peaks due to ibuprofen retain high resolution even when the drug is encapsulated in the nanosponges, thus proving that the

Table 1: Chemical shift (ppm), and proton relaxation $T_1\rho$ (ms) of the carbon atoms of CDNS(1:4), CDNS(1:8) polymers and pristine β-CD.

Carbon atoms	Chemical shift[a]	$T_1\rho$ CDNS(1:4)[a]	$T_1\rho$ CDNS(1:8)[a]	$T_1\rho$ β-CD[b]
CL (carbonyl)	170	3.3	3.0	
C(1)	102	3.3	5.0	2.6
C(4)	82	3.3	5.0	2.4–2.6
C(2), C(3), C(5)	72	3.3	5.0	2.2–2.5
C(6) + CL (methylene)	56	3.0	5.0	2.7

[a]This work. [b]From ref. [26].

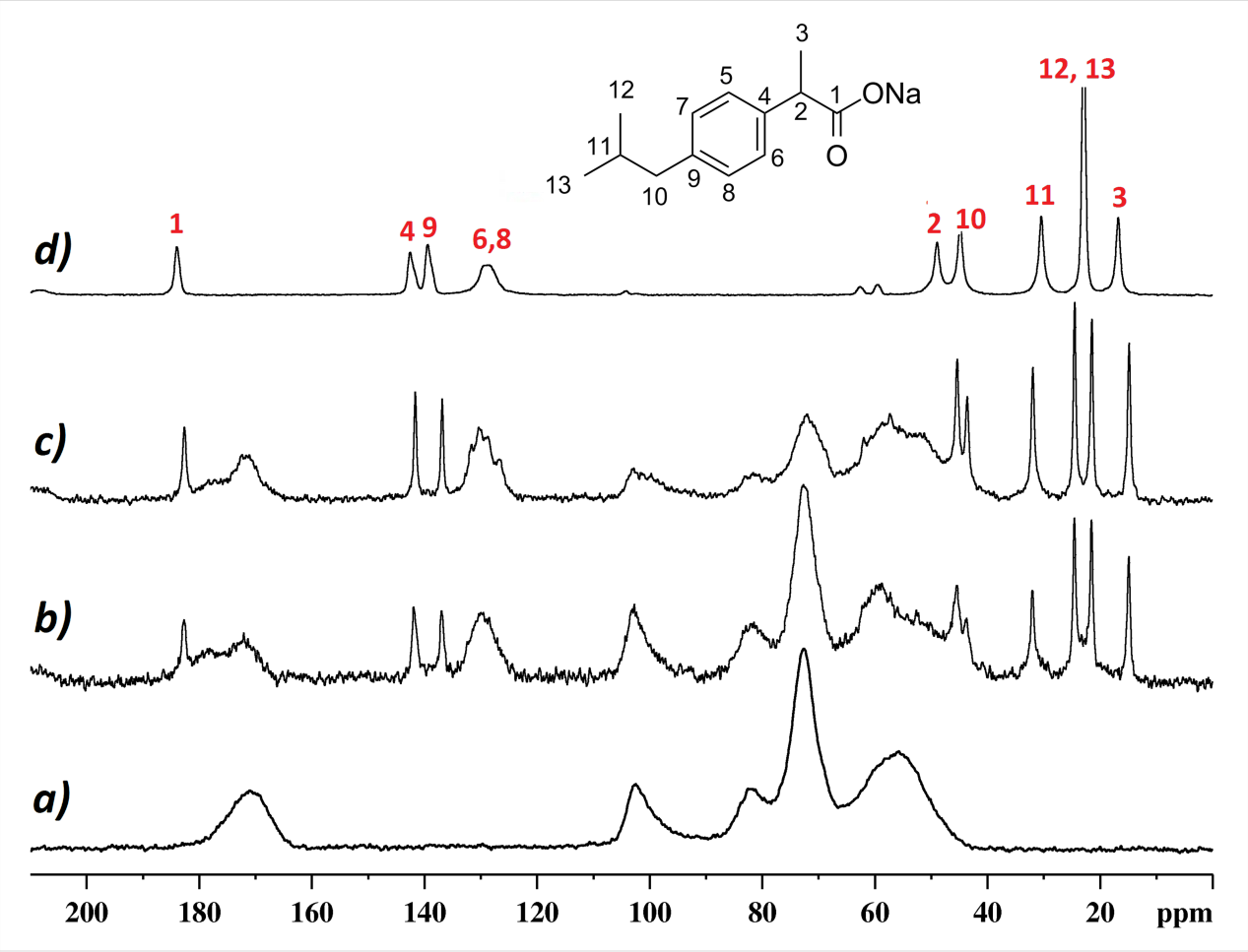

Figure 5: ^{13}C CP-MAS NMR spectrum of: a) CDNS(1:4) polymer; b) CDNS(1:4)-IbuNa system; c) CDNS(1:8)-IbuNa system; d) pure IbuNa (reference spectrum). The molecular structure and atom numbering of IbuNa are shown in the inset. The notation CDNS-IbuNa indicates the original preparation, irrespective of the conversion of the sodium salt into the undissociated acid.

drug is in a crystalline form inside the rigid polymeric network. However, two important findings should be highlighted here. The peaks assigned to C12 and C13 of IbuNa – which are isochronous in the reference sample (Figure 5d) and they give rise to a singlet at ca. 23 ppm – provide two separate signals when IbuNa is loaded onto the polymers, as clearly visible in Figure 5b and c. This finding further supports what described in the previous section: the guest molecule ibuprofen, originally added to the polymeric matrix as the sodium salt IbuNa, is present, in the CDNS(1:4) and CDNS(1:8) nanosponges, as the corresponding acid form IbuH. Indeed, the chemical shift of ibuprofen signals from the spectra of Figure 5b and 5c match with those reported in the literature for the ^{13}C CP-MAS NMR spectrum of crystalline IbuH [25]. The indication that IbuH is not significantly interacting with the polymeric backbone and that the ^{13}C CP-MAS NMR chemical shift of encapsulated IbuH match those of pure, crystalline IbuH provide useful, additional information to spot on the nature of the hydrogen bond network introduced in the previous section. As significant IbuH···CDNS interactions are not detected, the hydrogen bond detected via ^{1}H NMR and discussed in the previous section is likely to involve two IbuH units in the formation of dimers.

Dynamics of cross polarization

We applied variable contact time (VCT) ^{1}H-^{13}C CP-MAS NMR techniques to study the CP kinetics of both the CDNS polymers. As an example, the array of ^{13}C CP-MAS spectra acquired at the MAS rate of 10 kHz and with increasing contact time for cross-polarization is shown in Figure 6 in the case of CDNS(1:4). We can observe that at 100 μs all the carbon atoms are polarized, i.e., the signal intensity is high enough to generate an observable ^{13}C CP-MAS NMR spectrum. The maximum signal intensity S_{CPMAX} is observed around 750 μs for all the cyclodextrin carbon atoms and around 1100 μs for the carbonyl groups of the cross-linker. Such small values indicate a fast cross-polarization process, consistent with a rigid polymeric system. Therefore, strong heteronuclear dipolar interactions are present and capable to facilitate an effective magnetization

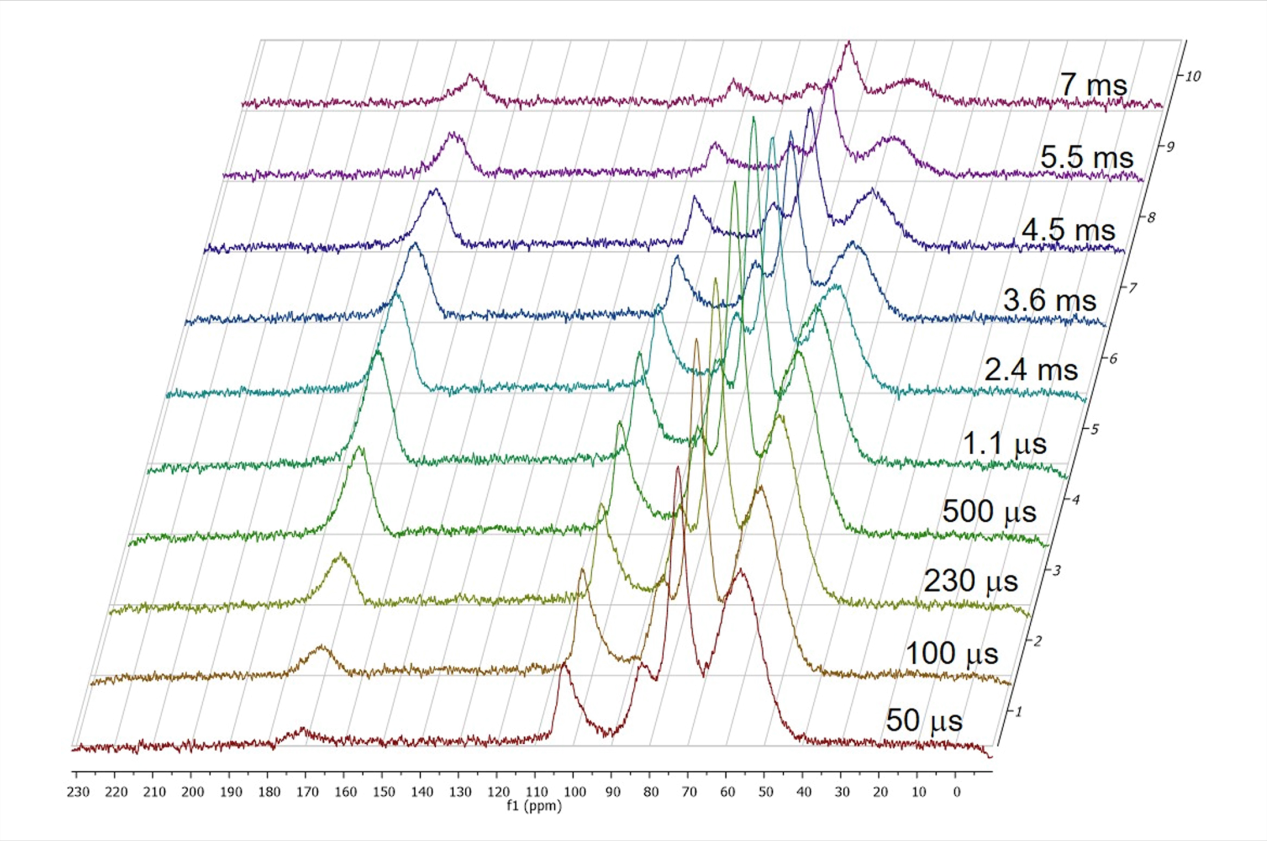

Figure 6: ^{13}C CP-MAS NMR spectra of CDNS(1:4) acquired with CP variable contact time in the range 50 µs–7 ms.

transfer from the proton reservoir to various carbon atoms. The CP kinetics in both CDNS systems follow the classical *I*–*S* model. The signal intensity *I*(t), expressed by the peak area, versus the CP contact time *t* are reported in Figure 7 for all the carbon atoms.

The experimental curves can be fitted by using Equation 2, thus providing the values of the proton relaxation parameter $T_{1\rho}$. The results are collected in Table 1 for CDNS(1:4), CDNS(1:8). For clarity, also the literature $T_{1\rho}$ values related to monomeric β-cyclodextrin are listed [26]. All the carbon atoms revealed

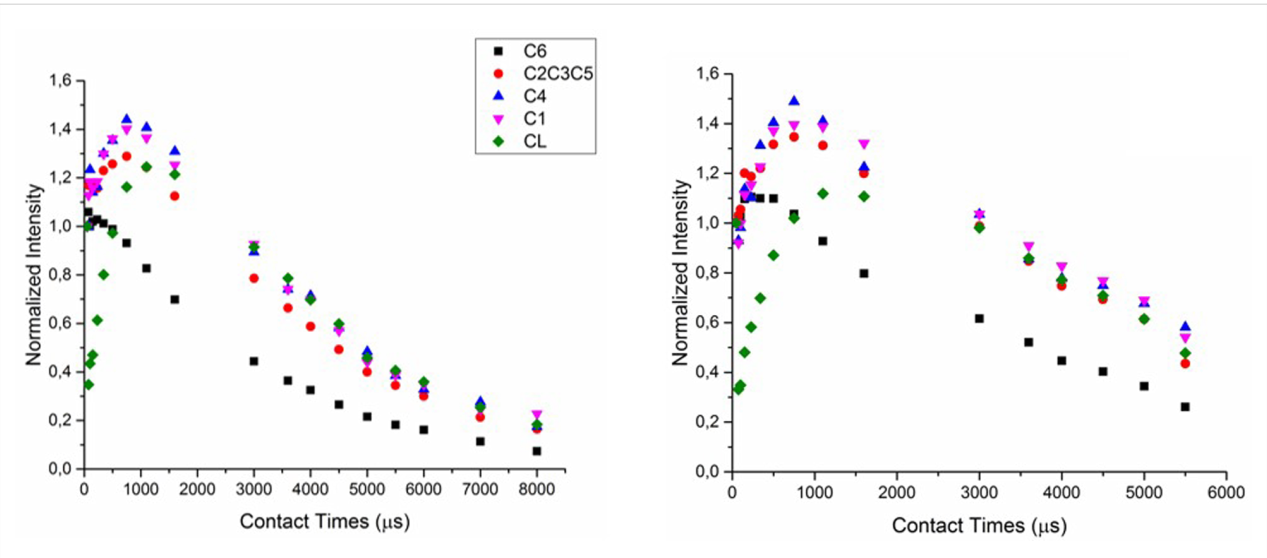

Figure 7: Time dependence of ^{13}C magnetization for CDNS(1:4) (left) and CDNS(1:8) (right) polymers.

short $T_{1\rho}$ values in the range of 3–5 ms and similar for β-CD C atoms and the carbonyl atom of the cross-linker, suggesting that their chemical environments are equally proximate to the ^{1}H reservoirs. This result is indicative of the homogeneous nature of the polymer sample. The only exception to this general trend is observed for the cross-linker C atom of CDNS(1:8). In such a case, $T_{1\rho}$ of 3 ms was detected, while all the other C atoms show the constant value of 5 ms. This finding confirms a certain degree of heterogeneity in CDNS(1:8) connected to the carbonyl groups of the CL in this polymer, in agreement with the observation previously reported for the same system in the gel state [9].

A different, more complex, kinetic behaviour is obtained for both the CDNS-IbuNa samples. For all the carbon atoms of the CDNS polymer as well as for all the carbons of ibuprofen, our VCT results followed a non-classical kinetic model (*I*–*I**–*S* model) corresponding to oscillatory polarization transfer. The results for the C(1), C(4) atoms of the CDNS(1:4) and CDNS(1:8) polymers are shown in Figure 8 and Figure 9, respectively. The dipolar oscillations modulate the magnetization build-up curve at short mixing times up to 750 μs, then the time constants (proton spin diffusion T_{diff} and proton spin–lattice relaxation in the rotating frame $T_{1\rho}$) determine the magnetization decay.

The CP kinetic curve of ibuprofen (aromatic carbons 6, 8) is shown in Figure 9. In this case, the magnetization intensity rises at short mixing times (in the range 50–1100 μs) and then approaches a plateau which means that $T_{1\rho}$ (H) is infinitely long.

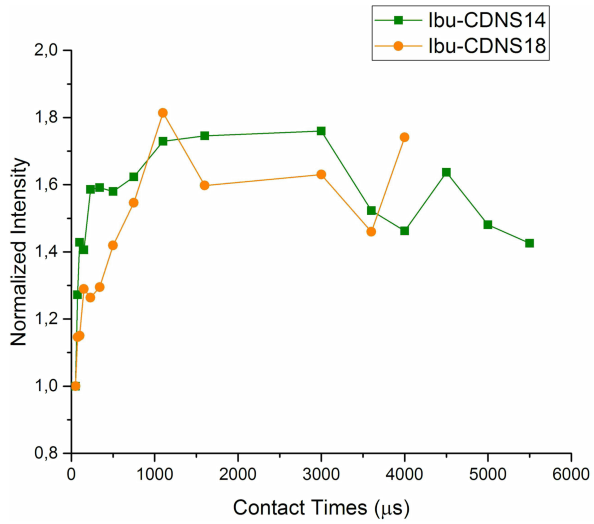

Figure 9: ^{1}H-^{13}C CP oscillatory kinetics for the ibuprofen aromatic carbon atoms C(6,8) in samples CDNS(1:4)-IbuNa and CDNS(1:8)-IbuNa. The notation CDNS-IbuNa indicates the original preparation, irrespective of the conversion of the sodium salt into the undissociated acid.

The process of drug loading in both CDNS polymers influences the dynamic behaviour of both the polymer and the drug due to strong heteronuclear dipolar interactions rising in a rigidly connected system. A more detailed analysis of these systems would need a deeper theoretical data treatment. Additionally, in order to achieve an accurate fitting, some relaxation parameters

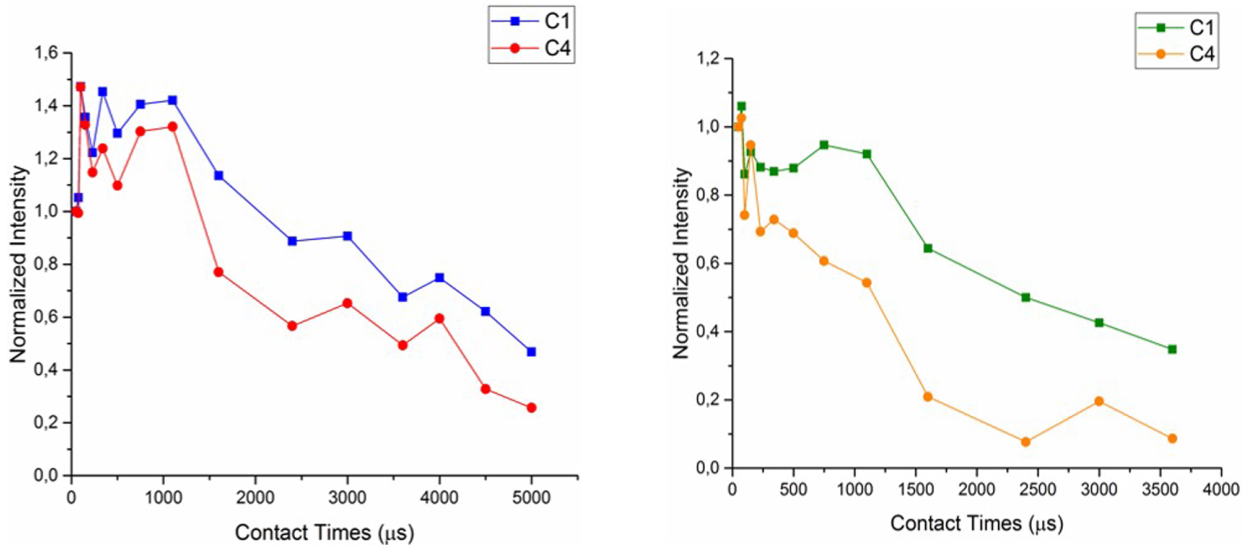

Figure 8: ^{1}H-^{13}C CP oscillatory kinetics for the carbon C(1) and C(4) of CDNS(1:4)-IbuNa sample *(left)* and CDNS(1:8)-IbuNa (right). The notation CDNS-IbuNa indicates the original preparation, irrespective of the conversion of the sodium salt into the undissociated acid.

need to be determined with different solid state experiments such as depolarization or the TORQUE [27] experimental method, which is beyond the aim of this work. In the economy of the present work, the most important conclusion of this section is that the VCT profiles of the free polymers – CDNS(1:4) and CDNS(1:8) – and the corresponding drug-loaded formulations – CDNS(1:4)-IbuNa and CDNS(1:8)-IbuNa – fit two different dynamic models: the commonly observed *I–S* scheme and the non-classic, less common *I–I*–S* model, respectively. The changes observed in the dynamics of the system after the drug loading point out that the polymer and the drug are in contact (dipolar contact) and that the magnetization is transferred from the protons (of both polymer and drug) to the CDNS carbons. This allows to conclude that a supramolecular architecture is formed, in spite of the fact that the initial structure of the CDNS polymer is retained.

Powder X-ray diffraction

The diffraction patterns of both CDNS used in the present work (Figure 10a and b) show a totally amorphous structure in agreement with the results of ^{13}C CP-MAS NMR. Once loaded with ibuprofen sodium salt, the PXRD profiles of both CDNS (Figure 10c and d) show the amorphous structure of CDNS along with peaks belonging to ibuprofen. The ibuprofen Bragg peaks are intense and sharp, typical for a high ordered crystalline structure. Their positions are in agreement with the diffraction pattern of the acidic racemic form of ibuprofen, thus confirming that, after the lyophilisation, the IbuNa originally added to the nanosponge is turned into the undissociated acid IbuH. For comparison, the spectrum of a standard sample of pure, racemic ibuprofen in its acidic form (IbuH) is also reported in the figure (Figure 10e). The peak positions match perfectly the literature reference [28] and they are clearly distinguishable from the reflexes of IbuNa, shown in upper traces of the figure (Figure 10f).

As a final remark, the PXRD patterns show that ibuprofen entrapped into the nanosponge network still retains crystallinity, thus confirming that the formation of the polymer-drug association is a mild process.

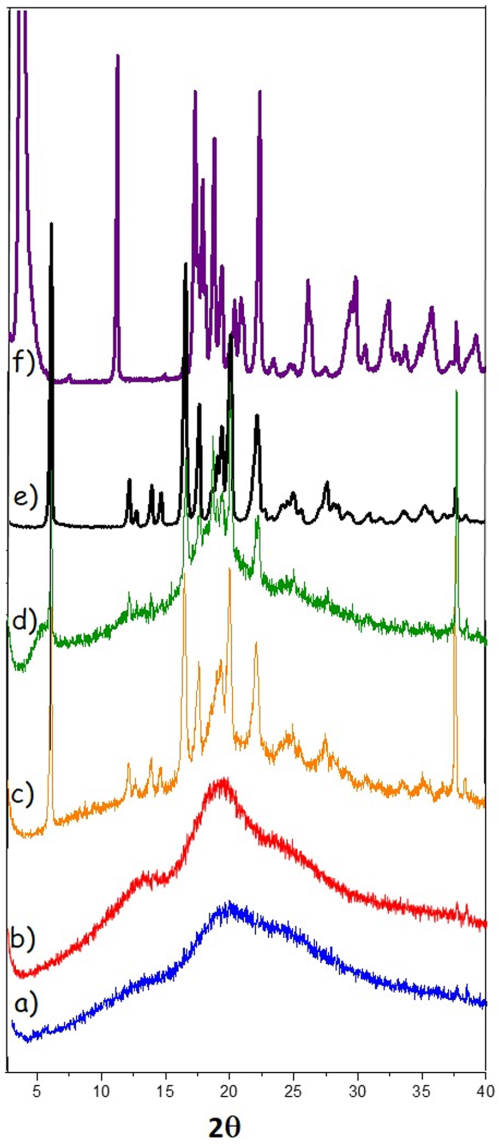

Figure 10: PXRD patterns of: a) CDNS(1:8), b) CDNS(1:4), c) CDNS(1:8)-IbuNa loaded, d) CDNS(1:4)-IbuNa loaded, e) IbuH, analytical standard, f) IbuNa, analytical standard, The notation CDNS-IbuNa indicates the original preparation, irrespective of the conversion of the sodium salt into the undissociated acid.

Conclusion

The mesoporous materials CDNS(1:4), CDNS(1:8) in their free form and loaded with ibuprofen sodium salt were prepared and thoroughly characterized using solid-state ^{1}H Fast MAS and ^{13}C CP-MAS NMR spectroscopy. The main conclusions can be summarized as follows:

1. Ibuprofen sodium salt is converted into its acid form IbuH after the lyophilisation of the hydrogels obtained by swelling CDNS(1:4) and CDNS(1:8) with aqueous IbuNa solutions.

2. ^{1}H Fast MAS NMR spectra reveal that ibuprofen loaded in the CDNS polymeric scaffold does not form H-bonds with the polymer, but rather it crystallizes as a dimer.

3. ^{13}C CP-MAS spectra allow the characterization of the free CDNS polymers as amorphous materials. ^{13}C CP-VCT experiments show that the investigated cyclodextrin nanosponges are rigid and homogeneous.

4. ^{13}C CP-MAS spectra of the CDNS and the CDNS-drug systems do not show observable chemical shift changes, thus ruling out significant structural changes (e.g., conformational or

structural) for the polymer backbone after the entrapment of the drug.

5. Conversely, ^{13}C CP-VCT NMR experiments provide evidence that the kinetic behaviour of all the carbon atoms of the CDNS polymers dramatically changes upon drug loading, thus providing a dynamic fingerprint of the formation of a supramolecular architecture. The latter is characterized by the formation of IbuH domanins in the pores of the 3D structure of the polymeric network. The experimental data show that the inclusion of IbuH in the CD cavity – namely the formation of a host–guest inclusion complex – does not occur, confirming the situation already described by HR-MAS NMR data for the same system in the gel state [9] and outlining a different scenario on passing from monomeric CD, capable to form well characterized inclusion complexes with IbuH [29-31] to CDNS of the present work. A possible explanation relies upon the availability of the CD cavity within the polymeric network. The importance of this factor is particularly clear in the case of polymers obtained by monomers containing cyclodextrin units as dangling groups, e.g., glycidylmethacrylate-mono-6-amino-6-deoxy-β-CD (GMA-NH_2-β-CD) co-polymerized with ethylene dimethacrylate [32]. The corresponding cross-linked polymers are thus decorated with cyclodextrin units, easily accessible to small molecules to give rise to inclusion complexes. This type of polymers showed excellent efficiency as chiral selectors for the enantioseparation of racemic ibuprofen [32]. In our case, the primary OH groups of CD units react with EDTA dianhydride to form a cross-linked polyester. As a matter of fact, this type of polycondensation makes the CD cavity less available compared to the former case. The overall result is that the guest molecules are mainly confined in the pores formed by the polycondensation process rather than forming a genuine inclusion complex with the single CD units. From a practical point of view, our class of polymerized cyclodextrins can be conveniently exploited as sorbent or scaffold by exploiting the pores of the polymer network to encapsulate the guest molecules. However, it should be stressed that CD nanosponges similar to ours and prepared by using citric acid as cross-linker, showed a different behaviour towards ibuprofen: the authors provided evidence of inclusion complex formation as the main mechanism of absorption [33]. We may conclude that the type of monomer and the cross-linker agent both play a key role in driving the absorption towards inclusion complexes or segregation in the polymer pores, although a sufficient number of data is still missing to formulate a general model.

As a final remark, the possibility of solid-state reactions involving the active components should be taken into account when designing scaffolds for in situ release. The methodologies here described can be conveniently included in the tool-case to monitor the molecular state and dynamics of the host–guest systems.

Experimental

Materials and measurements

The detailed procedures for the synthesis of CDNS and the preparation of the corresponding hydrogels containing IbuNa can be found and seen in [34]. In the following, we report the essential information on the synthesis and the experimental details for the NMR and XRD experiments.

Nanosponges preparation and drug loading procedure

The synthesis of CDNS(1:4) and CDNS(1:8) was done according to the protocol previously described [9]. The drug loading procedure consists of three fundamental steps:

1. A stock solution (0.27 M) of ibuprofen sodium salt was prepared by dissolving 308 mg of IbuNa together with 68 mg of Na_2CO_3 in 5 mL of water.
2. 3 mL of the solution (1) were then added to a weighted amount (400 mg) of CDNS polymer in both preparations.
3. Homogeneous hydrogels were then obtained in 1 h. The measured pH of the gels was 6.5. The samples are then freeze-dried overnight.

Solid state NMR spectroscopy

^1H NMR spectra were recorded on VNMRS spectrometer operating at 600 MHz (51 mm bore Oxford superconducting magnet) equipped with a 1.6 mm Triple Resonance Fast MAS probehead. Sample rotation frequencies were 20–40 kHz for ^1H Fast MAS NMR experiment.

^{13}C CP-MAS NMR spectra were collected at 125.77 MHz on the 500 MHz NMR Spectrometer AvanceTM 500 operating at a static field of 11.7 Tesla (superconducting ultrashield magnet) and equipped with a 4 mm MAS probe. All the samples were prepared by packing the powder in Zirconia rotors (ZrO_2), closed with Kel-F caps (80 μL internal volume); the spinning speed (MAS) was optimized at 10 kHz.

Cross-polarization (CP) spectra, under Hartmann–Hahn conditions, were recorded with a variable spin-lock sequence (ramp CP-MAS), a relaxation delay d1 = 4 s, and a ^1H $\pi/2$ pulse-width of 4.2 μs was employed. The contact time (CT) for the VCT experiments was varied in the range of 50 μs to 7.0 ms; 1200 scans for each experiment were acquired.

The CP-MAS signals were approximated by Lorentzian function curve fitting analysis. The baseline and the deconvolution

of the peaks were performed with OriginPro 2016 software. The accordance between experimental and deconvoluted curves is expressed as R^2 value which is >0.98 for all of the analyzed spectra.

X-ray diffraction experiments

The powder X-ray diffraction (PXRD) experiments were performed with a Bruker D2 Phaser X-ray powder diffractometer using CuKα radiation. The data were collected in the 2θ range 2.3–40° with a step size of 0.02° and a counting time of 0.4 s per step, a primary slit module of 0.6 mm, air scatter screen module 1 mm and secondary slit module 8 mm.

Acknowledgements

The authors acknowledge the CERIC-ERIC Consortium for the access to experimental facilities and financial support. The authors thank Dr Enrico Caneva (University of Milan) for helpful discussions.

References

1. Allabashi, R.; Arkas, M.; Hörmann, G.; Tsiourvas, D. *Water Res.* **2007,** *41,* 476–486. doi:10.1016/j.watres.2006.10.011
2. Li, D.; Ma, M. *Clean Prod. Process.* **2000,** *2,* 112–120. doi:10.1007/s100980000061
3. Trotta, F.; Zanetti, M.; Cavalli, R. *Beilstein J. Org. Chem.* **2012,** *8,* 2091–2099. doi:10.3762/bjoc.8.235
4. Castiglione, F.; Crupi, V.; Majolino, D.; Mele, A.; Panzeri, W.; Rossi, B.; Trotta, F.; Venuti, V. *J. Inclusion Phenom. Macrocyclic Chem.* **2013,** *75,* 247–254. doi:10.1007/s10847-012-0106-z
5. Rossi, B.; Caponi, S.; Castiglione, F.; Corezzi, S.; Fontana, A.; Giarola, M.; Mariotto, G.; Mele, A.; Petrillo, C.; Trotta, F.; Viliani, G. *J. Phys. Chem. B* **2012,** *116,* 5323–5327. doi:10.1021/jp302047u
6. Castiglione, F.; Crupi, V.; Majolino, D.; Mele, A.; Rossi, B.; Trotta, F.; Venuti, V. *J. Phys. Chem. B* **2012,** *116,* 7952–7958. doi:10.1021/jp303006a
7. Rossi, B.; Venuti, V.; D'Amico, F.; Gessini, A.; Mele, A.; Punta, C.; Melone, L.; Crupi, V.; Majolino, D.; Masciovecchio, C. *Soft Matter* **2016,** *12,* 8861–8868. doi:10.1039/C6SM01647B
8. Venuti, V.; Rossi, B.; Mele, A.; Melone, L.; Punta, C.; Majolino, D.; Masciovecchio, C.; Caldera, F.; Trotta, F. *Expert Opin. Drug Delivery* **2016,** *0,* 1–10. doi:10.1080/17425247.2016.1215301
9. Ferro, M.; Castiglione, F.; Punta, C.; Melone, L.; Panzeri, W.; Rossi, B.; Trotta, F.; Mele, A. *Beilstein J. Org. Chem.* **2014,** *10,* 2715–2723. doi:10.3762/bjoc.10.286
10. Rao, P.; Knaus, E. E. *J. Pharm. Pharm. Sci.* **2008,** *11,* 81s–110s. doi:10.18433/J3T886
11. Sörgel, F.; Fuhr, U.; Minic, M.; Siegmund, M.; Maares, J.; Jetter, A.; Kinzig-Schippers, M.; Tomalik-Scharte, D.; Szymanski, J.; Goeser, T.; Toex, U.; Scheidel, B.; Lehmacher, W. *Int. J. Clin. Pharmacol. Ther.* **2005,** *43,* 140–149. doi:10.5414/CPP43140
12. Kotar, A.; Kotar, M.; Sketa, P.; Plavec, J. *Curr. Pharm. Anal.* **2015,** *11,* 124–130. doi:10.2174/1573412910666141111231325
13. Mallard, I.; Baudelet, D.; Castiglione, F.; Ferro, M.; Panzeri, W.; Ragg, E.; Mele, A. *Beilstein J. Org. Chem.* **2015,** *11,* 2785–2794. doi:10.3762/bjoc.11.299
14. Kolodziejski, W.; Klinowski, J. *Chem. Rev.* **2002,** *102,* 613–628. doi:10.1021/cr000060n
15. Mehring, M. *Principles of High-Resolution NMR in Solids,* 2nd ed.; Springer-Verlag: Berlin, Germany, 1983. doi:10.1007/978-3-642-68756-3
16. Müller, L.; Kumar, A.; Baumann, T.; Ernst, R. R. *Phys. Rev. Lett.* **1974,** *32,* 1402–1406. doi:10.1103/PhysRevLett.32.1402
17. Hester, R. K.; Ackermann, J. L.; Cross, V. R.; Waugh, J. S. *Phys. Rev. Lett.* **1975,** *34,* 993–995. doi:10.1103/PhysRevLett.34.993
18. Kolmas, J.; Jaklewicz, A.; Zima, A.; Bućko, M.; Paszkiewicz, Z.; Lis, J.; Ślósarczyk, A.; Kolodziejski, W. *J. Mol. Struct.* **2011,** *987,* 40–50. doi:10.1016/j.molstruc.2010.11.058
19. Stejskal, E. O.; Memory, J. D. *High-Resolution NMR in the Solid State: Fundamentals of CP/MAS;* Oxford University Press: Oxford, U.K., 1994.
20. Schaefer, J.; Stejskal, E. O. *J. Am. Chem. Soc.* **1976,** *98,* 1031–1032. doi:10.1021/ja00420a036
21. Brown, S. P. *Solid State Nucl. Magn. Reson.* **2012,** *41,* 1–27. doi:10.1016/j.ssnmr.2011.11.006
22. Chu, P. J.; Potrzebowski, M. J.; Scott, A. I.; Gao, Y. *J. Am. Chem. Soc.* **1990,** *112,* 881–883. doi:10.1021/ja00158a066
23. Shankland, N.; Wilson, C. C.; Florence, A. J.; Cox, P. J. *Acta Crystallogr., Sect. C* **1997,** *C53,* 951–954. doi:10.1107/S0108270197003193
24. Geppi, M.; Guccione, S.; Mollica, G.; Pignatello, R.; Veracini, C. A. *Pharm. Res.* **2005,** *22,* 1544–1555. doi:10.1007/s11095-005-6249-5
25. Carignani, E.; Borsacchi, S.; Geppi, M. *J. Phys. Chem. A* **2011,** *115,* 8783–8790. doi:10.1021/jp202650n
26. Crini, G.; Cosentino, C.; Bertini, S.; Naggi, A.; Torri, G.; Vecchi, C.; Janus, L.; Morcellet, M. *Carbohydr. Res.* **1998,** *308,* 37–45. doi:10.1016/S0008-6215(98)00077-9
27. Tekely, P.; Gérardy, V.; Palmas, P.; Canet, D.; Retournard, A. *Solid State Nucl. Magn. Reson.* **1995,** *4,* 361–367. doi:10.1016/0926-2040(95)00018-L
28. Zhang, G. G. Z.; Paspal, S. Y. L.; Suryanarayanan, R.; Grant, D. J. W. *J. Pharm. Sci.* **2003,** *92,* 1356–1366. doi:10.1002/jps.10393
29. Mura, P.; Bettinetti, G. P.; Manderioli, A.; Faucci, M. T.; Bramanti, G.; Sorrenti, M. *Int. J. Pharm.* **1998,** *166,* 189–203. doi:10.1016/S0378-5173(98)00035-0
30. Braga, S. S.; Gonçalves, I. S.; Herdtweck, E.; Teixeira-Dias, J. J. C. *New J. Chem.* **2003,** *27,* 597–601. doi:10.1039/b207272f
31. Pereva, S.; Sarafska, T.; Bogdanova, S.; Spassov, T. *J. Drug Delivery Sci. Technol.* **2016,** *35,* 34–39. doi:10.1016/j.jddst.2016.04.006
32. Guo, J.; Xiao, Y.; Lin, Y.; Crommen, J.; Jiang, Z. *J. Chromatogr. A* **2016,** *1467,* 288–296. doi:10.1016/j.chroma.2016.05.078
33. Moulahcene, L.; Kebiche-Senhadji, O.; Skiba, M.; Lahiani-Skiba, M.; Oughlis-Hammache, F.; Benamor, M. *Desalin. Water Treat.* **2016,** *57,* 11392–11402. doi:10.1080/19443994.2015.1048734
34. Ferro, M.; Castiglione, F.; Punta, C.; Melone, L.; Panzeri, W.; Rossi, B.; Trotta, F.; Mele, A. *J. Visualized Exp.* **2016,** *114,* e53769. doi:10.3791/53769

License and Terms

BEILSTEIN JOURNAL OF ORGANIC CHEMISTRY

Structure–efficiency relationships of cyclodextrin scavengers in the hydrolytic degradation of organophosphorus compounds

Sophie Letort[1], Michaël Bosco[1], Benedetta Cornelio[1], Frédérique Brégier[1], Sébastien Daulon[2], Géraldine Gouhier[1] and François Estour[*1]

Full Research Paper

Open Access

Address:
[1]Normandie Univ, INSA Rouen, UNIROUEN, CNRS, COBRA (UMR 6014), 76000 Rouen, France and [2]DGA Maîtrise NRBC, Département Evaluation des effets des agents chimiques, 91710 Vert le Petit, France

Email:
François Estour[*] - francois.estour@univ-rouen.fr

* Corresponding author

Keywords:
cyclodextrin; decontamination; enzyme mimic; nerve agents; organophosphorus pesticides

Beilstein J. Org. Chem. **2017,** *13,* 417–427.
doi:10.3762/bjoc.13.45

Received: 22 November 2016
Accepted: 10 February 2017
Published: 06 March 2017

This article is part of the Thematic Series "Superstructures with cyclodextrins: Chemistry and applications IV".

Guest Editor: G. Wenz

Abstract

New derivatives of cyclodextrins were prepared in order to determine the relative importance of the structural key elements involved in the degradation of organophosphorus nerve agents. To avoid a competitive inclusion between the organophosphorus substrate and the iodosobenzoate group, responsible for its degradation, the latter group had to be covalently bound to the cyclodextrin scaffold. Although the presence of the α nucleophile iodosobenzoate was a determinant in the hydrolysis process, an imidazole group was added to get a synergistic effect towards the degradation of the agents. The degradation efficiency was found to be dependent on the relative position of the heterocycle towards the reactive group as well as on the nature of the organophosphorus derivative.

Introduction

Originally employed as pesticides, organophosphorus compounds were further developed as chemical warfare agents during the Second World War. These compounds act as potent irreversible inhibitors of cholinesterases [1-6] and are able to cause lethal intoxications [3]. Despite the measures adopted to reduce the risk of accidental poisoning by pesticides [7-11] and the Chemical Weapons Convention aiming at the non-proliferation of chemical weapons or their precursors, organophosphorus compounds still constitute a threat to civilian and military people. Moreover, due to the current geopolitical situation and the increasing number of terrorist attacks worldwide, more efficient means against nerve agents are required [12]. Four

steps have to be considered to reach this objective: detection, individual and collective protection, decontamination, and medical countermeasures. Because a contamination transfer can occur from victims or through contact with contaminated equipment, a rapid elimination of the toxic has to be envisaged. For this, a scavenging approach to trap and degrade the nerve agents seems especially promising and may consist in developing enzyme mimics able to hydrolyze the organophosphorus (OP) compounds under physiological conditions.

In this context, cyclodextrins (CD) constitute attractive starting materials because, due to the inclusion properties of their internal cavity, they can form host–guest complexes in aqueous media by weak interactions with small hydrophobic molecules. In particular, these macromolecular structures display the interesting capability to include organophosphorus pesticides into their cavity [13-17]. However, their intrinsic ability to transform these compounds into low or non-toxic metabolites at physiological pH is weak [18-20]. Therefore, in order to display such metabolic efficiency under mild conditions, various monofunctionalization strategies of β-CD were studied [21,22]. The attachment of an α-nucleophilic functional group on β-CD is a promising strategy to degrade G agents such as soman, sarin, cyclosarin or tabun (Figure 1) [23-30]. In fact, these β-CD derivatives play a dual role in this process: the macrocycle traps the organophosphorus whilst the bound α nucleophile reacts with the toxic agent leading to a non-toxic derivative. Other scavengers bearing several α nucleophilic groups were described [31,32].

Recently, our team developed a synthesis of heterodifunctionalized β-CD derivatives bearing an iodosobenzoate group and an imidazole substituent [33]. We have proven that the presence of both substituents increased the detoxification rate of soman as compared to the monofunctionalized derivatives. However, the synergistic effect was regiodependent and only observed with the imidazole substituent located in position 2 of one methylated glucose unit and the α nucleophile in position 3 of the adjacent methylated glucose unit (compound **1**, Figure 2).

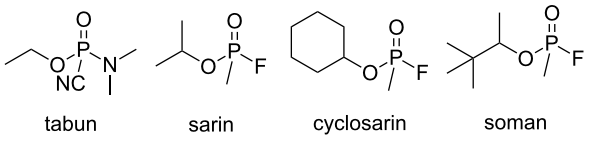

Figure 1: Structures of G agents.

Herein we present an extended study focusing on the impact of covalently bound functional groups to macrocyclic β-cyclodextrin that are involved in the OP hydrolysis. Four new derivatives **2**–**5** were prepared (Figure 3) for this purpose. Compared to analog **1**, scavenger **2** has a longer linker between the iodosobenzoate group and the methylated-β-cyclodextrin scaffold whilst scavenger **3** is characterized by a longer linker binding the imidazole ring to the CD derivative. Finally, compounds **4** and **5** are analogs of **2** bearing only one of these groups, either the α nucleophile or the imidazole ring, respectively.

All five derivatives **1**–**5** were tested for their degradation ability against methyl paraoxon (Figure 4), selected as the pesticide model, and their efficiencies were compared. To demonstrate the importance of functionalizing the CDs and the influence of

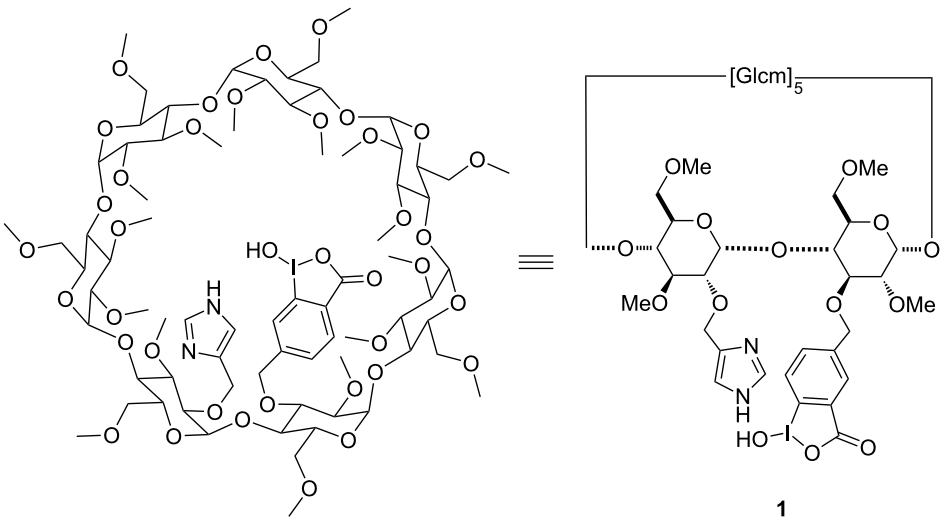

Figure 2: Scavenger based on a heterodifunctionalized β-cyclodextrin derivative.

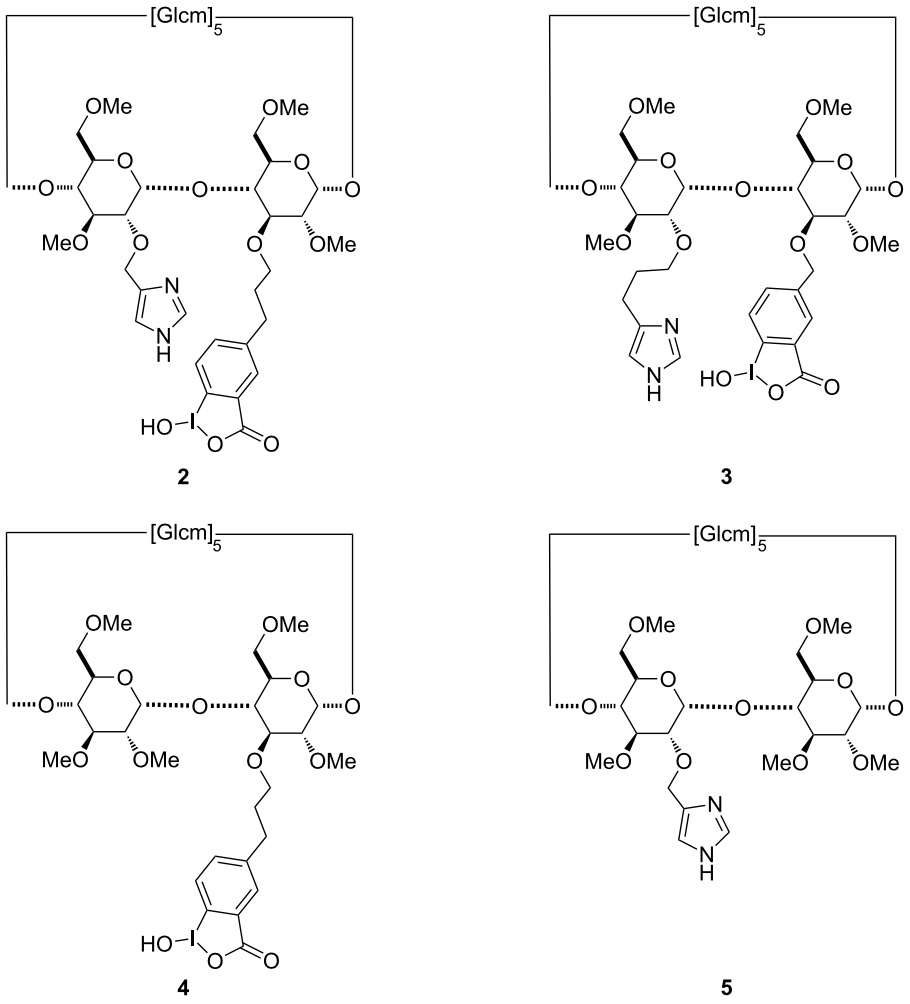

Figure 3: Structures of β-cyclodextrin derivatives **2**–**5**.

the individual moieties, the experiments were performed using the modified scavengers (with the groups covalently attached to the macrocycle) and with mixtures of heptakis(2,3,6-trimethyl)-β-cyclodextrin (TRIMEB) with 2-iodosobenzoic acid and/or imidazole, respectively. In addition, the degradation properties of the newly synthesized CD derivatives against methyl parathion and fenitrothion (Figure 4) were also investigated. Finally, compounds **1**–**4** were tested for their detoxification ability against the nerve agent soman.

Results and Discussion

Synthesis

The regioselective disubstitution of diol **6** (Scheme 1) was the key step to access derivatives **2** and **3**.

The synthetic methodology consisted first in the selective introduction of the imidazole substituent in position 2 in unit B of **6** by making use of the higher acidity of this hydroxy group compared to the OH groups in positions 3 and 6. As expected, the

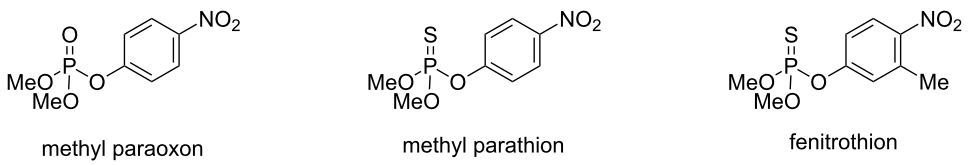

Figure 4: Structures of pesticides tested.

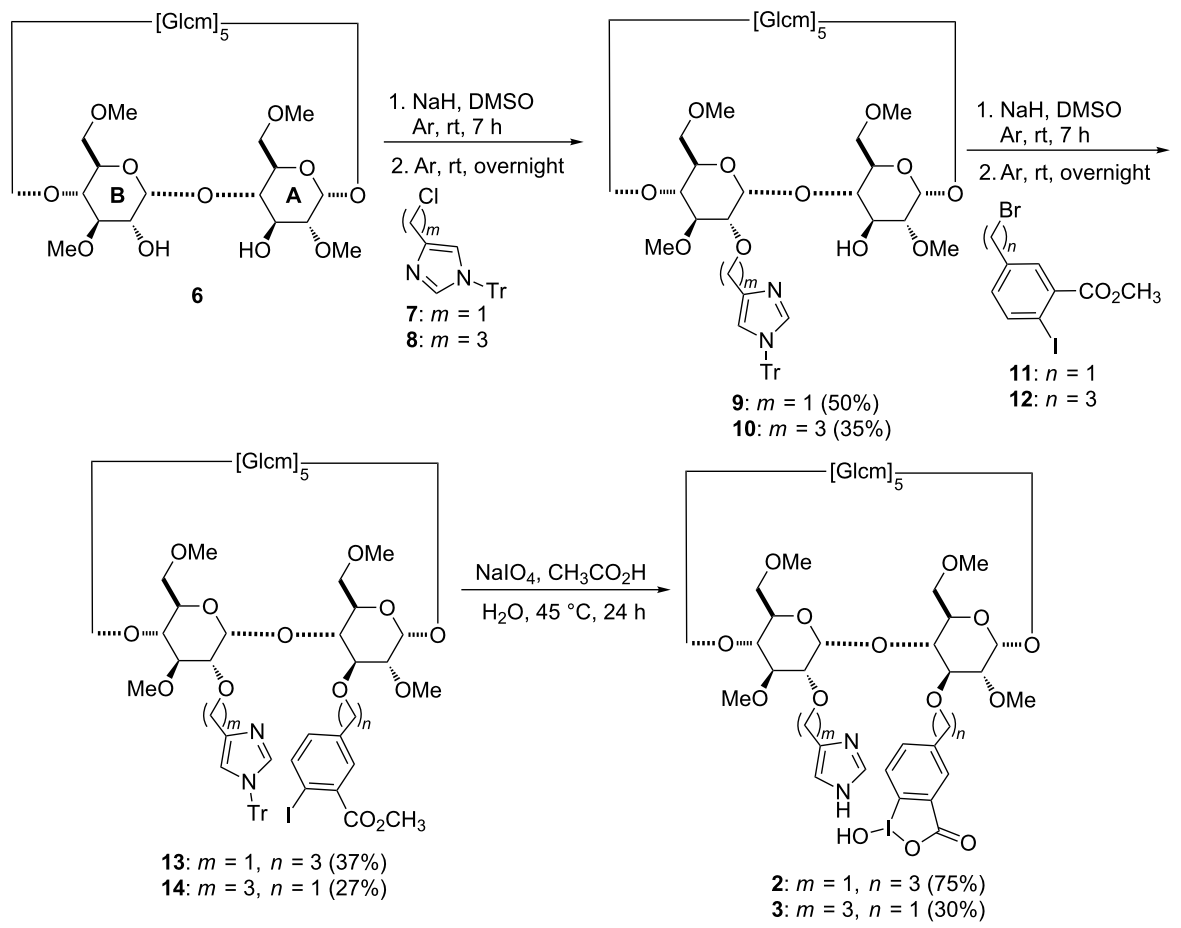

Scheme 1: Synthetic pathway to derivatives **2** and **3** (Tr = trityl).

substitution reaction with the benzyl-like reactant **7** led to a higher yield than the reaction with the propyl analog **8** (50% versus 35%), but suffered from a slightly lower regioselectivity. In fact, 4% of the 3-monosubstituted regioisomer of **9** was also formed, whereas less than 1% of the 3-monofunctionalized regioisomer of **10** was observed for the reaction with electrophile **8**. Once the first group was introduced in position 2, the substitution reaction at O-3 on the adjacent unit A was performed. Due to the lower reactivity of this alcohol group, an excess of base and electrophile was required for this step. In addition, the presence of the sterically hindered trityl-protected imidazole reduced the accessibility of substrates **11** and **12** to position 3. Thus, compounds **13** and **14** were isolated in comparable yields of 37% and 27%, respectively and this time without significantly different reactivities observed for the precursors **9** and **10**.

High resolution mass spectrometry (ESI^+ HRMS) analyses of compounds **13** and **14** confirmed the presence of the two substituents bound to the macrocycle. Also the ^1H and ^{13}C NMR spectra showed chemical shifts attributable to the CH_2 groups linked to the imidazole and iodobenzoate moieties, similar to those observed for the precursor of **1** [33]. The subsequent deprotection and oxidation–hydrolysis reactions of derivatives **13** and **14** afforded scavengers **2** and **3**, respectively and were performed in one step using sodium periodate in acidic medium. Compound **2** was obtained in good yield, but the steric hindrance of the benzylic group in derivative **14** decreased the yield of scavenger **3**.

The introduction of the methyl iodobenzoate substituent at O-3 was conducted starting from monohydroxy compound **15** [34]. After reaction with electrophile **12**, compound **4** was obtained through oxidation and hydrolysis of intermediate **16** (Scheme 2) using the same experimental conditions as applied for derivatives **13** and **14**. HSQC NMR analysis of **16** allowed the assignment of the three CH_2 groups of the propyl linker bearing the benzene ring. Correlation signals were observed for the diastereotopic protons at 3.59 and 3.90 ppm with the ^{13}C signal at 73.1 ppm belonging to the carbon connected to the oxygen atom

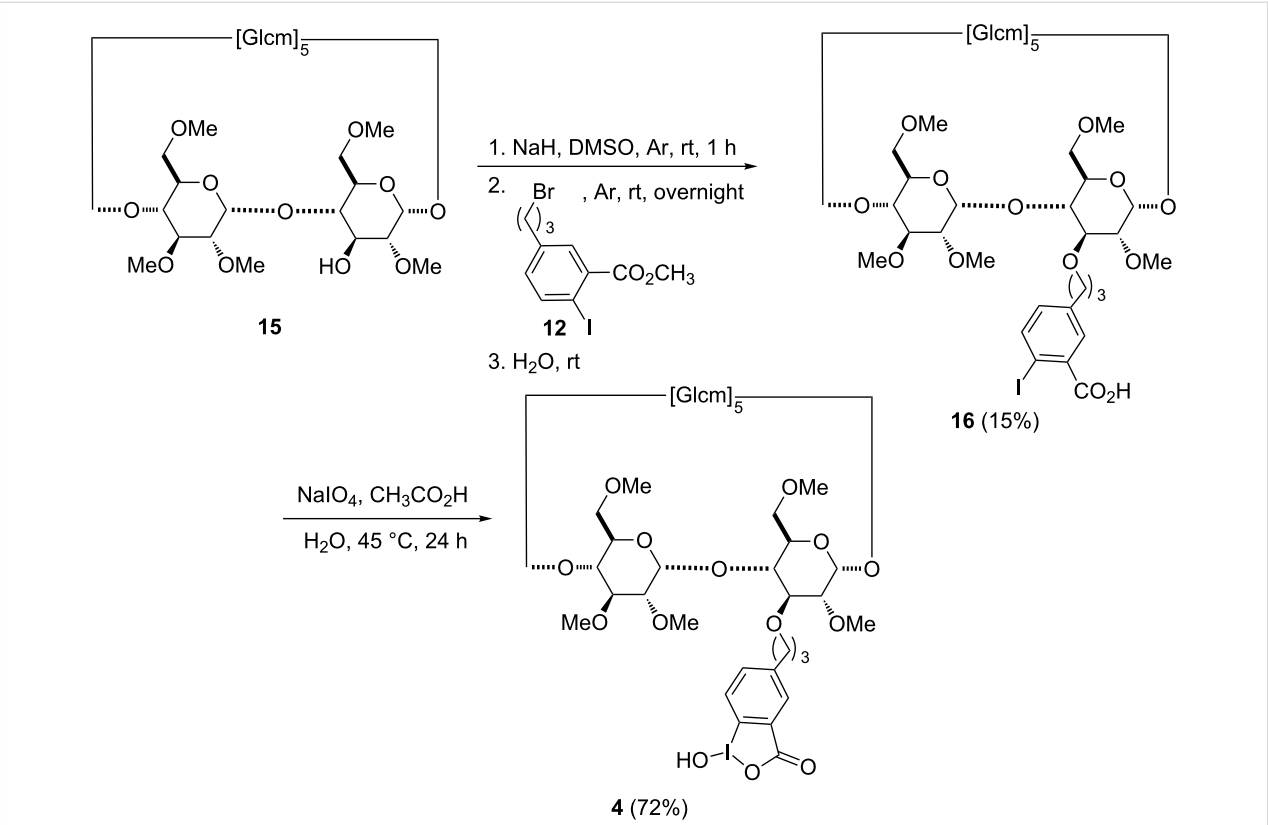

Scheme 2: Synthesis of compound **4**.

at the C-3 position. In the same way, the HSQC spectrum highlights a correlation between two other diastereotopic protons 2.50 and 2.75 ppm) and the benzylic carbon (31.9 ppm). Finally, the quintuplet at 1.99 ppm correlated with the ^{13}C signal at 31.4 ppm was assigned to the third methylene group.

The monosubstituted derivative **18** was prepared in good yield by reaction of the tritylated imidazole **7** with monohydroxy compound **17** in the presence of sodium hydride (Scheme 3) [35]. The ^{1}H NMR signals of the diastereotopic methylene protons in product **18** were respectively observed at 4.57 and 4.71 ppm, while the corresponding ^{13}C signal connected to the aromatic group was detected at 67.0 ppm. After deprotection under acidic conditions, the desired compound **5** was obtained in 94% yield.

OPasic assays

A series of tests was undertaken with the aim to: i) estimate whether the length and flexibility of the linker between the imidazole and iodosobenzoate groups and the cyclodextrin affects the OPasic activity, ii) compare the results obtained with the scavengers with those obtained with a mixture of CD and imidazole or iodosobenzoate, and iii) study the structural influence of the organophosphorus compounds on the hydrolysis process.

In a first step, 2-iodosobenzoic acid (IBA) was used as reference compound to assess the efficiencies of derivatives **1**, **2**, and **3** towards the hydrolysis of methyl paraoxon (Figure 5). All scavengers **1**–**3** accelerated the transformation of the organophosphorus compound into *p*-nitrophenol compared to IBA alone. Compound **2** was the most effective, while the slowest pesticide hydrolysis was observed in the presence of derivative **3**. These results provided evidence that the relative position of the reactive group towards the phosphorus atom and the vicinity of the imidazole affect the efficiency of the scavengers. In fact, the pesticide degradation was more effective for the derivative possessing an *n*-propyl linker of the α-nucleophile to the macrocycle (**2** versus **1**). On the other hand the highest synergistic effect of the imidazole group was observed for scavengers connected with this group through a methylene, CH_2 linker (**1** versus **3**).

At a higher concentration (0.5 mM) of scavengers **1**, **2** or **3**, we observed an improved efficiency for all three derivatives, compared to IBA (Figure 6) together with a reduced difference in their relative activities. For both studied concentrations

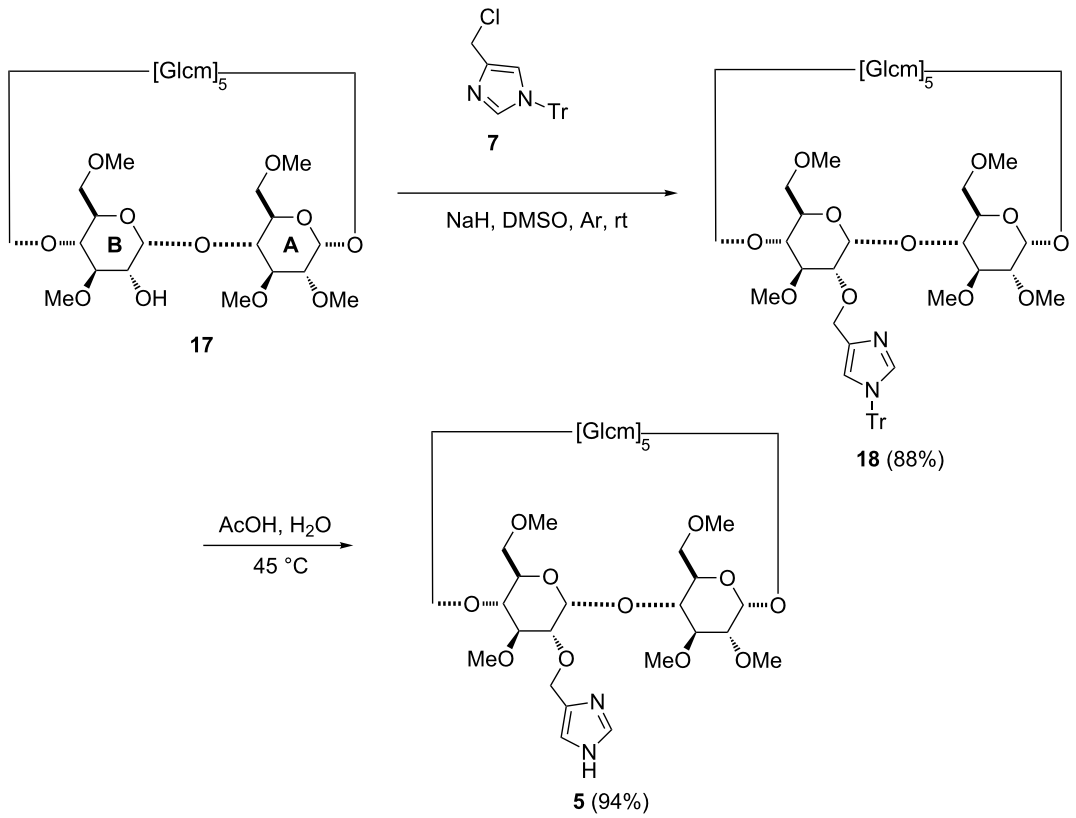

Scheme 3: Synthesis of compound **5** (Tr = trityl).

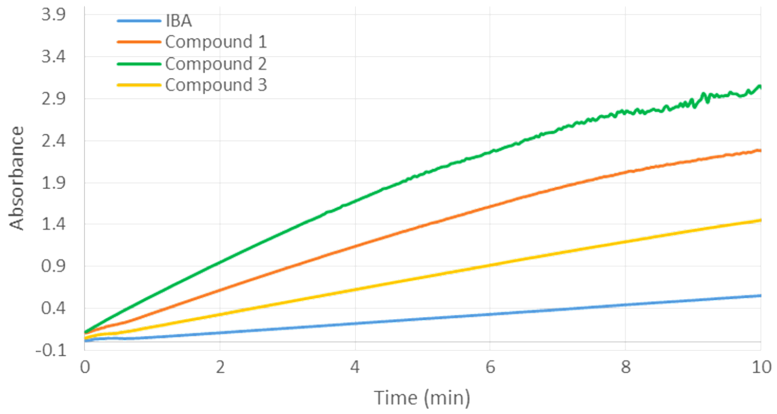

Figure 5: Hydrolysis of methyl paraoxon (0.5 mM) in the presence of compounds **1**, **2**, **3** or 2-iodosobenzoic acid (IBA) at 0.25 mM concentration.

(0.25 and 0.5 mM), the catalysts **1**–**3** were poisoned by the formed *p*-nitrophenol after a determined time. This phenomenon was already observed: the inclusion of the hydrolysis product in the cyclodextrin cavity limits the catalyst regeneration [27].

Additional investigations were then performed with the monosubstituted cyclodextrin derivatives **4** and **5** (Figure 7). In the case of compound **5**, no activity was observed. In contrast, scavenger **4**, bearing only the α-nucleophile through a three-carbon atom linker showed a similar efficiency than **2**. Therefore, it can be concluded for compound **2** that there is no synergistic effect between the imidazole and the reactive groups. Thus, the imidazole substituent is able to accelerate the degradation of methyl paraoxon, induced by the covalently attached α-nucleophile iodosobenzoate, only if IBA is bound close to the macrocycle (**1** versus **3**).

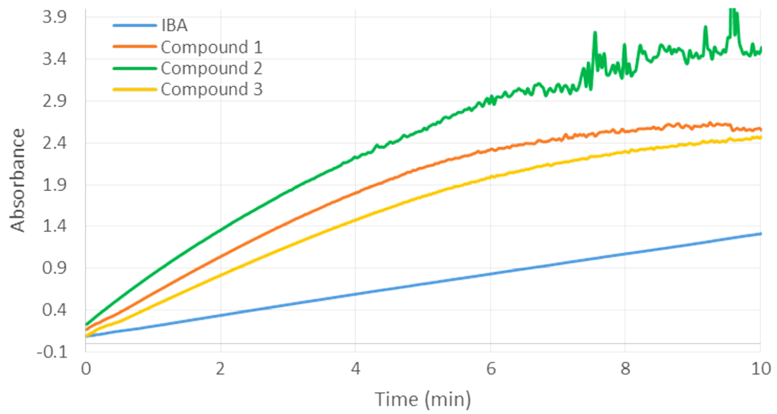

Figure 6: Hydrolysis of methyl paraoxon (0.5 mM) in the presence of compounds **1**, **2**, **3** or 2-iodosobenzoic acid (IBA) at 0.5 mM concentration.

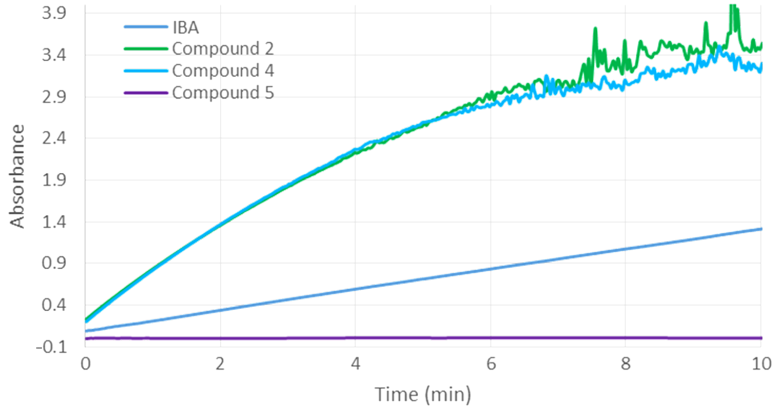

Figure 7: Hydrolysis of methyl paraoxon (0.5 mM) in the presence of compounds **2**, **4**, **5** or 2-iodosobenzoic acid (IBA) at 0.5 mM concentration.

In the presence of both, imidazole and compound **4** (Figure 8), the rate of methyl paraoxon degradation was marginally increased with respect to scavenger **4** alone. On the other hand, a mixture of IBA and compound **5** (Figure 8) led to a reduced hydrolysis efficiency of IBA. The same effect was observed for a mixture of IBA, imidazole and TRIMEB. Furthermore, adding

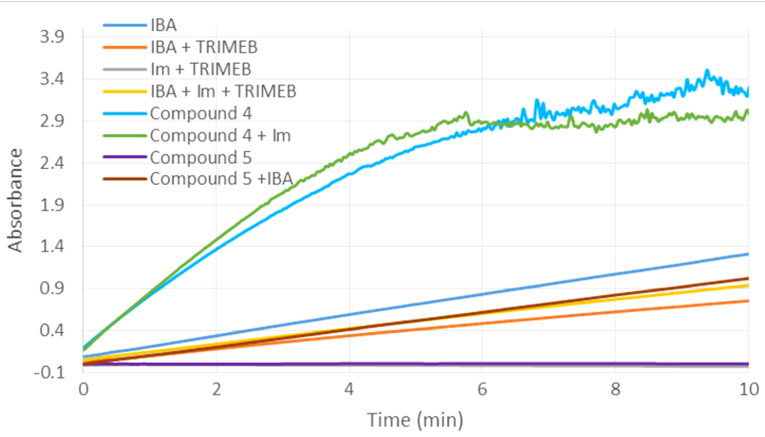

Figure 8: Hydrolysis of methyl paraoxon (0.5 mM) in the presence of mixtures of compounds **4**, **5** with IBA or imidazole and in the presence of a mixture of TRIMEB, 2-iodosobenzoic acid (IBA) and imidazole. The final concentrations of compounds **4**, **5**, 2-iodosobenzoic acid (IBA), imidazole and TRIMEB were 0.5 mM.

one molar equivalent of IBA to TRIMEB even strengthened the effect and it can be concluded that both, TRIMEB and compound **5** at least partially inhibited the pesticide hydrolysis by IBA. Therefore, when the α-nucleophile is not covalently bound to the macrocycle, the inclusion of paraoxon into the cyclodextrin cavity obviously protects the phosphate moiety of the pesticide from the external attack of the α-nucleophile. Clearly, the covalent binding of the α-nucleophile to the β-cyclodextrin scaffold leads to an increased hydrolytic activity.

The relative abilities of IBA and compounds **1**–**4** (0.25 mM) to accelerate the methyl paraoxon (0.5 mM) hydrolysis were then measured by determining the pseudo-first-order rate constants during the initial course of the process (Table 1). Under the conditions, the cyclodextrin derivatives **1**–**4** are fully active over the first 4 minutes. The absorbance increases linearly, thus indicating that no competitive inclusion of *p*-nitrophenol occurs as a side reaction and the catalyst is prevented from poisoning. In the presence of the most active compound **2**, 19.6% of paraoxon were hydrolyzed after 4 minutes whereas a conversion of only 2.6% was observed using IBA alone. The comparison with the reaction conducted in the presence of IBA revealed that scavengers **1**, **2**, **3** and **4** increased the catalytic factor by 5.5, 8.4, 2.9 and 8.2 times, respectively.

Derivative **2** appeared as the most promising disubstituted cyclodextrin for the degradation of methyl paraoxon. Therefore, this compound was subsequently used in the hydrolysis of other pesticides (Figure 9). Compound **2** was found to hydrolyze the organophosphorus compounds in the following order: fenitrothion < methyl parathion < methyl paraoxon while IBA alone displayed a generally lower and similar efficiency towards these three pesticides. This suggests that the electrophilic character of the phosphorus atom plays a role in the detoxification process (methyl parathion versus methyl paraoxon). Moreover, the strength and depth of the pesticide inclusion into the cyclodextrin cavity undeniably influence the degradation process. Indeed, it was shown that the lowest hydrolysis rates correspond to the highest dissociation constants from TRIMEB [36,37]. As methyl paraoxon represents the main and first metabolite of methyl parathion [38], scavenger **2** may be used in the late intervention after parathion intoxication.

The degradation of methyl parathion was also studied in presence of compound **4**. As already observed for methyl paraoxon compound **4** promoted the hydrolysis of methyl parathion with comparable efficiency than **2** (Figure 10). This suggests that the introduction of an imidazole group on the scavenger having the iodosobenzoate bound through an *n*-propyl linker has no effect

Table 1: Estimated pseudo-first-order rate constant (*k*) and amount (%) of hydrolyzed methyl paraoxon over the first 4 minutes.[a]

	IBA	**1**	**2**	**3**	**4**
k (10^{-3} min^{-1})	6.48	35.81	54.64	19.07	53.00
% of hydrolyzed methyl paraoxon	2.6	13.3	19.6	7.3	19.1

[a]Conditions: 20 mM phosphate buffer, 13 mM CTAC, 2.9 vol % DMSO, 3 vol % CH_3OH at 25 °C. The concentrations of 2-iodosobenzoic acid (IBA), compounds **1**, **2**, **3** and **4** were 0.25 mM. The concentration of methyl paraoxon was 0.5 mM. The reactions were followed by UV–vis determination of the released *p*-nitrophenol at 400 nm.

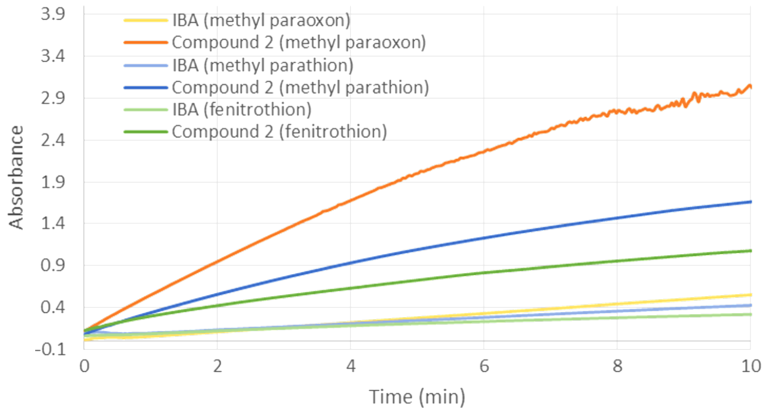

Figure 9: Influence of the pesticide structure on the hydrolytic efficiency of compound **2** (0.25 mM). Kinetic assays were carried out with methyl paraoxon, methyl parathion or fenitrothion (0.5 mM).

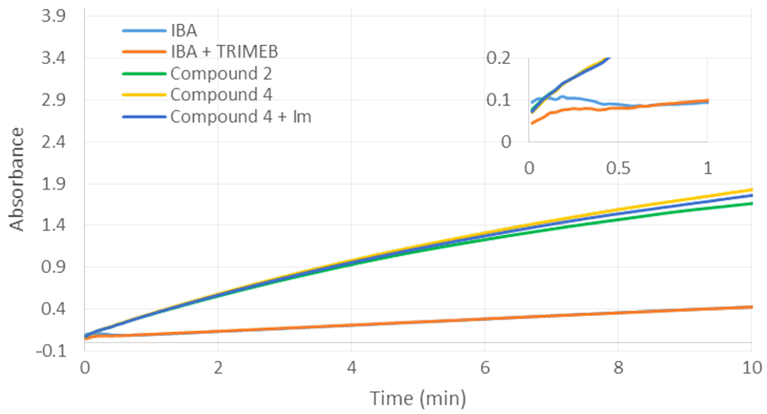

Figure 10: Influence of TRIMEB, IBA and imidazole on the hydrolysis of methyl parathion (0.5 mM). The final concentrations of compounds **2**, **4**, 2-iodosobenzoic acid (IBA), imidazole and TRIMEB were 0.25 mM.

on the hydrolytic activity, irrespective of the nature of the pesticide. Moreover, the hydrolysis rate of methyl parathion in the presence of imidazole and derivative **4** did not change when compared to scavenger **2**. This result confirms the importance to introduce the imidazole at a specific distance from the reactive group. It is important to note that, contrary to methyl paraoxon, in the case of methyl parathion, the use of an equimolar mixture of IBA and TRIMEB didn't affect the degradation of the pesticide compared to IBA alone. The influence of the intermolecular interactions between the pesticides and the methylated oligosaccharide is of fundamental importance towards the degradation process.

The degradation efficiency of IBA and compounds **1** and **4** towards methyl parathion was also studied in terms of rate constants (Table 2) within the initial 4 minutes. In the presence of derivatives **1** and **4**, 10–11% hydrolysis of the substrate were observed and the catalytic factor increased by 7.1 and 7.5 times, respectively, compared to free IBA.

Table 2: Estimated pseudo-first-order rate constant (k) and amount (%) of hydrolyzed methyl parathion over the first 4 minutes.[a]

	IBA	**1**	**4**
k (10^{-3} min^{-1})	3.99	28.17	29.79
% of hydrolyzed methyl parathion	1.6	10.7	11.2

[a]Conditions: 20 mM phosphate buffer, 13 mM CTAC, 2.9 vol % DMSO, 3 vol % CH_3OH at 25 °C. The concentrations of 2-iodosobenzoic acid (IBA), compounds **1** and **4** were 0.25 mM, respectively. The concentration of methyl parathion was 0.5 mM. The reactions were followed by UV–vis determination of the released *p*-nitrophenol at 400 nm.

Finally, the scavengers **1**–**4** were tested for their ability to prevent the inhibition of acetylcholinesterase by the chemical warfare agent soman (Figure 11). The heterodifunctionalized derivatives **1** and **3** were, this time, the most effective compounds. Preincubation of compounds **1** and **3** with soman for 60 minutes reduced the inhibition of the enzyme by 70% and 60%, respectively, whilst 40% and 50% reduction was observed with compounds **2** and **4** after the same pretreatment

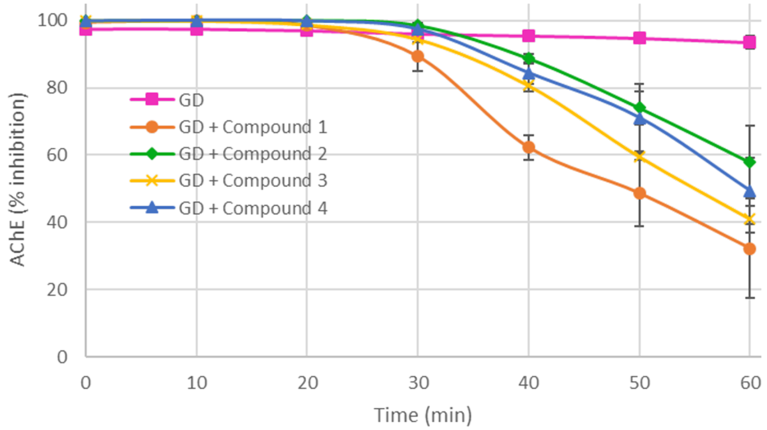

Figure 11: Ability of compounds **1**–**4** in preventing the inhibition of acetylcholinesterase by soman (GD).

time. Moreover, scavengers **1** and **3** exhibited a detectable activity only after approximately 20 minutes incubation with soman, whereas compounds **2** and **4** showed an even later effect reducing the inhibition by 30% after 50 minutes pretreatment. Comparing the efficiencies of compounds **1** and **2** with those obtained for methyl paraoxon, we observed a higher activity when the α-nucleophile is close to the macrocycle. Concerning compounds **1** and **3**, the vicinity of the imidazole substituent to the active group confirmed its benefit to accelerate the soman degradation [33]. However, many parameters are involved in the detoxification process. It is known that an aromatic group attached to a phosphorus atom can interact with the cyclodextrin cavity wherefore soman and organophosphorus pesticides having an aromatic group were not hydrolyzed with the same efficiency by the scavengers. In fact, this efficiency is highly substrate-dependent and it is difficult to strictly correlate the hydrolysis profiles to the cyclodextrin structures of the prepared derivatives. Therefore, the design of new scavengers will require further structural studies on the inclusion complexes and affinity measurements with carefully selected analogs of organophosphates.

Conclusion

New β-cyclodextrin derivatives were synthesized and their efficiency to degrade the organophosphorus pesticides and soman was evaluated. Some structural features of the scavengers could be identified as the key elements in charge to accelerate the decontamination of organophosphorus compounds: (1) the degradation kinetics of organophosphorus constituents is dependent on their affinity for the cyclodextrin cavity; (2) the α-nucleophile needs to be covalently bound to the macrocycle in order to enhance its activity towards the hydrolysis of organophosphorus compounds; (3) the hydrolysis process of pesticides bearing a phenyl group is mainly affected by the chain length of the linker between the iodosobenzoate group and the methylated oligosaccharide; (4) in case of soman, the degradation is enhanced by a cooperative effect observed between the imidazole and 2-iodosobenzoate when the latter is in close proximity to the macrocycle. A more extended structure–activity relationship study is envisaged to further investigate and better rationalize all parameters involved in this complex hydrolytic process.

Supporting Information

Supporting Information File 1

Experimental procedures, NMR spectra, hydrolytic and detoxification assays.
[http://www.beilstein-journals.org/bjoc/content/supplementary/1860-5397-13-45-S1.pdf]

Acknowledgements

Funding: DGA-MRIS and region Haute-Normandie are gratefully acknowledged for PhD scholarship. The authors thank DGA Maîtrise NRBC (contract n°2014910080), DGA (« ASTRID maturation », ANR-14-ASMA-0003), ANR (ANR BLAN06-1_134538) and ANR-LABEX SynOrg for postdoctoral fellowships (ANR-11-LABX-0029). Rouen University, INSA Rouen, CNRS, EFRD and Labex SynOrg (ANR-11-LABX-0029) are also acknowledged for their financial support.

References

1. Worek, F.; Thiermann, H.; Szinicz, L.; Eyer, P. *Biochem. Pharmacol.* **2004,** *68,* 2237–2248. doi:10.1016/j.bcp.2004.07.038
2. Tuovinen, K. *Toxicology* **2004,** *196,* 31–39. doi:10.1016/j.tox.2003.10.013
3. Benschop, H. P.; De Jong, L. P. A. *Acc. Chem. Res.* **1988,** *21,* 368–374. doi:10.1021/ar00154a003
4. Aragay, G.; Pino, F.; Merkoçi, A. *Chem. Rev.* **2012,** *112,* 5317–5338. doi:10.1021/cr300020c
5. Taylor, P.; Radic, Z.; Hosea, N. A.; Camp, S.; Marchot, P.; Berman, H. A. *Toxicol. Lett.* **1995,** *82–83,* 453–458. doi:10.1016/0378-4274(95)03575-3
6. Marrs, T. C. *Pharmacol. Ther.* **1993,** *58,* 51–66. doi:10.1016/0163-7258(93)90066-M
7. Gunnell, D.; Eddleston, M.; Phillips, M. R.; Konradsen, F. *BMC Public Health* **2007,** *7,* 357–372. doi:10.1186/1471-2458-7-357
8. Lee, B. K.; Jeung, K. W.; Lee, H. Y.; Jung, Y. H. *Clin. Toxicol.* **2011,** *49,* 828–833. doi:10.3109/15563650.2011.617309
9. Kwong, T. C. *Ther. Drug Monit.* **2002,** *24,* 144–149. doi:10.1097/00007691-200202000-00022
10. Bertolote, J. M.; Fleischmann, A.; Eddleston, M.; Gunnell, D. *Br. J. Psychiatry* **2006,** *189,* 201–203. doi:10.1192/bjp.bp.105.020834
11. Sultatos, L. G. *J. Toxicol. Environ. Health* **1994,** *43,* 271–289. doi:10.1080/15287399409531921
12. Kim, K.; Tsay, O. G.; Atwood, D. A.; Churchill, D. G. *Chem. Rev.* **2011,** *111,* 5345–5403. doi:10.1021/cr100193y
13. Bui, M.-P. N.; Makamba, H.; Seo, S. S. *Anal. Lett.* **2016,** *49,* 1600–1612. doi:10.1080/00032719.2015.1113418
14. Coscarello, E. N.; Barbiric, D. A.; Castro, E. A.; Vico, R. V.; Bujánm, E. I.; de Rossi, R. H. *J. Struct. Chem.* **2009,** *50,* 671–679. doi:10.1007/s10947-009-0103-2
15. Cruickshank, D. L.; Rougier, N. M.; Vico, R. V.; Bourne, S. A.; Buján, E. I.; Caira, M. R.; de Rossi, R. H. *Beilstein J. Org. Chem.* **2013,** *9,* 106–117. doi:10.3762/bjoc.9.14
16. Letort, S.; Balieu, S.; Erb, W.; Gouhier, G.; Estour, F. *Beilstein J. Org. Chem.* **2016,** *12,* 204–228. doi:10.3762/bjoc.12.23
17. Cruickshank, D.; Rougier, N. M.; Vico, R. V.; de Rossi, R. H.; Buján, E. I.; Bourne, S. A.; Caira, M. R. *Carbohydr. Res.* **2010,** *345,* 141–147. doi:10.1016/j.carres.2009.10.023
18. Saint André, S.; Désiré, B. *C. R. Acad. Sci., Ser. III* **1985,** *301,* 67–72.
19. Désiré, B.; Saint-André, S. *Experientia* **1987,** *43,* 395–397. doi:10.1007/BF01940424
20. Désiré, B.; Saint-André, S. *Fundam. Appl. Toxicol.* **1986,** *7,* 646–657. doi:10.1016/0272-0590(86)90114-4
21. Masurier, N.; Estour, F.; Lefèvre, B.; Brasme, B.; Masson, P.; Lafont, O. *Carbohydr. Res.* **2006,** *341,* 935–940. doi:10.1016/j.carres.2006.02.012

22. Masurier, N.; Lafont, O.; Le Provost, R.; Lesur, D.; Masson, P.; Djedaini-Pilard, F.; Estour, F. *Chem. Commun.* **2009,** 589–591. doi:10.1039/B812325J
23. Zengerle, M.; Brandhuber, F.; Schneider, C.; Worek, F.; Reiter, G.; Kubik, S. *Beilstein J. Org. Chem.* **2011,** *7,* 1543–1554. doi:10.3762/bjoc.7.182
24. Bierwisch, A.; Zengerle, M.; Thiermann, H.; Kubik, S.; Worek, F. *Toxicol. Lett.* **2014,** *224,* 209–214. doi:10.1016/j.toxlet.2013.10.024
25. Worek, F.; Seeger, T.; Zengerle, M.; Kubik, S.; Thiermann, H.; Wille, T. *Toxicol. Lett.* **2014,** *226,* 222–227. doi:10.1016/j.toxlet.2014.02.010
26. Kranawetvogl, A.; Müller, S.; Kubik, S.; Spruit, H.; Thiermann, H.; Worek, F.; Noort, D.; Reiter, G. *Toxicol. Lett.* **2015,** *239,* 41–52. doi:10.1016/j.toxlet.2015.08.007
27. Masurier, N.; Estour, F.; Froment, M.-T.; Lefèvre, B.; Debouzy, J.-C.; Brasme, B.; Masson, P.; Lafont, O. *Eur. J. Med. Chem.* **2005,** *40,* 615–623. doi:10.1016/j.ejmech.2005.02.008
28. Kalakuntla, R. K.; Wille, T.; Le Provost, R.; Letort, S.; Reiter, G.; Müller, S.; Thiermann, H.; Worek, F.; Gouhier, G.; Lafont, O.; Estour, F. *Toxicol. Lett.* **2013,** *216,* 200–205. doi:10.1016/j.toxlet.2012.11.020
29. Le Provost, R.; Wille, T.; Louise, L.; Masurier, N.; Müller, S.; Reiter, G.; Renard, P.-Y.; Lafont, O.; Worek, F.; Estour, F. *Org. Biomol. Chem.* **2011,** *9,* 3026–3032. doi:10.1039/c0ob00931h
30. Estour, F.; Letort, S.; Müller, S.; Kalakuntla, R. K.; Le Provost, R.; Wille, T.; Reiter, G.; Worek, F.; Lafont, O.; Gouhier, G. *Chem.-Biol. Interact.* **2013,** *203,* 202–207. doi:10.1016/j.cbi.2012.10.020
31. Brandhuber, F.; Zengerle, M.; Porwol, L.; Bierwisch, A.; Koller, M.; Reiter, G.; Worek, F.; Kubik, S. *Chem. Commun.* **2013,** *49,* 3425–3427. doi:10.1039/c3cc41290c
32. Brandhuber, F.; Zengerle, M.; Porwol, L.; Tenberken, O.; Thiermann, H.; Worek, F.; Kubik, S.; Reiter, G. *Toxicology* **2012,** *302,* 163–171. doi:10.1016/j.tox.2012.08.013
33. Letort, S.; Mathiron, D.; Grel, T.; Albaret, C.; Daulon, S.; Djedaini-Pilard, F.; Gouhier, G.; Estour, F. *Chem. Commun.* **2015,** *51,* 2601–2604. doi:10.1039/C4CC09189B
34. Xiao, S.; Yang, M.; Sinaÿ, P.; Blériot, Y.; Sollogoub, M.; Zhang, Y. *Eur. J. Org. Chem.* **2010,** 1510–1516. doi:10.1002/ejoc.200901230
35. Cousin, H.; Cardinael, P.; Oulyadi, H.; Pannecoucke, X.; Combret, J. C. *Tetrahedron: Asymmetry* **2001,** *12,* 81–88. doi:10.1016/S0957-4166(00)00499-7
36. Kamiya, M.; Nakamura, K. *Pest Manage. Sci.* **1994,** *41,* 305–309. doi:10.1002/ps.2780410404
37. Kamiya, M.; Nakamura, K.; Sasaki, C. *Chemosphere* **1995,** *30,* 653–660. doi:10.1016/0045-6535(94)00431-S
38. Boone, J. S.; Chambers, J. E. *Aquat. Toxicol.* **1997,** *39,* 333–343. doi:10.1016/S0166-445X(97)00019-2

License and Terms

BEILSTEIN JOURNAL OF ORGANIC CHEMISTRY

Novel β-cyclodextrin–eosin conjugates

Gábor Benkovics[1,2], Damien Afonso[3], András Darcsi[4], Szabolcs Béni[4], Sabrina Conoci[5], Éva Fenyvesi[1], Lajos Szente[1], Milo Malanga[*1] and Salvatore Sortino[*3]

Full Research Paper

Open Access

Address:
[1]CycloLab, Cyclodextrin R&D Ltd, Budapest, H-1097 Illatos út 7, Hungary, [2]Department of Organic Chemistry, Faculty of Science, Charles University in Prague, Hlavová 8, 128 43, Prague 2, Czech Republic, [3]Laboratory of Photochemistry, Department of Drug Sciences, University of Catania, I-95125 Viale A. Doria 6, Italy, [4]Department of Pharmacognosy, Semmelweis University, H-1085 Üllői út 26, Hungary and [5]STMicroelectronics, Stradale Primosole 50, I-95121, Catania, Italy

Email:
Milo Malanga* - malanga@cyclolab.hu; Salvatore Sortino* - ssortino@unict.it

* Corresponding author

Keywords:
β-cyclodextrins; fluorescence; photodynamic therapy; photosensitizers; singlet oxygen; xanthene

Beilstein J. Org. Chem. **2017,** *13,* 543–551.
doi:10.3762/bjoc.13.52

Received: 16 December 2016
Accepted: 23 February 2017
Published: 15 March 2017

This article is part of the Thematic Series "Superstructures with cyclodextrins: Chemistry and applications IV".

Guest Editor: G. Wenz

Abstract

Eosin B (EoB) and eosin Y (EoY), two xanthene dye derivatives with photosensitizing ability were prepared in high purity through an improved synthetic route. The dyes were grafted to a 6-monoamino-β-cyclodextrin scaffold under mild reaction conditions through a stable amide linkage using the coupling agent 4-(4,6-dimethoxy-1,3,5-triazin-2-yl)-4-methylmorpholinium chloride. The molecular conjugates, well soluble in aqueous medium, were extensively characterized by 1D and 2D NMR spectroscopy and mass spectrometry. Preliminary spectroscopic investigations showed that the β-cyclodextrin–EoY conjugate retains both the fluorescence properties and the capability to photogenerate singlet oxygen of the unbound chromophore. In contrast, the corresponding β-cyclodextrin–EoB conjugate did not show either relevant emission or photosensitizing activity probably due to aggregation in aqueous medium, which precludes any response to light excitation.

Introduction

Cyclodextrins (CDs) are cyclic oligosaccharides able to form host–guest inclusion complexes with drugs and this property can be utilized to protect the guest molecules from oxidation and degradation, to enhance their solubility and bioavailability, or to use the CD host as a drug carrier [1]. The potential application of these macrocyclic sugars in such pharmaceutical formulations required the understanding of the mechanism of their action and their fate inside living cells. The fluorescent labeling of CDs enables their tracking and visualization in biological media and provides useful information about their cell-membrane-penetration ability [2,3]. Besides, fluorophore-appended CDs have been extensively studied and successfully

utilized in photodynamic therapy (PDT). This minimally invasive therapeutic approach has proven to be very well-suited for cancer and bacterial diseases treatment. The PDT is based on the combination of three main components: visible light, a photosensitizer (PS) and molecular oxygen [4,5]. After being excited with visible light, the PS – while reverting to the ground state – transfers the energy of its lowest excited triplet state to nearby molecular oxygen. This leads to an in situ generation of singlet oxygen ($^1O_2$), which is the main responsible species for cytotoxic reactions in cells [6]. Singlet oxygen offers important advantages over conventional drugs as it: i) potentially attacks biological substrates of different nature (i.e., lipids, proteins, and DNA), ii) does not suffer from multidrug resistance (MDR) problems, and iii) due to its short half-life (<0.1 ms) and lack of charge, it diffuses in the cellular environment over short distances (few tens of nm) resulting in negligible systemic side effects.

For PDT applications CDs have been conjugated with porphyrin [7] and protoporphyrin (5-aminolevulinic acid) [8] in order to enhance the membrane penetration of the PS (or its prodrug), to increase the aqueous solubility and to prevent the undesired aggregation of the PS inside the cell. Another advantage offered by the covalently connected CD–PS systems is the encapsulation of hydrophobic photoactivatable drug molecules in the CD cavity, enabling thereby the application of these systems in combined phototherapies. This approach has recently led to self-assembled systems based on a porphyrin–β-CD conjugate and a tailored nitric oxide photoreleaser forming a strong inclusion complex with the β-CD cavity [9]. This supramolecular nanoassembly simultaneously releases cytotoxic $^1O_2$ and nitric oxide under illumination with visible light, resulting in amplified cancer-cell mortality [9]. By attaching porphyrin to γ-CD and dimeric β-CD, which are both able to form inclusion complexes with cytotoxic drug molecules such as doxorubicin and paclitaxel, nanocarriers with multimodal therapeutic effects (PDT and chemotherapy) have been developed by Král et al. [10,11]. The results achieved by these groups clearly demonstrated the numerous advantages of the PS–CD coupling. However, despite the number of porphyrinoid PSs conjugated with CDs [12-20], literature on xanthene-type PSs in conjugation with CDs is very scarce. The reasons behind this fact are most probably the difficulties in selective CD functionalization and limitations in xanthene-dye modification.

Xanthene dyes can be introduced into the CD scaffold most easily through an ester linkage between the available hydroxy groups of the CD and the carboxylic acid group of the dye [21]. These conjugates, however, cannot be used in biomedical applications because of the lability of the ester bond towards enzymatic degradation. Any cleavage of the conjugate would result in an increased free dye concentration in the studied medium and consequently it would lead to false positive results in microscopic studies or in undesired aggregation of the free PS. To circumvent this drawback and to ensure the stability of the dye-appended CD derivatives, different strategies using thioureido [3] or amide [22] connections have been developed. Fenyvesi and Jicsinszky applied thioureido chemistry to attach fluoresceinyl isothiocyanate to randomly methylated 6-monoamino-β-CD as a possible sensor for soluble contaminants in groundwater [23]. In the conjugate obtained, the stability of the formed thioureido moiety also made possible its biological application and since the introduction of this strategy a wide variety of xanthene-dye-appended CDs have been developed [24,25] using the same methodology. However, the major drawbacks of this approach is the extremely high price of the isothiocyanate pre-modified xanthene starting materials and the harsh reaction conditions (pyridine as a solvent, reflux, additional base) necessary for the successful coupling. These factors called for an easy-to-perform and widely applicable approach towards xanthene-dye-modified CDs. This was achieved with the aid of 4-(4,6-dimethoxy-1,3,5-triazin-2-yl)-4-methylmorpholinium chloride (DMTMMCl), a coupling reagent frequently used in peptide synthesis. Malanga et al. recently reported on the preparation of xanthene-dye-appended CDs with the most commonly used fluorescent probes rhodamine and fluorescein (Flu, **1**). The conjugation of the 6-monoamino-β-CD scaffold was achieved through amide-bond formation between the amino-CD and the carboxylic group of the xanthene dyes [26]. This strategy does not require the laborious isothiocyanate functionalization and it can be applied to all xanthene dyes having a carboxylic function. Encouraged by these results we decided to use this method for the coupling with xanthene dyes which upon light irradiation are able to generate cytotoxic $^1O_2$. The coupled products would thus represent a new family of photosensitizers, the eosin-CDs (Eo–CDs). Although the photobactericidal activity of Eo dyes is well known from the literature [27,28], to the best of our knowledge Eo–CD conjugates have not been prepared up to date.

Results and Discussion

Synthesis of eosin Y (EoY, **2**) and eosin B (EoB, **4**)

The purity of the commercially available dyes eosin Y and eosin B, purchased from different providers (two different sources for each dye were tested) was not suitable for the preparation of the β-CD conjugates. The ^1H NMR spectra and TLC analysis of the commercially available dyes are provided in Supporting Information File 1, Figures S1 and S2, Figures S8 and S9 and Figures S41 and S42, respectively. Therefore, both dyes were freshly synthesized starting from fluorescein (Flu, **1**). Although the described synthetic procedures for the preparation

of eosin dyes commonly use Br_2, herein the less hazardous *N*-bromosuccinimide (NBS) was used as the source of bromine. Thus, eosin Y (**2**) was prepared in a single step from **1** in ethanol in the presence of NBS (Figure 1). The detailed description of the syntheses is reported in Supporting Information File 1.

The synthesis of EoB (**4**) was performed in two steps: first, dibromofluorescein (**3**) was synthesized through partial bromination of **1** with NBS in acetic acid (Figure 1). However, under the selected reaction conditions, a three-component mixture of mono-, di- and tribromofluorescein was obtained and the isolation of the targeted dibrominated product **3** from this crude was extremely laborious and low yielding. On the other hand, when using NBS in a slight excess (2.5-fold molar excess with respect to **1**) only a two-component mixture of di- and tribromofluorescein was formed. The isolation of **3** from this crude was easily achieved through direct-phase silica gel column chromatography with isocratic chloroform/methanol elution. Herewith the overbrominated byproduct was permanently immobilized on the silica gel column and only the targeted dibromofluorescein (**3**) was eluted. The structure of compound **3** was elucidated with the aid of 1D and 2D NMR experiments (Supporting Information File 1, Figures S10–S14). In the following step, dibrominated fluorescein **3** was nitrated using standard nitration conditions to obtain the desired dye eosin B (**4**) (Figure 1). The NMR spectra showing the structure elucidation of the free dyes eosin Y (**2**) and eosin B (**4**) are shown in Supporting Information File 1, Figures S3–S7 and Figures S15–S19, respectively.

Synthesis of eosin Y–β-CD and eosin B–β-CD conjugates

The condensation reaction between 6-monoamino-β-CD and the synthesized dyes **2** and **4** is shown in Figure 2.

The reaction is promoted by the coupling agent DMTMMCl that enables an effective conjugation in water under mild reaction conditions (room temperature). Since a successful condensation requires the amino function to be in the free base form, an additional base *N*-methylmorpholine (NMM) was added. All reactants are well soluble in water resulting in a homogenous reaction mixture and in both cases the coupling proceeded at room temperature within 3 h for eosin Y (**2**) and 12 h in case of eosin B (**4**). TLC analysis of the crude reaction mixture gave the first unambiguous evidence for the successful conjugate formation as the formed products have an R_f value distinct from those of the other starting materials. Additionally the products show intensive absorbance after excitation at 254 nm and 366 nm and they are carbonizable. Thus the products exhibit the expected characteristics of a fluorescent CD conjugate (Figure 3). Work-up of the reactions included the concentration of the reaction mixtures and selective precipitation of the CD-related com-

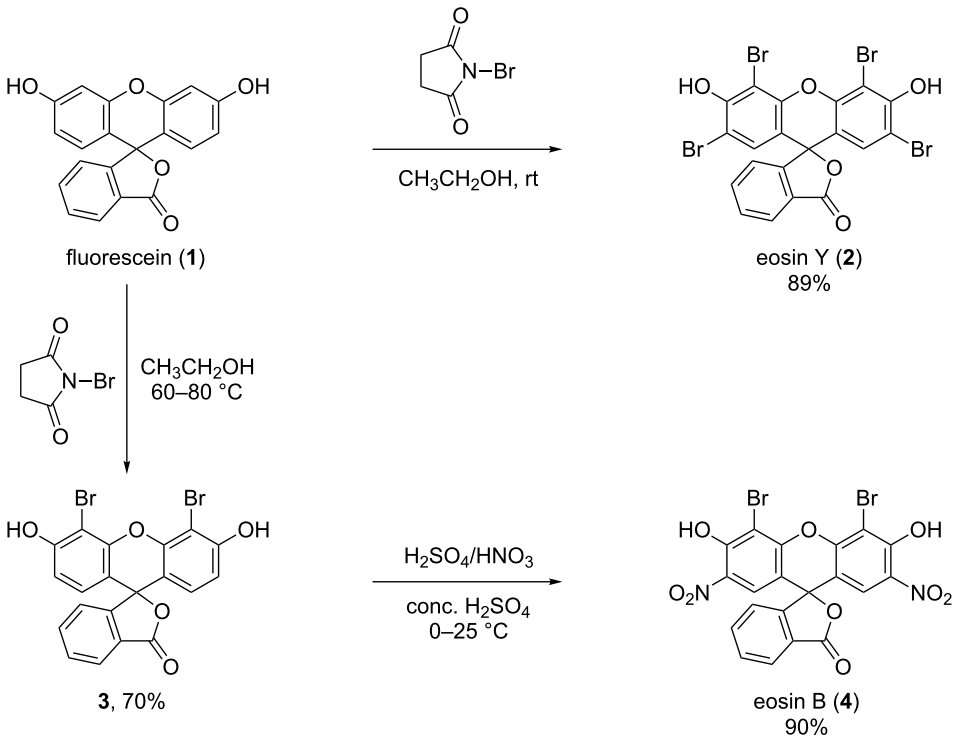

Figure 1: Reaction scheme for the synthesis of eosin Y (**2**) and eosin B (**4**).

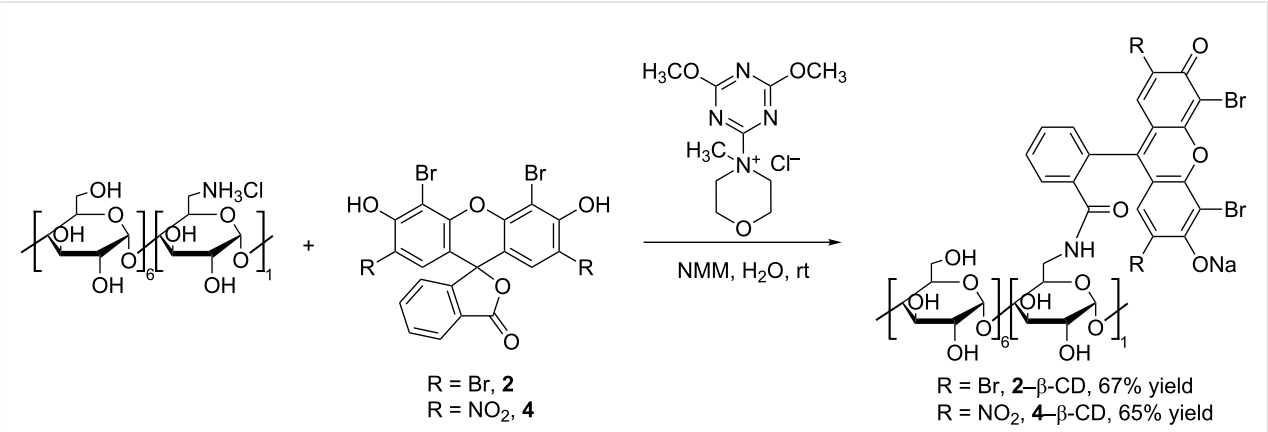

Figure 2: Reaction scheme for the synthesis of eosin-appended β-CDs, **2**–β-CD and **4**–β-CD (NMM: *N*-methylmorpholine).

pounds (conjugate and unreacted starting material) with acetone. As the free dyes, NMM, DMTMM-related products and other reaction impurities are all well soluble in a water/acetone mixture, they can easily be removed by washing the precipitates with sufficient amounts of these solvents. In order to separate the target conjugates from unreacted 6-monoamino-β-CD (5–10% based on TLC evaluation, see Figure 3), the precipitate was subjected to direct-phase column chromatography using an acetonitrile (ACN)/H_2O/NH_3 elution mixture, in which the faster eluting component is the conjugate and the slower is the unreacted aminocyclodextrin which can be eventually recovered.

NMR characterization of eosin-appended β-CDs, **2**–β-CD and **4**–β-CD

Solutions in deuterated DMSO (DMSO-d_6) were used for NMR measurements, in order to preserve a molecularly dispersed form of the CD derivatives during characterization. The ^{1}H NMR spectra of both conjugates have the typical fingerprint signals for the asymmetric, 6-monosubstituted β-cyclodextrins. Generally two sets of signals can be identified (Figure 4 and Figure S20 in Supporting Information File 1): the first set comprises the aromatic protons of the eosin dyes that are observed between 6.35–7.75 ppm, while the second one is formed by the CD resonances in the range of 3.0–5.9 ppm. The CD region also includes the proton resonances from the primary OH groups (4.34–4.49 ppm) and the resonances of the protons from the secondary OH groups (5.53–5.93 ppm) of the CD. DEPT-edited HSQC spectra for both products confirm the characteristic signal pattern of a 6-substituted β-CD, having the C6 carbon atom of the substituted glucose unit shifted towards lower fields (42.27 ppm) (Figure S24 and Figure S32 in Supporting Information File 1). This chemical shift of the C6 carbon atom of the substituted glucose unit is also a good indicator for the

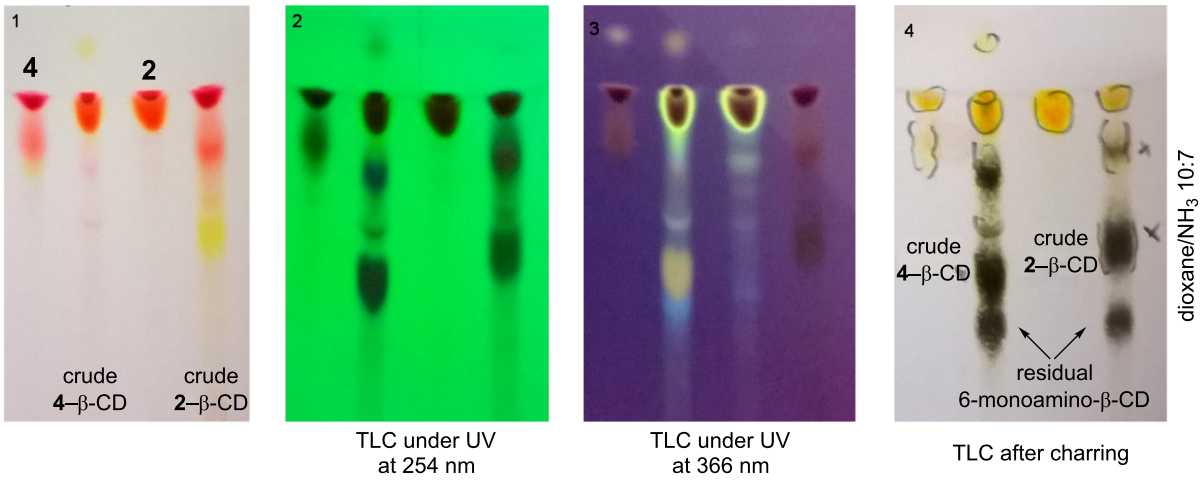

Figure 3: TLC analysis of the composition of the crude coupling reaction mixtures.

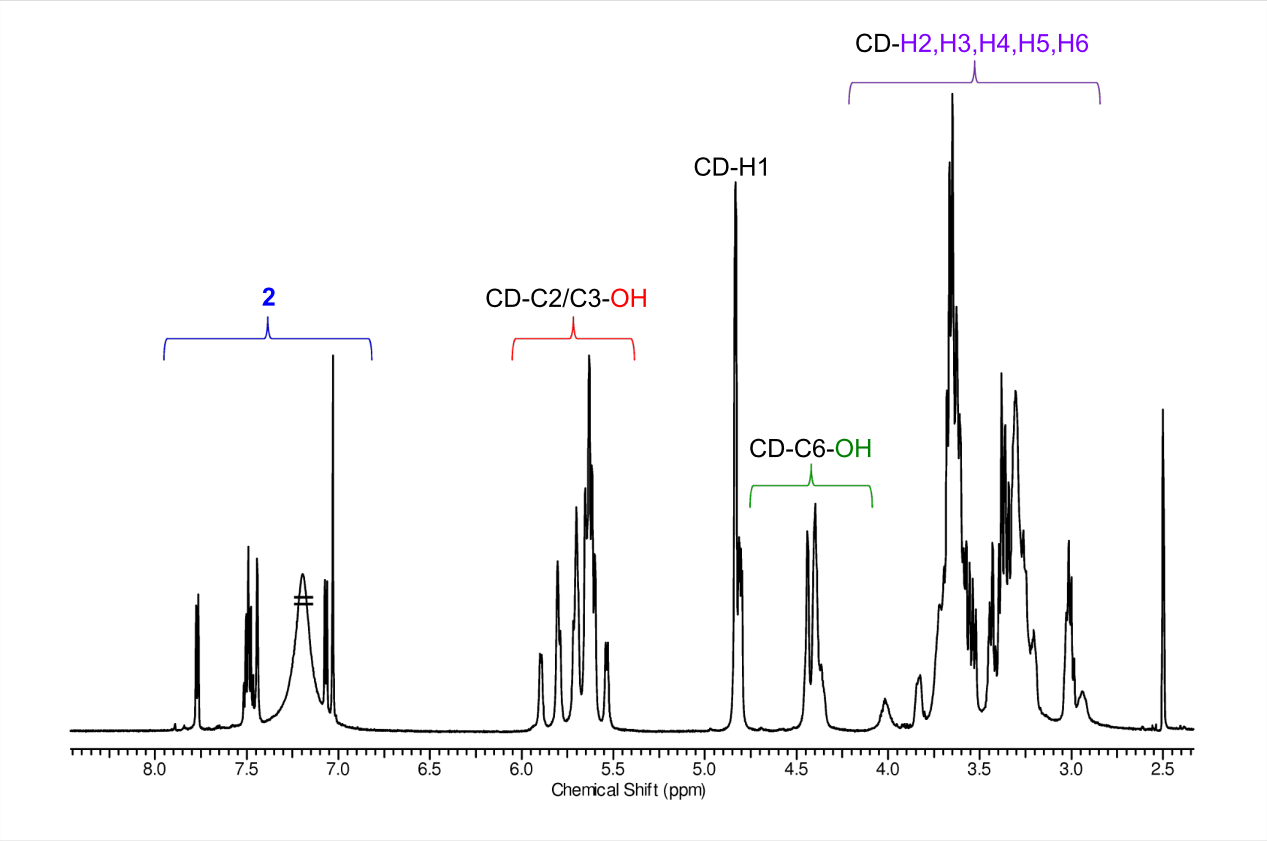

Figure 4: ^{1}H NMR spectrum of **2**–β-CD with partial assignment (DMSO-d_6, 600 MHz, 298 K).

successful amide-bond formation, as this signal in the starting material, 6-monoamino-β-CD, is found at slightly higher fields – around 40 ppm. The coupling effectivity is further confirmed by the presence of a single signal at around 168 ppm in the ^{13}C NMR spectra which is assigned to the carbon atom of the amide group of the conjugates (see Figures S21 and S29 in Supporting Information File 1).

In the ^{1}H NMR spectra of both conjugates, the signals of the anomeric protons are well separated from the aromatic protons and from other CD-related resonances (Figure 4 and for the spectrum of conjugate **4**–β-CD, see Figure S20 in Supporting Information File 1). Therefore these protons provide a good reference for the determination of the degree of substitution (DS) of the molecules. The comparison of the intensities of the anomeric protons with those of the aromatic protons unambiguously confirms the monosubstitution pattern (DS = 1) in both cases and was further proven by electrospray ionization mass spectrometry (ESIMS) analysis of the compounds (see Supporting Information File 1). The signals in the aromatic region are well resolved (see Figures S25 and S33, Supporting Information File 1) and the in-depth analysis of the DEPT-edited HSQC spectra supported by COSY data (Figures S23 and S31, Supporting Information File 1), allowed the complete assignment of the aromatic resonances. Additional 2D NMR spectra (HMBC and ROESY) for the eosin–β-CD conjugates are also included in Supporting Information File 1, Figures S26 and S27 and Figures S34–S36).

To summarize, the compounds were prepared in good purity and a thorough investigation by NMR spectroscopy revealed that the compounds are monosubstituted on the primary side.

Aggregation properties of eosin–β-CD conjugates by dynamic light scattering

For the investigation of the aggregation properties, solutions of the eosin–β-CD conjugates in water were used. A concentration of 1 mM of the conjugates Eo-β-CDs was applied to obtain reliably high scattered intensities for the characterization. Figure 5 shows that the aggregation behavior of eosin B (**4**)– and eosin Y (**2**)–β-CD conjugates significantly differ from each other. The size distribution of **2**–β-CD shows that the sample is essentially monodisperse with a peak at around 5 nm and this behavior is also observed by transforming the results into volume-related data (see Figure S39 in Supporting Information File 1). On the other hand, the conjugate **4**–β-CD is more likely to form large aggregates. Aggregate populations with sizes of approximately 100–300 nm as well as 5000–6000 nm were

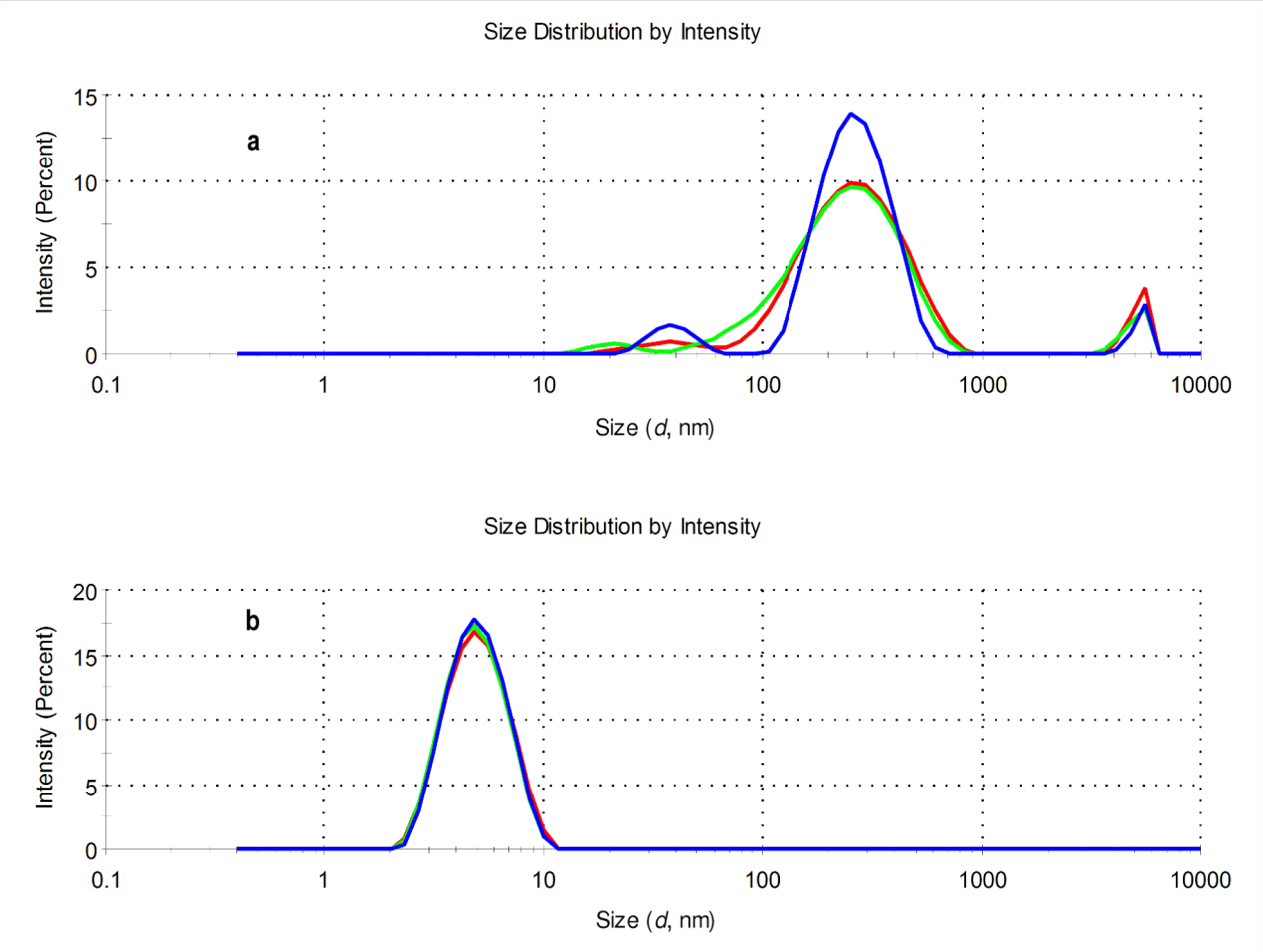

Figure 5: Size distributions of 1 mM aqueous solutions of conjugates **4**–β-CD (**a**) and **2**–β-CD (**b**) at 25.0 °C (pH 7) by intensity (three parallel measurements: blue, green and red lines).

found for cyclodextrin conjugate with dye **4** both in the intensity vs size-distribution plot as well as in the volume plot (see Figure S39 in Supporting Information File 1).

The aggregation properties of **4**–β-CD were further confirmed by the results obtained by nanoparticles tracking analysis (Figure S40, Supporting Information File 1). The sample, under the selected experimental conditions, is rather polydisperse and differently sized populations can be detected. The strong aggregation character of **4**–β-CD can remarkably influence the spectroscopic and photophysical properties of the conjugate.

UV–vis spectroscopic and photophysical properties of eosin–β-CD conjugates

Preliminary spectroscopic investigations on the conjugates were carried out in aqueous solutions. Figure 6 shows the absorption and fluorescence emission spectra of eosin Y conjugate **2**–β-CD and, for comparison, of the free dye **2**. Apart from a slight red shift of the absorption maximum, the absorption spectral profile in the visible region of the conjugate is similar to that of the free dye, ruling out any relevant aggregation phenomena. This hypothesis was well confirmed by the fluorescence emission spectrum, which exhibits an intense band maximum at 550 nm. The fluorescence quantum yield was $\Phi_f = 0.20$, which is very close to the value reported for free eosin Y (**2**) [29].

On the other hand, the fluorescence decay of the conjugate was different from that of the isolated dye **2**. Figure 7 illustrates the fluorescence decay traces observed in both cases. The analysis of the fluorescence decay in case of **2** was fitted by a biexponential kinetic with a longer, dominant lifetime (τ) of 1.44 ns (83%) and a minor shorter component of 0.48 ns (17%). The decay of the **2**–β-CD conjugate was more complex and was fitted by a triexponential fit with lifetimes of 4.26 ns (3%), 1.77 ns (45%) and below 0.2 ns (52%). This behavior may tentatively be attributed to populations of fluorophores probably interacting in a different way with the CD cavity.

As outlined in the introduction, singlet oxygen, $^1O_2$, is the key species involved in PDT and it is generated by energy transfer

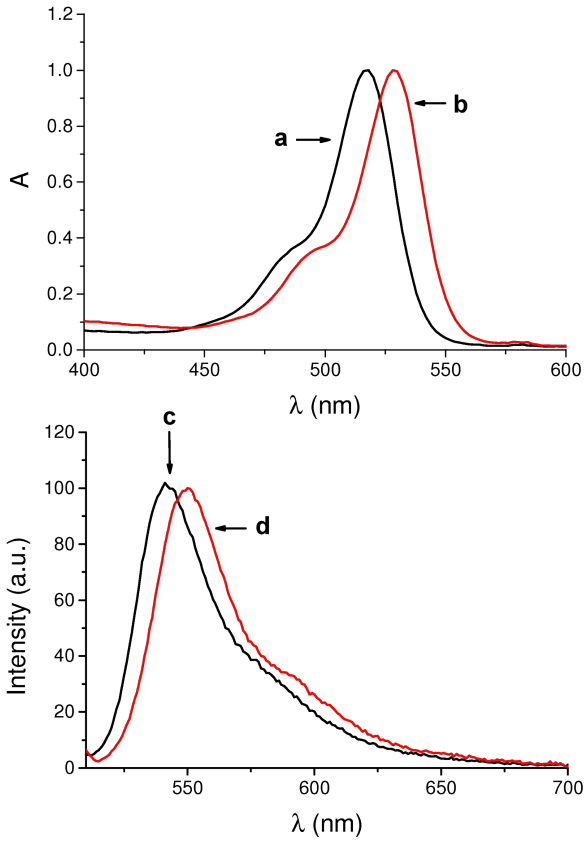

Figure 6: Normalized absorption spectra of aqueous solutions of (a) eosin Y (**2**) and (b) conjugate **2**–β-CD and fluorescence emission spectra of aqueous solutions of (c) **2** and (d) **2**–β-CD. λ_{exc} = 490 nm. The fluorescence spectra were recorded with the two samples having the same absorbance at the excitation wavelength.

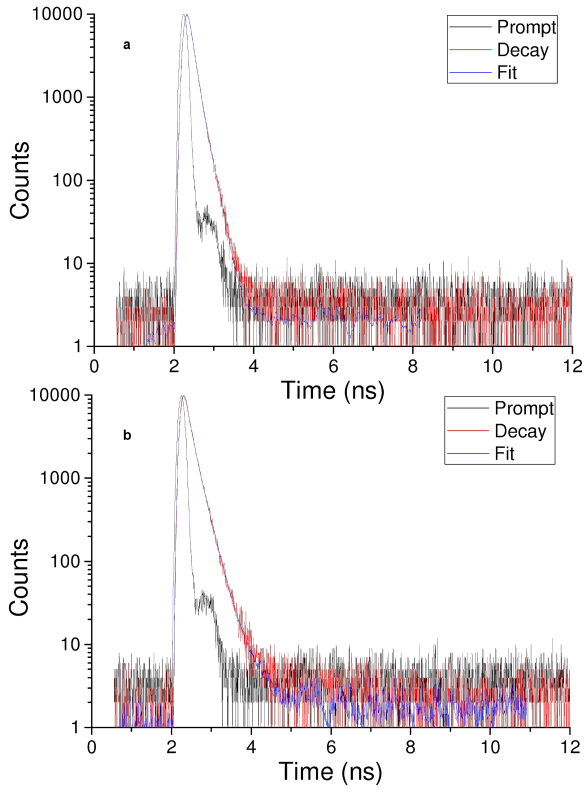

Figure 7: Time-resolved fluorescence observed for aqueous solutions of (a) eosin Y (**2**) and (b) the **2**–β-CD conjugate. λ_{exc} = 455 nm; λ_{em} = 570 nm.

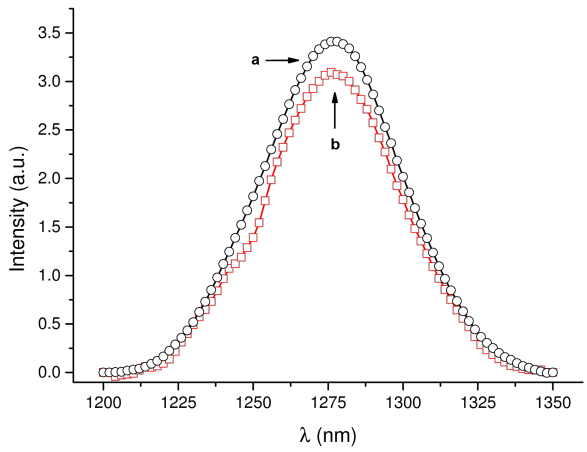

Figure 8: $^1O_2$ luminescence detected upon 528 nm light excitation of D_2O solutions of (a) eosin Y (**2**) and (b) **2**–β-CD conjugate having the same absorbance at the excitation wavelength.

from the excited triplet state of a PS and the nearby molecular oxygen. Although several indirect methodologies based on suitable chemical traps are well known to detect $^1O_2$ formation, the best experimental method to prove and quantify its production is its direct detection. It is based on the monitoring of the typical phosphorescence of $^1O_2$ in the near-IR spectral window [30]. As shown in Figure 8, excitation of the conjugate **2**–β-CD with visible green light generates the characteristic luminescence signals with a maximum at ca. 1270 nm analogously to what observed for free dye **2**. We obtained a $^1O_2$ quantum yield $\Phi_\Delta = 0.47$, that is very similar to that of the free dye in the same solvent ($\Phi_\Delta = 0.49$) [31]. This result excludes any significant intra- or interencapsulation of the excited triplet state of the dye within the β-CD. If this was the case, the reduced quenching by oxygen due to steric hindrance would have resulted in a much smaller value for Φ_Δ.

The corresponding **4**–β-CD conjugate did not show either detectable fluorescence emission or $^1O_2$ photogeneration. This is not surprising in light of the observed massive aggregation of this derivative in aqueous medium (see Figure 5). Studies currently in progress are addressed to better clarify this point and to design strategies to circumvent this drawback and results will be reported in the due course.

Conclusion

Two novel eosin–β-CD conjugates have been prepared through a DMTMMCl-promoted condensation under mild reaction conditions in water. The synthesis started from the xanthene dyes that were prepared in high purity through an improved synthetic route. The prepared CD conjugates have been thoroughly characterized by 1D and 2D NMR experiments. While the eosin B (**4**)-β-CD conjugate was not light responsive, probably due to self-aggregation phenomena, the eosin Y conjugate **2**–β-CD showed excellent preservation of the photophysical properties of the dye. In fact, this molecular hybrid exhibits satisfactory fluorescence and $^1O_2$ photogeneration quantum yields making it a suitable candidate for biomedical research studies in the field of imaging and PDT applications. The possibility to exploit the CD cavity as potential carrier site may also open intriguing prospect in multimodal therapy applications.

Supporting Information

Supporting Information File 1

Syntheses, NMR spectroscopic data, ESIMS spectra, DLS study and semi-quantitative TLC of eosin-appended β-CDs.
[http://www.beilstein-journals.org/bjoc/content/supplementary/1860-5397-13-52-S1.pdf]

Acknowledgements

We thank the Marie Curie Program (FP7-PEOPLE-ITN-2013, CYCLON-HIT 608407) for financial support to MC fellows G.B. and D.A., and funding of the research. The financial supports from NKFIH 109373 and from ÚNKP-16-4 New National Excellence Program of the Ministry of Human Capacities for S.B. are also acknowledged.

References

1. Szejtli, J. *Pure Appl. Chem.* **2004,** *76,* 1825–1845. doi:10.1351/pac200476101825
2. Réti-Nagy, K.; Malanga, M.; Fenyvesi, E.; Szente, L.; Vámosi, G.; Váradi, J.; Bácskay, I.; Fehér, P.; Ujhelyi, Z.; Róka, E.; Vecsernyés, M.; Balogh, G.; Vasvári, G.; Fenyvesi, F. *Int. J. Pharm.* **2015,** *496,* 509–517. doi:10.1016/j.ijpharm.2015.10.049
3. Mourtzis, N.; Paravatou, M.; Mavridis, I. M.; Roberts, M. L.; Yannakopoulou, K. *Chem. – Eur. J.* **2008,** *14,* 4188–4200. doi:10.1002/chem.200701650
4. Castano, A. P.; Mroz, P.; Hamblin, M. R. *Nat. Rev. Cancer* **2006,** *6,* 535–545. doi:10.1038/nrc1894
5. Celli, J. P.; Spring, B. Q.; Rizvi, I.; Evans, C. L.; Samkoe, K. S.; Verma, S.; Pogue, B. W.; Hasan, T. *Chem. Rev.* **2010,** *12,* 2795–2838. doi:10.1021/cr900300p
6. Hasan, T.; Moor, A. C. E.; Ortel, B. *Cancer Medicine,* 5th ed.; Decker BC, Inc.: Hamilton, Ontario, Canada, 2000.
7. Kirejev, V.; Gonçalves, A. R.; Aggelidou, C.; Manet, I.; Mårtensson, J.; Yannakopoulou, K.; Ericson, M. B. *Photochem. Photobiol. Sci.* **2014,** *13,* 1185–1191. doi:10.1039/C4PP00088A
8. Aggelidou, C.; Theodossiou, T. A.; Yannakopoulou, K. *Photochem. Photobiol. Sci.* **2013,** *89,* 1011–1019. doi:10.1111/php.12127
9. Fraix, A.; Goncalves, A. R.; Cardile, V.; Graziano, A. C. E.; Theodossiou, T. A.; Yannakopoulou, K.; Sortino, S. *Chem. – Asian J.* **2013,** *8,* 2634–2641. doi:10.1002/asia.201300463
10. Králová, J.; Kejík, Z.; Bříza, T.; Poučková, P.; Král, A.; Martásek, P.; Král, V. *J. Med. Chem.* **2010,** *53,* 128–138. doi:10.1021/jm9007278
11. Kejík, Z.; Bříza, T.; Poučková, P.; Kralová, J.; Král, V.; Martásek, P. *J. Controlled Release* **2008,** *132,* e27–e28. doi:10.1016/j.jconrel.2008.09.016
12. Breslow, R.; Zhang, X.; Huang, Y. *J. Am. Chem. Soc.* **1997,** *119,* 4535–4536. doi:10.1021/ja9704951
13. French, R. R.; Holzer, P.; Leuenberger, M. G.; Woggon, W.-D. *Angew. Chem., Int. Ed.* **2000,** *39,* 1267–1269. doi:10.1002/(SICI)1521-3773(20000403)39:7<1267::AID-ANIE1267>3.0.CO;2-7
14. Lang, K.; Král, V.; Kapusta, P.; Kubát, P.; Vašek, P. *Tetrahedron Lett.* **2002,** *43,* 4919–4922. doi:10.1016/S0040-4039(02)00954-1
15. Kuroda, Y.; Hiroshige, T.; Sera, T.; Shoroiwa, Y.; Tanaka, H.; Ogoshi, H. *J. Am. Chem. Soc.* **1989,** *111,* 1912–1913. doi:10.1021/ja00187a073
16. Kato, T.; Nakamura, Y. *Heterocycles* **1988,** *27,* 973–979. doi:10.3987/COM-87-4455
17. Kuroda, Y.; Ito, M.; Sera, T.; Ogoshi, H. *J. Am. Chem. Soc.* **1993,** *115,* 7003–7004. doi:10.1021/ja00068a080
18. Kano, K.; Nishiyabu, R.; Yamazaki, T.; Yamazaki, I. *J. Am. Chem. Soc.* **2003,** *125,* 10625–10634. doi:10.1021/ja035055q
19. Carofiglio, T.; Fornasier, R.; Lucchini, V.; Simonato, L.; Tonellato, U. *J. Org. Chem.* **2000,** *65,* 9013–9021. doi:10.1021/jo0010678
20. Puglisi, A.; Purrello, R.; Rizzarelli, E.; Sortino, S.; Vecchio, G. *New J. Chem.* **2007,** *31,* 1499–1506. doi:10.1039/b703680a
21. Wang, Y.; Ikeda, T.; Ueno, A.; Toda, F. *Tetrahedron Lett.* **1993,** *34,* 4971–4974. doi:10.1016/S0040-4039(00)74060-3
22. Nishimura, D.; Takashima, Y.; Aoki, H.; Takahashi, T.; Yamaguchi, H.; Ito, S.; Harada, A. *Angew. Chem., Int. Ed.* **2008,** *47,* 6077–6079. doi:10.1002/anie.200801431
23. Fenyvesi, E.; Jicsinszky, L. *Land Contam. Reclam.* **2009,** *17,* 405–412.
24. Malanga, M.; Jicsinszky, L.; Fenyvesi, E. *J. Drug Delivery Sci. Technol.* **2012,** *22,* 260–265. doi:10.1016/S1773-2247(12)50037-7
25. Malanga, M.; Bálint, M.; Puskás, I.; Tuza, K.; Sohajda, T.; Jicsinszky, L.; Szente, L.; Fenyvesi, É. *Beilstein J. Org. Chem.* **2014,** *10,* 3007–3018. doi:10.3762/bjoc.10.319
26. Malanga, M.; Darcsi, A.; Balint, M.; Benkovics, G.; Sohajda, T.; Beni, S. *Beilstein J. Org. Chem.* **2016,** *12,* 537–548. doi:10.3762/bjoc.12.53
27. Hettegger, H.; Gorfer, M.; Sortino, S.; Fraix, A.; Bandian, D.; Rohrer, C.; Harreither, W.; Potthast, A.; Rosenau, T. *Cellulose* **2015,** *22,* 3291–3304. doi:10.1007/s10570-015-0715-y
28. Johnson, G. A.; Ellis, E. A.; Kim, H.; Muthukrishnan, N.; Snavely, T.; Pellois, J.-P. *PLoS One* **2014,** *9,* e91220. doi:10.1371/journal.pone.0091220
29. Penzkofer, A.; Beidoun, A.; Daiber, M. *J. Lumin.* **1992,** *51,* 297–314. doi:10.1016/0022-2313(92)90059-I
30. Wilkinson, F.; Helman, W. P.; Ross, A. B. *J. Phys. Chem. Ref. Data* **1993,** *22,* 113–262. doi:10.1063/1.555934
31. Redmond, R. W.; Gamlin, J. N. *Photochem. Photobiol.* **1999,** *70,* 391–475. doi:10.1111/j.1751-1097.1999.tb08240.x

License and Terms

BEILSTEIN JOURNAL OF ORGANIC CHEMISTRY

Inclusion complexes of β-cyclodextrin with tricyclic drugs: an X-ray diffraction, NMR and molecular dynamics study

Franca Castiglione[1], Fabio Ganazzoli[1], Luciana Malpezzi[*1], Andrea Mele[*1,2], Walter Panzeri[2] and Giuseppina Raffaini[*1]

Full Research Paper

Open Access

Address:
[1]Dipartimento di Chimica, Materiali e Ingegneria Chimica 'G. Natta', Politecnico di Milano, via Mancinelli 7, 20131 Milano, Italy and [2]CNR-Istituto di Chimica del Riconoscimento Molecolare – Via Mancinelli 7, 20131 Milano, Italy

Email:
Luciana Malpezzi[*] - luciana.malpezzi@polimi.it; Andrea Mele[*] - andrea.mele@polimi.it; Giuseppina Raffaini[*] - giuseppina.raffaini@polimi.it

* Corresponding author

Keywords:
amitriptyline; β-cyclodextrin; crystal structure; cyclobenzaprine; molecular dynamics simulations; NOE

Beilstein J. Org. Chem. **2017,** *13,* 714–719.
doi:10.3762/bjoc.13.70

Received: 31 October 2016
Accepted: 27 March 2017
Published: 13 April 2017

This article is part of the Thematic Series "Superstructures with cyclodextrins: Chemistry and applications IV".

Guest Editor: G. Wenz

Abstract

Tricyclic fused-ring cyclobenzaprine (**1**) and amitriptyline (**2**) form 1:1 inclusion complexes with β-cyclodextrin (β-CD) in the solid state and in water solution. Rotating frame NOE experiments (ROESY) showed the same geometry of inclusion for both **1**/β-CD and **2**/β-CD complexes, with the aromatic ring system entering the cavity from the large rim of the cyclodextrin and the alkylammonium chain protruding out of the cavity and facing the secondary OH rim. These features matched those found in the molecular dynamics (MD) simulations in solution and in the solid state from single-crystal X-ray diffraction of **1**/β-CD and **2**/β-CD complexes. The latter complex was found in a single conformation in the solid state, whilst the MD simulations in explicit water reproduced the conformational transitions observed experimentally for the free molecule.

Introduction

The present paper reports on a multidisciplinary approach [1,2] based on single crystal X-ray diffraction, solution NMR spectroscopy and molecular dynamics (MD) simulations with explicit water to study the inclusion complexes of two tricyclic aromatic molecules – cyclobenzaprine (**1**) and amitriptyline (**2**, Figure 1) – with β-cyclodextrin (β-CD). Previous work already considered certain aspects of the interaction of **2** with β-CD [3-8], but no full characterization of the complex geometry in solution and in the solid state was carried out, while the only similation study of this complex was very limited both in scope and in the adopted methodology [6]. In addition, to the best of our knowledge no study was ever performed on the inclusion complex of the strictly related compound **1**. Compounds **1** and **2** are not planar and the exocyclic double bond prevents the free rotation of the side chain with respect to the ring system. Consequently, **1** and **2** show inherent chirality [9] as lacking of

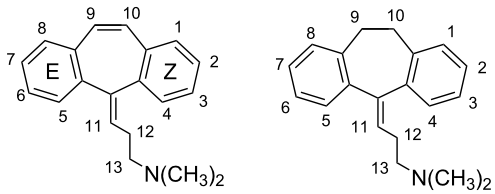

Figure 1: Molecular formulae and atom numbering of cyclobenzaprine (**1**, left) and amitriptyline (**2**, right). E and Z symbols are arbitrarily introduced to identify the two aromatic rings.

symmetry elements. The main purpose of the work is the comparison of the structural features obtained in the solid state and in D_2O solution by X-ray diffraction and NMR spectroscopy, respectively. The dynamic behaviour of the examined systems is simulated by MD runs of the complexes with explicit water. Suitable structural descriptors thus obtained as time averages are then compared to those found experimentally.

Results and Discussion

The guest molecules **1** and **2** form 1:1 inclusion complexes with β-CD in aqueous solution and in the solid state. The Job's plots are reported in Figure 2.

The plots of Figure 2 show that the maximum of the curves is obtained, in both cases, for $r = 0.5$, consistent with the 1:1 host–guest stoichiometry.

Some important structural features of the inclusion complexes of **1** and **2** can be outlined by the analysis of the ^{1}H NMR spectra: the spectrum of **1** shows that the AB quartet assigned to H9–H10 spin system is split into two AB quartets on passing from pure **1** to the corresponding **1**/β-CD complex, thus showing the formation of two diastereomeric inclusion complexes. Similar behaviour can be reported for **2**. The geometry of inclusion can be inferred by analysis of intermolecular NOEs obtained from ROESY spectra (Figure 3).

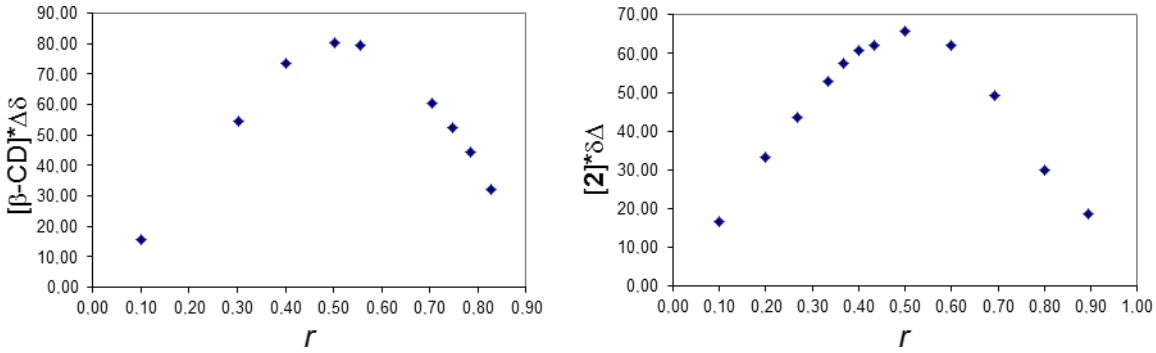

Figure 2: Left: Job's plot for H3' chemical shift variations of the complex β-CD/**1**. Right: Job's plot for H11 (see Figure 1 for atom numbering) chemical shift variations of the complex β-CD/**2**.

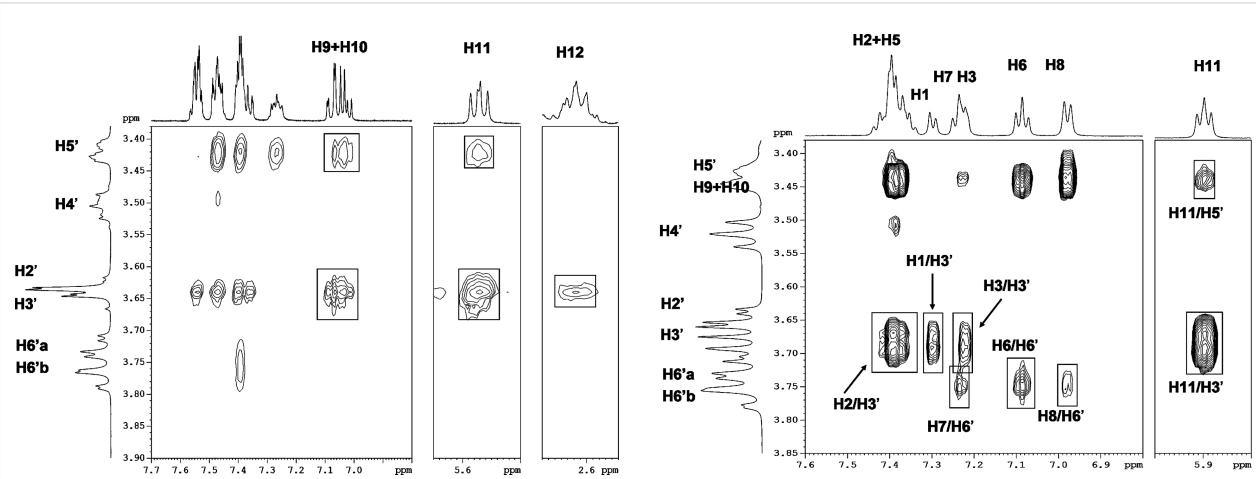

Figure 3: Expansion of 2D-ROESY of **1**/β-CD (left) and **2**/β-CD (right) complexes. Atom numbering is referred to Figure 1. Primed numbers are used for glucose units.

The signals of H9, H10 and H11 of **1** show intermolecular contacts with H5' and H3' of the β-CD, indicating that the ring system of **1** is deeply inserted into the cavity of the β-CD. The selective NOE between H12 and H3' suggests that the alkylammonium chain is protruding out of the β-CD cavity from the secondary OH rim. The analysis of intermolecular NOEs within the **2**/β-CD complex points out that the overall geometry is very much similar to that described for **1**/β-CD. The approximate and qualitative picture derived from NOE restraints is in good agreement with the solid state structure of the two complexes obtained from single crystal X-ray diffraction. The refined structures are shown in Figure 4.

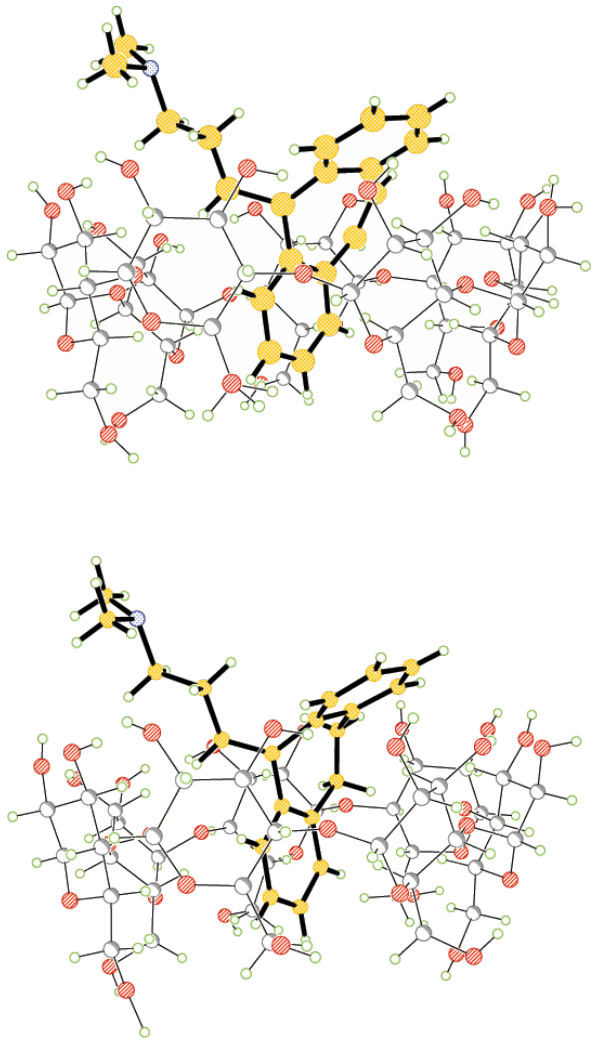

Figure 4: X-ray diffraction structures of **1**/β-CD (top) and **2**/β-CD (bottom) complexes.

As expected, the most significant difference between the two structures involves the C9–C10 bond. The C9–C10 bond distances for **1** and **2** are 1.312(14) Å and 1.420(8) Å, respectively, while the torsion angles around this bond are 0.6(19)° and 51.3(10)° for **1** and **2**, respectively, where the figures in parentheses give the standard errors.

The β-CD macrocyclic rings appear slightly distorted upon inclusion of the guest molecule. In the crystal, the arrangement of the complexes formed by **1** and **2** with β-CD are similar, being stacked head-to-head to form antiparallel columns along the crystallographic *b* axis. Within each column, the molecules are linked by hydrogen bonding involving both the macrocycles and the guest molecules, while interactions between macrocycles link adjacent columns. A large network of H-bonds involving the water molecules contribute to the crystal stability.

In both cases the crystal structures are non-centrosymmetric, indicating that the crystal contains a single enantiomer of **1** and **2**. The overall topology of inclusion matches that found in solution and through molecular simulations. In both cases the complex structures do not show any disorder: this finding is largely predictable for the rigid tricyclic moiety of **1** but it is remarkable in **2**. Indeed, literature data on isolated amitriptyline point out that the fused ring system of **2** shows conformational transitions [10], especially those involving the torsion about the C9–C10 single bond. The lack of disorder in the C9–C10 segment suggests that complexation constrains **2** in a single conformation in the solid state.

The MD simulations led to the formation of a 1:1 inclusion complex of β-CD with molecules **1** and **2** both in vacuo and in explicit water. In both cases, the complex formation was relatively fast, and allowed us to find the most stable geometry eventually achieved from the trial starting arrangements [17] mentioned in the Materials and Methods section. The most stable complex yielded inclusion of an aromatic ring in the β-CD, with the seven-membered ring, the side chain and the other aromatic ring protruding above the secondary rim, quite similar to the arrangement experimentally determined in the solid state by X-ray diffraction with a very similar depth of inclusion. In view of the geometrical similarity achieved in the two different simulation environments, in the following we will only discuss the results obtained for the simulations in explicit water. In water, the inclusion process was relatively fast, as it can be gauged by Figure 5, which shows the distance between the center of mass (c.o.m.) of molecule **1** and **2** and of the β-CD.

It is interesting to note that the inclusion is much faster in the case of molecule **2**, being essentially complete within the initial 20–30 ps of the MD run, apart from some smaller and lengthier rearrangements at longer times. Such very fast process is

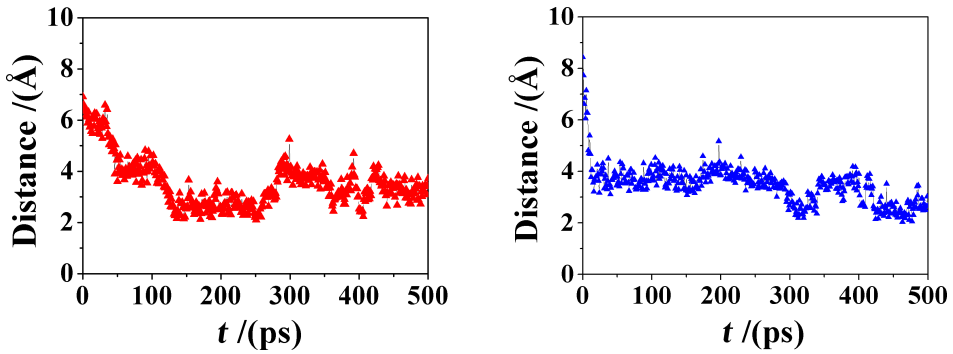

Figure 5: The distance between the center of mass (c.o.m.) of molecule **1** (at left) and of molecule **2** (at right) from the c.o.m. of the β-CD.

possibly related to the larger or smaller rigidity of the central ring in the tricyclic system: in fact, molecule **2** requires a smaller time interval before inclusion thanks to its larger fluctuations, related in turn to the flexibility of the central cycle, not constrained by the C9–C10 double bond present in molecule **1**. The larger flexibility of molecule **2** is best shown through the torsional degree of freedom around its C9–C10 bond that is experimentally observed in solution for uncomplexed **2** [10], and is also preserved in the included state, according to the present MD simulations in water. This torsional freedom is reported in Figure 6, where we show the value of the C9–C10 dihedral angle as a function of time for both complexes. It may be clearly seen that this dihedral angle fluctuates around a value of 0° in molecule **1**, being constrained by the double bond. Conversely, in molecule **2** it undergoes a sharp and very fast change from an average value of (−52.3(5) ± 8.9)° to a value of (+57.7(6) ± 8.0)°, where the value in parenthesis is the standard error on the last significant digit of the mean, and the ± sign indicates the standard deviation around the mean, indicating relatively large fluctuations. In this connection, we also note that this conformational transition between two gauche states is very fast, being completed within 3 ps only. Figure 7 shows three

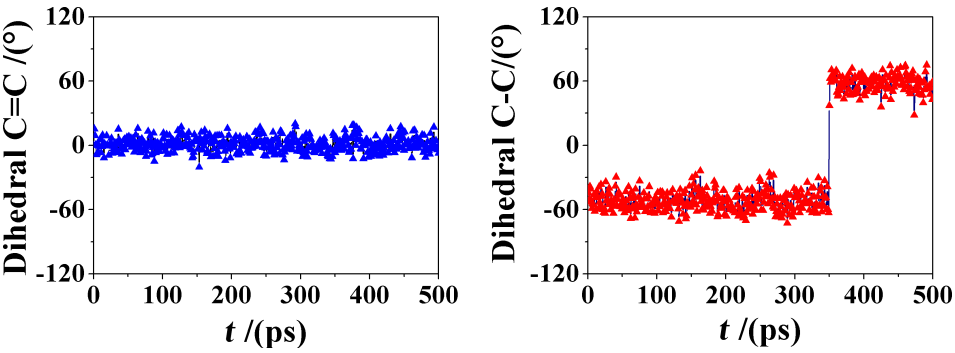

Figure 6: The value of the C9–C10 dihedral angle as a function of time for the complexes of molecule **1** and **2** (left and right, respectively).

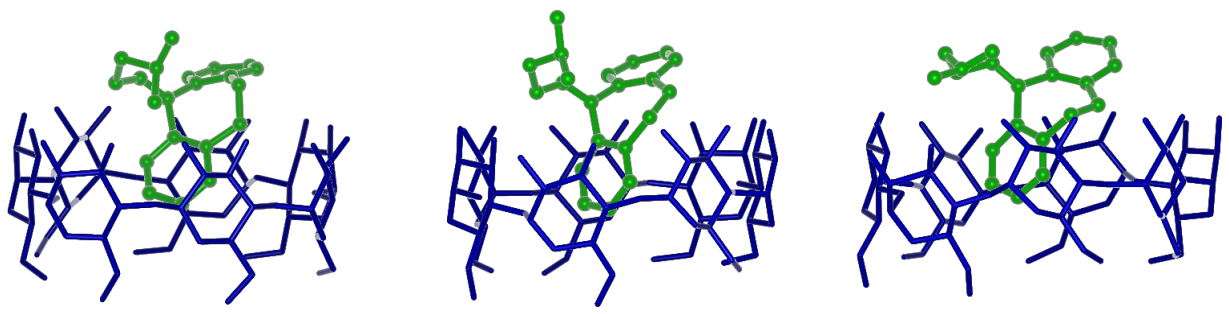

Figure 7: Snapshots of the conformational transition in **2**/β-CD in water taken at a 1 ps interval.

snapshots of the complex taken at a 1 ps interval during this conformational transition, showing the quite large rearrangement in water of the moiety protruding over the secondary rim. It is interesting to note that this change in the C9–C10 dihedral angle can only takes place when the thermal fluctuations of the complex lead to some small upward displacement of the guest molecule with respect to β-CD thus allowing for a larger conformational freedom of the central ring of molecule **2** not constrained by the secondary rim of the host.

Conclusion

The integrated approach X-ray/NMR/MD was successfully applied to the structure assessment of **1**/β-CD and **2**/β-CD complexes. The crystallization of a single enantiomer of **1** encapsulated into β-CD showed that the latter acts as chiral selector towards racemic **1**. The comparison of the X-ray structure and the MD simulations in water of **2**/β-CD complex showed that **2** is present as single conformer in the crystal and in two conformations in the solution state.

Materials and Methods

X-ray diffraction

Single crystals of **1**/β-CD and **2**/β-CD were obtained after many attempts by slow evaporation of the solvent from an aqueous solution. The **1**/β-CD complex appeared extremely unstable in the air and finally a poor quality crystal, just enough suitable for the X-ray diffraction, was sealed in a glass capillary in the presence of the mother liquor. Data collection was performed on a Siemens P4 diffractometer using Cu Kα (λ = 1.54178 Å) radiation for **1** and on a Bruker SMART APEX II diffractometer equipped with APEX II CCD detector using Mo Kα (λ = 0.71073 Å) radiation for **2**. The structures were solved by direct methods with the SIR97 program [11] and refined by full-matrix-least-squares procedure with the SHELX97 program [12]. The refinement of **1**, owing to the low ratio of data/refined parameters, was refined by block full-matrix-least-squares procedure. All non H atoms of both complexes were refined anisotropically. The H atoms were positioned in the calculated positions and refined with a riding model. Both complexes were found to crystallize in the solid state in 1:1 host–guest ratio with many partially disordered water molecules distributed in the intermolecular space outside the macrocyclic cavities. Full molecular and crystal data, together with the structural refinement details, are given in Supporting Information File 1 (Tables S1–S14 and Figures S1–S4 for the complexed guest geometry and for the packing diagrams) and Supporting Information Files 2 and 3 (cif files).

NMR spectroscopy

The NMR spectra were recorded in D_2O on a Bruker Avance 500 spectrometer at 305 K. The stoichiometry of complexes was assessed by the Job's method [13]. A typical procedure was as follows: (i) two stock solutions of host (β-CD) and guest (compound **1** or **2**) were prepared at given concentrations; (ii) accurately measured volumes of host and guest solutions were mixed in different volumes ratios in the NMR tubes and in such a way that the total volume was 750 μL for all the solutions; (iii) the NMR spectra were collected for each sample and the chemical shift variation Δδ were measured for some target proton signal; (iv) the data were used for the plot of [β-CD]*Δδ vs r or [guest]*Δδ vs r where r = [host]/[host]+[guest] (or related expression in the case the guest's chemical shift variations are reported), providing the Job's plot with the typical bell shape. The abscissa of the maximum provides the stoichiometry of the host–guest complex in solution. 2D NOE correlation experiments in the rotating frame (ROESY) were acquired on 4 mM solutions by using a suitable pulse sequence with two different transmitter offsets for spin-lock and pulse [14] in order to minimize artefacts due to the J-coupling magnetization transfer (HOHAHA). The typical experimental set-up was as follows: 2K points acquired in the F2 domain, 512 increments and subsequent zero-filling to 1K to process data.

Molecular dynamics simulations

The simulations employed InsightII/Discover [15] with the CVFF force field [16]. The structure of molecules **1** and **2** were first subjected to an MD run in vacuo and finally optimized up to an energy gradient lower than 4×10^{-3} kJ mol^{-1} Å^{-1}. The simulation protocol closely followed the strategy proposed by some of us for modeling the inclusion complex formation without any a priori assumption about its possible geometry [17-21]. Thus, the optimized molecules were placed close to β-CD in 12 unbiased trial geometries with the main sides close to the two rims and the outer surface of β-CD in different orientations: no inclusion complex was assumed at the beginning of the simulations. The simulations in water were carried out in a large cell with periodic boundary conditions. The outer adducts were separately optimized in vacuo and in explicit water adopting a box of water with a size of 33 Å adopting periodic boundary conditions, and then subjected to MD runs (2 ns in vacuo, 500 ps in water) at room temperature (300 K). The dynamic equations were integrated using the Verlet algorithm with a time step of 1 fs at a temperature of 300 K, controlled through the Berendsen thermostat. Equilibration of the resulting adducts was monitored through the time change of the total energy and of its components (including also the van der Waals components) and of the distance between the centers of mass of the host and of the guest molecule [17]. Final optimizations (up to an energy gradient lower than 4×10^{-3} kJ mol^{-1} Å^{-1}) of many conformations generated during the MD runs yielded the most stable host–guest geometries discussed in the main text.

Supporting Information

Supporting Information File 1

Crystallographic data for cyclobenzaprine (**1**) and amitriptyline (**2**).
Tables with the crystallographic data, the atomic coordinates, the bond distances and angles, the torsion angles and the hydrogen bonds (Tables S1–S14) and the geometry of the complexed guest and the the packing diagram in the crystalline state (Figures S1–S4).
[http://www.beilstein-journals.org/bjoc/content/supplementary/1860-5397-13-70-S1.pdf]

Supporting Information File 2

Chemical information file for cyclobenzaprine (**1**).
[http://www.beilstein-journals.org/bjoc/content/supplementary/1860-5397-13-70-S2.cif]

Supporting Information File 3

Chemical information file for amitriptyline (**2**).
[http://www.beilstein-journals.org/bjoc/content/supplementary/1860-5397-13-70-S3.cif]

References

1. Mele, A.; Raffaini, G.; Ganazzoli, F.; Juza, M.; Schurig, V. *Carbohydr. Res.* **2003,** *338,* 625–635. doi:10.1016/S0008-6215(02)00493-7
2. Malpezzi, L.; Fronza, G.; Fuganti, C.; Mele, A.; Brückner, S. *Carbohydr. Res.* **2004,** *339,* 2117–2125. doi:10.1016/j.carres.2004.05.029
3. Ali, M. S.; Rub, M. A.; Khan, F.; Al-Lohedan, H. A.; Kabir-Ud-Din. *J. Mol. Liq.* **2012,** *167,* 115–118. doi:10.1016/j.molliq.2012.01.004
4. Cano, J.; Rodriguez, A.; Aicart, E.; Junquera, E. *J. Inclusion Phenom. Macrocyclic Chem.* **2007,** *59,* 279–285. doi:10.1007/s10847-007-9328-x
5. Wei, W.; Zhang, Z. J.; Ju, H. X. *Chromatographia* **2004,** *59,* 513–516.
6. Junquera, E.; Romero, J. C.; Aicart, E. *Langmuir* **2001,** *17,* 1826–1832. doi:10.1021/la000819q
7. Georgiou, M. E.; Koupparis, M. A.; Georgiou, C. A. *Analyst* **1999,** *124,* 391–396. doi:10.1039/a808426b
8. Valsami, G. N.; Koupparis, M. A.; Macheras, P. E. *Pharm. Res.* **1992,** *9,* 94–100. doi:10.1023/A:1018940013006
9. Dalla Cort, A.; Mandolini, L.; Pasquini, C.; Schiaffino, L. *New J. Chem.* **2004,** *28,* 1198–1199. doi:10.1039/b404388j
10. Casarotto, M. G.; Craik, D. J. *J. Pharm. Sci.* **2001,** *90,* 713–721. doi:10.1002/jps.1027
11. Altomare, A.; Burla, M. C.; Camalli, M.; Cascarano, G. L.; Giacovazzo, C.; Guagliardi, A.; Moliterni, A. G. G.; Polidori, G.; Spagna, R. *J. Appl. Crystallogr.* **1999,** *32,* 115–119. doi:10.1107/S0021889898007717
12. Sheldrick, G. M.; *SHELXL97: Program for the Refinement of Crystal Structures.* University of Gottingen, Germany, 1997.
13. Connors, K. A. Binding Constants. *The Measurement of Molecular Complex Stability;* John Wiley & Sons: New York, 1987; pp 24–28.
14. Desvaux, H.; Berthault, P.; Birlirakis, N.; Goldman, M.; Piotto, M. *J. Magn. Reson., Ser. A* **1995,** *113,* 47–52. doi:10.1006/jmra.1995.1054
15. *InsightII*. Accelrys Inc.: San Diego, CA, 2000; http://www.accelrys.com.
16. Dauber-Osguthorpe, P.; Roberts, V. A.; Osguthorpe, D. J.; Wolff, J.; Genest, M.; Hagler, A. T. *Proteins: Struct., Funct., Genet.* **1988,** *4,* 31–47. doi:10.1002/prot.340040106
17. Raffaini, G.; Ganazzoli, F.; Malpezzi, L.; Fuganti, C.; Fronza, G.; Panzeri, W.; Mele, A. *J. Phys. Chem. B* **2009,** *113,* 9110–9122. doi:10.1021/jp901581e
18. Raffaini, G.; Ganazzoli, F. *J. Inclusion Phenom. Macrocyclic Chem.* **2007,** *57,* 683–688. doi:10.1007/s10847-006-9265-0
19. Raffaini, G.; Ganazzoli, F. *J. Inclusion Phenom. Macrocyclic Chem.* **2013,** *76,* 213–221. doi:10.1007/s10847-012-0193-x
20. Raffaini, G.; Ganazzoli, F. *Chem. Phys.* **2007,** *333,* 128–134. doi:10.1016/j.chemphys.2007.01.015
21. Raffaini, G.; Ganazzoli, F. *J. Phys. Chem. B* **2010,** *114,* 7133–7139. doi:10.1021/jp911812j

License and Terms

BEILSTEIN JOURNAL OF ORGANIC CHEMISTRY

The effect of cyclodextrin complexation on the solubility and photostability of nerolidol as pure compound and as main constituent of cabreuva essential oil

Joyce Azzi[1,2], Pierre-Edouard Danjou[2], David Landy[2], Steven Ruellan[2], Lizette Auezova[1], Hélène Greige-Gerges[1] and Sophie Fourmentin[*2]

Full Research Paper

Open Access

Address:
[1]Bioactive Molecules Research Group, Doctoral School of Sciences and Technologies, Faculty of Sciences, Jdaidet El-Matn, Lebanese University, Lebanon and [2]Unité de Chimie Environnementale et Interactions sur le Vivant (UCEIV, EA 4492), SFR Condorcet FR CNRS 3417, ULCO, F-59140 Dunkerque, France

Email:
Sophie Fourmentin[*] - lamotte@univ-littoral.fr

* Corresponding author

Keywords:
cabreuva essential oil; cyclodextrins; nerolidol; photostability; solubility

Beilstein J. Org. Chem. **2017,** *13,* 835–844.
doi:10.3762/bjoc.13.84

Received: 05 December 2016
Accepted: 07 April 2017
Published: 05 May 2017

This article is part of the Thematic Series "Superstructures with cyclodextrins: Chemistry and applications IV".

Guest Editor: G. Wenz

Abstract

Nerolidol (Ner), a major component of many plant essential oils, is known for its various biological properties. However, the low solubility of Ner in water and its susceptibility to degradation limit its application. The aim of our study was to improve the solubility and photostability of Ner through its encapsulation in different cyclodextrins (CDs). The formation constants of *cis*-, *trans*-Ner and their commercial mixture with various CDs (α-CD, β-CD, γ-CD, HP-β-CD, RAMEB, CRYSMEB and SBE-β-CD) were determined by phase solubility studies and confirmed by the spectral displacement UV-visible method. The solubility of cabreuva essential oil (EO) rich in *trans*-Ner was also evaluated by total organic carbon (TOC) analysis. The encapsulation efficiency (EE %) of Ner in HP-β-CD solid complexes was assessed by HPLC. The structural characterization of CD/*trans*-Ner inclusion complex was then conducted by NMR spectroscopy followed by molecular modelling studies. The effect of encapsulation on the Ner photostability was also carried out over time under UVB irradiation. A_L-type phase-solubility diagrams were obtained, suggesting the formation of 1:1 CD/Ner inclusion complexes. The solubility of Ner was enhanced by approximately 70-fold in the presence of 10 mM HP-β-CD. Moreover, high EE % values were obtained for 5:1 and 10:1 HP-β-CD:Ner molar ratios. NMR and molecular modelling studies revealed the most stable structure for *trans*-Ner inside the CD cavity with the OH group oriented towards the wider rim of the CD. Finally, CD encapsulation of Ner as pure compound or as main component of the cabreuva EO, protected it from degradation. This effect was more pronounced as the concentration of CD increased. These findings suggested that CDs are promising encapsulating carriers for Ner by enhancing its solubility and stability and thereby its application in food industry.

Introduction

Nerolidol (Ner, 3,7,11-trimethyl-1,6,10-dodecatrien-3-ol), an acyclic sesquiterpene obtained from fresh flowers of bitter orange and found in many other plants [1], is extensively used in perfumery. It was also approved by the U.S. Food and Drug Administration as a food flavoring agent and included by the Council of Europe in the list of substances granted A [2]. In nature, Ner occurs as a mixture of two isomers: *cis* and *trans*, with *trans* being the most abundant. The two isomers are distributed differently in various plant parts and among species. *trans*-Ner is present in high percentage (58–80%) in cabreuva essential oil (EO) (*Myrocarpus fastigiatus*) [3]. Due to its antimicrobial effects against a wide range of microorganisms such as *Staphylococcus aureus*, *Salmonella enterica* and *Aspergillus niger* [4], Ner can be employed as natural alternative to traditional synthetic food preservatives. To achieve this goal, Ner should be dissolved partially or totally in aqueous media to provide an efficient interaction with the pathogens [5]. However, Ner is poorly soluble in water and is also subject to degradation during storage. Nanoencapsulation techniques may improve Ner solubility and stability allowing to produce functional foods with enhanced functionality and stability [6]. Various encapsulation materials are used for food applications such as liposomes, phytosomes, cyclodextrins, dendrimers and many others [7-9]. The use of cyclodextrins (CDs) in food industry is currently flourishing due to their high potential to solubilize, stabilize and protect flavors and food ingredients [10-13]. CDs are non-toxic water-soluble cyclic oligosaccharides composed of six, seven or eight α-(1→4) glucopyranose units giving rise, respectively, to α-, β- and γ-CDs [14]. Their most notable characteristic is their ability to form inclusion complexes with poorly soluble guest molecules which are entrapped in the hydrophobic cavity of CDs. Chemical modifications of the hydroxy groups of CDs can be performed to obtain water-soluble CD derivatives like hydroxypropyl-β-CD (HP-β-CD), methylated CDs (randomly methylated β-CD, RAMEB, or a low 2-O-methylated-β-CD, CRYSMEB) and sulfobutylether-β-CD (SBE-β-CD) (Figure 1). Molecular complexation in CDs has been widely proposed for EOs to limit their degradation during processing and storage and to offer a good dispersion of compounds in the aqueous media thus enhancing their biological properties [15,16].

To the best of our knowledge, no literature data reported the encapsulation of Ner in CDs. In this study, for the first time, CD/Ner inclusion complexes were characterized in solution and in solid state. Formation constants (K_f) were determined for Ner with seven CDs: α-CD, β-CD, γ-CD, HP-β-CD, RAMEB, CRYSMEB and SBE-β-CD using phase solubility studies coupled to HPLC. The K_f values were determined for the separate isomers and their commercial mixture. To confirm the K_f values obtained for the isomeric mixture, UV-visible spectroscopy was employed using a competition method. The solubility of cabreuva EO rich in *trans*-Ner was also assessed with HP-β-CD using the total organic carbon method developed in our laboratory [17]. In addition, ^{1}H and 2D ROESY NMR experiments and molecular modelling were performed to investigate the orientations of *trans*-Ner inside the CD cavity. Next, the effect of encapsulation on the Ner photodegradation rate under UVB irradiation was examined. Solid HP-β-CD/Ner complexes were also prepared and the encapsulation efficiency (EE %) was determined.

Results and Discussion

Phase solubility studies

Considering the low aqueous solubility of Ner, phase-solubility studies were conducted to examine the ability of different CDs (α-CD, β-CD, γ-CD, HP-β-CD, RAMEB, CRYSMEB and SBE-β-CD) to solubilize Ner. All concentrations were determined for each isomer from their commercial mixture by HPLC. The mean intrinsic solubility (S_0) of *cis*- and *trans*-Ner in water at room temperature was estimated to be about 5 and 7 μg/mL, respectively. The phase-solubility diagrams showed that the solubility of both isomers increased linearly with CD concentration. Thus, an about 60- and 80-fold increase in solubility is

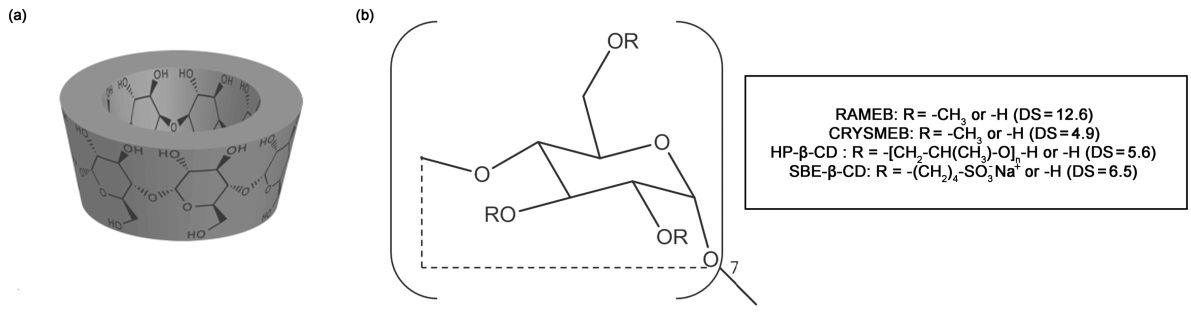

Figure 1: Chemical structure of β-CD (a) and β-CD derivatives (b).

achieved, in the presence of 10 mM HP-β-CD, for *cis*- and *trans*-Ner (284 µg/mL and 578 µg/mL, respectively). Moreover, the curves obtained for all CDs/Ner inclusion complexes followed an A_L-type profile except for β and γ-CD where B_s-type profiles were obtained (Figure 2). For A_L-type phase solubility diagrams, the slope was less than unity which indicates the formation of 1:1 inclusion complexes [18]. The K_f values (Table 1) were then calculated as indicated in Equation 1 (experimental part). For β-CD and γ-CD, precipitation occurred at concentrations above 1 mM.

We can notice from Table 1, that the K_f values of CD/*cis*-Ner were generally lower than those of CD/*trans*-Ner. This is evidently attributed to the different spatial orientations of the isomers: *trans*-Ner adopts a linear conformation while *cis*-Ner has a more twisted one. Consequently, the interaction with the CD cavity is more favorable for the *trans*-Ner isomer leading to a more stable inclusion complex [16]. An exception is observed for γ-CD, where *cis*-Ner is better encapsulated than *trans*-Ner, owing to the larger cavity of this CD.

Phase-solubility studies also allow the determination of the complexation efficiency (CE) permitting to evaluate the solubilizing potential of CDs. CE is obtained either from the slope of phase solubility curve or by dividing the concentration of CD in its complexed form ([CD/Ner]) by its concentration in its free

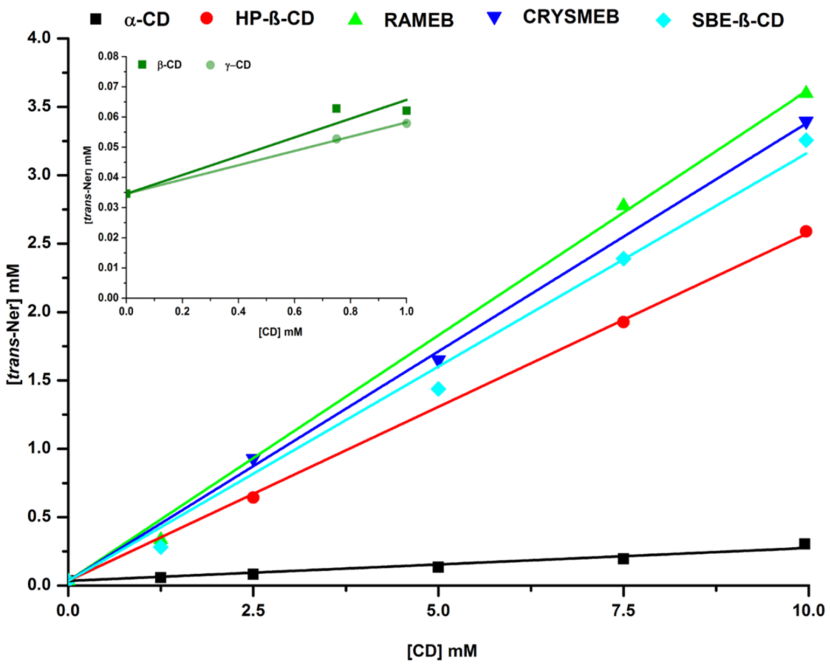

Figure 2: Phase solubility diagrams of CD/*trans*-Ner inclusion complexes.

Table 1: Formation constants (K_f), solubility enhancement ratio (S_t/S_0) (in the presence of 10 mM CD, except for β-CD and γ-CD, 1mM) and complexation efficiency (CE) of *cis* and *trans*-Ner with different CDs.

	cis-Ner			trans-Ner			Ner[b]
CDs	K_f (M^{-1})	S_t/S_0	CE[a]	K_f (M^{-1})	S_t/S_0	CE	K_f (M^{-1})
α-CD	81	1.85	0.002	619	8.80	0.021	418
β-CD	769	1.49	0.019	1233	1.80	0.043	1238
γ-CD	1866	2.76	0.046	752	1.68	0.026	1435
HP-β-CD	5540	51.53	0.137	9515	75.37	0.328	10365
RAMEB	8149	72.62	0.202	15577	104.40	0.537	19450
CRYSMEB	8787	72.77	0.217	14036	98.80	0.484	15412
SBE-β-CD	9240	80.20	0.229	13264	94.66	0.457	17768

[a]CE: complexation efficiency ([CD/Ner])/[CD]).
[b]Ner: formation constant for the commercial mixture.

form ([CD]) (Equation 2) [19]. For both isomers, the CE values of CD derivatives were higher than those of native CDs. For instance, the CE values of *trans*-Ner for HP-β-CD, RAMEB and SBE-β-CD were, respectively, 0.328, 0.537 and 0.457 versus 0.043 for β-CD (Table 1). These results showed that RAMEB is the best solubilizer among the studied CDs. The solubility enhancement of this CD towards many compounds has been reported in the literature [20-22]. However, HP-β-CD is the only β-CD derivative cited in the FDA's list of Inactive Pharmaceutical Ingredients among the studied derivatives, therefore, further studies will focus on this CD.

UV–visible spectroscopy

Formation constants between Ner (mixture of *cis* and *trans* isomers) and HP-β-CD was also evaluated by a UV-visible competition method with methyl orange (MO) as a competitor [23]. Before starting the competition experiment, the K_f value of the HP-β-CD/MO inclusion complex was determined by direct titration; the data were consistent with those reported in the literature [24]. The competition method measures the spectral variation of MO upon the addition of Ner to a solution containing HP-β-CD and MO. The addition of Ner induced an increase in MO absorbance, which indicates the formation of inclusion complex between Ner and HP-β-CD. The obtained spectral variations revealed once again the formation of 1:1 inclusion complexes (data not shown). The K_f values of HP-β-CD/Ner inclusion complexes (Table 2) were in good agreement with the phase solubility results. However, a slight increase was observed in K_f values obtained from the phase solubility studies. Indeed, formation constants determined by this method are generally overestimated since several effects are combined and not only complexation [25].

Table 2: Formation constants (K_f) of HP-β-CD inclusion complexes with Ner obtained by phase solubility and UV-visible competition method.

Formation constants (M^{-1})		HP-β-CD
Phase solubility	Ner	10365
UV–visible	MO	7429
	Ner	8168

Phase solubility studies of cabreuva essential oil

Phase solubility studies were also performed for the cabreuva EO, an EO rich in *trans*-Ner (64.54%), at different HP-β-CD concentrations (0, 1.25, 2.5, 5, 7.5 and 10 mM). The phase solubility profile was obtained by the Total Organic Carbon (TOC) method [17]. The mass concentration of EO (g/L) obtained from the EO standard calibration curves, was plotted against CD concentration (Figure 3). As illustrated in Figure 3, the intrinsic solubility of EO was found to be of about 0.63 g/L. A linear increase in EO solubility was observed with HP-β-CD concentration (R^2 = 0.996). The solubility of cabreuva EO increased from 0.63 to 1.7 g/L in the presence of 10 mM HP-β-CD (≈3-fold increase). These results showed that HP-β-CD is able to enhance the aqueous solubility of cabreuva EO. Other studies have also demonstrated that CD could significantly increase the solubility of EO components [26].

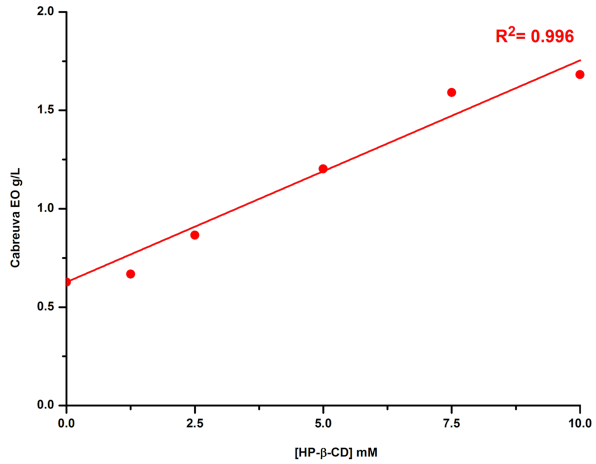

Figure 3: Phase solubility profile of cabreuva EO obtained by the TOC method.

Characterization of solid inclusion complexes

HP-β-CD/Ner mixture was prepared as a solid inclusion complex by the freeze-drying method in the presence of 50 and 100 mM CD and a fixed Ner concentration (10 mM). The encapsulation efficiency (EE %) of the Ner mixture in CD at 5:1 and 10:1 CD/Ner molar ratios was evaluated by HPLC. A high EE % was obtained for both HP-β-CD/Ner molar ratios (99 and 100% for 5:1 and 10:1, respectively) in good agreement with phase solubility results. The Ner contents were equal to 0.032 and 0.020 $mg_{Ner}/mg_{solid\ complex}$ for 5:1 and 10:1 molar ratios, respectively. These results showed that a 5:1 ratio is enough to have a high EE %.

NMR study

In order to elucidate the possible orientations of *trans*-Ner within the CD cavity, NMR spectroscopy was used. Because HP-β-CD is a heterogeneous mixture of isomers, NMR was conducted only with β-CD. ^{1}H NMR and ROESY spectra were recorded for β-CD and β-CD/*trans*-Ner solutions in D_2O. The induced shift (Δδ) which is the difference between chemical shifts of β-CD protons in the presence and absence of *trans*-Ner, was calculated as follows: $\Delta\delta = \delta_{(complex)} - \delta_{(free)}$. Positive and negative signs showed downfield and upfield displace-

ment, respectively. The inclusion of the guest into the CD cavity is generally proved by the chemical shift variations of the guest or the CD. Particularly, a shielding of inner protons of the CD is induced after inclusion of a guest into the CD cavity while protons of the outside are generally unchanged [27]. It should be noted that in our study, the NMR spectra of *trans*-Ner alone in D_2O could not be obtained due to its low aqueous solubility. The proton chemical shifts of β-CD and β-CD/*trans*-Ner inclusion complex solutions are shown in Table 3. As expected, the presence of *trans*-Ner shifted upfield the protons located inside the CD hydrophobic cavity (H_3, H_5 and H_6) more effectively than those located at the surface (H_1, H_2 and H_4). These observations confirmed that *trans*-Ner is included into the CD cavity without evidence for outside complexation. Besides, the higher upfield shift value of 0.12 ppm was assigned to H_5 (Table 3). This probably means that the complexation of *trans*-Ner within the CD cavity involves hydrophobic interactions and that Ner penetrates the cavity from the wider side [28].

Furthermore, a ROESY experiment was performed to gain further insight into the dynamic structure of the β-CD/*trans*-Ner inclusion complex. The two-dimensional spectrum indicates a strong intermolecular cross-peaks between H_3 and H_5 protons of β-CD and the protons of *trans*-Ner's methyl groups (Figure 4a). As can be seen in Figure 4a, the H-16 proton of *trans*-Ner interacted only with H_3 proton of β-CD. Additionally, H-14 proton signals of *trans*-Ner showed intense cross-peaks with the inner CD protons, in particular with H_5. However, H-1 and H-4 of *trans*-Ner did not interact with any of CD interior protons. Based on these data, we suggested that *trans*-Ner is included in the β-CD cavity where the hydroxy group is oriented towards the wider rim of β-CD and the methyl groups located at positions 1 and 4 are present outside the narrow side of CD.

Table 3: ^{1}H NMR chemical shifts (δ, ppm) for free β-CD and β-CD/*trans*-Ner inclusion complex solutions in D_2O in the presence of 0.5 mM β-CD and 3.28 mM *trans*-Ner.

β-CD ^{1}H	$\delta_{(free)}$ (ppm)	$\delta_{(complex)}$ (ppm)	Δ δ (ppm)
H_1	5.11	5.08	−0.03
H_2	3.70	3.67	−0.03
H_4	3.62	3.61	−0.01
H_3	4.00	3.93	−0.07
H_5	3.89	3.77	−0.12
H_6	3.91	3.83	−0.08

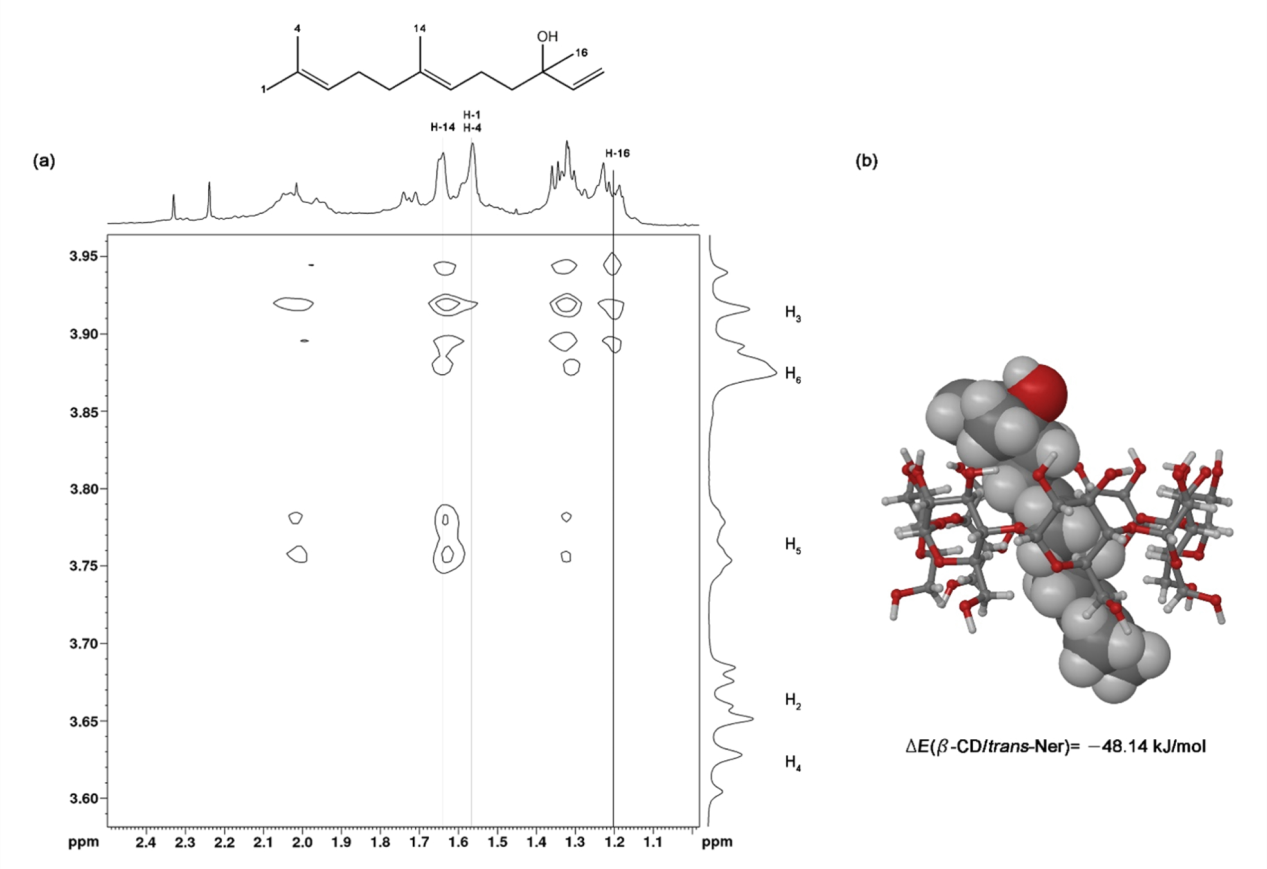

Figure 4: a) 2D ROESY spectrum of β-CD/*trans*-Ner inclusion complex in D_2O and b) representation of the most stable inclusion complex conformer.

Molecular modelling

The theoretical molecular modelling is useful to illustrate the most energetically favorable three-dimensional structure of the inclusion complex in solution. The inclusion complex conformer that presents the weakest relative binding energies (ΔE) (i.e., the most stable conformer) is represented in Figure 4b. The results showed that the formation of the β-CD/*trans*-Ner inclusion complex is an energetically favorable process and that the inclusion mode is coherent with the experimental NMR results.

Photodegradation studies of Ner

To the best of our knowledge, no studies were performed on the photodegradation of Ner under UV-light. Nonetheless, we can assume that the presence of three C=C double bonds may indicate the susceptibility of Ner to be photodegradable [29]. Therefore, the photostability of Ner was carried out in aqueous solution, in the absence and the presence of different CDs (α-CD, β-CD, HP-β-CD and SBE-β-CD) after its irradiation with UVB light. The concentration of each isomer was determined by HPLC. The effect of HP-β-CD on the photostability of *trans*-Ner in the cabreuva EO was also assessed upon UVB exposure. The photodegradation reaction of all samples followed a first-order kinetics. First, a constant concentration of Ner (0.1 mM) was added to various concentrations of HP-β-CD (0.1, 1 and 10 mM). Figure 5 represents the percentage of *cis*, *trans*-Ner and the mixture remaining in the solution after irradiation in function of time. It can be observed that Ner was rapidly degraded in the absence of CD; after 120 min of UVB exposure, only about 17% of Ner remained in the solution (Figure 5a). However, its degradation was slowed down as the HP-β-CD concentration increased. For example, after 120 min of irradiation, about 60 and 90% of Ner was still remaining in the solution in the presence of 0.5 and 10 mM HP-β-CD, respectively. The inclusion of Ner into the CD cavity exhibited a protective effect against photodegradation. This effect was more impor-

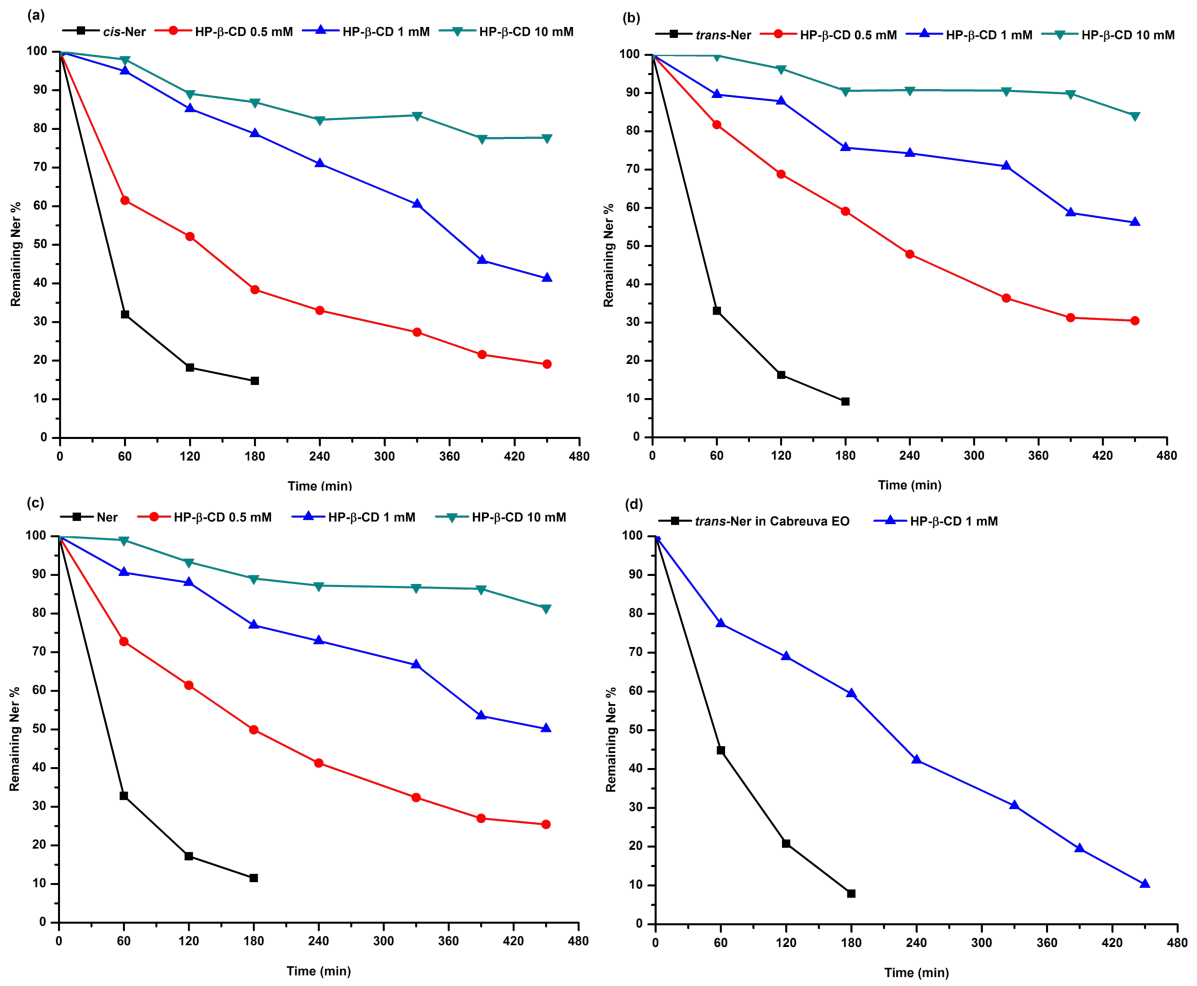

Figure 5: Photodegradation kinetics of *cis*-Ner (a), *trans*-Ner (b), the isomer mixture Ner (c) in the absence and presence of increasing concentrations of HP-β-CD (0.5, 1 and 10 mM) and of *trans*-Ner in cabreuva EO (d) in the absence and presence of 1 mM HP-β-CD under UV light irradiation.

tant as the concentration of HP-β-CD increased, due to the larger amount of complexed Ner. Furthermore, the photostability of *trans*-Ner in the cabreuva EO was investigated with 1 mM HP-β-CD (Figure 5b). We can observe that *trans*-Ner in cabreuva EO was totally degraded after 180 min of irradiation; whereas the complexation of EO with HP-β-CD enhanced the stability of *trans*-Ner (only 40% of *trans*-Ner was degraded in HP-β-CD solution after 180 min, Figure 5b). The existing literature also showed the protective effect of CD towards other guests [13,30-33]. When comparing the photostability of *trans*-Ner in its pure form and in the EO, it can be noted that the degradation of *trans*-Ner alone (K = 0.0145 min^{-1}) was slightly different than *trans*-Ner in EO (K = 0.0127 min^{-1}). This finding could be explained by the presence of other chemical compounds in the EO that may be influence the degradation of *trans*-Ner [34].

Then, we compared the effect of different CDs at a fixed concentration (1 mM) on the photostability of Ner upon UVB irradiation. From Table 4, we can notice that in the absence of CD, *trans*-Ner is more rapidly degraded than *cis*-Ner (K = 0.0145 min^{-1} and K = 0.0121 min^{-1} for *trans* and *cis* isomers, respectively). The main reason behind its instability is that *trans*-Ner isomerizes to its *cis* form during irradiation [34,35]. However, the presence of CD improved the photostability of *trans*-Ner more efficiently compared to *cis*-Ner (Table 4). This could be explained by the fact that *trans*-Ner is better encapsulated in CD than *cis*-Ner (Table 1). For example, in the presence of SBE-β-CD, the K value of *trans*-Ner was 0.0007 min^{-1} while that of *cis*-Ner was 0.0012 min^{-1}. This difference could be attributed to the difference in K_f values between the two isomers ($K_{f\ cis\text{-Ner}}$ = 9240 M^{-1} and $K_{f\ trans\text{-Ner}}$ = 13264 M^{-1}). It is worth noting that the higher the K_f value, the higher the photoprotective effect of CD; thus, SBE-β-CD (K_f = 17768 M^{-1}) > HP-β-CD (K_f = 10365 M^{-1}) > β-CD (K_f = 1238 M^{-1}) > α-CD (K_f = 418 M^{-1}).

Table 4: Photodegradation rate constants (K, min^{-1}, Equation 5) of CD/Ner inclusion complexes upon UVB irradiation.

K (min^{-1})	*cis*-Ner	*trans*-Ner	Ner
No CD	0.0121	0.0145	0.0134
α-CD	0.0051	0.0051	0.0051
β-CD	0.0019	0.0010	0.0013
HP-β-CD	0.0017	0.0012	0.0014
SBE- β-CD	0.0012	0.0007	0.0009

Conclusion

In this study, inclusion complexes of Ner (*cis*, *trans* and the isomer mixture) with seven CDs were successfully formed in aqueous solution. All inclusion complexes exhibited an 1:1 (CD:Ner) stoichiometry, with K_f values of CD/*trans*-Ner superior to those of CD/*cis*-Ner. The solubility of Ner and of the cabreuva EO (containing 64.54% of *trans*-Ner) was greatly enhanced in the presence of CDs. Moreover, solid HP-β-CD/Ner inclusion complexes were obtained with a high encapsulation efficiency (EE %). Structural characterization by NMR and molecular modelling confirmed once again the formation of the inclusion complex between *trans*-Ner and β-CD. The most stable structure was obtained for the hydroxy group oriented towards the wide rim of the CD. Finally, the photostability of Ner and of *trans*-Ner in cabreuva EO was remarkably improved upon CD complexation, thereby proving the protective effect of CD. From the above results, we could conclude that CDs are effective encapsulating agents for Ner, able to enhance its solubility and photostability.

Experimental

Materials

Nerolidol (98%, mixture of *cis* (40%) and *trans* (60%) isomers), *trans*-nerolidol (≥85%, analytical standard) and thymol (>99%) were purchased from Sigma-Aldrich (Missouri, United States). Cabreuva (*Myrocarpus fastigiatus*) essential oil (64.54% of *trans*-Ner) was purchased from Herbes et Traditions (Comines, France). Methylorange (MO) was provided by Acros Organics (Massachusetts, United States). α-CD, β-CD, HP-β-CD (DS = 5.6) and RAMEB (DS = 12.6) were purchased from Wacker-Chemie (Lyon, France). CRYSMEB (DS = 4.9) was provided from Roquette Frères (Lestrem, France). SBE-β-CD (DS = 6.5, Captisol®) was donated by Ligand Pharmaceuticals Incorporated (La Jolla, USA). Methanol HPLC-grade was purchased from VWR Chemicals (Atlanta, United States).

Methods

HPLC assay

Chromatographic analysis was performed with a Waters 600E multisolvent delivery system HPLC. The method development for estimation of Ner quantity in CD was carried out using the analytical column Xterra RP C18 (150 × 4.6 mm, 5 µm). The column temperature was maintained at 25 °C. The mobile phase consisted of methanol/water (70:30 v/v). The flow rate was set at 1 mL/min. The injection volume was 20 µL. The wavelength of UV detector was set at 212 nm. Stock solutions of Ner (1 mg/mL) and thymol (1 mg/mL) were prepared in methanol. Then, diluted concentrations of Ner ranged from 5 to 250 µg/mL and 100 µg/mL thymol, used as internal standard, were prepared in methanol. For HPLC measurement, 100 µL of each sample was added to thymol (100 µL) and methanol (200 µL). The mixture was then sonicated at 4 °C and centrifuged at 15000 rpm at 4 °C. The HPLC method was validated in terms of linearity, repeatability and limit of detection.

Formation constants determination

UV–visible spectroscopy

The UV–visible competition method described by Landy et al. [23] was used to determine the formation constants (K_f) of HP-β-CD/Ner inclusion complexes. Methylorange (MO), an azo dye, was used as a competitor. First, the K_f of the HP-β-CD/MO inclusion complex was calculated by a direct titration method. Then, a spectral displacement method was performed by adding Ner to a solution containing constant concentrations of HP-β-CD and MO. The expulsion of MO from HP-β-CD cavity induced an absorbance increment. The spectrum of MO solution (0.1 mM) was recorded between 520 and 530 nm. In this range of wavelengths, there was an optimal difference in absorbance between the free and encapsulated forms of MO. The HP-β-CD/Ner K_f values were calculated by an algorithmic treatment to minimize the difference between the experimental and theoretical values of the peak area. The K_f calculation is based on 1:1 stoichiometry for HP-β-CD/MO and HP-β-CD/Ner. All measurements were done using a UV–visible dual-beam spectrophotometer with a 1 cm thick quartz cuvette (Perkin Elmer Lambda 2S).

Phase solubility studies

Phase solubility studies were performed according to Higuchi and Connors [36]. Excess amounts of Ner were added to 2 mL of CD solution (α-CD, RAMEB, CRYSMEB, HP-β-CD or SBE-β-CD) at concentrations varying from 0 to 10 mM, except for γ- and β-CD where lower concentrations were used (0–1 mM). The mixtures were shaken for 24 h at 25 °C. After the equilibrium was reached, the solution was filtered through a 0.45 μm filter. The concentrations of *cis* and *trans*-Ner were determined using the HPLC method described above. The solubility of Ner was plotted against CD concentration. Formation constant (K_f) values of CD:Ner inclusion complexes were calculated from phase-solubility diagrams using the following equation:

$$K_f = \frac{slope}{S_0\ (1 - slope)} \tag{1}$$

where S_0 is the intrinsic solubility of Ner in aqueous solution without CD.

The solubilizing effect of CD was also determined by calculating complexation efficiency (*CE*) parameter which is the concentration ratio between CD in a complex and free CD:

$$CE = S_0 \times K_{1:1} = \frac{[CD/Ner]}{[CD]} = \frac{slope}{1 - slope} \tag{2}$$

Total organic carbon (TOC) analysis

Phase solubility studies of cabreuva EO with HP-β-CD were investigated by TOC analysis using a Shimadzu TOC-VCSH analyzer. It is based on the production of carbon dioxide (CO_2) following oxidation of organic compounds. CO_2 is then detected using a high-sensitivity infrared gas analyzer (NDIR). First, TOC was measured for the CD solution (TOC_{CD}). Then, the amount of EO in the filtrate was calculated using the following equation: $TOC_{EO} = TOC_T - TOC_{CD}$, where TOC_T is the TOC value obtained for the filtrate by the TOC analyzer. Results were reported in g/L of organic carbon. The solubility of EO was determined from standard curves constructed with known EO concentrations.

Preparation of the solid inclusion complex by freeze-drying

Ner (10 mM) was added to different HP-β-CD (50 and 100 mM) aqueous solutions. Solutions were stirred at 300 rpm for 24 h at 25 °C. After equilibrium was reached, the suspensions were filtered, frozen at −20 °C for 24 h and lyophilized. The lyophilization process was carried out at −85 °C and 0 Pa in a Christ Alpha 2-4 LD Freeze dryer until all moisture had been sublimated.

Encapsulation efficiency

Encapsulation efficiency (EE %) of Ner as a mixture (10 mM) into HP-β-CD (50 and 100 mM CD) was carried out by dissolving 10 mg of solid inclusion complexes in ethanol (10 mL). An aliquot of each sample was taken and analyzed by the HPLC method described above.

The EE % was calculated as follows:

$$EE\ \% = \frac{m_{exp}\ (\text{mg})}{m_t\ (\text{mg})} \tag{3}$$

where m_{exp} and m_t are the experimental and theoretical (amount of Ner initially added to prepare the solid inclusion complex) quantities of Ner in the solid inclusion complexes, respectively.

Molecular modelling studies

Molecular mechanics simulation was done using the Macromodel-MMFFs force field in the presence of water (GB/SA implicit model) as implemented in the Schrodinger software (release 2014). The CD hosts were based on a non-distorted monomeric β-CD with C7 symmetry. *trans*-Ner were constructed manually. Fifty conformations of *trans*-Ner/CD complexes were selected (Monte Carlo conformational searches: Mixed torsional/low mode sampling, 10000 structures generated, FMNR conjugate gradient minimization,

convergence fixed to 0.01 kJ $Å^{-1}$ mol^{-1}). The total energy difference (ΔE, kJ/mol) between the inclusion complex and the sum of their individual components in their optimized fundamental states was calculated ($\Delta E = E_{CD/Ner} - (E_{CD} + E_{Ner})$) and used as the theoretical parameter to evaluate the complexation energy of the inclusion complex.

NMR spectroscopy

NMR experiments were realized for β-CD/*trans*-Ner inclusion complex solution. ^{1}H NMR spectra were acquired on a 400 MHz Bruker Avance III spectrometer at room temperature equipped with a multinuclear z-gradient PABBO probe head capable of producing magnetic field pulse gradients in the z-direction of 48.15 G·cm^{-1}. *trans*-Ner and β-CD were dissolved in 99.98% D_2O. Two-dimensional (2D) ROESY off resonance spectra were acquired at 25 °C with presaturation of the residual water resonance and a mixing (spin-lock) time of 600 ms, using the States-TPPI method with a 2048 K time domain in F2 and 512 experiments in F1. Sixty-four scans were recorded to obtain a good resolution 2D ROESY spectra.

Photostability study

The Ner photodegradation experiment was realized under an artificial UV source (UVB, 310 nm) in a 100 mL quartz reactor, with continuous stirring, using a Multirays apparatus (Heliosquartz, Italy). The photostability of Ner, cabreuva EO and their inclusion complexes with CDs was investigated under UVB irradiation as a function of time.

Ner (0.1 mM) was added to solutions of various HP-β-CD concentrations (0.5, 1 and 10 mM) and to 1 mM solutions of α-, β- and SBE-β-CD. Cabreuva EO (1.27 µL) was also added to 1 mM HP-β-CD aqueous solution. Ner and cabreuva EO aqueous solutions without CD were also prepared. Irradiated aliquots were withdrawn every 60 min, over 8 h of total irradiation and the remaining Ner concentration was then determined by HPLC.

The percentage of Ner remaining was calculated as follows:

$$\%\,\text{Ner remaining} = \frac{C_t}{C_i} \times 100 \quad (4)$$

where C_t is Ner concentration in solution after irradiation at time t and C_i is Ner concentration before irradiation.

The photodegradation constant (K, min^{-1}) was also calculated using the following equation:

$$\ln[\text{Ner}] = -Kt + b \quad (5)$$

Supporting Information

Supporting Information File 1

^{1}H NMR spectra.
[http://www.beilstein-journals.org/bjoc/content/supplementary/1860-5397-13-84-S1.pdf]

Acknowledgments

Authors are grateful to the Lebanese University and the Université du Littoral Côte d'Opale for the financial support of J. Azzi's PhD thesis. The study was supported by the Agence Universitaire de la Francophonie (Projet de Coopération Scientifique Inter-universitaire 2015-2017).

References

1. Mc Ginty, D.; Letizia, C. S.; Api, A. M. *Food Chem. Toxicol.* **2010,** *48* (Suppl. 3), S43–S45. doi:10.1016/j.fct.2009.11.008
2. Lapczynski, A.; Bhatia, S. P.; Letizia, C. S.; Api, A. M. *Food Chem. Toxicol.* **2008,** *46* (Suppl. 11), S247–S250. doi:10.1016/j.fct.2008.06.063
3. Schubert, V.; Dietrich, A.; Ulrich, T.; Mosandl, A. *Z. Naturforsch., C: J. Biosci.* **1992,** *47,* 304–307.
4. Tao, R.; Wang, C.-Z.; Kong, Z.-W. *Molecules* **2013,** *18,* 2166–2182. doi:10.3390/molecules18022166
5. Nardello-Rataj, V.; Leclercq, L. *Beilstein J. Org. Chem.* **2014,** *10,* 2603–2622. doi:10.3762/bjoc.10.273
6. Sekhon, B. S. *Nanotechnol., Sci. Appl.* **2010,** *3,* 1–15. doi:10.2147/NSA.S8677
7. Mozafari, R. M.; Khosravi-Darani, K.; Borazan, G. G.; Cui, J.; Pardakhty, A.; Yurdugul, S. *Int. J. Food Prop.* **2008,** *11,* 833–844. doi:10.1080/10942910701648115
8. Nedovic, V.; Kalusevic, A.; Manojlovic, V.; Levic, S.; Bugarski, B. *Procedia Food Sci.* **2011,** *1,* 1806–1815. doi:10.1016/j.profoo.2011.09.265
9. Rodríguez, J.; Martín, M. J.; Ruiz, M. A.; Clares, B. *Food Res. Int.* **2016,** *83,* 41–59. doi:10.1016/j.foodres.2016.01.032
10. Astray, G.; Gonzalez-Barreiro, C.; Mejuto, J. C.; Rial-Otero, R.; Simal-Gándara, J. *Food Hydrocolloids* **2009,** *23,* 1631–1640. doi:10.1016/j.foodhyd.2009.01.001
11. Kfoury, M.; Landy, D.; Auezova, L.; Greige-Gerges, H.; Fourmentin, S. *Beilstein J. Org. Chem.* **2014,** *10,* 2322–2331. doi:10.3762/bjoc.10.241
12. Wang, X.; Yuan, Y.; Yue, T. *Starch/Staerke* **2015,** *67,* 225–236. doi:10.1002/star.201400163
13. Kfoury, M.; Lounès-Hadj Sahraoui, A.; Bourdon, N.; Laruelle, F.; Fontaine, J.; Auezova, L.; Greige-Gerges, H.; Fourmentin, S. *Food Chem.* **2016,** *196,* 518–525. doi:10.1016/j.foodchem.2015.09.078
14. Szejtli, J. *Chem. Rev.* **1998,** *98,* 1743–1754. doi:10.1021/cr970022c
15. Marques, H. M. C. *Flavour Fragrance J.* **2010,** *25,* 313–326. doi:10.1002/ffj.2019
16. Kfoury, M.; Balan, R.; Landy, D.; Nistor, D.; Fourmentin, S. *Supramol. Chem.* **2015,** *27,* 620–628. doi:10.1080/10610278.2015.1051977
17. Kfoury, M.; Auezova, L.; Greige-Gerges, H.; Fourmentin, S. *Anal. Chim. Acta* **2016,** *918,* 21–25. doi:10.1016/j.aca.2016.03.013
18. Del Valle, E. M. M. *Process Biochem.* **2004,** *39,* 1033–1046. doi:10.1016/S0032-9592(03)00258-9

19. Loftsson, T.; Hreinsdóttir, D.; Másson, M. *J. Inclusion Phenom. Macrocyclic Chem.* **2007,** *57,* 545–552. doi:10.1007/s10847-006-9247-2
20. Mathiron, D.; Marçon, F.; Dubaele, J.-M.; Cailleu, D.; Pilard, S.; Djedaïni-Pilard, F. *J. Pharm. Sci.* **2013,** *102,* 2102–2111. doi:10.1002/jps.23558
21. Kfoury, M.; Auezova, L.; Greige-Gerges, H.; Ruellan, S.; Fourmentin, S. *Food Chem.* **2014,** *164,* 454–461. doi:10.1016/j.foodchem.2014.05.052
22. Fenyvesi, E.; Szemán, J.; Csabai, K.; Malanga, M.; Szente, L. *J. Pharm. Sci.* **2014,** *103,* 1443–1452. doi:10.1002/jps.23917
23. Landy, D.; Fourmentin, S.; Salome, M.; Surpateanu, G. *J. Inclusion Phenom. Macrocyclic Chem.* **2000,** *38,* 187–198. doi:10.1023/A:1008156110999
24. Decock, G.; Fourmentin, S.; Surpateanu, G. G.; Landy, D.; Decock, P.; Surpateanu, G. *Supramol. Chem.* **2006,** *18,* 477–482. doi:10.1080/10610270600665749
25. Messner, M.; Kurkov, S. V.; Jansook, P.; Loftsson, T. *Int. J. Pharm.* **2010,** *387,* 199–208. doi:10.1016/j.ijpharm.2009.11.035
26. Samperio, C.; Boyer, R.; Eigel, W. N., III; Holland, K. W.; McKinney, J. S.; O'Keefe, S. F.; Smith, R.; Marcy, J. E. *J. Agric. Food Chem.* **2010,** *58,* 12950–12956. doi:10.1021/jf103275a
27. Schneider, H.-J.; Hacket, F.; Rüdiger, V. *Chem. Rev.* **1998,** *98,* 1755–1786. doi:10.1021/cr970019t
28. Fernandes, C. M.; Carvalho, R. A.; Pereira da Costa, S.; Veiga, F. J. B. *Eur. J. Pharm. Sci.* **2003,** *18,* 285–296. doi:10.1016/S0928-0987(03)00025-3
29. Hayashi, N.; Nakata, Y.; Yazaki, A. *Antimicrob. Agents Chemother.* **2004,** *48,* 799–803. doi:10.1128/AAC.48.3.799-803.2004
30. Villaverde, J.; Maqueda, C.; Undabeytia, T.; Morillo, E. *Chemosphere* **2007,** *69,* 575–584. doi:10.1016/j.chemosphere.2007.03.022
31. Fir, M. M.; Smidovnik, A.; Milivojevic, L.; Zmitek, J.; Prosek, M. *J. Inclusion Phenom. Macrocyclic Chem.* **2009,** *64,* 225–232. doi:10.1007/s10847-009-9555-4
32. Carlotti, M. E.; Sapino, S.; Ugazio, E.; Caron, G. *J. Inclusion Phenom. Macrocyclic Chem.* **2011,** *70,* 81–90. doi:10.1007/s10847-010-9864-7
33. Hădărugă, D. I.; Hădărugă, N. G.; Costescu, C. I.; David, I.; Gruia, A. T. *Beilstein J. Org. Chem.* **2014,** *10,* 2809–2820. doi:10.3762/bjoc.10.298
34. Turek, C.; Stintzing, F. C. *Compr. Rev. Food Sci. Food Saf.* **2013,** *12,* 40–53. doi:10.1111/1541-4337.12006
35. Ahmad, I.; Ahmed, S.; Anwar, Z.; Sheraz, M. A.; Sikorski, M. *Int. J. Photoenergy* **2016,** No. 8135608. doi:10.1155/2016/8135608
36. Higuchi, T.; Connors, A. K. Phase solubility techniques. In *Advances in Analytical Chemistry and Instrumentation;* Reilly, C. N., Ed.; Wiley-Interscience: New York, 1965; Vol. 4, pp 117–212.

License and Terms

BEILSTEIN JOURNAL OF ORGANIC CHEMISTRY

Molecular recognition of *N*-acetyltryptophan enantiomers by β-cyclodextrin

Spyros D. Chatziefthimiou, Mario Inclán, Petros Giastas, Athanasios Papakyriakou, Konstantina Yannakopoulou* and Irene M. Mavridis*

Full Research Paper

Open Access

Address:
Institute of Nanoscience & Nanotechnology, National Center for Scientific Research "Demokritos", Patriarchou Gregoriou E' & Neapoleos 27, 15310 Aghia Paraskevi Attikis, Greece

Email:
Konstantina Yannakopoulou* - k.yannakopoulou@inn.demokritos.gr;
Irene M. Mavridis* - e.mavridis@inn.demokritos.gr

* Corresponding author

Keywords:
β-cyclodextrin; enantiomeric discrimination; *N*-acetyltryptophan; NMR; X-ray structure

Beilstein J. Org. Chem. **2017,** *13,* 1572–1582.
doi:10.3762/bjoc.13.157

Received: 14 February 2017
Accepted: 18 July 2017
Published: 09 August 2017

This article is part of the Thematic Series "Superstructures with cyclodextrins: Chemistry and applications IV".

Guest Editor: G. Wenz

Abstract

The enantioselectivity of β-cyclodextrin (β-CD) towards L- and D-*N*-acetyltryptophan (NAcTrp) has been studied in aqueous solution and the crystalline state. NMR studies in solution show that β-CD forms complexes of very similar but not identical geometry with both L- and D-NAcTrp and exhibits stronger binding with L-NAcTrp. In the crystalline state, only β-CD–L-NAcTrp crystallizes readily from aqueous solutions as a dimeric complex (two hosts enclosing two guest molecules). In contrast, crystals of the complex β-CD–D-NAcTrp were never obtained, although numerous conditions were tried. In aqueous solution, the orientation of the guest in both complexes is different than in the β-CD–L-NAcTrp complex in the crystal. Overall, the study shows that subtle differences observed between the β-CD–L,D-NAcTrp complexes in aqueous solution are magnified at the onset of crystallization, as a consequence of accumulation of many soft host–guest interactions and of the imposed crystallographic order, thus resulting in very dissimilar propensity of each enantiomer to produce crystals with β-CD.

Introduction

Cyclodextrins (CDs) are cyclic, water-soluble carbohydrates with a rather non-polar cavity that can host a variety of organic molecules (guests) and form inclusion complexes [1]. The guest molecules may be completely or partly enclosed inside the cavity depending on their size and the CD macrocycle's dimensions. The host–guest interactions established in the cavity are of van der Waals type, whereas between parts of the guest extending out of the cavity and the host's hydroxy groups are H-bonding interactions and/or of electrostatic nature. CDs have been studied and used for the enhancement of solubility, bioavailability and stability of drugs [2-5]. Moreover, being oligomers of α-D-glucopyranose, CDs possess an intrinsic

chirality, thus they form diastereomeric inclusion complexes with enantiomeric pairs and frequently they exhibit enantioselectivity in aqueous solution or they can co-precipitate with only one enantiomer (enantioseparation). The separation of enantiomers via cyclodextrin inclusion is particularly important in the case of guests of pharmaceutical interest, since enantiomerically pure drugs are crucial for the pharmaceutical industry [1,6,7].

It has been proven difficult so far to explain and to predict the recognition abilities of specific CDs towards enantiomers, especially in solution. An interesting attempt is a thermodynamic study in aqueous solution with microcalorimetry of a large number (43) and variety of chiral organic compounds [8] with β-CD at room temperature. It was shown that properties and interactions important for chiral recognition include (i) weak non-bonding interactions rather than polar, (ii) nonsymmetrical non-polar penetrating guests and (iii) large distance of the chiral center from charged/hydrophilic groups. Moreover, trends in enantioselectivity do not follow trends in association constants, i.e., the association constants for the β-CD complexes of both enantiomers of *N*-acetyltyrosine, *N*-acetylphenylalanine and *N*-acetyltryptophan are in decreasing order, whereas their enantioselectivity (ratio of the binding constants, *K*, of the L- to the D-enantiomer) shows an increasing order (1.04, 1.1 and 1.34, respectively). X-ray crystallography, on the other hand, can improve our understanding of chiral recognition by CDs at the atomic level by providing insight into the interactions and the fit of the guest in the cavity, taking into account that crystal lattice forces may introduce additional and more stringent parameters for the enantiodiscrimination [9,10]. However, the crystallographic structures of diastereomeric complexes of CDs with chiral guest molecules in the literature are scarce. For β-CD with fenoprofen [7], a partial chiral resolution of the racemic mixture occurs, since the obtained crystals contain discrete β-CD dimers enclosing (*R*)- or (*S*)-enantiomers in a *S*/*R* ratio = 3:1. The enantiomers adopt different orientations in the β-CD dimers and preference of the (*S*) complex is dictated both by stronger H-bonding of the carboxyl group, as well as more favorable methyl–phenyl interactions inside the cavity. In contrast, no discrimination is shown by β-CD for (*R*)- and (*S*)-flurbiprofen [11], since the crystals grown from the racemic mixture have both enantiomers enclosed (as a head-to-head dimer) in a β-CD dimer. In the case of substituted CDs, 2,3,6-tri-*O*-methyl-α-CD discriminates between (*R*)- and (*S*)-mandelic acid [12] as it forms very different crystals from a racemic mixture. The same host crystallizes exclusively with (*R*)-(−)-1,7-dioxaspiro[5.5]undecane, the *Dacus Oleae* pheromone, from an aqueous solution of the racemic mixture (enantioseparation) [13] also exhibiting high enantioselectivity in solution. Likewise, heptakis-(2,3,6-tri-*O*-methyl)-β-CD displays high enantioselectivity in solution towards (*S*)-(+)-1,7-dioxaspiro[5.5]undecane and under certain conditions it co-crystallizes only with the (*S*)-enantiomer [14]. Induced host–guest fit, made possible by the macrocyclic flexibility of the permethylated CDs plays a crucial role in their capacity for chiral discrimination.

Chiral recognition of amino acids and their derivatives by CDs has been also tested using phase-solubility diagrams [15], NMR spectroscopy [16] and electrochemical methods [17], as well as by X-ray crystallography [18]. Detailed structures of β-CD with L- and D-*N*-acetylphenylalanine (NAcPhe) grown separately [18] has shown that although the two complexes are isomorphous (same space group, very similar unit cell dimensions and same packing of β-CD dimers) there are differences regarding the positioning of the guest molecules, the D-enantiomer being ordered, whereas the L- enantiomer extensively disordered. This disparity seems to be determined by subtle hydrophobic differences and H-bonding interactions among guests themselves and with the host and co-crystallized water molecules in the lattice. Additional structures of β-CD with different L-phenylalanine derivatives [19,20] confirm the above general result. In the present study, we report on the inclusion of the L- and D-enantiomers of *N*-acetyltryptophan (NAcTrp) in β-CD (Scheme 1) in an effort to contribute to the study of chiral recognition of amino acid derivatives by CDs in the crystalline state and in solution. The guest NAcTrp has been selected because of its large aromatic side chain with appropriate dimensions to fit tightly in the β-CD cavity thus expected to have restricted mobility and limited disorder. Indicative of the interest and possible applications of the CD use in chiral selectivity/discrimination of tryptophan are studies in aqueous solution [21], in electrochemistry for sensor development [17,22,23], as components of solid phases in chromatography [24], or in capillary electrophoresis [25].

Results and Discussion

NMR studies

In deuterium oxide (D_2O), each of the NAcTrp enantiomers induced significant chemical shift displacements (shielding) in the ^{1}H NMR signals of the β-CD cavity protons, namely H3 (near the wider, secondary side) and H5, H6,6’ (at the narrower, primary side), signifying cavity inclusion of each enantiomer (Scheme 1). When a racemic mixture of NAcTrp was added to a β-CD solution no differentiation in the signals was observed due to in situ formation of diastereomers, except for a very small splitting of the methyl signal of the *N*-acetyl group. No differentiation was detected in the ^{13}C NMR spectrum either. In order to determine the stoichiometry of the complexes continuous variation (Job) plots [26] were drafted. For β-CD protons only the cavity signals due to H5, H3 and H6,6’ showed significant shifts upon complexation (Supporting Information File 1,

Figure S1). The inflection point of the graphs at 0.5 indicates a 1:1 stoichiometry for both enantiomers. The tryptophan protons were affected differently upon complexation (Supporting Information File 1, Figure S2), i.e., the graphs due to shifts of the indole's benzene ring protons (H3, H4, H5 and H6) indicate a 1:1 host/guest stoichiometry, whereas those of the indole moiety (H8) and of the aliphatic protons (H9,9', H10, H12), with an inflection point at ≈0.3, suggest a host/guest ratio close to 2:1. This behavior reveals the existence of two different complexation modes, one involving the indole phenyl ring with one host only and the aliphatic chain with two host molecules. The fact that the second mode takes place mainly when there is an excess of host concentration indicates that the inclusion of the indole moiety is the predominant mode of interaction. Moreover, it is observed that the magnitude of the shifts of the L-enantiomer are always larger and the slopes of the Job plots steeper than those of the D-enantiomer, suggesting stronger binding of β-CD with L- than with D-NAcTrp.

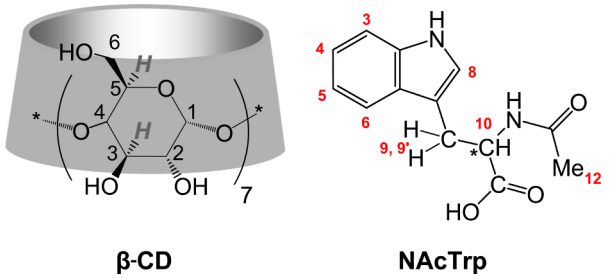

Scheme 1: Numbering scheme of one glucopyranose residue (G) of β-CD and the NAcTrp molecule; specific atom labels of β-CD are denoted in the text/tables as Cmn, Omn, m being the atom number and n the glucopyranose residue (Gn) of β-CD.

2D ROESY spectra of each enantiomer with β-CD at a 1:1 mole ratio in D_2O were obtained under identical conditions (temperature, concentration, acquisition parameters). Strong intermolecular dipolar interactions were observed between indole protons (H3, H4, H5, H6, H8) and the β-CD cavity protons (H5, H6,6', H3) in both enantiomeric guests, confirming full inclusion of the Trp side chain. To facilitate the comparison of the two in situ formed diastereomers and to visualize the small differences (Supporting Information File 1, Figure S3) in dipolar through space intermolecular interactions in each case, 3D correlation maps were employed. They were displayed carefully so as to ensure the same intensity for the reference intramolecular correlations between NAcTrp H9,9' with H6 (average distance ≈3.5 Å) and with H8 (average distance ≈4.0 Å) in each of the enantiomers (Figure 1a), enlarging the points of difference in the magnified maps (Figure 1b). Thus (i) guest-H6,H3,H5–host-H5,H66',H3 interactions are very similar in both enantiomers with guest-H5–host-H3 clearly weaker than the others, and guest-H6/host-H6,6' stronger in L- than in D-, suggesting that guest-H6,H3 are embedded inside the cavity, guest-H5 is closer to the narrow β-CD rim and L-H6 is closer to it than D-H6. (ii) Guest-H8–host-H3 interactions are equally strong in both enantiomers, stronger than the guest-H8/host-H5,H6,6' ones, which in turn are stronger in L- than in D-. Moreover, interactions between guest-Me12–host-H3 are strong for both enantiomers (Supporting Information File 1, Figure S3b), suggesting that the *N*-acetyl group is in both cases at the wide secondary opening of β-CD, and L-H8, is closer to the primary opening than D-H8 suggesting a difference in tilting. (iii) Guest-H4–host-H5 interactions are similar in both enantiomers but this of guest-H4–host-H6,6' is considerably stronger in D- than in L-, while guest-H4–host-H3 interactions are practically absent for both enantiomers, implying that L-H4 is extended further out of the primary side than D-H4. (iv) Guest-H9,9' and H10 show weak interactions with host-H3 thus they reside mostly closer to the wide opening of the host.

The above interactions detected by NMR suggest that in the aqueous environment the inclusion modes in each diastereomeric complex are very similar but non-identical. D-H4 is located near the primary side of the host, while L-H4 is completely outside (scarcely communicates with the cavity). On the other hand H8 (at a ≈7 Å distance from H4) is at the secondary side in both enantiomers, slightly closer to H5 of the host only in the L-enantiomer. These interactions suggest a common binding model, with the indole part included in the direction H4 to H8 from primary to secondary opening and with the L-enantiomer having its H4 end exposed and its NAc group at the secondary side in contact with CD-H3. A different degree of tilting with respect to the β-CD axis to accommodate the hydrophobic NAc group in the cavity is inferred by the NMR data in each case, thus explaining the small differences observed in solution. However, as the Job plots suggested, the aliphatic part is influenced by a second host molecule presumably via its secondary side. This implies that in solution, host–guest association is possible through additional orientations and stoichiometry, thus the presence of alternative arrangements in low percentage cannot be excluded.

X-ray crystallography studies

In the crystalline state, the structure of the inclusion complex of L-NAcTrp in β-CD comprises dimers. The asymmetric unit of the complex contains two crystallographically independent β-CD hosts (**A** and **B**) forming a dimer (Figure 2), in which two guest molecules of L-NAcTrp are enclosed in a head-to-head fashion (host:guest ratio, 1:1). The pair of L-NAcTrp molecules inside the dimer are found in orientational disorder, i.e., the guest exhibits a major orientation, molecules **C** and **D** (occupancy 65%), and a co-existing minor orientation (molecules **E** and **F**, occupancy 35%) in a statistical fashion. The

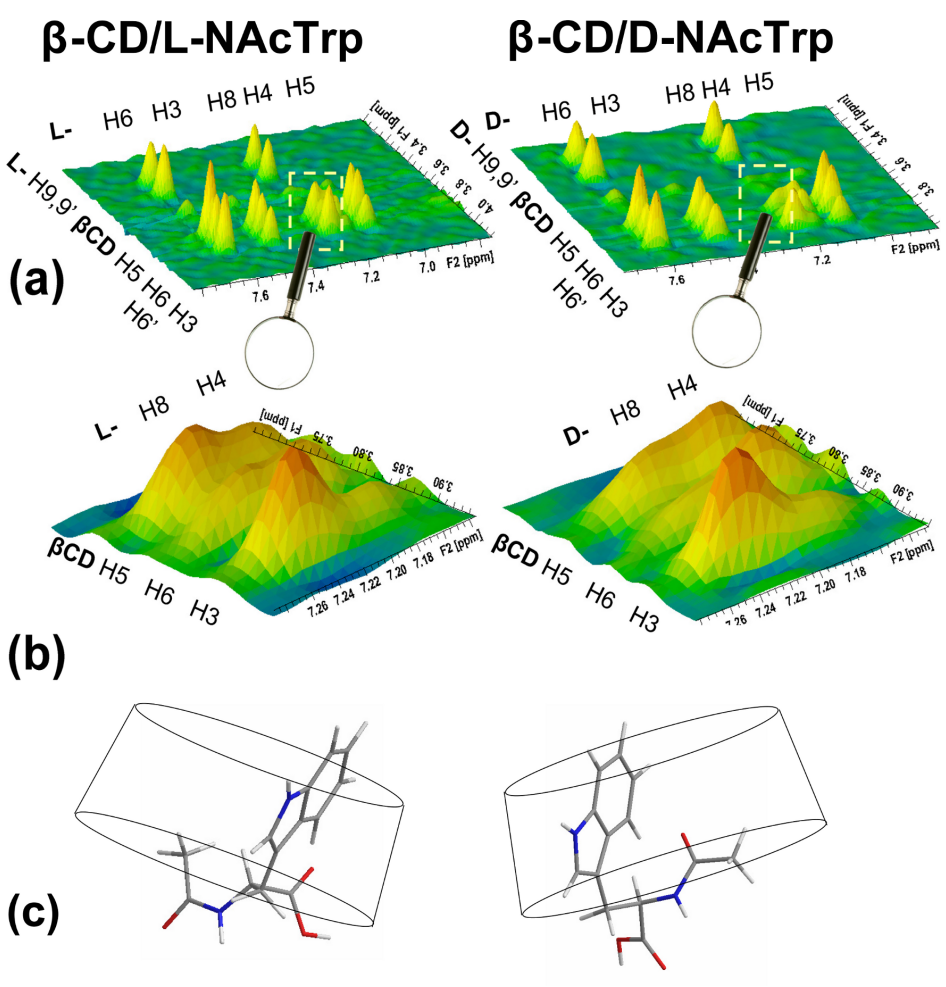

Figure 1: 3D maps of the observed dipolar, through-space host–guest interactions depicted so as to (a) reflect ≈equally strong cross-peaks in each L- and D-NAcTrp enantiomer for intramolecular correlations, namely guest H9,9' with guest H6 and H8; (b) the few differences observed in the intermolecular interactions have been magnified and reflect somewhat different binding modes of the two enantiomers revealed by intermolecular interactions of guest protons H8 and H4 only; (c) schematic representation of the respective solution models for each 1:1 complex.

dimers pack along the axis *a* at an angle of 19° thus forming a broken channel (Intermediate packing) [10,27]. The mean distance of the centers of mass of two consecutive β-CD dimers is 5.78 Å. Co-crystallized with each dimer, 21.45 water molecules are found distributed over 36 sites. The water molecules form the usual water networks of H-bonds, one linking the primary and the other the secondary hydroxy groups [28], many of them stabilizing the crystal lattice (structural water molecules).

The glucopyranose residues (in $^4C_1$ chair) of both **A** and **B** β-CD have a rather undistorted conformation (Supporting Information File 1, Table S1) (angles between the glycosidic oxygen atoms O-4n similar to these of the regular heptagon, 128.57°, deviations of the O-4n atoms from their mean plane, close to zero). The tilt of the mean glucopyranose planes towards their 7-fold axis are small and close to their average values (7.1 and 7.7°, respectively). As in all β-CD dimeric complexes [28], the macrocycles' conformation is stabilized by hydrogen bonds connecting (i) intramolecularly, the O-3n and O-2(n+1) atoms of neighboring glucopyranose units (mean 2.73 Å and 2.75 Å for **A** and **B**, respectively, 2.78 Å in hydrated β-CD) and (ii) intermolecularly, the O-3n**A** and O-(8−n)**B** atoms of monomers **A** and **B**, respectively (range of distances 2.7–2.8 Å, Supporting Information File 1, Table S2). At the primary side, only β-CD molecule **B** exhibits disorder of the C-O63**B** bond in two conformations, the major (−)-gauche C-O63Ba (occupancy 78%) pointing outward and the minor (+)-gauche C-O63Bb (22%) pointing towards the interior of the cavity, the latter interacting with guests **C** and **D** of neighboring dimers (Figure 3a).

The aromatic moieties of both guest orientations maintain the same relative position with the host, their planes interacting in a π···π fashion (Figure 2 and Figure 3) (dihedral angle between

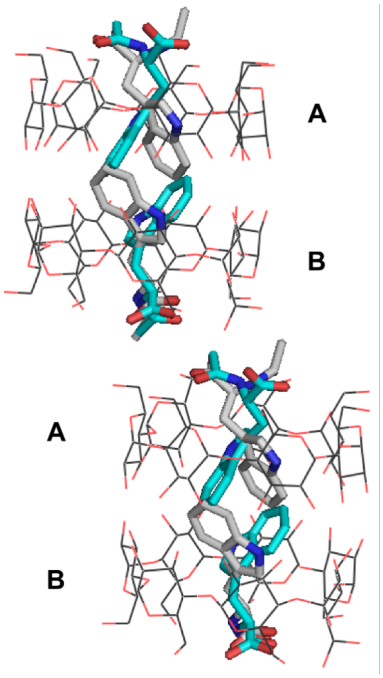

Figure 2: Two dimers of β-CD–L-NAcTrp, stacked along the *a*-axis, are shown. Each β-CD dimer (**A**, **B**) encloses a pair of guest molecules distributed in two orientations, the major (**C** and **D** in cyan) and the minor (**E** and **F**, in grey) respectively.

the **C** and **D** indole planes, 17.3(1)°, smallest distance 3.5 Å; dihedral angle between **E** and **F**, 14.0(2)°, smallest distance 3.3 Å). The relative positions between major guest **C** and minor **E** enclosed in β-CD **A** are very similar to the relative positions of **D** and **F** enclosed in β-CD **B** (dihedral angles 69.8(6)° and 65.4(7)°, respectively). The dihedral angles between the β-CD mean O-4n planes and indole planes **C** and **D** are the same (57.8(1)° and 57.5(2)°) and very close to the dihedral angles for the minor guests **E** and **F** (58(1) and 61(1)°). The indole nitrogen atoms N1 of guests (**C**, **E**) enclosed in β-CD **A** are almost at the level of the glycosidic oxygen atoms O-4n and close to atoms O42A and O45A, respectively, whereas N1 of the guests (**D**, **F**) in cavity **B** are close to the secondary hydroxy level, apparently in order to optimize the π···π interactions between the indole planes (Figure 2 and Figure 3, Table 1). The above suggest a tight fit of the guest inside the cavity. On the other hand, the aliphatic part of NAcTrp, positioned in the space between dimers, exhibits more freedom: the carboxylic and acetylamino groups of guests **D** and **F** inside β-CD **B** are close and parallel, whereas in β-CD monomer **A** the acetylamino moiety of the major guest **C** is close to the carboxyl group of minor guest **E**, their respective carboxyl and acetylamino groups pointing to opposite directions (Figure 2 and Figure 3). These differences maximize the strong interactions between major guests **C** and **D** (Figure 3, Table 1).

Numerous trials to crystallize the inclusion complex of β-CD with D-NAcTrp have failed to give anything but hydrated β-CD crystals [29], as described in detail in the experimental section, however, some crystals were grown after hydrothermal treatment of the solution (65 °C for duration of 6 days) [30,31]. The structure of the latter could not be solved by isomorphous replacement (using the coordinates of β-CD–glutaric acid complex [32], that is isomorphous to hydrated β-CD [29]. This was an indication that the structure should be quite different from hydrated β-CD. However, no guest could be located during the refinement and the present structure (henceforth "β-CD–D-

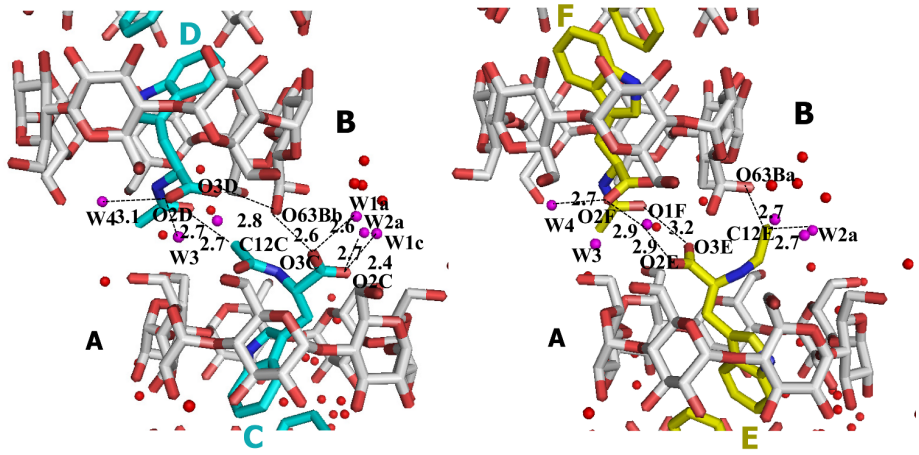

Figure 3: β-CD–L-NAcTrp complex at the interface between two β-CD dimers along the *a*-axis (major orientation guest molecules **C**, **D** in cyan and minor **E**, **F** in yellow). Note that the major guests **C**, **D** interact (a) directly by O1**D** and C12**C** through non-conventional H-bonding and (b) indirectly by mutual H-bonding of O3**C** and O3**D** with the only inward pointing hydroxy O63**B**b. Moreover, they are stabilized by the H-bonds of carboxylic oxygen atoms with the structural water molecules OW2a, OW3 and OW4, which interact also with hydroxy groups of the neighbor β-CD hosts. In contrast, the minor guests **E** and **F** interact weakly via the carboxylic O3**E** and acetyl O1**F** atoms and indirectly via a low occupancy water molecule W5, whereas the acetylamino methyl group is exposed to the water molecules in the exterior of the broken channel.

Table 1: H-bond distances of β-CD–L-NAcTrp complex: (1) between guest molecules themselves and with the host (2) with water molecules, (3) between structural water molecules and the host.

	Distance (Å)	C_1-A_1···O_2 (°)	A_1···O_2-C_2 (°)	Symmetry[i]
1. guest···guest and guest···host interactions				
Major-occupancy guests **C** and **D**				
C12**C**···O1**D**[i]	2.75 (2)	138 (1)	136 (1)	x−1,y,z
O3**C**···O63**B**b[i]	2.60 (2)	121 (1)	132 (1)	x−1,y,z
N1**C**···O42**A**	3.09 (1)	136.9 (8) 110.4 (8)	106.2 (3) 137.0 (4)	–
O3**D**[i]···O63**B**b[i]	2.81 (3)	154 (2)	94 (1)	x−1,y,z
N1**D**[i]···O45**B**[i]	3.38 (2)	138 (2) 90 (2)	101.9 (5) 137.3 (5)	–
Minor-occupancy guests **E** and **F**				
O3**E**···O1**F**[i]	3.18 (8)	132 (1)	131 (1)	x−1,y,z
C12**E**···O63**B**a[i]	2.72 (5)	130 (1)	119 (1)	x−1,y,z
N1**E**···O45**A**	3.06 (6)	147.5 (2) 103.0 (3)	99.8 (3) 142.8 (2)	–
2. guest···water molecules interactions				
Major-occupancy guests **C** and **D**				
O3**C**···OW1a	2.61 (2)	114 (1)		
O2**C**···OW2a	2.71 (2)	120 (1)		
O2**D**[i]···OW3	2.74 (2)	131 (1)		x−1,y,z
O2**D**[i]···OW4	3.15 (2)	111 (1)		x−1,y,z
N2**D**[i]···OW4	2.89 (2)	113 (1) 114 (1)		x−1,y,z
Minor-occupancy guests **E** and **F**				
O3**F**[i]···OW5	2.81	96 (1)		x−1,y,z
O2**F**[i]···OW4	2.67	131 (1)		x−1,y,z
3. structural water molecules···host interactions				
OW2a···O61**B**	2.58 (2)		116 (1)	x−1,y−1,z
OW3···O64**A**	2.70 (2)		115 (1)	x,y+1,z
OW3···O67**A**	2.68 (2)		109 (1)	x,y,z
OW4···O64**A**	2.89 (2)		105 (1)	x,y+1,z

[i]Atomic position equivalent by symmetry; a or b on atom names refer to different disordered positions of the atom.

NAcTrp") was refined as a β-CD–water complex (Table 2). "β-CD–D-NAcTrp" exhibits the "herringbone" packing of the β-CD monomers (Figure 4) as the hydrated β-CD structures reported so far [29,33-35], as well as several monomeric β-CD complexes [32,36,37]. The conformation of the β-CD macrocycle (Supporting Information File 1, Table S3) is similar to the monomeric β-CD structures [29], but more distorted than in the dimeric β-CD–L-NAcTrp complex: The glucopyranose residues adopt the regular $^4C_1$ chair conformation, but the angles between them deviate from the angle of the regular heptagon and the tilt of their average planes towards the 7-fold β-CD axis varies between 5.0 and 25.8°. At the primary side, two hydroxy groups (O61 and O65) point towards the interior of the cavity and two exhibit two-way disorder of the C-O63 and C-O67 bonds.

Comparison of the "β-CD–D-NAcTrp" structure to this of hydrated β-CD [29] pinpoints the difficulty of solving the struc-

Table 2: Details of crystal and structure refinement data of the complexes. β-CD–L-NAcTrp and the β-CD–H2O ("β-CD–D-NAcTrp").

	β-CD–L-NAcTrp	"β-CD–D-NAcTrp"
molecular formula	$C_{110}H_{113.6}N_4O_{97.45}$	$C_{42}H_{49}O_{46.76}$
formula weight	3050.85	1301.98
temperature	100 K	100 K
radiation/wavelength	0.8015	0.80
space group	*P*1	*P*21
a, α	17.760(6) Å, 102.77(3)°	14.970(5) Å
b, β	15.158(6) Å, 99.35(4)°	10.175(2) Å, 112.37(1)°
c, γ	15.237(7) Å, 113.00(3)°	21.298 (4) Å
volume/Z	3538(3) $Å^3$/1	3000(1) $Å^3$/2
density (calculated)	1.432 mg/m^3	1.436 mg/m^3
2θ range for data collection	9.28–57.74°	3.0–47.16°
index ranges	0 < h < 21, −18 < k < 16, −18 < l < 17	−14 < h < 14, −10 < k < 10, −21 < l < 21
reflections collected/unique	26878/11889	9397/5511
solution method	isomorphous replacement	molecular replacement
refinement method	full-matrix least-squares on F^2	full-matrix least-squares on F^2
data[Fo > 4σ(Fo)]/restraints/parameters	11771/184/1983	5516/683/801
goodness-of-fit on F^2	1.076	1.065
R indices [F_o>4σ(F_o)]	R1 = 0.0609, wR2 = 0.1663	R1 = 0.0815, wR2 = 0.1989
R indices (all data)	R1 = 0.0613, wR2 = 0.1674	R1 = 0.0815, wR2 = 0.1989
largest diff. peak and hole	0.87 and −0.52	0.59 and −0.62

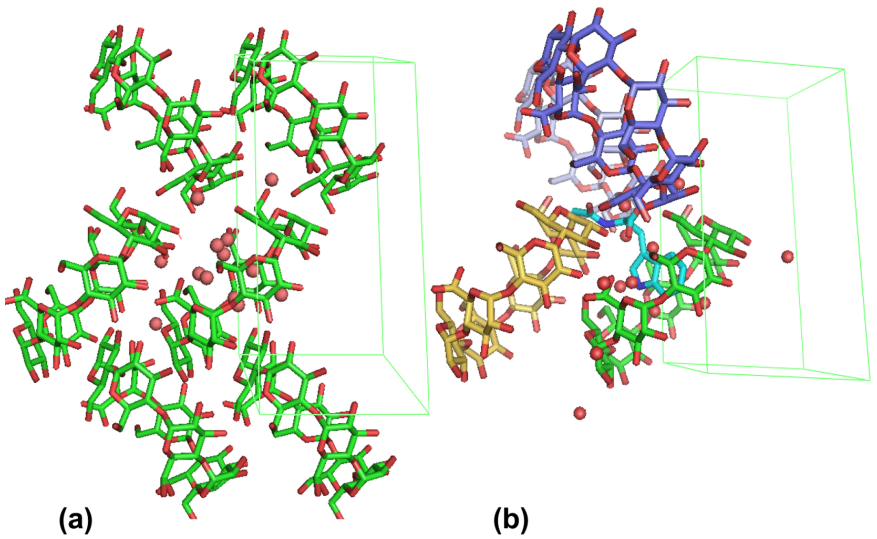

Figure 4: "β-CD–D-NAcTrp" structure. (a) The herring bone packing of β-CD along the *c*-axis; (b) The guest (cyan) can be accommodated in the "β-CD–D-NAcTrp" monomeric structure as indicated by molecular modeling studies (water molecules of the asymmetric unit are shown as spheres).

ture as an isomorph. It can be seen (after the appropriate transformation of coordinates due to different origin and axes; Supporting Information File 1, Figures S4 and S5) that the hydrated β-CD macrocycle does not superpose exactly in the lattice of "β-CD–D-NAcTrp", which may render the two structures not quite isomorphous. It is worth noting that many of the hydrated β-CD structures [29,33-35], as well as several monomeric β-CD complexes [32,36,37] are determined in lattices with different origin or interchanged crystallographic axes or even inverse coordinates (Supporting Information File 1, Figure S4). Further, by superposition of one glucopyranose unit of "β-CD–D-NAcTrp" to the equivalent unit of hydrated β-CD [29] the

difference in coordinates of the two structures is more apparent (Supporting Information File 1, Figure S6). In contrast, the same kind of superposition applied to monomeric structures mentioned above shows that they superpose completely on hydrated β-CD.

Although the NMR results have shown that β-CD forms complexes with both L- and D-NAcTrp in aqueous solution at room temperature, it was not possible to crystallize the β-CD–D-NAcTrp complex. In contrast, the β-CD complexes of both enantiomers of *N*-acetylphenylalanine (NAcPhe) have been determined [18] and they are isomorphous with β-CD–L-NAcTrp. Although the isomorphous complexes of L-NAcPhe and D-NAcPhe exhibit identical packing of the β-CD dimers, the relative stability of the guest molecules enclosed in them is controlled by subtle changes in the guest positioning. L-NAcPhe is highly disordered even at 20 K probably due to very weak non-polar and polar interactions, whereas D-NAcPhe is highly ordered, although the non-polar interactions between the phenyl moieties are also weak. Its stability is gained by the *N*-acetyl group of one D-NAcPhe guest, which rotates and "hides" inside the dimer cavity [18] (probably because of unfavourable exposure to the aqueous environment). Similarly, β-CD–L-NAcTrp is also more stable than β-CD–L-NAcPhe due to the larger side chain of the guest. L-NAcPhe is shorter than in L-NAcTrp, which has two consequences for the stability of the complex (a) no strong π···π interactions at 3.5 Å can be established in the middle of the β-CD dimer as in L-NAcTrp (Figure 5); (b) the aliphatic moieties of β-CD–L-NAcPhe protruding from the primary sides between dimers do not interact directly or even indirectly via β-CD hydroxy groups along the channels, as in the L-NAcTrp complex. Modeling the possibility of formation of a dimer β-CD–D-NAcTrp complex by energy minimization of the interactions of D-NAcTrp inside the β-CD dimer (as determined in the β-CD–L-NAcTrp structure) revealed a complex similar to β-CD–L-NAcTrp (Supporting Information File 1, Figure S7). The positioning of the **D**-indole groups is very similar to these of the L-enantiomer (closest distance 3.46 Å between the aromatic planes). The approaching aliphatic moieties between two β-CD dimers along the channel could be stabilized possibly by an inward pointing hydroxy group O63Bb of β-CD (assuming that the β-CD host remains unchanged), which H-bonds to the carboxylic oxygen atom of the **D** guest and the acetyl O1 atom of the **C** guest, however, the acetyl methyl group of **C** is exposed to the water environment. "Hiding" of the latter group inside the cavity, as in the case of the β-CD–D-NAcPhe complex, is not possible due to the bulkier indole group of D-NAcTrp that fills the cavity. This unfavorable environment might be a factor that forbids the formation of a β-CD–D-NAcTrp dimer structure.

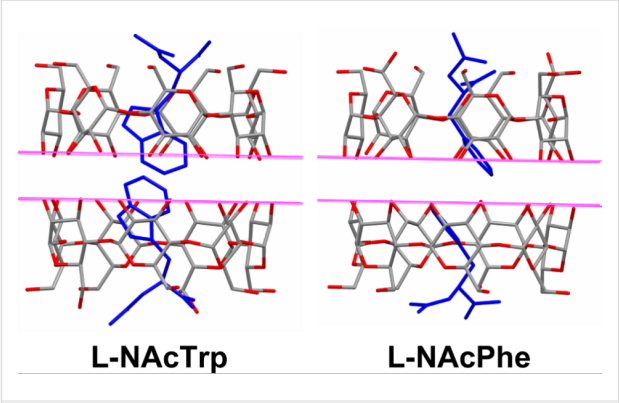

Figure 5: L-NAcTrp and L-NAcPhe in β-CD dimers (the lines indicate the levels of the O2 and O3 secondary hydroxy groups.

The difficulty in crystallizing the β-CD–D-NAcTrp may arise from a higher free energy barrier of crystal nucleation compared to other competing processes in solution at room temperature, but under the higher temperature and pressure conditions of the hydrothermal cell the presence of D-NAcTrp or of the complex β-CD–D-NAcTrp may influence the initial crystal nuclei which eventually lead to the grown crystals and differentiates them slight from hydrated β-CD. It is worth noting that hydrothermal treatment in crystallization trials has yielded uncommon structures such as, novel packing of β-CD–ethanol crystals [31] during trials to crystallize the β-CD–*N*-(1-adamantyl)salicylaldimine complex in ethanol, novel association of β-CD monomers in structures of β-CD complexes, e.g., with 4-pyridinealdazine [30], polyethylene glycol [38] or adamantane [39].

Conclusion

This work has been focused on the ability of β-CD to discriminate between the enantiomers of *N*-acetyltryptophan. NMR studies in aqueous solution show that both enantiomers form similar, but not identical complexes with β-CD. L-NAcTrp induces larger shifts of β-CD cavity protons, suggesting stronger binding. For both enantiomers the prevailing complexation mode involves insertion in the cavity with the *N*-acetyl group in the secondary side and the indole moiety exiting the primary side, more exposed in L- than in D-NAcTrp. The tendency of the *N*-acetyl group to hide in the cavity is considered as the major cause for the differences between the two complexes that also results in somewhat folded NAcTrp structures, compared to the conformation observed in the crystal. In addition, both complexes are in contact with a second β-CD molecule suggesting presence of higher stoichiometries and possibility of different inclusion modes at low concentration. Overall, the orientation of both enantiomeric guests with respect to the macrocycle in the solution structures is opposite to the orientation of L-NAcTrp in ther crystal.

On the other hand, only the complex β-CD–L-NAcTrp crystallizes readily forming a dimeric complex (two host and two guest molecules) packed in broken channels, isomorphous to the known β-CD complexes of the NAcPhe enantiomers. Numerous crystallization trials failed to produce crystals of the β-CD–D-NAcTrp complex yielding only hydrated β-CD crystals. The fact that β-CD–D-NAcTrp could not be crystallized in dimers as the β-CD–L-NAcTrp might be due to destabilization of the interface between dimers, because of exposure of the acetyl group to the water environment of the exterior and the inability to "hide" in the cavity, due to the bulky indole group occupying it. Trials to employ more energetic crystallization conditions resulted in crystals of a slightly different structure than hydrated β-CD crystals. The disagreement between solution and crystal structure in terms of complex formation and orientation/conformation of the guest indicates that the lattice forces and organization in the crystal prevail by far over the soft host–guest contacts established in solution and determines the final orientation of the guest inside the host and the formation of the crystals per se.

Experimental

Materials and methods

N-Acetyl-L-tryptophan (L-NAcTrp), *N*-acetyl-D-tryptophan (D-NAcTrp) and β-CD were obtained from Sigma-Aldrich. Deuterium oxide was a product of Deutero GmbH.

NMR spectroscopy

The spectra were carried out on a 500 MHz Bruker Avance instrument at 300 K using a BBI probe, the library pulse sequences and 300 ms mixing time for the 2D ROESY runs. The compounds were dissolved in unbuffered D_2O. The data was processed with Topspin.

X-ray crystallography

Crystallisation of β-CD–L-NAcTrp. In an aqueous solution of β-CD (6 mM) an equimolar quantity of L-NAcTrp was added and stirred for an hour until the solution became clear, which indicated formation of a complex. Then the solution was placed in an incubator at 23 °C, where by slow evaporation of the solvent, single crystals appropriate for X-ray data collection were obtained. The crystals had a diamond shape and a slightly pink color.

Crystallisation trials of β-CD–D-NAcTrp. Trials to crystallize the complex of β-CD with D-NAcTrp under various conditions, including the above, did not result to single crystals of the complex. D-NAcTrp in the presence of β-CD (6 mM) at 50–60 °C, required a small quantity of ethanol in order to obtain a clear solution, from which crystals of hydrated native β-CD precipitated. This was proved from data collection from several crystals and structure determination based on isomorphous replacement using the coordinates of the β-CD–glutaric acid complex [32], which is isomorphous to hydrated β-CD [29]. Use of racemic mixtures of NAcTrp produced also native β-CD crystals. However, use of a hydrothermal cell [30,31], in which β-CD (0.050 mM) and D-NAcTrp (0.025 mM) were placed in 2 mL of water and left at 65 °C for 5–7 days, produced crystals that could not be refined by isomorphous replacement using the coordinates of hydrated β-CD or other isomorphous crystals, as above.

Structure determination. Low temperature X-ray data were collected at synchrotron radiation light sources. A single crystal, covered with a drop of paraffin oil, was mounted on a hair fiber loop and was instantly frozen to 100 K. Crystal data and analysis details are given in Table 2.

β-CD–L-NAcTrp. Data of the β-CD–L-NAcTrp complex were collected at the beamline X13 of EMBL at DESY, Hamburg, by the oscillation method using a CCD of 165 mm radius detector. The DENZO and SCALEPACK [40] software were used for data processing and scaling, respectively. The unit cell parameters and their esds were determined by the least square method from the high resolution frames of the collected data. The structure was solved by the isomorphous replacement method using the host coordinates of the β-CD–1,12-dodecanodioic acid complex [28]. The structure solution and the refinement were carried out with the SHELXL97 program [41]. The coordinates of the guest and solvent atoms were determined by successive cycles of difference maps and refinement. The non-hydrogen β-CD atoms and the oxygen atoms of the co-crystallized water molecules were treated anisotropically. Hydrogen atoms were placed at idealized positions and refined by the riding model (UH = 1.25 UC). The refinement of the structure, by full matrix least squares, converged to R1 = 0.0609, wR2 = 0.1663 and Goodness-of-fit = 1.076, for Fo > 4σ(Fo). Refinement details appear in CCDC 1531988. The structures were rendered in PyMOL [42].

"β-CD–D-NAcTrp". Diffraction data were collected at the X06DA beamline, Swiss Light Source, Paul Scherrer Institut, Villigen, Switzerland. The XDS [43] software package was used to reduce data and determine the unit cell parameters and space group, which were the same as hydrated β-CD. Trials to use isomorphous replacement (using the coordinates of β-CD–glutaric acid complex [32], which is isomorphous to hydrated β-CD [29], to refine the structure was unsuccessful (vide supra). The structure was solved finally by molecular replacement methods [44] using the β-CD–glutaric acid complex coordinates. The refinement was carried out with the same strategy as in β-CD–L-NAcTrp complex. Early in the refine-

ment numerous peaks appeared mainly at the primary hydroxy side of the cavity. Some were at bonding distances with each other, but by introducing the strongest of them as water molecules into the refinement did not result in a model of the guest (Table 2). Refinement details appear in CCDC 1531987. The structures were rendered in PyMOL [42].

Molecular modeling

The molecular models of D-NAcTrp complexes were based (a) on the geometry of the major orientation of β-CD–L-NAcTrp by changing the chirality of the Cα atom and (b) on β-CD non-hydrogen atoms of the corresponding lattice. To relieve steric clashes, restrained energy minimization of D-NAcTrp have been performed, while non-hydrogen atoms of β-CD are kept fixed in space. The XLEaP module of the AMBER 16 suite [45] was used and the GAFF parameters were applied to the β-CD molecules with AM1-BCC atomic charges using the Antechamber module [46], while the ff99SB parameters were employed for NAcTrp. Restraint energy minimizations in implicit solvent were performed for 1,000 steps using a pairwise generalized Born model [47], while all β-CD non-hydrogen atoms were kept fixed in space using harmonic restraints of 10 kcal/mol $Å^2$. For the "β-CD–D-NAcTrp" complex, the indole moiety was placed inside the β-CD cavity with the aliphatic part protruding from its primary side towards the empty space formed by three neighboring β-CD monomers of the lattice (Figure 4b), whereas for the β-CD–D-NAcTrp dimer model the crystallographic coordinates of the β-CD–L-NAcTrp dimer were employed after changing the chirality of the L-NAcTrp Cα atom only to generate the D-NAcTrp guest molecule.

Supporting Information

Supporting Information File 1

Experimental data containing geometry data of the β-CD hosts; H-bonding interactions in the β-CD dimer; NMR data (Job plots and 2D maps of the observed dipolar interactions); packing, origin selection and comparison of monomeric β-CD complexes; modeling results of D-NAcTrp/β-CD.
[http://www.beilstein-journals.org/bjoc/content/supplementary/1860-5397-13-157-S1.pdf]

Acknowledgements

The financial support of the following programs is kindly acknowledged: European Program FP7-PEOPLE-ITN-2013 "CycloN Hit", project #608407 (M.I.), Empirikion Foundation, Greece and the European MC (HPMT-CT-2000-00174) training site programme (S.D.C.).

References

1. Dodziuk, H. *Cyclodextrins and their complexes. Chemistry, analytical methods, applications;* Wiley-VCH Verlag GmbH & Co. KGaA: Weinheim, 2006. doi:10.1002/3527608982
2. Davis, M. E.; Brewster, M. E. *Nat. Rev. Drug Discovery* **2004,** *3,* 1023–1035. doi:10.1038/nrd1576
3. Kurkov, S. V.; Loftsson, T. *Int. J. Pharm.* **2013,** *453,* 167–180. doi:10.1016/j.ijpharm.2012.06.055
4. Loftsson, T.; Duchêne, D. *Int. J. Pharm.* **2007,** *329,* 1–11. doi:10.1016/j.ijpharm.2006.10.044
5. Stella, V. J.; He, Q. *Toxicol. Pathol.* **2008,** *36,* 30–42. doi:10.1177/0192623307310945
6. Rubin, A.; Knadler, M. P.; Ho, P. P. K.; Bechtol, L. D.; Wolen, R. L. *J. Pharm. Sci.* **1985,** *74,* 82–84. doi:10.1002/jps.2600740122
7. Hamilton, J. A.; Chen, L. *J. Am. Chem. Soc.* **1988,** *110,* 5833–5841. doi:10.1021/ja00225a039
8. Rekharsky, M.; Inoue, Y. *J. Am. Chem. Soc.* **2000,** *122,* 4418–4435. doi:10.1021/ja9921118
9. Mavridis, I. M. Influence of the Guest on the Packing of Dimeric ß-Cyclodextrin Complexes. In *Current Challenges on Large Supramolecular Assemblies;* Tsoucaris, G., Ed.; Part of the NATO Science Series book series, Vol. 519; Kluwer Acad. Publ., 1999; pp 393–403. doi:10.1007/978-94-011-5284-6_28
10. Giastas, P.; Yannakopoulou, K.; Mavridis, I. M. *Acta Crystallogr., Sect. B* **2003,** *B59,* 287–299. doi:10.1107/S010876810300257X
11. Harata, K. *Chem. Rev.* **1998,** *98,* 1803–1828. doi:10.1021/cr9700134
12. Harata, K.; Uekama, K.; Otagiri, M.; Hirayama, F. *Bull. Chem. Soc. Jpn.* **1987,** *60,* 497–502. doi:10.1246/bcsj.60.497
13. Yannakopoulou, K.; Mentzafos, D.; Mavridis, I. M.; Dandika, K. *Angew. Chem., Int. Ed. Engl.* **1996,** *35,* 2480–2482. doi:10.1002/anie.199624801
14. Makedonopoulou, S.; Yannakopoulou, K.; Mentzafos, D.; Lamzin, V.; Popov, A.; Mavridis, I. M. *Acta Crystallogr., Sect. B* **2001,** *B57,* 399–409. doi:10.1107/S0108768101001963
15. García Méndez, S.; Otero Espinar, F. J.; Luzardo Alvarez, A.; Longhi, M. R.; Quevedo, M. A.; Zoppi, A. *J. Inclusion Phenom. Macrocyclic Chem.* **2016,** *85,* 33–48. doi:10.1007/s10847-016-0603-6
16. Aachmann, F. L.; Larsen, K. L.; Wimmer, R. *J. Inclusion Phenom. Macrocyclic Chem.* **2012,** *73,* 349–357. doi:10.1007/s10847-011-0071-y
17. Tao, Y.; Dai, J.; Kong, Y.; Sha, Y. *Anal. Chem.* **2014,** *86,* 2633–2639. doi:10.1021/ac403935s
18. Alexander, J. M.; Clark, J. L.; Brett, T. J.; Stezowski, J. J. *Proc. Natl. Acad. Sci. U. S. A.* **2002,** *99,* 5115–5120. doi:10.1073/pnas.072647599
19. Clark, J. L.; Stezowski, J. J. *J. Am. Chem. Soc.* **2001,** *123,* 9880–9888. doi:10.1021/ja003717v
20. Clark, J. L.; Booth, B. R.; Stezowski, J. J. *J. Am. Chem. Soc.* **2001,** *123,* 9889–9895. doi:10.1021/ja0100221
21. Lipkowitz, K. B.; Raghothama, S.; Yang, J. A. *J. Am. Chem. Soc.* **1992,** *114,* 1554–1562. doi:10.1021/ja00031a003
22. Xiao, Q.; Lu, S.; Huang, C.; Su, W.; Huang, S. *Sensors* **2016,** *16,* 1874. doi:10.3390/s16111874
23. Xu, J.; Wang, Q.; Xuan, C.; Xia, Q.; Lin, X.; Fu, Y. *Electroanalysis* **2016,** *28,* 868–873. doi:10.1002/elan.201500548
24. Qin, L.; He, X.-W.; Li, W.-Y.; Zhang, Y.-K. *J. Chromatogr. A* **2008,** *1187,* 94–102. doi:10.1016/j.chroma.2008.02.004

25. Malta, L. F. B.; Cordeiro, Y.; Tinoco, L. W.; Campos, C. C.; Medeiros, M. E.; Antunes, O. A. C. *Tetrahedron: Asymmetry* **2008,** *19,* 1182–1188. doi:10.1016/j.tetasy.2008.04.035
26. Job, P. *C. R. Hebd. Seances Acad. Sci.* **1925,** *180,* 928–930.
27. Mentzafos, D.; Mavridis, I. M.; Le Bas, G.; Tsoucaris, G. *Acta Crystallogr., Sect. B* **1991,** *B47,* 746–757. doi:10.1107/S010876819100366X
28. Makedonopoulou, S.; Mavridis, I. M. *Acta Crystallogr., Sect. B* **2000,** *B56,* 322–331. doi:10.1107/S0108768199014494
29. Steiner, T.; Koellner, G. *J. Am. Chem. Soc.* **1994,** *116,* 5122–5128. doi:10.1021/ja00091a014
30. Chatziefthimiou, S. D.; Yannakopoulou, K.; Mavridis, I. M. *CrystEngComm* **2007,** *9,* 976–979. doi:10.1039/b709155a
31. Hadjoudis, E.; Yannakopoulou, K.; Chatziefthimiou, S. D.; Paulidou, A.; Mavridis, I. M. *J. Photochem. Photobiol., A: Chem.* **2011,** *217,* 293–298. doi:10.1016/j.jphotochem.2010.10.022
32. Paulidou, A.; Yannakopoulou, K.; Mavridis, I. M. *J. Inclusion Phenom. Macrocyclic Chem.* **2010,** *68,* 297–303. doi:10.1007/s10847-010-9787-3
33. Zabel, V.; Saenger, W.; Mason, S. A. *J. Am. Chem. Soc.* **1986,** *108,* 3664–3673. doi:10.1021/ja00273a020
34. Ivanova, B.; Spiteller, M. *Int. J. Biol. Macromol.* **2014,** *64,* 383–391. doi:10.1016/j.ijbiomac.2013.12.026
35. Ilin, A. *CSD Communication* **2016**, CCDC 1510220.
36. Steiner, T.; Koellner, G.; Gessler, K.; Wolfram, S. *J. Chem. Soc., Chem. Commun.* **1995,** 511–512. doi:10.1039/C39950000511
37. Gessler, K.; Steiner, T.; Koellner, G.; Saenger, W. *Carbohydr. Res.* **1993,** *249,* 327–344. doi:10.1016/0008-6215(93)84098-Q
38. Udachin, K. A.; Wilson, L. D.; Ripmeester, J. A. *J. Am. Chem. Soc.* **2000,** *122,* 12375–12376. doi:10.1021/ja002189k
39. Enright, G. D.; Udachin, K. A.; Ripmeester, J. A. *CrystEngComm* **2010,** *12,* 1450–1453. doi:10.1039/B920581K
40. Otwinowski, Z.; Minor, W. *Methods Enzymol.* **1997,** *276,* 307–326. doi:10.1016/S0076-6879(97)76066-X
41. Sheldrick, G. M.; Schneider, T. R. *Methods Enzymol.* **1997,** *277,* 319–343. doi:10.1016/S0076-6879(97)77018-6
42. DeLano, W. L. *The PyMOL Molecular Graphics System*. DeLano Scientific LLC: San Carlos, CA, USA, 2002; http://www.pymol.org.
43. Kabsch, W. *Acta Crystallogr., Sect. D* **2010,** *D66,* 125–132. doi:10.1107/S0907444909047337
44. Navaza, J. *Acta Crystallogr., Sect. A* **1994,** *A50,* 157–163. doi:10.1107/S0108767393007597
45. Salomon-Ferrer, R.; Case, D. A.; Walker, R. C. *Wiley Interdiscip. Rev.: Comput. Mol. Sci.* **2013,** *3,* 198–210. doi:10.1002/wcms.1121
46. Wang, J.; Wolf, R. M.; Caldwell, J. W.; Kollamn, P. A.; Case, D. A. *J. Comput. Chem.* **2004,** *25,* 1157–1174. doi:10.1002/jcc.20035
47. Tsui, V.; Case, D. A. *Biopolymers* **2000,** *56,* 275–291. doi:10.1002/1097-0282(2000)56:4<275::AID-BIP10024>3.0.CO;2-E

License and Terms

BEILSTEIN JOURNAL OF ORGANIC CHEMISTRY

β-Cyclodextrin- and adamantyl-substituted poly(acrylate) self-assembling aqueous networks designed for controlled complexation and release of small molecules

Liang Yan[1], Duc-Truc Pham[1], Philip Clements[1], Stephen F. Lincoln[*1], Jie Wang[2], Xuhong Guo[*2] and Christopher J. Easton[3]

Full Research Paper

Open Access

Address:
[1]Department of Chemistry, University of Adelaide, Adelaide, SA 5005, Australia, [2]State Key Laboratory of Chemical Engineering, East China University of Science and Technology, Shanghai 200237, China and [3]Research School of Chemistry, Australian National University, Canberra, ACT 0200, Australia

Email:
Stephen F. Lincoln[*] - stephen.lincoln@adelaide.edu.au;
Xuhong Guo[*] - guoxuhong@ecust.edu.cn

* Corresponding author

Keywords:
controlled release; cyclodextrin; network; poly(acrylate); self-assembly

Beilstein J. Org. Chem. **2017,** *13,* 1879–1892.
doi:10.3762/bjoc.13.183

Received: 19 April 2017
Accepted: 21 August 2017
Published: 07 September 2017

This article is part of the Thematic Series "Superstructures with cyclodextrins: Chemistry and applications IV".

Guest Editor: G. Wenz

Abstract

Three aqueous self-assembling poly(acrylate) networks have been designed to gain insight into the factors controlling the complexation and release of small molecules within them. These networks are formed between 8.8% 6^A-(2-aminoethyl)amino-6^A-deoxy-6^A-β-cyclodextrin, β-CDen, randomly substituted poly(acrylate), PAAβ-CDen, and one of the 3.3% 1-(2-aminoethyl)amidoadamantyl, ADen, 3.0% 1-(6-aminohexyl)amidoadamantyl, ADhn, or 2.9% 1-(12-aminododecyl)amidoadamantyl, ADddn, randomly substituted poly(acrylate)s, PAAADen, PAAADhn and PAAADddn, respectively, such that the ratio of β-CDen to adamantyl substituents is ca. 3:1. The variation of the characteristics of the complexation of the dyes methyl red, methyl orange and ethyl orange in these three networks and by β-cyclodextrin, β-CD, and PAAβ-CDen alone provides insight into the factors affecting dye complexation. The rates of release of the dyes through a dialysis membrane from the three aqueous networks show a high dependence on host–guest complexation between the β-CDen substituents and the dyes as well as the structure and the viscosity of the network as shown by ITC, ^{1}H NMR and UV–vis spectroscopy, and rheological studies. Such networks potentially form a basis for the design of controlled drug release systems.

Introduction

The formation of self-assembling aqueous polymer networks through the complexation of hydrophobic polymer substituents by cyclodextrin oligomers [1-4] and cyclodextrin substituted polymers [5-19] to form cross-links between polymer strands is well-established. Depending upon their composition, these networks and related systems retain drug and similar molecules to varying extents which renders them of interest as potential drug delivery systems [20-47]. Generally, the retention and the release of the drug is controlled by the thermodynamics of drug complexation and in some systems the drug release is stimu-

lated by either pH variation [28,30,34] or light irradiation [38,45]. The drug types include small molecular species, exemplified by diflunisal, fluconazole [40] and curcumin [37], along with larger species exemplified by RNA and DNA segments [26,32,33,36,39,47]. Some systems are designed to target specific tissues [26,35].

We are particularly interested in the extent to which small molecule guest complexation and release characteristics may be designed into the structure of aqueous networks formed between a β-cyclodextrin-substituted poly(acrylate) and three adamantyl-substituted poly(acrylate)s. Accordingly, we report an ITC, ^{1}H NMR and UV–vis spectroscopic and rheological study of three self-assembling networks formed between the 8.8% 6^A-(2-aminoethyl)amino-6^A-deoxy-6^A-β-cyclodextrin, β-CDen, randomly substituted poly(acrylate), PAAβ-CDen [13], and 3.3% 1-(2-aminoethyl)amido-adamantyl, ADen, 3.0% 1-(6-aminohexyl)amidoadamantyl, ADhn, or 2.9% 1-(12-aminododecyl)amidoadamantyl, ADddn, randomly substituted poly(acrylate)s, PAAADen [11], PAAADhn [15] and PAAADddn [15], respectively, where the poly(acrylate) is of 250 kDa average molecular weight prior to substitution (Figure 1). The network formation is driven by the β-CDen substituents complexing the adamantyl substituents, ADen, ADhn or ADddn, to form cross-links between the PAAβ-CDen strands and the PAAADen, PAAADhn or PAAADddn strands. The adamantyl group is selected as the guest substituent as it is strongly complexed by β-CD [48], β-CD oligomers [3,4] and β-CD-substituted polymers [10,14,16], and drives the self-assembly of aqueous chitosan [1,5,9], hyaluronic acid [8,9] and poly(acrylate) networks [14,15,19]. In aqueous solutions equimolar in PAAβ-CDen strands and PAAADen, PAAADhn or PAAADddn strands, the concentration of the β-CDen substituents is in ca. three-fold excess over that of the adamantyl substituents as a consequence of the ca. three-fold greater percentage substitution of PAAβ-CDen. Thus, when host–guest complexation between the poly(acrylate) substituents of the network is complete, ca. two thirds of the β-CDen substituents remain available to complex other hydrophobic species exemplified by the dyes methyl red, MR, methyl orange, MO, and ethyl orange, EO, chosen for this study (Figure 1).

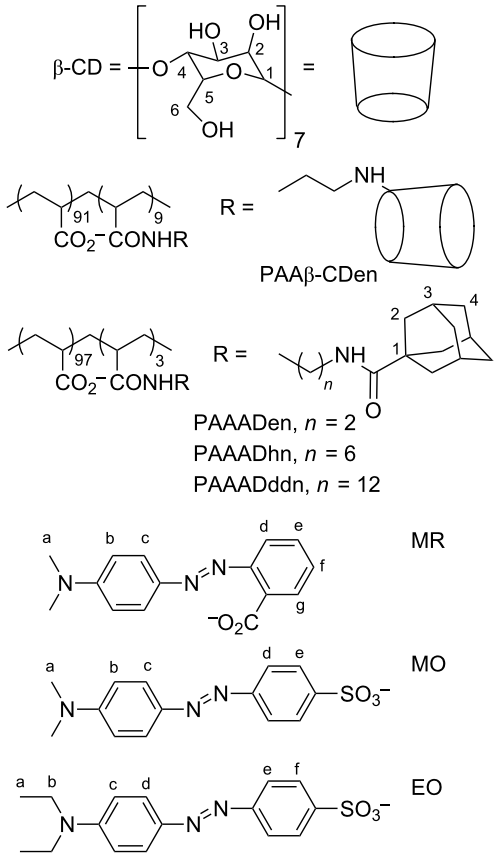

Figure 1: β-Cyclodextrin- and adamantyl-substituted poly(acrylate)s PAAβ-CDen, PAAADen, PAAADhn, and PAAADddn (carbon atoms labelled numerically), and the anionic dyes methyl red, MR, methyl orange, MO, and ethyl orange, EO (carbon atoms labelled alphabetically).

Results and Discussion

Isothermal titration calorimetry (ITC) studies of substituted poly(acrylate) network formation

In aqueous solution, the host β-CDen substituents of PAAβ-CDen complex the guest adamantyl substituents of PAAADen, PAAADhn and PAAADddn to form poly(acrylate) networks as exemplified by the PAAβ-CDen/PAAADen system according to Equation 1. The complexation constant, K, for the host–guest complexation between the β-CDen and ADen substituents within the network is given by Equation 2. The data for the titration of a PAAβ-CDen solution into a PAAADen, a PAAADhn, or a PAAADddn solution together with the best-fit of an algorithm for a single complexation (Equation 1) for the PAAβ-CDen/PAAADen system (and analogous equations for the other two systems) to these data appear in Figure 2 and Figure 3 and Figure S1 in Supporting Information File 1. The derived K and the corresponding ΔH, $T\Delta S$, and N values are given in Table 1. The ratio of the number of ADen substituents of PAAADen complexed by a single β-CDen substituent of PAAβ-CDen, N, is expected to be unity for unhindered 1:1 complexation and corresponds to the ratio of complexed β-CDen substituents to complexed adamantyl substituents at the inflexion point of the ITC titration curve (Equation 3). However, the N = 0.78 and 0. 87 derived for each β-CDen substituent complexing either a ADen or ADhn substituent, respectively, are less than unity as also observed in other studies [1,3-5,8].

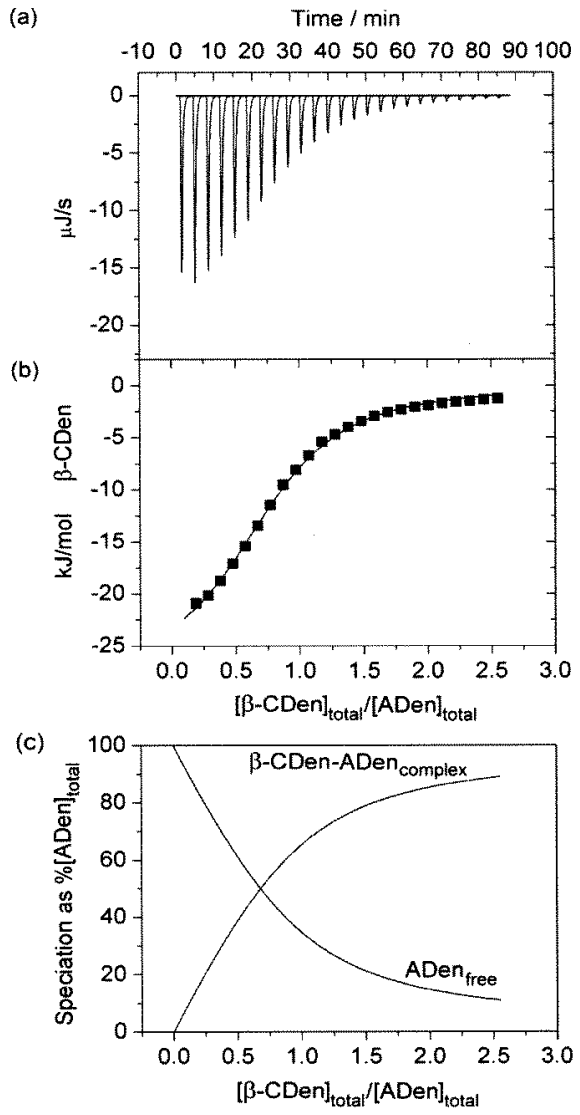

Figure 2: ITC data for the PAAβ-CDen/PAAADen, system obtained in aqueous Na_2HPO_4/KH_2PO_4 pH 7.0 buffer at I = 0.10 mol dm^{-3}. (a) Titration of 10 mm^3 aliquots of 0.62 wt % PAAβ-CDen ([β-CDen] = 2.84 × 10^{-3} mol dm^{-3}) into 1.46 cm^3 of 0.062 wt % PAAADen ([ADen] = 2.06 × 10^{-4} mol dm^{-3}). (b) The solid curve shows the best fit of an algorithm for host–guest complexation between the β-CDen and ADen substituents to the titration data points. (c) Speciation plots showing for the variation of the $[β\text{-CDen–ADen}]_{complex}$ and of the $[ADen]_{free}$ as percentage a of $[ADen]_{total}$ = 100%.

This is attributed to either steric hindrance by the poly(acrylate) backbone, or hydrophobic association of the adamantyl substituents, or both, hindering complexation.

$$\beta\text{-CDen} + \text{ADen} \underset{}{\overset{K}{\rightleftharpoons}} \beta\text{-CDen–ADen} \qquad (1)$$

$$K = [\beta\text{-CDen–ADen}]/([\beta\text{-CDen}][\text{ADen}]) \qquad (2)$$

$$N = [\beta\text{-CDen}]_{complexed}/[\text{ADen}]_{complexed} \qquad (3)$$

The PAAβ-CDen/PAAADddn system contrasts with the other two systems in that N = 1.45 is consistent with one β-CDen substituent complexing the adamantyl group of the ADddn substit-

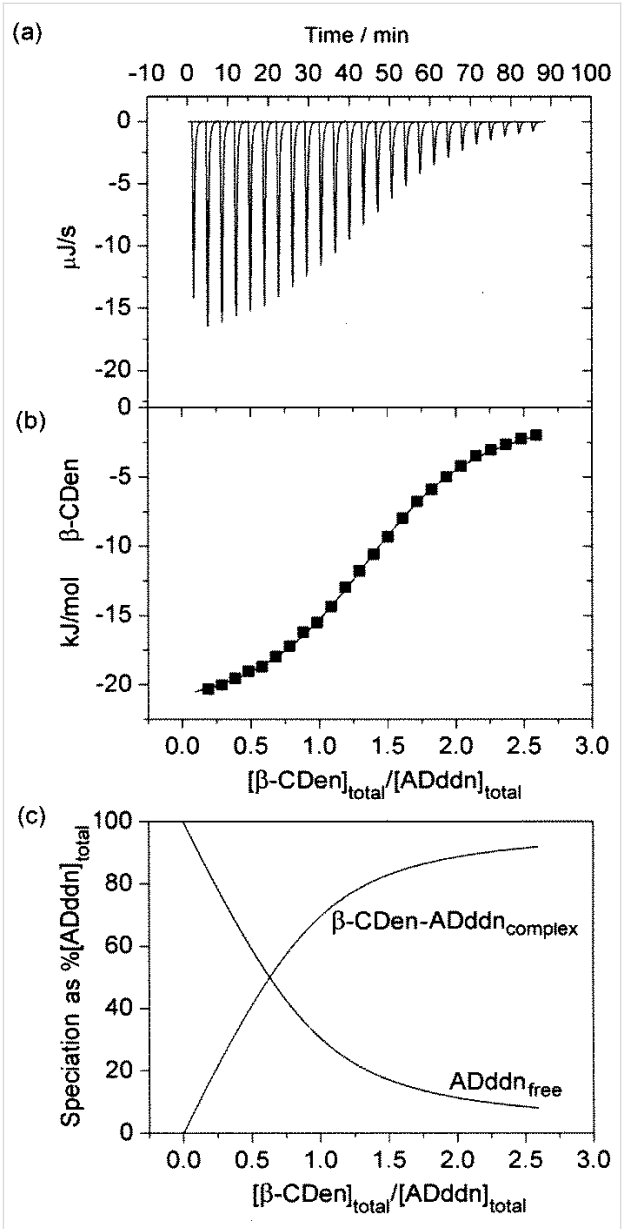

Figure 3: ITC data for the PAAβ-CDen/PAAADddn system obtained in aqueous Na_2HPO_4/KH_2PO_4 pH 7.0 buffer at I = 0.10 mol dm^{-3}. (a) Titration data: for each system 10 mm^3 aliquots of a 0.62 wt % PAA β-CDen solution ([β-CDen] = 2.84 × 10^{-3} mol dm^{-3}) into 1.46 cm^3 of 0.064 wt % PAAADddn ([ADddn] = 1.91 × 10^{-4} mol dm^{-3}). (b) The solid curve shows the best fit of an algorithm for host–guest complexation between the β-CDen and ADddn substituents to the titration data. (c) Speciation plot showing the variation of $[β\text{-CDen–ADddn}]_{complex}$ and of $[ADen]_{free}$ as a percentage of $[ADddn]_{total}$ = 100%.

Table 1: Parameters for host–guest complexation between PAAβ-CDen and PAAADen, PAAADhn, or PAAADddn.[a]

Host	PAAβ-CDen[b]		
Guest	PAAADen	PAAADhn	PAAADddn
$10^{-3}K$ dm^3 mol^{-1}	28.2 ± 0.15	28.4 ± 0.15	39.5 ± 0.08
ΔH kJ mol^{-1}	−27.81 ± 0.55	−25.74 ± 0.48	−22.36 ± 0.09
$T\Delta S$ kJ mol^{-1}	−2.42 ± 0.05	−0.35 ± 0.01	3.85 ± 0.08
N	0.78 ± 0.01	0.87 ± 0.01	1.45 ± 0.01
Host		β-CD[c]	
Guest	PAAADen	PAAADhn	PAAADddn
$10^{-3}K$ dm^3 mol^{-1}	8.77 ± 0.24	14.4 ± 0.06	5.77 ± 0.18
ΔH kJ mol^{-1}	−20.81 ± 0.12	−15.45 ± 0.09	−16.58 ± 0.17
$T\Delta S$ kJ mol^{-1}	1.72 ± 0.18	8.29 ± 0.18	4.89 ± 0.24
N	0.86 ± 0.07	0.85 ± 0.06	0.83 ± 0.05

[a]In aqueous Na_2HPO_4/KH_2PO_4 buffer at pH 7.0 and I = 0.10 mol dm^{-3}. [b]This study. [c]Data from [3] obtained under identical conditions to those of this study. The errors shown are the fitting errors, and the experimental error is ≤5% in both studies.

uent and a second β-CDen substituent complexing its dodecyl tether in the sequence shown in Figure 4. (Alternatively, the dodecyl tether may be complexed first followed by complexation of the adamantyl group. A further possibility is that the adamantyl group may pass through the annulus of one β-CDen substituent to be complexed by a second β-CDen substituent.) The titration curve (Figure 3) could not be resolved into two separate curves consistent with the two complexations being akin to a chelation process which arises from the greater length and flexibility of the dodecyl tether. Ideally, N = 2 should be observed for such a process, but it appears that either the steric hindrance or hydrophobic association of the adamantyl substituents, or both, restrict N to <2. The 2D NOESY ^{1}H NMR spectrum of the PAAβ-CDen/PAAADddn system confirms the complexation of both the adamantyl group and its dodecyl tether as is discussed below.

The large K for the PAAβ-CDen/PAAADen and PAAβ-CDen/PAAADhn systems are mainly due to substantial ΔH contributions (Table 1). The negative $T\Delta S$ for the PAAβ-CDen/PAAADen system is attributable to the entropy loss arising from the combination of the β-CDen and ADen substituents into a single complex and network formation outweighing the entropy gain [49,50] anticipated for the displacement of water from the β-CDen annulus by the ADen substituent. This offset is smaller for the PAAβ-CDen/PAAADhn system possibly because the ADhn substituent hexyl tether allows more network flexibility. The K for the PAAβ-CDen/PAAADddn system is the largest observed as a consequence of a smaller ΔH being offset by a positive $T\Delta S$. This probably arises from the entropy loss expected for complexation of the adamantyl group and the dodecyl tether of the ADddn substituent and network formation being outweighed by the entropy gain arising from displacement of water from the β-CDen annulus by the adamantyl group of ADddn and its dodecyl tether (under the titration conditions the solutions remain fluid whereas at higher concentrations the solution viscosity increases as the network formation becomes more extensive as discussed in the Rheological studies section).

A comparison with the complexation parameters for the β-CD/PAAADen, β-CD/PAAADhn and β-CD/PAAADddn systems from the literature (Table 1) shows these systems to be characterized by significantly smaller K and ΔH and more positive $T\Delta S$ [3]. (The N = 0.86 − 0.83 are also consistent with either the steric hindrance by the poly(acrylate) backbone, or the hydrophobic association of the adamantyl substituents, or both, hindering complexation). The greater stabilities of the PAAβ-CDen/PAAADen and PAAβ-CDen/PAAADhn systems are attributable to the cooperative stabilizing effect of network formation facilitated by β-CDen, ADen and ADhn being substituents on the poly(acrylate) backbone, and an accompanying decrease in entropy. The N = 1.45 and 0.83 (Table 1) for the PAAβ-CDen/PAAADddn and β-CD/PAAADddn systems, respectively, indicate the greater effect of the dodecyl tether on complexation in the first system by comparison with the second system where some complexation of the dodecyl tether occurs as indicated by ^{1}H NMR spectroscopy but does not result in significant network formation [14].

^{1}H NMR studies of substituted poly(acrylate) network formation

Further insight into the complexation process is gained from the 2D NOESY ^{1}H NMR spectrum of a D_2O solution of PAAβ-CDen and PAAADen in which the β-CDen and ADen substitu-

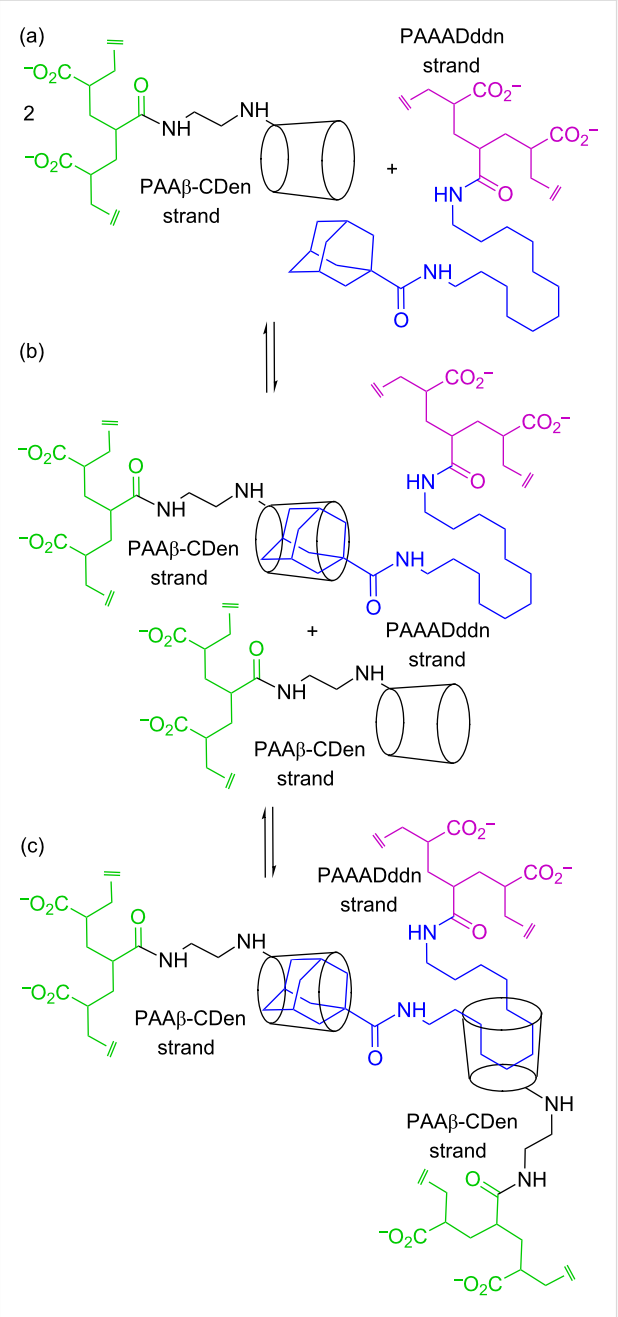

Figure 4: Representation of ditopic complexation of an ADddn substituent of PAAADddn, by two β-CDen substituents of PAAβ-CDen through initial complexation of the adamantyl group followed by complexation of the dodecyl linker in the sequence (a) to (b) to (c).

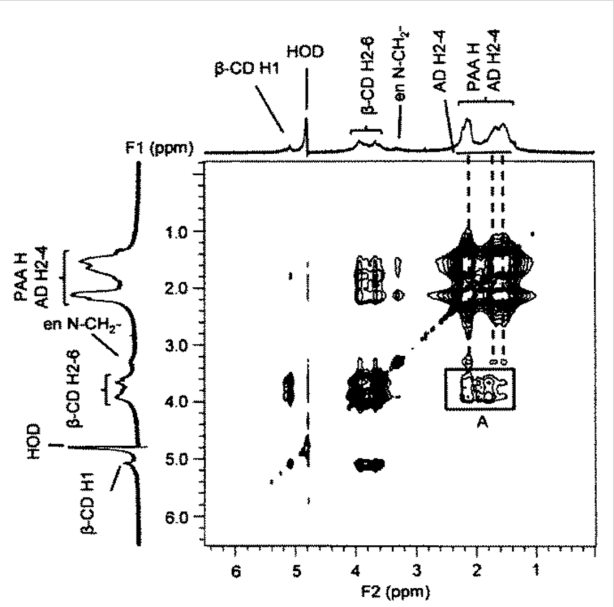

Figure 5: 2D NOESY ^{1}H NMR spectrum of 0.44 wt % PAAβ-CDen ([β-CDen] = 2.0 × 10^{-3} mol dm^{-3}) and 0.60 wt % PAAADen ([ADen] = 2.0 × 10^{-3} mol dm^{-3}) in D_2O Na_2HPO_4/KH_2PO_4 buffer at pD 7.0 and I = 0.10 mol dm^{-3} at 298.2 K. The cross-peaks in box A are attributed to dipolar interactions between the annular H3,5,6 protons of the β-CD of the β-CDen substituents and the H2–4 protons of the ADen substituents.

ents are equimolar (Figure 5). Substitution of β-CD at $C6^A$, as in PAAβ-CDen, renders all of the D-glucopyranose subunits inequivalent such that distinction between the H2–6 resonances is not possible as a consequence of small differences in the chemical shifts of the resonances of each D-glucopyranose subunit which results in a loss of definition in the β-CDen substituent spectrum. Thus, the cross-peaks in box A in Figure 5 cannot be unequivocally assigned to the anticipated dominant dipolar interactions between the β-CDen annular H3,5,6 protons and the H2–4 ADen protons of the host–guest complex, but they are consistent with such an interaction. The analogous spectrum for the PAAβ-CDen/PAAADhn system (Figure S2, Supporting Information File 1) also shows cross-peaks attributable to dipolar interactions between the β-CDen annular H3,5,6 protons and the H2–4 ADhn protons. (The 2D NOESY ^{1}H NMR spectrum of PAAβ-CDen alone (Figure S3, Supporting Information File 1) shows no cross-peaks in the region where those assigned to β-CDen/ADen substituent dipolar interactions arise (Figure 5) indicating that β-CDen substituent proton dipolar interactions with PAAβ-CDen backbone protons are insignificant.) The similarity of the spectra in Figure 5 and Figure S2 (Supporting Information File 1) and the K, ΔH, $T\Delta S$ and N data (Table 1) for the PAAβ-CDen/PAAADen and PAAβ-CDen/PAAADhn systems is consistent with their host–guest interactions being similar in nature.

The 2D NOESY ^{1}H NMR spectrum of a D_2O solution of PAAβ-CDen and PAAADddn in which the β-CDen and ADddn substituents are equimolar shows cross-peaks arising from dipolar interactions between the annular H3,5,6 protons of the β-CDen substituent and also those of the H2–4 ADddn protons and the methylene protons of its dodecyl tether (Figure S4, Supporting Information File 1). This is consistent with complexation of both the adamantyl group and the dodecyl tether of the

ADddn substituent by the β-CDen substituent, and thereby the likelihood of simultaneous complexation by two β-CDen substituents as previously discussed. (It has been reported that NOESY ^{1}H NMR cross-peaks between the β-CD annular H3,H5,H6 annular protons and both the H2–4 ADddn protons and the methylene protons of its dodecyl tether are also observed for solutions of β-CD and PAAADddn [14].)

UV–vis dye complexation studies

The complexations of the three dyes by β-CD alone in aqueous solution are used as a basis for assessing the effects of the substitution of β-CDen onto poly(acrylate) in PAAβ-CDen and the subsequent network formation with PAAADen, PAAADhn and PAAADddn on dye complexation. The variation of absorbance of all three dyes with added β-CD is consistent with the dominant formation of 1:1 β-CD–dye complexes (Equation 4 and Equation 5 where A, ε_{dye} and $\varepsilon_{\beta\text{-CD–dye}}$ represent the observed absorbance and the molar absorbance of the dye and the β-CD–dye complex, respectively) as seen for EO, MO and MR in Figures S5–S7 (Supporting Information File 1), respectively. The wavelengths at which the maximum absorbances occur for the three dyes in their free and complexed states, λ_{max}, and the derived K_{11} (Table 2) were determined by best-fitting an algorithm derived from Equations 4–6 to the titration absorbance data using a nonlinear least-squares program, HypSpec [51,52]. The largest and smallest K_{11} characterize the β-CD–EO and β-CD–MR host–guest complexes, respectively, and probably reflect the favorable stereochemistry of EO for complexation and its greater hydrophobicity.

$$\beta\text{-CD} + \text{dye} \overset{K_{11}}{\rightleftharpoons} \beta\text{-CD–dye} \quad (4)$$

$$K_{11} = [\beta\text{-CD–dye}]/([\beta\text{-CD}][\text{dye}]) \quad (5)$$

$$A = \varepsilon_{dye}[\text{dye}] + \varepsilon_{\beta\text{-CD–dye}}[\beta\text{-CD–dye}] \quad (6)$$

Systematic UV–vis absorbance changes also occur for the dyes upon addition of PAAβ-CDen as seen for EO in Figure 6 and MO and MR in Figures S8 and S9 (Supporting Information File 1), respectively. The K_{11}, determined through an algorithm derived from equations analogous to Equations 4–6 in which β-CD is replaced by the β-CDen substituent, are substantially decreased in magnitude by comparison with those derived in the presence of β-CD, particularly for MR (Table 2). This is attributable to a combination of steric hindrance caused by the poly(acrylate) backbone and repulsion between the PAAβ-CDen carboxylate groups and the negatively charged dyes.

Table 2: Dye UV–vis absorption λ_{max} and complexation constants, K_{11}, for complexation of MR, MO and EO by β-CD, β-CDen substituents of PAAβ-CDen and β-CDen substituents of PAAβ-CDen substituted poly(acrylate) in binary mixtures with PAAADen, PAAADhn or PAAADddn.

Host	Dye	Dye λ_{max} [nm]	K_{11}[a] [dm^3 mol^{-1}]
None	MR	430	–
	MO	464	–
	EO	474	–
β-CD	MR	414	772 ± 10
	MO	455	3255 ± 35
	EO	466	10515 ± 110
PAAβ-CDen	MR	415	76 ± 1
	MO	458	1454 ± 20
	EO	463	2230 ± 30
PAAβ-CDen/PAAADen	MR	–	–
	MO	457	1000 ± 10
	EO	463	1475 ± 20
PAAβ-CDen/PAAADhn	MR	–	–
	MO	457	875 ± 10
	EO	463	1411 ± 20
PAAβ-CDen/PAAADddn	MR	–	–
	MO	457	713 ± 10
	EO	467	986 ± 20

[a]In aqueous Na_2HPO_4/KH_2PO_4 buffer at pH 7.0 and I = 0.10 mol dm^{-3} at 298.2 K. The errors shown are fitting errors. The experimental error is ≤5%.

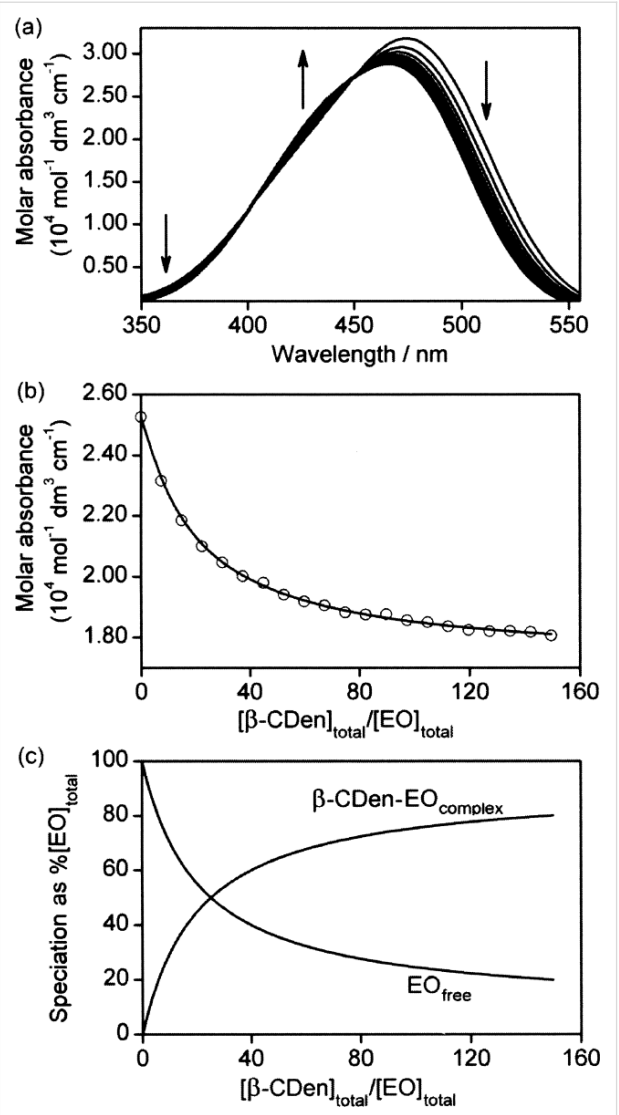

Figure 6: (a) Molar absorbance variation of 1.5 cm^3 of a EO solution ([EO] = 2.00 × 10^{-5} mol dm^{-3}) with 20 sequential additions of a PAAβ-CDen solution (50 mm^3 each, 0.98 wt %, [β-CDen] = 4.49 × 10^{-3} mol dm^{-3}) at 298.2 K. Both solutions were prepared in aqueous Na_2HPO_4/KH_2PO_4 buffer at pH 7.0 and I = 0.10 mol dm^{-3}. The arrows indicate the direction of molar absorbance variation upon each addition of PAAβ-CDen solution. (b) Molar absorbance variation at 500 nm and the line representing the best fit of an algorithm for a 1:1 host–guest complexation of EO by β-CDen substituents of PAAβ-CDen over the wavelength range 475–525 nm. (c) Speciation plot with $[EO]_{total}$ = 100% as the ratio $[\beta\text{-CDen}]_{total}/[EO]_{total}$ increases.

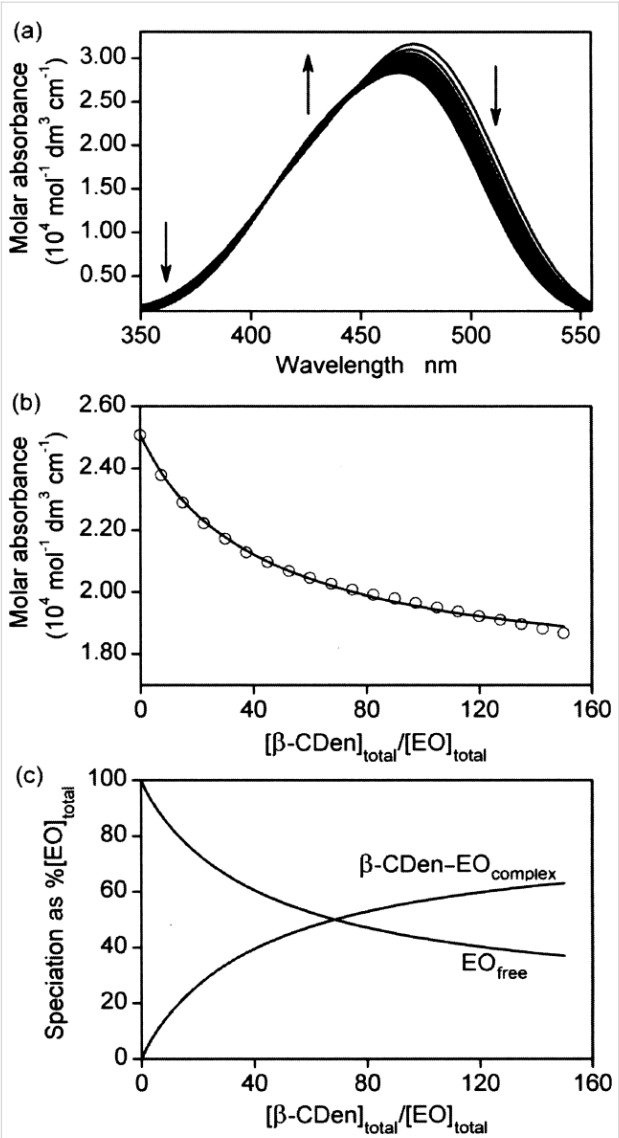

Figure 7: (a) Molar absorbance variation of 1.5 cm^3 of a EO solution ([EO] = 2.00 × 10^{-5} mol dm^{-3}) with 20 sequential additions of a PAAβ-CDen solution (25 mm^3 each, 1.93 wt %, [β-CDen] = 9.03 × 10^{-3} mol dm^{-3}) and a PAAADhn solution (25 mm^3 each, 0.98 wt %, [ADhn] = 3.00 × 10^{-3} mol dm^{-3}) at 298.2 K. All solutions were prepared in aqueous Na_2HPO_4/KH_2PO_4 buffer solutions at pH 7.0 and I = 0.10 mol dm^{-3}. The arrows indicate the direction of molar absorbance variation upon each addition of the PAAβ-CDen and PAAADhn solutions. (b) Molar absorbance variation at 500 nm and the line representing the best-fit of an algorithm for a 1:1 host–guest complexation of EO by β-CDen substituents in the self-assembled PAAβ-CDen/PAAADhn network over the wavelength range 475–525 nm. (c) Speciation plot with $[EO]_{total}$ = 100% as the ratio $[\beta\text{-CDen}]_{total}/[EO]_{total}$ increases.

The UV–vis variations observed for titration of the dyes with PAAβ-CDen and PAAADen, PAAADhn, or PAAADddn, as exemplified by the ternary PAAβ-CDen/PAAADhn/EO system (Figure 7), reflect the competition between the dye and the adamantyl substituent groups (and also the dodecyl tether for PAAADddn) and the dye for complexation by the β-CDen substituents of PAAβ-CDen, as do the derived K_{11} (Table 2). Thus, there are two competing equilibria for complexation by the β-CDen substituent in the PAAβ-CDen/PAAADhn network as shown in Equation 1 and Equation 7. The K_{11} for the host–guest complexation between the β-CDen substituents in the self-assembled PAAβ-CDen/PAAADhn network and the dye is defined by Equation 8 where [β-CDen], [dye] and [β-CDen–dye] represent the concentration of the β-CDen substituents in the PAAβ-CDen/PAAADhn network, the dye, and

the dye complex at equilibrium, respectively. Given that $[\beta\text{-CDen}]_{total}$ and $[dye]_{total}$ are the total concentrations; mass balances are given by Equation 9 and Equation 10. The UV–vis absorbance at a particular wavelength is given by Equation 11 where A, ε_{dye} and $\varepsilon_{PAA\beta\text{-CDen–dye}}$ represent the observed absorbance and molar absorbance of the dye and the host–guest complex, respectively. The K_{11} (Table 2) were derived by best-fitting an algorithm based on Equations 1–3 and 7–11 to the UV–vis absorbance data using the HypSpec protocol [51,52].

$$\beta\text{-CDen} + dye \rightleftharpoons \beta\text{-CDen–dye} \quad (7)$$

$$K_{11} = [\beta\text{-CDen–dye}]/([\beta\text{-CDhn}][dye]) \quad (8)$$

$$[\beta\text{-CDen}]_{total} = [\beta\text{-CDen}] + [\beta\text{-CDen–ADhn}] + [\beta\text{-CDen–dye}] \quad (9)$$

$$[dye]_{total} = [dye] + [\beta\text{-CDen–dye}] \quad (10)$$

$$A = \varepsilon_{dye}[dye] + \varepsilon_{PAA\beta\text{-CDen–dye}}[\beta\text{-CDen–dye}] \quad (11)$$

The variation of the β-CDen–EO complex concentration in the PAAβ-CDen/PAAADhn/EO network occurring during the course of titration is shown in Figure 7, and the accompanying changes in free β-CDen, β-CDen–ADhn complex and β-CDen–EO complex concentrations are shown in Figure 8.

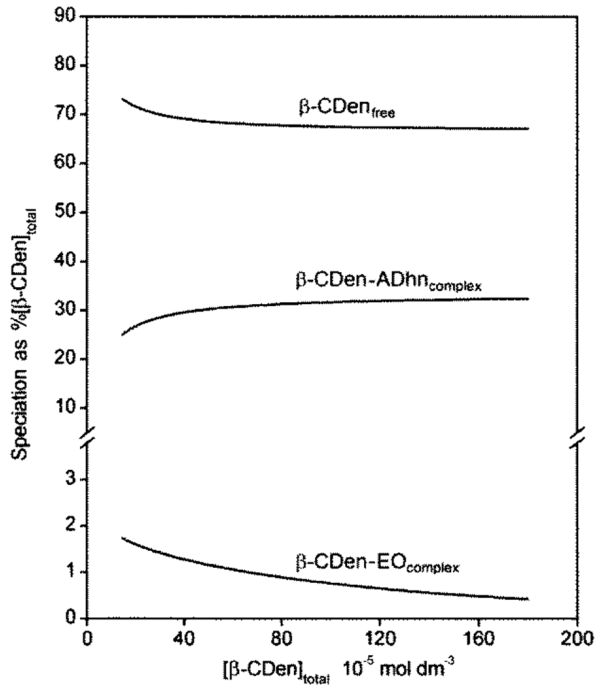

Figure 8: Speciation plot with $[\beta\text{-CDen}]_{total}$ = 100% for the PAAβ-CDen/PAAADhn/EO system.

The analogous data for PAAβ-CDen/PAAADen/EO are quite similar (Figures S10 and S11, Supporting Information File 1) whereas those for PAAβ-CDen/PAAADddn/EO (Figures S12 and S13, Supporting Information File 1) differ considerably. The corresponding data for the PAAβ-CDen/PAAADen/MO, PAAβ-CDen/PAAADhn/MO and PAAβ-CDen/PAAADddn/MO systems appear in Figures S14–S19 (Supporting Information File 1). Collectively, these data facilitate determination of K_{11} for these six systems (Table 2) from which it is seen that in each case K_{11} is further decreased by comparison with that determined for complexation by β-CD and PAAβ-CDen, probably because of increased steric crowding within the network. The largest decreases in K_{11} occur for the PAAβ-CDen/PAAADddn/MO and PAAβ-CDen/PAAADddn/EO systems; decreases which may reflect the additional competition between the ADddn substituent dodecyl tether and the dyes for complexation by the β-CDen substituents. (The UV–vis absorbance changes observed for MR in the three networks (Figures S20–S22, Supporting Information File 1) are too small for derivation of K_{11} consistent with further decreases in K_{11} as also observed for the complexation of EO and MO in the analogous systems.)

Equimolar D_2O solutions of β-CD and each of the three dyes show 2D ^{1}H ROESY NMR cross-peaks arising from dipolar interactions between the β-CD annular H3,5,6 protons and those of the dye (Figures S23–S25, Supporting Information File 1) consistent with dye complexation. The 2D ^{1}H NOESY NMR spectra of solutions of PAAβ-CDen/dye, PAAβ-CDen/PAAADen/dye, PAAβ-CDen/PAAADhn/dye or PAAβ-CDen/PAAADddn/dye, where the β-CDen concentration is 3.6×10^{-3} mol dm^{-3}, the adamantyl substituent concentration is 1.2×10^{-3} mol dm^{-3} in the last three systems and the dye concentration is 2.0×10^{-3} mol dm^{-3} show cross-peaks arising from dipolar interactions between the β-CDen annular H3,5,6 protons and those of the dye, as seen for the PAAβ-CDen/PAAADen/MR system in Figure 9 (analogous cross-peaks occur in the spectra for the other eleven systems as shown in Figures S26–S36, Supporting Information File 1), consistent with dye complexation in all twelve systems. Thus, despite the K_{11} for complexation of MR by the PAAβ-CDen/PAAADen, PAAβ-CDen/PAAADhn and PAAβ-CDen/PAAADddn networks being too small for reliable determination in the UV–vis studies, the observation of significant cross-peaks arising from dipolar interactions between the β-CDen substituent annular H3,5,6 protons and the MR Ha–g protons indicate the occurrence of complexation.

Rheological studies

At higher solution concentrations than those studied by UV–vis spectroscopy, the networks formed by the three combinations:

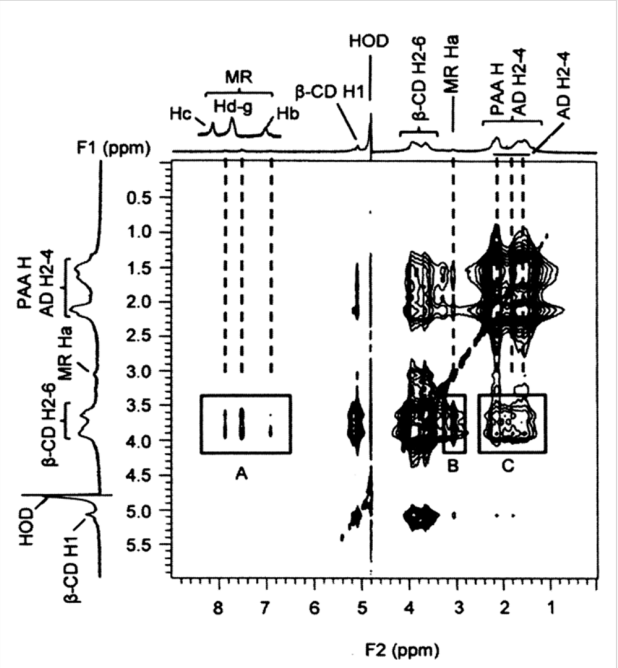

Figure 9: 2D NOESY ^{1}H NMR spectrum of MR ([MR] = 2.0×10^{-3} mol dm^{-3}) in solution with PAAβ-CDen (0.78 wt %, [β-CDen] = 3.6×10^{-3} mol dm^{-3}) and PAAADen (0.40 wt %, [ADen] = 1.2×10^{-3} mol dm^{-3}) in D_2O Na_2HPO_4/KH_2PO_4 buffer solution at pD 7.0 and I = 0.10 mol dm^{-3} at 298.2 K. Cross-peaks in boxes A and B are attributed to dipolar interactions of the annular H3,5,6 protons of β-CDen and the aromatic (Hb–g) and methyl (Ha) protons of MR, respectively. Cross-peaks in box C arise from dipolar interactions between the annular H3,5,6 protons of β-CDen and the H2–4 protons of ADen.

PAAβ-CDen/PAAADen, PAAβ-CDen/PAAADhn and PAAβ-CDen/PAAADddn separately and when complexing MR, MO or EO form hydrogels, the viscosities of which were determined by rheology. In each hydrogel [β-CDen] = 3.60×10^{-3} mol dm^{-3} and [ADen, ADhn or ADddn] = 1.20×10^{-3} mol dm^{-3}, the concentration of each dye was 2.00×10^{-3} mol dm^{-3} and the overall concentration of substituted poly(acrylate)s was 1.14–1.20 wt %. (These hydrogel compositions are identical to those used in the dye release studies discussed below, and are presented in Table S1, Supporting Information File 1.) The viscosity variation of each system with the shear rate is shown for the binary systems PAAβ-CD/PAAADen, PAAβ-CD/PAAADhn and PAAβ-CD/PAAADddn in Figure S37 (Supporting Information File 1), and for the ternary systems in which each of the binary systems complexes the three dyes in Figure S38, Supporting Information File 1). The viscosities show small variations in the shear rate and those determined at 0.03 s^{-1} shear rate are selected for comparison purposes. (Because it was necessary to quantitatively determine the rates of dye release from these hydrogels, their fluidities must be sufficient to allow their quantitative transfer into the dye release measurement apparatus (Figure S39, Supporting Information File 1), and this determined their maximum component concentrations.)

The viscosity variations at a 0.03 s^{-1} shear rate for all twelve systems are shown in Figure 10 from which it is seen that, in the absence of dyes, the viscosities of the binary systems increase in the sequence: 1.14 w % PAAβ-CDen/PAAADen (1.44 Pa s) < 1.18 wt % 1.20 wt % PAAβ-CDen/PAAADhn (1.75 Pa s) < PAAβ-CDen/PAAADddn (4.85 Pa s). Thus, it appears that the two-fold β-CDen complexation of both the adamantyl group and the dodecyl tether of the ADddn substituent in the PAAβ-CDen/PAAADddn system (Figure 4), deduced to be present from the ITC and 2D NOESY ^{1}H NMR studies, increases the viscosity and extent of network formation of the 1.20 wt % solutions of this system by comparison with those of the PAAβ-CDen/PAAADen and PAAβ-CDen/PAAADhn systems.

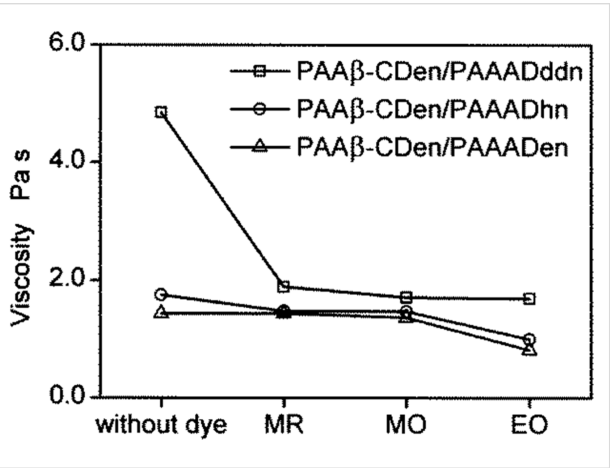

Figure 10: Viscosity variations at a 0.03 s^{-1} shear rate of 1.14 wt % PAAβ-CDen/PAAADen, 1.18 wt % PAAβ-CDen/PAAADhn, or 1.20 wt % PAAβ-CDen/PAAADddn in the absence and presence of MR, MO, or EO at 298.2 K in aqueous Na_2HPO_4/KH_2PO_4 buffer at pH 7.0 and I = 0.10 mol dm^{-3}. In each system, the concentrations of the β-CDen and adamantyl substituents were 3.60×10^{-3} mol dm^{-3} and 1.20×10^{-3} mol dm^{-3}, respectively, and the dye concentration was 2.00×10^{-3} mol dm^{-3}.

Upon addition of MR, MO or EO, a substantial decrease in the viscosities of the ternary PAAβ-CDen/PAAADddn/dye solutions occurs (viscosities = 4.85, 1.89, 1.71 and 1.59 Pa s in the presence of no dye, MR, MO and EO, respectively) whereas the changes in the 0.03 s^{-1} shear rate viscosities of the PAAβ-CDen/PAAADen (1.44, 1.49, 1.37 and 0.87 Pa s in the presence of no dye, MR, MO and EO, respectively) and PAAβ-CDen/PAAADhn (1.75, 1.48, 1.53 and 1.00 Pa s in the presence of no dye, MR, MO and EO, respectively) solutions are smaller. This is consistent with the dye complexation competing with that of the dodecyl tether of the ADddn substituent for a second β-CDen substituent in the PAAβ-CDen/PAAADddn/dye systems, even with the β-CDen substituent concentration being

1.8 times greater than that of the dyes, whereas this option is not available in the PAAβ-CDen/PAAADen/dye and PAAβ-CDen/PAAADhn/dye systems. Nevertheless, the 0.03 s^{-1} shear rate viscosities of the PAAβ-CDen/PAAADddn/dye systems are still greater than those of the PAAβ-CDen/PAAADen/dye and PAAβ-CDen/PAAADhn/dye systems consistent with some residual complexation of the dodecyl tether of the ADddn substituent and a consequent viscosity enhancement.

The viscosities of the PAAβ-CDen/PAAADen/dye and PAAβ-CDen/PAAADhn/dye systems show little variation in the presence of MR and MO, but a small decrease occurs in the presence of EO consistent with it showing the largest K_{11} for both systems (as determined in the UV–vis studies) and competing more strongly with ADen and ADhn for complexation by β-CDen. The general picture which emerges for dye complexation in the PAAβ-CDen/PAAADen/dye and PAAβ-CDen/PAAADhn/dye systems is shown in Figure 11. In the PAAβ-CDen/PAAADddn/dye systems the dodecyl tether of the ADddn substituent is complexed by the β-CDen substituent as shown by 2D ^{1}H NOESY NMR (Figures S34–S36, Supporting Information File 1) consistent with it competing with the dyes for complexation by β-CDen.

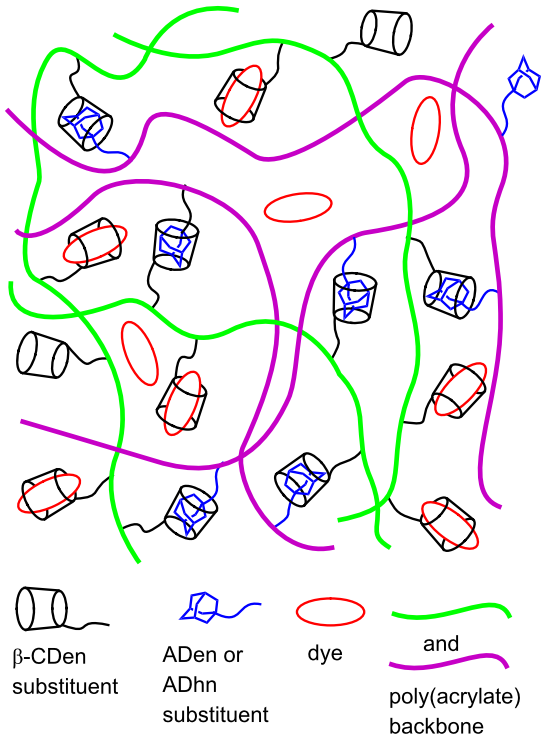

Figure 11: Representation of dye complexation in the PAAβ-CDen/PAAADen and PAAβ-CDen/PAAADhn networks.

Dye release studies

Dye release through a dialysis membrane with pores allowing passage of species with a molecular weight up to 3.5 kDa into an aqueous Na_2HPO_4/KH_2PO_4 buffer at pH 7.0, I = 0.10 mol dm^{-3} and 298.2 K was characterized for each system. Reference solutions of MR, MO and EO were prepared in aqueous Na_2HPO_4/KH_2PO_4 buffer at pH 7.0 and I = 0.10 mol dm^{-3}. All other dye solutions were prepared in the same buffer. To render the dye environment as similar as possible with respect to poly(acrylate), PAA, backbone concentration, those solutions containing neither PAAβ-CDen/PAAADen, PAAβ-CDen/PAAADhn nor PAAβ-CDen/PAAADddn had an appropriate amount of PAA added. The compositions of the thirty-six solutions studied appear in the caption to Figure 12 and in more detail in Table S1 (Supporting Information File 1.

The profiles of dye released with time for EO, MR and MO shown in Figure 12 exhibit informative trends. The solutions of EO in (a) Na_2HPO_4/KH_2PO_4 buffer alone, (b) 1.20 wt % PAA, (e) 1.14 wt % PAA/PAAADen, (d) 1.18 wt % PAA/PAAADhn and (c) 1.20 wt % PAA/PAAADddn show very similar release profiles (Figure 12(i)) with 90% of EO released within 20 h indicative of little interaction between EO and the other solutes. This is consistent with the major factors determining the appearance of EO in the receiving solution being its diffusion within the particular EO sample and its interaction with the dialysis membrane as it passes through its pores. Similar profiles characterize the release of MO and MR from PAA and adamantyl substituted PAA (Figure 12(ii) and 12(iii), respectively,) and a similar interpretation applies. However, the release of EO from a solution of (f) 1.20 wt % PAA/β-CD is slower reaching 87% after 48 h consistent with substantial formation of the β-CD–EO complex which, although of lower molecular weight than the membrane 3.5 kDa limit, is likely to pass through the membrane less readily than EO alone and is less mobile than free EO. An even slower release of EO from the (j) 1.18 wt % PAA/PAAβ-CDen solution occurs reaching only 69% after 48 h consistent with substantial formation of the β-CDen–EO complex within the PAAβ-CDen/EO solution which is of too high molecular weight to pass through the membrane such that the passage is limited to free EO alone. These data are consistent with complexation of EO by either β-CD alone or a β-CDen substituent within PAAβ-CDen controlling the amount of free EO in solution and thereby the rate of release through the membrane. A similar slowing of release is seen for the analogous MO and MR solutions (Figure 12(ii) and 12(iii)).

The EO release rate profiles for the (i) 1.14 wt % PAAβ-CDen/PAAADen, h) 1.18 wt % PAAβ-CDen/PAAADhn and (g) 1.20 wt % PAAβ-CDen/PAAADddn networks fall between

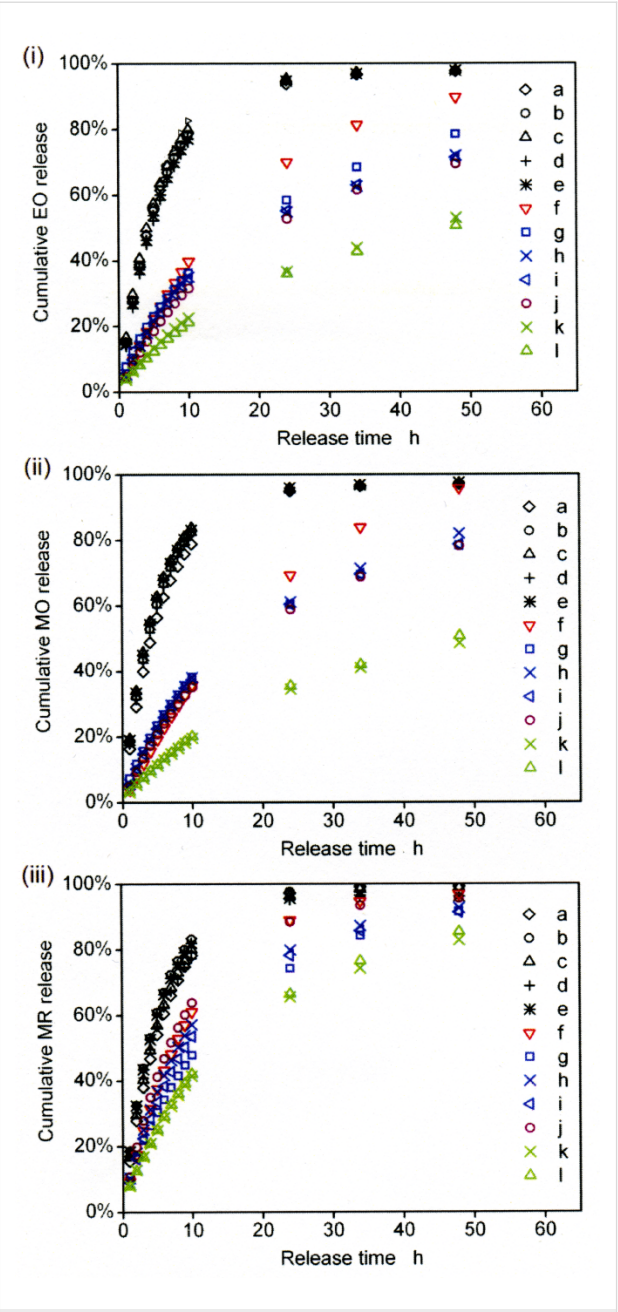

Figure 12: Release profiles for EO (i), MO (ii) and MR (iii) from aqueous (a) Na_2HPO_4/KH_2PO_4 buffer alone, (b) 1.20 wt % PAA, (c) 1.20 wt % PAA/PAAADddn, (d) 1.18 wt % PAA/PAAADhn, (e) 1.14 wt % PAA/PAAADen, (f) 1.20 wt % PAA/β-CD, (g) 1.20 wt % PAAβ-CDen/PAAADddn, (h) 1.18 wt % PAAβ-CDen/PAAADhn, (i) 1.14 wt % PAAβ-CDen/PAAADen, (j) 1.18 wt % PAA/PAAβ-CDen, (k) 1.96 wt % PAAβ-CDen/PAAADhn, and (l) 1.89 wt % PAAβ-CDen/PAAADen all in aqueous Na_2HPO_4/KH_2PO_4 buffer at pH 7.0, I = 0.10 mol dm^{-3} and 298.2 K. Initial [dye] = 2.00 × 10^{-3} mol dm^{-3}.

those for the (f) 1.20 wt % PAA/β-CD and (j) 1.18 wt % PAA/PAAβ-CDen solutions consistent with EO complexation by the β-CDen substituents being of major importance in controlling the rate of EO release. The release of EO is significantly more rapid from the (g) 1.20 wt % PAAβ-CDen/PAAADddn solution than from the (h) 1.18 wt % PAAβ-CDen/PAAADhn and (i) 1.14 wt % PAAβ-CDen/PAAADen solutions, but this variation is much less for MR and MO (Figure 12(ii) and 12(iii)). This coincides with the (g) 1.20 wt % PAAβ-CDen/PAAADddn/EO solution being substantially more viscous than the (h) 1.18 wt % PAAβ-CDen/PAAADhn/EO and (i) 1.14 wt % PAAβ-CDen/PAAADen/EO solutions whereas the viscosities of the three corresponding MR and MO solutions are more similar (Figure 10). This indicates that viscosity is a significant rate determining factor for dye release.

The effect of increasing network extension and viscosity on the rate of EO release is illustrated by the profiles for the more viscous (l) 1.89 wt % PAAβ-CDen/PAAADen and (k) 1.96 wt % PAAβ-CDen/PAAADhn solutions from which 50% of EO is released in 48 h, and is attributable to an increase in β-CDen substituent concentration increasing the proportion of EO complexed and the more extensive network slowing free EO movement. A slowing of dye release for the analogous MO and MR solutions (Figure 12(ii) and 12(iii), respectively) is similarly explained. (A 1.90 wt % PAAβ-CDen/PAAADddn solution was too viscous to transfer quantitatively to the release apparatus.)

While the release of MR in (a) Na_2HPO_4/KH_2PO_4 buffer alone, (b) 1.20 wt % PAA, (e) 1.14 wt % PAA/PAAADen, (d) 1.18 wt % PAA/PAAADhn and (c) 1.20 wt % PAA/PAAADddn solutions (Figure 12(iii)) show profiles similar to those observed for EO (Figure 12(i)), the profiles for MR release from the (f) 1.20 wt % PAA/β-CD solution and the six solutions, (g)–(l), containing PAAβ-CDen are compressed into a shorter time-frame of more rapid release than that observed for the corresponding EO solutions. This is consistent with the weaker complexing of MR by comparison with EO (Table 2) and the higher proportion of free MR facilitating more rapid release. The release profiles for MO (Figure 12(ii)) more closely resemble those of EO as anticipated from the strength of complexing of MO being between that of EO and MR (Table 2).

The release rates of the three dyes from their (j) 1.18 wt % PAA/PAAβ-CDen/dye, (i) 1.14 wt % PAAβ-CDen/PAAADen/dye and (h) 1.18 wt % PAAβ-CDen/PAAADhn/dye solutions decrease in the order MR > MO > EO (Figures S40–S42, Supporting Information File 1) consistent with the same order of decrease in K_{11} for dye complexation (Table 2) largely determining the relative release rates. While the release of MR from the (g) 1.20 wt % PAAβ-CDen/PAAADddn/dye solution is the most rapid, the release profiles of MO and EO are more similar (Figure S43, Supporting Information File 1). This indicates that the dodecyl tether of the ADddn substituent diminishes the

effect of the magnitude of K_{11} on the relative release rates of MO and EO possibly as a result of variations in the network structure as MO and EO compete with the dodecyl tether for complexation in the β-CDen substituent annuli. Finally, while the rate of MR release from the (f) 1.20 wt % PAA/β-CD/dye solution (Figure S44, Supporting Information File 1) is the most rapid, the two analogous but less rapid release profiles for MO and EO overlap which probably reflects a combination of the abilities of MO, EO and the β-CD–MO and β-CD–EO complexes to pass through the pores of the dialysis membrane.

Conclusion

The self-assembly of the β-CDen and ADen, ADhn and ADddn substituted poly(acrylate) networks, PAAβ-CDen/PAAADen, PAAβ-CDen/PAAADhn and PAAβ-CDen/PAAADddn, and their complexation and release of the dyes, ethyl orange, methyl orange and methyl red have been characterized in aqueous solution. The factors controlling the dye release from these networks are the strength of complexation of the dye, which is dependent upon the structure of the dye, and the structure of the network and its viscosity. Potentially, these systems form the basis for the development of controlled drug delivery systems for topical and wound applications, where the factors for drug release are likely to be similar to those controlling the dye release.

Experimental

Materials

The sodium salts of methyl red (BDH), methyl orange (BDH), ethyl orange (Sigma-Aldrich), and β-cyclodextrin (Nihon Shokuhin Kako Co.) were used as received. Poly(acrylic acid) (M_w = 250 kDa, $M_w/M_n \approx 2$) was purchased from Aldrich as a 35 wt % aqueous solution and freeze-dried to a constant weight. The substituted poly(acrylate)s: PAAβ-CDen [15], PAAADen [13], PAAADhn [17] and PAAADddn [17] (Figure 1) were synthesized according to literature procedures, and the extent of random substitution of poly(acrylate) with the β-CDen, ADen, ADhn and ADddn substituents was determined from their ^{1}H NMR spectra to be 8.8 ± 0.2%, 3.3 ± 0.1%, 3.0 ± 0.1% and 2.9 ± 0.1%, respectively.

NMR spectroscopy

A Varian Inova 600 spectrometer operating at 599.96 MHz was used to run 1D, 2D NOESY and 2D ROESY ^{1}H NMR spectra using standard pulse sequences with a mixing time of 0.3 s in the last two cases. All sample solutions were prepared in D_2O Na_2HPO_4/KH_2PO_4 buffer solutions at pD 7.0 and I = 0.10 mol dm^{-3} and were equilibrated at the thermostated probe temperature of 298.2 ± 0.1 K for 30 min in 5 mm diameter NMR tubes prior to their spectra being recorded. Chemical shifts (δ, ppm) were internally referenced to HOD at δ = 4.79 ppm. The substitution percentage of the β-CDen substituents on the PAAβ-CDen backbone was determined from a comparison of the resonance areas of the β-CD H1 protons and the poly(acrylate) protons. The substitution percentages of the adamantyl substituents on the PAAADen, PAAADhn and PAAADddn backbones were determined through a comparison of the resonance area of the methylene protons of both -$NHCH_2$ tether groups with that of the superimposed resonance areas of the poly(acrylate), adamantyl H2–4 and other tether methylene protons. The compositions of all solutions appear in the corresponding figure captions.

Isothermal titration calorimetry (ITC)

ITC measurements were made using a MicroCal VP isothermal titration calorimeter. In each titration, 10 mm^3 aliquots of a 0.62 wt % PAAβ-CDen solution ([β-CDen] = 2.84 × 10^{-3} mol dm^{-3}) were titrated into 1.46 cm^3 of either a 0.062 wt % PAAADen ([ADen] = 2.06 × 10^{-4} mol dm^{-3}), 0.064 wt % PAAADhn ([ADhn] = 1.91 × 10^{-4} mol dm^{-3}), or 0.072 wt % PAAADddn ([ADddn] = 2.03 × 10^{-4} mol dm^{-3}) solution at 298.2 K using a computer-controlled micro-syringe at intervals of 210 s. All solutions were prepared in aqueous Na_2HPO_4/KH_2PO_4 buffer at pH 7.0 and I = 0.10 mol dm^{-3}. The heats of dilution were determined by titrating aqueous Na_2HPO_4/KH_2PO_4 buffer (pH 7.0 and I = 0.10 mol dm^{-3}) into similarly buffered PAAADen, PAAADhn and PAAADddn solutions and by titrating similarly buffered PAAβ-CDen solution into the buffer solution. The heats of dilution were subtracted from the total heats evolved to give the heats of host–guest complexation from which the complexation constant, K, and the corresponding ΔH, $T\Delta S$ and N were calculated using the Origin 7.0 MicroCal protocol [53] as described in the Results and Discussion section.

UV–vis spectroscopy

The UV–vis spectra were recorded with a Cary-Varian 5000 UV–vis spectrophotometer using 1 cm path length matched quartz cells. All UV–vis titrations were performed in aqueous Na_2HPO_4/KH_2PO_4 buffer at pH 7.0 and I = 0.10 mol dm^{-3} at 298.2 K. For the β-CD/dye titrations, 50 mm^3 aliquots of a β-CD solution were sequentially titrated into 1.5 cm^3 of each dye solution and 1.5 cm^3 of each reference solution. The UV–vis absorbance spectra were recorded prior to and after each of 20 sequential additions of β-CD solution. The PAAβ-CDen/dye titrations where carried out in a similar manner using the same solution volumes. For the PAAβ-CDen/adamantyl-substituted PAA/dye studies, a 25 mm^3 aliquot of a PAAβ-CDen solution followed by 25 mm^3 aliquots of a PAAADen, PAAADhn, or PAAADddn solution were sequentially titrated in a twenty-fold sequence into 1.5 cm^3 of each dye solution and 1.5 cm^3 of each reference solution. The UV–vis

absorbance spectra were recorded prior to and after each of the twenty sequential additions of PAAβ-CDen solution and a PAAADen, PAAADhn, or PAAADddn solution. The concentrations of all solutions used in the UV–vis titrations are given in the figure captions. The complexation constants for dye complexation, K_{11}, and the corresponding ΔH and $T\Delta S$ were derived from the UV–vis data as described in the Results and Discussion section.

Rheology

Rheological measurements were carried out with a Physica MCR 501 (Anton Parr GmbH) stress-controlled rheometer with a 25 mm cone and plate geometry. The temperature was controlled at 298.2 K by a Peltier plate. All solutions were prepared in aqueous Na_2HPO_4/KH_2PO_4 buffer at pH 7.0 and $I = 0.10$ mol dm^{-3}. The compositions of sample solutions are shown in the corresponding figure captions.

Dye release

Dye release studies were performed using a membrane diffusion apparatus (Figure S37, Supporting Information File 1) in which a 3.5 kDa molecular weight cut-off dialysis membrane (Spectr/Por 3) of surface area 7.0 cm^2 separated 5.0 cm^3 of the dye containing solution (made up in Na_2HPO_4/KH_2PO_4 buffer at pH 7.0 and $I = 0.10$ mol dm^{-3} with MR, MO or EO concentration = 2.00×10^{-3} mol dm^{-3}) from 200 cm^3 of aqueous Na_2HPO_4/KH_2PO_4 buffer at pH 7.0 and $I = 0.10$ mol dm^{-3} which acted as the receiving solution. During the release experiments, the receiving solution was stirred at 298.2 K. At appropriate time intervals, a 2.0 cm^3 sample of the receptor solution was withdrawn, its UV–vis spectrum was measured and the sample was then returned to the receiving solution. The dye concentration in the receiving solution was calculated by reference to its molar absorbance spectrum determined under the same conditions. Each dye solution composition is given in Table S1 (Supporting Information File 1). All solutions were stirred and equilibrated at 298.2 K before dye release measurements commenced.

Supporting Information

Supporting Information File 1

Additional titrations, spectra and data.
[http://www.beilstein-journals.org/bjoc/content/supplementary/1860-5397-13-183-S1.pdf]

Acknowledgements

We gratefully acknowledge the support of this research by the Australian Research Council through Discovery Project DP110103177 (SFL and CJE) and by the National Science Foundation of China through Grants 20774028 and 20774030 (XG).

References

1. Lecourt, T.; Sinay, P.; Chassenieux, C.; Rinaudo, M.; Auzély-Velty, R. *Macromolecules* **2004,** *37,* 4635–4642. doi:10.1021/ma049822x
2. Wenz, G. *Adv. Polym. Sci.* **2009,** *222,* 204–254. doi:10.1007/12_2008_13
3. Nguyen, H.-T.; Pham, D.-T.; Lincoln, S. F.; Wang, J.; Guo, X.; Easton, C. J.; Prud'homme, R. K. *Polym. Chem.* **2013,** *4,* 820–829. doi:10.1039/C2PY20746J
4. Wang, J.; Xu, Y.; Wang, Y.; Liu, J.; Xu, J.; Li, L.; Nguyen, H.-T.; Pham, D.-T.; Lincoln, S. F.; Guo, X. *RSC Adv.* **2015,** *5,* 46067–46073. doi:10.1039/C5RA06163F
5. Auzély-Velty, R.; Rinaudo, M. *Macromolecules* **2002,** *35,* 7955–7962. doi:10.1021/ma020664o
6. Guo, X.; Abdala, A. A.; May, B. L.; Lincoln, S. F.; Khan, S. A.; Prud'homme, R. K. *Macromolecules* **2005,** *38,* 3037–3040. doi:10.1021/ma050071o
7. Guo, X.; Abdala, A. A.; May, B. L.; Lincoln, S. F.; Khan, S. A.; Prud'homme, R. K. *Polymer* **2006,** *47,* 2976–2983. doi:10.1016/j.polymer.2006.03.006
8. Charlot, A.; Auzély-Velty, R. *Macromolecules* **2007,** *40,* 1147–1158. doi:10.1021/ma062322e
9. Semenov, A.; Charlot, A.; Auzély-Velty, R.; Rinaudo, M. *Rheol. Acta* **2007,** *46,* 541–568. doi:10.1007/s00397-006-0149-4
10. Koopmans, C.; Ritter, H. *Macromolecules* **2008,** *41,* 7418–7422. doi:10.1021/ma801202f
11. Li, L.; Guo, X.; Wang, J.; Liu, P.; Prud'homme, R. K.; May, B. L.; Lincoln, S. F. *Macromolecules* **2008,** *41,* 8677–8681. doi:10.1021/ma8020147
12. Li, L.; Guo, X.; Fu, L.; Prud'homme, R. K.; Lincoln, S. F. *Langmuir* **2008,** *24,* 8290–8296. doi:10.1021/la800859w
13. Wang, J.; Li, L.; Ke, H.; Liu, P.; Zheng, L.; Guo, X.; Lincoln, S. F. *Asia-Pac. J. Chem. Eng.* **2009,** *4,* 537–543. doi:10.1002/apj.279
14. Guo, X.; Wang, J.; Li, L.; Pham, D.-T.; Clements, P.; Lincoln, S. F.; May, B. L.; Chen, Q.; Zheng, L.; Prud'homme, R. K. *J. Polym. Sci., Part B: Polym. Phys.* **2010,** *48,* 1818–1825. doi:10.1002/polb.22052
15. Guo, X.; Wang, J.; Li, L.; Pham, D.-T.; Clements, P.; Lincoln, S. F.; May, B. L.; Chen, Q.; Zheng, L.; Prud'homme, R. K. *Macromol. Rapid Commun.* **2010,** *31,* 300–304. doi:10.1002/marc.200900560
16. Stadermann, J.; Komber, H.; Erber, M.; Däbritz, F.; Ritter, H.; Voit, B. *Macromolecules* **2011,** *44,* 3250–3259. doi:10.1021/ma200048a
17. Wang, J.; Pham, D.-T.; Kee, T. W.; Clafton, S. N.; Guo, X.; Clements, P.; Lincoln, S. F.; Prud'homme, R. K.; Easton, C. J. *Macromolecules* **2011,** *44,* 9782–9791. doi:10.1021/ma202055a
18. Pham, D.-T.; Nguyen, H.-T.; Lincoln, S. F.; Wang, J.; Guo, X.; Easton, C. J.; Prud'homme, R. K. *J. Polym. Sci., Part A: Polym. Chem.* **2015,** *53,* 1278–1286. doi:10.1002/pola.27563
19. Wang, J.; Qiu, Z.; Wang, Y.; Li, L.; Guo, X.; Pham, D.-T.; Lincoln, S. F.; Prud'homme, R. K. *Beilstein J. Org. Chem.* **2016,** *12,* 50–72. doi:10.3762/bjoc.12.7
20. Hirayama, F.; Uekama, K. *Adv. Drug Delivery Rev.* **1999,** *36,* 125–141. doi:10.1016/S0169-409X(98)00058-1
21. Bibby, D. C.; Davies, N. M.; Tucker, I. G. *Int. J. Pharm.* **2000,** *197,* 1–11. doi:10.1016/S0378-5173(00)00335-5

22. Davis, M. E.; Brewster, M. E. *Nat. Rev. Drug Discovery* **2004,** *3,* 1023–1035. doi:10.1038/nrd1576
23. Loftsson, T.; Duchêne, D. *Int. J. Pharm.* **2007,** *329,* 1–11. doi:10.1016/j.ijpharm.2006.10.044
24. van de Manakkar, F.; Vermonden, T.; van Nostrum, C. F.; Hennink, W. E. *Biomacromolecules* **2009,** *10,* 3157–3175. doi:10.1021/bm901065f
25. Layre, A.-M.; Volet, G.; Wintgens, V.; Amiel, C. *Biomacromolecules* **2009,** *10,* 3283–3289. doi:10.1021/bm900866p
26. Davis, M. E. *Mol. Pharmaceutics* **2009,** *6,* 659–668. doi:10.1021/mp900015y
27. Thiele, C.; Auerbach, D.; Jung, G.; Qiong, L.; Schneider, M.; Wenz, G. *Polym. Chem.* **2010,** *2,* 209–215. doi:10.1039/C0PY00241K
28. Gao, W.; Chan, J. M.; Farokhzad, O. C. *Mol. Pharmaceutics* **2010,** *7,* 1913–1920. doi:10.1021/mp100253e
29. Maciollek, A.; Munteanu, M.; Ritter, H. *Macromol. Chem. Phys.* **2010,** *211,* 245–249. doi:10.1002/macp.200900436
30. Böhm, I.; Kreth, S. K.; Ritter, H. *Beilstein J. Org. Chem.* **2011,** *7,* 1130–1134. doi:10.3762/bjoc.7.130
31. Yhaya, F.; Lim, J.; Kim, Y.; Liang, M.; Gregory, A. M.; Stenzel, M. H. *Macromolecules* **2011,** *44,* 8433–8445. doi:10.1021/ma2013964
32. Mellet, C. O.; García Fernández, J. M.; Benito, J. M. *Chem. Soc. Rev.* **2011,** *40,* 1586–1608. doi:10.1039/C0CS00019A
33. Albuzat, T.; Keil, M.; Ellis, J.; Alexander, C.; Wenz, G. *J. Mater. Chem.* **2012,** *22,* 8558–8565. doi:10.1039/c2jm16425f
34. Luo, G.-F.; Xu, X.-D.; Zhang, J.; Yang, J.; Gong, Y.-H.; Lei, Q.; Jia, H.-Z.; Li, C.; Zhuo, R.-X.; Zhang, X.-Z. *ACS Appl. Mater. Interfaces* **2012,** *4,* 5317–5324. doi:10.1021/am301258a
35. Trotta, F.; Zanetti, M.; Cavalli, R. *Beilstein J. Org. Chem.* **2012,** *8,* 2091–2099. doi:10.3762/bjoc.8.235
36. Li, Z.; Yin, H.; Zhang, Z.; Liu, K. L.; Li, J. *Biomacromolecules* **2012,** *13,* 3162–3172. doi:10.1021/bm300936x
37. Harada, T.; Giorgio, L.; Harris, T. J.; Pham, D.-T.; Ngo, H. T.; Need, E. F.; Coventry, B. J.; Lincoln, S. F.; Easton, C. J.; Buchanan, G.; Kee, T. W. *Mol. Pharmaceutics* **2013,** *10,* 4481–4490. doi:10.1021/mp400309s
38. Wang, D.; Xie, D.; Shi, W.; Sun, S.; Zhao, C. *Langmuir* **2013,** *29,* 8311–8319. doi:10.1021/la401201w
39. Kanasty, R.; Dorkin, J. R.; Vegas, A.; Anderson, D. *Nat. Mater.* **2013,** *12,* 967–977. doi:10.1038/nmat3765
40. Kutyła, M. J.; Lambert, L. K.; Davies, N. M.; McGeary, R. P.; Shaw, P. N.; Ross, B. P. *Int. J. Pharm.* **2013,** *444,* 175–184. doi:10.1016/j.ijpharm.2013.01.005
41. Jing, J.; Szarpak-Jankowska, A.; Guillot, R.; Pignot-Paintrand, I.; Picart, C.; Auzély-Velty, R. *Chem. Mater.* **2013,** *25,* 3867–3873. doi:10.1021/cm4019925
42. Harada, T.; McTernan, H. L.; Pham, D.-T.; Lincoln, S. F.; Kee, T. W. *J. Phys. Chem. B* **2015,** *119,* 2425–2433. doi:10.1021/jp507272f
43. Zhao, Y.; Tian, W.; Yang, G.; Fan, X. *Beilstein J. Org. Chem.* **2014,** *10,* 2696–2703. doi:10.3762/bjoc.10.284
44. Li, Y.; Guo, H.; Gan, J.; Zheng, J.; Zhang, Y.; Wu, K.; Lu, M. *J. Polym. Res.* **2015,** *22,* 91. doi:10.1007/s10965-015-0720-8
45. Sharker, S. M.; Kim, S. M.; Kim, S. H.; In, I.; Lee, H.; Park, S. Y. *J. Mater. Chem. B* **2015,** *3,* 5833–5841. doi:10.1039/C5TB00779H
46. Duchene, D.; Cavalli, R.; Gref, R. *Curr. Pharm. Biotechnol.* **2016,** *17,* 248–255. doi:10.2174/1389201017666151030104944
47. Liu, J.; Hennink, W. E.; van Steenbergen, M. J.; Zhuo, R.; Jiang, X. *Bioconjugate Chem.* **2016,** *27,* 1143–1152. doi:10.1021/acs.bioconjchem.6b00094
48. Eftink, M. R.; Andy, M. L.; Bystrom, K.; Perlmutter, H. D.; Kristol, D. S. *J. Am. Chem. Soc.* **1989,** *111,* 6765–6772. doi:10.1021/ja00199a041
49. Rekharsky, M. V.; Inoue, Y. *Chem. Rev.* **1998,** *98,* 1875–1918. doi:10.1021/cr970015o
50. Harries, D.; Rau, D. C.; Parsegian, V. A. *J. Am. Chem. Soc.* **2005,** *127,* 2184–2190. doi:10.1021/ja045541t
51. Gans, P.; Sabatini, A.; Vacca, A. *Talanta* **1996,** *43,* 1739–1753. doi:10.1016/0039-9140(96)01958-3
52. *HypSpec;* Protonic Software: 2 Templegate Avenue, Leeds LS15 0HD, UK.
53. MicroCal, 22 Industrial Drive East, Northampton, MA01060, USA.

License and Terms

BEILSTEIN JOURNAL OF ORGANIC CHEMISTRY

Synthesis and supramolecular properties of regioisomers of mononaphthylallyl derivatives of γ-cyclodextrin

Markéta Bláhová[1], Sergey K. Filippov[2], Lubomír Kováčik[3], Jiří Horský[2], Simona Hybelbauerová[4], Zdenka Syrová[3], Tomáš Křížek[5] and Jindřich Jindřich[*1]

Full Research Paper

Open Access

Address:
[1]Department of Organic Chemistry, Faculty of Science, Charles University, Hlavova 8, 128 43 Prague 2, Czech Republic, [2]Institute of Macromolecular Chemistry, Academy of Sciences of the Czech Republic, Heyrovsky Sq. 2, 162 06 Prague 6, Czech Republic, [3]Institute of Biology and Medical Genetics, First Faculty of Medicine, Charles University, Albertov 4, 128 01 Prague 2, Czech Republic, [4]Department of Teaching and Didactics of Chemistry, Faculty of Science, Charles University, Hlavova 8, 128 43, Prague 2, Czech Republic and [5]Department of Analytical Chemistry, Faculty of Science, Charles University, Hlavova 8, 128 43, Prague 2, Czech Republic

Email:
Jindřich Jindřich[*] - jindrich@natur.cuni.cz

* Corresponding author

Keywords:
γ-cyclodextrin; naphthylallyl derivatives; regioselective alkylation; supramolecular properties; synthesis

Beilstein J. Org. Chem. **2017,** *13,* 2509–2520.
doi:10.3762/bjoc.13.248

Received: 08 July 2017
Accepted: 03 November 2017
Published: 27 November 2017

This article is part of the Thematic Series "Superstructures with cyclodextrins: Chemistry and applications IV".

Guest Editor: G. Wenz

Abstract

Monosubstituted derivatives of γ-cyclodextrin (γ-CD) are suitable building blocks for supramolecular polymers, and can also serve as precursors for the synthesis of other regioselectively monosubstituted γ-CD derivatives. We prepared a set of monosubstituted 2^I-*O*-, 3^I-*O*-, and 6^I-*O*-(3-(naphthalen-2-yl)prop-2-en-1-yl) derivatives of γ-CD using two different methods. A key step of the first synthetic procedure is a cross-metathesis between previously described regioisomers of mono-*O*-allyl derivatives of γ-CD and 2-vinylnaphthalene which gives yields of about 16–25% (2–5% starting from γ-CD). To increase the overall yields, we have developed another method, based on a direct alkylation of γ-CD with 3-(naphthalen-2-yl)allyl chloride as the alkylating reagent. Highly regioselective reaction conditions, which differ for each regioisomer in a used base, gave the monosubstituted isomers in yields between 12–19%. Supramolecular properties of these derivatives were studied by DLS, ITC, NMR, and Cryo-TEM.

Introduction

Cyclodextrins [1] (CDs) are cyclic oligosaccharides with a cone-shaped cavity formed by α-1,4-linked D-glucopyranose units. The most widely used CDs are α-, β-, and γ-CD with 6, 7 or 8 glucose units, respectively. Both chemically modified and native CDs are used in numerous applications, e.g., in separation methods [2,3] or in the pharmaceutical industry [4,5]. CDs

are well-known as host molecules for various guest substances in aqueous solutions [4]. Derivatives of CDs are attractive building blocks for various types of supramolecular structures [6,7]. Necessary non-covalent interactions depend on the type and derivatization of CD, on lipophilicity, shape, and size of the guest molecule, and on conditions such as temperature, pH, or solvent used [8]. In supramolecular polymers [9] multifunctional molecules are assembled in a regular manner. To avoid branching, monosubstituted CDs are required for a linear supramolecular polymer of CDs with guest groups attached.

Monosubstituted derivatives of CDs [10] include three regioisomers, namely 2^I-*O*-, 3^I-*O*-, and 6^I-*O*-substituted ones. To separate pure regioisomers from their mixture is tricky. Their direct regioselective synthesis is possible, although not easy, because hydroxy groups at different positions of CD have different properties; the hydroxy group at position 6 is the most nucleophilic and basic one, the hydroxy group at position 2 is the most acidic, and the group at position 3 is most sterically hindered. Therefore, regioselective monosubstitution to positions 2 and 6 can be controlled by the amount and strength of the base used in the reaction, whereas monosubstitution at position 3 can be achieved by complexation of the alkylation agent to the CD cavity and orientation of the agent´s reactive center towards the 3-OH group [11-13].

Here, we report the preparation of regioisomers of novel mononaphthylallyl γ-CD (NA-CD), i.e., 3-(naphthalene-2-yl)prop-2-en-1-yl γ-CD, which is interesting for several reasons. Compared to α- or β-CD, the number of publications dealing with γ-CD is quite small, e.g., [14,15]. The naphthyl group is well known for its ability to make inclusion complexes with CDs [16]. The allyl connecting linker is relatively rigid and should support the formation of supramolecular polymers of CD–guest type [17]. Moreover, the double bond of the allyl group allows a subsequent conversion of these compounds to other regiospecifically monosubstituted γ-CD derivatives. Naphthylallyl derivatives of any CD have not been described yet.

Supramolecular properties of the prepared derivatives were studied by a set of methods allowing characterization of supramolecular behavior at various levels – from binary complexation, over supramolecular oligomers to large assemblies; namely by isothermal titration calorimetry (ITC) [16], ^{1}H nuclear magnetic resonance spectroscopy (^{1}H NMR), dynamic light scattering (DLS) [18-21] and cryo-transmission electron microscopy (Cryo-TEM) [22-24].

Results and Discussion

Synthesis

We present two approaches for the synthesis of naphthylallyl (NA) derivatives. The first approach is a cross-metathesis of peracetylated allyl derivatives of γ-CD with 2-vinylnaphthalene. The main advantage of this procedure is that a pure regioisomer of the product is obtained due to the regio-purity of the starting material. Unfortunately, this reaction is quite low-yielding, and the isolation of the products is hard to perform. Moreover, the starting compound for this reaction has to be prepared from γ-CD in two steps involving complicated chromatographic separations. Thus, the overall yields of the pure NA regioisomers were only 2–5%. Therefore, we turned our focus to developing another method for the preparation of naphthylallyl derivatives, which is based on a direct alkylation of γ-CD with 2-(3-chloroprop-1-enyl)naphthalene.

Cross-metathesis

Mono 2^I-*O*-, 3^I-*O*- and 6^I-*O*-naphthylallyl-γ-CDs (2-*O*-NA-γ-CD, **2a**, 3-*O*-NA-γ-CD, **2b**, 6-*O*-NA-γ-CD, **2c**) were prepared from peracetylated *O*-allyl derivatives [14] by cross-metathesis with 2-vinylnaphthalene (Scheme 1) in the presence of the Hoveyda–Grubbs 2nd generation catalyst. After deacetylation, column chromatography afforded the naphthylallyl derivatives in yields between 16–25%, which is comparable to

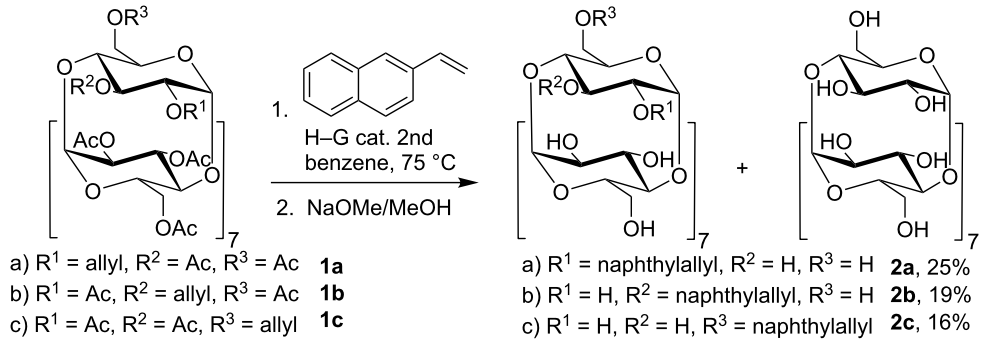

Scheme 1: Preparation of 2^I-*O*-, 3^I-*O*- and 6^I-*O*-naphthylallyl derivatives of γ-CD by cross-metathesis.

the results of other metathesis reactions of allylated CDs [11,25]. In all cases, only the isomer with *E* configuration of the NA double bond was observed by ^{1}H NMR. Reactions were performed in benzene at 75 °C or dichloromethane at 45 °C, the latter giving lower yields. Prior to the isolation, it was necessary to perform deacetylation of the reaction mixture because the product had the same R_f as the starting material. After the deprotection, a substantial amount of the pure γ-CD was isolated as the only byproduct containing CD. Apparently, a concurrent reaction – the cleavage of allyl ether – also took place. The use of similar ruthenium complexes as catalysts for the cleavage of allyl ethers and allyl esters was described before by Tanaka et al. [26,27].

Naphthylallylation

The same naphthylallyl derivatives of γ-CD **2a**–**c** were also prepared by direct alkylation of γ-CD with 2-(3-chloroprop-1-enyl)naphthalene [28] as the alkylation reagent (Scheme 2). This reagent is easy to prepare on a large scale without a need of purification by chromatography. Yields of the NA regioisomers **2a**–**c** were, after isolation by column chromatography, in the range 1–24% (Table 1). The optimization experiments for this procedure, followed by TLC, revealed that the products are formed in all cases, but the yields and regioselectivity depend substantially on the amount and the type of a base. Anhydrous DMSO was selected as a solvent because it often proved to be superior to DMF in our previous experiments in alkylations of CDs.

Direct alkylation methods have been studied in CD chemistry over last twenty years [11,14,29-34]. As mentioned before, it is possible to direct the alkylation to the specific position just by changing the amount of a base used for the reaction. For example, the alkylation of the secondary rim of CDs can be achieved by using an equimolar amount of the base. In these cases, perdominantly the 2-*O*-substituted product is formed, but a small amount of the 3-*O*-derivative can be present in the reaction mixture as well. However, in the case of NA derivatives, the 3-*O*-derivative is formed preferentially (Table 1, entries 1 and 4), which is the same outcome we have observed earlier in the case of the 3-*O*-cinnamyl-β-CD [35].

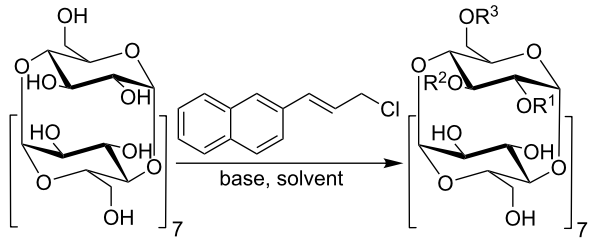

a) R^1 = naphthylallyl, R^2 = H, R^3 = H **2a**
b) R^1 = H, R^2 = naphthylallyl, R^3 = H **2b**
c) R^1 = H, R^2 = H, R^3 = naphthylallyl **2c**

Scheme 2: Preparation of 2-*O*-, 3-*O*- and 6-*O*-NA derivatives of γ-CD by direct alkylation (see Table 1 for the yields and conditions).

Table 1: Preparation of 2-*O*- (**2a**), 3-*O*- (**2b**) a 6-*O*- (**2c**) NA derivatives of γ-CD by direct alkylation with 2-(3-chloroprop-1-enyl)naphthalene.

entry	base, solvent	yields[a] (%)		
		2a	**2b**	**2c**
1	1.5 equiv EtONa, DMSO	1	19	–
2	4 equiv EtONa, DMSO	6	<1	–
3	15 equiv EtONa, DMSO	15	–	23
4	1.5 equiv LiH, LiI, DMSO	3	24	–
5	15 equiv LiH, LiI, DMF	13	<1	–
6	10 equiv NaOH, DMSO	14	<1	–
7	15 equiv NaOH, DMSO	16	–	5
8	20 equiv LDA, DMSO	11	<1	–
9	15 equiv NaH, DMSO	<1	–	12

[a]Isolated yields; <1 no isolated yield, – not observed.

During the attempts to prepare the 6-*O*-substituted derivative, we came across unusual changes in the regioselectivity of the substitution. In previous publications, we have shown that the substitution to the position 6 can be achieved by using an excess of NaOH (30 equiv) in aqueous solvents [11,30,35]. Unfortunately, this method is not applicable for the reaction described in this paper because the alkylation reagent hydrolyzes too fast and the desired product is not formed. Attempts to use 30 equiv of a base in nonaqueous solvents also lead only to decomposition of the alkylation agent. Therefore, a new set of optimization experiments for developing suitable reaction conditions for the preparation of the 6-*O*-derivative had to be made. Different amounts (1.5–20 equiv) and types of bases were used. Interestingly, the highest yields of 6-*O*-isomer gave 15 equiv of a base; however, the same conditions gave unexpectedly also the 2-*O*-derivative. In experiments with more than 1.5 equiv of a base (Table 1, entries 2, 5, 6, 8), the 2-*O*-derivative was obtained almost regiospecifically, but entries 3 and 7 gave mixtures of 2-*O*- and 6-*O*-derivatives. However, the 6-*O*-derivative can be obtained regioselectively with 15 equiv of NaH (Table 1, entry 9). The robustness of this method was confirmed by an experiment using just 12 equiv of NaH resulting in practically the same outcome.

The 2-*O*-, 3-*O*- and 6-*O*-NA regioisomers of γ-CD offer a significant advantage – they are separable by column chromatography in the elution mixture $PrOH/H_2O/NH_3$, which cannot be achieved for other monoderivatives of α-, β- and γ-CD with

smaller substituents such as allyl and propargyl having similar R_f and must be peracetylated prior to other separation processes.

Dynamic light scattering (DLS)

The supramolecular properties of all regioisomers of NA-γ-CD (2-*O*-, 3-*O*-, 6-*O*-) were investigated by DLS. We analyzed the dependence of self-assembling of the isomers on external stimuli such as agitation and temperature. The 3-*O*-isomer **2b** shows co-existence of two types of aggregates: large aggregates (around 600 nm in diameter) and smaller aggregates (around 140 nm in diameter, Figure 1). Aggregates formed by 2-*O*-isomer **2a** were similar to those of the 3-*O*-sample. On the other hand, the 6-*O*-isomer **2c** produced different results. Since the measurement of this isomer was complicated due to its low solubility in water, the sample was first dispersed in water and then heated to 120 °C in a sealed ampule. The solution became turbid after cooling, which manifests the presence of large particles. Indeed, the DLS experiments revealed large particles of the 6-*O*-sample with sizes larger than 1 μm, exceeding the limit of the instrument used.

To assess the influence of filtration on the self-assembly of naphthylallyl regioisomers, samples were then passed through 0.22 μm pores. The volume-weighted DLS distribution function of the 2-*O*- and 3-*O*-samples show a dominant presence of 2.5 nm particles immediately after the filtration. The sample of the 6-*O*-isomer showed the distribution of sizes ranging from 30 nm to 200 nm after filtration through 0.22 μm pores and 200 nm aggregates after filtration through 1 μm pores. In either case, the 6-*O*-isomer formed aggregates with a broader distribution of sizes than the 2-*O*- and 3-*O*-isomers and no 2–3 nm particles were observed in the sample. Nevertheless, small particles still may be present in solution because the intensity of light scattered by hard spheres is proportional to R^6 (R being the radius) which means that large particles scatter significantly more light than the same mass of small particles. Thus, a fairly small amount of large aggregates might dominate the scattering making the contribution of small particles negligible.

The long-time evolution of all the isomers after filtration was evaluated according to the approach of Bonini [22] and González-Gaitano [21]. The distribution function of the 3-*O*-isomer shows the presence of a dominant mode with 2.5 nm particles immediately after the filtration, which stays intact throughout the experiment. A minor fraction of larger aggregates is formed in solution shortly after filtration whose size continuously fluctuate (Supporting Information File 1, Figure S5), which could be easily monitored by scattering intensities behavior. The evolution of the 2-*O*-isomer in time has also been investigated, but no trend was observed in this case (Supporting Information File 1, Figure S6). The long-time evolution of the 6-*O*-filtered sample revealed that the size of particles continuously increased with time (Supporting Information File 1, Figure S6), starting from 2 nm particles appearing immediately after the filtration and reaching larger particles that grew in the sample standing overnight.

Subsequently, the effect of different solvents on the size of aggregates was investigated by a method proposed by us for monocinnamyl-α-CD (Cin-α-CD) derivatives [20]. Two other water-solvent mixtures were tested. In 50% MeOH (v/v) solution 2-*O*- and 3-*O*-isomer formed aggregates with diameters around 200 nm, but the 2-*O*-derivative contained 50 nm aggregates as well. Interestingly, the 6-*O*-isomer formed aggregates with a broad size distribution with a peak at 100 nm (Figure 2).

We observed that the 6-*O*-isomer has a low solubility in water and 50% MeOH solution, but it is more soluble in 50% PrOH (v/v). Consequently, the assembling of the 6-*O*-derivative was investigated in 50% PrOH, which revealed that just 1.4 nm particles were present in the solution. This means that the 6-*O*-derivative does not form any aggregates in 50% PrOH.

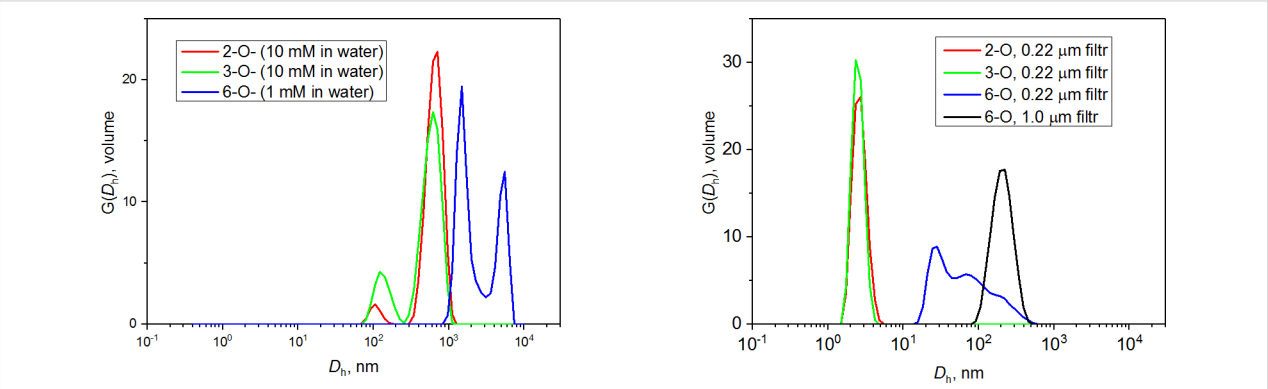

Figure 1: Volume-weighted distribution functions for water solutions of 2-*O*- (**2a**), 3-*O*- (**2b**), and 6-*O*- (**2c**) NA-γ-CD regioisomers before (left) and after (right) filtration.

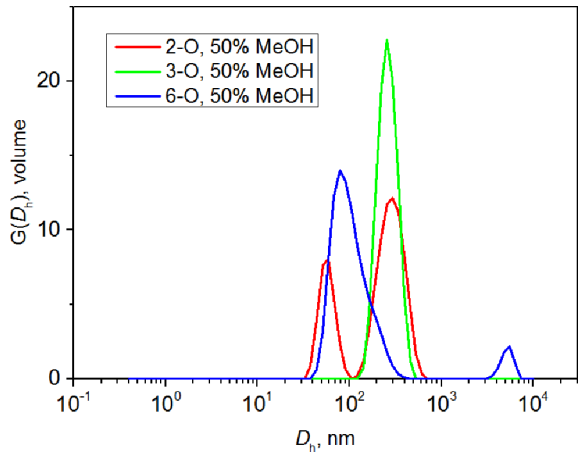

Figure 2: Distribution functions for 2-*O*- (**2a**), 3-*O*- (**2b**), and 6-*O*- (**2c**) NA-γ-CD regioisomers in 50% MeOH (v/v).

We investigated the temperature dependence of the aggregate size of the regioisomers in similar ways as González-Gaitano [21] and as we did for Cin-α-CD [20]. The temperature was raised from 5 °C to 65 °C (5 °C steps) across 2.5 h, which led to substantial changes in sizes of the aggregates (Figure 3). A shift of the correlation curve, caused by the change of viscosity, is noticeable for the 3-*O*-isomer (Supporting Information File 1, Figure S4). Up to 30 °C, two peaks around 150 nm and 600–700 nm were detected, whereas at 35 °C and above, just one peak around average size (300–400 nm) appeared. The increase in hydrophobic interaction at the higher temperature may be responsible for the observed behavior. The effect of temperature was not as pronounced as in the case of Cin-α-CD [20]. The sample of the 6-*O*-isomer had to be filtered through 1 µm pores because of its high turbidity. The sample was equilibrated for 3 h before the measurement. The temperature behavior of the 6-*O*-derivative was similar to the 3-*O*-isomer. At the low temperature (25 °C), two peaks are visible on the distribution function (Figure 3) corresponding to sizes of aggregates around 80 nm and 400 nm. At 40 °C, just one peak around 300 nm appeared, and at 65 °C, two peaks appeared again, around 100 nm and 300 nm. The 2-*O*-sample did not show any temperature dependence.

Transmission cryo-electron microscopy (Cryo-TEM)

The supramolecular properties of the individual regioisomers (2-*O*-, 3-*O*-, 6-*O*-) of NA-γ-CD **2a–c** and the dependence of the formation of the self-assembled structures on their concentration were also determined by Cryo-TEM.

While the 2 mM sample of the 3-*O*-derivative **2b** formed irregular clumps of fibers of the thicknesses 1–2 and 4–7 nm having a size of 50 to 100 nm (Figure 4A), the 20 mM sample contained

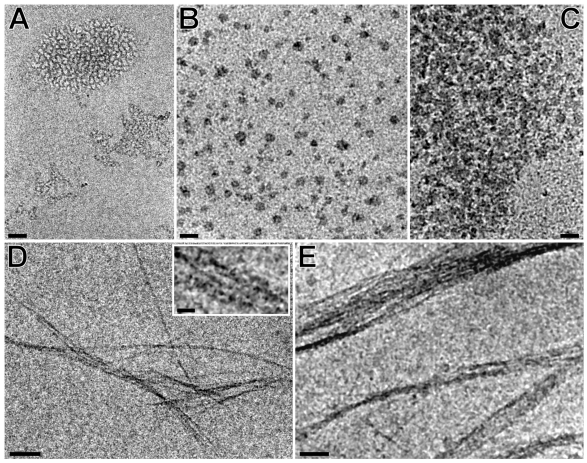

Figure 4: Effect of increasing concentration and sonication on the morphology of the 3-*O*-derivative **2b**. A to C: 2 mM, 20 mM, and 100 mM unsonicated specimens; D: fibers of the 2 mM specimen after sonication. Inset: high-magnification detail of the fibers; E: fibers and aggregates of the 100 mM specimen. Scale bars: A–C: 50 nm, D–E: 100 nm, inset: 20 nm.

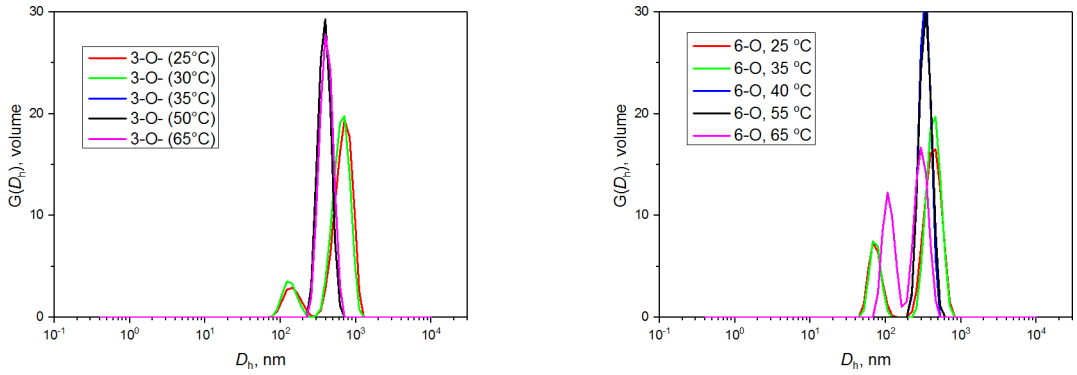

Figure 3: Volume-weighted distribution functions for the 3-*O*- (**2b**) and 6-*O*- (**2c**) NA-γ-CD regioisomer at different temperatures.

smaller spherical clusters of size 20 to 30 nm (Figure 4B), which formed large aggregates with the size of hundreds of nm in the 100 mM sample (Figure 4C). It is evident that the method of aggregation and the morphology of the specimen vary with increasing concentration. Sonication, conducted for 2 mM and 100 mM samples, resulted in a diametrically different arrangement of the fibers (Figure 4D and E). Both sonicated solutions contained several μm long bundles of fibers with thicknesses of 1.5–10 nm; in the 100 mM sample, also particles having diameters from 30 to 120 nm were present.

Smaller spherical particles of β-CD, which tend to combine into larger aggregates, were also observed by Bonini et al. [22], who described the presence of clusters of different sizes and shapes in one sample as well as the dependence of the cluster properties on the concentration. The 2 mM and 20 mM solution of 2-*O*-derivative **2a** formed clusters of similar shape and size as the 3-*O*-derivative **2b** (Figure 5A and B). In the 100 mM sample, the presence of large quantities of material rarely forming large particles, was evident (Figure 5C). A 10-minute sonication led just to the disappearance of the larger aggregates, no fibers in a μm scale were detected.

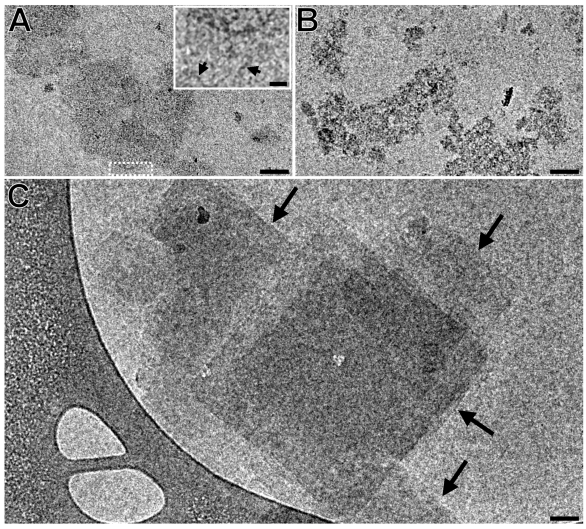

Figure 6: Effect of increasing concentration and sonication on the morphology of the 6-*O*-derivative **2c**. A: 0.5 mM specimen after sonication. Inset: enlarged area indicated by the white dashed rectangle. Arrows indicate the NA-γ-CD fibers; B: 5 mM sonicated specimen; C: 5 mM unsonicated specimen. Scale bars: 50 nm, inset: 10 nm.

The 6-*O*-derivative **2c**, due to its low solubility, was measured only at low concentrations of 0.5 mM and 5 mM (Figure 6A, B). In the 0.5 mM solution, only short fibers were found, whereas in the 5 mM sonicated solution, fibrous aggregates, similar to those of 2 mM unsonicated samples 2-*O*- and 3-*O*-derivatives, were observed. In an unsonicated 5 mM preparation, we observed many sheet-like structures (Figure 6C), corresponding to the observations of Bonini et al [22].

Isothermal titration calorimetry (ITC)

ITC experiments on NA-γ-CD cannot be carried out as classical titration experiments, i.e., by injecting the ligand solution into a solution of the receptor [36], because complementary complexing moieties are covalently bonded. Instead, the so-called dissociation [37] or release [38] experiment had to be used, in which a solution of a complex is injected initially into a pure solvent and to the dilute solution in subsequent injections (see Supporting Information File 1 for more details and the model description).

The fit of experimental and calculated values of the normalized heat per injection (NDH) was quite satisfactory for 2-*O*- (**2a**) and 3-*O*- (**2b**) NA-γ-CD at all measured temperatures. Fits for the less soluble 6-*O*- (**2c**) were less satisfactory at 10 and 25 °C and failed at 45 °C. Results at 10 °C are shown in Figure 7.

Estimated thermodynamic parameters and average degrees of polymerization at various temperatures are collected in Table 2. The values for 6-*O*-NA-γ-CD at 45 °C are omitted and the values for 6-*O*-NA-γ-CD at 10 °C and 25 °C are given in parentheses because of their low reliability. Nevertheless, even those values, as well as those for 2-*O*-NA-γ-CD and 3-*O*-NA-γ-CD at

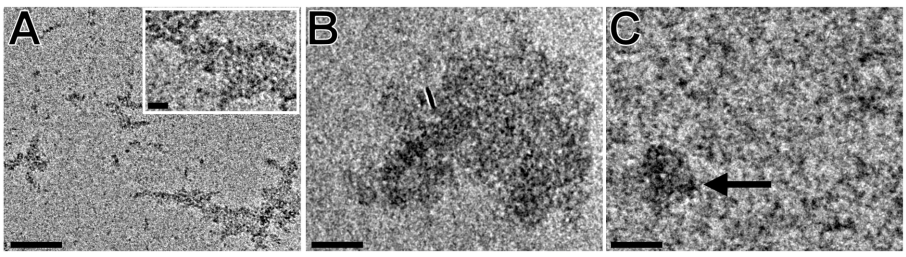

Figure 5: Effect of increasing concentration and sonication on the morphology of the 2-*O*-derivative **2a**. A: 2 mM unsonicated specimen; B: 20 mM unsonicated specimen; C: 100 mM sonicated specimen. The arrow indicates an aggregated particle. Scale bars: 50 nm, inset: 10 nm.

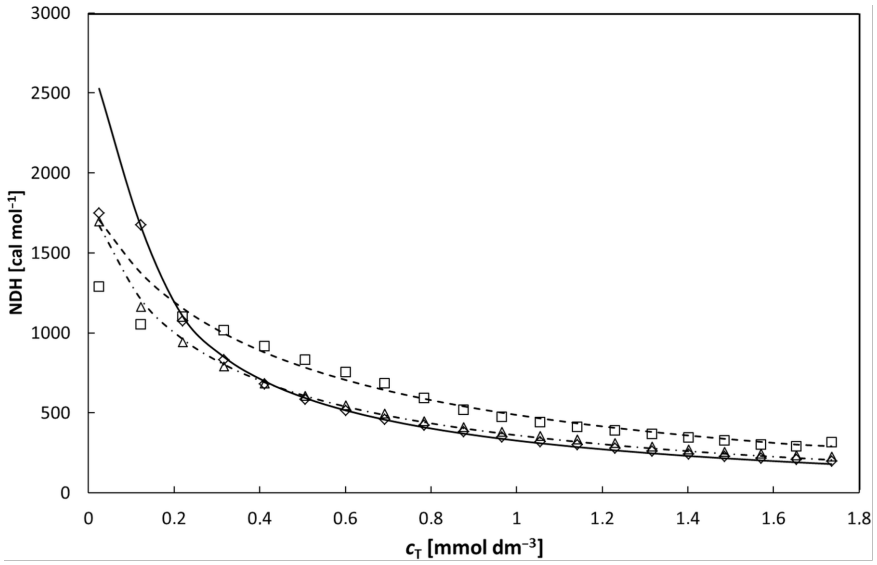

Figure 7: Heat change for injection per mole of NA-γ-CD added as a function of the total concentration of NA-γ-CD at 10 °C. Symbols are used for experimental values; lines for fits: 6-*O*-NA-γ-CD **2c** squares and a dashed line; 2-*O*-NA-γ-CD **2a** diamonds and a full line; 3-*O*-NA-γ-CD **2b** triangles and a dashed-dotted line.

Table 2: Estimated thermodynamic parameters for complexation of NA-γ-CD regioisomers.

sample	*T* (°C)	*K* (dm^3/mol)	Δ*H* (cal mol^{-1})	*T*Δ*S* (cal mol^{-1})	n_n[a]	n_w[b]
2c	10	(1215)	(−2783)	(1395)	(4.02)	(7.04)
	25	(418)	(−2439)	(1176)	(2.60)	(4.20)
	45	–	–	–	–	–
2b	10	2857	−2903	1795	5.87	10.74
	25	2644	−3654	1328	5.67	10.33
	45	1193	−4463	317	3.99	6.98
2a	10	5657	−3303	1806	8.04	15.08
	25	3489	−3667	1490	6.43	11.86
	45	1619	−4466	533	4.55	8.11

[a]Number-average degree of polymerization calculated for 10 mM solution. [b]Weight-average degree of polymerization calculated for 10 mM solution.

all three temperatures correspond to values found for γ-CD and aromatic compounds [39]. Binding of the 2-*O*-regioisomer is stronger than that of the 3-*O*-regioisomer, and consequently, longer oligomers can be expected for it.

The fraction of suprapolymer with polymerization degree n is then given for negligible cyclisation as

$$x_n = (1-\theta)\theta^{n-1} \quad (1)$$

where θ is the degree of occupation, i.e., the probability that the particular group, either naphthyl or CD, is in a bound state. θ is determined by the binding constant and NA-γ-CD concentration (see Supporting Information, File 1). Number average and weight average degrees of polymerization (n_n and n_w) are given by standard relations derived for polycondensation [40]

$$n_n = \frac{1}{1-\theta} \qquad n_w = \frac{1+\theta}{1-\theta} \quad (2)$$

The values of n_n and n_w calculated from ITC results for 10 mM solutions of NA-γ-CD are also presented in Table 2.

NMR spectroscopy

The supramolecular behavior of the regioisomers was further examined by ^{1}H NMR. The measurements were performed in

D_2O, where the strongest intermolecular interactions are expected. The concentration dependence of chemical shifts was taken as their indicator. The 6-*O*-isomer **2c** was excluded from these experiments because its solubility in water is very limited; samples cannot be prepared at concentrations greater than 5 mM.

Spectra for 2-*O*- (**2a**) and 3-*O*- (**2b**) derivatives were measured at concentrations of 100, 10, and 1 mM. Although these regioisomers are quite soluble in water, turbidity becomes noticeable after a longer time, and in the case of 100 mM specimens, even precipitation of a solid was observed. The turbidity caused the worse quality of ^{1}H NMR spectra; however, chemical shifts and changes in the shape of the peaks are clearly visible.

For the 2-*O*-derivative, chemical shifts of hydrogens of the aromatic region and hydrogens of the double bond moved upfield with increasing concentration; therefore, their values are lower (Figure 8). The change in the signal shapes, especially of aromatic hydrogens (A), is also evident. With increasing concentration, the distance between signals B and C of the double bond hydrogens is reduced (about 0.05 ppm), as well as the extent of the area of aromatic hydrogens A (0.13 ppm).

Chemical shifts of hydrogen signals of 3-*O*-derivative at concentrations 100 and 10 mM do not significantly differ (Figure 9). However, a change in the shape of signals and the narrowing (0.12 ppm) of the signals are apparent in the aromatic region (A). For the 1 mM sample, chemical shifts in the aromatic and double bond areas evidently move downfield; however, shapes of peaks do not much differ from the 10 mM sample. It is also worth noting, that while the distance between signals B and C increased (by about 0.07 ppm), the area of aromatic protons A narrowed (about 0.21 ppm).

For all of the above cases, the changes of chemical shifts and shapes of signals in the CD hydrogens' area were minimal. Also, NOESY and ROESY experiments did not indicate any interaction between the NA group and the CD cavity (data not shown).

Summarization and discussion of results of different methods

We have successfully employed two synthetic approaches to 2^I-*O*-, 3^I-*O*- a 6^I-*O*-NA derivatives of γ-CD. The first approach is based on a cross-metathesis reaction between corresponding regioisomers of mono-*O*-allyl derivatives of γ-CD and 2-vinyl-

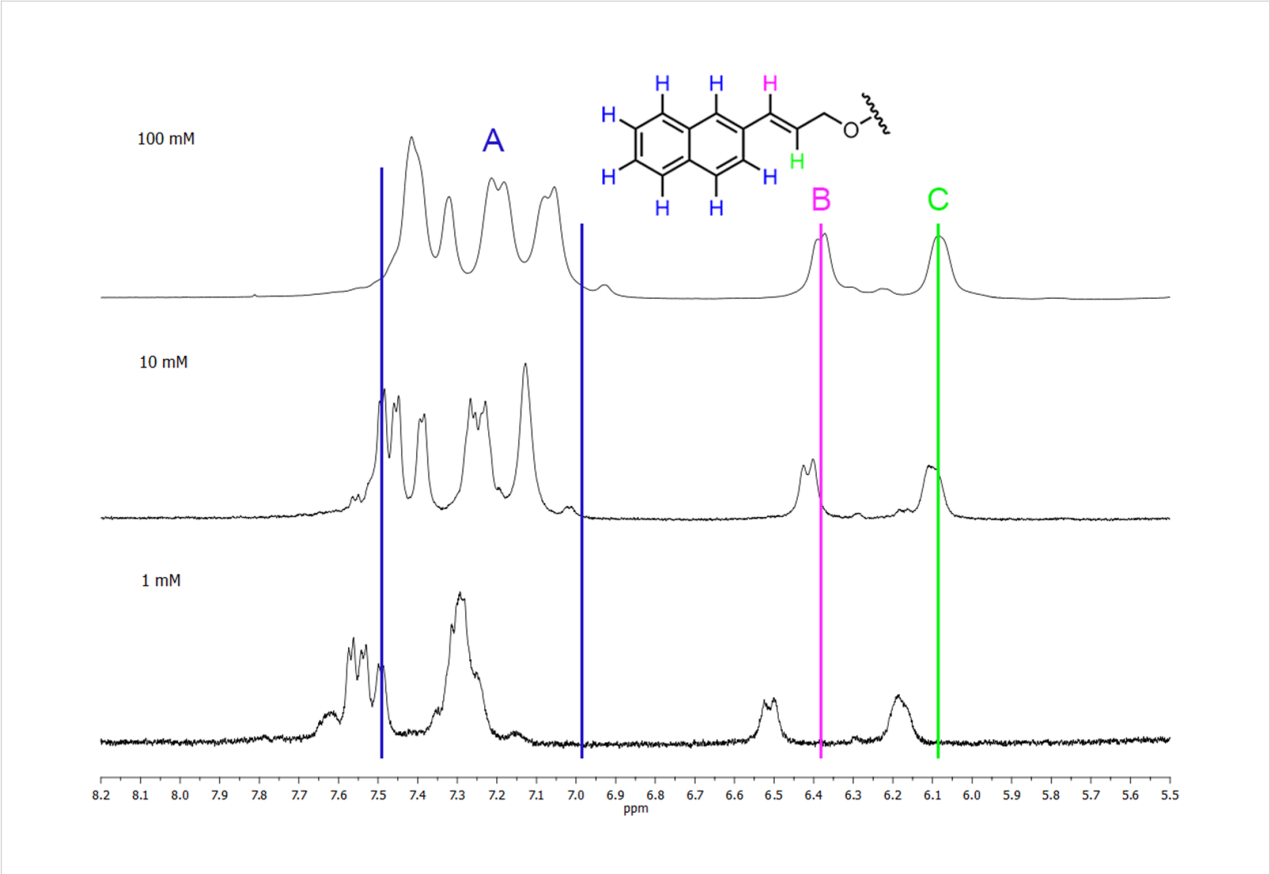

Figure 8: ^{1}H NMR spectra of 2-*O*-derivative **2a** in D_2O at concentrations of 100, 10, and 1 mM.

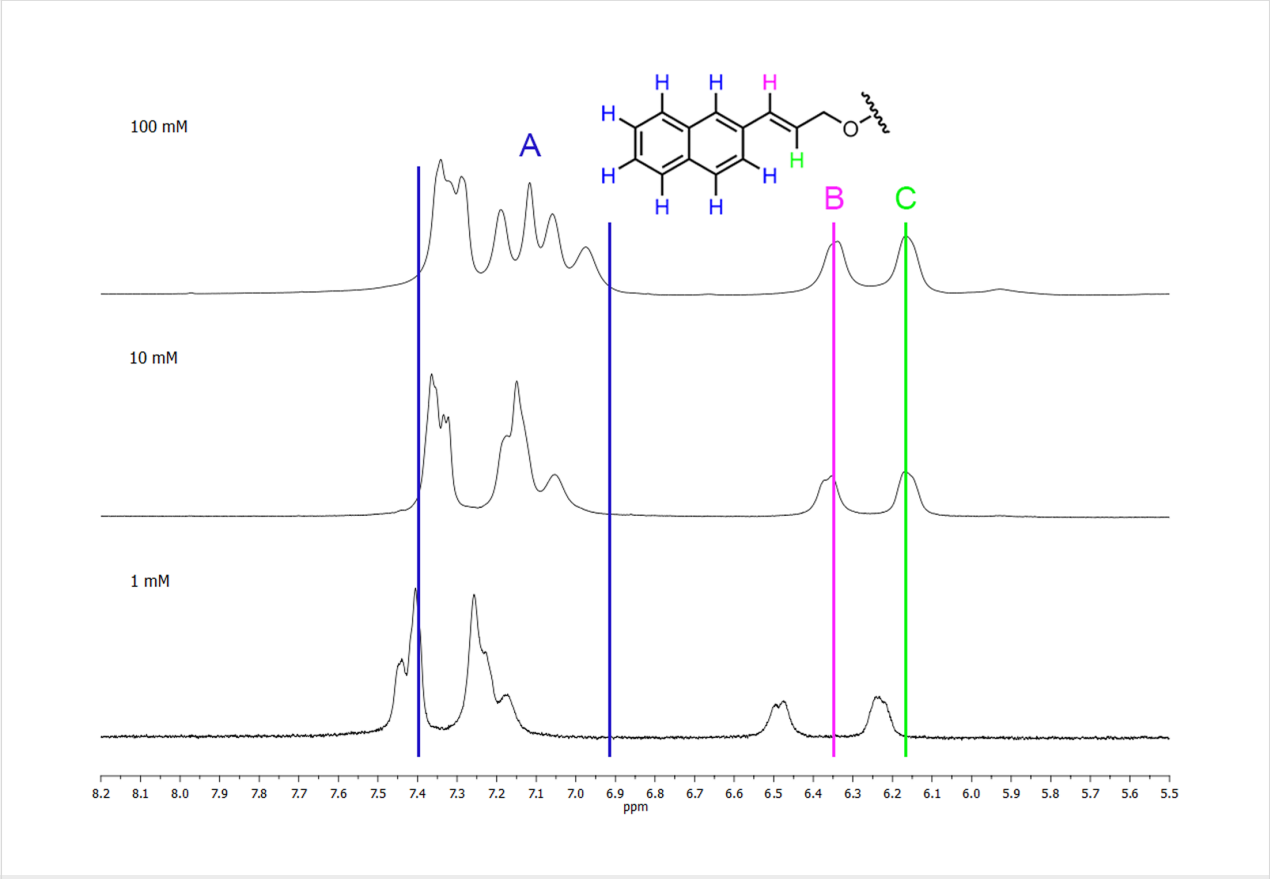

Figure 9: ^{1}H NMR spectra of 3-*O*-derivative **2b** in D_2O at concentrations of 100, 10, and 1 mM.

naphthalene yielding 16–25%; however, the overall yield from γ-CD is only 2–5%. The second approach is based on the direct alkylation of γ-CD, with easy to prepare 3-(naphth-2-yl)allyl alkylation reagent, yielding up to 24%. Moreover, we achieved high regioselectivity in preparations of all regioisomers using the second approach, so this method proved to be superior.

From the NMR experiments, we conclude that the signals of hydrogens of the naphthylallyl group of 2-*O*- and 3-*O*-derivatives differ not only in the shape of peaks, but also in the value of the chemical shifts. For both regioisomers the concentration dependence of chemical shifts in aromatic and allyl areas indicates intermolecular association such as inclusion of the naphthylallyl moiety into the cavity of γ-CD or π stacking of naphthyls. The absence of the significant concentration dependence of chemical shifts of the CD hydrogens does not disqualify inclusion complexation because changes of chemical shifts by 0.01 ppm or less were observed upon inclusion of an aromatic guest into the γ-CD cavity [41]. To reconcile the absence of interactions CD/NA in NOESY and ROESY experiments with NA inclusion into CD is more difficult. Nevertheless, the change in chemical shifts was observed also for the allyl hydrogens which indicates that the allyl group might be also inserted into the CD cavity which would increase the distance between CD and NA hydrogens. Thus, the co-existence of various interactions such as inclusion of NA to various depths of the CD cavity, stacking of naphthyl rings either inside or outside the CD cavity (possibly leading to micellization or aggregation) must be expected.

The intermolecular interactions were quantified by ITC. The obtained values of binding constants were in the upper range of values usually found for the inclusion complexation of γ-CD [42] and decreased in the order (i) 2-*O*-, (ii) 3-*O*-, and (iii) 6-*O*-, as well as with temperature. The values were obtained from the fit to the model in which NA-γ-CD is taken as a ditopic monomer of the AB type with groups A and B undergoing an association of 1:1. However, a number of alternate or competing interactions may occur, as mentioned above, γ-CD is known to form also inclusion complexes of 2:1 stoichiometry and formation of cyclic supramolecular structures my also occur. Moreover to make the situation more complex, the change of the stoichiometry from 1:1 to 2:2 upon the increase in concentration has been reported for a naphthalene–β-CD complex; the concurrently observed increase in excimer indicated close pairing of naphthalene molecules [43]. Nevertheless, the good fit, observed at

least for the 2-*O*- and 3-*O*-regioisomers, identifies the 1:1 complexation as the probably dominant associative process.

The presence of unimers and/or short oligomers was confirmed by DLS even though objects with corresponding hydrodynamic diameters of a few nm were observed only in solutions of the 2-*O*- and 3-*O*-regioisomers after filtration through a filter with 0.22 μm pores. Indeed, larger particles with diameter in the range of tens and hundreds nm dominate the scattering, and such large objects of various morphologies were also detected by cryo-TEM. In this respect, the behavior of NA-γ-CD regioisomers is similar to native CDs for which unstable large objects are also observed [22]. Thus, the supramolecular behavior of NA-γ-CD seems to be determined not only by the interactions of NA and γ-CD but also by interactions of the subparts of the same type, i.e., NA/NA and γ-CD/γ-CD. In Figure 10 various putative interactions of NA-γ-CD are schematically depicted indicating how small supramolecular structures such as supramolecular oligomers or micelles as well as large one such as aggregates can originate.

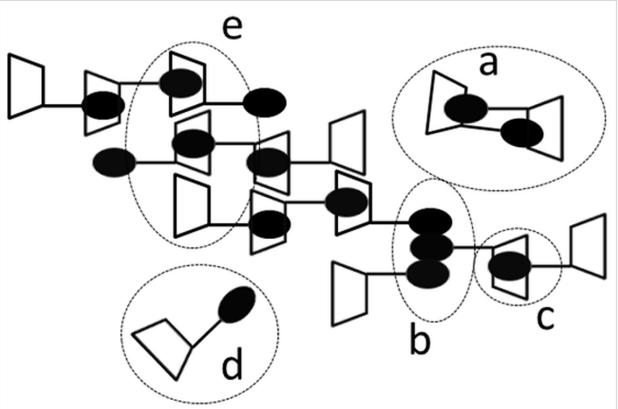

Figure 10: Putative objects and interactions in naphthylallyl-γ-CD solution, depicted schematically for 6^{I}-*O*-naphthylallyl-γ-CD (**2c**). (a) Cyclic supramolecular dimer based on inclusion complexation. (b) Interactions between naphthyl groups (stacking) leading to micellization or aggregation. (c) Inclusion complexation of naphthyl into the CD cavity leading to supramolecular polymerization. (d) Free **2c**. (e) Interaction between CD moieties leading to aggregation or precipitation.

As all three NA-γ-CD regioisomers were prepared, the effect of the substituent position could be assessed. Particularly, different behavior was observed especially between the 2-*O*-, 3-*O*-regioisomers on the one hand and the 6-*O*-one on the other. There are two underlying structural differences: (i) NA groups face the wider CD side in the head-tail arrangement of 6-*O*-isomers, (ii) the spacer of the 6-*O*-isomer is elongated by a CH_2 group of glucose unit. The details of differences in behavior in water could not be fully assessed due to the low solubility of the 6-*O*-regioisomer. In fact, the low solubility of the 6-*O*-regioisomer is the most striking difference in behavior of investigated regioisomers. The difference is easier to explain considering inclusion complexation of NA-γ-CD rather than interaction of NA groups only. Consequently, even though no direct evidence for inclusion complexation of NA-γ-CD was obtained it should not be omitted from considerations, especially because the inclusion complexation of naphthalene derivatives with CDs (including γ-CD) is so well established [42].

The experiments performed clearly demonstrate the supramolecular behavior of newly synthesized NA-γ-CDs in solution; at the same time, the experiments showed the anticipated formation of linear NA-γ-CD suprapolymers based on inclusion complexation as a somewhat naive concept – other interactions, e.g., naphthalene stacking may occur between two NA-γ-CD molecules; in addition, mutual interactions of more than two NA-γ-CD molecules may occur, leading to branched supramolecular structures or aggregation. It is to be hoped that the future research not only reveals details of NA-γ-CD interactions but also show how to utilize them in construction of functional supramolecular assemblies.

Conclusion

New methods for highly regioselective mononaphthylallylation of γ-CD to positions 2-*O*-, 3-*O*-, and 6-*O*- were developed. The alkylation reagent 2-(3-chloroprop-1-enyl)naphthalene, used for the reactions, can be easily prepared in large quantities without the need for chromatographic separation. The method originally expected to be used for the preparation of the regioisomers based on the metathesis of allyl-γ-CD derivatives proved to be inferior, giving about a 6 times lower overall yield than the mononaphthylallylation procedure. Compared to allyl derivatives, the NA-γ-CD derivatives are easy to prepare and purify. Due to the presence of the double bond in the NA group, they can be used as starting compounds for preparation of other monosubstituted γ-CD derivatives.

We demonstrated that the supramolecular properties of individual NA-γ-CD regioisomers substantially differ. The largest difference is being observed between 2-*O*- and 3-*O*-isomers on one hand and the 6-*O*- on the other. To explain the differences in the size of objects observed by different methods, various types of interactions have to be taken into account.

Supporting Information

Supporting Information File 1

Experimental part and data for compounds **2a**, **2b**, and **2c**: copies of NMR spectra and DLS.
[http://www.beilstein-journals.org/bjoc/content/supplementary/1860-5397-13-248-S1.pdf]

Acknowledgements

The work has been supported by the Czech Science Foundation (project No. 13-01440S and 17-07164S), the Charles University (project No. UNCE 204022), and the Ministry of Education, Youth and Sports of the Czech Republic (project No. 7F14009).

References

1. Crini, G. *Chem. Rev.* **2014,** *114,* 10940–10975. doi:10.1021/cr500081p
2. Řezanka, P.; Navrátilová, K.; Řezanka, M.; Král, V.; Sýkora, D. *Electrophoresis* **2014,** *35,* 2701–2721. doi:10.1002/elps.201400145
3. Xiao, Y.; Ng, S.-C.; Tan, T. T. Y.; Wang, Y. *J. Chromatogr. A* **2012,** *1269,* 52–68. doi:10.1016/j.chroma.2012.08.049
4. Li, S.; Purdy, W. C. *Chem. Rev.* **1992,** *92,* 1457–1470. doi:10.1021/cr00014a009
5. Szejtli, J. *J. Mater. Chem.* **1997,** *7,* 575–587. doi:10.1039/A605235E
6. Harada, A.; Takashima, Y.; Yamaguchi, H. *Chem. Soc. Rev.* **2009,** *38,* 875–882. doi:10.1039/b705458k
7. Miyauchi, M.; Kawaguchi, Y.; Harada, A. *J. Inclusion Phenom. Macrocyclic Chem.* **2004,** *50,* 57–62. doi:10.1007/s10847-003-8839-3
8. Yuen, F.; Tam, K. C. *Soft Matter* **2010,** *6,* 4613–4630. doi:10.1039/C0SM00043D
9. Brunsveld, L.; Folmer, B. J. B.; Meijer, E. W.; Sijbesma, R. P. *Chem. Rev.* **2001,** *101,* 4071–4098. doi:10.1021/cr990125q
10. Řezanka, M. *Eur. J. Org. Chem.* **2016,** 5322–5334. doi:10.1002/ejoc.201600693
11. Řezanka, M.; Eignerová, B.; Jindřich, J.; Kotora, M. *Eur. J. Org. Chem.* **2010,** 6256–6262. doi:10.1002/ejoc.201000807
12. Khan, A. R.; Forgo, P.; Stine, K. J.; D'Souza, V. T. *Chem. Rev.* **1998,** *98,* 1977–1996. doi:10.1021/cr970012b
13. Rong, D.; D'Souza, V. T. *Tetrahedron Lett.* **1990,** *31,* 4275–4278. doi:10.1016/S0040-4039(00)97599-3
14. Bláhová, M.; Bednářová, E.; Řezanka, M.; Jindřich, J. *J. Org. Chem.* **2013,** *78,* 697–701. doi:10.1021/jo301656p
15. Zhu, X.; Quaranta, A.; Bensasson, R. V.; Sollogoub, M.; Zhang, Y. *Chem. – Eur. J.* **2017,** *23,* 9462–9466. doi:10.1002/chem.201700782
16. Inoue, Y.; Hakushi, T.; Liu, Y.; Tong, L.; Shen, B.; Jin, D. *J. Am. Chem. Soc.* **1993,** *115,* 475–481. doi:10.1021/ja00055a017
17. Harada, A.; Takashima, Y.; Nakahata, M. *Acc. Chem. Res.* **2014,** *47,* 2128–2140. doi:10.1021/ar500109h
18. Puskás, I.; Schrott, M.; Malanga, M.; Szente, L. *J. Inclusion Phenom. Macrocyclic Chem.* **2012,** *75,* 269–276. doi:10.1007/s10847-012-0127-7
19. Coleman, A. W.; Nicolis, I.; Keller, N.; Dalbiez, J. P. *J. Inclusion Phenom. Mol. Recognit. Chem.* **1992,** *13,* 139–143. doi:10.1007/BF01053637
20. Benkovics, G.; Hodek, O.; Havlikova, M.; Bosakova, Z.; Coufal, P.; Malanga, M.; Fenyvesi, E.; Darcsi, A.; Beni, S.; Jindrich, J. *Beilstein J. Org. Chem.* **2016,** *12,* 97–109. doi:10.3762/bjoc.12.11
21. González-Gaitano, G.; Rodríguez, P.; Isasi, J. R.; Fuentes, M.; Tardajos, G.; Sánchez, M. *J. Inclusion Phenom. Macrocyclic Chem.* **2002,** *44,* 101–105. doi:10.1023/A:1023065823358
22. Bonini, M.; Rossi, S.; Karlsson, G.; Almgren, M.; Lo Nostro, P.; Baglioni, P. *Langmuir* **2006,** *22,* 1478–1484. doi:10.1021/la052878f
23. Peroche, S.; Parrot-Lopez, H. *Tetrahedron Lett.* **2003,** *44,* 241–245. doi:10.1016/S0040-4039(02)02539-X
24. Gèze, A.; Aous, S.; Baussanne, I.; Putaux, J.; Defaye, J.; Wouessidjewe, D. *Int. J. Pharm.* **2002,** *242,* 301–305. doi:10.1016/S0378-5173(02)00192-8
25. Šnajdr, I.; Janoušek, Z.; Jindřich, J.; Kotora, M. *Beilstein J. Org. Chem.* **2010,** *6,* 1099–1105. doi:10.3762/bjoc.6.126
26. Tanaka, S.; Saburi, H.; Hirakawa, T.; Seki, T.; Kitamura, M. *Chem. Lett.* **2009,** *38,* 188–189. doi:10.1246/cl.2009.188
27. Tanaka, S.; Hirakawa, T.; Oishi, K.; Hayakawa, Y.; Kitamura, M. *Tetrahedron Lett.* **2007,** *48,* 7320–7322. doi:10.1016/j.tetlet.2007.08.032
28. Bouziane, A.; Hélou, M.; Carboni, B.; Carreaux, F.; Demerseman, B.; Bruneau, C.; Renaud, J.-L. *Chem. – Eur. J.* **2008,** *14,* 5630–5637. doi:10.1002/chem.200702030
29. Tojima, T.; Katsura, H.; Nishiki, M.; Nishi, N.; Tokura, S.; Sakairi, N. *Carbohydr. Polym.* **1999,** *40,* 17–22. doi:10.1016/S0144-8617(99)00030-2
30. Řezanka, M.; Jindřich, J. *Carbohydr. Res.* **2011,** *346,* 2374–2379. doi:10.1016/j.carres.2011.08.011
31. Hanessian, S.; Benalil, A.; Laferriere, C. *J. Org. Chem.* **1995,** *60,* 4786–4797. doi:10.1021/jo00120a023
32. Masurier, N.; Lafont, O.; Le Provost, R.; Lesur, D.; Masson, P.; Djedaini-Pilard, F.; Estour, F. *Chem. Commun.* **2009,** 589–591. doi:10.1039/B812325J
33. Jindrich, J.; Pitha, J.; Bengt, L. *Carbohydr. Res.* **1995,** *275,* 1–7. doi:10.1016/0008-6215(95)00071-Z
34. Wenz, G.; Höfler, T. *Carbohydr. Res.* **1999,** *322,* 153–165. doi:10.1016/S0008-6215(99)00224-4
35. Jindřich, T.; Tišlerová, I. *J. Org. Chem.* **2005,** *70,* 9054–9055. doi:10.1021/jo051339c
36. Bertaut, E.; Landy, D. *Beilstein J. Org. Chem.* **2014,** *10,* 2630–2641. doi:10.3762/bjoc.10.275
37. Lovatt, M.; Cooper, A.; Camilleri, P. *Eur. Biophys. J.* **1996,** *24,* 354–357. doi:10.1007/BF00180377
38. Heerklotz, H. H.; Binder, H.; Epand, R. M. *Biophys. J.* **1999,** *76,* 2606–2613. doi:10.1016/S0006-3495(99)77413-8
39. Illapakurthy, A. C.; Wyandt, C. M.; Stodghill, S. P. *Eur. J. Pharm. Biopharm.* **2005,** *59,* 325–332. doi:10.1016/j.ejpb.2004.08.006
40. Munk, P.; Aminabhavi, T. M. *Introduction to Macromolecular Science,* 2nd ed.; Wiley-Interscience: New York, 2002.
41. Pessine, F. B. T.; Calderini, A.; Alexandrino, G. L. *Magnetic Resonance Spectroscopy;* InTechOpen, 2012; pp 237–264.
42. Rekharsky, M. V.; Inoue, Y. *Chem. Rev.* **1998,** *98,* 1875–1918. doi:10.1021/cr970015o
43. Sau, S.; Solanki, B.; Orprecio, R.; Stam, J. V.; Evans, C. H. *J. Inclusion Phenom. Macrocyclic Chem.* **2004,** *48,* 173–180. doi:10.1023/B:JIPH.0000022556.47230.c8